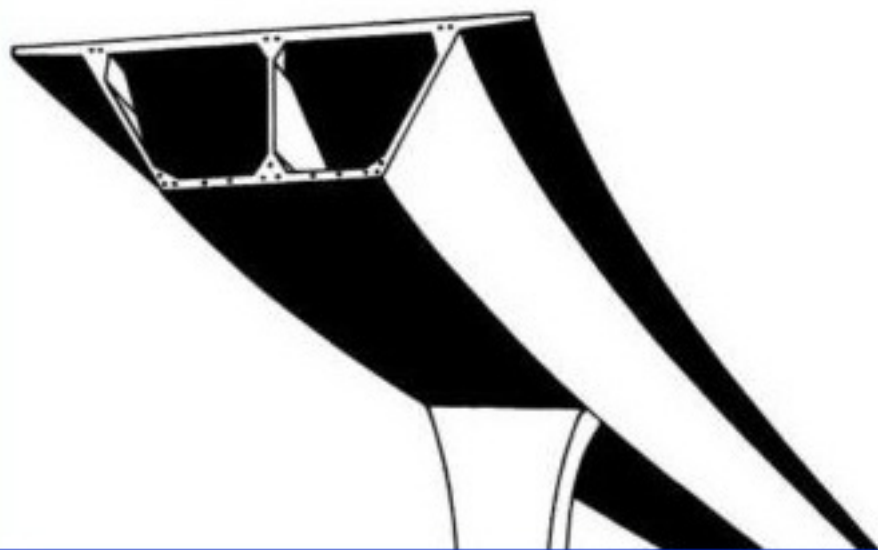


# DESIGN OF PRESTRESSED CONCRETE

R. I. GILBERT  
N. C. MICKLEBOROUGH



# DESIGN OF PRESTRESSED CONCRETE



This page intentionally left blank.

# DESIGN OF PRESTRESSED CONCRETE

## TITLES OF RELATED INTEREST

*Analytical and computational methods in engineering rock mechanics*  
E.T.Brown (ed.)

*Boundary element methods in elastodynamics*  
G.D.Manolis & D.E.Beskos

*Boundary element methods in solid mechanics*  
S.L.Crouch & A.M.Starfield

*Computers in construction planning and control*  
M.J.Jackson

*A concise introduction to engineering economics*  
P.Cassimatis

*Distribution-free tests*  
H.R.Neave & P.B.Worthington

*Earth structures engineering*  
R.J.Mitchell

*The finite element method in thermomechanics*  
T.-R.Tsu

*Hemispherical projection methods in rock mechanics*  
S.D.Priest

*Hydraulic structures*  
P.Novak *et al.*

*Hydraulics in civil engineering*  
A.Chadwick & J.Morfett

*Intelligent planning*  
R.Wyatt

*Marine geotechnics*  
H.Poulos

*Numerical methods in engineering and science*  
G.deV.Davis

*Planning and design of engineering systems*  
R.Warner & G.Dandy

*Plastic design*

P.Zeman & H.M.Irvine

*Rock mechanics for underground mining*

B.H.G.Brady & E.T.Brown

*Structural dynamics*

H.M.Irvine

# DESIGN OF PRESTRESSED CONCRETE

*R.I.Gilbert & N.C.Mickleborough*

*School of Civil Engineering*

*The University of New South Wales, Sydney, Australia*



LONDON AND NEW YORK

First published in 1990 by Unwin Hyman Ltd

Transferred to Digital Printing 2004

*Spon Press is an imprint of the Taylor & Francis Group*

This edition published in the Taylor & Francis e-Library, 2005.

To purchase your own copy of this or any of Taylor & Francis or Routledge's collection of thousands of eBooks please go to [www.eBookstore.tandf.co.uk](http://www.eBookstore.tandf.co.uk).

© R.I.Gilbert & N.C.Mickleborough, 1990

This book is copyright under the Berne Convention. No reproduction without permission. All rights reserved.

**British Library Cataloguing in Publication Data**

Gilbert, R.I.

Design of prestressed concrete.

1. Prestressed concrete

I. Title II. Mickleborough, N.C.

666.893

ISBN 0-203-98586-9 Master e-book ISBN

ISBN 0-419-16160-0 (Print Edition)

**Library of Congress Cataloging-in-Publication Data**

Gilbert, R.I., 1950–

Design of prestressed concrete/R.I.Gilbert, N.C.Mickleborough.

p. cm.

Includes bibliographical references.

ISBN 0-04-445402-3 (alk. paper)

ISBN 0-04-445403-1 (pbk.: alk. paper)

1. Prestressed concrete construction. 2. Structural design.

I.Mickleborough, N.C. (Neil C.) II. Title.

TA683.9.G52 1990

624.1' 83412–dc20 89–77745

CIP

## Preface

The design of structures in general, and prestressed concrete structures in particular, requires considerably more information than is contained in building codes. A sound understanding of structural behaviour at all stages of loading is essential. The aim of this book is to present a detailed description and explanation of the behaviour of prestressed concrete members and structures both at service loads and at ultimate loads and, in doing so, provide a comprehensive guide to design. The design criteria and procedures contained in several major building codes, including ACI 318–83, BS 8110:1985, and AS 3600–1988, are also presented.

Each aspect of the analysis and design of fully prestressed and partially prestressed concrete members is approached from first principles and illustrated by numerous worked examples. The text is written for senior undergraduate and postgraduate students of civil and structural engineering, and also for practising structural engineers.

The book began as notes for a series of lectures to structural engineers in a short course on prestressed concrete design conducted in Sydney in 1985 and has been further developed over the past 5 years as part of the authors' involvement in research and the teaching of prestressed concrete to graduate students at the University of New South Wales. The work has also gained much from the membership of Professor Gilbert on committees of the Standards Association of Australia and his involvement in the development of the Australian Standard for Concrete Structures, AS 3600–1988.

The scope of the work ranges from an introduction to the fundamentals of prestressed concrete to in-depth treatments of more advanced topics. [Chapter 1](#) introduces the basic concepts of prestressed concrete and the limit states design philosophies used in North American, British, European, and Australian practice. Material properties relevant to design are discussed in [Chapter 2](#). A comprehensive treatment of the design of prestressed concrete beams for serviceability is presented in [Chapter 3](#). The instantaneous and time-dependent behaviour of cross-sections under service loads are discussed in considerable detail. Both uncracked and cracked cross-sections are considered. Techniques for determining the section size, the magnitude and eccentricity of prestress, the losses of prestress and the deflection of members are outlined. Each aspect of design is illustrated by numerical examples.

Chapters [4](#) and [5](#) deal with the design of members for strength in bending, shear, and torsion, and [Chapter 6](#) covers the design of the anchorage zones

in both pretensioned and post-tensioned members. A guide to the design of composite prestressed concrete beams is provided in [Chapter 7](#), and includes a detailed worked example of the analysis of a composite trough girder footbridge. [Chapter 8](#) discusses design procedures for statically determinate beams. Comprehensive self-contained design examples are provided for fully prestressed and partially prestressed, post-tensioned, and pretensioned concrete members.

The analysis and design of statically indeterminate beams and frames is covered in [Chapter 9](#), and provides guidance on the treatment of secondary effects at all stages of loading. Chapters [10](#) and [11](#) provide a detailed discussion of the analysis and design of two-way slab systems. [Chapter 10](#) is concerned with the behaviour and strength of slabs, whilst [Chapter 11](#) deals with serviceability. Complete design examples are provided for panels of an edge-supported slab and a flat slab. The behaviour of axially loaded members is dealt with in [Chapter 12](#). Compression members, members subjected to combined bending and compression, and prestressed concrete tension members are discussed and design aspects are illustrated by examples.

A special feature of the book is the treatment of serviceability aspects of design. Concrete structures are prestressed to improve behaviour at service loads and thereby increase the economical range of concrete as a construction material. In conventional prestressed structures, the level of prestress and the position of the tendons are usually based on considerations of serviceability. Practical methods for accounting for the non-linear and time-dependent effects of cracking, creep, shrinkage, and relaxation are presented in a clear and easy-to-follow format.

The authors hope that *Design of Prestressed Concrete* will be a valuable source of information and a useful guide to design.

R.I.Gilbert & N.C.Mickleborough  
Sydney, 1990



# Contents

<a href="#">Preface</a>	<a href="#">vii</a>
<a href="#">Notation</a>	<a href="#">xiii</a>
<a href="#">1 Basic concepts</a>	<a href="#">1</a>
<a href="#">1.1 Introduction</a>	<a href="#">1</a>
<a href="#">1.2 Methods of prestressing</a>	<a href="#">2</a>
<a href="#">1.3 Introductory example</a>	<a href="#">4</a>
<a href="#">1.4 Transverse forces caused by draped tendons</a>	<a href="#">6</a>
<a href="#">1.5 Calculation of elastic stresses</a>	<a href="#">9</a>
<a href="#">1.6 Flexural behaviour—from initial to ultimate loads</a>	<a href="#">15</a>
<a href="#">1.7 Design procedures</a>	<a href="#">17</a>
<a href="#">1.8 References</a>	<a href="#">28</a>
<a href="#">2 Design properties of materials</a>	<a href="#">29</a>
<a href="#">2.1 Introduction</a>	<a href="#">29</a>
CONCRETE	
<a href="#">2.2 Composition of concrete</a>	<a href="#">30</a>
<a href="#">2.3 Strength of concrete</a>	<a href="#">30</a>
<a href="#">2.4 Deformation of concrete</a>	<a href="#">34</a>
<a href="#">2.5 Predictions of the creep coefficient and shrinkage</a>	<a href="#">42</a>
<a href="#">2.6 Thermal expansion</a>	<a href="#">47</a>
STEEL	
<a href="#">2.7 Steel used for prestressing</a>	<a href="#">48</a>
<a href="#">2.8 Steel relaxation</a>	<a href="#">52</a>
<a href="#">2.9 Non-prestressed reinforcement</a>	<a href="#">54</a>
<a href="#">2.10 References</a>	<a href="#">58</a>

<u>3 Design for serviceability</u>	<u>60</u>
<u>3.1 Introduction</u>	<u>60</u>
<u>3.2 Stress limits</u>	<u>61</u>
<u>3.3 Determination of prestress and eccentricity in flexural members</u>	<u>64</u>
<u>3.4 Cable profiles</u>	<u>75</u>
<u>3.5 Short-term analysis of cross-sections</u>	<u>77</u>
<u>3.6 Time-dependent analysis of cross-sections</u>	<u>89</u>
<u>3.7 Losses of prestress</u>	<u>102</u>
<u>3.8 Deflection calculations</u>	<u>108</u>
<u>3.9 References</u>	<u>120</u>
<u>4 Ultimate flexural strength</u>	<u>121</u>
<u>4.1 Introduction</u>	<u>121</u>
<u>4.2 Flexural behaviour at overloads</u>	<u>122</u>
<u>4.3 Flexural strength theory</u>	<u>124</u>
<u>4.4 Approximate code-oriented procedures</u>	<u>140</u>
<u>4.5 Design calculations</u>	<u>147</u>
<u>4.6 Flanged sections</u>	<u>153</u>
<u>4.7 References</u>	<u>159</u>
<u>5 Design for shear and torsional strength</u>	<u>160</u>
<u>5.1 Introduction</u>	<u>160</u>
<u>SHEAR IN BEAMS</u>	
<u>5.2 Inclined cracking</u>	<u>161</u>
<u>5.3 Effect of prestress</u>	<u>162</u>
<u>5.4 Web reinforcement</u>	<u>163</u>
<u>5.5 Shear strength</u>	<u>165</u>
<u>TORSION IN BEAMS</u>	
<u>5.6 Compatibility torsion and equilibrium torsion</u>	<u>182</u>
<u>5.7 Effects of torsion</u>	<u>183</u>
<u>5.8 Design provisions for torsion in AS 3600–1988</u>	<u>185</u>

<u>SHEAR IN SLABS AND FOOTINGS</u>	
<u>5.9 Punching shear</u>	<u>195</u>
<u>5.10 Design procedures for punching shear in AS 3600–1988</u>	<u>198</u>
<u>5.11 References</u>	<u>208</u>
<u>6 Anchorage zones</u>	<u>209</u>
<u>6.1 Introduction</u>	<u>209</u>
<u>6.2 Pretensioned concrete—force transfer by bond</u>	<u>210</u>
<u>6.3 Post-tensioned concrete anchorage zones</u>	<u>214</u>
<u>6.4 References</u>	<u>238</u>
<u>7 Composite members</u>	<u>240</u>
<u>7.1 Types and advantages of composite construction</u>	<u>240</u>
<u>7.2 Behaviour of composite members</u>	<u>242</u>
<u>7.3 Stages of loading</u>	<u>243</u>
<u>7.4 Determination of prestress</u>	<u>246</u>
<u>7.5 Methods of analysis at service loads</u>	<u>249</u>
<u>7.6 Ultimate flexural strength</u>	<u>265</u>
<u>7.7 Horizontal shear transfer</u>	<u>265</u>
<u>7.8 Ultimate shear strength</u>	<u>275</u>
<u>7.9 References</u>	<u>280</u>
<u>8 Design procedures for determinate beams</u>	<u>281</u>
<u>8.1 Introduction</u>	<u>281</u>
<u>8.2 Types of section</u>	<u>281</u>
<u>8.3 Initial trial section</u>	<u>283</u>
<u>8.4 Design procedures—fully prestressed beams</u>	<u>286</u>
<u>8.5 Design procedures—partially prestressed beams</u>	<u>312</u>
<u>9 Statically indeterminate members</u>	<u>319</u>
<u>9.1 Introduction</u>	<u>319</u>
<u>9.2 Tendon profiles</u>	<u>321</u>
<u>9.3 Continuous beams</u>	<u>323</u>
<u>9.4 Statically indeterminate frames</u>	<u>350</u>
<u>9.5 Design of continuous beams</u>	<u>354</u>
<u>9.6 References</u>	<u>375</u>

<u>10 Two-way slabs—behaviour and design</u>	<u>376</u>
<u>10.1 Introduction</u>	<u>376</u>
<u>10.2 Effects of prestress</u>	<u>378</u>
<u>10.3 Design approach—general</u>	<u>381</u>
<u>10.4 One-way slabs</u>	<u>382</u>
<u>10.5 Two-way edge-supported slabs</u>	<u>382</u>
<u>10.6 Flat plate slabs</u>	<u>394</u>
<u>10.7 Flat slabs with drop panels</u>	<u>415</u>
<u>10.8 Band-beam and slab systems</u>	<u>416</u>
<u>10.9 References</u>	<u>417</u>
<u>11 Two-way slabs—serviceability</u>	<u>418</u>
<u>11.1 Introduction</u>	<u>418</u>
<u>11.2 The balanced load stage</u>	<u>419</u>
<u>11.3 Initial sizing of slabs</u>	<u>421</u>
<u>11.4 A review of simplified slab deflection models</u>	<u>429</u>
<u>11.5 Cracking in prestressed slabs</u>	<u>438</u>
<u>11.6 Long-term deflections</u>	<u>442</u>
<u>11.7 Worked examples</u>	<u>443</u>
<u>11.8 References</u>	<u>452</u>
<u>12 Compression and tension members</u>	<u>454</u>
<u>12.1 Types of compression members</u>	<u>454</u>
<u>12.2 Classification and behaviour of compression members</u>	<u>455</u>
<u>12.3 Cross-sectional analysis—compression and bending</u>	<u>457</u>
<u>12.4 Slenderness effects</u>	<u>471</u>
<u>12.5 Reinforcement requirements in compression members</u>	<u>481</u>
<u>12.6 Tension members</u>	<u>483</u>
<u>12.7 References</u>	<u>489</u>
<u>Appendix I Alternative models for creep and shrinkage</u>	<u>490</u>
<u>A.1 Introduction</u>	<u>490</u>
<u>A.2 The ACI Committee 209 Method (1978)</u>	<u>490</u>
<u>A.3 The CEB–FIP Method (1978)</u>	<u>493</u>
<u>A.4 References</u>	<u>497</u>
<u>Index</u>	<u>498</u>



## Notation

All symbols are defined in the text where they first appear. The more frequently used symbols and those that appear throughout the book are listed below. Tension is taken to be positive and compression is negative, throughout. Positive bending about a horizontal axis causes tension in the bottom fibres of a cross-section.

$A$	area
$A_c$	area of concrete
$A_g$	area of gross cross-section
$A_{min}$	minimum required area of a cross-section
$A_{pc}$	area of the precast element of a composite cross-section
$A_{pt}$	area of prestressed steel in the tensile zone
$A_s, A_p$	areas of the non-prestressed and prestressed steel, respectively
$A_{si}, A_{pi}$	areas of non-prestressed and prestressed steel at the $i$ th steel level, respectively
$A_{sb}, A_{ss}$	area of the transverse non-prestressed reinforcement required for bursting and spalling, respectively, in an anchorage zone (Eqns 6.11 and 6.12)
$A_{st}, A_{sc}$	areas of the non-prestressed tensile and compressive reinforcement, respectively
$A_{sv}$	area of shear reinforcement at each stirrup location
$A_{sw}$	area of bar used for closed torsional stirrup
$(A_s)_{min}$	minimum area of non-prestressed reinforcement
$A'$	area of concrete under idealized rectangular compressive stress block
$A_1$	bearing area
$A_2$	largest area of the concrete surface geometrically similar to $A_1$
$a$	width of the torsion strip
$B$	first moment of area of the transformed cross-section about the top fibre
$B_c, \bar{B}_c$	property $B$ of the concrete part of the cross-section and of the age-adjusted transformed section, respectively
$b$	width of the compressive zone of the cross-section of a beam or slab
$b_{ef}$	effective width of the flange of a flanged cross-section
$b_f$	width of the contact surface between the precast and <i>in situ</i> parts of a composite cross-section

$b_o$	width of an opening adjacent to the critical shear perimeter ( <a href="#">Fig. 5.12</a> )
$b_{tr}$	width of the transformed flange of a composite cross-section (Eqn 7.1)
$b_v$	effective width of the web for shear calculations ( $b_w - 0.5d_d$ )
$b_w$	width of the web of a flanged cross-section
$C$	resultant compressive force carry over factor
$C_b$	transverse compressive force behind an anchorage plate caused by bursting
$C_c$	compressive force carried by the concrete
$C_m$	factor to account for the effect of the magnitude and direction of end moments on the moment magnification factor for a slender column
$C_s$	compressive force in the non-prestressed steel
$c_1, c_2$	side dimensions of a column
$D$	overall depth of a cross-section
$D_b$	overall depth of the beam in a beam and slab system
$D_e$	depth of the symmetrical prism within an anchorage zone
$D_{min}$	minimum overall depth
$D_s$	depth of a slab
$d$	effective depth from the extreme compressive fibre to the resultant tensile force at the ultimate strength in bending
$d_b$	bar diameter
$d_c$	depth to the top layer of non-prestressed steel
$d_d$	diameter of a prestressing duct
$d_n$	depth from the extreme compressive fibre to the neutral axis
$d_o$	depth to the bottom layer of tensile reinforcement
$d_s, d_p$	depths to the non-prestressed and prestressed steel, respectively
$d_{si}, d_{pi}$	depths to the $i$ th level of non-prestressed and prestressed steel, respectively
$d_z$	depth to the compressive force in the concrete
$E_c, E_s, E_p$	elastic moduli of concrete, non-prestressed steel, and prestressed steel, respectively
$E_{ci}$	initial elastic modulus of concrete
$E_{c,28}$	static elastic modulus at 28 days (Eqn 2.17)
$E_{c1}, E_{c2}$	elastic moduli of concrete in precast and <i>in situ</i> elements, respectively, of a composite cross-section
$E_e, \bar{E}_e$	effective modulus of concrete (Eqn 2.12) and age-adjusted effective modulus of concrete (Eqn 2.14), respectively
$e$	eccentricity of prestress eccentricity of load in a compression member
$e$	base of the natural logarithm

$e^*$	eccentricity of the pressure line from the centroidal axis
$e_{max}$	maximum possible eccentricity of prestress
$e_{min}$	minimum acceptable eccentricity of prestress
$e_o$	initial eccentricity of load in a slender column
$e_{pc}$	eccentricity of prestress measured from the centroidal axis of the precast part of a composite cross-section
$F(x), \bar{F}(x)$	functions of $x$ (Eqn 9.4)
$F_b$	design strength of concrete in bearing
$F_c, F_{ci}$	compressive stress limits for concrete under full load and immediately after transfer, respectively
$F_{ep}$	force caused by earth pressure
$F_{eq}$	force caused by earthquake
$F_{lp}$	force caused by liquid pressure
$F_s$	force caused by snow loads
$F_b, F_{ti}$	tensile stress limits for concrete under full load and immediately after transfer, respectively
$F_c^*$	absolute value of the design force in the compressive zone due to bending
$f_B$	flexibility coefficient associated with a release at point B
$f_c(t)$	mean compressive strength of concrete at time $t$
$f_{cv}$	permissible concrete shear stress on the critical shear perimeter
$f_c'$	characteristic compressive strength of concrete at 28 days
$f_c'(t)$	characteristic compressive strength of concrete at time $t$
$f_{ci}'$	characteristic compressive strength of concrete at transfer
$f_{cu}$	cube strength of concrete
$f_p$	ultimate strength of the prestressing steel
$f_{py}$	0.2% proof stress for prestressing steel
$f_{ft}$	flexural tensile strength of concrete (Eqn 2.3)
$f_{td}$	direct tensile strength of concrete (Eqn 2.4)
$f_y$	yield stress of non-prestressed steel
$G$	dead load
$g$	dead load per unit area
$h$	dimension of anchorage plate drape of tendon
$h_x, h_y$	drape of the tendons running in the $x$ and $y$ directions, respectively
$I$	second moment of area (moment of inertia) about centroidal axis
$I_{av}$	average second moment of area after cracking
$I_{c1}, I_{c2}$	second moments of area of precast and <i>in situ</i> elements on a composite cross-section
$I_{cr}$	second moment of area of a cracked cross-section



$I_e$  effective second moment of area after cracking  
 $I_g$  second moment of area of the gross cross-section

$\bar{I}$	second moment of area of the transformed section about the top fibre of the section
$\bar{I}_c, \bar{I}_e$	property $\bar{I}$ of the concrete part of the cross-section and of the age-adjusted transformed section, respectively
$i, j, k$	integers
$J_t$	torsional constant
$kl_u$	effective length of a column
$k_{AB}$	stiffness coefficient for member AB
$k_u$	ratio of the depth to the neutral axis to the effective depth at the ultimate bending moment
$k_1, k_2$	factors used for the determination of stress in the prestressing steel at ultimate (Eqn 4.18)
$k_1, k_2, k_3$	material multiplication constants
$K$	slab system factor
$L$	span
$L_a$	length of anchorage zone measured from the loaded face ( <a href="#">Fig. 6.3b</a> )
$L_b, L_c$	length of a beam and a column, respectively
$L_{di}$	length of tendon associated with draw-in losses (Eqn 3.61)
$L_e$	effective span, i.e. the lesser of the centre to centre distance between the supports and the clear span plus depth ( $L_n + D$ )
$L_o$	distance between points of zero bending moment in a beam
$L_n$	clear span
$L_{pa}$	distance along a tendon from the jack
$L_t$	transverse span
$L_x, L_y$	shorter and longer orthogonal span lengths, respectively, in two-way slabs
$l$	internal level arm
$l_b, l_s$	lever arms associated with bursting and spalling moment, respectively
$l_c, l_s$	lever arm distance of compressive forces in the concrete and in the steel, respectively, above the non-prestressed tensile steel ( <a href="#">Fig. 4.6</a> )
$l_d$	development length for a pretensioned tendon (Eqn 6.2)
$l_t$	transmission length for a pretensioned tendon (Eqn 6.2)
$l_t$	additional length required to develop $(\sigma_{pu} - \sigma_{pe})$ in a pretensioned tendon (Eqn 6.2)
$l_u$	unsupported length of a column
$\ln$	natural logarithm
$M$	bending moment
$\bar{M}$	virtual bending moment
$M_b$	bursting moment moment transferred to front face of a column
$M_{cr}$	cracking moment
$M^F$	fixed-end moment

$M_G, M_Q$	moment caused by the dead and live loads, respectively
$M_i$	initial moment about top fibre of the transformed cross-section
$M_o$	moment at a cross-section at transfer total static moment in a two-way flat slab decompression moment
$M_{pp}, M_{ps}$	total and secondary moments due to prestress in a continuous member
$M_s$	spalling moment moment transferred to side face of a column
$M_{sus}$	moment caused by the sustained loads
$M_{sw}$	moment caused by self-weight
$M_T$	moment caused by total service loads
$M_u$	ultimate flexural strength
$M_{ub}$	unbalanced moment
$M^*$	factored design moment for the strength limit state
$M_m^*$	magnified design moment
$M_v^*$	design moment transferred to a column through the critical shear perimeter
$m_u, m'_u$	ultimate moment of resistance per unit length along a positive and a negative yield line, respectively
$N$	axial force
$\bar{N}$	virtual axial force
$N_c$	critical buckling load
$N_{cr}$	tensile axial force at cracking
$N_i$	initial axial force on the transformed cross-section
$N_u$	ultimate axial strength
$N_{ub}$	ultimate axial force at the balanced failure point
$N^*$	factored design axial force for the strength limit state
$\Delta N_i, \Delta M_i$	increments of axial force and moment about the top fibre of the cross-section, respectively
$\delta N, \delta M$	restraining actions which develop during a time interval due to restrained creep, shrinkage and relaxation (Eqns 3.41–3.48)
$n, n_s$	modular ratio for non-prestressed steel ( $E_s/E_c$ )
$n, n_p$	modular ratio for prestressed steel ( $E_p/E_c$ )
$\bar{n}$	age-adjusted modular ratio ( $E_s/\bar{E}_c$ or $E_p/\bar{E}_c$ )
$n_c$	modular ratio for the <i>in situ</i> concrete on a composite cross-section ( $E_{c2}/E_{c1}$ )
$P$	prestressing force
$P_e$	effective prestressing force after time-dependent losses
$P_i$	prestressing force immediately after transfer
$P_j$	prestressing force at the jack before transfer
$P_v$	vertical component of prestress
$Q$	live load

first moment of an area about the centroidal axis

$q$	live load per unit area
$q_p, q_s$	reinforcement indices for prestressed and non-prestressed steel
$R$	relaxation force in the prestressing steel relaxation of prestress (in percent) time-dependent loss parameter ( $P_e/P_i$ ) reaction force ratio of cube and cylinder strengths radius of curvature
$R_u$	ultimate strength
$R^*$	factored design action for the strength limit state
$R_{1000}, R_\infty$	relaxation of prestressing steel (in percent) after 1000 h and at time infinity, respectively
$r$	radius of gyration
$s$	spacing between stirrups or ties
$T$	resultant tensile force twisting moment or torque temperature
$T_b$	tension resulting from bursting
$T_{cr}$	twisting moment at first cracking
$T_p$	tension in the prestressed steel
$T_s$	tension in the non-prestressed steel twisting moment transferred to side face of column
$T_u$	ultimate strength in torsion
$T_{uc}$	torsional strength of a beam without torsional reinforcement (Eqn 5.28)
$T_{us}$	torsional strength of a beam containing torsional reinforcement (Eqn 5.29)
$T_{u,max}$	maximum torsional strength of a cross-section
$T_1$	twisting moment carried by the torsion strip
$T^*$	factored design torsion for the strength limit state
$\Delta T$	restraining force at level of non-prestressed steel
$\Delta T_c$	tensile force increment imposed on concrete
$\Delta T_p$	restraining force at level of prestressed steel
$t$	time
$U$	internal work
$u$	perimeter of the critical section for punching shear
$V$	shear force
$V_b, V_s$	shear transferred to the front and side faces of a column, respectively
$V_{cr}$	shear force acting with torque $T_{cr}$ at first cracking
$V_o$	shear force corresponding to the decompression moment $M_o$
$V_t$	shear force required to produce a web-shear crack
$V_u$	ultimate shear strength
$V_{uc}$	contribution of concrete to the shear strength

$V_{uo}$	shear strength of the critical shear perimeter with no moment transferred
$V_{us}$	contribution of transverse steel to the shear strength
$V_{u,max}$	maximum shear strength of a beam (Eqn 5.7)
$V_{u,min}$	shear strength of a beam containing the minimum shear reinforcement (Eqn 5.6)
$V_1$	shear carried by the torsion strip
$V^*$	factored design shear force for the strength limit state
$V_f^*, v_f^*$	design horizontal shear force and nominal shear stress; respectively
$v$	deflection
$v_C$	deflection at midspan
$v_{cr}$	deflection due to creep
$v_{cx}, v_{mx}$	deflection of the column strip and the middle strip in the $x$ -direction
$v_{cy}, v_{my}$	deflection of the column strip and the middle strip in the $y$ -direction
$v_i$	deflection immediately after transfer
$v_{LT}$	time-dependent part of the total deflection
$v_{max}$	maximum permissible total deflection maximum deflection of a flat plate (Eqn 11.11)
$v_{sh}$	deflection due to shrinkage
$v_{sus}$	short-term deflection caused by the sustained loads
$v_{tot}$	total deflection
$v_v, v_{var}$	deflection due to variable loads
$W$	wind load external work
$w$	uniformly distributed load
$w_b$	the balanced load
$w_G, w_Q$	uniformly distributed dead and live loads, respectively
$w_p$	uniformly distributed transverse load exerted on a member by a parabolic tendon profile
$w_{px}, w_{py}$	transverse loads exerted by tendons in the $x$ - and $y$ -directions, respectively (Eqn 10.3)
$w_{sw}$	self-weight
$w_t$	total equivalent long-term load (Eqn 8.4)
$w_{ub}, w_u$	unbalanced load
$w_{us}$	sustained part of the unbalanced load
$w_v$	variable or transient part of the uniform load
$w^*$	factored design load for the strength limit state
$x$	direction of member axis
$x, y$	shorter and longer overall dimensions of the rectangular parts of a solid section
$x_1, y_1$	shorter and larger dimension of a closed rectangular tie

$y$	direction perpendicular to the member axis depth below reference level (either centroidal axis or top fibre)
$y_b, y_t$	distance from centroidal axis to bottom and top fibre, respectively
$Z$	section modulus
$Z_b, Z_t$	bottom and top fibre section moduli ( $I/y_b, I/y_t$ ) respectively
$Z_{b,pc}, Z_{t,pc}$	bottom and top fibre section moduli of the precast part of a composite cross-section
$Z_{b,comp}$	bottom fibre section modulus of a composite cross-section
$(Z_b)_{min}$	minimum bottom fibre section modulus (Eqn 3.9)
$\alpha$	a parameter to account for the effect of cracking and reinforcement quantity on the restraint to creep (Eqn 3.76) twice the slope of the prestress line ( <a href="#">Fig. 3.21b</a> ) constant associated with the development of concrete strength with time (Eqn 2.2) factor that depends on the support conditions of a two-way edge-supported slab
$\alpha_b, \alpha_t$	section properties relating to bottom and top fibres ( $A/Z_b$ and $A/Z_t$ , respectively)
$\alpha_n$	factor to define the shape of a biaxial bending contour (Eqn 12.18)
$\alpha_t$	sum of the successive angular deviations of a tendon (Eqn 3.60)
$\alpha_v$	angle between shear reinforcement and longitudinal tensile steel
$\beta$	deflection coefficient shrinkage deflection coefficient constant associated with the development of concrete strength with time (Eqn 2.2)
$\beta_c$	ratio of long side to short side of the loaded area (in punching shear calculations)
$\beta_h$	ratio of the longest overall dimension of the effective loaded area to the overall dimension measured in the perpendicular direction (Eqn 5.52)
$\beta_p$	angular deviation term (Eqn 3.60)
$\beta_x, \beta_y$	moment coefficients in a two-way slab (Eqn 10.8)
$\beta_1, \beta_2$	tension stiffening constants (Eqn 3.74)
$\beta_4, \beta_5$	coefficients related to the surface of the shear plane (Eqn 7.29)
$\gamma$	ratio of the depth of the idealized rectangular compressive stress block to the depth of the neutral axis at the ultimate strength in bending or combined bending and compression
$\gamma_c, \gamma_s$	partial safety factor for concrete and steel, respectively
$\gamma_m$	partial material safety factor
$\gamma_v$	fraction of unbalanced moment transferred to a column by eccentricity of shear (Eqn 5.49)

$\Delta$	an increment or a change lateral displacement (sway) at the top of a column slip or draw-in (in mm) at the anchorage of a tendon
$\delta_b, \delta_s$	moment magnification factor for a braced and for an unbraced column, respectively
$\delta_i, \Delta\delta$	initial and time-dependent lateral displacement, respectively, of a slender column
$\varepsilon$	strain
$\varepsilon_c, \varepsilon_c(t)$	creep strain of concrete at time $t$
$\varepsilon_c(t, \tau_0)$	creep strain at time $t$ due to a stress first applied at $\tau_0$
$\varepsilon_c^*$	final creep strain at time infinity
$\varepsilon_{ce}$	strain in the concrete at the level of the prestressed steel due to the effective prestress
$\varepsilon_{cu}$	extreme concrete fibre compressive strain at the ultimate limit state
$\varepsilon_e, \varepsilon_e(t)$	instantaneous or elastic component of concrete strain at time $t$
$\varepsilon_{oi}$	initial strain in the top concrete fibre
$\varepsilon_p, \varepsilon_s$	strain in the prestressed and non-prestressed steel, respectively
$\varepsilon_{pe}$	strain in the prestressed steel due to the effective prestress (Eqn 3.31)
$\varepsilon_{pt}$	tensile strain in the concrete at the level of the prestressed steel in the post-cracking range and at the ultimate moment
$\varepsilon_{pu}$	strain in the prestressed steel at ultimate
$\varepsilon_s$	strain in the non-prestressed steel
$\varepsilon_{sc}, \varepsilon_{st}$	strain in the non-prestressed compressive and tensile steel, respectively
$\varepsilon_{sh}, \varepsilon_{sh}(t)$	shrinkage strain at time $t$
$\varepsilon_{sh}^*$	final shrinkage strain at time infinity
$\varepsilon_{sh}(28)$	shrinkage strain after 28 days of drying
$\varepsilon_y$	yield strain
$\Delta\varepsilon$	change in strain with time $t$
$\Delta\varepsilon_o$	change in top fibre strain with time
$\theta$	slope
$\theta_p$	angle between the direction of the prestressing tendon and the horizontal
$\theta_v, \theta_t$	angles of the inclined crack caused by shear (Eqn 5.4) and by torsion (Eqn 5.30) respectively
$x$	curvature
$x_i$	initial curvature
$x_p$	curvature of prestressing tendon
$x_{sh}$	curvature induced by shrinkage
$x_{sus}$	curvature caused by the sustained loads
$x_u$	curvature at ultimate
$(x_u)_{min}$	minimum curvature at ultimate for a ductile cross-section (Eqn 4.6)



$\Delta x$	change in curvature with time
$\lambda$	long-term deflection multiplication factor
$\mu$	friction curvature coefficient (Eqn 3.60) friction coefficient on the surface of a crack (Eqn 7.33)
$\nu$	Poisson's ratio for concrete
$\pi$	3.141593
$\rho$	reinforcement ratio, $A_{st}/A_c$ density of concrete
$\Sigma$	sum of
$\sigma$	stress in the concrete
$\sigma_b$	bearing stress
$\sigma_{cp}$	stress in the concrete at the level of the prestressing steel
$\sigma_{cu}$	maximum compressive concrete stress cube strength of concrete
$\sigma_i$	initial stress in the concrete
$\sigma_o$	stress at the time of first loading
$\sigma_{oi}$	initial concrete stress in the top fibre
$\sigma_p, \sigma_s$	stress in the prestressed and non-prestressed steel, respectively
$\sigma_{pe}$	stress in the prestressed steel due to the effective prestressing force
$\sigma_{pi}$	stress in the prestressed steel immediately after transfer
$\sigma_{pu}$	stress in the prestressed steel at ultimate
$\sigma_s$	permissible steel stress
$\sigma_{sc}, \sigma_{st}$	stress in the non-prestressed compressive and tensile steel, respectively
$\sigma_t, \sigma_b$	top and bottom fibre concrete stresses, respectively
$\sigma_x, \sigma_y$	longitudinal and transverse stress in the anchorage zone average stress imposed by the longitudinal prestress in each direction of a two-way slab
$\sigma_1, \sigma_2$	principal stresses in the concrete
$\tau_o$	age of concrete at first loading
$\phi$	strength reduction factor creep coefficient
$\phi(t, \tau_o)$	creep coefficient at time $t$ due to stress first applied at $\tau_o$
$\phi_{cc.b}$	a reference creep coefficient (Eqn 2.20)
$\phi^*$	final creep coefficient at time infinity
$\Delta\phi$	increment of the creep coefficient associated with a particular time interval
$\chi, \chi(t, \tau_o)$	ageing coefficient at time $t$ for concrete first loaded at $\tau_o$
$\chi^*$	final ageing coefficient at time infinity
$\psi$	serviceability load factor
$\psi_s, \psi_1$	short-term serviceability load factor
$\phi$	long-term serviceability load factor

$\zeta$  coefficient associated with the effective moment of inertia (Eqn 3.74).

# 1

## Basic concepts

### 1.1 Introduction

Reinforced concrete is the most widely used structural material of the 20th century. Because the tensile strength of concrete is low, steel bars are embedded in the concrete to carry all internal tensile forces. Tensile forces may be caused by imposed loads or deformations, or by load-independent effects such as temperature changes or shrinkage.

Consider the simple reinforced concrete beam shown in [Figure 1.1](#). The external loads cause tension in the bottom fibres which may lead to cracking, as shown. Practical reinforced concrete beams are usually cracked under the day-to-day service loads. On a cracked cross-section, the applied moment is resisted by compression in the concrete above the crack and tension in the bonded reinforcing steel. Although the steel reinforcement provides the cracked concrete beam with flexural strength, it does not prevent cracking and does not prevent the loss of stiffness caused by cracking. Crack widths are approximately proportional to the strain, and hence stress, in the reinforcement. Steel stresses must therefore be limited to some appropriately low value in order to avoid excessively wide cracks. Similarly, large steel strain is the result of large curvature, which in turn is associated with large deflection. There is little benefit to be gained, therefore, by using higher strength steel or concrete, since in order to satisfy serviceability requirements, the increased strain capacity afforded by higher strength steel cannot be utilized.

Prestressed concrete is a particular form of reinforced concrete. Prestressing involves the application of an initial compressive load on a structure to reduce or eliminate the internal tensile forces and thereby control or eliminate cracking. The initial compressive load is imposed and sustained by highly tensioned steel reinforcement reacting on the concrete. With cracking reduced or eliminated, a prestressed section is considerably stiffer than the equivalent (usually cracked) reinforced section. Prestressing may also impose internal forces which are of opposite sign to the external loads and may therefore significantly reduce or even eliminate deflection.

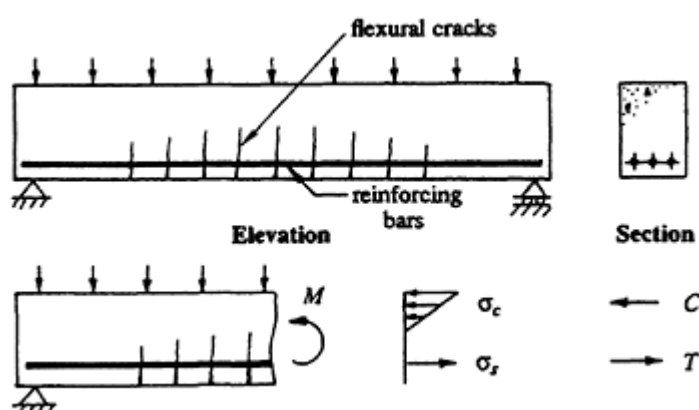


**Figure 1.1** A reinforced concrete beam.

With service load behaviour improved, the use of high-strength steel reinforcement and high-strength concrete becomes both economical and structurally efficient. As will be seen subsequently, only steel which can be tensioned with large initial elastic strains is suitable for prestressing concrete. The use of high-strength steel is therefore not only an advantage to prestressed concrete, it is a necessity. Prestressing results in lighter members, longer spans, and an increase in the economical range of application of reinforced concrete.

## 1.2 Methods of prestressing

As mentioned in the previous section, prestress is usually imparted to a concrete member by highly tensioned steel reinforcement (wire, strand, or bar) reacting on the concrete. The high-strength prestressing steel is most often tensioned using hydraulic jacks. The tensioning operation may occur before or after the concrete is cast and, accordingly, prestressed members are classified as either *pretensioned* or *post-tensioned*.

### 1.2.1 Pretensioned concrete

[Figure 1.2](#) illustrates the procedures for pretensioning a concrete member. The prestressing tendons are initially tensioned between fixed abutments and anchored. With the formwork in place, the concrete is cast around the highly stressed steel tendons and cured. When the concrete has reached its required strength, the wires are cut or otherwise released from the abutments. As the highly stressed steel attempts to contract, the concrete is compressed. Prestress is imparted via bond between the steel and the concrete.

Pretensioned concrete members are often precast in pretensioning beds long enough to accommodate many identical units simultaneously. To decrease the construction cycle time, steam curing may be employed to

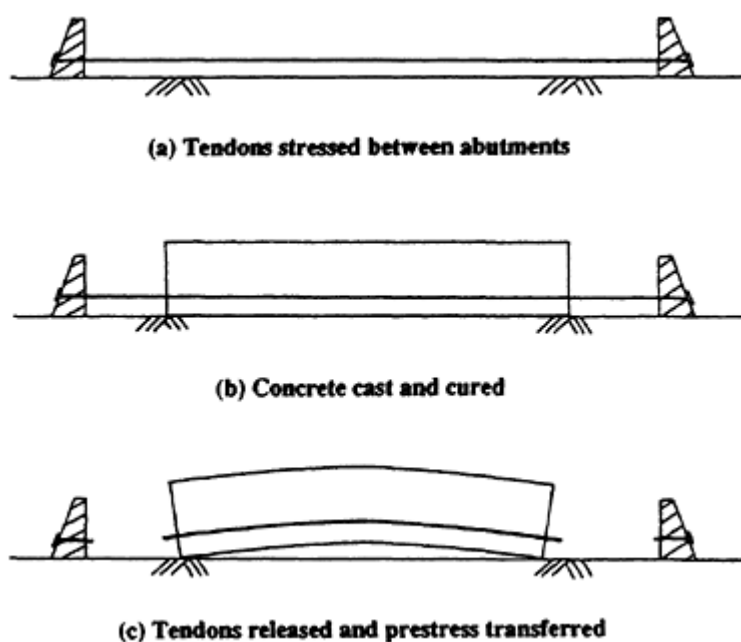


**Figure 1.2** Pretensioning procedure.

facilitate rapid concrete strength gain and the concrete is often stressed within 24 hours of casting. Because the concrete is usually stressed at such an early age, elastic shortening of the concrete and subsequent creep strains tend to be high. This relatively high time-dependent shortening of the concrete causes a significant reduction in the tensile strain in the bonded, prestressing steel and a relatively high loss of prestress.

### *1.2.2 Post-tensioned concrete*

The procedures for post-tensioning a concrete member are shown in [Figure 1.3](#). With the formwork in position, the concrete is cast around hollow ducts which are fixed to any desired profile. The steel tendons are usually in place, unstressed in the ducts during the concrete pour, or alternatively may be threaded through the ducts at some later time. When the concrete has reached its required strength, the tendons are tensioned. Tendons may be stressed from one end with the other end anchored or may be stressed from both ends, as shown in [Figure 1.3b](#). The tendons are then anchored at each stressing end.

The concrete is compressed during the stressing operation and the prestress is maintained after the tendons are anchored by bearing of the end anchorage plates onto the concrete. The post-tensioned tendons also impose a transverse force to the member wherever the direction of the cable changes.

After the tendons have been anchored and no further stressing is

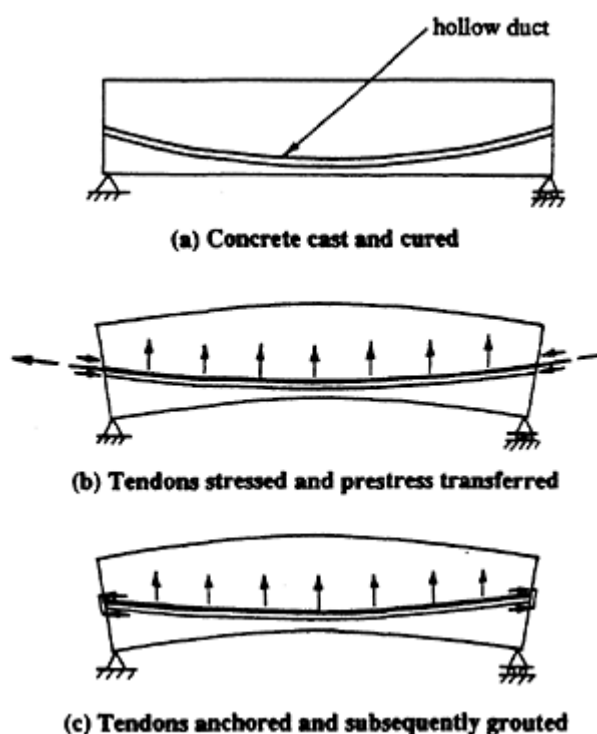


**Figure 1.3** Post-tensioning procedure.

required, the ducts containing the tendons are often filled with grout under pressure. In this way, the tendons are bonded to the concrete and are more efficient in controlling cracks and providing ultimate strength. Bonded tendons are also less likely to corrode or lead to safety problems if a tendon is subsequently lost or damaged. In some situations, however, particularly in North America and Europe, tendons are not grouted for reasons of economy and remain permanently unbonded.

Most *in situ* prestressed concrete is post-tensioned. Relatively light and portable hydraulic jacks make on-site post-tensioning an attractive proposition. Post-tensioning is also used for segmental construction of large-span bridge girders.

Prestress may also be imposed on new or existing members using external tendons or such devices as *flat jacks*. These systems are useful for temporary prestressing operations but may be subject to high time-dependent losses.

### 1.3 Introductory example

Consider an unreinforced concrete beam of rectangular section, simply supported over a span  $L$ , and carrying a uniform load  $w$ , as shown in [Figure 1.4a](#). When the tensile strength of concrete is reached in the bottom fibre

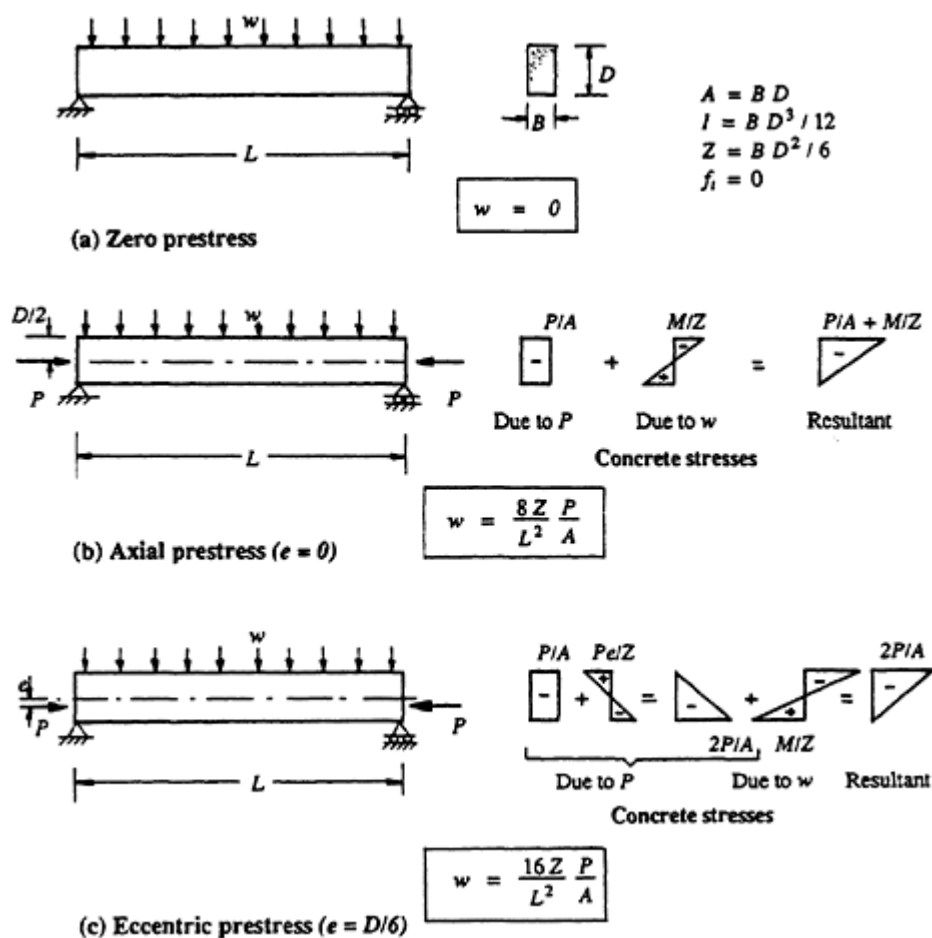


Figure 1.4 Introductory example.

at mid-span, cracking and a sudden brittle failure occur. If it is assumed that the concrete possesses zero tensile strength, then no load can be carried and at failure  $w=0$ .

An axial compressive force  $P$  applied to the beam, as shown in Figure 1.4b, induces a uniform compressive stress of intensity  $P/A$ . For failure to extreme fibre tensile stress at mid-span equal to  $P/A$ . If linear-elastic behaviour is assumed, simple beam theory gives

$$\frac{M}{Z} = \frac{wL^2}{8Z} = \frac{P}{A}$$

and therefore

$$w = \frac{8Z P}{L^2 A}$$

If the prestressing force  $P$  is applied at an eccentricity of  $D/6$ , as shown in [Figure 1.4c](#), the compressive stress caused by  $P$  in the bottom fibre at mid-span is equal to

$$\begin{aligned}\frac{P}{A} + \frac{Pe}{Z} &= \frac{P}{A} + \frac{PD/6}{BD^2/6} \\ &= \frac{2P}{A}\end{aligned}$$

and the external load at failure  $w$  must now produce a tensile stress of  $2P/A$  in the bottom fibre. That is

$$\frac{M}{Z} = \frac{wL^2}{8Z} = \frac{2P}{A}$$

and therefore

$$w = \frac{16Z}{L^2} \frac{P}{A}$$

By locating the prestress at an eccentricity of  $D/6$ , the load-carrying capacity is effectively doubled.

The eccentric prestress induces an internal bending moment  $Pe$  which is opposite in sign to the moment caused by the external load. An improvement in behaviour is obtained by using a variable eccentricity of prestress along the member. This may be achieved using a draped cable profile.

If the prestress *countermoment*  $Pe$  is equal and opposite to the load-induced moment all along the span, each cross-section is subjected only to axial compression, i.e. each section suffers a uniform compressive stress of  $P/A$ . No cracking can occur and, since the curvature on each section is zero, the beam does not deflect. This is the *balanced load stage*.

## 1.4 Transverse forces caused by draped tendons

In addition to the longitudinal force  $P$  exerted on a prestressed member at the anchorages, transverse forces are also exerted on the member wherever curvature exists in the tendons. Consider the simply supported beam in [Figure 1.5a](#) which is prestressed by a cable with a *kink* at mid-span. The eccentricity of the cable is zero at each end and  $e$  at mid-span. The slope of the two straight segments of cable is  $\theta$ , and because  $\theta$  is small

$$\theta \doteq \sin \theta \doteq \tan \theta = \frac{e}{L/2} \quad (1.1)$$



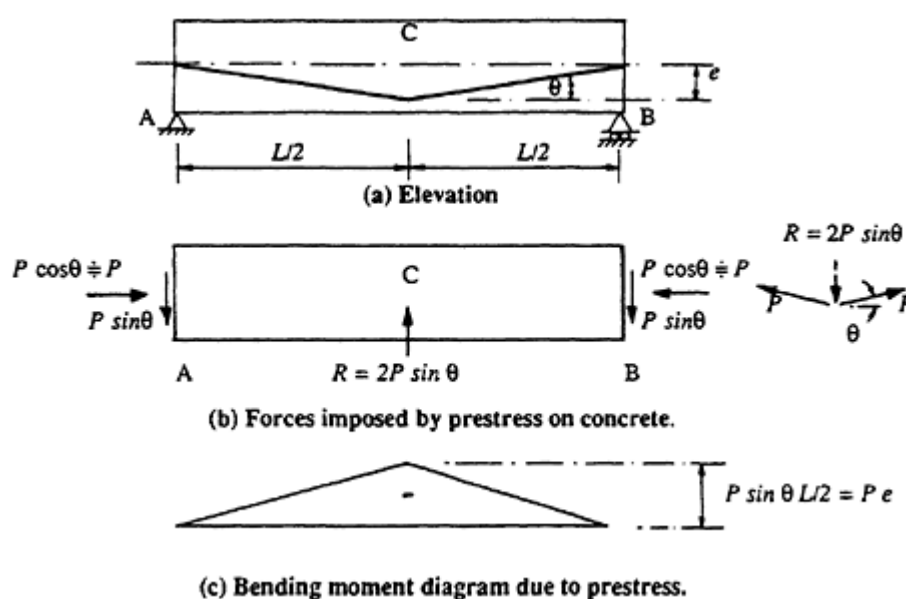


Figure 1.5 Beam with centrally depressed tendon.

In [Figure 1.5b](#), the forces exerted by the tendon on the concrete are shown. At mid-span, the cable exerts an upward force  $R$  on the concrete. From statics,  $R$  equals the sum of the vertical component of the prestressing force in the tendon on both sides of the *kink*:

$$R = 2P \sin \theta = \frac{4Pe}{L} \quad (1.2)$$

At each anchorage, the cable has a horizontal component of  $P \cos \theta$  ( $\approx P$  for small  $\theta$ ) and a vertical component of  $P \sin \theta = 2Pe/L$ .

The beam is said to be *self-stressed*. No external reactions are induced at the supports. However, the beam suffers curvature and deflects upward owing to the internal bending moment caused by prestress. As illustrated in [Figure 1.5c](#), the internal bending moment at any section can be calculated from statics and equals the product of the prestressing force  $P$  and the eccentricity.

If the prestressing cable has a curved profile, the cable exerts transverse forces on the concrete throughout its length. Consider the prestressed beam with the parabolic cable profile shown in [Figure 1.6](#). The shape of the parabolic cable is

$$y = 4e \left[ \frac{x}{L} - \left( \frac{x}{L} \right)^2 \right] \quad (1.3)$$

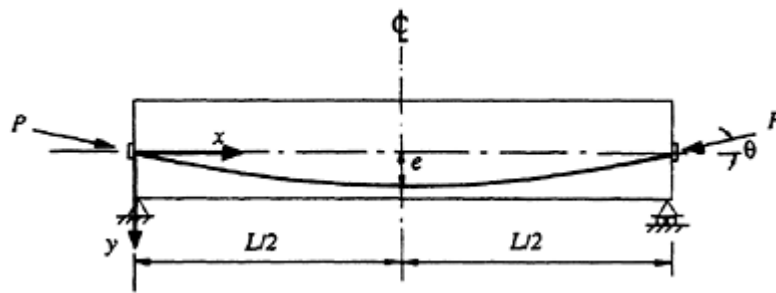


Figure 1.6 Simple beam with parabolic tendon profile.

and its slope and curvature are, respectively,

$$\frac{dy}{dx} = \frac{4e}{L} \left(1 - \frac{2x}{L}\right) \tag{1.4}$$

and

$$\frac{d^2y}{dx^2} = -\frac{8e}{L^2} = x_p \tag{1.5}$$

From Equation 1.4, the slope of the cable at each anchorage when  $x=0$  and  $x=L$  is

$$\theta = \frac{dy}{dx} = \pm \frac{4e}{L} \tag{1.6}$$

and therefore the horizontal and vertical components of the prestressing force at each anchorage are  $P$  and  $4Pe/L$ , respectively.

Equation 1.5 indicates that the curvature of the parabolic cable is constant along its length. The curvature  $x_p$  is the angular change in direction of the cable per unit length, as illustrated in [Figure 1.7a](#).

From the freebody diagram in [Figure 1.7b](#), the cable exerts an upward transverse force  $w_p = Px_p$  per unit length. This upward force is an equivalent distributed load along the member and, for a parabolic cable with the

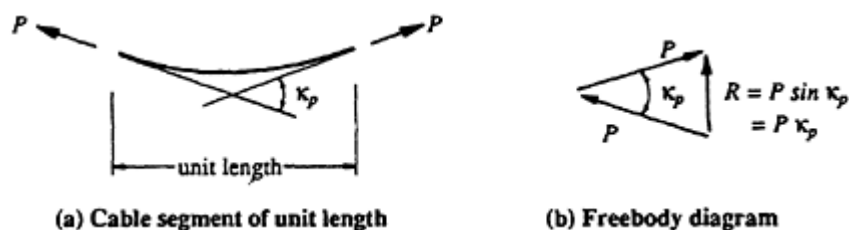
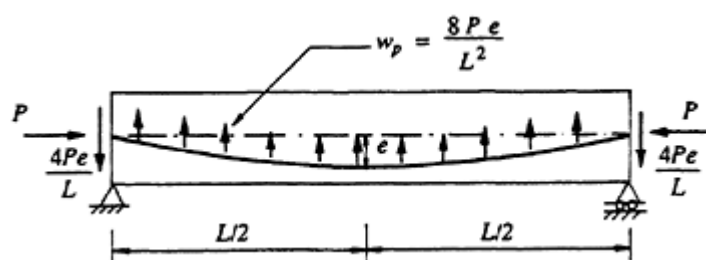


Figure 1.7 Forces on a curved cable of unit length.



**Figure 1.8** Forces exerted on a concrete beam by a parabolic tendon.

constant curvature given in Equation 1.5,  $w_p$  is given by

$$w_p = P x_p = \frac{8Pe}{L^2} \quad (1.7)$$

If  $P$  is constant, which is never quite the case in practice,  $w_p$  is uniformly distributed.

A freebody diagram of the concrete beam showing the forces exerted by the cable is illustrated in [Figure 1.8](#). Once again, the beam is self-stressed. No external reactions are induced by the prestress. With the maximum eccentricity usually known, Equation 1.7 may be used to calculate the value of  $P$  required to cause an upward force  $w_p$  which exactly balances a selected portion of the external load. Under this *balanced load*, the beam suffers no curvature and is subjected only to the longitudinal compressive force  $P$ . This is the basis of a useful design approach sensibly known as *load balancing*.

## 1.5 Calculation of elastic stresses

The components of stress on a prestressed cross-section caused by the prestress, the self-weight, and the external loads are usually calculated using simple beam theory and assuming linear-elastic material behaviour. In addition, the properties of the gross concrete section are usually used in the calculations, provided the section is not cracked. Indeed, these assumptions have already been made in the calculations for the introductory example in [Section 1.3](#).

Concrete, however, does not behave in a linear-elastic manner. Linear-elastic calculations provide, at best, only an approximation of the state of stress on a concrete section immediately after the application of the load. Inelastic creep and shrinkage strains may cause a substantial redistribution of stresses with time, particularly on a section containing significant amounts of bonded reinforcement.

Elastic calculations are useful, however, in determining, for example, if

tensile stresses occur at service loads, and therefore if cracking is likely, or if compressive stresses are excessive and large time-dependent shortening may be expected. Elastic stress calculations may therefore be used to indicate potential serviceability problems.

If an elastic calculation indicates that cracking may occur at service loads, the cracked section analysis presented in [Section 3.5](#) should be used to determine appropriate section properties for all serviceability calculations. A more comprehensive picture of the variation of concrete stresses with time can be obtained using the time analysis described in [Section 3.6](#).

In the following sub-sections, several different approaches to the calculation of elastic concrete stresses on an uncracked cross-section are described.

### 1.5.1 Combined load approach

The stress distributions on a cross-section caused by prestress, self-weight, and the applied loads may be calculated separately and summed to obtain the combined stress distribution at any particular load stage. Consider first the stresses caused by prestress and ignore all other loads. On a section, such as that shown in [Figure 1.9](#), equilibrium requires that the resultant of the concrete stresses is a compressive force which is equal and opposite to the tensile force in the steel tendon and located at the level of the steel, i.e. at an eccentricity  $e$  below the centroidal axis. This is statically equivalent to an axial compressive force  $P$  and a moment  $Pe$  located at the centroidal axis, as shown.

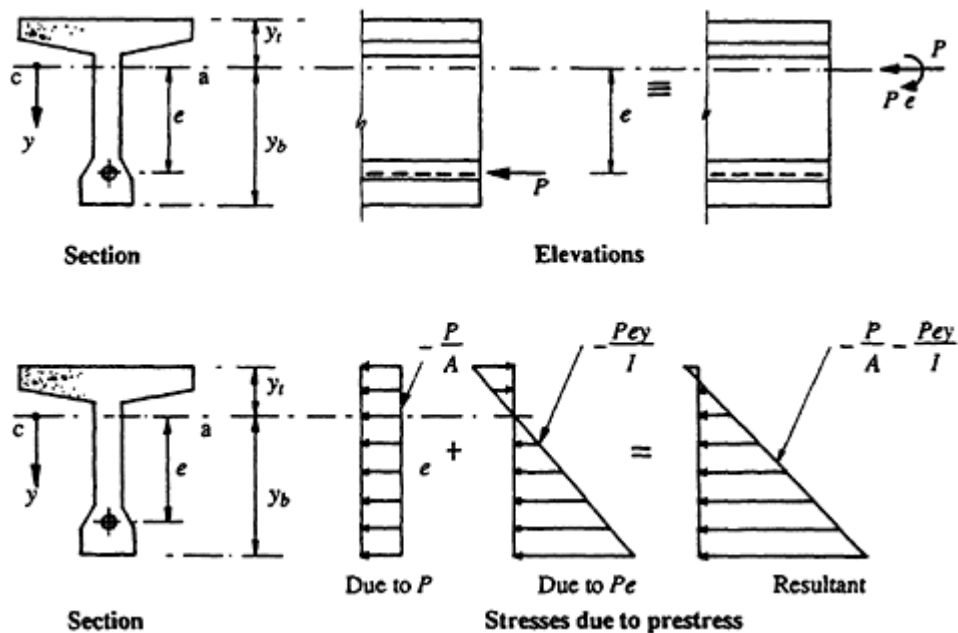


Figure 1.9 Concrete stress resultants and stresses caused by prestress.

The stresses caused by the compressive force  $P$  and the hogging (–ve) moment  $Pe$  are also shown in [Figure 1.9](#). The resultant stress induced by the prestress is given by

$$\sigma = -\frac{P}{A} - \frac{Pe y}{I} \quad (1.8)$$

where  $A$  and  $I$  are the area and second moment of area about the centroidal axis of the cross-section, respectively, and  $y$  is the distance from the centroidal axis (positive downward). It is common in elastic stress calculations to ignore the stiffening effect of the reinforcement and to use the properties of the gross cross-section. For cross-sections containing significant amounts of bonded steel reinforcement, however, the steel should be included in the determination of the section properties.

The elastic stresses caused by an applied positive moment  $M$  on the uncracked section are

$$\sigma = \frac{My}{I} \quad (1.9)$$

and the combined stress distribution due to prestress plus applied moment is shown in [Figure 1.10](#) and given by

$$\sigma = -\frac{P}{A} - \frac{Pe y}{I} + \frac{My}{I} \quad (1.10)$$

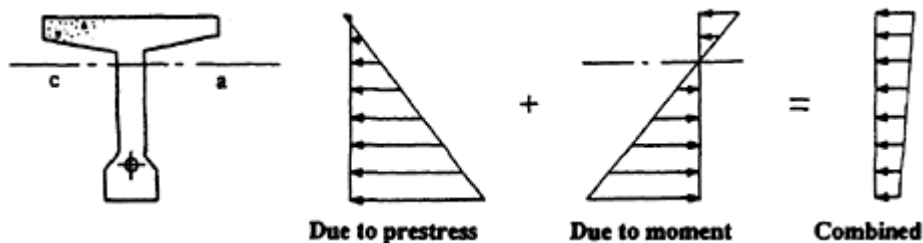


**Figure 1.10** Combined stresses.

### 1.5.2 Internal couple concept

The resultant of the combined stress distribution shown in [Figure 1.10](#) is a compressive force of magnitude  $P$  located at a distance  $l$  above the level of the steel tendon, as shown in [Figure 1.11](#). The compressive force in the concrete and the tension force in the steel form a couple with magnitude equal to the applied bending moment, i.e.

$$M = Pl \quad (1.11)$$

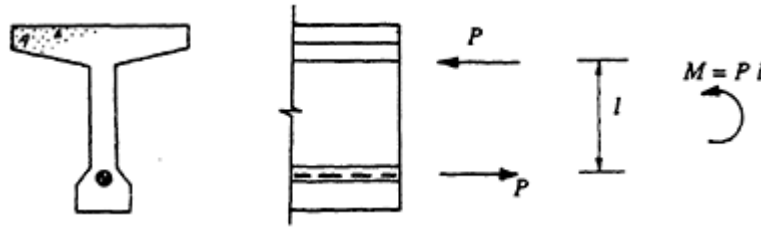


**Figure 1.11** Internal couple.

When  $M=0$ , the lever arm  $l$  is zero and the resultant concrete compressive force is located at the steel level. As  $M$  increases and compressive stresses in the top fibres increase and those in the bottom fibres decrease, the location of the resultant compressive force moves upward.

It is noted that provided the section is uncracked, the magnitude of  $P$  does not change appreciably as the applied moment increases. The lever arm  $l$  is therefore almost directly proportional to the applied moment. If the magnitude and position of the resultant of the concrete stresses are known, the stress distribution can be readily calculated.

### 1.5.3 Load balancing approach

In [Figure 1.8](#), the forces exerted on a prestressed beam by a parabolic cable were shown and the uniformly distributed transverse load  $w_p$  may be calculated from Equation 1.7. In [Figure 1.12](#), all the loads acting on the beam, including the external gravity loads  $w$ , are shown.

If  $w=w_p$ , the bending moment and shear force caused by the gravity load on every cross-section are balanced by the equal and opposite values caused by  $w_p$ . With the transverse loads balanced, the beam is subjected only to the longitudinal prestress  $P$  applied at the anchorage. If the anchorage is located at the centroid of the section, a uniform stress distribution of intensity  $P/A$  occurs on each section and the beam does not deflect.

If  $w \neq w_p$ , the bending moment  $M_{ub}$  caused by the unbalanced load  $(w-w_p)$  must be calculated and the resultant stress distribution (given by Equation 1.9) must be added to the stresses, caused by the axial prestress  $(P/A)$ .

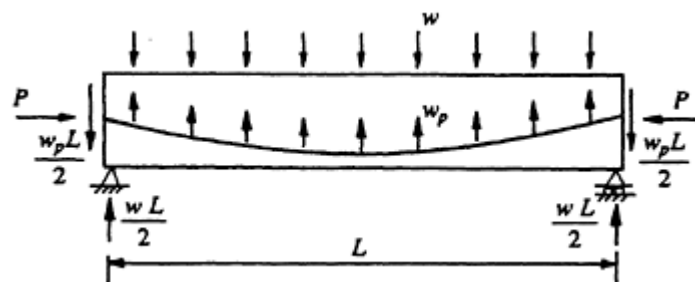


**Figure 1.12** Forces imposed on a concrete beam with a parabolic tendon.

## 1.5.4 Example 1.1

The elastic stress distribution at mid-span of the simply supported beam shown in [Figure 1.13](#) is to be calculated. Each of the procedures discussed in [Sections 1.5.1–3](#) are illustrated in the following calculations.

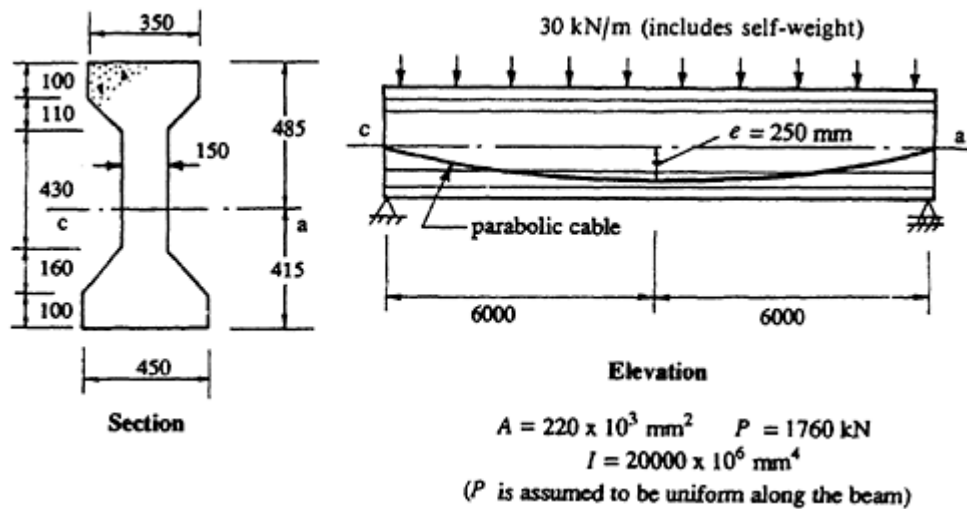


Figure 1.13 Beam of [Example 1.1](#).

## Combined load approach

The extreme fibre stresses at mid-span ( $\sigma_t$ ,  $\sigma_b$ ) due to  $P$ ,  $Pe$  and  $M$  are calculated separately and summed.

$$P = 1760 \text{ kN}; \quad Pe = 1760 \times 250 \times 10^{-3} = 440 \text{ kN m};$$

$$M = \frac{wL^2}{8} = \frac{30 \times 12^2}{8} = 540 \text{ kN m}$$

Due to  $P$ :

$$\sigma_t = \sigma_b = -\frac{P}{A} = -\frac{1760 \times 10^3}{220 \times 10^3} = -8.0 \text{ MPa}$$

Due to  $Pe$ :

$$\sigma_t = +\frac{Pe y_t}{I} = \frac{440 \times 10^6 \times 485}{20000 \times 10^6} = +10.67 \text{ MPa}$$

$$\sigma_b = -\frac{Pe y_b}{I} = \frac{440 \times 10^6 \times 415}{20000 \times 10^6} = -9.13 \text{ MPa}$$

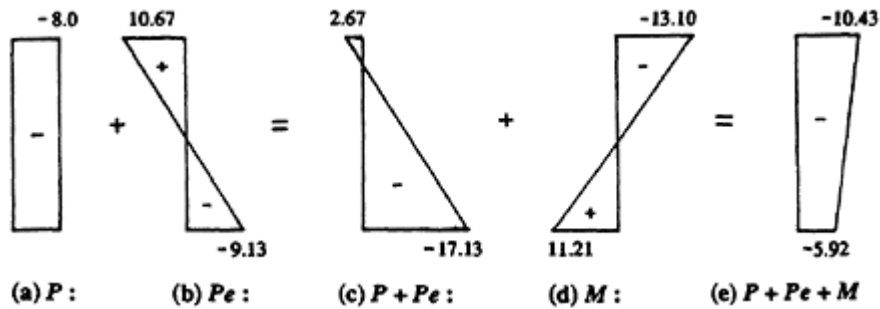


Figure 1.14 Component stress distributions in [Example 1.1](#).

Due to  $M$ :

$$\sigma_t = -\frac{My_t}{I} = -\frac{540 \times 10^6 \times 485}{20000 \times 10^6} = -13.10 \text{ MPa}$$

$$\sigma_b = +\frac{My_b}{I} = \frac{540 \times 10^6 \times 415}{20000 \times 10^6} = +11.21 \text{ MPa}$$

The corresponding concrete stress distributions are shown in [Figures 1.14a, b](#) and [d](#), respectively, and the combined elastic stress distribution on the concrete section at mid-span is shown in [Figure 1.14e](#).

### Internal couple concept

An alternative approach for the calculation of elastic stresses is based on the internal couple concept of [Section 1.5.2](#). From Equation 1.11,

$$l = \frac{M}{P} = \frac{540 \times 10^6}{1760 \times 10^3} = 306.8 \text{ mm}$$

The resultant compressive force on the concrete section is 1760 kN and is located  $306.8 - 250 = 56.8$  mm above the centroidal axis. This is statically equivalent to an axial compressive force of 1760 kN (applied at the centroid) plus a moment  $M_{ub} = 1760 \times 56.8 \times 10^{-3} = 100$  kNm.

The extreme fibre concrete stresses are therefore

$$\sigma_t = -\frac{P}{A} - \frac{M_{ub}y_t}{I} = -\frac{1760 \times 10^3}{220 \times 10^3} - \frac{100 \times 10^6 \times 485}{20000 \times 10^6} = -10.43 \text{ MPa}$$

$$\sigma_b = -\frac{P}{A} + \frac{M_{ub}y_b}{I} = -\frac{1760 \times 10^3}{220 \times 10^3} + \frac{100 \times 10^6 \times 415}{20000 \times 10^6} = -5.92 \text{ MPa}$$

as shown in [Figure 1.14e](#).



### Load balancing approach

The elastic concrete stresses can also be determined using the load balancing procedure outlined in [Section 1.5.3](#). The transverse force imposed on the concrete by the parabolic cable is obtained using Equation 1.7. That is,

$$w_p = \frac{8Pe}{L^2} = \frac{8 \times 1760 \times 10^3 \times 250}{12000^2} = 24.4 \text{ kN/m}$$

The unbalanced load is therefore

$$w_{ub} = 30.0 - 24.4 = 5.55 \text{ kN/m} \quad \downarrow$$

and the resultant unbalanced moment at mid-span is

$$M_{ub} = \frac{w_{ub}L^2}{8} = \frac{5.55 \times 12^2}{8} = 100 \text{ kNm}$$

which, of course, is identical to the moment  $M_{ub}$  calculated using the internal couple concept. Once again, the elastic stresses at mid-span are obtained by adding the  $P/A$  stresses to those caused by  $M_{ub}$ :

$$\sigma_t = -\frac{P}{A} - \frac{M_{ub}y_t}{I} = -10.43 \text{ MPa}$$

$$\sigma_b = -\frac{P}{A} + \frac{M_{ub}y_b}{I} = -5.92 \text{ MPa}$$

## 1.6 Flexural behaviour—from initial to ultimate loads

The choice between reinforced and prestressed concrete for a particular structure is one of economics. For relatively short-span beams and slabs, reinforced concrete is usually the most economical alternative. As the span increases, however, reinforced concrete design is more and more controlled by the serviceability requirements. Strength and ductility can still be economically achieved but, in order to prevent excessive deflection, cross-sectional dimensions become uneconomically large. Excessive deflection is usually the governing *limit state*.

For medium- to long-span beams and slabs, the introduction of prestress improves both serviceability and economy. The optimum level of prestress depends on the span, the load history, and the serviceability requirements. Until recently, the level of prestress was usually selected so that cracking at service loads did not occur. Frequently, this resulted in unnecessarily high initial prestressing forces and, consequently, uneconomical designs. The

high initial prestress also often led to excessively large camber and/or axial shortening. Members designed to remain uncracked at service loads are termed *fully prestressed*.

In building structures, there are relatively few situations in which it is necessary to avoid cracking at service loads. In fact, the most economic design often results in significantly less prestress than is required for a *fully prestressed* member. Frequently, such members are designed to remain uncracked under the sustained or permanent load, with cracks opening and closing as the variable live load is applied and removed. Prestressed concrete members behave well in the post-cracking load range, provided they contain sufficient bonded reinforcement to control the cracks. A cracked prestressed concrete section under service loads is significantly stiffer than a cracked reinforced concrete section of similar size and containing similar quantities of bonded reinforcement. Members that are designed to crack at the full service load are called *partially prestressed*.

The elastic stress calculations presented in the previous section are applicable only if material behaviour is linear-elastic and the principle of superposition is valid. These conditions may be assumed to apply on a prestressed section prior to cracking, but only immediately after the loads are applied. As was mentioned in the introduction to [Section 1.5](#), the gradual development of inelastic creep and shrinkage strains in the concrete can cause a marked redistribution of stress between the bonded steel and the concrete on the cross-section. The greater the quantity of bonded reinforcement, the greater is the time-dependent redistribution of stress. For the determination of the long-term stress and strain distributions, elastic stress calculations are not meaningful and may be misleading.

If the external loads are sufficient to cause cracking (i.e. the extreme fibre stress exceeds the tensile strength of concrete), the short-term behaviour also becomes non-linear and the principle of superposition is no longer applicable. As the applied moment on a cracked, prestressed section increases, the crack depth gradually increases from the tension surface towards the compression zone and the size of the uncracked part of the cross-section in compression above the crack decreases. This is different to the post-cracking behaviour of a conventionally reinforced concrete section. At first cracking on a reinforced section, the crack suddenly propagates deep into the beam and the crack height and the depth of the concrete compression zone remains approximately constant as the applied moment is subsequently varied.

As the moment increases further into the overload region, the material behaviour becomes increasingly non-linear, Permanent deformation occurs in the bonded prestressing tendons as the stress approaches its ultimate value, the non-prestressed conventional reinforcement yields, and the compressive concrete in the ever decreasing region above the crack enters the non-linear range. The external moment is resisted by an internal couple,

with tension in the reinforcement crossing the crack and compression in the concrete and in any reinforcement in the compressive zone. At the *ultimate load stage*, the prestressed section behaves in the same way as a reinforced concrete section, except that the stress in the high-strength steel reinforcement is very much higher. A significant portion of the very high steel stress and strain is due to the initial prestress or, more precisely, the initial prestrain. If the same higher strength steel were to be used without being initially prestrained, excessive deformation and unacceptably wide cracks would result at only a small fraction of the ultimate load (well below normal service loads).

The ultimate strength of a prestressed section depends on the quantity and strength of the steel reinforcement. The level of prestress, however, and therefore the quantity of prestressing steel are determined from serviceability considerations. In order to provide a suitable factor of safety for strength, additional conventional reinforcement may be required to supplement the prestressing steel in the tension zone. This is particularly so in the case of partially prestressed members and may even apply for fully prestressed construction. The avoidance of cracking at service loads and the satisfaction of selected elastic stress limits do not ensure adequate strength. Strength must be determined from a rational analysis which accounts for the non-linear material behaviour of both steel and concrete. Flexural strength analysis is described and illustrated in [Chapter 4](#), and analyses for shear and torsional strength are contained in [Chapter 5](#).

## 1.7 Design procedures

### 1.7.1 Limit states requirements

A structure and its components must simultaneously satisfy a number of different *limit states* or design requirements. It must possess adequate strength, be stable, and perform satisfactorily under service loads. Further, it must be durable, have adequate fire protection, resist fatigue loading, and satisfy any special requirements which are related to its intended use. Codes of practice specify design criteria which provide a suitable margin of safety against a structure becoming unfit for service in any of these ways.

If a structure becomes unfit for service in any way, it is said to have entered a *limit state*. Limit states are the undesirable consequences associated with each possible mode of failure. In order to satisfy the design criteria set down in codes of practice, methods of design and analysis should be used which are appropriate to the limit state being considered. For example, if the strength of a cross-section is to be calculated, *ultimate strength* analysis and design procedures are usually adopted. Collapse load methods of analysis and design (plastic methods) may be suitable for calculating the

strength of ductile, indeterminate structures. If the serviceability limit states of excessive deflection (or camber) or excessive cracking are considered, an analysis which accounts for the non-linear and inelastic nature of concrete is usually required. The sources of this concrete material non-linearity include cracking, tension stiffening, creep, and shrinkage. In addition, creep of the high-strength prestressing steel (more commonly referred to as *relaxation*) may affect in-service behaviour.

Each limit state must be considered and designed for separately. Satisfaction of one does not ensure satisfaction of others. All undesirable consequences should be avoided. For each limit state, the designer must compare the structure's capacity with the appropriate external loads. In the following sections, the design requirements for prestressed concrete are discussed, including the specified loads and load combinations and the treatments of structural safety contained in several major codes of practice.

### 1.7.2 Loads on structures

In the design of a concrete structure, the internal actions arising from the following loads should be considered if applicable. The notation used here is based, where possible, on the recommendations of ISO 3898:

Dead load (G); Live load (Q); Wind load (W); Prestress (P); Earthquake ( $F_{eq}$ ); Earth pressure ( $F_{ep}$ ); Liquid pressure ( $F_{lp}$ ); and Snow load ( $F_s$ ).

In addition, possible accidental loading and construction loads should be considered where they may adversely affect the limit states requirements. Other actions which may cause either stability, strength or serviceability failures include, creep of concrete, shrinkage (or expansion) of concrete, temperature changes and gradients, foundation movements, and dynamic effects.

Dead loads are usually defined as loads imposed by both the structural and non-structural components of a structure. Dead loads include the self-weight of the structure and the forces imposed by all walls, floors, roofs, ceilings, permanent partitions, service machinery, and other permanent construction. Dead loads are usually permanent, fixed in position, and can be estimated reasonably accurately from the mass of the relevant material or type of construction. Normal weight prestressed (or reinforced) concrete, for example, weighs about  $24 \text{ kN/m}^3$ . Lightweight reinforced concrete weighs between  $15$  and  $20 \text{ kN/m}^3$ .

Live loads are the loads which are assumed to arise from the intended use or purpose of the structure and are generally specified by regional or national codes and specifications. A number of these references are listed at the end of this chapter. Specified live loads depend on the expected use

or occupancy of the structure and usually include allowances for impact and inertia loads (where applicable) and for possible overload. In general, both uniformly distributed and concentrated live loads are specified. At the design stage, the magnitude of the maximum live load is never accurately known, and there is a small, but significant, probability that the specified live load will be exceeded at some stage during the life of the structure. Live loads may or may not be present at any particular time; they are not constant and their position can vary. Although part of the live load is transient, some portion may be permanently applied to the structure and have effects similar to dead loads. Live loads also occur during construction due to stacking of building materials, the use of equipment, or the construction procedure (such as the loads induced by floor-to-floor propping in multistorey construction).

Specified wind, earthquake, snow and temperature loads depend on the geographical location and the relative importance of the structure (the mean return period). Wind loads also depend on the surrounding terrain, the degree of shielding, and the height of the structure above the ground. These *environmental* loads are also usually specified by regional or national codes and specifications.

### 1.7.3 Load combinations for the strength limit states

The loads used in the design for strength are the specified values discussed above multiplied by minimum load factors contained in the various codes of practice. With the built-in allowance for overloads in most loading specifications, the specified loads will not often be exceeded in the life of a structure. The load factors applied to each load type ensure that the probability of strength failure is extremely low. Load factors provide only part of the overall factor of safety against strength failure and are referred to in Europe as *partial safety factors for load*. As will subsequently be seen, partial safety factors, in one form or another, are also applied to the calculated strength of the structure.

The load factors depend on the type of load and the load combination under consideration. For example, the load factors associated with dead loads are less than those for live or wind loads, because the dead load is known more reliably and therefore less likely to be exceeded.

The load factors specified in several widely used concrete codes for particular load combinations are summarized below. The most severe factored load combination should be used in the design for strength.

#### ACI 318–83 (1983)

Dead+Live:	$1.4G+1.7Q$
Wind:	$0.75(1.4G+1.7Q+1.7W)$ or $0.9G+1.3W$

Earthquake: As for wind, except that  $1.1F_{eq}$  is substituted for  $W$   
 Earth pressure:  $1.4G+1.7Q+1.7F_{ep}$  or  
 $0.9G+1.7F_{ep}$

### BS 8110: Part 1 (1985)

Dead+Live:  $1.4G+1.6Q$   
 Wind:  $1.2G+1.2Q+1.2W$  or  
 $1.4G+1.4W$  or  
 $1.0G+1.4W$   
 Earth pressure:  $1.4G+1.6Q+1.4F_{ep}$  or  
 $1.0G+1.4F_{ep}$   
 Liquid pressure: As for earth pressure

### CEB–FIP Model Code (1978)

Dead+Live:  $1.35G+1.5Q$   
 Wind:  $1.35G + 1.5\psi_0Q + 1.5W$  or  
 $1.0G+1.5W$

For earthquake, earth pressure, or liquid pressure, the same two load combinations as for wind are used except that  $W$  is replaced by  $F_{eq}$ ,  $F_{ep}$  or  $F_{lp}$ , respectively.  $\psi_0$  is a combination factor which depends on the type of structure and accounts for the reduced probability that the specified live load will be acting when the design wind (or earthquake) occurs. For example,  $\psi_0 = 0.3$  for dwellings and highway bridges and  $\psi_0 = 0.6$  for offices, retail stores, and parking areas.

### CAN3–A23.3–M84 (1984)

Dead+Live:  $1.25G+1.5Q$   
 Wind:  $1.25G+1.5W$  or  
 $0.85G+1.5W$  or  
 $1.25G + 0.7(1.5Q+1.5W)$

Earthquake loads are treated similarly to wind loads. Earth and liquid pressures are taken as live loads and factored accordingly.

### AS 3600 (1988)

Dead+Live:  $1.25G+1.5Q$  or  
 $0.8G+1.5Q$

Wind:  $1.25G + \psi_c Q + 1.5W$  or  
 $0.8G + 1.5W$

Earthquake:  $1.25G + 1.6F_{eq} + \psi_c Q$  or  
 $0.8G + 1.6F_{eq}$

Earth pressure:  $1.25G + 1.5Q + 1.5F_{ep}$  or  
 $0.8G + 1.5F_{ep}$

Liquid pressure is factored similarly to earth pressure.  $\psi_c$  depends on the type of occupancy:  $\psi_c = 0.4$  for domestic, office, and parking areas, 0.5 for retail stores, and 0.6 for storage areas. In addition to the above load combinations, AS 3600–1988 specifies the following factored combination of prestressed and dead load when considering compressive failure at transfer:  $1.15G+1.15P$  or  $0.8G+1.15P$ .

#### 1.7.4 Load combinations for the stability limit states

All structures should be designed such that the factor of safety against instability due to overturning, uplift, or sliding is suitably high. In general, most codes require that the structure remains stable under the most severe of the load combinations for the strength limit states (see [Section 1.7.3](#)). The Australian Standard for Concrete Structures AS 3600–1988 suggests that the loads causing instability should be separated from those tending to resist it. The *design action effect* is then calculated from the most severe of the load combinations for the strength limit state. The *design resistance effect* is calculated from 0.8 times the loads and other forces tending to resist instability. The structure should be so proportioned that its design resistance effect is not less than the design action effect.

Consider, for example, the case of a standard cantilever retaining wall. When checking for overturning in accordance with AS 3600–1988, the overturning moment caused by both the lateral earth pressure and the lateral thrust of any dead and live load surcharge would be calculated using the worst factored load combination of [Section 1.7.3](#). To provide a suitable margin of safety against stability failure, the overturning moment should not be greater than 0.8 times the restoring moment caused by the wall self-weight and the weight of the backfill and other permanent surcharge above the wall.

#### 1.7.5 Load combinations for the serviceability limit states

The design loads to be used in serviceability calculations are the day-to-day *service loads* which may be considerably less than the *specified loads*. The specified live load  $Q$ , for example, has a built-in allowance for overload and impact, and there is a relatively low probability that this value will be exceeded. It is usually not necessary, therefore, to ensure acceptable deflections and crack widths under the full specified live loads. The day-to-day load combinations that exist under *normal* conditions of service are more appropriate.

ACI 318–83 (1983) does not make specific recommendations regarding load combinations for serviceability calculations, except that adequate stiffness is required to limit the deformation of a structure at service loads to a specified maximum value. Where the long-term deformation is calculated,



only the dead load and the permanent portion of the live load need be considered.

BS 8110: Part 2 (1985) differentiates between the *characteristic* (or specified) loads and the *expected* loads. Depending on the type of structure, the expected loads may be significantly less than the characteristic loads. If the aim of the serviceability calculation is to produce a *best estimate* of the likely behaviour, then expected loads should be used. The actual values of these expected live loads are not specified and are deemed to be a matter for engineering judgement. If the aim is to satisfy a particular serviceability limit state, and the consequences of failure to do so are high, then the specified or characteristic service loads may be more appropriate. Once again, the decision should be based on engineering judgement and experience. BS 8110 specifies that for dead load the expected and the characteristic values are the same and, therefore, the characteristic dead load should be used in all serviceability calculations. For normal domestic or office occupancy, BS 8110 specifies that 25% of the live load should be considered as permanent or sustained and the remainder may be assumed to be transitory in nature. For storage areas, when an upper limit to the final long-term deflection is required, 75% of the live load should be considered to be permanent.

The CEB–FIP Model Code (1978) specifies live load factors,  $\psi$  and  $\psi$  for serviceability calculations. The following service load combinations should be considered:

The quasi-permanent loads:

$$G + P + \psi_2 Q$$

The frequent (day-to-day) loads:

$$G + P + \psi_1 Q$$

The infrequent (one-off) loads:

$$G + P + Q$$

$P$  is the mean prestressing force.  $\psi_1$  is the short-term service load factor and equals 0.4 for dwellings, 0.6 for offices and retail stores, 0.7 for parking areas, and for highway bridges may be linearly interpolated between 0.7 for spans of 10 m and 0.5 for spans of 100 m.  $\psi_2$  is the long-term service load factor and equals 0.2 for dwellings, 0.3 for offices and retail stores, 0.6 for parking areas, and zero for highway bridges. For wind and snow loads,  $\psi_1$  lies between 0.2 and 0.5 and  $\psi_2 = 0$ .

The Canadian code CAN3–A23.3–M84 (1984) suggests that the specified loads should be used in serviceability calculations, except that for the estimate of long-term deflections, the sustained loads only are to be considered. A load combination factor  $\psi$  is introduced when combinations of dead load and each of the following loads are considered: (a) live load,  $Q$ ; (b) wind or earthquake load,  $W$ ; and (c) the cumulative effects of temperature, creep, shrinkage, and differential settlement,  $T$ . The load combination for serviceability is therefore

$$G + \psi(Q + W + T)$$

where  $\psi = 1.0$  when only one of  $Q$ ,  $W$ , or  $T$  is acting, 0.7 when two of  $Q$ ,  $W$ , or  $T$  are acting, and 0.6 when all three are acting.

The Australian code AS 3600–1988 adopts a similar approach to the CEB–FIP model code. Live load factors,  $\psi_s$  and  $\psi_l$  are used in the following service load combinations:

$$\begin{aligned} \text{Short-term loads:} & \quad G + P + \psi_s Q \quad \text{or} \quad G + P + \psi_l Q + 0.5W \\ \text{Long-term loads:} & \quad G + P + \psi_l Q \end{aligned}$$

$\psi_s$  is the minimum fraction of  $Q$  which is considered to be appropriate for short-term serviceability calculations and is equal to 0.7 for dwellings, 0.5 for offices and parking areas, 0.6 for retail stores, 1.0 for storage areas, and for bridges varies linearly from 0.7 for spans of 10 m to 0.5 for spans of 100 m.  $\psi_l$  is the minimum fraction of  $Q$  which may reasonably be expected to be sustained or permanent in nature and is equal to 0.3 for dwellings and retail stores, 0.25 for parking areas, 0.2 for offices, between 0.5 and 0.8 for storage areas, and zero for bridges.

### 1.7.6 Design for the strength limit states

The *design strength* of a member or connection must always be greater than the *design action* produced by the most severe factored load combination (as outlined in [Section 1.7.3](#)). On a particular cross-section, the design action may be the axial load  $N^*$ , shear force  $V^*$ , the bending moment  $M^*$ , or the twisting moment  $T^*$ , or combinations thereof.

The design strength of a cross-section is a conservative estimate of the actual strength. In modern concrete codes, one of two alternative design philosophies is used to determine the design strength. The first involves the use of *strength (or capacity) reduction factors* and the second approach involves the use of *partial safety factors for material strengths*.

#### Design strength using strength reduction factors

The design strength of a cross-section is taken as the product of the *ultimate strength*,  $R_u$ , and a strength reduction factor,  $\phi$ . The strength reduction factor is a factor of safety introduced to account for the variability of the material properties controlling strength and the likelihood of underperformance;  $\phi$  also accounts for possible variations in steel positions and concrete dimensions, inaccuracies in design procedures and workmanship, and the degree of ductility of the member.

Both ACI 318–83 (1983) and AS 3600 (1988) adopt this approach and the strength reduction factors contained therein are summarized in [Table 1.1](#).  $\phi$  varies between 0.7 and 0.9 in ACI 318–83 (and 0.6 and 0.8 in AS 3600–1988), the lower end of the range being applicable when concrete directly controls the strength and the upper end of the range when strength depends primarily on the properties of the steel.

**Table 1.1** Strength reduction factors (ACI 318–83 and AS 3600–1988).

Type of Action	ACI 318–83	AS 3600–1988
(a) Flexure (with or without axial tension) and Axial tension	0.9	0.8
(b) Axial Compression and Axial Compression with Flexure		
(i) Spiral reinforcement	0.75	0.6
(ii) Tied reinforcement	0.70	0.6
For small axial compression, $\phi$ may be increased linearly from the value given in (b) to the value given in (a) as the axial compression tends to zero.		
(c) Shear and torsion	0.85	0.7
(d) Bearing on Concrete	0.7	0.6

The determination of the ultimate strength  $R_u$  of a prestressed concrete section is based on the characteristic strengths of the materials and their idealized constitutive relationships, the principles of ultimate strength theory, and the fundamental concepts of mechanics. Procedures for calculating the ultimate bending strength  $M_u$  are discussed in [Chapter 4](#), the ultimate shear strength  $V_u$  and torsional strength  $T_u$  in [Chapter 5](#), and the ultimate strength of members in axial compression and tension  $N_u$  in [Chapter 12](#).

The design requirement for the strength limit state on each cross-section and at each connection throughout the structure is

$$\phi R_u \geq R^* \quad (1.12)$$

The design strength must be greater than or equal to the most severe design action.

### Design strength using partial safety factors

The strength reduction factor is a safety factor which is applied to the ultimate strength of a section, the ultimate strength being calculated from the characteristic or specified material strengths. An alternative approach to

the determination of the design strength of a section is to apply the safety factors directly to the material strengths.

For concrete, reinforcement bars, and prestressing tendons, the design strength of the material is obtained from the characteristic strength divided by the appropriate partial safety factor,  $\gamma_m$ . These reduced material strengths are then used to determine the design strength of the section directly (using similar procedures to those used for calculating the ultimate strength,  $R_u$ ).

The partial safety factors for the constituent materials,  $\gamma_m$ , take account of the variability of the material, the differences between actual material properties and laboratory-measured values, local weaknesses, and inaccuracies in the methods of assessment of the resistance of cross-sections. They serve the same function as strength reduction factors, but do so in, arguably, a more rational way and provide a more consistent level of safety.

BS 8110: Part 1 (1985), the CEB–FIP Model Code (1978) and CAN3–A23.3–M84 (1984) all use this approach. The partial safety factors for materials specified in each code are summarized below:

### **BS 8110: Part 1 (1985)**

For reinforcement (all types):	$\gamma_m=1.15$
Concrete in flexure or axial load:	$\gamma_c=1.5$
Shear strength without shear reinforcement:	$\gamma_c=1.25$
Bond strength:	$\gamma_c=1.4$
Others (e.g. bearing stress):	$\gamma_c \geq 1.5$

### **CEB–FIP Model Code (1978)**

For concrete:	$\gamma_c=1.5$
For steel:	$\gamma_s=1.15$

### **CAN3–A23.3–M84 (1984)**

For concrete:	$\gamma_c=1/0.6$
For prestressing tendons (and structural steel):	$\gamma_s=1/0.9$
For conventional reinforcing bar:	$\gamma_s=1/0.85$

#### *1.7.7 Design for the serviceability limit states*

When designing for serviceability, the designer must ensure that the structure behaves satisfactorily and can perform its intended function at service loads. Deflection (or camber) must not be excessive, cracks must be adequately controlled, and no portion of the structure should suffer excessive vibration.

The design for serviceability is possibly the most difficult and least well understood aspect of the design of concrete structures. Service load behaviour depends primarily on the properties of the concrete which are

often not known reliably. Moreover, concrete behaves in a non-linear and inelastic manner at service loads. The non-linear behaviour of concrete which complicates serviceability calculations is caused by cracking, tension stiffening, creep, and shrinkage.

In [Chapter 3](#), design procedures for determining the in-service behaviour of beams are presented, and [Chapter 11](#) deals with serviceability aspects of the design of prestressed concrete slabs. The level of prestress in beams and slabs is generally selected to satisfy the serviceability requirements.

The control of cracking in a prestressed concrete structure is usually achieved by limiting the stress increment in the bonded reinforcement to some appropriately low value and ensuring that the bonded reinforcement is suitably distributed. Many codes of practice specify maximum steel stress increments after cracking and maximum spacing requirements for the bonded reinforcement. For example, for the control of flexural cracking in partially prestressed concrete beams, AS 3600 (1988) requires that the increment of stress in the steel near the tension face is limited to 200 MPa as the load is increased from its value when the extreme concrete tensile fibre is at zero stress to the full short-term service load. In addition, the centre to centre spacing of reinforcement (including bonded tendons) must not exceed 200 mm.

For deflection control, the structural designer should select *maximum deflection limits* which are appropriate to the structure and its intended use. The calculated deflection (or camber) must not exceed these limits. Codes of practice give general guidance for both the selection of the maximum deflection limits and the calculation of deflection. However, the simplified procedures for calculating deflection in most codes were developed from tests on simply supported reinforced concrete beams and often produce grossly inaccurate predictions when applied to more complex structures. Reliable procedures for calculating deflections of partially prestressed concrete beams are presented in some detail in [Chapter 3](#).

Deflection problems which may affect the serviceability of prestressed concrete structures can be classified into three main types:

- (a) Where excessive deflection causes either aesthetic or functional problems.
- (b) Where excessive deflection results in damage to either structural or non-structural elements attached to the member.
- (c) Where dynamic effects due to insufficient stiffness cause discomfort to occupants.

Examples of deflection problems of type (a) include objectionable visual sagging (or hogging), and ponding of water on roofs. In fact, any deflection which prevents a member fulfilling its intended function causes a problem of this type. Type (a) problems are generally overcome by limiting the total

deflection to some appropriately low value. The total deflection is the sum of the short-term and time-dependent deflection caused by the dead load (including self-weight), the prestress, the expected in-service live load, and the load-independent effects of shrinkage and temperature changes.

Some codes (including ACI 318–83, BS 8110 1985, and CAN3–A23.3– M84) place no maximum limit on the total deflection. However, when the total deflection exceeds about span/200 below the horizontal, it may become visually unacceptable. Total deflection limits which are appropriate for the particular member and its intended function must be decided by the designer. A total deflection limit of span/200, for example, may be appropriate for the floor of a carpark, but is inadequate for a gymnasium floor which may be required to remain essentially plane under service conditions.

Examples of type (b) problems include deflections which result in cracking of masonry or other partitions, damage to ceiling or floor finishes, and improper functioning of sliding windows and doors. To avoid these problems, a limit must be placed on that part of the total deflection that occurs after the attachment of such elements. This *incremental deflection* is usually the sum of the long-term deflection due to all the sustained loads and shrinkage, the short-term deflection due to the transitory live load, and any temperature-induced deflection.

For roof or floor construction supporting or attached to non-structural elements that are unlikely to be damaged by large deflection, ACI 318–83 (1983) limits the incremental deflection to span/240. Where such elements are likely to be damaged by large deflection, the incremental deflection limit is reduced to span/480. Incremental deflections of span/480 can cause cracking of supported masonry walls, particularly when doorways or corners prevent arching and no provisions are made to minimize the effect of movement. AS 3600 (1988) limits the incremental deflection for members supporting masonry partitions to between span/500 and span/1000, depending on the provisions made to minimize the effect of movement.

Type (c) deflection problems include the perceptible springy vertical motion of floor systems and other vibration-related problems. Very little quantitative information for controlling this type of deflection problem is available in codes of practice. ACI 318–83 (1983) places a limit of span/360 on the short-term deflection of a floor due to live load (and span/180 for a flat roof). This limit provides a minimum requirement on the stiffness of members which may, in some cases, be sufficient to avoid problems of type (c). For prestressed concrete floors, type (c) problems are potentially the most common. Load balancing is often employed to produce a nearly horizontal floor under the sustained load. Such structures are generally uncracked at service loads, total deflection is small, and types (a) and (b) deflection problems are easily avoided.

Where a structure supports vibrating machinery (or any other significant dynamic load) or where a structure may be subjected to ground motion

caused by earthquake, blasting, or adjacent road or rail traffic, vibration control becomes an important design requirement. This is particularly so for slender structures, such as tall buildings or long-span beams and slabs.

Vibration is best controlled by isolating the structure from the source of vibration. Where this is not possible, vibration may be controlled by limiting the frequency of the fundamental mode of vibration of the structure to a value which is significantly different from the frequency of the source of vibration. When a structure is subjected only to pedestrian traffic, 5 Hz is often taken as the minimum frequency of the fundamental mode of vibration of a beam or slab (Irwin 1978, Mickleborough & Gilbert 1986).

## 1.8 References

- AASHTO 1983. *Standard specifications for highway bridges*. Washington, DC: American Association of State Highway and Transportation Officials.
- ACI 318–83 1983. *Building code requirements for reinforced concrete*. Detroit: American Concrete Institute.
- ACNBC 1985. *National building code of Canada*. Ottawa: National Research Council of Canada.
- ANSI A58.1 1982. *Minimum design loads for buildings and other structures*. New York: American National Standards Institute.
- AS 1170.1 1989. *SAA loading code, Part 1—Dead and live loads and load combinations*. Sydney: Standards Association of Australia.
- AS 1170.2 1989. *SAA loading code, Part 2—Wind loads*. Sydney: Standards Association of Australia.
- AS 3600 1988. *Australian standard for concrete structures*. Sydney: Standards Association of Australia.
- BS 8110 1985. *Structural use of concrete—parts 1 and 2*. London: British Standards Institution.
- CAN3–A23.3–M84 1984. *Design of concrete structures for buildings*. Rexdale, Canada: Canadian Standards Association.
- CEB–FIP 1978. *Model code for concrete structures*. Paris: Comité Euro-International du Béton—Fédération Internationale de la Précontrainte.
- Irwin, A.W. 1978. Human response to dynamic motion of structures. *Structural Engineer* **56A**, No. 9, 237–44.
- ISO 3898. *Basis for the design of structures*. Geneva: International Standards Organization.
- Mickleborough, N.C. & R.I.Gilbert 1986. Control of concrete floor slab vibration by L/D limits. *Proceedings of the 10th Australasian Conference on the Mechanics of Structures and Materials*. Adelaide: University of Adelaide, 51–6.
- Ministry of Transportation and Communications 1983. *Ontario highway bridge design code (OHBDC–1983)*, 2nd edn. Downsview, Ontario: Ministry of Transportation and Communications.
- NAASRA 1976. *Bridge design specification*. Sydney: National Association of Australian State Road Authorities.
- Structural Engineers Association of California 1980. *Recommended lateral force requirements and commentary*. San Francisco: Seismology Committee.

## 2

# Design properties of materials

### 2.1 Introduction

The behaviour of a prestressed concrete member throughout the full range of loading depends on the properties and behaviour of the constituent materials. In order to satisfy the design objective of adequate structural strength, the ultimate strengths of both concrete and steel need to be known. In addition, factors affecting material strength and the non-linear behaviour of each material in the overload range must be considered. In order to check for serviceability, the instantaneous and time-dependent properties of concrete and steel at typical in-service stress levels are required.

As was mentioned in [Chapter 1](#), the prestressing force in a prestressed member gradually decreases with time. This *loss* of prestress, which is usually 10–25% of the initial value, is mainly caused by inelastic creep and shrinkage strains which develop with time in the concrete at the level of the bonded steel. Reasonable estimates of the creep and shrinkage characteristics of concrete and procedures for the *time analysis* of prestressed structures are essential for an accurate prediction and a clear understanding of in-service behaviour. Relaxation of the prestressing steel also causes a time-dependent loss of prestress. With the current trend towards the use of low relaxation steels, however, this component of prestress loss is usually small (less than 5%).

The intention in this chapter is to present a broad outline of material behaviour and to provide sufficient quantitative information on material properties to complete most design tasks.

### CONCRETE

A more comprehensive treatment of the properties of concrete and the factors affecting them was given by Neville (1981).



## 2.2 Composition of concrete

Concrete is a mixture of cement, water, and aggregates. It may also contain one or more chemical admixtures. Within hours of mixing and placing, concrete sets and begins to develop strength and stiffness as a result of chemical reactions between the cement and water. These reactions are known as *hydration*. Calcium silicates in the cement react with water to produce calcium silicate hydrate and calcium hydroxide. The resultant alkalinity of the concrete helps to provide corrosion protection for the reinforcement.

The relative proportions of cement, water, and aggregates may vary considerably depending on the chemical properties of each component and the desired properties of the concrete. A typical mix used for prestressed concrete by weight might be coarse aggregate 44%, fine aggregate 31%, cement 18%, and water 7%.

In most countries, several different types of Portland cement are available, including normal cements, high early strength cements, low heat of hydration cements, and various cements which provide enhanced sulphate resistance. In order to alter and improve the properties of concrete, other cementitious materials may be used to replace part of the Portland cement, e.g. fly ash, natural pozzolans, blast furnace slag, and condensed silica fume.

The ratio of water to cement by weight that is required to hydrate the cement completely is about 0.25, although larger quantities of water are required in practice in order to produce a workable mix. For the concrete typically used in prestressed structures, the water-to-cement ratio is about 0.4. It is desirable to use as little water as possible, since water not used in the hydration reaction causes voids in the cement paste that reduce the strength and increase the permeability of the concrete.

The use of chemical admixtures to improve one or more properties of the concrete is now commonplace. In recent years, high-strength concretes with low water-to-cement ratios have been made more workable by the inclusion of superplasticizers in the mix. These polymers greatly improve the flow of the wet concrete and allow very high-strength, low-permeability concrete to be used with conventional construction techniques.

The rock and sand aggregates used in concrete should be properly graded and inert. Expansive and porous aggregates should not be used and aggregates containing organic matter or other deleterious substances, such as salts or sulphates, should also be avoided.

## 2.3 Strength of concrete

In structural design, the quality of concrete is usually controlled by the specification of a minimum *characteristic compressive strength* at 28 days,

$f_c$ . The characteristic strength is the stress which is exceeded by 95% of the uniaxial compressive strength measurements taken from standard compression tests. Such tests are most often performed on 150 mm concrete cubes (in Europe and the UK) and on 150 mm diameter by 300 mm long concrete cylinders (in North America and Australia). Because the restraining effect at the loading surfaces is greater for the cube than for the longer cylinder, strength measurements taken from cubes are higher than those taken from cylinders. The ratio between cylinder and cube strength,  $R$ , is about 0.8 for low-strength concrete (i.e. cylinder strengths of 20–30 MPa) and increases as the strength increases. The following expression for  $R$  is often used (Neville 1981):

$$R = 0.76 + 0.2 \log_{10} \left( \frac{\sigma_{cu}}{c} \right) \quad (2.1)$$

where  $\sigma_{cu}$  is the cube strength in MPa (psi) and  $c=19.6$  (2480). Throughout this book,  $f_c$  refers to the characteristic compressive strength obtained from *cylinder* tests.

In practice, the concrete used in prestressed construction is usually of better quality and higher strength than that required for ordinary reinforced concrete. Values of  $f_c$  in the range 30–40 MPa are most often used, but strengths as high as 60 MPa are not uncommon. In some recent structures in North America, concrete strengths of over 100 MPa have been used successfully. The forces imposed on a prestressed concrete section are relatively large and the use of high-strength concrete keeps section dimensions to a minimum. High-strength concrete also has obvious advantages in the anchorage zone of post-tensioned members where bearing stresses are large, and in pretensioned members where a higher bond strength better facilitates the transfer of prestress. As the compressive strength of concrete increases, so too does the tensile strength. The use of higher strength concrete may therefore delay (or even prevent) the onset of cracking in a member.

High-strength concrete is considerably stiffer than low-strength concrete. The elastic modulus is higher and elastic deformations due to both the prestress and the external loads are lower. In addition, high-strength concrete generally creeps less than low-strength concrete. This results in smaller losses of prestress and smaller long-term deformations.

The effect of concrete strength on the shape of the stress-strain curve for concrete in uniaxial compression is shown in [Figure 2.1](#). The modulus of elasticity (the slope of the ascending portion of each curve) increases with increasing strength and each curve reaches its maximum stress at a strain of about 0.002.

The shape of the unloading portion of each curve (after the peak stress has been reached) depends on, among other things, the characteristics of the testing machine. By applying deformation to a specimen, instead of load,

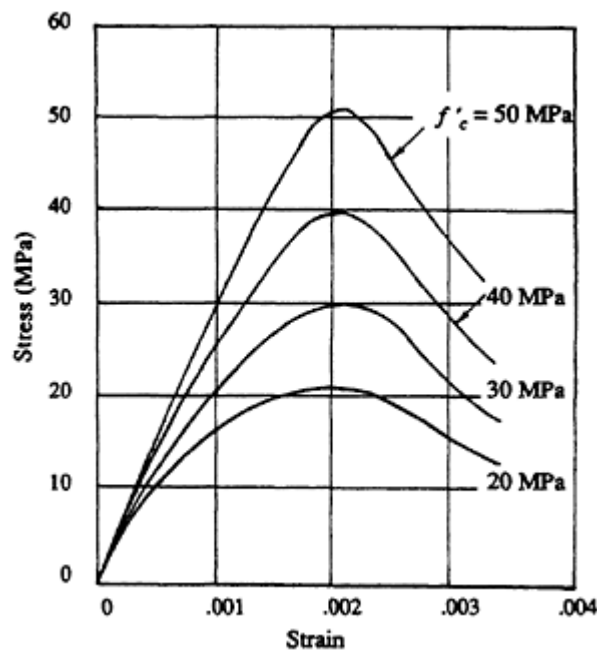


**Figure 2.1** Effect of strength on the compressive stress-strain curve.

in a testing machine which is stiff enough to absorb all the energy of a failing specimen, an extensive unloading branch of the stress-strain curve can be obtained. Concrete can undergo very large compressive strains and still carry load. This *deformability* of concrete tends to decrease with increasing strength.

The strength of properly placed and well compacted concrete depends primarily on the water-to-cement ratio, the size of the specimen, the size, strength, and stiffness of the aggregate, the cement type, the curing conditions, and the age of the concrete. As mentioned in [Section 2.2](#), the strength of concrete increases as the water-to-cement ratio decreases.

The compressive strength of concrete increases with time, a rapid initial strength gain (in the first day or so after casting) and a much slower, gradually decreasing rate thereafter. The rate of development of strength with time depends on the type of curing and the type of cement. In prestressed concrete construction, a rapid initial gain in strength is usually desirable in order to apply the prestress as early as possible. This is particularly so in the case of precast, pretensioned production. Steam curing and high early strength cement are often used to this end.

The following expression is recommended by ACI-209 (1978) for predicting the strength at any time from the measured or specified 28 day value:

$$f'_c(t) = \frac{t}{\alpha + \beta t} f'_c(28) \quad (2.2)$$

where  $f'_c(t)$  is the strength of the concrete at age  $t$  in days,  $f'_c(28)$  is the concrete strength at age 28 days, and  $\alpha$  and  $\beta$  are constants:

For normal Portland cement:

For moist cured concrete:  $\alpha=4.0$   $\beta=0.85$

For steam cured concrete:  $\alpha=1.0$   $\beta=0.95$

For high early strength cement:

For moist cured concrete:  $\alpha=2.3$   $\beta=0.92$

For steam cured concrete:  $\alpha=0.7$   $\beta=0.98$

The strength of concrete in tension is an order of magnitude less than the compressive strength and is far less reliably known. A reasonable estimate is required, however, in order to predict service-load behaviour in the post-cracking range. The flexural tensile strengths of concrete (or modulus of rupture,  $f'_t$ ) is the extreme fibre stress calculated from the results of standard flexural strength tests on plain concrete prisms and usually lies within the range  $0.6\sqrt{f'_c}$ – $1.0\sqrt{f'_c}$  (in MPa). Because of the relatively large scatter of measured tensile strengths, the lower end of this range is usually specified in building codes [such as ACI 318–83 (1983) and AS 3600 (1988)]. For design purposes, the *flexural tensile strength* of normal weight concrete may be taken as

$$f'_t = 0.6\sqrt{f'_c} \quad (2.3)$$

In direct tension, where the tensile stress is uniform (or nearly so) over the section, the tensile strength of concrete,  $f'_{td}$ , is lower and may be taken as

$$f'_{td} = 0.4\sqrt{f'_c} \quad (2.4)$$

For lightweight aggregate concrete, these tensile strengths should be reduced by a factor of about 0.67.

In practice, concrete is often subjected to multi-axial states of stress. For example, a state of biaxial stress exists in the web of a beam, or in a shear wall, or a deep beam. Triaxial stress states exist within connections, in confined columns, in two-way slabs, and other parts of a structure. A number of experimental studies of the behaviour of concrete under multi-axial states of stress (particularly biaxial stress) have been undertaken, including those by Kupfer *et al.* (1975) and Tasuji *et al.* (1978). The results of such studies have been particularly useful in the formulation of material modelling laws for use in finite element studies of concrete structures, such as by Darwin & Pecknold (1977), Gilbert (1979), and many more. A typical biaxial strength envelope is shown in [Figure 2.2](#). The strength of concrete under biaxial compression is greater than for uniaxial compression. Transverse compression improves the longitudinal compressive strength by confining

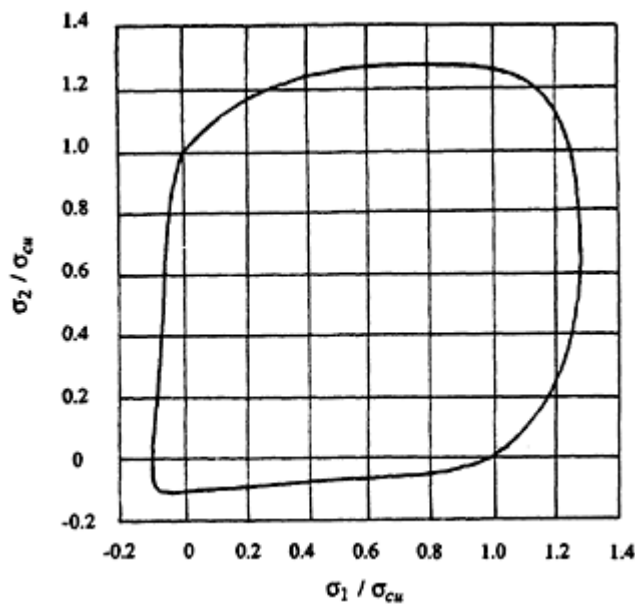


**Figure 2.2** Typical biaxial strength envelope for concrete.

the concrete, thereby delaying (or preventing) the propagation of internal microcracks. [Figure 2.2](#) also shows that transverse compression reduces the tensile strength of concrete, due mainly to the Poisson's ratio effect. Similarly, transverse tension reduces the compressive strength. In triaxial compression, both the strength of concrete and the strain at which the peak stress is reached are greatly increased and even small confining pressures can increase strength significantly. Correctly detailed transverse reinforcement provides confinement to produce a triaxial stress state in the compressive zone of columns and beams, thereby improving both strength and ductility.

## 2.4 Deformation of concrete

### 2.4.1 Discussion

The deformation of a loaded concrete specimen is both instantaneous and time dependent. If the load is sustained, the deformation of the specimen gradually increases with time and may eventually be several times larger than the instantaneous value.

The gradual development of strain with time is caused by creep and shrinkage. Creep strain is produced by sustained stress. Shrinkage is independent of stress and results primarily from the loss of water as the concrete dries. Creep and shrinkage cause increases in axial deformation and curvature on reinforced and prestressed concrete cross-sections, losses of

prestress, local redistribution of stress between the concrete and the steel reinforcement, and redistribution of internal actions in statically indeterminate members. Creep and shrinkage are often responsible for excessive deflection (or camber) and excessive shortening of prestressed members. In addition, shrinkage may cause unsightly cracking which could lead to serviceability or durability problems. On a more positive note, creep relieves concrete of stress concentrations and imparts a measure of deformability to concrete. A comprehensive treatment of the effects of creep and shrinkage on the behaviour of concrete structures is available elsewhere (Gilbert 1988).

Researchers have been investigating the time-dependent deformation of concrete ever since it was first observed and reported almost a century ago, and an enormous volume of literature has been written on the topic. Detailed summaries of the time-dependent properties of concrete and the factors which affect them are contained in the books by Neville (1970, 1981) and Neville *et al.* (1983).

The time-varying deformation of concrete may be illustrated by considering a uniaxially loaded concrete specimen subjected to a constant sustained stress  $\sigma_0$  first applied at time  $\tau_0$ . The total strain at any time  $t > \tau_0$  may be assumed to be the sum of the instantaneous, creep, and shrinkage components, as represented by the equation

$$\varepsilon(t) = \varepsilon_e(t) + \varepsilon_c(t) + \varepsilon_{sh}(t) \quad (2.5)$$

The components of strain are illustrated diagrammatically in [Figure 2.3](#).

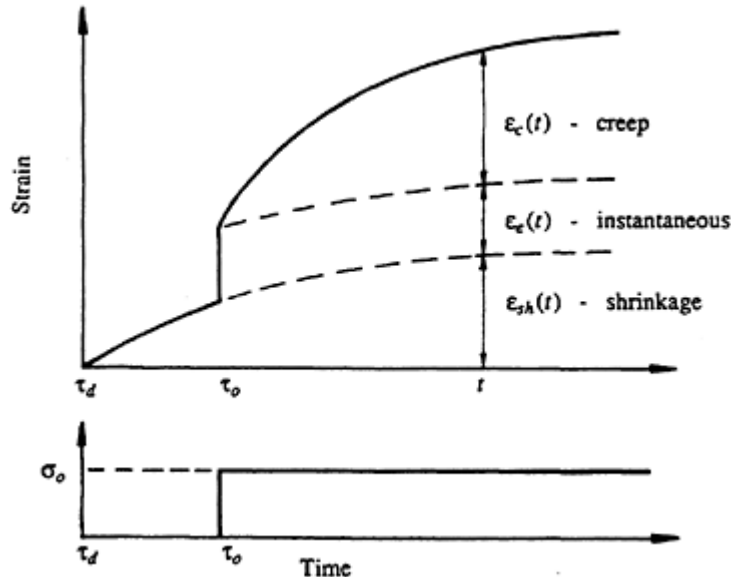


**Figure 2.3** Strain vs time for specimen under constant compressive stress.

Shrinkage strains begin to develop as soon as drying commences at time  $\tau_d$  (immediately after setting or at the end of moist curing). Shrinkage continues to increase with time at a gradually decreasing rate, as shown. When the stress is first applied at  $\tau_o$ , the instantaneous strain component causes a sudden jump in the strain diagram, which is followed by a further increase in strain due to creep. Creep also increases with time at a gradually decreasing rate.

To predict accurately the time-varying behaviour of concrete, a knowledge of the magnitude and rate of development of each of these strain components is required. In a concrete structure, prediction of time-dependent deformation is complicated by the restraint to creep and shrinkage provided by both the reinforcement and the external supports, and the continuously varying concrete stress history that inevitably results. In [Sections 2.4.2–4](#), the material properties that influence each of the strain components in [Figure 2.3](#) are summarized. Methods for predicting the time-dependent behaviour of prestressed concrete cross-sections and members are discussed in detail in [Section 3.6](#).

#### 2.4.2 Instantaneous strain

The magnitude of the instantaneous strain  $\varepsilon_e(t)$  caused by either compressive or tensile stress depends on the magnitude of the applied stress, the rate at which the stress is applied, the age and the properties of the concrete and the proportions of its constituent materials. Consider the uniaxial instantaneous strain versus compressive stress curve shown in [Figure 2.4](#). When the applied stress is less than about half of the compressive strength, the curve is essentially linear, and the instantaneous strain is usually considered to be elastic (fully recoverable). In this low-stress range, the secant

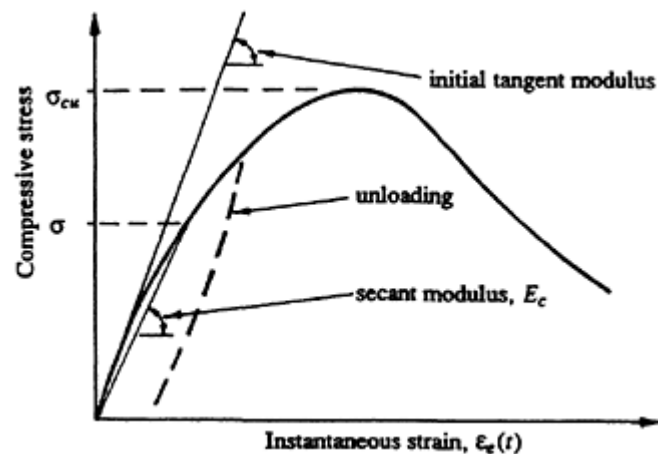


**Figure 2.4** Typical stress vs instantaneous strain curve for concrete in compression.

modulus  $E_c$  does not vary significantly with stress and is only slightly smaller than the initial tangent modulus. At higher stress levels, the curve is decidedly non-linear and a significant proportion of the instantaneous strain is irrecoverable.

In concrete structures, compressive concrete stresses caused by the day-to-day service loads rarely exceed half of the compressive strength. It is therefore reasonable to assume that the instantaneous behaviour of concrete at service loads is linear-elastic and that instantaneous strain is given by

$$\epsilon_e(t) = \frac{\sigma(t)}{E_c} \quad (2.6)$$

The value of the elastic modulus  $E_c$  increases with time as the concrete gains strength and stiffness.  $E_c$  also depends on the rate of application of the stress and increases as the loading rate increases. For most practical purposes, these variations are usually ignored and it is common practice to assume that  $E_c$  is constant with time and equal to its initial value calculated at the time of first loading,  $\tau_0$ . For stress levels less than about  $0.4f'_c$ , and for stresses applied over a relatively short period (say up to 5 min), a numerical estimate of the elastic modulus may be obtained from Pauw's well known expression (Pauw 1960):

$$E_c = \rho^{1.5} 0.043 \sqrt{f'_c(\tau_0)} \quad (\text{MPa}) \quad (2.7)$$

where  $\rho$  is the density of concrete (about  $2400 \text{ kg/m}^3$  for normal weight concrete) and  $f'_c(\tau_0)$  is the average compressive strength in MPa at the time of first loading. Equation 2.7 is specified in both ACI 318–83 (1983) and AS 3600 (1988).

When the stress is applied more slowly, say over a period of 1 day, significant additional deformation occurs owing to the rapid early development of creep. For the estimation of short-term deformation in such a case, it is recommended that the elastic modulus given by Equation 2.7 be reduced by about 20% (Gilbert 1988).

The in-service performance of a concrete structure is very much affected by concrete's ability (or lack of it) to carry tension. It is therefore necessary to consider the instantaneous behaviour of concrete in tension, as well as in compression. Prior to cracking, the instantaneous strain of concrete in tension consists of both elastic and inelastic components. In design, however, concrete is usually taken to be elastic-brittle in tension, i.e. at stress levels less than the tensile strength of concrete the instantaneous strain versus stress relationship is assumed to be linear. Although the initial elastic modulus in tension is a little higher than that in compression, it is usual to assume that both values are equal and given by Equation 2.7. Prior to



cracking, therefore, the instantaneous strain in tension may be calculated using Equation 2.6. When the tensile strength is reached, cracking occurs and the concrete stress perpendicular to the crack is usually assumed to be zero. In reality, if the rate of tensile deformation is controlled, and crack widths are small, concrete can carry some tension across a crack owing to friction on the rough, mating surfaces.

Poisson's ratio for concrete,  $\nu$ , lies within the range 0.15–0.22 and for most practical purposes may be taken equal to 0.2.

### 2.4.3 Creep strain

For concrete subjected to a constant sustained stress, the gradual development of creep strain was illustrated in [Figure 2.3](#). In the period immediately after first loading, creep develops rapidly, but the rate of increase slows appreciably with time. Creep is generally thought to approach a limiting value as the time after first loading approaches infinity. Approximately 50% of the final creep develops in the first 2–3 months and about 90% after 2–3 years. After several years under load, the rate of change of creep with time is very small. Creep of concrete has its origins in the hardened cement paste and is caused by a number of different mechanisms. A comprehensive treatment of creep in plain concrete was given by Neville *et al.* (1983).

Many factors influence the magnitude and rate of development of creep, including the properties of the concrete mix and its constituent materials. In general, as the concrete quality increases, the capacity of concrete to creep decreases. At a particular stress level, creep in higher-strength concrete is less than that in lower-strength concrete. An increase in either the aggregate content or the maximum aggregate size reduces creep, as does the use of a stiffer aggregate type. Creep also decreases as the water-to-cement ratio is reduced.

Creep depends on the environment, and increases as the relative humidity decreases. Creep is therefore greater when accompanied by shrinkage (drying). Creep is also greater in thin members with large surface area to volume ratios, such as slabs. Near the surface of a member, creep takes place in a drying environment and is therefore greater than in regions remote from a drying surface. In addition to the relative humidity, creep is dependent on the ambient temperature. A temperature rise increases the deformability of the cement paste and accelerates drying, and thus increases creep. At 40°C, creep in concrete is about 25% higher than that at 20°C. The dependence of creep on temperature is much more significant at more elevated temperatures.

In addition to the environment and the characteristics of the concrete mix, creep depends on the loading history, in particular the magnitude of the stress and the age of the concrete when the stress was first applied. When the sustained concrete stress is less than about  $0.5f_c'$  (and this is usually the

case in real structures at service loads), creep is proportional to stress and is sensibly known as *linear creep*. At higher sustained stress levels, creep increases at a faster rate and becomes non-linear with respect to stress. From a structural design point of view, non-linear creep is of little interest and only the effects of linear creep are considered here. The age of the concrete when the stress is first applied  $\tau_0$  has a marked influence on the magnitude of creep. Concrete loaded at an early age creeps more than concrete loaded at a later age.

Creep strain is made up of a recoverable component [called the *delayed elastic strain*,  $\varepsilon_d(t)$ ] and an irrecoverable component [called *flow*,  $\varepsilon_f(t)$ ]. These components are illustrated by the creep strain versus time curve in [Figure 2.5a](#), which is caused by the stress history shown in [Figure 2.5b](#). The delayed elastic strain develops rapidly and is of the order of 40% of the elastic strain. The flow component is sometimes further sub-divided into *basic flow* and *drying flow* components; however, in structural analysis, it is not usually necessary to distinguish between these components.

The capacity of concrete to creep is usually measured in terms of the *creep coefficient*  $\phi(t, \tau)$ . In a concrete specimen subjected to a constant sustained compressive stress  $\sigma_0$  first applied at age  $\tau$ , the creep coefficient at time  $t$  is the ratio of creep strain to instantaneous strain and is represented by

$$\phi(t, \tau) = \frac{\varepsilon_c(t, \tau)}{\varepsilon_e} \quad (2.8)$$

and therefore

$$\varepsilon_c(t, \tau) = \varepsilon_e \phi(t, \tau) = \frac{\sigma_0}{E_c} \phi(t, \tau) \quad (2.9)$$

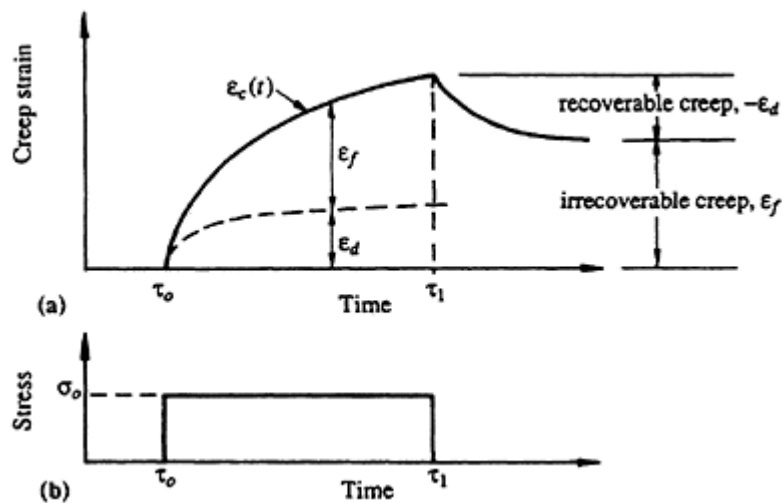


Figure 2.5 Recoverable and irrecoverable creep components.

For stress levels less than about  $0.5f_c'$ , the creep coefficient is a pure time function, independent of the applied stress, and has the same shape as the creep-time curve in [Figure 2.3](#). As time approaches infinity, the creep coefficient is assumed to approach a final value  $\phi^*(\tau) = \phi(\infty, \tau)$  which usually falls within the range 1.5–4.0. A number of the well known methods for predicting the creep coefficient were described and compared by Gilbert (1988). Two of the simpler (and, therefore, more useful) approaches for making numerical estimates of  $\phi(t, \tau)$  are presented in [Section 2.5](#).

The effect of ageing is illustrated in [Figure 2.6](#). The magnitude of the final creep coefficient  $\phi^*(\tau)$  decreases as the age at first loading  $\tau$  increases. That is,

$$\phi^*(\tau_i) > \phi^*(\tau_j) \quad \text{for} \quad \tau_i < \tau_j \quad (2.10)$$

This time-hardening or ageing of concrete complicates the calculation of creep strain caused by a time-varying stress history.

The load-dependent strain at time  $t$  caused by a *constant sustained stress*  $\sigma_o$  is the sum of the elastic and creep components and, using Equation 2.9, is given by

$$\epsilon_e(t) + \epsilon_c(t) = \frac{\sigma_o}{E_c} [1 + \phi(t, \tau)] = \frac{\sigma_o}{E_e(t, \tau)} \quad (2.11)$$

where  $E_e(t, \tau)$  is known as the effective modulus and is given by

$$E_e(t, \tau) = \frac{E_c}{1 + \phi(t, \tau)} \quad (2.12)$$

If the stress is gradually applied to the concrete, rather than suddenly applied, the subsequent creep strain is reduced significantly, since the concrete ages during the period of application of the stress. This can be accom-

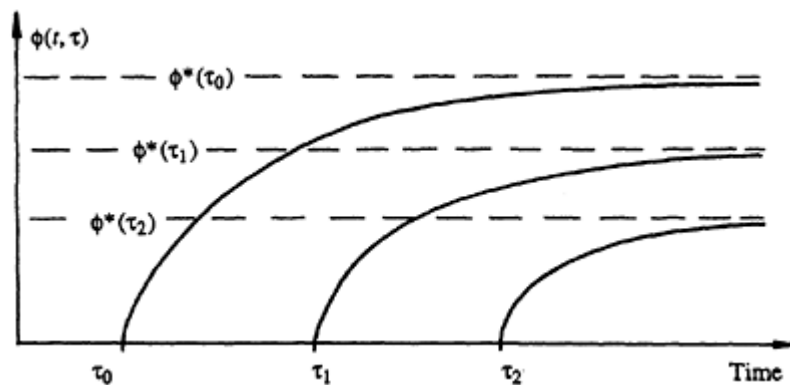


**Figure 2.6** Effect of age at first loading on the creep coefficient (Gilbert 1988).

modated analytically by the use of a reduced or *adjusted* creep coefficient. For an increment of stress,  $\Delta\sigma$ , applied gradually to the concrete, the load-dependent strain may be obtained by modifying Equation 2.11 as follows:

$$\varepsilon_e(t) + \varepsilon_c(t) = \frac{\Delta\sigma}{E_c} [1 + \chi\phi(t, \tau)] = \frac{\Delta\sigma}{\bar{E}_e(t, \tau)} \quad (2.13)$$

where

$$\bar{E}_e(t, \tau) = \frac{E_c}{1 + \chi\phi(t, \tau)} \quad (2.14)$$

$\bar{E}_e(t, \tau)$  is often called the age-adjusted effective modulus, and  $\chi$  is an ageing coefficient first introduced by Trost (1967) and later used by Bazant (1972). Like the creep coefficient, the ageing coefficient depends on the duration of loading and the age at first loading and varies between 0.6 and 1.0. For most practical purposes,  $\chi$  can be taken as 0.8. More accurate estimates of  $\chi$  based on the creep predictive models of ACI 209 (1978) and the CEB Model Code (1978) have been made by Bazant (1972) and Neville *et al.* (1983), respectively.

The above discussion is concerned with compressive creep. In many practical situations, however, creep of concrete in tension is also of interest. Tensile creep, for example, plays an important part in delaying the onset of cracking caused by restrained shrinkage. The mechanisms of tensile creep are thought to be different from those of compressive creep, but at the same stress levels the magnitudes are similar. In design, it is usual to assume that the creep coefficients in tension and in compression are identical. Although not strictly correct, this assumption simplifies calculations and does not usually introduce serious inaccuracies. A comprehensive comparison between tensile and compressive creep was made by Neville *et al.* (1983).

#### 2.4.4 Shrinkage strain

Shrinkage is the time-dependent strain measured in an unloaded and unrestrained specimen at constant temperature. Concrete begins shrinking when drying commences and continues to increase with time at a decreasing rate, as illustrated in [Figure 2.3](#). Shrinkage is assumed to approach a final value  $\varepsilon_{sh}^*$  as time approaches infinity and is dependent on all the factors which affect the drying of concrete, including the relative humidity, the mix characteristics (in particular, the water content and water-to-cement ratio), and the size and shape of the member.

Shrinkage increases as the relative humidity of the surrounding air decreases. The drier the atmosphere, the more rapid is the rate of drying

of the concrete and the larger are both the magnitude and rate of development of shrinkage strain. A temperature rise accelerates drying and therefore increases the rate of shrinkage.

The amount of drying depends on the initial water content. A concrete specimen with a high initial water-to-cement ratio will shrink more than a similar specimen made from concrete with a lower water-to-cement ratio and kept under the same atmospheric conditions. In addition, the volume and type of aggregate also affect shrinkage. Aggregate provides restraint to deformation of the cement paste, so that shrinkage tends to decrease if the volume of aggregate is increased or if a stiffer aggregate is used. Shrinkage in lightweight concrete is therefore considerably greater (up to 50%) than in normal weight concrete.

The size and shape of the concrete member have a major influence on the magnitude and rate of development of shrinkage. For a thin member with a large drying surface to volume ratio, such as a suspended slab or wall, drying takes place rapidly and may be essentially complete after several years. For the concrete in the interior of thicker members, such as beams or columns, drying takes place more slowly and may continue throughout the lifetime of the member. Shrinkage strain therefore varies across the depth (and width) of structural members and is highest at the surfaces exposed to the atmosphere. In fact, for more massive members, there is no significant drying (shrinkage) except in the concrete located within about 300 mm of a drying surface.

Procedures for estimating the mean shrinkage on a cross-section are contained in many building codes and other technical specifications. Two of the more simple approaches for making rough estimates of shrinkage strain are presented in [Section 2.5](#).

## **2.5 Predictions of the creep coefficient and shrinkage**

### *2.5.1 Discussion*

Great accuracy in the prediction of the creep coefficient and shrinkage strain is not possible. The variability of these material characteristics is high. Reasonable estimates can be made, however, by extrapolation from short-term test results, using one of a number of mathematical expressions which have been proposed to model the shape of the creep-time and shrinkage-time curves. Creep strain is measured over a relatively short time period in laboratory specimens subjected to constant stress. Shrinkage is also measured during the same period in identical unloaded specimens. The longer the initial period of measurement, the better are the long-term predictions.

Based on 28 day measurements  $[\phi(28), \varepsilon_{sh}(28)]$ , the ACI Committee 209 (1978) suggests the following expressions for the creep coefficient at any time  $t$  after first loading and the shrinkage strain in moist cured concrete at any time  $T$  after the commencement of drying:

$$\phi(t) = \frac{2.35t^{0.6}}{10 + t^{0.6}} \phi(28) \quad (2.15)$$

and

$$\varepsilon_{sh}(T) = \frac{2.25T}{35 + T} \varepsilon_{sh}(28) \quad (2.16)$$

In practice, structural designers seldom have the time or resources to commission laboratory testing to determine material properties. Design predictions are more often made using one of many numerical methods which are available for predicting the creep coefficient and shrinkage strain. These methods vary in complexity, ranging from relatively complicated methods, involving the determination of numerous coefficients that account for the many factors affecting creep and shrinkage, to much simpler procedures. Comparisons between predictions made using several of the more well known procedures were made by Gilbert (1988) and Neville *et al.* (1983). Although the properties of concrete vary from country to country as the mix characteristics and environmental conditions vary, the agreement between the procedures for estimating both creep and shrinkage is still remarkably poor, particularly for shrinkage. In addition, the comparisons between predictive models show that the accuracy of a particular model is not directly proportional to its complexity, and predictions made using several of the best known methods differ widely.

In the following sections, two simple methods for the estimation of the creep and shrinkage characteristics of concrete are outlined. The first is that recommended in BS 8110 (1985) and the second is similar to that recommended in AS 3600 (1988). In [Appendix I](#), two of the most widely used (and considerably more complex) alternative procedures are presented, namely the recommendations of ACI 209 (1978) and CEB–FIP (1978). The variability of the time-dependent properties of concrete is highlighted by the large differences in the predictions made by each of these methods. From the point of view of the structural designer, there is much to recommend a simple, approximate method which will provide a rough estimate of the creep coefficient and shrinkage strain. After all, a rough estimate is all that is possible. Predictions made using the following procedures will, in general, lead to estimates of structural behaviour which are satisfactory for most practical purposes.

### 2.5.2 British standard—structural use of concrete, BS 8110: Part 2 (1985)

British Standard BS 8110 (1985) specifies a simple method for estimating the final (30 year) creep and shrinkage.

#### Creep

The procedure outlined in BS 8110 is similar to an earlier proposal by the British Concrete Society (1978) and is in fact based on the CEB–FIP (1970) recommendations. The static modulus of elasticity of normal weight concrete at 28 days is specified as

$$E_{c,28} = K_o + 0.2f_{cu}(28) \quad (2.17)$$

where  $K_o$  is a constant that depends on the stiffness of the aggregate and may be taken as 20 GPa for normal weight concrete, and  $f_{cu}(28)$  is the 28 day cube strength in MPa. For lightweight concrete of density  $\rho$  (in  $\text{kg/m}^3$ ), the right-hand side of Equation 2.17 should be multiplied by  $(\rho/2400)^2$ . The elastic modulus at any time  $t$  may be derived from  $E_{c,28}$  using the equation

$$E_c(t) = E_{c,28} \left[ 0.4 + 0.6 \frac{f_{cu}(t)}{f_{cu}(28)} \right] \quad (2.18)$$

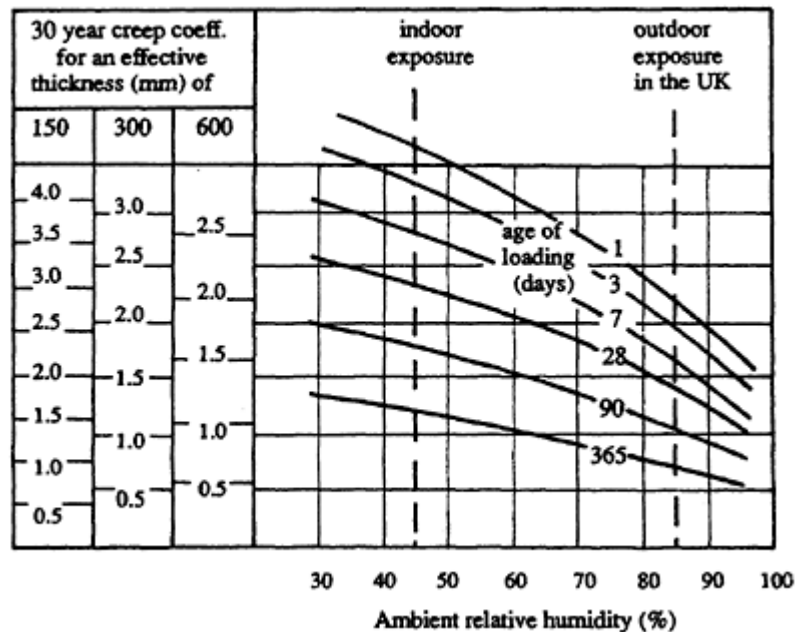


Figure 2.7 Final creep coefficient (BS 8110 1985).

The Standard suggests that the final creep strain may be predicted from

$$\epsilon_{cc} = \frac{\sigma}{E_c(\tau)} \phi^* \tag{2.19}$$

where  $E_c(\tau)$  is the elastic modulus at the time of loading and  $\phi^*$  is the final creep coefficient. Numerical estimates of  $\phi^*$  may be obtained from [Figure 2.7](#) [which is based on the CEB–FIP (1970) recommendations]. Equation 2.19 implies that the final creep strain depends only on the current concrete stress  $\sigma$  and not on the previous stress history, which of course is wrong. If reliable estimates of long-term deformation are required, Equation 2.19 should *not* be used. A more reliable procedure for predicting creep strain, which better accounts for the previous stress history, is presented in [Section 3.6](#). The Standard points out that 40%, 60%, and 80% of the final creep may be assumed to develop during 1, 6, and 30 months, respectively, under load.

### Shrinkage

Shrinkage strains after 6 months and after 30 years may be estimated from [Figure 2.8](#) for concrete of *normal* workability, without water reducing admixtures. [Figure 2.8](#) was proposed originally by Parrott (1979) and applies to concrete with a water content of about 190 l/m<sup>3</sup>. For concrete

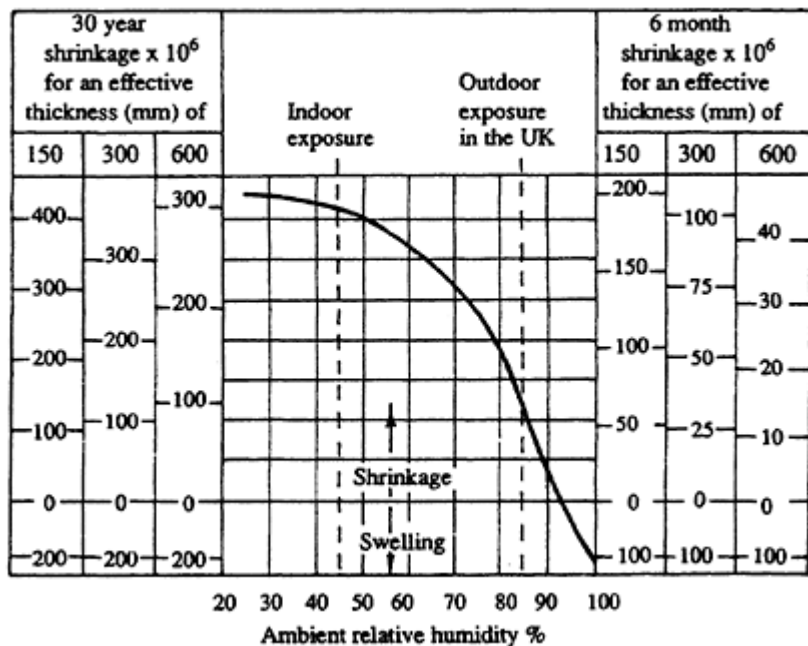


Figure 2.8 Shrinkage for normal weight concrete (BS 8110 1985).



with a different water content, shrinkage may be regarded as proportional to water content within the range 150–230 l/m<sup>3</sup>.

### 2.5.3 Australian standard AS 3600–1988

#### Creep

The creep coefficient at time  $t$  due to a sustained stress first applied at age  $\tau$  is expressed as

$$\phi(t, \tau) = k_2 k_3 \phi_{cc.b} \quad (2.20)$$

In the absence of more reliable test data, the reference creep coefficient  $\phi_{cc.b}$  may be taken as follows:

$f'_c$ (MPa)	20	25	32	40	50
$\phi_{cc.b}$	5.2	4.2	3.4	2.5	2.0

The constant  $k_2$  depends on the hypothetical thickness  $t_h$ , the environment, and the duration of load  $(t - \tau)$  and can be determined from [Figure 2.9](#). The hypothetical thickness of a member is the ratio of its cross-sectional area to half of that part of the perimeter of the section which is exposed to the atmosphere (the drying perimeter).  $k_3$  depends on the age of the concrete at the time of loading and is obtained from the strength ratio  $f_c(\tau)/f_c(28)$  using [Figure 2.10](#).

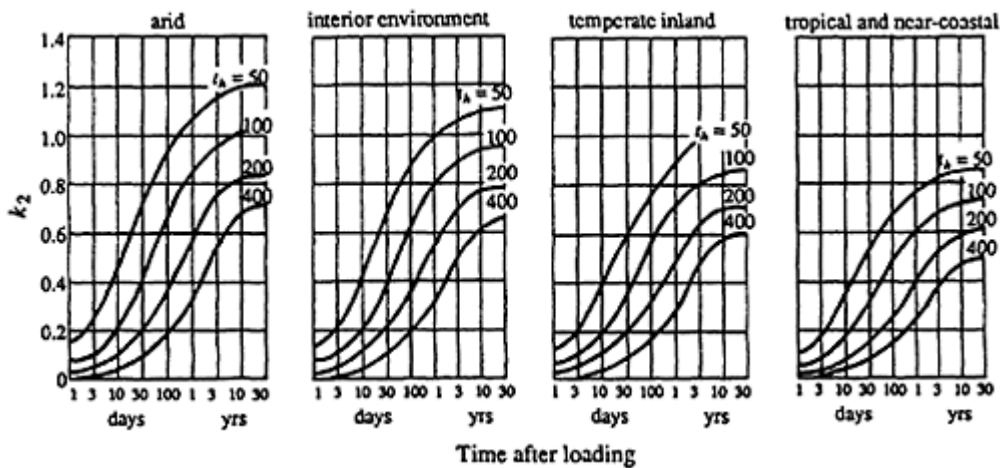


Figure 2.9 Creep coefficient,  $k_2$  (AS 3600–1988).

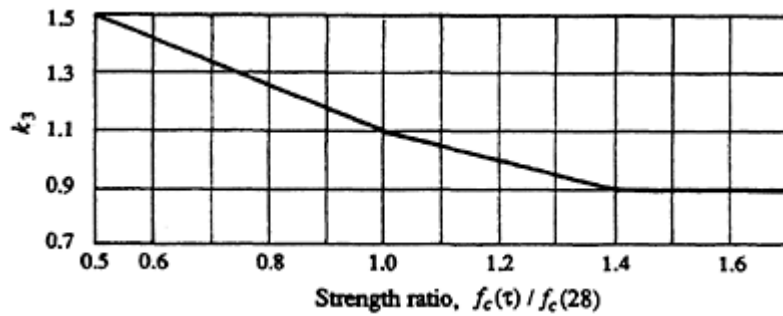


Figure 2.10 Creep coefficient,  $k_3$  (AS 3600–1988).

### Shrinkage

The shrinkage strain at any time after the commencement of drying is given by

$$\epsilon_{sh}(t) = 0.0007k_1 \tag{2.21}$$

where  $k_1$  is obtained from [Figure 2.11](#) and depends on the environment and the hypothetical thickness.

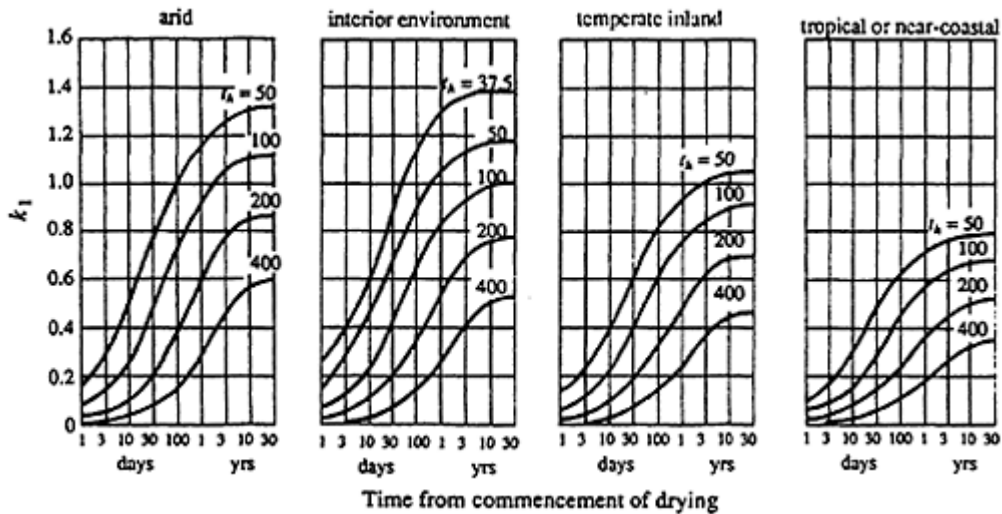


Figure 2.11 Shrinkage coefficient,  $k_1$  (AS 3600–1988).

## 2.6 Thermal expansion

The coefficient of thermal expansion of concrete depends on the coefficient of thermal expansion of the coarse aggregate and on the mix proportions in general. For most types of coarse aggregate, the coefficient lies within the

range  $5 \times 10^{-6}$ – $13 \times 10^{-6}$  per °C (Neville, 1981). For design purposes and in the absence of more detailed information, a coefficient of thermal expansion for concrete of  $10 \times 10^{-6}$  per °C is often recommended (AS 3600–1988).

## STEEL

### 2.7 Steel used for prestressing

The shortening of the concrete caused by creep and shrinkage in a prestressed member causes a corresponding shortening of the prestressing steel which is physically attached to the concrete either by bond or by anchorages at the ends of the tendon. This shortening can be significant and usually results in a loss of stress in the steel of between 150 and 350 MPa. Significant additional losses of prestress can result from other sources, such as friction along a post-tensioned tendon or draw-in at an anchorage at the time of prestressing.

For an efficient and practical design, the total loss of prestress should be a relatively small portion of the initial prestressing force. The steel used to prestress concrete must therefore be capable of carrying a very high initial stress. A tensile strength of between 1000 and 1900 MPa is typical for modern prestressing steels. The early attempts to prestress concrete with low-strength steels failed because the entire prestressing force was rapidly lost owing to the time-dependent deformations of the poor-quality concrete in use at that time.

There are three basic types of high-strength steel commonly used as tendons in modern prestressed concrete construction:

- (a) cold-drawn, stress-relieved round wire;
- (b) stress-relieved strand; and
- (c) high-strength alloy steel bars.

#### 2.7.1 Wires

Cold-drawn wires are manufactured to conform to the requirements of the relevant local code or specification (such as ASTM A421 in the USA and AS 1310 in Australia). These specifications outline the minimum required mechanical properties (such as ultimate tensile strength, yield stress, and elongation at rupture) and dimensional tolerances. Wires are produced by drawing hot-rolled steel rods through dies to produce wires of the required diameter. The drawing process cold works the steel, thereby altering its mechanical properties and increasing its strength. The wires are then

stress-relieved by a process of continuous heat treatment and straightening to produce the required material properties. Wires are sometimes indented or crimped to improve their bond characteristics.

Available sizes of wires vary from country to country, with diameters of 5–7 mm being the most often used. Data for some commonly used wires in Australia are given in [Table 2.1](#) and a typical stress-strain curve is shown in [Figure 2.12](#). The curve is typical of stress-strain curves for high-strength prestressing steel, with no distinct yield point. Nevertheless, the so-called *yield stress* is often referred to in codes and specifications and, unfortunately, is often defined differently. Frequently, yield stress is defined as the stress at the 0.2% offset (AS 1310), as shown in [Figure 2.12](#). The ASTM specification A421 specifies minimum yield strengths for wire at 1% extension. For design purposes, the yield strength of stress-relieved wires may be taken as 0.85 times the minimum tensile strength (i.e.  $0.85f_p$ ) and the modulus of elasticity of the wires may be taken as  $E_p=200\times 10^3$  MPa.

**Table 2.1** Tensile strengths of Australian prestressing steels (AS 3600–1988).

Material type and Standard	Nominal diameter mm	Area mm <sup>2</sup>	Minimum breaking load kN	Minimum tensile strength ( $f_p$ ) MPa
Wire	5	19.6	30.4	1550
	5	19.6	33.3	1700
	7	38.5	65.5	1700
7-wire strand super grade	9.3	54.7	102	1860
	12.7	100	184	1840
	15.2	143	250	1750
7-wire strand regular grade	12.7	94.3	165	1750
Bars (super grade)	23	415	450	1080
	26	530	570	1080
	29	660	710	1080
	32	804	870	1080
	38	1140	1230	1080

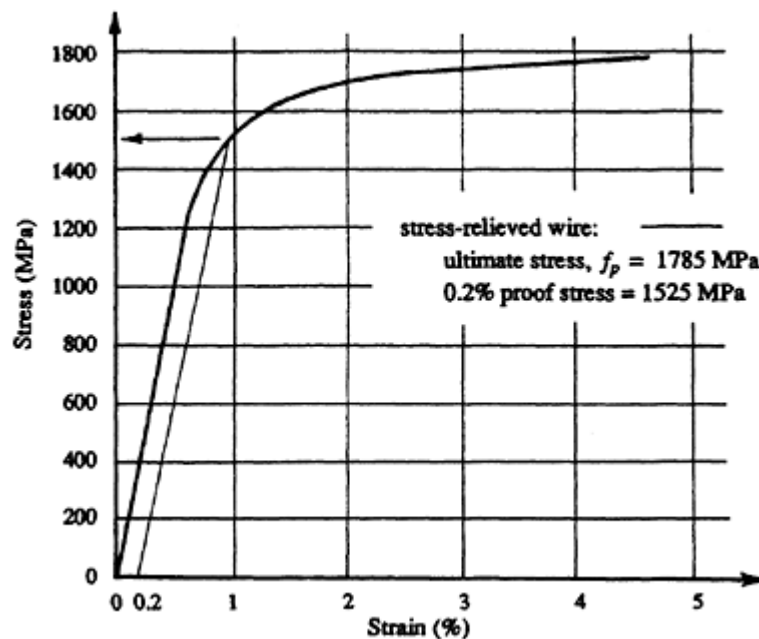


**Figure 2.12** Typical stress-strain curve for stress-relieved wire.

In recent years, the use of wires in prestressed concrete construction has declined, with 7-wire strand being preferred in most applications. Where wires are used in post-tensioned applications, tendons consisting of many individual wires are generally employed.

### 2.7.2 Strands

Stress-relieved strand is the most commonly used prestressing steel. Strand must comply with the requirements of the relevant local specifications (such as ASTM A416 and AS 1311–1312). Strand is fabricated from a number of prestressing wires, usually seven (although 19-wire strand is also available in some countries). Seven-wire strand consists of six wires tightly wound around a seventh, slightly larger diameter, central wire. The pitch of the six spirally wound wires is between 12 and 16 times the nominal diameter of the strand. After stranding, the tendon is further stress-relieved. Low-relaxation (or stabilized) strand is most often used by today's prestressing industry.

Seven-wire strand is generally available in two grades, normal and super grade (Grades 250 and 270 in the USA). Diameters ranging from 7.9 to 15.2 mm are typical. Data for some commonly used Australian strand are given in [Table 2.1](#) and a typical stress-strain curve for a 12.7 mm diameter, super grade, 7-wire strand is shown in [Figure 2.13](#).

The mechanical properties of the strand are slightly different from those of the wire from which it is made. This is because the stranded wires tend

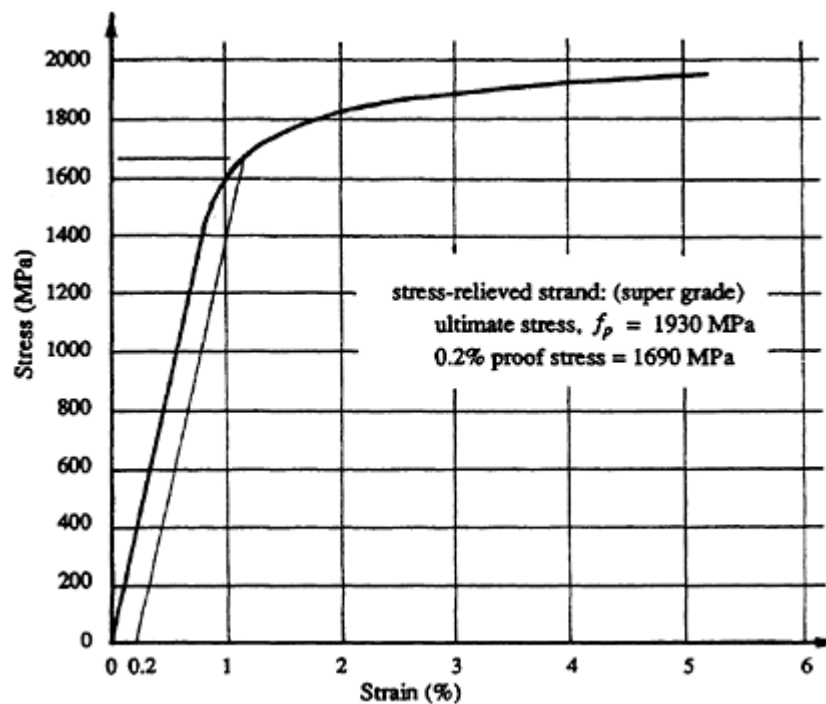


**Figure 2.13** Typical stress-strain curve for 7-wire strand.

to straighten slightly when subjected to tension. For design purposes, the yield stress of stress-relieved strand may be taken to be  $0.85f_p$  and the elastic modulus to be  $E_p=195\times 10^3$  MPa.

Strand may be compacted by being drawn through a die, thereby compressing the outer six wires more tightly around the central one. The cross-sectional area is therefore maintained but the strand diameter is significantly reduced.

### 2.7.3 Bars

The high strength of alloy steel bars is obtained by the introduction of alloying elements in the manufacture of the steel and by cold working (stretching) the bars. The bars are then stress-relieved to obtain properties which meet the requirements of the relevant local specification (e.g. ASTM A722 and AS 1313).

In the USA, both plain and deformed bars are available in two grades ( $f_p=1000$  and 1100 MPa) with diameters which range from 12.7 mm ( $\frac{1}{2}$  in) to 35 mm ( $1\frac{3}{8}$  in). Some sizes and properties of bars commonly used in Australia are presented in Table 2.1 and a typical stress-strain curve is shown in [Figure 2.14](#).

The elastic modulus for bars is generally lower than those for strand and wire. For design purposes  $E_p$  may be taken to be  $170\times 10^3$  MPa and the yield stress (0.2% offset) may be taken to be  $0.85f_p$ .

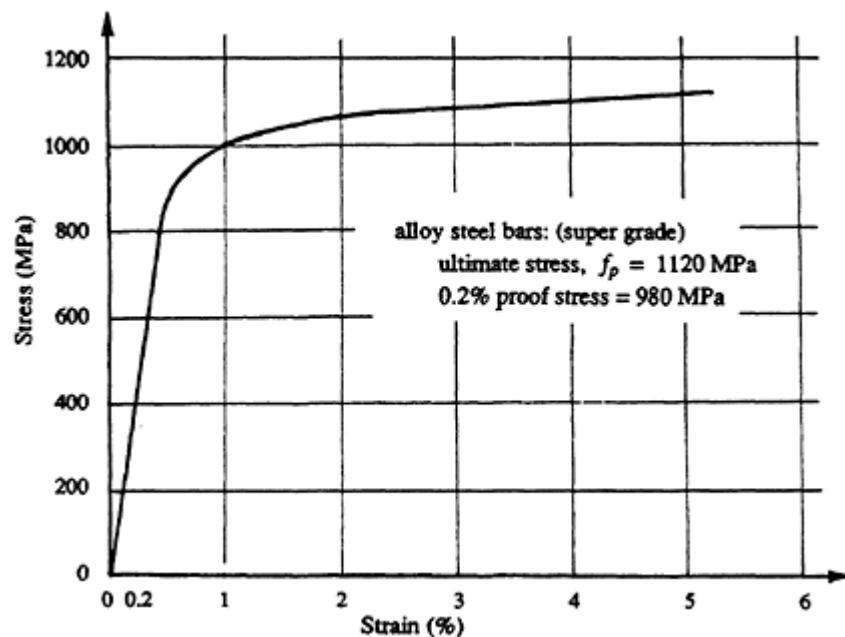


**Figure 2.14** Typical stress-strain curve for alloy steel bars.

The stress-strain curves shown in [Figures 2.12–2.14](#) exhibit similar characteristics. There is no well defined yield point (as exists for lower strength reinforcing steels). Each curve has a relatively high proportional limit. When the curves become non-linear as loading continues, the stress gradually increases monotonically until the steel fractures. The elongation at fracture is usually about 5%. High-strength steel is therefore considerably less ductile than conventional, non-prestress reinforcing steel. Nevertheless, the material is ductile enough to permit the design of ductile prestressed concrete flexural members which suffer large deformations prior to failure.

## 2.8 Steel relaxation

The initial stress level in prestressing steel after transfer is usually high, often in the range 60–75% of the tensile strength of the material. At such stress levels, high-strength steel creeps. If a tendon is stretched and held at a constant length (constant strain), the development of creep strain in the steel is exhibited as a loss of elastic strain, and hence a loss of stress. This loss of stress in a specimen subjected to constant strain is known as *relaxation*. Relaxation in steel is highly dependent on the stress level and increases at an increasing rate as the stress level increases. Relaxation (creep) in steel increases rapidly with temperature. Both *normal-relaxation* and *low-relaxation* steels are available. In recent years, low-relaxation steel has

**Table 2.2** Basic Relaxation  $R_{1000}$  for Australian steel (AS 3600–1988).

Type of Steel	$R_{1000}$ (%) Low Relaxation	$R_{1000}$ (%) Normal Relaxation
Stress-relieved wire	2.0	6.5
Stress-relieved strand	2.5	7.0
Alloy steel bars	2.5	7.0

become the most popular because of the reduced time-dependent losses of prestress that result from its use. Low relaxation steel has been stabilized by prestretching at an appropriate temperature.

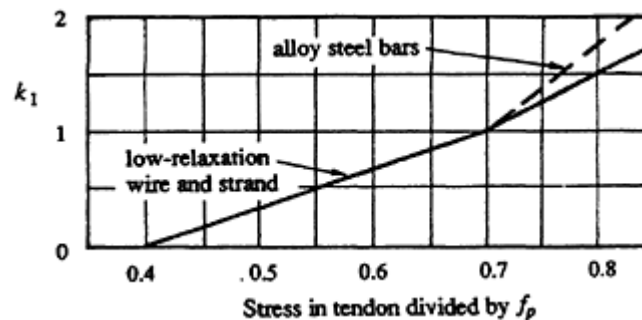
Relaxation measurements are often made over a test period of 1000 hours on a specimen subjected to constant strain at a constant temperature of 20°C. The initial stress levels usually vary from 60 to 80% of the ultimate tensile strength. For an initial stress of 0.7 times the ultimate tensile strength (i.e.  $\sigma_{pi}=0.7f_p$ ), the relaxation of a tendon (i.e. the loss of stress due to relaxation as a percentage of the initial stress) after 1000 h at 20°C is represented by  $R_{1000}$ . For Australian steels,  $R_{1000}$  may be taken from [Table 2.2](#).

The design relaxation  $R$  (in percent) after a period of  $t$  days may be obtained from Equation 2.22 (AS 3600–1988):

$$R = k_1 k_2 R_{1000} [\log(5.38t^{0.167})] \quad (2.22)$$

The coefficient  $k_1$  depends on the initial stress level in the tendon and is obtained from [Figure 2.15](#). The term  $k_2$  depends on the average annual temperature  $T$  and may be taken as  $T/20$  but not less than 1.0.

Very long-term relaxation values for prestressing steels were proposed by the CEB–FIP (1978) and are given in [Table 2.3](#).

**Figure 2.15** Relaxation coefficient,  $k_1$  (AS 3600–1988).



**Table 2.3** Very long-term relaxation  $R_\infty$  (in percent) [CEB-FIP (1978)].

$\sigma_{pi}/f_p$	0.6	0.7	0.8
Normal relaxation steel	6	12	25
Low relaxation steel	3	6	10

Ghali & Favre (1986) proposed an equation of the following form to approximate the data in [Table 2.3](#):

$$R_\infty = \eta \left( \frac{\sigma_{pi}}{f_p} - 0.4 \right)^2 \quad (2.23)$$

where  $\eta=150$  for normal-relaxation steel and 67 for low-relaxation steel.

When elevated temperatures exist during steam curing or at other times, relaxation is increased and occurs rapidly during the period of high temperature. For low-relaxation steel in a concrete member subjected to an initial period of steam curing, it is recommended that the design relaxation should be at least double the value given by Equation 2.22 (calculated with  $T=20^\circ\text{C}$ ).

## 2.9 Non-prestressed reinforcement

Conventional, non-prestressed reinforcement in the form of bars, cold-drawn wires, or welded wire mesh is used in prestressed concrete structures for the same reasons as it is used in conventional reinforced concrete construction. These include the following:

- (a) To provide additional tensile strength and ductility in regions of the structure where sufficient tensile strength and ductility are not provided by the prestressing steel. Non-prestressed, longitudinal bars, for example, are often included in the tension zone of beams to supplement the prestressing steel and increase the flexural strength. Non-prestressed reinforcement in the form of stirrups is most frequently used to carry the diagonal tension caused by shear and torsion in the webs of prestressed concrete beams.
- (b) To control flexural cracking at service loads in partially prestressed concrete beams and slabs where some degree of cracking under full service loads is expected.
- (c) To control shrinkage and temperature cracking in regions and directions of low (or no) prestress.

- (d) To carry compressive forces in regions where the concrete alone may not be adequate, such as in columns or in the compressive zone of heavily reinforced beams.
- (e) Lateral ties or helices are used to provide restraint to bars in compression (i.e. to prevent lateral buckling of compressive reinforcement prior to the attainment of full strength) and to provide confinement for the compressive concrete in columns, beams, and connections, thereby increasing both the strength and deformability of the concrete.
- (f) To reduce long-term deflection and shortening due to creep and shrinkage by the inclusion of longitudinal bars in the compression region of the member.
- (g) To provide resistance to the transverse tension that develops in the anchorage zone of post-tensioned members and to assist the concrete to carry the high bearing stresses immediately behind the anchorage plates.
- (h) To reinforce the overhanging flanges in T-, I-, or L-shaped cross-sections in both the longitudinal and transverse directions.

Non-prestressed reinforcement is manufactured to meet the requirements of the relevant local codes or specifications. Types and sizes vary from country to country. In Australia, for example, reinforcing bars are available in two grades, Grade 230 and 410 (which correspond to characteristic yield

**Table 2.4** Types and sizes of non-prestressed reinforcing bar in Australia.

Steel Grade and Guaranteed Minimum Yield Stress	Bar Size $d_b$ (mm)	Nominal Mass per metre (kg/m)	Nominal Area $A_s$ (mm <sup>2</sup> )
Grade 230 (R-bars) $f_y=230$ MPa	R6	0.245	31
	R10	0.632	80
Grade 410 $f_y=410$ MPa Y-bars	12	0.910	110
	16	1.618	200
	20	2.528	310
	24	3.640	450
	28	4.955	620
	32	6.471	800
	36	8.190	1020

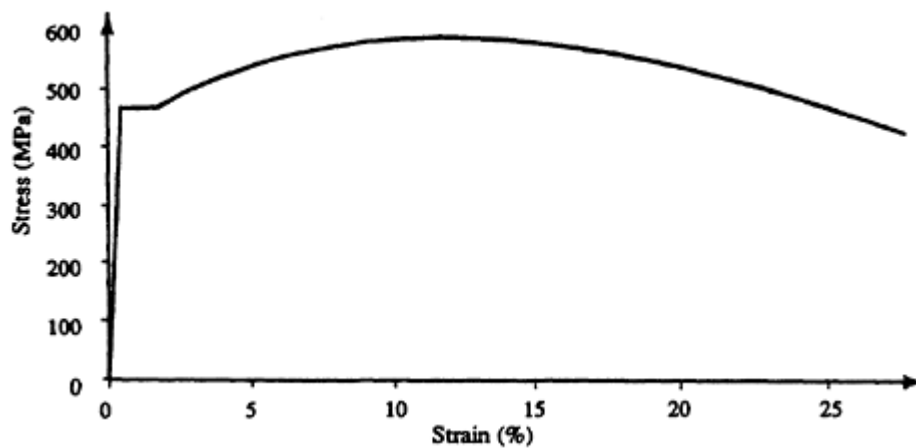


**Figure 2.16** Stress-strain curve for Grade 410 Y-bars (Broken Hill Proprietary Company 1983).

**Table 2.5** Types and sizes of Australian welded wire mesh (Humes ARC 1985).

Mesh Type ( $f_y=450$ MPa)	Cross-Sectional Area of Wires		Mesh Specification			
			Longitudinal Wire		Cross Wire	
	Longitud. ( $\text{mm}^2/\text{m}$ )	Cross ( $\text{mm}^2/\text{m}$ )	Size (mm)	Pitch (mm)	Size (mm)	Pitch (mm)
Rectangular						
F1218	1227	251	12.5	100	8	200
F1118	985	251	11.2	100	8	200
F1018	785	251	10	100	8	200
F918	636	251	9	100	8	200
F818	503	251	8	100	8	200
F718	396	251	7.1	100	8	200
Square						
F81	503	503	8	100	8	100
F102	393	393	10	200	10	200
F92	318	318	9	200	9	200
F82	251	251	8	200	8	200
F72	198	198	7.1	200	7.1	200
F62	156	156	6.3	200	6.3	200
F52	98	98	5	200	5	200
F42	63	63	4	200	4	200
Trench Mesh						
F11TM	985	82	11.2	100	5.6	300
F8TM	503	42	8	100	4	300

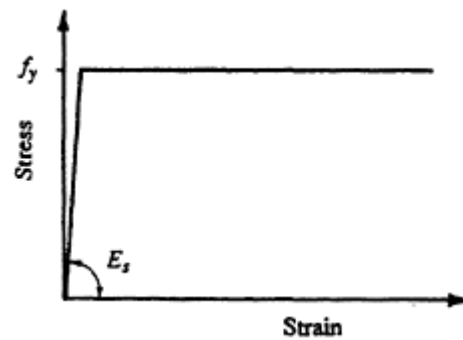


**Figure 2.17** Stress-strain curve for non-prestressed steel usually assumed in design.

stresses of 230 and 410 MPa, respectively). Bars must comply with Australian Standard AS 1302, *Steel reinforcing bars for concrete*. Grade 230 bars are hot-rolled plain round bars 6 or 10 mm diameter (designated R6 and R10 bars) and are commonly used for fitments, such as ties and stirrups. Grade 410 bars (known as *tempcore* or Y-bars) are hot-rolled deformed bars with diameters ranging from 12 to 36 mm (in 4 mm increments). Available bar sizes and properties are shown in [Table 2.4](#). The regularly spaced, rib-shaped deformations on the surface of a deformed bar provide a far better bond between the concrete and the steel and greatly improve the anchorage potential of the bar. It is for this reason that deformed bars rather than plain round bars are used as longitudinal reinforcement in most reinforced and partially prestressed concrete members.

In reality, the actual yield stress of a reinforcing bar is usually significantly higher than the guaranteed minimum indicated in [Table 2.4](#). A typical stress-strain curve for Grade 410 steel is shown in [Figure 2.16](#). Note the distinct yield point and the large total elongation. Although possessing less than one third of the strength of prestressing wire or strand, Grade 410 bars are far more ductile.

Welded wire mesh is sometimes used in prestressed concrete slabs and is manufactured from hard-drawn wire. In Australia, the characteristic yield strength of the wire is 450 MPa and it is manufactured to comply with AS 1303, *Hard-drawn reinforcing wire for concrete*, and AS 1304, *Hard-drawn steel wire reinforcing fabric for concrete*. The properties and designations of available mesh sizes in Australia are given in [Table 2.5](#).

In design calculations, non-prestressed steel is usually assumed to be elastic-plastic, that is  $f_y$  is taken to be the *strength* of the material. When  $f_y$  is reached, the stress-strain curve is assumed to be horizontal (perfectly plastic), as shown in [Figure 2.17](#). The stress-strain curve in compression is assumed to be similar to that in tension. The elastic modulus for non-prestressed steel is taken to be  $E_s=200\times 10^3$  MPa.

## 2.10 References

- ACI 318–83 1983. *Building code requirements for reinforced concrete*. Detroit: American Concrete Institute.
- ACI Committee 209, Subcommittee II 1978. *Prediction of creep, shrinkage and temperature effects, 2, Draft Report*. Detroit: American Concrete Institute.
- AS 1310 1987. *Steel wire for tendons in prestressed concrete*. Sydney: Standards Association of Australia.
- AS 1311 1987. *Steel tendons for prestressed concrete 7-wire stress-relieved strand for tendons in prestressed concrete*. Sydney: Standards Association of Australia.
- AS 1313 1989. *Steel tendons for prestressed concrete, cold-worked high tensile alloy steel bars for prestressed concrete*. Sydney: Standards Association of Australia.
- AS 3600–1988. *Australian standard for concrete structures*. Sydney: Standards Association of Australia.
- ASTM Specification A416 1988. *Steel strand, uncoated seven-wire stress-relieved strand for prestressed concrete*. Philadelphia: American Society for Testing and Materials.
- ASTM Specification A421 1980. *Uncoated stress-relieved steel wire for prestressed concrete*. Philadelphia: American Society for Testing and Materials.
- ASTM Specification A722 1988. *Uncoated high strength steel bar for prestressed concrete*. Philadelphia: American Society for Testing and Materials.
- Bažant, Z.P. 1972. Prediction of concrete creep effects using age-adjusted effective modulus method. *Journal of the American Concrete Institute (ACI Journal)* **69**, April, 212–7.
- British Concrete Society 1978. *A simple design method for predicting the elastic modulus and creep of structural concrete*. Technical Report. London: British Concrete Society.
- Broken Hill Proprietary Company 1983. *Tempcore—Summarised technical information based on European Tempcore*. Data Sheets Sydney.
- BS 8110 1985. *Structural use of concrete, part 2, code of practice for special circumstances*. London: British Standards Institution.
- CEB–FIP 1970. *International recommendations for the design and construction of concrete structures*. Paris: Comité Euro-International du Béton.
- CEB–FIP 1978. *Model code for concrete structures*. English Translation, April. Paris: Comité Euro-International du Béton.
- Darwin, D. & D.A. Pecknold 1977. Nonlinear biaxial stress-strain law for concrete. *Journal of the Engineering Mech. Division, ASCE* **103**, 229–41.
- Ghali, A. & R. Favre, 1986. *Concrete structures: stresses and deformations*. London: Chapman and Hall.
- Gilbert, R.I. 1979. Time-dependent behaviour of structural concrete slabs. *PhD Thesis*. Sydney: School of Civil Engineering, University of New South Wales.
- Gilbert, R.I. 1988. *Time effects in concrete structures*. Amsterdam: Elsevier.
- Humes ARC Engineering Services 1985. *Properties of reinforcing fabric and bar*. Melbourne: Humes ARC Engineering Services.
- Kupfer, H.B., H.K. Hilsdorf & H. Rüschi 1975. Behaviour of concrete under biaxial stresses. *ACI Journal*, **66**, 656–66.
- Neville, A.M. 1970. *Creep of concrete: plain, reinforced and prestressed*. Amsterdam: North-Holland.
- Neville, A.M. 1981. *Properties of concrete*. London: Pitman.
- Neville, A.M., W.H. Dilger & J.J. Brooks 1983. *Creep of plain and structural concrete*. London: Construction Press.

- Parrott, L.J. 1979. Simplified methods for predicting the deformation of structural concrete. *Development Report No. 3*. London: Cement and Concrete Association.
- Pauw, A. 1960. Static modulus of elasticity of concrete as affected by density. *ACI Journal* **57**, 679–87.
- Rüsch, H. & D.Jungwirth 1976. *Stahlbeton-Spannbeton*, Band 2. Düsseldorf: Werner-Verlag.
- Tasuji, M.E., F.O.Slate & A.H.Nilson 1978. Stress-strain response and fracture of concrete in biaxial loading. *ACI Journal* **75**, 306–12.
- Trost, H. 1967. Auswirkungen des Superpositionsprinzips auf Kriech- und Relaxations Probleme bei Béton und Spannbeton. *Beton- und Stahlbetonbau* **62**, 230–8, 261–9.
- Trost, H. 1978. Creep and creep recovery of very old concrete. *RILEM Colloquium on Creep of Concrete, Leeds*.

# 3

## Design for serviceability

### 3.1 Introduction

The level of prestress and the layout of the tendons in a member are usually determined from the serviceability requirements for that member. If a water-tight and crack-free slab is required, for example, tension in the slab must be eliminated or limited to some appropriately low value. If, on the other hand, the deflection under a particular service load is to be minimized, a load-balancing approach may be used to determine the prestressing force and cable drape (see [Section 1.5.3](#)).

For the serviceability requirements to be satisfied in each region of a member and at all times after first loading, a reasonably accurate estimate of the magnitude of prestress is needed in design. This requires reliable procedures for the determination of both the instantaneous and the time-dependent losses of prestress. Instantaneous losses of prestress occur during the stressing (and anchoring) operation and include elastic shortening of the concrete, friction along a post-tensioned cable, and slip at the anchorages. As has been mentioned in the previous chapters, the time-dependent losses of prestress are caused by creep and shrinkage of the concrete and stress relaxation in the steel. Procedures for calculating both the instantaneous and time-dependent losses of prestress are presented in [Section 3.7](#).

There are two critical stages in the design of prestressed concrete for serviceability. The first stage is immediately after the prestress is transferred to the concrete, i.e. when the prestress is at a maximum and the external load is usually at a minimum. The instantaneous losses have taken place but no time-dependent losses have yet occurred. At this stage, the concrete is usually young and the concrete strength may be relatively low. The prestressing force immediately after *transfer* at a particular section is designated  $P_i$ . The second critical stage is after the time-dependent losses have taken place and the full-service load is applied, i.e. when the prestress is at a minimum and the external service load is at a maximum. The prestressing force at this stage is designated  $P_e$ .

At each of these stages (and at all intermediate stages), it is necessary to ensure that the serviceability requirements of the member are satisfied. It is even more important, of course, to make sure that strength requirements at each stage are also satisfied. It is not strength, however, that determines the level of prestress, but serviceability. When the prestressing force and the amount and distribution of the prestressing steel have been determined, the flexural strength may be readily increased, if necessary, by the addition of non-prestressed conventional reinforcement. This is discussed in considerably more detail in [Chapter 4](#). Shear strength may be improved by the addition of transverse stirrups (as discussed in [Chapter 5](#)). As will be seen throughout this chapter, the presence of bonded conventional reinforcement also greatly influences both the short- and long-term behaviour at service loads, particularly for partially prestressed members. The design for strength and serviceability therefore cannot be performed independently, as the implications of one affect the other.

General design requirements for the serviceability limit states, including load combinations for serviceability, were discussed in [Section 1.7](#). It is necessary to ensure that the instantaneous and time-dependent deflection and the axial shortening under service loads are acceptably small and that any cracking is well controlled by suitably detailed, bonded reinforcement. To determine the in-service behaviour of a member, it is therefore necessary to establish the extent of cracking, if any, by checking the magnitude of elastic tensile stresses. If a member remains uncracked (i.e. the maximum tensile stress at all stages is less than the tensile strength of concrete), the properties of the gross section may be used in all deflection and camber calculations. If cracking occurs, a cracked section analysis may be performed to determine the properties of the cracked section and the post-cracking behaviour of the member. Such an analysis is described in [Section 3.5.2](#).

## 3.2 Stress limits

Depending on the serviceability requirements for a particular structure, a designer may set limits on the tensile and compressive stresses in concrete both at transfer and under the full service loads. For the design of *fully prestressed* members (i.e. members in which cracking is not permitted), some codes of practice (e.g. ACI 318–83) set mandatory maximum limits on the magnitude of the concrete stress, both tensile and compressive. For *partially prestressed* members, where cracking is permitted under normal service loads and the tensile stress limits (often called *permissible stresses*) are exceeded, a detailed non-linear analysis is required to determine behaviour in the post-cracking range.

The concrete stress limits specified in ACI 318–83 (here converted to SI



units) are as follows:

Immediately after transfer (before time-dependent losses):

In compression:  $0.6 f'_{ci}$   
 In tension:  $0.25 \sqrt{f'_{ci}}$   
 (or  $0.5 \sqrt{f'_{ci}}$  at the ends of a simple member)

The quantity  $f'_{ci}$  is the characteristic compressive strength of concrete at transfer. Where the tensile stress exceeds these values, bonded reinforcement should be provided in the tensile zone to resist the total tensile force in the concrete.

Under full service loads (after all losses):

In compression:  $0.45 f'_c$   
 In tension:  $0.5 \sqrt{f'_c}$

When an analysis based on transformed cracked sections shows that both short- and long-term deflections are acceptable, ACI 318–83 allows the tensile stress limit to be increased to  $1.00 \sqrt{f'_c}$ , provided the minimum concrete cover to the tendons is increased by 50% when the cracked surface is exposed to earth, weather, or other corrosive environments.

Other codes (e.g. AS3600–1988) impose no mandatory concrete permissible stresses. The choice of stress limit is left entirely to the designer and should be based on the appropriate serviceability requirements. There is much to recommend this approach. Satisfaction of any set of stress limits does not guarantee serviceability. Camber and deflection calculations are still required. It is therefore appropriate to discuss the reasons for and the implications of selecting particular stress limits.

Firstly, consider whether or not stress limits are required at transfer. There can be little doubt that the magnitudes of both compressive and tensile concrete stresses at transfer need to be carefully considered. It is important that the concrete compressive stress at the steel level at transfer should not exceed about  $0.5 f'_{ci}$ . At higher stress levels, large non-linear creep strains develop with time, resulting in large creep deformation and high losses of prestress. Designers must also check strength at transfer and the satisfaction of the above compressive stress limit will usually, although not necessarily, lead to an adequate factor of safety against compressive failure at transfer.

It is also advisable to limit the tensile stress at transfer, particularly in unreinforced regions. The regions of a member which are subjected to tension at transfer are often those which are later subjected to compression when the full service load is applied. If these regions are unreinforced and uncontrolled cracking is permitted at transfer, an immediate serviceability

problem exists. When the region is later compressed, cracks may not close completely, local spalling may occur, and even a loss of shear strength could result. If cracking is permitted at transfer, bonded reinforcement should be provided to carry all the tension and to ensure that the cracks are fine and well behaved.

In some cases, stress limits may also be required under full service loads when all prestress losses have taken place. If cracking is to be avoided, some tensile stress limit must be adopted. A value in the range  $0.25\sqrt{f'_c}$ – $0.5\sqrt{f'_c}$  is appropriate. If the upper end of this range is adopted, some cracking may occur under full loads, particularly if the load-independent tension induced by restrained shrinkage or temperature effects has not been adequately assessed. Provided bonded reinforcement or tendons are provided near the tensile face, however, the cracks will be well controlled and the resulting loss of stiffness will not be significant.

For many prestressed concrete situations, there is no reason why tensile cracking should be avoided at service loads and, therefore, no reason why a limit should be placed on the elastic tensile stress. If cracking is permitted, the resulting loss of stiffness must be accounted for in deflection calculations and crack widths must be acceptably small. Crack control may be achieved by limiting both the spacing of and the change of stress in the bonded reinforcement. Where the cracked surface is not exposed to a corrosive environment, crack control may be achieved by limiting the increment of stress in the bonded reinforcement after cracking to about 200 MPa, and by limiting the centre-to-centre spacing of bonded reinforcement to about 200 mm for beams and 500 mm for slabs (AS 3600–1988). In order to calculate the loss of stiffness caused by cracking or the increment of steel stress after cracking, a cracked section analysis is required.

Under full service loads, which occur infrequently, there is often no practical reason why compressive stress limits should be imposed. Separate checks for flexural strength, ductility and shear strength are obviously necessary. Excessive compressive stresses may, however, occur under full service loads in some types of members, such as trough girders or inverted T-beams, and in the design of these members care should be taken to limit the extreme fibre compressive stress at service loads. If a large portion of the total service load is permanent, compressive stress levels in excess of  $0.5f'_c$  should be avoided.

The primary objective in selecting concrete stress limits is to obtain a serviceable structure. As was discussed in [Section 1.5](#), elastic stress calculations are not strictly applicable to prestressed concrete. Creep and shrinkage cause a gradual transfer of compression from the concrete to the bonded steel. Nevertheless, elastic stress calculations may indicate potential serviceability problems and the satisfaction of concrete tensile stress limits is a useful procedure to control the extent of cracking. It should be understood, however, that the satisfaction of a set of elastic concrete stress limits does

not, in itself, ensure serviceability and it certainly does not ensure adequate strength. The designer must check separately both strength and serviceability, irrespective of the stress limits selected. In the end, provided a structure is strong enough and is serviceable, the value adopted for each stress limit is largely irrelevant.

Codes of practice also set mandatory limits on the tensile stress in the prestressing steel at various stages of construction. ACI 318–83 specifies that the maximum stress applied to a tendon during the jacking operation is  $0.94f_{py}$  (but not greater than  $0.85f_p$ ). The relationships between  $f_{py}$  and  $f_p$  for the various steel types were given in [Section 2.7](#). ACI 318–83 also requires that the steel stress immediately after transfer does not exceed  $0.82f_{py}$  (but not greater than  $0.74f_p$ ) and, for post-tensioned tendons at anchorages and couplers,  $0.70f_p$ .

### 3.3 Determination of prestress and eccentricity in flexural members

There are a number of possible starting points for the determination of the prestressing force  $P$  and eccentricity  $e$  required at a particular cross-section. The starting point depends on the particular serviceability requirements for the member. The quantities  $P$  and  $e$  are often determined to satisfy pre-selected stress limits. Cracking may or may not be permitted under service loads. As was mentioned in the previous section, satisfaction of concrete stress limits does not necessarily ensure that deflection, camber, and axial shortening are within acceptable limits. Separate checks are required for each of these serviceability limit states. Alternatively, the prestressing force and the cable layout may be selected to minimize deflection under some portion of the applied load (i.e. a load-balancing approach to design). With such an approach, cracking may occur when the applied load is substantially different from the selected balanced load, such as at transfer or under the full service loads, and this needs to be checked and accounted for in serviceability calculations.

#### 3.3.1 Satisfaction of stress limits

Numerous design approaches have been proposed for the satisfaction of concrete stress limits, including analytical and graphical techniques (e.g. Magnel 1954, Lin 1963, Warner & Faulkes 1979). A simple and convenient approach is described here.

If the member is required to remain uncracked throughout, suitable stress limits should be selected for the tensile stress at transfer,  $F_{ti}$ , and the tensile stress under full load,  $F_t$ . In addition, limits should also be placed on the concrete compressive stress at transfer,  $F_{ci}$  and under full loads,  $F_c$ . If

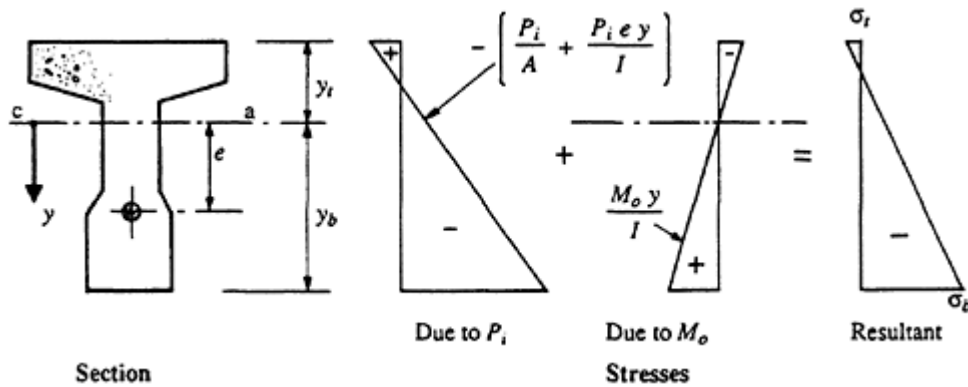


**Figure 3.1** Concrete stresses at transfer.

cracking under the full loads is permitted, the stress limit  $F_t$  is relaxed and the remaining three limits are enforced.

Consider the uncracked cross-section of a beam at the critical moment location, as shown in [Figure 3.1](#). Also shown in [Figure 3.1](#) are the concrete stresses at transfer caused by the prestress  $P_i$  (located at an eccentricity  $e$  below the centroidal axis of the concrete section) and by the external moment  $M_o$  resulting from the loads acting at transfer. Often self-weight is the only load (other than prestress) acting at transfer.

At transfer, the concrete stress in the top fibre must not exceed the tensile stress limit. That is,

$$\sigma_t = -\frac{P_i}{A} + \frac{P_i e y_t}{I} - \frac{M_o y_t}{I} \leq F_{ti} \quad \text{or} \quad -\frac{P_i}{A} + \frac{(P_i e - M_o)}{Z_t} \leq F_{ti}$$

and rearrangement gives

$$F_{ti} \geq -\frac{P_i}{A} \left(1 - \frac{Ae}{Z_t}\right) - \frac{M_o}{Z_t} \quad (3.1)$$

where  $A$  is the area of the section,  $I$  is the second moment of area of the section about the centroidal axis, and  $Z_t$  is the elastic section modulus, with respect to the top fibre ( $=I/y_t$ ).

Similarly, the concrete stress in the bottom fibre must be greater than the negative compressive stress limit at transfer:

$$\sigma_b = -\frac{P_i}{A} - \frac{P_i e}{Z_b} + \frac{M_o}{Z_b} \geq F_{ci}$$

where  $F_{ci}$  is a negative quantity. Rearrangement gives

$$F_{ci} \leq -\frac{P_i}{A} \left(1 + \frac{Ae}{Z_b}\right) + \frac{M_o}{Z_b} \quad (3.2)$$

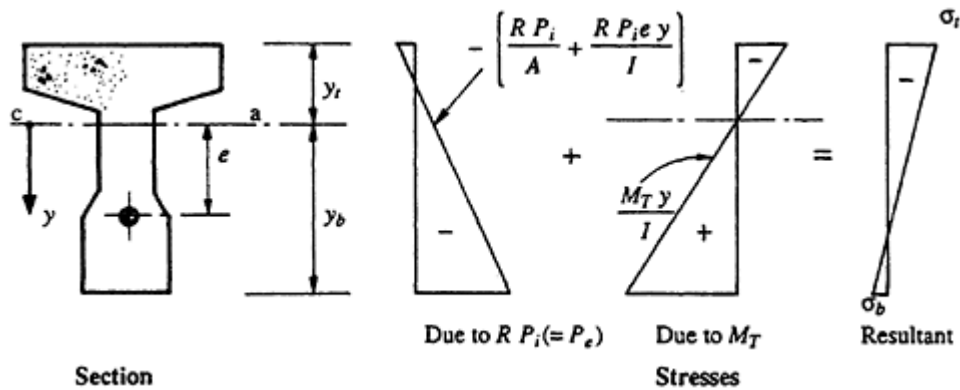


**Figure 3.2** Concrete stresses under full loads (after all prestress losses).

[Figure 3.2](#) shows the concrete stresses caused by the effective prestress after all losses have taken place ( $P_e = RP_i$ ) and by the applied moment  $M_T$  resulting from the full service load.

For a fully prestressed member, the concrete stress in the bottom fibre must be less than the selected tensile stress limit  $F_t$ :

$$\sigma_b = -\frac{RP_i}{A} - \frac{RP_i e}{Z_b} + \frac{M_T}{Z_b} \leq F_t$$

or

$$F_t \geq -\frac{RP_i}{A} \left(1 + \frac{Ae}{Z_b}\right) + \frac{M_T}{Z_b} \quad (3.3)$$

The compressive stress in the top fibre must also satisfy the appropriate stress limit. Therefore,

$$\sigma_t = -\frac{RP_i}{A} + \frac{RP_i e}{Z_t} - \frac{M_T}{Z_t} \geq F_c$$

or

$$F_c \leq -\frac{RP_i}{A} \left(1 - \frac{Ae}{Z_t}\right) - \frac{M_T}{Z_t} \quad (3.4)$$

Equations 3.1–3.4 can be rearranged to express  $1/P_i$  as a linear function of  $e$ . Rearrangement of Equation 3.1 gives

$$A \left( F_{ti} + \frac{M_o}{Z_t} \right) \geq -P_i \left( 1 - \frac{Ae}{Z_t} \right)$$

or

$$\frac{1}{P_i} \geq \frac{-1 + Ae/Z_t}{A(F_{ti} + M_o/Z_t)}$$

and if  $a_t = A/Z_t$ , then

$$\frac{1}{P_i} \geq \frac{\alpha_t e - 1}{AF_{ti} + \alpha_t M_o} \quad (3.5)$$

Similarly, from Equations 3.2, 3.3 and 3.4, the following equations are obtained:

$$\frac{1}{P_i} \geq \frac{\alpha_b e + 1}{-AF_{ci} + \alpha_b M_o} \quad (3.6)$$

$$\frac{1}{P_i} \leq \frac{R(\alpha_b e + 1)}{-AF_t + \alpha_b M_T} \quad (3.7)$$

and

$$\frac{1}{P_i} \leq \frac{R(\alpha_t e - 1)}{AF_c + \alpha_t M_T} \quad (3.8)$$

where  $\alpha_b = A/Z_b$  and  $F_{ci}$  in Equation 3.6 and  $F_c$  in Equation 3.8 are negative numbers.

Each of the linear relationships in Equations 3.5–3.8 may be plotted on a graph of  $1/P_i$  versus  $e$ , as shown in [Figure 3.3](#). The intercept of each straight line on the horizontal axis is obtained by setting  $1/P_i$  equal to zero in each equation. When  $1/P_i = 0$ , the eccentricity  $e$  equals  $1/\alpha_t$  for Equations 3.5 and 3.8 and  $-1/\alpha_b$  for Equations 3.6 and 3.7. A graphical interpretation of the stress conditions on a prestressed section similar to that shown in [Figure 3.3](#) was first proposed by Magnel (1954) and may be a useful aid in design.

On one side of each straight line in [Figure 3.3](#), the relevant stress limit is satisfied. The wedge-shaped area in which all four stress limits are satisfied represents suitable combinations of  $P_i$  and  $e$ . In order to minimize prestressing costs, the smallest possible value for  $P_i$  would generally be selected. This corresponds to the value at the intersection of Equations 3.5 and 3.7. However, the corresponding value of  $e$  may not be practical. The maximum eccentricity  $e_{max}$  is governed by concrete cover and tendon spacing requirements. As is seen in [Figure 3.3](#), the smallest possible value for  $P_i$  is obtained by substituting the appropriate maximum eccentricity into Equation 3.7.

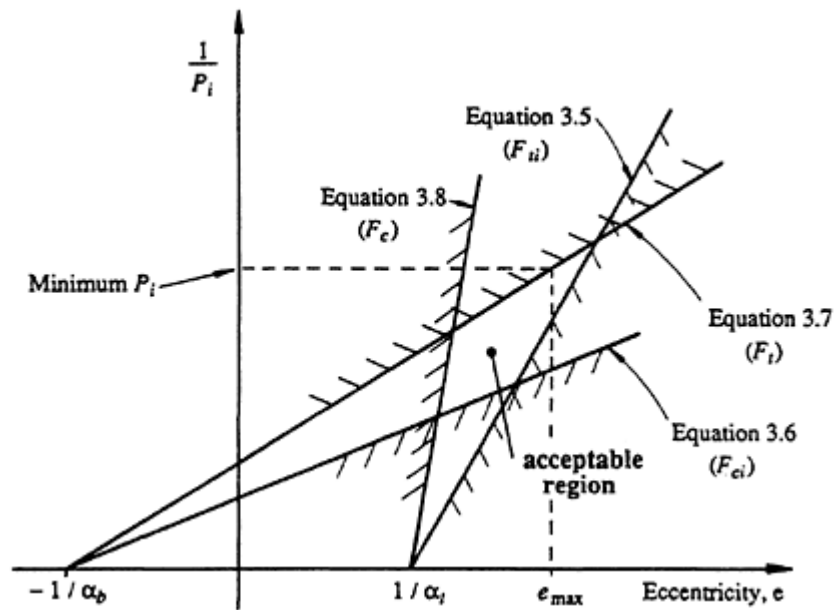


Figure 3.3 Magnel's design diagram.

If a particular cross-section is too small, the plot of Equation 3.6 in Figure 3.3 will lie above the plot of Equation 3.7 and no acceptable region exists. Similarly, if the line representing Equation 3.5 is steeper than that of Equation 3.8, no acceptable region exists. It is therefore not possible to satisfy all four stress limits and a larger section is clearly required. If, on the other hand, the angle between the plots of Equations 3.6 and 3.7 in Figure 3.3 is large, a large acceptable region exists and a smaller section may prove more economical.

When the minimum-sized cross-section is used, Equations 3.6 and 3.7 plot on the same line. By equating Equations 3.2 and 3.3, the section modulus of this minimum-sized section  $(Z_b)_{min}$  can be readily found. If the minimum-sized section is used, Equation 3.2 becomes

$$F_{ci} - \frac{M_o}{(Z_b)_{min}} = -\frac{P_i}{A_{min}} \left( 1 + \frac{A_{min}e}{(Z_b)_{min}} \right)$$

Similarly, from Equation 3.3,

$$\frac{1}{R} \left[ F_t - \frac{M_T}{(Z_b)_{min}} \right] = -\frac{P_i}{A_{min}} \left[ 1 + \frac{A_{min}e}{(Z_b)_{min}} \right]$$

By subtracting these two equations, an expression for the minimum permissible section modulus is obtained:

$$(Z_b)_{min} = \frac{M_T - RM_o}{F_t - RF_{ci}} \quad (3.9)$$

It must be remembered that  $F_{ci}$  is always negative. Equation 3.9 is a useful starting point in the selection of an initial cross-section.

In order to use Equation 3.9 and to be able to plot Equation 3.7 on [Figure 3.3](#), some estimate of the time-dependent losses must be made so that the loss parameter  $R$  can be determined. As  $R$  is varied, the angle between the plots of Equations 3.6 and 3.7 varies and hence the range of acceptable combinations of  $P_i$  and  $e$  also varies. Usually, a first estimate of  $R$  within the range 0.75–0.85 is adopted when low-relaxation steel is used. The lower end of this range (i.e.  $R \approx 0.75$ ) is more appropriate for a heavily stressed girder with high sustained compressive stresses in the concrete at the tendon level. In such a member, creep losses will be relatively high. For lightly stressed members, such as slabs, and for members in which the sustained compressive stress in the concrete at the tendon level is low, the upper end of the range is more appropriate (i.e.  $R \approx 0.85$ ). Any initial estimate of  $R$  must be checked after the prestress, the eccentricity, and the quantity of bonded reinforcement have been determined. Suitable procedures for determining the time-dependent losses are described in Sections [3.6](#) and [3.7](#).

For a limited amount of well controlled cracking, ACI 318–83 allows the tensile stress limit  $F_t$  to be set as high as  $1.0\sqrt{f'_c}$  provided bonded reinforcement is placed near the tensile face. In general, however, if cracking is permitted under full service loads, a tensile stress limit  $F_t$  is not specified and Equation 3.7 does not apply. Tensile and compressive stress limits at transfer are usually enforced and, therefore, Equations 3.5 and 3.6 are still applicable and continue to provide an upper limit on the level of prestress. The only minimum limit on the level of prestress is that imposed by Equation 3.8 and, for more practical cross-sections, this does not influence the design. When there is no need to satisfy a tensile stress limit under full loads, the plot of Equation 3.7 no longer appears on [Figure 3.3](#). Any level of prestress which satisfies Equations 3.5, 3.6, and 3.8 may be used, including  $P_i=0$  (which corresponds to a reinforced concrete member). In such a situation, [Figure 3.3](#) is no longer of much use in design.

Often partially prestressed members are designed such that cracking does not occur under the sustained or permanent service loads. It is the variable live load that causes cracking. Cracks therefore open and close as the variable load is applied and removed. The selection of prestress in such a case can still be made conveniently using a figure similar to [Figure 3.3](#). If the maximum total service moment  $M_T$  is replaced in Equation 3.7 by the sustained or permanent moment  $M_{sus}$ , Equation 3.7 becomes

$$\frac{1}{P_i} \leq \frac{R(\alpha_b e + 1)}{-AF_t + \alpha_b M_{sus}} \quad (3.10)$$

The plot of Equation 3.10 now replaces the plot of Equation 3.7 in [Figure 3.3](#). The line representing Equation 3.10 crosses the horizontal axis at the



same point (i.e.  $e = -1/\alpha_b$ ), but is steeper and therefore the acceptable region shown in [Figure 3.3](#) is larger. For a given eccentricity, the minimum prestress  $P_i$  is less. The tensile stress limit  $F_t$  will not be exceeded under the sustained loads, but cracking may occur under peak live loads. If after the variable load has been removed the cracks are required to close completely,  $F_t$  in Equation 3.10 should be set to zero.

If less prestress is used and cracking occurs, the cross-section required for a partially prestressed member may need to be larger than that required for a fully prestressed member for a particular deflection limit. In addition, the quantity of non-prestressed reinforcement is usually significantly greater. Often, however, the reduction in prestressing costs more than compensates for the additional concrete and non-prestressed reinforcement costs and partially prestressed members are the most economical structural solution in a wide range of applications.

### Example 3.1

A one-way slab is simply supported over a span of 12 m and is to be designed to carry a service load of 7 kPa ( $\text{kN/m}^2$ ) in addition to its own self-weight. The slab is post-tensioned by regularly spaced tendons with parabolic profiles. The material properties are:

$$f'_{ci} = 25 \text{ MPa}; f'_c = 32 \text{ MPa}; E_{ci} = 25300 \text{ MPa}; E_c = 28600 \text{ MPa}; \\ \text{and } f_p = 1840 \text{ MPa}.$$

The prestressing force and eccentricity are to be determined to satisfy the following concrete stress limits:

$$F_{ti} = 0.25\sqrt{25} = 1.25 \text{ MPa} \\ F_{ci} = -0.5 \times 25 = -12.5 \text{ MPa} \\ F_t = 0.25\sqrt{32} = 1.41 \text{ MPa} \\ F_c = -0.5 \times 32 = -16.0 \text{ MPa}$$

At mid-span, the instantaneous and time-dependent losses are taken to be 8% and 16%, respectively. In order to obtain an estimate of the slab self-weight (which is the only load other than the prestress at transfer), a trial slab thickness of 300 mm (span/40) is assumed initially. For a 1 m wide strip of slab, the self-weight is

$$w_{sw} = 24 \times 0.3 = 7.2 \text{ kN/m}$$

and the moments at mid-span both at transfer and under the full service load are

$$M_o = \frac{7.2 \times 12^2}{8} = 129.6 \text{ kNm/m} \quad \text{and}$$

$$M_T = \frac{(7.0 + 7.2) \times 12^2}{8} = 255.6 \text{ kN m/m}$$

From Equation 3.9,

$$(Z_b)_{min} = \frac{[255.6 - (0.84 \times 129.6)] \times 10^6}{1.41 - (0.84 \times -12.5)} = 12.3 \times 10^6 \text{ mm}^3/\text{m}$$

and the corresponding minimum slab depth is therefore

$$D_{min} = \sqrt{6(Z_b)_{min}/1000} = 272 \text{ mm}$$

Select a slab thickness  $D=300$  mm. The relevant section properties are:

$$A = 300 \times 10^3 \text{ mm}^2/\text{m}; \quad I = 2250 \times 10^6 \text{ mm}^4/\text{m};$$

$$Z = Z_t = Z_b = 15 \times 10^6 \text{ mm}^3/\text{m};$$

$$\alpha_t = \alpha_b = A/Z = 0.02; \quad \text{and } 1/\alpha_t = 1/\alpha_b = 50 \text{ mm.}$$

Equation 3.5 becomes

$$\frac{1}{P_i} \geq \frac{0.02e - 1}{(300 \times 10^3 \times 1.25) + (0.02 \times 129.6 \times 10^6)} = \frac{0.02e - 1}{2967 \times 10^3}$$

Similarly, the following expressions are obtained from Equations 3.6, 3.7 and 3.8, respectively:

$$\frac{1}{P_i} \geq \frac{0.02e + 1}{(-300 \times 10^3 \times -12.5) + (0.02 \times 129.6 \times 10^6)} = \frac{0.02e + 1}{6342 \times 10^3}$$

$$\frac{1}{P_i} \leq \frac{0.84(0.02e + 1)}{(-300 \times 10^3 \times 1.41) + (0.02 \times 255.6 \times 10^6)} = \frac{0.02e + 1}{5582 \times 10^3}$$

and

$$\frac{1}{P_i} \leq \frac{0.84(0.02e - 1)}{(300 \times 10^3 \times -16.0) + (0.02 \times 255.6 \times 10^6)} = \frac{0.02e - 1}{371.4 \times 10^3}$$

Each of these four equations is plotted on [Figure 3.4](#).

If 12.7 mm diameter strand is used with 30 mm minimum concrete cover, then

$$e_{max} \approx 150 - 36 = 114 \text{ mm}$$

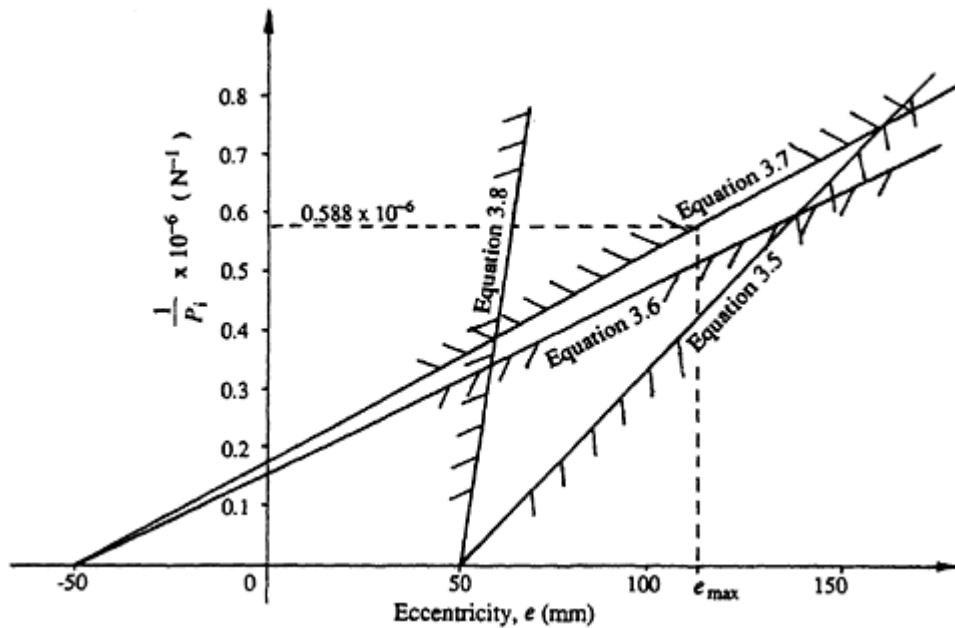


Figure 3.4 Design diagram for [Example 3.1](#).

and, from [Figure 3.4](#) (or Equation 3.7), the corresponding minimum permissible value of  $P_i$  is found to be

$$\frac{1}{P_i} = 0.588 \times 10^{-6} \quad \text{and} \quad \therefore P_i = 1700 \text{ kN/m}$$

At the jacking point, the required prestressing force is

$$P_j = \frac{1700}{0.92} = 1850 \text{ kN/m} \quad (8\% \text{ instantaneous losses})$$

From [Table 2.1](#), a 12.7 mm diameter 7-wire, low-relaxation strand has a cross-sectional area of  $100 \text{ mm}^2$  and a minimum breaking load of 184 kN. A flat duct containing four 12.7 mm strands can therefore be stressed with a maximum jacking force of

$$0.85 \times 4 \times 184 = 626 \text{ kN}$$

The minimum number of cables required in each metre width of slab is therefore

$$\frac{1850}{626} = 2.96$$

and the maximum spacing between cables is

$$\frac{1000}{2.96} = 338 \text{ mm}$$

Use 1–4 strand tendon every 330 mm.

To check deflection, the properties of the gross section can be used in all calculations, since cracking has been avoided both at transfer and under the full service loads. It is assumed that of the 7 kPa service load, 3 kPa is sustained or permanent and 4 kPa is temporary.

*At transfer:*

$$E_{ci} = 25300 \text{ MPa} \quad \text{and} \quad I = 2250 \times 10^6 \text{ mm}^4/\text{m}$$

The uniformly distributed upward load caused by the parabolic cables with drapes equal to 114 mm is obtained from Equation 1.7 as

$$w_p = \frac{1700 \times 0.114 \times 8}{12^2} = 10.8 \text{ kN/m} \uparrow$$

The resultant upward load is  $w_p - w_{sw} = 10.8 - 7.2 = 3.6 \text{ kN/m} \uparrow$  and the deflection (camber) at transfer is

$$v_i = \frac{5}{384} \times \frac{3.6 \times 12000^4}{25300 \times 2250 \times 10^6} = 17.0 \text{ mm} \uparrow \text{ (span/700)}$$

*Under full loads:*

$$E_c = 28600 \text{ MPa}$$

After the time-dependent losses, the prestressing force has decreased by 16% and therefore

$$w_p = 0.84 \times 10.8 = 9.1 \text{ kN/m} \uparrow$$

The sustained external load is  $(7.2 + 3.0) = 10.2 \text{ kN/m} \downarrow$  and the short-term deflection due to the permanent loads is

$$v_{sus} = \frac{5}{384} \times \frac{(10.2 - 9.1) \times 12000^4}{28600 \times 2250 \times 10^6} = 4.8 \text{ mm} \downarrow$$

For this uncracked slab, the long-term deflection caused by creep and

shrinkage is likely to be at least three times the short-term deflection due to all the sustained loads. Therefore,

$$v_{LT} \approx 3 \times \Delta_{sus} = 14.4 \text{ mm} \downarrow$$

A far more accurate and reliable estimate of the effects of creep and shrinkage is outlined in [Section 3.6](#).

The instantaneous deflection caused by the variable portion of the service load,  $w_v=4.0$  kN/m, is

$$v_v = \frac{5}{384} \times \frac{4.0 \times 12000^4}{28600 \times 2250 \times 10^6} = 16.8 \text{ mm} \downarrow$$

and the maximum total deflection is therefore

$$v_{tot} = v_{sus} + v_{LT} + v_v = 36.0 \text{ mm} \downarrow (\text{span}/333)$$

This may or may not be acceptable depending on the deflection requirements for this particular structure.

To complete this design, strength checks must be made, losses must be checked, and the anchorage zones must be designed.

### 3.3.2 Load-balancing

Using the load-balancing approach, the effective prestress after losses  $P_e$  and the eccentricity  $e$  are selected such that the transverse load imposed by the prestress  $w_p$  balances a selected portion of the external load. The effective prestress  $P_e$  in a parabolic cable of drupe  $e$  required to balance a uniformly distributed external load  $w_b$  is obtained from Equation 1.7. That is,

$$P_e = \frac{w_b L^2}{8e} \quad (3.11)$$

Concrete stresses are checked under the remaining unbalanced service loads to identify regions of possible cracking and regions of high compression. Deflection under the unbalanced loads may need to be calculated and controlled. Losses are calculated and stresses immediately after transfer are also checked. Having determined the amount and layout of the prestressing steel (and the prestressing force) to satisfy serviceability requirements, the design for adequate strength can then proceed.

Load balancing is widely used for the design of indeterminate members and also for simple determinate beams and slabs. It is only strictly applicable, however, prior to cracking when the member behaves linearly and the principle of superposition, on which load balancing relies, is valid.

### Example 3.2

For the 300 mm thick, 12 m span one-way slab of [Example 3.1](#), the prestress required to balance the slab self-weight (7.2 kPa) is to be determined. The parabolic tendons have zero eccentricity at each support and  $e=114$  mm at mid-span.

With  $w_b=7.2$  kPa and  $e=0.114$  m, Equation 3.11 gives

$$P_e = \frac{7.2 \times 12^2}{8 \times 0.114} = 1140 \text{ kN/m}$$

If at mid-span the time-dependent losses are 16% and the instantaneous losses are 8% (as was stated in [Example 3.1](#)),

$$P_i = \frac{1140}{0.84} = 1350 \text{ kN/m} \quad \text{and} \quad P_j = \frac{1350}{0.92} = 1470 \text{ kN/m}$$

which corresponds to 1–4 strand flat ducted cable every 425 mm.

In [Example 3.1](#), the tensile stress limit under full loads was  $F_t=1.41$  MPa. In this example, the prestress is lower and  $F_t$  will therefore be exceeded. The bottom fibre elastic stress at mid-span after all losses and under the full service loads is

$$\sigma_b = -\frac{1140 \times 10^3}{300 \times 10^3} - \frac{1140 \times 10^3 \times 114}{15 \times 10^6} + \frac{255.6 \times 10^6}{15 \times 10^6} = 4.61 \text{ MPa}$$

which would almost certainly cause cracking. The resulting loss of stiffness must be included in subsequent deflection calculations using the procedures outlined in Sections [3.5](#) and [3.6](#). In addition, the smaller quantity of prestressing steel required in this example, in comparison with the slab in [Example 3.1](#), results in reduced flexural strength. A layer of non-prestressed bottom reinforcement may be required to satisfy strength requirements.

## 3.4 Cable profiles

When the prestressing force and eccentricity are determined for the critical sections, the location of the cable at every section along the member must be specified. For a member which has been designed to be uncracked throughout, the tendons must be located so that the stress limits are observed on every section. At any section, Equations 3.1–3.4 may be used to establish a range of values for eccentricity which satisfy the selected stress limits.

If  $M_o$  and  $M_T$  are the moments caused by the external loads at transfer and under full service loads, respectively, and  $P_i$  and  $P_e$  are the corresponding prestressing forces at the same section, the extreme fibre stresses must

satisfy the following:

$$-\frac{P_i}{A} + \frac{(P_i e - M_o)}{Z_t} \leq F_{ti} \quad (3.12)$$

$$-\frac{P_i}{A} - \frac{(P_i e - M_o)}{Z_b} \geq F_{ci} \quad (3.13)$$

$$-\frac{P_e}{A} - \frac{(P_e e - M_T)}{Z_b} \leq F_t \quad (3.14)$$

$$-\frac{P_e}{A} + \frac{(P_e e - M_T)}{Z_t} \geq F_c \quad (3.15)$$

Equations 3.12–3.15 can be rearranged to provide limits on the tendon eccentricity, as follows:

$$P_i e \leq M_o + Z_t \left( F_{ti} + \frac{P_i}{A} \right) \quad (3.16)$$

$$P_i e \leq M_o - Z_b \left( F_{ci} + \frac{P_i}{A} \right) \quad (3.17)$$

$$P_e e \geq M_T - Z_b \left( F_t + \frac{P_e}{A} \right) \quad (3.18)$$

$$P_e e \geq M_T + Z_t \left( F_c + \frac{P_e}{A} \right) \quad (3.19)$$

It should be remembered that  $F_{ci}$  and  $F_c$  are negative numbers.

After  $P_i$  and  $P_e$  have been determined at the critical sections, the friction losses along the member are estimated (see [Section 3.7.3](#)) and the corresponding prestressing forces at intermediate sections are calculated. At each intermediate section, the maximum eccentricity that will satisfy both stress limits at transfer is obtained from either Equation 3.16 or 3.17. The minimum eccentricity required to satisfy the tensile and compressive stress limits under full loads is obtained from either Equation 3.18 or 3.19. A permissible zone is thus established in which the line of action of the resulting prestressing force must be located. Such a permissible zone is shown in [Figure 3.5](#). Relatively few intermediate sections need to be considered to determine an acceptable cable profile.

When the prestress and eccentricity at the critical sections are selected using the load-balancing approach, the cable profile should match, as

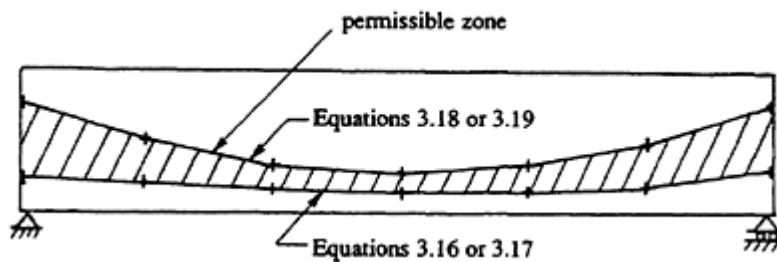


**Figure 3.5** Typical permissible zone for location of cable profile.

closely as practicable, the bending moment diagram caused by the balanced load. In this way, deflection will be minimized. For cracked, partially prestressed members, Equations 3.16 and 3.17 are usually applicable and fix the maximum eccentricity. The cable profile should then be selected according to the loading type and moment diagram.

### 3.5 Short-term analysis of cross-sections

#### 3.5.1 Uncracked cross-sections

The short-term behaviour of a prestressed concrete cross-section can be determined by transforming the bonded reinforcement into equivalent areas of concrete and performing a simple, elastic analysis on the equivalent concrete section. The following mathematical formulation of the short-term analysis of an uncracked cross-section forms the basis of the time-dependent analysis described in [Section 3.6](#) and was described by Gilbert (1988).

Consider a prestressed concrete cross-section with a vertical axis of symmetry. For a section containing both non-prestressed and prestressed reinforcement, the transformed section may be similar to that shown in [Figure 3.6](#). The top surface of the cross-section, rather than the centroidal axis, is selected here as the reference surface. This is a convenient selection, but not a necessary one. The position of the centroidal axis of a prestressed concrete cross-section varies with time owing to the gradual development of creep and shrinkage in the concrete. The centroidal axis also depends on the quantity of bonded reinforcement and may change position when unbonded tendons are subsequently grouted. It is convenient, therefore, to select a fixed reference point that can be used in all stages of the analysis and, for this reason, reference to any point on the cross-section in [Figure 3.6](#) is made in terms of its distance  $y$  from the top surface.

In [Figure 3.6](#), the non-prestressed reinforcement is transformed into equivalent areas of concrete ( $=A_s E_s / E_c = n A_s$ ), i.e. an *additional* area of concrete equal to  $(n-1)A_s$  is added to the section at each bonded steel



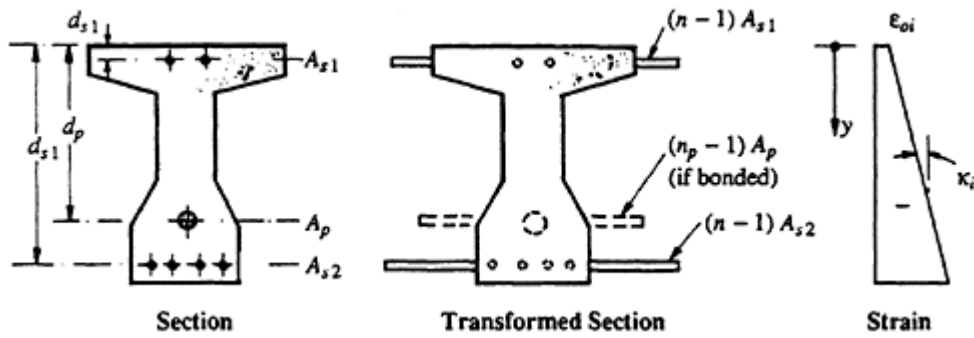


Figure 3.6 Transformed section at transfer.

level, as shown;  $n$  is the short-term *modular ratio* ( $E_s/E_c$ ). If the prestressed steel in [Figure 3.6](#) is bonded to the concrete at transfer, it too should be transformed into an equivalent area of concrete. Also shown in [Figure 3.6](#) is the strain distribution on the section immediately after transfer. The strain at a depth  $y$  below the top of the cross-section is defined in terms of the top fibre strain  $\epsilon_{oi}$  and the initial curvature  $\kappa_i$ , as follows:

$$\epsilon_i = \epsilon_{oi} + y\kappa_i \quad (3.20)$$

If the short-term behaviour of concrete is assumed to be linear-elastic, the initial concrete stress at  $y$  below the top fibre is

$$\sigma_i = E_c \epsilon_i = E_c (\epsilon_{oi} + y\kappa_i) \quad (3.21)$$

The resultant axial force on the section  $N_i$  is obtained by integrating the stress block over the depth of the section, as shown in Equation 3.22. For a prestressed section in pure bending, the initial axial force on the transformed concrete section immediately after transfer is compressive and equal in magnitude to the prestressing force, i.e.  $N_i = -P_i$ .

$$\begin{aligned} N_i &= \int \sigma_i \, dA \\ &= E_c \epsilon_{oi} \int dA + E_c \kappa_i \int y \, dA \\ &= E_c \epsilon_{oi} A + E_c \kappa_i B \end{aligned} \quad (3.22)$$

where  $A$  ( $= \int dA$ ) is the area of the transformed section and  $B$  ( $= \int y \, dA$ ) is the first moment of the transformed area about the top surface of the section.

If the first moment of the stress block about the top fibre is integrated

over the depth of the section, as shown in Equation 3.23, the resultant moment about the top surface,  $M_i$ , is found. For a prestressed concrete beam section,  $M_i = M_o - P_i d_p$ , where  $M_o$  is the external moment at the section at transfer and  $d_p$  is the depth to the prestressing steel as shown in [Figure 3.6](#). Therefore,

$$\begin{aligned} M_i &= \int \sigma_i y \, dA \\ &= E_c \epsilon_{oi} \int y \, dA + E_c \kappa_i \int y^2 \, dA \\ &= E_c \epsilon_{oi} B + E_c \kappa_i \bar{I} \end{aligned} \quad (3.23)$$

where  $\bar{I} (= \int y^2 \, dA)$  is the second moment of the transformed area *about the top surface* of the transformed section.

By rearranging Equations 3.22 and 3.23, expressions are obtained for the initial top fibre strain and curvature in terms of  $N_i$  and  $M_i$ :

$$\epsilon_{oi} = \frac{BM_i - \bar{I}N_i}{E_c(B^2 - A\bar{I})} \quad (3.24)$$

and

$$\kappa_i = \frac{BN_i - AM_i}{E_c(B^2 - A\bar{I})} \quad (3.25)$$

For any combination of external load and prestress, the corresponding values of  $N_i$  and  $M_i$  are readily calculated and may be substituted into Equations 3.24 and 3.25 to obtain the strain distribution immediately after transfer. Equations 3.24 and 3.25 may also be used to obtain the increment of elastic strain due to the application of any subsequent load increment.

### Example 3.3

The short-term behaviour of the post-tensioned cross-section shown in [Figure 3.7a](#) is to be determined immediately after transfer. The section contains a single unbonded cable containing 10–12.7 mm diameter strands ( $A_p = 1000 \text{ mm}^2$ ) located within a 60 mm diameter duct, and two layers of non-prestressed reinforcement, as shown. The force in the prestressing steel is  $P_i = 1350 \text{ kN}$  and the applied moment is  $M_o = 100 \text{ kNm}$ . The elastic moduli for concrete and steel are  $E_c = 30 \times 10^3 \text{ MPa}$  and  $E_s = E_p = 200 \times 10^3 \text{ MPa}$ , and therefore  $n = 6.67$ .

The transformed section is shown in [Figure 3.7b](#). Because the prestressing steel is not bonded to the concrete, it does not form part of the transformed

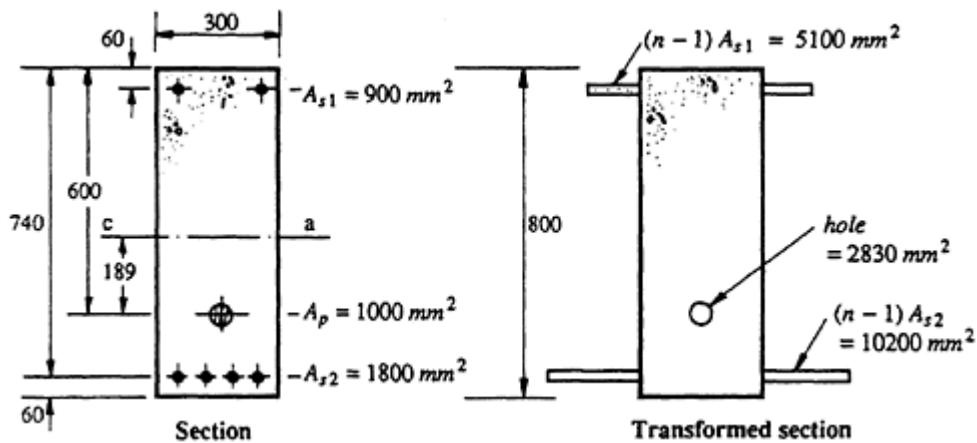


Figure 3.7 Post-tensioned cross-section of [Example 3.3](#).

section. In addition, the hole created on the concrete section by the hollow duct must also be taken into account. The properties of the transformed section with respect to the top reference surface are

$$A = (300 \times 800) + 5100 + 10200 - 2830 = 252.5 \times 10^3 \text{ mm}^2$$

$$B = (300 \times 800 \times 400) + (5100 \times 60) + (10200 \times 740) - (2830 \times 600) \\ = 102.2 \times 10^6 \text{ mm}^3$$

$$\bar{I} = \frac{300 \times 800^3}{3} + (5100 \times 60^2) + (10200 \times 740^2) - (2830 \times 600^2) \\ = 55.79 \times 10^9 \text{ mm}^4$$

The axial force and moment about the top surface at transfer are

$$N_i = -P_i = -1350 \text{ kN} \quad \text{and} \quad M_i = M_o - P_i d_p = -710 \text{ kNm}$$

The top fibre strain and curvature immediately after transfer are obtained from Equations 3.24 and 3.25:

$$\epsilon_{oi} = \frac{-(102.2 \times 10^6 \times 710 \times 10^6) + (55.79 \times 10^9 \times 1350 \times 10^3)}{30 \times 10^3 [(102.2 \times 10^6)^2 - (252.5 \times 10^3 \times 55.79 \times 10^9)]} \\ = -25.4 \times 10^{-6}$$

$$\chi_i = \frac{-(102.2 \times 10^6 \times 1350 \times 10^3) + (252.5 \times 10^3 \times 710 \times 10^6)}{30 \times 10^3 [(102.2 \times 10^6)^2 - (252.5 \times 10^3 \times 55.79 \times 10^9)]} \\ = -0.378 \times 10^{-6} \text{ mm}^{-1}$$

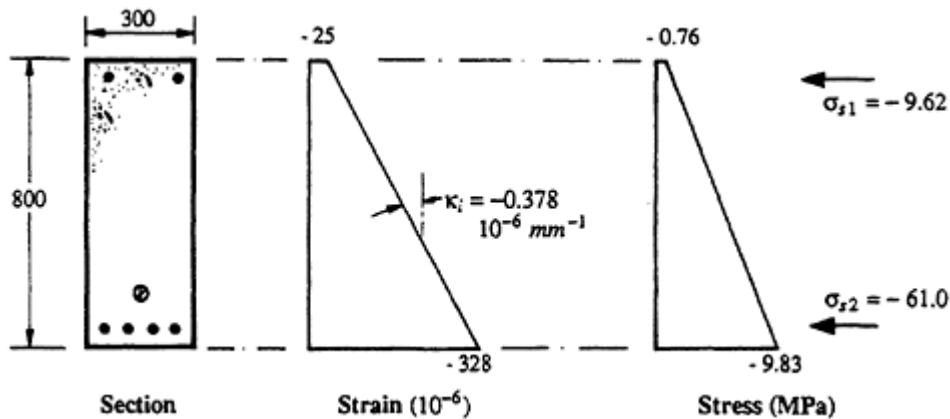


**Figure 3.8** Strains and stresses immediately after transfer ([Example 3.3](#)).

The concrete stresses are found using Equation 3.21. When  $y=0$ , the top fibre stress is  $\sigma_{oi}=-0.76\text{MPa}$ , and when  $y=800\text{ mm}$ , the bottom fibre stress is  $\sigma_{bi}=-9.83\text{ MPa}$ . The stress in the steel reinforcement is determined from the strain at the level of the steel. For the top layer of non-prestressed reinforcement (at  $y=60\text{ mm}$ ),

$$\sigma_{s1i} = E_s(\epsilon_{oi} + 60\kappa_i) = -9.62\text{ MPa}$$

and for the bottom steel (at  $y=740\text{ mm}$ ),

$$\sigma_{s2i} = E_s(\epsilon_{oi} + 740\kappa_i) = -61.0\text{ MPa}.$$

The distributions of strain and stress on the cross-section immediately after transfer are shown in [Figure 3.8](#).

### 3.5.2 Cracked cross-sections

When the tensile stress produced by the external moment at a particular section overcomes the compression caused by prestress, and the extreme fibre stress reaches the tensile strength of concrete, cracking occurs. The moment at which cracking first occurs is called the *cracking moment*,  $M_{cr}$ . As the compressive force on the concrete gradually decreases with time due to creep and shrinkage, the cracking moment also decreases with time. If the applied moment at any time is greater than the cracking moment, cracking will occur and, at each crack, the concrete below the neutral axis is ineffective. The short-term behaviour of the cracked cross-section may be calculated approximately using a simple elastic analysis which is based on the following assumptions:

- (a) Plane sections remain plane and therefore the strain distribution is linear over the depth of the section.

- (b) Perfect bond exists between the concrete and both the prestressed and non-prestressed steel. At service loads, this is a reasonable assumption.
- (c) Instantaneous material behaviour is linear-elastic. This includes the concrete in compression, the conventional reinforcement and the prestressing steel. Once again, this is a reasonable assumption at service loads.
- (d) Short-term behaviour only is required, i.e. the analysis does not include the inelastic effects of creep and shrinkage.
- (e) Tensile stresses in the concrete are ignored. This is a conservative assumption. An empirical adjustment to the second moment of area of the cracked section may be made to account for the contribution of the tensile concrete to the stiffness of the cross-section. This is the so-called *tension stiffening effect*.

The instantaneous strains and stresses on a cracked section are shown in [Figure 3.9](#). For an applied moment  $M$  greater than the cracking moment, there are two unknowns associated with the strain diagram in [Figure 3.9b](#): the depth to the neutral axis  $d_n$  and the extreme fibre instantaneous compressive strain  $\epsilon_{oi}$ . When  $\epsilon_{oi}$  and  $d_n$  are known, the strain diagram is defined and the concrete and steel stresses are readily determined. To find these two unknowns, there are two equations of equilibrium. Horizontal equilibrium dictates that

$$T_p + T_s + C + C_s = 0 \tag{3.26}$$

and moment equilibrium requires that

$$M = T_p d_p + T_s d_{s2} + C d_z + C_s d_{s1} \tag{3.27}$$

where  $C$ ,  $C_s$ ,  $T_p$ , and  $T_s$  may all be expressed as functions of  $d_n$  and  $\epsilon_{oi}$ .

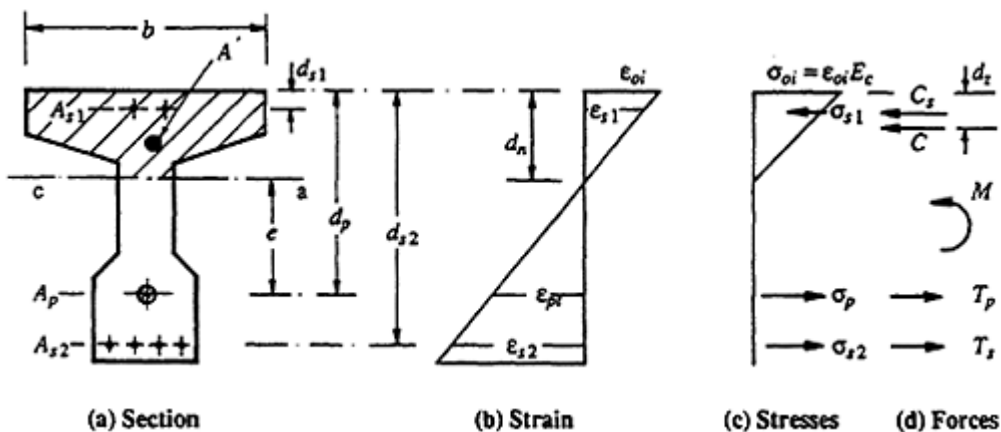


**Figure 3.9** Cracked section analysis.

$C$  is the volume of the triangular compressive stress block acting over the area  $A'$  above the neutral axis. If  $A'$  is rectangular ( $b$  wide and  $d_n$  deep), then

$$C = \frac{1}{2} \sigma_{oi} b d_n = \frac{1}{2} E_c \epsilon_{oi} b d_n \quad (3.28)$$

From similar triangles, the strains at the levels of the non-prestressed steel are

$$\epsilon_{s2} = \frac{-\epsilon_{oi}(d_{s2} - d_n)}{d_n} \quad \text{and} \quad \epsilon_{s1} = \frac{\epsilon_{oi}(d_n - d_{s1})}{d_n}$$

and therefore the forces in the conventional reinforcement are

$$T_s = \sigma_{s2} A_{s2} = \epsilon_{s2} E_s A_{s2} = E_s A_{s2} \frac{-\epsilon_{oi}(d_{s2} - d_n)}{d_n} \quad (3.29)$$

$$C_s = \sigma_{s1} A_{s1} = \epsilon_{s1} E_s A_{s1} = E_s A_{s1} \frac{-\epsilon_{oi}(d_n - d_{s1})}{d_n} \quad (3.30)$$

The strain in the bonded prestressing steel is equal to the sum of three strain components. The first component is the tensile strain caused by the effective prestress,  $\epsilon_{pe}$  i.e. the strain that exists in the steel prior to the application of any external moment:

$$\epsilon_{pe} = \frac{P_e}{A_p E_p} \quad (3.31)$$

Before the external moment is applied, the instantaneous compressive strain in the concrete at the level of the prestressing steel is

$$\epsilon_{ce} = \frac{1}{E_c} \left( -\frac{P_e}{A} - \frac{P_e e^2}{I} \right) \quad (3.32)$$

As the external moment increases, the strain in the concrete at the steel level increases from compressive ( $\epsilon_{ce}$ ) to tensile ( $\epsilon_{pt}$ ). If perfect bond exists between the tendon and the concrete, the prestressing steel strain increases by this same amount, i.e.  $|\epsilon_{ce}| + \epsilon_{pt}$ . From similar triangles,

$$\epsilon_{pt} = \frac{-\epsilon_{oi}(d_p - d_n)}{d_n} \quad (3.33)$$

The total strain in the prestressed steel is therefore given by

$$\epsilon_p = \epsilon_{pe} + |\epsilon_{ce}| + \epsilon_{pt} \quad (3.34)$$

and the force in the prestressing steel is

$$T_p = E_p A_p \left( \epsilon_{pe} + |\epsilon_{ce}| + \frac{-\epsilon_{oi}(d_p - d_n)}{d_n} \right) \quad (3.35)$$

By substituting Equations 3.28, 3.29, 3.30, and 3.35 into Equations 3.26 and 3.27 and solving the simultaneous equations,  $\epsilon_{oi}$  and  $d_n$  are found. For manual solution, the following trial and error procedure may be used:

- (a) Select a reasonable value for  $\epsilon_{oi}$  (say  $-0.5f'_c/E_c$ ). This will correspond to one particular value of applied moment.
- (b) Select a value for  $d_n$ .
- (c) Calculate strains, stresses, and forces in the steel and concrete.
- (d) Check horizontal equilibrium. Is Equation 3.26 satisfied?
  - If yes:  $d_n$  is correct.
  - If no: adjust  $d_n$  and go to (c).
- (e) When the correct value of  $d_n$  has been determined, calculate the moment corresponding to the initial selection of  $\epsilon_{oi}$ , using Equation 3.27.

The above procedure may be repeated for several values of  $\epsilon_{oi}$  to determine the change in elastic behaviour as a function of moment. Behaviour at intermediate values of  $M$  may be determined by interpolation.

From such an analysis, variations in steel stresses after cracking can be found in order to check for crack control. Estimates of the section stiffness can also be made for use in deflection calculations. It is noted that after cracking the neutral axis gradually rises as the applied moment increases. With the area of concrete above the crack becoming smaller, the second moment of area of the cracked section decreases as the applied moment increases. This is not the case for reinforced concrete sections where  $d_n$  remains approximately constant with increasing moment and the cracked moment of inertia of the section is constant in the post-cracking range.

In [Figure 3.10](#), a typical moment-curvature diagram for a prestressed concrete section is shown. At any moment  $M > M_{cr}$ , the curvature is

$$\kappa_i = -\frac{\epsilon_{oi}}{d_n} = \frac{M - P_e e}{E_c I_{av}} \quad (3.36)$$

where  $E_c I_{av}$  is the secant stiffness and  $e$  is the depth of the prestressing steel below the centroidal axis of the cross-section. From Equation 3.36,

$$E_c I_{av} = \frac{(M - P_e e)d_n}{-\epsilon_{oi}} \quad (3.37)$$

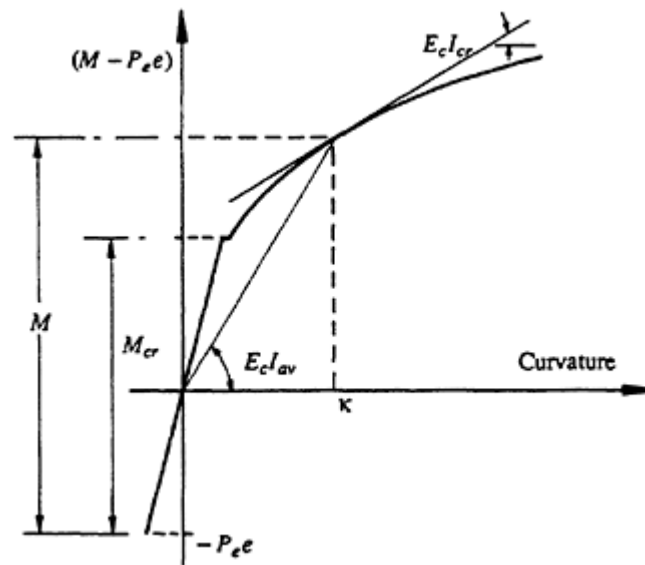


**Figure 3.10** Typical moment-curvature diagram for a prestressed section.

A conservative estimate of deflection is obtained if the value of  $E_c I_{av}$  for the section of maximum moment is taken as the flexural rigidity of the member.

The tangent stiffness  $E_c I_{cr}$  is also shown in [Figure 3.10](#).  $I_{cr}$  is the second moment of area of the cracked section, which may be obtained from a transformed section analysis. For small variations in applied moment, curvature increments should be calculated using  $I_{cr}$ . In reinforced concrete construction,  $I_{cr}$  is constant and equal to  $I_{av}$ , but this is not so for prestressed concrete.

### Example 3.4

The cross-section analysed in [Example 3.3](#) and shown in [Figure 3.7](#) is to be re-analysed to determine its post-cracking behaviour. It is assumed that the duct has been grouted, thereby bonding the tendon to the surrounding concrete. The force in the prestressing steel at the time of application of the external moment is  $P_e = 1200$  kN. Material properties are as follows:

$$E_c = 30 \times 10^3 \text{ MPa}; E_p = E_s = 200 \times 10^3 \text{ MPa};$$

$$f'_c = 40 \text{ MPa}; f_y = 400 \text{ MPa}; f_p = 1840 \text{ MPa}.$$

Sample calculations are provided for the particular applied moment that produces a top fibre stress  $\sigma_o = -20$  MPa, as shown in [Figure 3.11](#).

When  $\sigma_{oi} = -20$  MPa, the instantaneous top fibre strain is

$$\epsilon_{oi} = \frac{\sigma_{oi}}{E_c} = -667 \times 10^{-6}$$



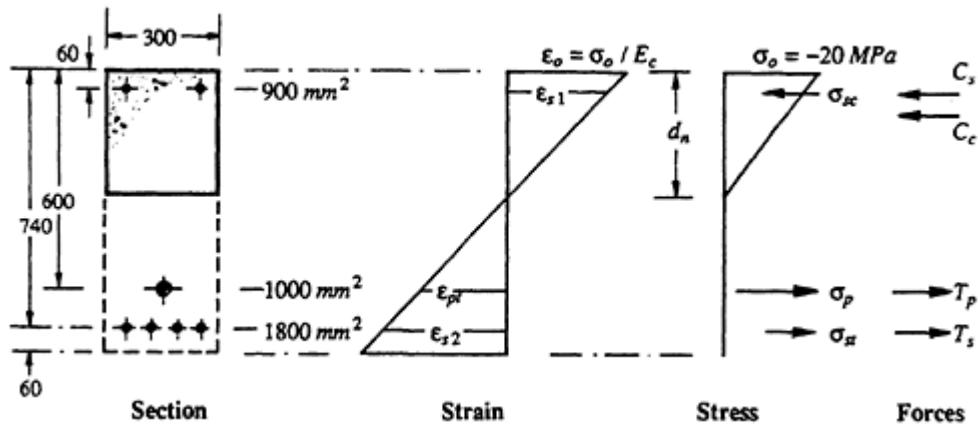


Figure 3.11 Short-term strain and stress on the cracked section of [Example 3.4](#).

The area of the transformed cross-section prior to cracking and the second moment of area about the centroidal axis are  $A=261 \times 10^3 \text{ mm}^2$  and  $I=14760 \times 10^6 \text{ mm}^4$ , respectively. The various strain components in the prestressing steel are obtained from Equations 3.31–3.33:

$$\epsilon_{pe} = \frac{1200 \times 10^3}{1000 \times 200\,000} = 6000 \times 10^{-6}; \quad \epsilon_{pi} = \frac{667 \times 10^{-6}(600 - d_n)}{d_n};$$

$$\epsilon_{ce} = \frac{1}{30 \times 10^3} \left( -\frac{1200 \times 10^3}{261 \times 10^3} - \frac{1200 \times 10^3 \times 189^2}{14760 \times 10^6} \right) = -250 \times 10^{-6}$$

and from Equation 3.35,

$$T_p = 200 \times 10^3 \times 1000 \left[ 6000 + 250 + \frac{667(600 - d_n)}{d_n} \right] \times 10^{-6}$$

Similarly from Equations 3.29 and 3.30:

$$T_s = 200\,000 \times 1800 \times \frac{667(740 - d_n)}{d_n} \times 10^{-6} = \frac{240 \times 10^3(740 - d_n)}{d_n}$$

and

$$C_s = 200\,000 \times 900 \times \frac{-667(d_n - 60)}{d_n} = \frac{-120 \times 10^3(d_n - 60)}{d_n}$$

The compression in the concrete above the neutral axis is obtained from Equation 3.28:

$$C = \frac{1}{2} \times -20 \times 300 \times d_n = -3000d_n$$

Trial values of  $d_n$  are considered below:

$d_n$ (mm)	$T_p$ (kN)	$T_s$ (kN)	$\Sigma T$ (kN)	$C$ (kN)	$C_s$ (kN)	$\Sigma C$ (kN)	$\Sigma T + \Sigma C$ (kN)
460	1291	146	1437	1380	104	1484	-47
440	1299	164	1463	1320	104	1424	+39
FROM LINEAR INTERPOLATION							
449	1295	155	1450	1347	104	1451	-1
CLOSE ENOUGH							

With  $d_n=449$  mm when  $\varepsilon_{oi}=-667 \times 10^{-6}$ , the moment and curvature on the section are obtained from Equations 3.27 and 3.36, respectively.

$$M = (1295 \times 0.6) + (155 \times 0.74) - \left(1347 \times \frac{0.449}{3}\right) - (104 \times 0.06)$$

$$= 684 \text{ kNm}$$

and

$$x_i = -\frac{\varepsilon_{oi}}{d_n} = \frac{667 \times 10^{-6}}{449} = 1.49 \times 10^{-6} \text{ mm}^{-1}$$

The secant stiffness is obtained from Equation 3.37:

$$E_c I_{av} = \frac{[(684 \times 10^6) - (1200 \times 10^3 \times 189)] \times 449}{667 \times 10^{-6}} = 308 \times 10^{12} \text{ N mm}^2$$

(cf.  $E_c I = 443 \times 10^{12} \text{ N mm}^2$  for the uncracked section). The stresses in the prestressed and the non-prestressed tensile steel under this applied moment are

$$\sigma_p = \frac{T_p}{A_p} = 1295 \text{ MPa} \quad \text{and} \quad \sigma_{s2} = \frac{T_s}{A_{s2}} = 86.1 \text{ MPa}$$

The change in stress in the prestressing steel and the tensile stress in the non-prestressed steel caused by the applied moment are much less than the tensile stress limits usually specified in codes of practice for crack control.

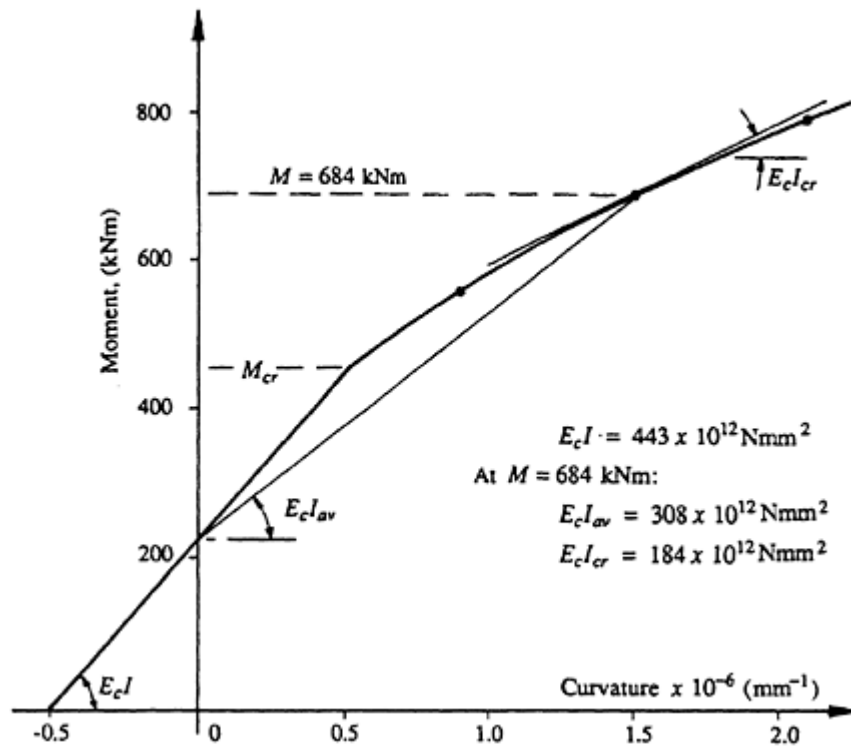


Figure 3.12 Moment vs curvature for section of [Example 3.4](#).

For example, AS 3600 (1988) specifies a maximum increment of tensile steel stress equal to 200 MPa between decomposition and the full in-service moment. With the closely spaced bonded reinforcement near the tension face of the section analysed here, cracks should be well controlled at this level of applied moment.

Similar calculations can be performed for other values of  $\sigma_{oi}$ . For example,

When  $\sigma_{oi} = -15 \text{ MPa}$ :

$$d_n = 555 \text{ mm}; M = 568 \text{ kNm}; x_i = 0.902 \times 10^{-6} \text{ mm}^{-1}$$

When  $\sigma_{oi} = -25 \text{ MPa}$ :

$$d_n = 395 \text{ mm}; M = 798 \text{ kNm}; x_i = 2.11 \times 10^{-6} \text{ mm}^{-1}$$

A plot of the moment-curvature relationship for the section is shown in [Figure 3.12](#).

### 3.6 Time-dependent analysis of cross-sections

#### 3.6.1 Introduction

The time-dependent behaviour of a partially prestressed member is greatly affected by the quantity and location of conventional, non-prestressed reinforcement. Bonded reinforcement provides restraint to the time-dependent shortening of concrete caused by creep and shrinkage. As the concrete creeps and shrinks, the reinforcement is gradually compressed. An equal and opposite tensile force  $\Delta T$  is applied to the concrete at the level of the bonded reinforcement, thereby reducing the compression caused by prestress. It is the tensile forces that are applied gradually at each level of bonded reinforcement which result in significant time-dependent changes in curvature and deflection. An accurate estimate of these forces ( $\Delta T$ ) is essential if reliable predictions of long-term behaviour are required.

Procedures specified in codes of practice for predicting losses of prestress due to creep and shrinkage are usually too simplified to be reliable and often lead to significant error, particularly for members containing non-prestressed reinforcement. In the following section, a simple analytical technique is presented for estimating the time-dependent behaviour of a general, partially prestressed cross-section. The procedure has been described in more detail by Ghali and Favre (1986) and Gilbert (1988), and makes use of the *age-adjusted effective modulus method* to model the effects of creep in concrete (see Equations 2.11–2.14 and the associated discussion).

#### 3.6.2 Uncracked cross-sections

During any time period, creep and shrinkage strains develop in the concrete and relaxation occurs in the prestressing steel. The gradual change in strain in the concrete with time causes changes of stress in the bonded reinforcement. The gradual change in force in the steel is opposed by an equal and opposite force on the concrete (usually tensile) at each steel location, as shown in [Figure 3.13](#). These forces are induced in the concrete at each level of bonded reinforcement and result in increments of axial force  $\Delta N(t)$  and moment about the top reference surface  $\Delta M(t)$  given by

$$\Delta N(t) = \sum_{j=1}^n \Delta T_j + \sum_{k=1}^m \Delta T_{pk} \quad (3.38)$$

and

$$\Delta M(t) = \sum_{j=1}^n \Delta T_j d_j + \sum_{k=1}^m \Delta T_{pk} d_{pk} \quad (3.39)$$

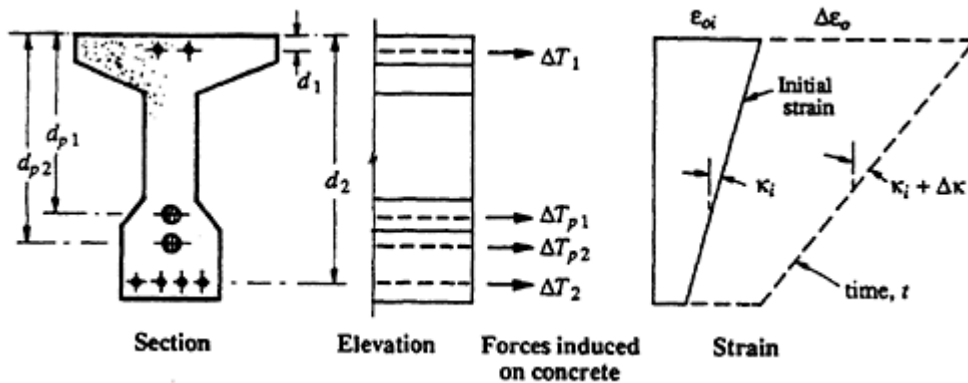


Figure 3.13 Time-dependent actions and deformations.

where  $n$  is the number of layers of conventional, non-prestressed reinforcement and  $m$  is the number of layers of bonded prestressed steel. Equal and opposite actions  $-\Delta N(t)$  and  $-\Delta M(t)$  are applied to the bonded steel portions of the cross-section.

The time-dependent change of strain at any depth  $y$  below the top of the cross-section ( $\Delta \epsilon$ ) may be expressed in terms of the change in top fibre strain ( $\Delta \epsilon_o$ ) and the change of curvature ( $\Delta \kappa$ ):

$$\Delta \epsilon = \Delta \epsilon_o + y \Delta \kappa \quad (3.40)$$

The magnitude of  $\Delta \epsilon$  is the sum of each of the following components:

- The free shrinkage strain  $\epsilon_{sh}$  (which is usually considered to be uniform over the section).
- The creep strain caused by the initial concrete stress  $\sigma_i$  existing at the beginning of the time period, i.e.  $\epsilon_c = \Delta \phi \sigma_i / E_c$  (from Equation 2.9), where  $\Delta \phi$  is the increment of the creep coefficient associated with the time period under consideration.
- The creep and elastic strain caused by  $\Delta N(t)$  and  $\Delta M(t)$  gradually applied to the concrete section. This term accounts for the internal restraint to creep and shrinkage provided by the bonded reinforcement.
- The tensile creep strain in the high-strength prestressing steel (relaxation).

A convenient approach for the determination of the change of strain during any particular time period ( $\Delta \epsilon_o$  and  $\Delta \kappa$  in Equation 3.40) involves a relaxation solution procedure first proposed by Bresler and Selna (1964). During the time interval, the strain at any point on the cross-section is initially assumed to remain unchanged, i.e. the change of strain due to creep and shrinkage is artificially prevented. If the total strain is held constant and the creep and shrinkage components change, then the instantaneous compo-

ment of strain must also change by an equal and opposite amount. As the instantaneous strain changes, so too does the concrete stress. The concrete stress on the cross-section is therefore allowed to vary due to relaxation. As a result, the internal actions change and equilibrium is not maintained. To restore equilibrium, an axial force  $\delta N$  and a bending moment  $\delta M$  must be applied to the section.

The forces required to restrain the section,  $-\delta N$  and  $-\delta M$ , are easily determined. If creep of the concrete was not restrained by bonded reinforcement and the concrete stress remained constant throughout the time period, the top fibre strain and curvature would increase by  $\Delta\phi\epsilon_{oi}$  and  $\Delta\phi\kappa_i$ , respectively. The restraining forces required to prevent this deformation are determined using expressions similar to Equation 3.22 and 3.23:

$$-\delta N_{\text{creep}} = -\bar{E}_e \Delta\phi (A_c \epsilon_{oi} + B_c \kappa_i) \quad (3.41)$$

$$-\delta M_{\text{creep}} = -\bar{E}_e \Delta\phi (B_c \epsilon_{oi} + \bar{I}_c \kappa_i) \quad (3.42)$$

where  $A_c$ ,  $B_c$ , and  $\bar{I}_c$  are the concrete area, the first moment of the concrete area and the second moment of the concrete area about the top surface of the section, respectively. The properties of the concrete section alone (without any contribution from the steel reinforcement) are used in Equations 3.41 and 3.42 since only the concrete is subject to creep. The age-adjusted effective modulus  $\bar{E}_e$  (as defined in Equation 2.14) is used in Equations 3.41 and 3.42 because the restraining forces  $\delta N$  and  $\delta M$  are gradually applied throughout the time period.

If shrinkage is uniform over the depth of the section and completely unrestrained, the shrinkage-induced top fibre strain which develops during the time interval is  $\epsilon_{sh}$  and there is no induced curvature. The restraining forces required to prevent this uniform deformation are again obtained using expressions similar to Equations 3.22 and 3.23:

$$-\delta N_{\text{shrinkage}} = -\bar{E}_e \epsilon_{sh} A_c \quad (3.43)$$

$$-\delta M_{\text{shrinkage}} = -\bar{E}_e \epsilon_{sh} B_c \quad (3.44)$$

For a prestressed concrete section, restraining forces required to prevent the relaxation  $R_k$  in each layer of tendons must also be included. The restraining forces required to prevent the tensile creep (which causes relaxation) in the  $m$  layers of prestressing steel are

$$-\delta N_{\text{relaxation}} = \sum_{k=1}^m R_k \quad (3.45)$$

and

$$-\delta M_{\text{relaxation}} = \sum_{k=1}^m R_k d_{pk} \quad (3.46)$$

The *total* restraining forces are the sum of the creep, shrinkage, and relaxation components:

$$-\delta N = -\bar{E}_e [\Delta\phi (A_c \epsilon_{oi} + B_c \chi_i) + \epsilon_{sh} A_c] + \sum_{k=1}^m R_k \quad (3.47)$$

$$-\delta M = -\bar{E}_e [\Delta\phi (B_c \epsilon_{oi} + \bar{I}_c \chi_i) + \epsilon_{sh} B_c] + \sum_{k=1}^m R_k d_{pk} \quad (3.48)$$

For a reinforced concrete section, the relaxation forces  $R_k$  in the above equations obviously do not exist.

The increments of top fibre strain ( $\Delta\epsilon_o$ ) and curvature ( $\Delta\chi$ ) produced by the axial force  $\delta N$  and the moment  $\delta M$ , gradually applied about the top reference level, may be obtained from the following equations (which are similar to Equations 3.24 and 3.25):

$$\Delta\epsilon_o = \frac{\bar{B}_e \delta M - \bar{I}_e \delta N}{\bar{E}_e (\bar{B}_e^2 - \bar{A}_e \bar{I}_e)} \quad (3.49)$$

$$\Delta\chi = \frac{\bar{B}_e \delta N - \bar{A}_e \delta M}{\bar{E}_e (\bar{B}_e^2 - \bar{A}_e \bar{I}_e)} \quad (3.50)$$

where  $\bar{A}_e$  is the area of the *age-adjusted transformed section* and  $\bar{B}_e$  and  $\bar{I}_e$  are the first and second moments of the area of the age-adjusted transformed section about the top surface. For the determination of  $\bar{A}_e$ ,  $\bar{B}_e$ , and  $\bar{I}_e$ , the age-adjusted effective modulus  $\bar{E}_e$  is used instead of the elastic modulus for concrete  $E_c$  in the calculation of the transformed area of the bonded reinforcement.  $\bar{E}_e$  is used in Equations 3.49 and 3.50 because  $\delta N$  and  $\delta M$  produce both elastic and creep strains on the cross-section.

The loss of stress in the concrete at any distance  $y$  below the top fibre, which occurs while the strain state is initially held constant (i.e. the initial stress relaxation), is given by

$$\Delta\sigma_{\text{relax}} = -\bar{E}_e [\Delta\phi (\epsilon_{oi} + y\chi_i) + \epsilon_{sh}] \quad (3.51)$$

and the change of stress which occurs when  $\delta N$  and  $\delta M$  are applied to the section to restore equilibrium is

$$\Delta\sigma_{\text{restore}} = \bar{E}_e (\Delta\epsilon_o + y \Delta\chi) \quad (3.52)$$

The actual change of concrete stress  $\Delta\sigma$  that occurs during the time interval due to the effects of creep, shrinkage, and relaxation is obtained by adding Equations 3.51 and 3.52:

$$\Delta\sigma = \Delta\sigma_{\text{relax}} + \Delta\sigma_{\text{restore}} \quad (3.53)$$

For non-prestressed steel, the change of stress in the  $j$ th layer is

$$\Delta\sigma_{sj} = E_s(\Delta\varepsilon_o + d_{sj} \Delta\kappa) \quad (3.54)$$

and, for the  $k$ th layer of prestressed steel, the change of stress is

$$\Delta\sigma_{pk} = E_p(\Delta\varepsilon_o + d_p \Delta\kappa) + \frac{R_k}{A_{pk}} \quad (3.55)$$

### Example 3.5

The time-dependent behaviour of the cross-section shown in [Figure 3.7](#) is to be determined. The short-term behaviour of the section immediately after transfer was calculated in [Example 3.3](#). The post-tensioned duct is filled with grout soon after transfer, thereby bonding the tendon to the concrete and ensuring compatibility of concrete and steel strains throughout the period of the time analysis. The material properties for the time period under consideration are

$$E_c = 30 \times 10^3 \text{ MPa}; E_s = E_p = 200 \times 10^3 \text{ MPa}; \Delta\phi = 2.0; \chi = 0.8;$$

$$\varepsilon_{sh} = -450 \times 10^{-6}; \text{ and } R = -30 \text{ kN.}$$

The strain and stress distributions immediately after transfer are shown in [Figure 3.8](#), and for  $M_o=100$  kNm,

$$\varepsilon_{oi} = -25.4 \times 10^{-6} \quad \text{and} \quad \kappa_i = -0.378 \times 10^{-6} \text{ mm}^{-1}$$

It is assumed in this example that the external moment remains constant and equals 100 kNm throughout the period of the time analysis.

From Equation 2.14,

$$\bar{E}_e = \frac{30 \times 10^3}{1 + (0.8 \times 2.0)} = 11\,540 \text{ MPa}$$

and with the post-tensioning duct fully grouted, the properties of the concrete section are

$$A_c = 236\,500 \text{ mm}^2; B_c = 94.01 \times 10^6 \text{ mm}^3; \bar{I}_c = 49\,850 \times 10^6 \text{ mm}^4$$



The forces required to restrain the cross-section are determined using Equations 3.41–3.46:

$$\begin{aligned}
 -\delta N_{\text{creep}} &= -11\,540 \times 2.0 [(236\,300 \times -25.4 \times 10^{-6}) \\
 &\quad + (94.01 \times 10^6 \times -0.378 \times 10^{-6})] \times 10^{-3} = 959 \text{ kN} \\
 -\delta M_{\text{creep}} &= -11\,540 \times 2.0 [(94.01 \times 10^6 \times -25.4 \times 10^{-6}) \\
 &\quad + (49\,850 \times 10^6 \times -0.378 \times 10^{-6})] \times 10^{-6} = 490 \text{ kNm} \\
 -\delta N_{\text{shrinkage}} &= -11\,540 \times -450 \times 10^{-6} \times 236\,300 \times 10^{-3} \\
 &= 1227 \text{ kN} \\
 -\delta M_{\text{shrinkage}} &= -11\,540 \times -450 \times 10^{-6} \times 94.01 \times 10^6 \times 10^{-6} \\
 &= 488 \text{ kNm} \\
 -\delta N_{\text{relaxation}} &= -30 \text{ kN} \\
 -\delta M_{\text{relaxation}} &= -30\,000 \times 600 \times 10^{-6} = -18.0 \text{ kNm}
 \end{aligned}$$

The total restraining forces are obtained by summing the individual components using Equations 3.47 and 3.48:

$$\delta N = -959 - 1227 + 30 = -2156 \text{ kN}$$

$$\delta M = -490 - 488 + 18 = -960 \text{ kNm}$$

The age-adjusted modular ratio is  $\bar{n} = E_s/\bar{E}_c = 17.33$  and the age-adjusted transformed section and its properties about the top reference surface are shown in [Figure 3.14](#).

The increments of top fibre strain and curvature which develop during the

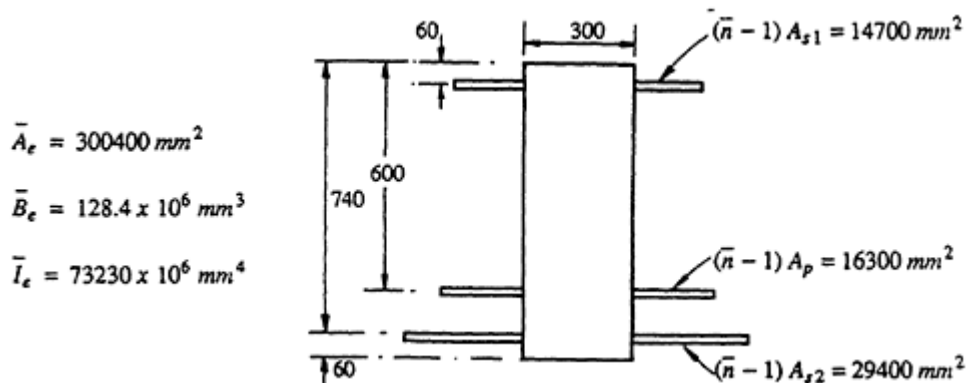


**Figure 3.14** Age-adjusted transformed section and properties ([Example 3.5](#)).

time interval are obtained from Equations 3.49 and 3.50:

$$\begin{aligned}\Delta \epsilon_o &= \frac{(128.4 \times 10^6 \times -960 \times 10^6) - (73\,230 \times 10^6 \times -2156 \times 10^3)}{11\,540[(128.4 \times 10^6)^2 - (300\,400 \times 73\,230 \times 10^6)]} \\ &= -544 \times 10^{-6} \\ \Delta x &= \frac{(128.4 \times 10^6 \times -2156 \times 10^3) - (300\,400 \times -960 \times 10^6)}{11\,540[(128.4 \times 10^6)^2 - (300\,400 \times 73\,230 \times 10^6)]} \\ &= -0.182 \times 10^{-6} \text{ mm}^{-1}\end{aligned}$$

The final top fibre strain and curvature are therefore

$$\begin{aligned}\epsilon_o &= \epsilon_{oi} + \Delta \epsilon_o = -569 \times 10^{-6} \quad \text{and} \\ x &= x_i + \Delta x = -0.561 \times 10^{-6} \text{ mm}^{-1}\end{aligned}$$

The time-dependent changes of the top and bottom fibre concrete stresses are calculated using Equations 3.51–3.53:

$$\begin{aligned}\Delta \sigma_o &= -11\,540[(2.0 \times -25.4) - 450 + 544] \times 10^{-6} = -0.50 \text{ MPa} \\ \Delta \sigma_b &= -11\,540[2.0[-25.4 + (800 \times -0.378)] - 450 \\ &\quad - [-544 + (800 \times -0.182)]] \times 10^{-6} = 4.80 \text{ MPa}\end{aligned}$$

and therefore the final concrete stresses are

$$\sigma_o = \sigma_{oi} + \Delta \sigma_o = -1.26 \text{ MPa} \quad \text{and} \quad \sigma_b = \sigma_{bi} + \Delta \sigma_b = -5.03 \text{ MPa}$$

From Equation 3.54, the change of stress in the non-prestressed steel is

$$\begin{aligned}\Delta \sigma_{s1} &= 200 \times 10^3 [-544 + (60 \times -0.182)] \times 10^{-6} = -111 \text{ MPa} \\ \Delta \sigma_{s2} &= 200 \times 10^3 [-544 + (740 \times -0.182)] \times 10^{-6} = -136 \text{ MPa}\end{aligned}$$

and from Equation 3.55, the loss of stress in the prestressed steel is

$$\begin{aligned}\Delta \sigma_p &= 200 \times 10^3 [-544 + (600 \times -0.182)] \times 10^{-6} + \frac{-30\,000}{1000} \\ &= -161 \text{ MPa}\end{aligned}$$

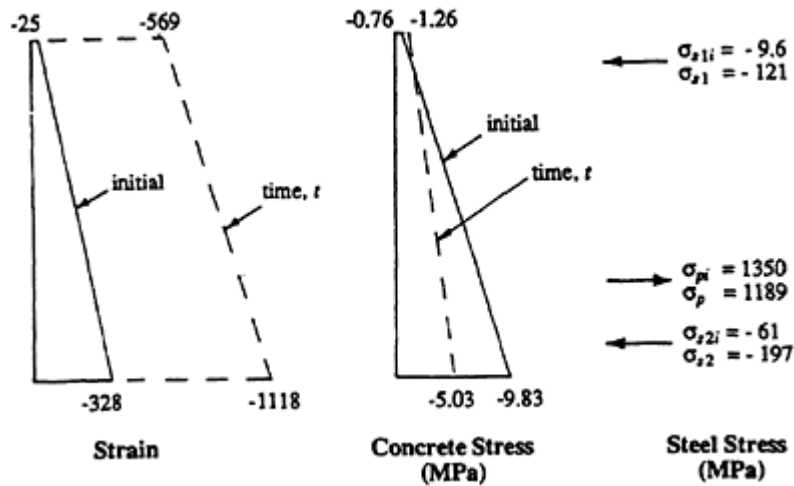


Figure 3.15 Initial and final strains and stresses for [Example 3.5](#).

The final steel stresses in each layer at time  $t$  are therefore

$$\sigma_{s1} = \sigma_{s1i} + \Delta\sigma_{s1} = -121 \text{ MPa}; \sigma_{s2} = \sigma_{s2i} + \Delta\sigma_{s2} = -197 \text{ MPa};$$

$$\text{and } \sigma_p = \sigma_{pi} + \Delta\sigma_p = 1189 \text{ MPa}$$

The initial and final strains and stress on the cross-section are illustrated in [Figure 3.15](#).

### Discussion

The results of several time analyses on the cross-section shown in [Figure 3.7](#) are presented in [Tables 3.1](#) and [3.2](#). The effects of varying the quantities of

**Table 3.1** Effect of varying tensile steel  $A_{s2}$  ( $A_{s1}=0$ ).

$M_s$ (kNm)	$A_{s1}$ (mm <sup>2</sup> )	$\epsilon_{oi}$ ( $\times 10^{-6}$ )	$\kappa_i$ ( $\times 10^{-6}$ mm <sup>-1</sup> )	$\Delta T_{c1}$ (kN)	$\Delta T_{c2}$ (kN)	$\Delta T_{cp1}$ (kN)	$\Delta \epsilon_o$ ( $\times 10^{-6}$ )	$\Delta \kappa$ ( $\times 10^{-6}$ mm <sup>-1</sup> )
100	0	-8.8	-0.455	0	0	206	-505	-0.629
	1800	-28.9	-0.372	0	233	160	-673	+0.035
	3600	-44.8	-0.306	0	337	135	-765	+0.402
270	0	-186	-0.008	0	0	174	-854	+0.221
	1800	-198	+0.038	0	169	143	-970	+0.677
	3600	-206	+0.075	0	248	125	-1034	+0.932
440	0	-364	+0.438	0	0	142	-1204	+1.071
	1800	-366	+0.448	0	105	125	-1267	+1.319
	3600	-368	+0.455	0	159	115	-1303	+1.463

**Table 3.2** Effect of varying compressive steel  $A_{s1}$  ( $A_{s2}=1800 \text{ mm}^2$ ).

$M_s$ (kNm)	$A_{s1}$ ( $\text{mm}^2$ )	$\varepsilon_{oi}$ ( $\times 10^{-6}$ )	$\kappa_i$ ( $\times 10^{-6}$ $\text{mm}^{-1}$ )	$\Delta T_{c1}$ (kN)	$\Delta T_{c2}$ (kN)	$\Delta T_{cp1}$ (kN)	$\Delta \varepsilon_o$ ( $\times 10^{-6}$ )	$\Delta \kappa$ ( $\times 10^{-6}$ $\text{mm}^{-1}$ )
100	0	-28.9	-0.372	0	233	160	-673	+0.035
	900	-25.4	-0.378	100	244	161	-544	-0.182
	1800	-22.3	-0.383	170	253	161	-450	-0.339
270	0	-198	+0.038	0	169	143	-970	+0.677
	900	-184	+0.014	136	186	143	-776	+0.353
	1800	-172	-0.007	227	198	143	-639	+0.121
440	0	-366	+0.448	0	105	125	-1267	+1.319
	900	-343	+0.407	172	127	125	-1009	+0.887
	1800	-322	+0.370	285	143	126	-827	+0.581

the compressive and tensile non-prestressed reinforcement ( $A_{s1}$  and  $A_{s2}$ , respectively) on the time-dependent deformation can be seen for three different values of sustained bending moment. At  $M=100$  kNm, the initial concrete stress distribution is approximately triangular with higher compressive stresses in the bottom fibres (as determined in Examples 3.3 and 3.5). At  $M=270$  kNm, the initial concrete stress distribution is approximately uniform over the depth of the section and the curvature is small. At  $M=440$  kNm, the initial stress distribution is again triangular with high compressive stresses in the top fibres.

From the results in Table 3.1, the effect of increasing the quantity of non-prestressed tensile reinforcement,  $A_{s2}$ , is to increase the change in positive or *sagging* curvature with time. The increase is most pronounced when the initial concrete compressive stress at the level of the steel is high, i.e. when the sustained moment is low and the section is initially subjected to a negative or *hogging* curvature. When  $A_{s2}=3600 \text{ mm}^2$  and  $M=100$  kNm in Table 3.1,  $\Delta x$  is positive despite a large initial negative curvature. Table 3.1 indicates that the addition of non-prestressed steel in the *tensile zone* will reduce the time-dependent camber which often causes problems in precast members subjected to low sustained loads. For sections on which  $M$  is sufficient to cause an initial positive curvature, an increase in  $A_{s2}$  causes an increase in time-dependent curvature and hence an increase in final deflection (e.g. when  $M=440$  kNm in Table 3.1).

The inclusion of non-prestressed steel in the *compressive zone*,  $A_{s1}$ , increases the change in negative curvature with time, as indicated in Table 3.2. For sections where the initial curvature is positive, such as when  $M=440$  kNm, the inclusion of  $A_{s1}$  reduces the time-dependent change in curvature (and hence the deflection of the member). However, when  $x_i$  is

negative,  $A_{s1}$  causes an increase in negative curvature and hence an increase in the camber of the member with time.

The significant unloading of the concrete with time on the sections containing non-prestressed reinforcement should be noted. In [Table 3.2](#), when  $M=270$  kNm and  $A_{s1}=1800$  mm<sup>2</sup>, the concrete is subjected to a total gradually applied tensile force ( $\Delta T_{c1}+\Delta T_{c2}+\Delta T_{cp1}$ ) of 568 kN. More than 42% of the initial compression in the concrete is shed into the bonded reinforcement with time. The loss of prestress in the tendon, however, is only 143 kN (10.6%). It is evident that an accurate picture of the time-dependent behaviour of a partially prestressed section cannot be obtained unless the restraint provided to creep and shrinkage by the non-prestressed steel is adequately accounted for. It is also evident that the presence of non-prestressed reinforcement significantly reduces the cracking moment with time and may in fact relieve the concrete of much of its initial prestress.

### 3.6.3 Cracked cross-sections

Under sustained loading, creep causes a change in position of the neutral axis on a cracked cross-section. In general, the depth to the neutral axis increases with time and, hence, so too does the area of concrete in compression. An iterative numerical solution procedure is required to account accurately for this gradual change in the properties of the cracked section with time. The time period is divided into small intervals and structural behaviour is calculated at the end of each time increment. The properties of the cross-section are modified or updated at the end of each time increment. Such a procedure is not suitable for manual solution and is often too complex for routine use in structural analysis and design.

The procedure described in the previous section for the time analysis of uncracked cross-sections can be extended to cracked sections, if it is assumed that the cross-sectional area of the section remains constant with time, that is, if the depth of the concrete above the neutral axis ( $d_n$  in [Figure 3.16a](#)) is assumed to remain constant throughout the time analysis. This assumption is in fact necessary if the short-term and time-dependent stress and strain increments are to be calculated separately and added together to obtain final stresses and deformations, i.e. if the principle of superposition is to be applied to fully cracked sections in the same way as it has been applied to uncracked cross-sections. The assumption also greatly simplifies the analysis and usually results in relatively little error.

Consider a fully cracked cross-section subjected to a sustained bending moment  $M$ , as shown in [Figure 3.16a](#). The short-term and time-dependent strain distributions are illustrated in [Figure 3.16b](#).

The restraining actions,  $-\delta N$  and  $-\delta M$ , that are required to prevent the free development of creep and shrinkage in the concrete and relaxation in the bonded prestressing tendons are calculated using Equations 3.47 and

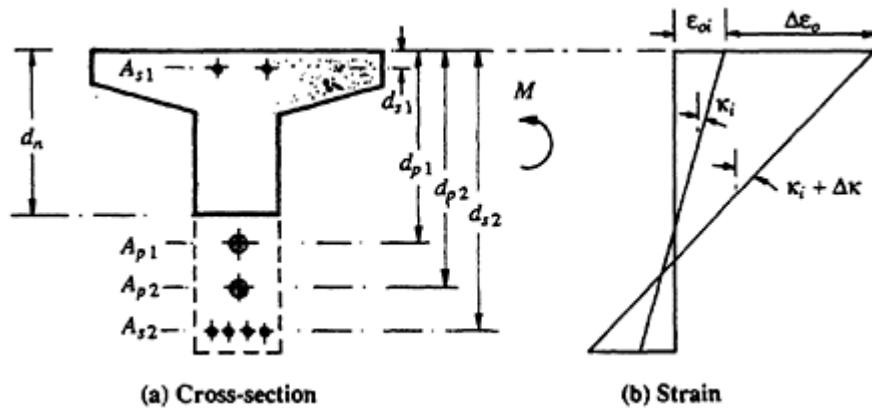


**Figure 3.16** Time-dependent behaviour of a fully cracked cross-section.

3.48. For a fully cracked cross-section, the terms  $A_c$ ,  $B_c$ , and  $\bar{I}_c$  in these equations are the properties of the uncracked part of the concrete cross-section with respect to the top fibre. The depth of the uncracked concrete  $d_n$  is calculated from the short-term analysis presented in [Section 3.5.2](#).

The change of the strain distribution with time is calculated using Equations 3.49 and 3.50 and  $\bar{A}_e$ ,  $\bar{B}_e$ , and  $\bar{I}_e$  are now the properties of the fully cracked age-adjusted transformed section, i.e. the properties of the cross-section consisting of the concrete compressive zone and a transformed area of  $\bar{n}A_s$  (or  $\bar{n}A_p$ ) at each bonded steel level, where  $\bar{n} = E_s/\bar{E}_e$  (or  $E_p/\bar{E}_e$ ).

The change of concrete stress with time at any depth  $y \leq d_n$  may be determined using Equations 3.51–3.53 and the change of stress in the  $j$ th layer of non-prestressing reinforcement and in the  $k$ th layer of prestressing steel may be found from Equations 3.54 and 3.55, respectively.

### Example 3.6

The change of stress and strain with time on the cross-section shown in [Figure 3.17a](#) is to be determined. The sustained bending moment is  $M=700$  kNm and the initial prestressing force is  $P=1350$  kN.

The material properties for the time period under consideration are:

$$E_c = 30\,000 \text{ MPa}; E_s = E_p = 200\,000 \text{ MPa}; \Delta\phi = 2.0; \chi = 0.8;$$

$$\epsilon_{sh} = -450 \times 10^{-6}; R = -30 \text{ kN}; \text{ and } f'_c = 40 \text{ MPa}.$$

The depth of the neutral axis immediately after the application of the applied moment  $M$  is calculated using the iterative short-term analysis outlined in [Section 3.5.2](#). In this example,

$$d_n = 474 \text{ mm}$$

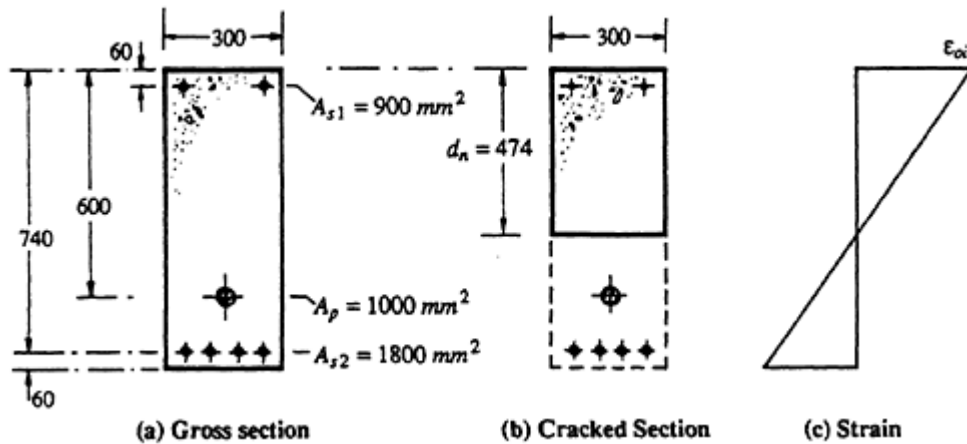


**Figure 3.17** Cross-sectional details and initial strains ([Example 3.6](#)).

(as shown in [Figure 3.17b](#)). The initial top fibre strain and curvature are  $\epsilon_{oi} = -671 \times 10^{-6}$  and  $x_i = 1.415 \times 10^{-6} \text{ mm}^{-1}$ , respectively.

The cracked cross-section and the strain distribution immediately after the application of  $M$  are shown in [Figures 3.17b](#) and [c](#).

The age-adjusted effective modulus is obtained from Equation 2.14:

$$\bar{E}_e = \frac{30\,000}{1 + (0.8 \times 2.0)} = 11\,540 \text{ MPa}$$

and the properties of the uncracked part of the concrete cross-section (i.e. the concrete compressive zone) with respect to the top fibre are

$$\bar{A}_c = 141\,300 \text{ mm}^2; \bar{B}_c = 33.66 \times 10^6 \text{ mm}^3; \text{ and } \bar{I}_c = 10\,650 \times 10^6 \text{ mm}^4$$

From Equations 3.47 and 3.48,

$$-\delta N = -11\,540 \{ 2.0 [ (141\,300 \times -671) + (33.66 \times 10^6 \times 1.415) ] - (450 \times 141\,300) \} \times 10^{-6} - 30 = 1793 \text{ kN}$$

$$-\delta M = -11\,540 \{ 2.0 [ (33.66 \times 10^6 \times -671) + (10\,650 \times 10^6 \times 1.415) ] - (450 \times 33.66 \times 10^6) \} \times 10^{-6} - (30\,000 \times 600) \times 10^{-6} = 330 \text{ kNm}$$

With the areas of the bonded steel reinforcement transformed into equivalent areas of concrete of modulus  $\bar{E}_e$ , the properties of the age-adjusted transformed section are

$$\bar{A}_e = 205\,450 \text{ mm}^2; \bar{B}_e = 68.08 \times 10^6 \text{ mm}^3; \text{ and } \bar{I}_e = 34\,030 \times 10^6 \text{ mm}^4.$$

The time-dependent increments of top fibre strain and curvature produced by  $\delta N$  and  $\delta M$  are found using Equations 3.49 and 3.50:

$$\begin{aligned}\Delta \epsilon_o &= \frac{(68.08 \times 10^6 \times -330 \times 10^6) - (34\,030 \times 10^6 \times -1793 \times 10^3)}{11\,540[(68.08 \times 10^6)^2 - (205\,450 \times 34\,030 \times 10^6)]} \\ &= -1417 \times 10^{-6} \\ \Delta \kappa &= \frac{(68.08 \times 10^6 \times -1793 \times 10^3) - (205\,450 \times -330 \times 10^6)}{11\,540[(68.08 \times 10^6)^2 - (205\,450 \times 34\,030 \times 10^6)]} \\ &= 1.995 \times 10^{-6} \text{ mm}^{-1}\end{aligned}$$

The change of stress in the concrete compression zone is obtained from Equations 3.51–3.53:

At  $y=0$ :

$$\begin{aligned}\Delta \sigma_o &= -11\,540[2.0(-671) - 450 + 1417] \times 10^{-6} \\ &= 4.33 \text{ MPa}\end{aligned}$$

At  $y=474$  mm:

$$\begin{aligned}\Delta \sigma_n &= -11\,540\{2.0[-671 + (474 \times 1.415)] - 450 \\ &\quad - [-1417 + (474 \times 1.995)]\} \times 10^{-6} \\ &= -0.24 \text{ MPa}\end{aligned}$$

and from Equations 3.54 and 3.55, the change of stress in the steel is

$$\begin{aligned}\Delta \sigma_{s1} &= 200 \times 10^3[-1417 + (60 \times 1.995)] \times 10^{-6} = -259 \text{ MPa} \\ \Delta \sigma_{s2} &= 200 \times 10^3[-1417 + (740 \times 1.995)] \times 10^{-6} = +12 \text{ MPa} \\ \Delta \sigma_p &= 200 \times 10^3[-1417 + (600 \times 1.995)] \times 10^{-6} - \frac{30\,000}{1000} = -74 \text{ MPa}\end{aligned}$$

The final stresses and strains are illustrated in [Figure 3.18](#).

There is a relatively small time-dependent change of stress in the prestressing steel on this cracked cross-section. If the concrete surrounding a bonded prestressing tendon is cracked under the sustained load, the loss of steel stress due to creep and shrinkage of the concrete is generally small. Most practical, partially prestressed concrete members are designed to



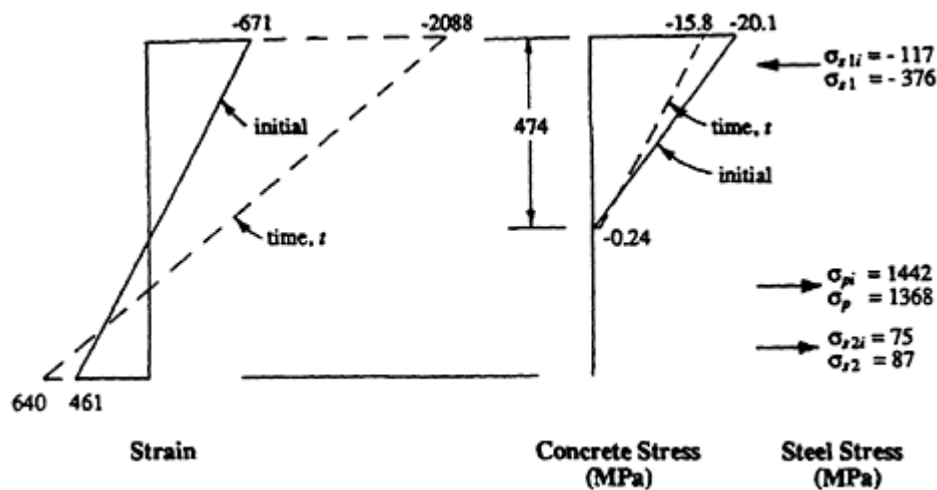


Figure 3.18 Stresses and strains on cross-section of [Example 3.6](#).

remain uncracked under the sustained or permanent in-service loads. Cracking occurs under the application of the variable live loads. Cracks therefore open and close as the variable live load is applied and removed. For most of the life of such members, the entire concrete cross-section is in compression (uncracked) and the time analysis for a general uncracked cross-section, as outlined in [Section 3.6.2](#), is appropriate.

### 3.7 Losses of prestress

#### 3.7.1 Definitions

The losses of prestress that occur in a prestressed member are illustrated in [Figure 3.19](#). When the prestress is transferred to the concrete, *immediate losses* of prestress occur. The difference between the prestressing force imposed at the jack,  $P_j$ , and the force in the steel immediately after transfer at a particular section,  $P_i$ , is the immediate loss:

$$\text{Immediate loss} = P_j - P_i \quad (3.56)$$

The gradual loss of prestress that takes place with time is called the *time-dependent* or *deferred loss*. If  $P_e$  is the force in the prestressing tendon after all losses, then

$$\text{Time-dependent loss} = P_i - P_e \quad (3.57)$$

Both of these losses are made up of several components. The immediate losses are caused by elastic deformation of the concrete as the prestress is

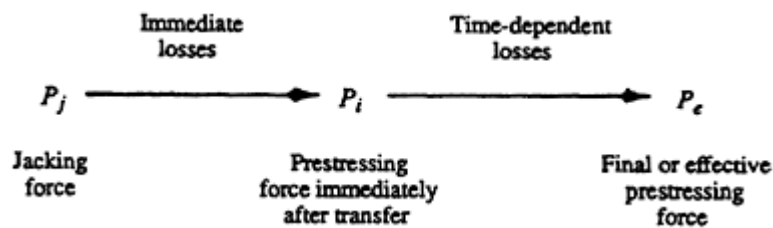


**Figure 3.19** Losses of prestress.

transferred, friction along the draped tendon in a post-tensioned member, and slip at the anchorage. Other sources of immediate loss of prestress which may need to be accounted for in some situations include deformation of the forms of precast members, temperature changes between the time of stressing the tendons and casting the concrete, deformation in the joints of precast members assembled in sections, and relaxation of the tendons prior to transfer. The time-dependent losses are caused by the gradual shortening of the concrete at the steel level due to creep and shrinkage, and by relaxation of the steel itself. Additional losses may occur due to time-dependent deformation of the joints in segmental construction.

### 3.7.2 Elastic deformation losses

#### Pretensioned members

Immediately after transfer, the change in strain in the prestressing steel  $\Delta\epsilon_p$  caused by elastic shortening of the concrete is equal to the strain in the concrete at the steel level,  $\epsilon_{cp}$ . The compatibility equation can be expressed as follows:

$$\epsilon_{cp} = \frac{\sigma_{cp}}{E_c} = \Delta\epsilon_p = \frac{\Delta\sigma_p}{E_p}$$

The loss of stress in the steel,  $\Delta\sigma_p$ , is therefore

$$\Delta\sigma_p = \frac{E_p}{E_c} \sigma_{cp} \quad (3.58)$$

where  $\sigma_{cp}$  is the concrete stress at the steel level immediately after transfer.

#### Post-tensioned members

For post-tensioned members with one cable or with two or more cables stressed simultaneously, the elastic deformation of the concrete occurs during the stressing operation before the tendons are anchored. In this case, elastic shortening losses are zero. In a member containing more than one tendon and where the tendons are stressed sequentially, the elastic deformation losses vary from tendon to tendon and are a maximum in the tendon

stressed first and a minimum (zero) in the tendon stressed last. It is relatively simple to calculate the elastic deformation losses in any tendon provided the stressing sequence is known. However, these losses are usually small and, for practical purposes, the average elastic shortening loss is often taken as half the value obtained from Equation 3.58:

$$\Delta\sigma_p = 0.5 \frac{E_p}{E_c} \sigma_{cp} \quad (3.59)$$

### 3.7.3 Friction along the tendon

Friction occurs in the jack and anchorage and depends on the type of jack and anchorage system used. This loss is usually allowed for during stressing and need not unduly concern the designer.

In *post-tensioned members*, friction losses occur along the tendon during the stressing operation. Friction between the tendon and the duct causes a gradual reduction in prestress with the distance along the tendon  $L_{pa}$  from the jacking end. The magnitude of the friction loss depends on the total angular change of the tendon, the distance from the jacking point and the size and type of the sheathing containing the tendons. A reliable estimate of friction losses may be obtained from Equation 3.60. An equation of similar form is recommended by numerous building codes, including ACI 318–83, BS 8110 (1985), and AS 3600–1988.

$$P_a = P_j e^{-\mu(\alpha_t + \beta_p L_{pa})} \quad (3.60)$$

where

$P_a$  is the force in the tendon at any point  $L_{pa}$  (in metres) from the jacking end.

$P_j$  is the force in the tendon at the jacking end.

$\mu$  is a friction curvature coefficient which depends on the type of duct. For strand in bright and zinc-coated metal ducts,  $\mu \approx 0.2$ ; for greased and wrapped wire or strand,  $\mu \approx 0.15$ ; and for strand in an unlined concrete duct,  $\mu \approx 0.50$ . Higher values should be used if either the tendon or the duct are rusted.

$\alpha_t$  is the sum in radians of the absolute values of all successive angular deviations of the tendon over the length  $L_{pa}$ .

$\beta_p$  is an angular deviation or wobble term and depends on the sheath (or duct) diameter:

For ducts containing strand and having an internal diameter as follows:

$\leq 50$ mm	$0.016 \leq \beta_p \leq 0.024$
$>50$ and $\leq 90$ mm	$0.012 \leq \beta_p \leq 0.016$
$>90$ and $\leq 140$ mm	$0.008 \leq \beta_p \leq 0.012$

For flat metal ducts:

$$0.016 \leq \beta_p \leq 0.024$$

For greased and wrapped bars:

$$\beta_p = 0.008.$$

### Example 3.7

The friction losses in the cable in the end-span of the post-tensioned girder of [Figure 3.20](#) are to be calculated. For this cable,  $\mu=0.2$  and  $\beta_p=0.01$ .

From Equation 3.60:

$$\begin{aligned} \text{At B: } P_a &= P_j e^{-0.2(0.105 + 0.01 \times 9)} \\ &= 0.962 P_j \quad \text{i.e. 3.8\% losses.} \\ \text{At C: } P_a &= P_j e^{-0.2(0.210 + 0.01 \times 18)} \\ &= 0.925 P_j \quad \text{i.e. 7.5\% losses.} \\ \text{At D: } P_a &= P_j e^{-0.2(0.315 + 0.01 \times 25)} \\ &= 0.893 P_j \quad \text{i.e. 10.7\% losses.} \end{aligned}$$

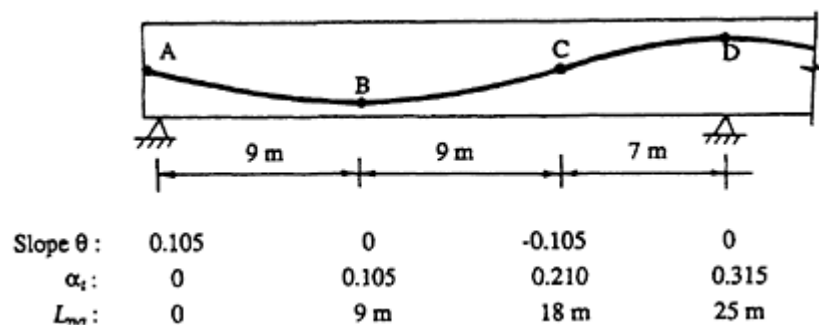


Figure 3.20 Tendon profile for end span of [Example 3.7](#).

#### 3.7.4 Anchorage losses

In post-tensioned members, some slip or *draw-in* occurs when the prestressing force is transferred from the jack to the anchorage. This causes an additional loss of prestress. The amount of slip depends on the type of anchorage. For wedge-type anchorages for strand, the slip  $\Delta$  may be as high as 6 mm. The loss of prestress caused by  $\Delta$  decreases with distance from the anchorage owing to friction and may be negligible at the critical design section. However, for short tendons, this loss may be significant and should not be ignored in design.

The loss of tension in the tendon caused by slip is opposed by friction in the same way as the initial prestressing force was opposed by friction, but in the opposite direction, i.e.  $\mu$  and  $\beta_p$  are the same. The graph of variation in prestressing force along a member due to friction (calculated using Equation 3.60) is modified in the vicinity of the anchorage by the mirror image reduction shown in [Figure 3.21](#). The slope of the *draw-in* line adjacent to the anchorage has the same magnitude as the friction loss line but the opposite sign.

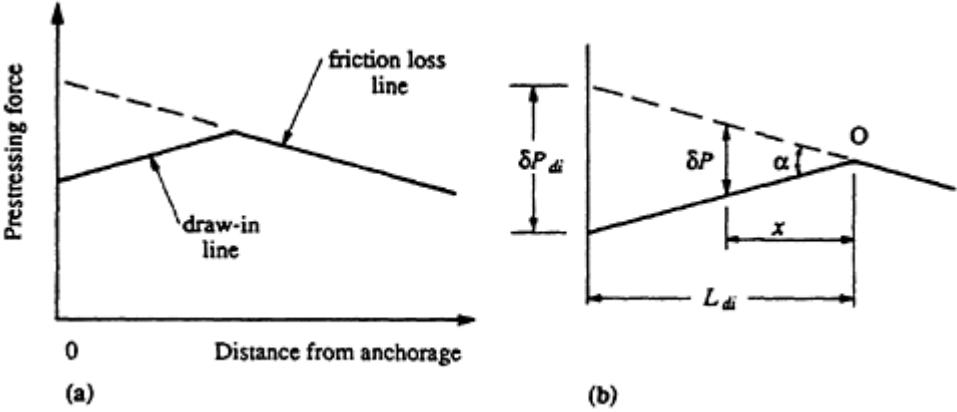


Figure 3.21 Variation in prestress due to draw-in at the anchorage.

In order to calculate the draw-in loss at the anchorage  $\delta P_{di}$ , the length of the draw-in line  $L_{di}$  must be determined. By equating the anchorage slip  $\Delta$  with the integral of the change in strain in the steel tendon over the length of the draw-in line,  $L_{di}$  may be determined. From [Figure 3.21b](#), the loss of prestress due to draw-in  $\delta P$  at distance  $x$  from point O is

$$\delta P = \alpha x$$

where  $\alpha$  is twice the slope of the prestress line as shown in [Figure 3.21](#). Therefore,

$$\Delta = \int_0^{L_{di}} \frac{\alpha x}{E_p A_p} \delta x = \frac{\alpha L_{di}^2}{2E_p A_p}$$

Rearrangement gives

$$L_{di} = \sqrt{\frac{2E_p A_p \Delta}{\alpha}} \tag{3.61}$$

and

$$\delta P_{di} = \alpha L_{di}$$

The magnitude of the slip that should be anticipated in design is usually supplied by the anchorage manufacturer and should be checked on site. Cautious overstressing at the anchorage is often an effective means of compensating for slip.

3.7.5 Time-dependent losses of prestress

In [Section 3.6](#), a time analysis was presented for determining the effects of creep, shrinkage, and relaxation on the behaviour of a prestressed concrete

beam section of any shape and containing any layout of prestressed and non-prestressed reinforcement. In this section, the approximate procedures which are often specified in codes of practice for calculating time-dependent losses of prestress are outlined. These methods are of limited value and often give misleading results because they do not adequately account for the significant loss of precompression in the concrete that occurs when non-prestressed reinforcement is present. For a realistic estimate of the time-dependent behaviour of a prestressed section, the method described in [Section 3.6](#) is recommended.

### Shrinkage losses

The loss of stress in a tendon due to shrinkage of concrete may be approximated by

$$\Delta\sigma_p = \varepsilon_{sh}E_p \quad (3.62)$$

where  $\varepsilon_{sh}$  is the shrinkage strain at the time under consideration and may be estimated using the procedures outlined in [Section 2.5](#). When non-prestressed reinforcement is present and offers restraint to shrinkage, the stress loss in the tendon will be smaller than that indicated by Equation 3.62. However, the non-prestressed reinforcement also relieves the concrete of compression, and the change in the resultant compression in the concrete may be much greater than the change in tensile force in the tendon. As time increases, more and more of the compression exerted on the beam by the tendon is carried by the non-prestressed steel and less and less by the concrete.

### Creep losses

Creep strain in the concrete at the level of the tendon depends on the stress in the concrete at that level. Because the concrete stress varies with time, a reliable estimate of creep losses requires a detailed time analysis (such as that presented in [Section 3.6](#)). An approximate and conservative estimate can be made by assuming that the concrete stress at the tendon level remains constant with time and equal to its initial (usually high) value,  $\sigma_c$  (caused by  $P_i$  and the permanent part of the load). With this assumption, the creep strain at any time  $t$  after transfer (at age  $\tau_0$ ) may be calculated from an expression similar to Equation 2.9):

$$\varepsilon_c(t) = \frac{\sigma_c}{E_c} \phi(t, \tau_0) \quad (3.63)$$

where  $\phi(t, \tau_0)$  is the creep coefficient, which may be estimated using the procedures outlined in [Section 2.5](#).

If the tendon is bonded to the surrounding concrete, the change of steel

strain caused by creep is equal to  $\varepsilon_c(t)$  and the creep loss in the tendon may be approximated by

$$\Delta\sigma_p = \varepsilon_c(t)E_p \quad (3.64)$$

Again, the presence of conventional steel will cause a decrease in the concrete compressive stress at the steel level and a consequent decrease in creep. In this case, Equation 3.64 will overestimate creep losses, often significantly.

### Relaxation of steel

The loss of stress in a tendon due to relaxation depends on the sustained stress in the steel. Owing to creep and shrinkage in the concrete, the stress in the tendon decreases with time at a faster rate than would occur due to relaxation alone. This decrease in stress level in the tendon affects (reduces) the magnitude of the relaxation losses. An equation similar to Equation 3.65 is often used to modify the *design relaxation* to include the effects of creep and shrinkage. The loss of prestress due to relaxation (as a percentage of the initial prestress) may be approximated by

$$R \left( 1 - \frac{2 \Delta\sigma_p}{\sigma_{pi}} \right) \quad (3.65)$$

where  $R$  is the design relaxation, which may be obtained from either Equation 2.22 or 2.23;  $\Delta\sigma_p$  is the loss of stress in the tendon due to creep plus shrinkage (from Equations 3.62 and 3.64); and  $\sigma_{pi}$  is the stress in the tendon immediately after transfer.

## 3.8 Deflection calculations

### 3.8.1 Discussion

The slope  $\theta$  and deflection  $v$  at any point  $x$  along a member may be calculated by integrating the curvature  $\kappa(x)$  over the length of the member. Provided that deformations are small compared with the beam dimensions, simple beam theory gives

$$\theta = \int \kappa(x) dx \quad (3.66)$$

$$v = \iint \kappa(x) dx dx \quad (3.67)$$

These equations are general and apply for both elastic and inelastic material

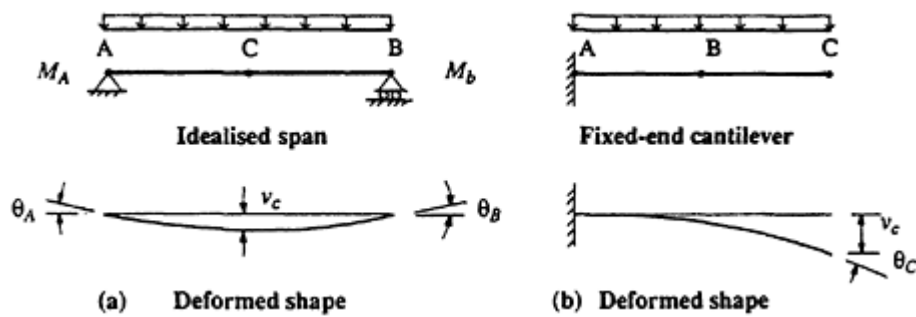


Figure 3.22 Deformation of a typical span and cantilever.

behaviour. For a prestressed concrete beam, the curvature at any point along the span at any time after first loading can be calculated using the procedures outlined in Sections 3.5 and 3.6.

Consider the span shown in Figure 3.22a. If the curvature at each end of the span ( $x_A$  and  $x_B$ ) and at mid-span ( $x_C$ ) are known and the variation in curvature along the member is parabolic, then the slope at each support ( $\theta_A$  and  $\theta_B$ ) and the deflection at mid-span ( $v_C$ ) are given by

$$\theta_A = \frac{L}{6} (x_A + 2x_C) \quad (3.68a)$$

$$\theta_B = -\frac{L}{6} (2x_C + x_B) \quad (3.68b)$$

$$v_C = \frac{L^2}{96} (x_A + 10x_C + x_B) \quad (3.68c)$$

Similarly, if the variation of curvature along a fixed-end cantilever (such as shown in Figure 3.22b) is parabolic, the slope and deflection at the free end are given by

$$\theta_C = -\frac{L}{6} (x_A + 4x_B + x_C) \quad (3.69a)$$

$$v_C = -\frac{L^2}{6} (x_A + 2x_B) \quad (3.69b)$$

If only the curvatures at each end of the cantilever are known, then

$$\theta_C = -\frac{L}{3} (x_A + 2x_C) \quad (3.70a)$$

$$v_C = -\frac{L^2}{4} (x_A + x_C) \quad (3.70b)$$



For practical members subjected to usual load configurations, deflection estimates made using Equations 3.68–3.70 are accurate enough for most design purposes, even where the variation of curvature along the member is not parabolic.

### 3.8.2 Short-term deflection

For any uncracked cross-section, the initial curvature may be calculated using Equation 3.25. A typical numerical example was illustrated in [Example 3.3](#). For a cracked cross-section, the initial curvature may be found from Equation 3.36 using the procedure presented in [Section 3.5.2](#) and illustrated in [Example 3.4](#). If the initial curvature at each end of the span of a beam or slab and at the mid-span are calculated, the short-term deflection can be estimated using Equations 3.68c, 3.69b or 3.70b, whichever is appropriate.

For uncracked, prestressed concrete members, codes of practice generally suggest that the gross moment of inertia  $I_g$  may be used in deflection calculations. The initial curvature at any cross-section may therefore be approximated by

$$\kappa_i = \frac{M - P_i e}{E_c I_g} \quad (3.71)$$

where  $P_i$  is the initial prestressing force and  $e$  is its eccentricity below the centroidal axis of the section.

After cracking, the stiffness of the cracked cross-section calculated using Equation 3.37 may underestimate the stiffness of the member in the cracked region. The intact concrete between adjacent cracks carries tensile force, mainly in the direction of the reinforcement, due to the bond between the steel and the concrete. The average tensile stress in the concrete is therefore not zero and may be a significant fraction of the tensile strength of concrete. The stiffening effect of the uncracked tensile concrete is sensibly known as *tension stiffening* and is usually accounted for in design by an empirical adjustment to the stiffness of the fully cracked cross-section.

For conventionally reinforced members, tension stiffening contributes significantly to the member stiffness, particularly when the maximum moment is not much greater than the cracking moment. However, as the moment level increases, the tension stiffening effect decreases owing to additional secondary cracking at the level of the bonded reinforcement. Shrinkage-induced cracking and tensile creep cause a reduction of the tension stiffening effect with time. Repeated or cyclic loading also causes a gradual breakdown of tension stiffening.

For a partially prestressed member (or a reinforced member subjected to significant axial compression), the effect of tension stiffening is less pro-

nounced because the loss of stiffness due to cracking is more gradual and significantly smaller.

In codes of practice, the simplified techniques specified for estimating the deflection of a cracked concrete member usually involve the determination of an effective moment of inertia  $I_e$  for the member. A number of empirical equations are available for  $I_e$ . Most have been developed specifically for reinforced concrete, where for a cracked member  $I_e$  lies between the gross moment of inertia of the critical section  $I_g$  and the moment of inertia of the cracked transformed section  $I_{cr}$ . For a prestressed concrete section,  $I_{cr}$  varies with the applied moment as the depth of the crack gradually changes. The value of  $I_{cr}$  is usually considerably less than  $I_{av}$ , as illustrated in [Figure 3.10](#). The equations used for estimating  $I_e$  for a reinforced section are not therefore directly applicable to prestressed concrete.

The following two well known procedures for modelling tension stiffening may be applied to prestressed concrete provided  $I_{av}$  replaces  $I_{cr}$  in the original formulations:

- (a) The empirical equation for  $I_e$  proposed by Branson (1963) is perhaps the best known method and has been adopted in many codes and specifications for reinforced concrete members, including ACI 318–83 and AS 3600–1988. For a prestressed concrete section, the following form of the equation can be used:

$$I_e = I_{av} + (I_g - I_{av}) \left( \frac{M_c}{M} \right)^3 \leq I_g \quad (3.72)$$

where  $M_c$  is the moment required to cause first cracking and  $M$  is the maximum in-service moment at the section under consideration.

- (b) The CEB (1983) has proposed an alternative approach for reinforced concrete which accounts for the effect of the reinforcement type on tension stiffening and also accounts for the breakdown of tension stiffening with time due to shrinkage induced tension, tensile creep, and repeated loading. The CEB proposal may be modified for cracked, prestressed sections as follows:

$$I_e = (1 - \zeta)I_g + \zeta I_{av} \quad (3.73)$$

where

$$\begin{aligned} \zeta &= 1 - \beta_1\beta_2(M_c/M)^2 \\ &= 0 \quad \text{for } M < M_c \end{aligned} \quad (3.74)$$

and

- $\beta_1 = 1.0$  when deformed non-prestressed bars are present;  
 $= 0.5$  when plain round bars or bonded tendons only are present;  
 $= 0.0$  when unbonded tendons only are present;  
 $\beta_2 = 1.0$  for initial loading;  
 $= 0.5$  for long-term sustained loads or cycles of load.

Numerous other approaches have been developed for modelling the tension stiffening phenomenon. Of the two approaches outlined above, the CEB approach is recommended because it best accounts for the breakdown of tension stiffening under long-term or cyclic loading and allows for the reduction in tension stiffening when plain bars or bonded tendons only are present and the steel-concrete bond might not be perfect.

For most practical prestressed or partially prestressed members, however, tension stiffening is not very significant and a reasonable, conservative estimate of deflection can be obtained by ignoring tension stiffening and using  $E_c I_{av}$  (from Equation 3.37) in the calculations.

### Example 3.8

The *short-term* deflection of a uniformly loaded, simply supported, post-tensioned beam of span 12m is to be calculated. An elevation of the member is shown in [Figure 3.23](#), together with details of the cross-section at mid-span (which is identical with that analysed in [Example 3.3](#)). The

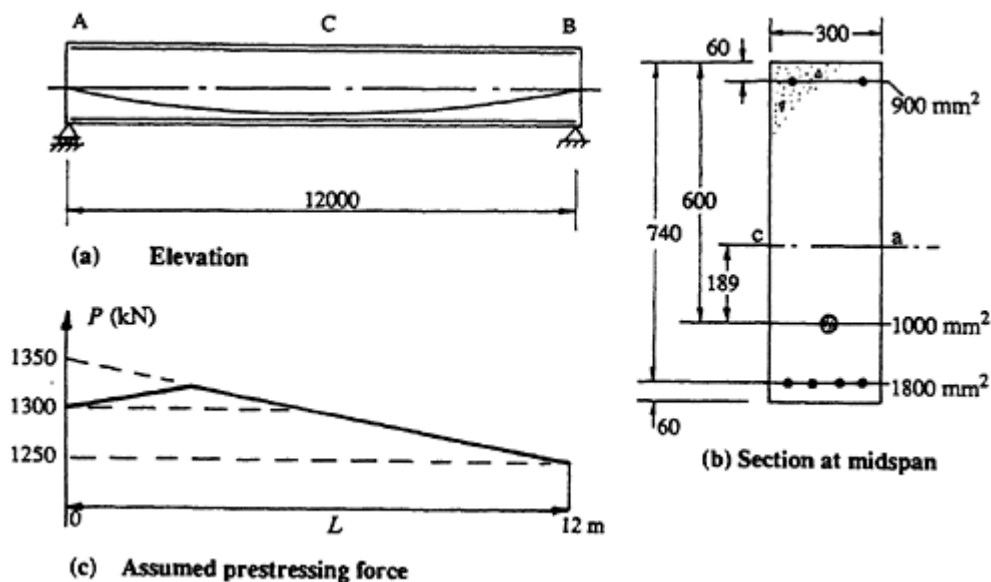


Figure 3.23 Beam details for [Example 3.8](#).

prestressing cable is parabolic with the depth of the tendon below the top fibre at each support  $d_p=400$  mm and at mid-span  $d_p=600$  mm, as shown. The non-prestressed reinforcement is constant throughout the span. Owing to friction and draw-in losses, the prestressing force at the left support is  $P=1300$  kN, at mid-span  $P=1300$  kN, and at the right support  $P=1250$  kN, as shown in [Figure 3.23c](#). The tendon has previously been bonded to the surrounding concrete by filling the duct with grout.

Two service load cases are to be considered:

- (a) a uniformly distributed load of 6 kN/m (which is the self-weight of the member);
- (b) a uniformly distributed load of 36 kN/m.

The material properties are

$$E_c = 30 \times 10^3 \text{ MPa}; E_p = E_s = 200 \times 10^3 \text{ MPa};$$

$$f'_c = 40 \text{ MPa}; f_y = 400 \text{ MPa}; f_p = 1840 \text{ MPa};$$

and the flexural tensile strength is taken to be  $0.6\sqrt{f'_c} = 3.8$  MPa.

**At support A** The applied moment is zero for both load cases and the prestressing tendon is located at the mid-depth of the section ( $d_p=400$  mm) with a prestressing force  $P=1300$  kN. Using the cross-sectional analysis described in [Section 3.5.1](#), the initial top fibre strain and curvature calculated using Equations 3.24 and 3.25 are

$$\epsilon_{oi} = -174 \times 10^{-6} \quad \text{and} \quad \kappa_i = 0.020 \times 10^{-6} \text{ mm}^{-1}$$

**At support B** The prestressing force is  $P=1250$  kN at  $d_p=400$  mm and  $M=0$ . As calculated at support A, the initial top fibre strain and curvature are

$$\epsilon_{oi} = -167 \times 10^{-6} \quad \text{and} \quad \kappa_i = 0.019 \times 10^{-6} \text{ mm}^{-1}$$

**At mid-span C** The prestressing force is  $P=1300$  kN at a depth of  $d_p=600$  mm. For load case (a),

$$M = \frac{6 \times 12^2}{8} = 108 \text{ kN m}$$

The cross-section is uncracked and from Equations 3.24 and 3.25

$$\epsilon_{oi} = -38 \times 10^{-6} \quad \text{and} \quad \kappa_i = -0.311 \times 10^{-6} \text{ mm}^{-1}$$

for load case (b),

$$M = \frac{36 \times 12^2}{8} = 648 \text{ kNm}$$

The section at mid-span is cracked and, using the iterative procedure outlined in [Section 3.5.2](#), the depth to the neutral axis is  $d_n=495$  mm. The initial top fibre strain and curvature are

$$\varepsilon_{oi} = -608 \times 10^{-6} \quad \text{and} \quad \kappa_i = 1.229 \times 10^{-6} \text{ mm}^{-1}$$

The value of  $I_{av}$  calculated from Equation 3.37 is

$$I_{av} = \frac{[(648 \times 10^6) - (1300 \times 10^3 \times 189)] \times 495}{30\,000 \times 608 \times 10^{-6}} = 10\,920 \times 10^6 \text{ mm}^4$$

**Deflection** With the initial curvature calculated at each end of the member and at mid-span, the short-term deflection for each load case is determined using Equation 3.68c. For load case (a),

$$v_c = \frac{12\,000^2}{96} [0.020 + (10 \times -0.311) + 0.019] \times 10^{-6} = -4.6 \text{ mm } (\uparrow)$$

For load case (b),

$$v_c = \frac{12\,000^2}{96} [0.020 + (10 \times 1.229) + 0.019] \times 10^{-6} = 18.5 \text{ mm } (\downarrow)$$

For load case (b), tension stiffening in the cracked region of the member near mid-span was ignored. To include tension stiffening, the moment required to cause first cracking (i.e. the moment required to produce a bottom fibre tensile stress of 3.8 MPa) is required. From an analysis of the uncracked transformed section, the cracking moment  $M_{cr}$  is 579 kN m. Using the procedure specified by the CEB (1983) for calculating  $I_e$  the  $\beta$  coefficients are  $\beta_1=1.0$  and  $\beta_2=0.5$  (assuming the member is subjected to load repetitions) and from Equations 3.74 and 3.73, respectively,

$$\zeta = 1 - 1.0 \times 0.5 \times \left(\frac{579}{648}\right)^2 = 0.601$$

$$\begin{aligned} I_e &= [(1 - 0.601) \times 14\,760 \times 10^6] + (0.601 \times 10\,920 \times 10^6) \\ &= 12\,450 \times 10^6 \text{ mm}^4 \end{aligned}$$

The revised curvature at mid-span for load case (b) is

$$\begin{aligned} \kappa_i &= \frac{M - Pe}{E_c I_{av}} = \frac{(648 \times 10^6) - (1300 \times 10^3 \times 189)}{30\,000 \times 12\,450 \times 10^6} \\ &= 1.078 \times 10^{-6} \text{ mm}^{-1} \end{aligned}$$

and the revised mid-span deflection for load case (b) is

$$v_c = \frac{12\,000^2}{96} [0.020 + (10 \times 1.078) + 0.019] \times 10^{-6} = 16.2 \text{ mm } (\downarrow)$$

### 3.8.3 Long-term deflection

Long-term deflections due to concrete creep and shrinkage are affected by many variables, including load intensity, mix proportions, member size, age at first loading, curing conditions, total quantity of compressive and tensile steel, level of prestress, relative humidity, and temperature. To account accurately for these parameters, a time analysis similar to that described in Sections 3.6.2 and 3.6.3 is required. The change in curvature during any period of sustained load may be calculated using Equation 3.50. Typical calculations are illustrated in Example 3.5 for an uncracked cross-section and in Example 3.6 for a cracked cross-section.

When the final curvature has been determined at each end of the member and at mid-span, the long-term deflection can be calculated using either Equations 3.68c, 3.69b, or 3.70b.

For reinforced concrete members, codes of practice offer simple approximate methods for obtaining ball-park estimates of long-term deflection. The long-term deflection is often taken to be equal to the short-term deflection due to the sustained or permanent loads times a multiplication factor. For example, the *long-term deflection multiplication factor* specified in ACI 318–83 for the long-term deflection after 5 years under load is

$$\lambda = \frac{2.0}{1 + 50\rho'} \quad (3.75)$$

where  $\rho'$  is the non-prestressed compressive reinforcement ratio ( $A_{sc}/bd$ ) at the mid-span for simple and continuous spans and at the support for cantilevers.

In prestressed concrete construction, a large proportion of the sustained external load is often balanced by the transverse force exerted by the tendons. Under this balanced load, the short-term deflection may be zero, but the long-term deflection is not. The restraint to creep and shrinkage offered by non-symmetrically placed, bonded reinforcement on a section can cause

significant time-dependent curvature and, hence, significant deflection of the member. The use of a simple deflection multiplier to calculate long-term deflection from the short-term deflection is therefore not satisfactory.

In this section, approximate procedures are presented which allow a rough estimate of long-term deflection. In some situations, this is all that is required. However, for most applications, the procedures in Sections 3.6.2 and 3.6.3 are recommended.

The final creep induced deflection may be approximated by

$$v_{cr} = \frac{\phi^*}{\alpha} v_{sus} \quad (3.76)$$

where  $v_{sus}$  is the short-term deflection produced by the sustained portion of the unbalanced load and  $\phi^*$  is the final creep coefficient. If a beam initially hogs upward under sustained loads (i.e.  $v_{sus}$  is upward), in general it will continue to hog upwards with time and  $v_{cr}$  will also be upward.

As seen in [Section 2.5](#), the final creep coefficient  $\phi^*$  varies from about 2.0 to 4.0, the upper end of the range for low to medium strength concrete loaded at early ages and located in a relatively dry environment. For prestressed concrete beams of average size, with  $f'_c \approx 40$  Mpa, exposed to the open air and initially loaded at ages greater than 7 days,  $\phi^*$  is typically about 2.5.

The factor  $\alpha$  in Equation 3.76 depends on the extent of cracking and the reinforcement quantity (Gilbert 1983) and may vary from 1.0 to about 3.5. For uncracked, lightly reinforced prestressed members, such as slabs, the increase in curvature due to creep is nearly proportional to the increase in strain due to creep and  $\alpha$  is little more than 1.0. For more heavily reinforced, uncracked members  $\alpha$  may be taken as 1.5. For cracked, partially prestressed members,  $\alpha$  is usually about 2.5. For members containing compression steel,  $A_{sc}$ , the creep deflection, is significantly smaller. This may be taken into account by multiplying  $\alpha$  by the factor  $1 + A_{sc}/A_s$ , where  $A_s$  is the total area of steel in the tension zone.

The deflection caused by shrinkage warping may be approximated by

$$v_{sh} = \beta \kappa_{sh}^* L^2 \quad (3.77)$$

where  $\kappa_{sh}^*$  is the shrinkage induced curvature at mid-span (or at the support of a cantilever);  $L$  is the beam span and  $\beta$  depends on the support conditions:

$\beta=0.50$	for a cantilever;
$\beta=0.125$	for a simply supported member;
$\beta=0.090$	for an end span of a continuous beam;
$\beta=0.065$	for an interior span of a continuous beam.

$\chi_{sh}^*$  is greater than zero for a non-symmetric steel layout and varies along the span as the eccentricity of the bonded tendon and the layout of non-prestressed steel varies. For uncracked prestressed members with small quantities of tensile reinforcement, an approximate estimate of the final shrinkage curvature is

$$\chi_{sh}^* = \frac{0.5\epsilon_{sh}^*}{D} \quad (3.78)$$

For cracked, partially prestressed members, with significant quantities of conventional reinforcement, the final shrinkage curvature is significantly higher and may be approximated by

$$\chi_{sh}^* = \frac{\epsilon_{sh}^*}{D}. \quad (3.79)$$

For members containing compressive reinforcement, shrinkage deflection is significantly lower and may be accounted for by multiplying  $\chi_{sh}^*$  by  $1 - A_{sc}/A_s$ .

### Example 3.9

The final time-dependent deflection of the beam described in [Example 3.8](#) and illustrated in [Figure 3.23](#) is to be calculated. As in [Example 3.8](#), two load cases are to be considered:

- (a) a uniformly distributed constant sustained load of 6 kN/m;
- (b) a uniformly distributed constant sustained load of 36 kN/m.

For each load case, the time-dependent material properties are

$$\Delta\phi = 2.5; \chi = 0.8; \epsilon_{sh} = -450 \times 10^{-6}; \text{ and } R = -30 \text{ kN}$$

All other material properties are as specified in [Example 3.8](#).

**At support A** The sustained moment at *A* is zero for both load cases and the initial prestress is  $P=1300$  kN at  $d_p$  400 mm. The time-dependent changes of top fibre strain and curvature calculated using Equations 3.49 and 3.50 are

$$\Delta\epsilon_o = -754 \times 10^{-6} \quad \text{and} \quad \Delta\chi = 0.250 \times 10^{-6} \text{ mm}^{-1}$$

The final top fibre strain and curvature are

$$\epsilon_{oi} + \Delta\epsilon_o = -928 \times 10^{-6} \quad \text{and} \quad \chi_i + \Delta\chi = 0.270 \times 10^{-6} \text{ mm}^{-1}$$



**At support B** As for support A, the sustained moment is zero, but the initial prestress is  $P=1250$  kN. Equations 3.49 and 3.50 give

$$\Delta \epsilon_o = -740 \times 10^{-6} \quad \text{and} \quad \Delta \kappa = 0.245 \times 10^{-6} \text{ mm}^{-1}$$

and therefore

$$\epsilon_{oi} + \Delta \epsilon_o = -907 \times 10^{-6} \quad \text{and} \quad \kappa_i + \Delta \kappa = 0.264 \times 10^{-6} \text{ mm}^{-1}$$

**At mid-span** For load case (a),  $M=108$  kNm and  $P=1300$  kN at  $d_p=600$  mm. For this uncracked section,

$$\Delta \epsilon_o = -586 \times 10^{-6} \quad \text{and} \quad \Delta \kappa = -0.129 \times 10^{-6} \text{ mm}^{-1}$$

and therefore

$$\epsilon_{oi} + \Delta \epsilon_o = -624 \times 10^{-6} \quad \text{and} \quad \kappa_i + \Delta \kappa = -0.440 \times 10^{-6} \text{ mm}^{-1}$$

For load case (b), the sustained moment is  $M=648$  kNm and for the cracked cross-section, Equations 3.49 and 3.50 give

$$\Delta \epsilon_o = -1520 \times 10^{-6} \quad \text{and} \quad \Delta \kappa = 2.13 \times 10^{-6} \text{ mm}^{-1}$$

and therefore

$$\epsilon_{oi} + \Delta \epsilon_o = -2130 \times 10^{-6} \quad \text{and} \quad \kappa_i + \Delta \kappa = 3.36 \times 10^{-6} \text{ mm}^{-1}$$

**Deflection** With the final curvature calculated at each end of the member and at mid-span, the long-term deflection at mid-span for each load case is found using Equation 3.68c. For load case (a),

$$v_c = \frac{12\,000^2}{96} [0.270 + (10 \times -0.440) + 0.264] \times 10^{-6} = -5.8 \text{ mm } (\uparrow)$$

For load case (b),

$$v_c = \frac{12\,000^2}{96} [0.270 + (10 \times 3.36) + 0.264] \times 10^{-6} = 51.1 \text{ mm } (\downarrow)$$

Consider the more approximate predictions made using Equations 3.76–3.79. The creep induced deflection is estimated using Equation 3.76. For load case (a), the member is uncracked with significant quantities of

non-prestressed steel. The factor  $\alpha$  is taken to be

$$\alpha = 1.5 \left( 1 + \frac{A_{sc}}{A_s} \right) = 1.5 \left( 1 + \frac{900}{2800} \right) = 2.0$$

From [Example 3.8](#),  $v_{sus} = -4.6$  mm and with  $\phi^* = 2.5$ , Equation 3.76 gives

$$v_{cr} = \frac{2.5}{2.0} \times -4.6 = -5.8 \text{ mm } (\uparrow)$$

For load case (b), the cross-section at mid-span is cracked and the factor  $\alpha$  is taken as

$$\alpha = 2.5 \left( 1 + \frac{A_{sc}}{A_s} \right) = 2.5 \left( 1 + \frac{900}{2800} \right) = 3.3$$

From [Example 3.8](#),  $v_{sus} = 18.5$  mm and therefore

$$v_{cr} = \frac{2.5}{3.3} \times 18.5 = 14.0 \text{ mm } (\downarrow)$$

For load case (a), the shrinkage induced curvature is given by Equation 3.78:

$$\kappa_{sh} = \frac{0.5 \times 450 \times 10^{-6}}{800} \left( 1 - \frac{900}{2800} \right) = 0.191 \times 10^{-6} \text{ mm}^{-1}$$

and from Equation 3.77,

$$v_{sh} = 0.125 \times 0.191 \times 10^{-6} \times 12\,000^2 = 3.4 \text{ mm } (\downarrow)$$

For load case (b), Equations 3.79 and 3.77 give, respectively,

$$\kappa_{sh} = \frac{450 \times 10^{-6}}{800} \left( 1 - \frac{900}{2800} \right) = 0.382 \times 10^{-6} \text{ mm}^{-1}$$

and

$$v_{sh} = 0.125 \times 0.382 \times 10^{-6} \times 12\,000^2 = 6.9 \text{ mm } (\downarrow)$$

The final long-term deflection for each load case is the sum of the initial deflection and the creep and shrinkage deflection increments.

For load case (a),

$$v_c = -4.6 - 5.8 + 3.4 = -7.0 \text{ mm } (\uparrow)$$

(cf.  $v_c = -5.8$  mm from the more accurate approach).

For load case (b),

$$v_c = 18.5 + 14.0 + 6.9 = 39.4 \text{ mm } (\downarrow)$$

which is almost 30% smaller than the estimate made using the more accurate procedure.

### 3.9 References

- ACI 318–83 1983. *Building code requirements for reinforced concrete*. Detroit: American Concrete Institute.
- AS 1481–1978. *SAA prestressed concrete code*. Sydney: Standards Association of Australia.
- AS 3600–1988. *Australian standard for concrete structures*. Sydney: Standards Association of Australia.
- Bazant, Z.P. 1972. Prediction of concrete creep effects using age-adjusted effective modulus method. *ACI Journal* **69**, 212–17.
- Branson, D.E. 1963. *Instantaneous and time-dependent deflection of simple and continuous reinforced concrete beams*. Alabama Highway Research Report, No. 7. Alabama: Bureau of Public Roads.
- Bresler, B. & L.Selna 1964. *Analysis of time dependent behaviour of reinforced concrete structures*. Symposium on Creep of Concrete, ACI Special Publication SP-9, Detroit, American Concrete Institute, pp. 115–28.
- Comité Euro-International du Béton (CEB) 1983. *Fissuration et deformations*. Manuel du CEB. Lausanne: Ecole Polytechnique Fédérale de Lausanne.
- Ghali, A. & M.K.Tadros 1985. Partially prestressed concrete structures. *Journal of Structural Engineering, ASCE* **111**, 1846–65.
- Ghali, A. & R.Favre 1986. *Concrete structures: stresses and deformations*. London: Chapman and Hall.
- Gilbert, R.I. 1983. Deflection calculations for reinforced concrete beams, *Civil Engineering Transactions, Institution of Engineers, Australia* **CE25**, 128–34.
- Gilbert, R.I. 1986. Prestress losses in partially-prestressed concrete beams. *Proceedings of the 10th Australasian Conference on the Mechanics of Structures and Materials, Adelaide, University of Adelaide, South Australia*, pp. 409–16.
- Gilbert, R.I. 1988. *Time effects in concrete structures*. Amsterdam: Elsevier.
- Khachaturian, N. & G.Gurfinkel 1969. *Prestressed concrete*. New York: McGraw-Hill.
- Lin, T.Y. 1963. *Prestressed concrete structures*. New York: Wiley.
- Magnel, G. 1954. *Prestressed concrete, 3rd edition*. London: Concrete Publications Ltd.
- Neville, A.M., W.H.Dilger & J.J.Brooks 1983. *Creep of plain and structural concrete*. London: Construction Press.
- Warner, R.F. & K.A.Faulkes 1979. *Prestressed concrete*. Melbourne: Pitman Australia.

## 4

# Ultimate flexural strength

### 4.1 Introduction

The single most important design objective for a structure or a component of a structure is the provision of adequate strength. The consequences and costs of strength failures are large and therefore the probability of such failures must be very small.

The satisfaction of concrete and steel stress limits at service loads does not necessarily ensure adequate strength and does not provide a reliable indication of either the actual strength or the safety of a structural member. It is important to consider the non-linear behaviour of the member in the over-loaded range to ensure that it has an adequate structural capacity. Only by calculating the ultimate capacity of a member can a sufficient margin between the service load and the ultimate load be guaranteed.

In the 1950s and 1960s, there was a gradual swing away from the use of elastic stress calculations for the satisfaction of the design objective of adequate strength. The so-called *ultimate strength design approach* emerged as the most appropriate procedure. The ultimate strength of a cross-section in bending  $M_u$  is calculated from a rational and well established *flexural strength theory*, which involves consideration of the strength of both the concrete and the steel in the compressive and tensile parts of the cross-section. The prediction of ultimate flexural strength is described and illustrated in this chapter. When  $M_u$  is determined, the design requirements for the strength limit state (as discussed in [Section 1.7.6](#)) may be checked and satisfied.

In addition to calculating the strength of a section, a measure of the ductility of each section must also be established. Ductility is an important objective in structural design. Ductile members undergo large deformations prior to failure, thereby providing warning of failure and allowing indeterminate structures to establish alternative load paths. In fact, it is only with adequate ductility that the predicted strength of indeterminate members and structures can be achieved in practice.

### 4.2 Flexural behaviour at overloads

The load at which collapse of a flexural member occurs is called the *ultimate load*. If the member has sustained large deformations prior to collapse, it is said to have ductile behaviour. If, on the other hand, it has only undergone small deformations prior to failure, the member is said to have brittle behaviour. There is no defined deformation or curvature which distinguishes ductile from brittle behaviour. Codes of practice, however, usually impose a ductility requirement by limiting the curvature at ultimate to some minimum value, thereby ensuring that significant deformation occurs in a flexural member prior to failure. Since beam failures that result from a breakdown of bond between the concrete and the steel reinforcement, or from excessive shear, or from failure of the anchorage zone tend to be brittle in nature, every attempt should be made to ensure that the region of maximum moment is the *weakest link*. The design philosophy should ensure therefore that a member does not fail before the required design moment capacity of the section is attained.

Consider the prestressed concrete cross-section shown in [Figure 4.1](#). The section contains non-prestressed reinforcement in the compressive and tensile zones and bonded tensile prestressing steel. Also shown in [Figure 4.1](#) are typical strain and stress distributions for four different values of applied

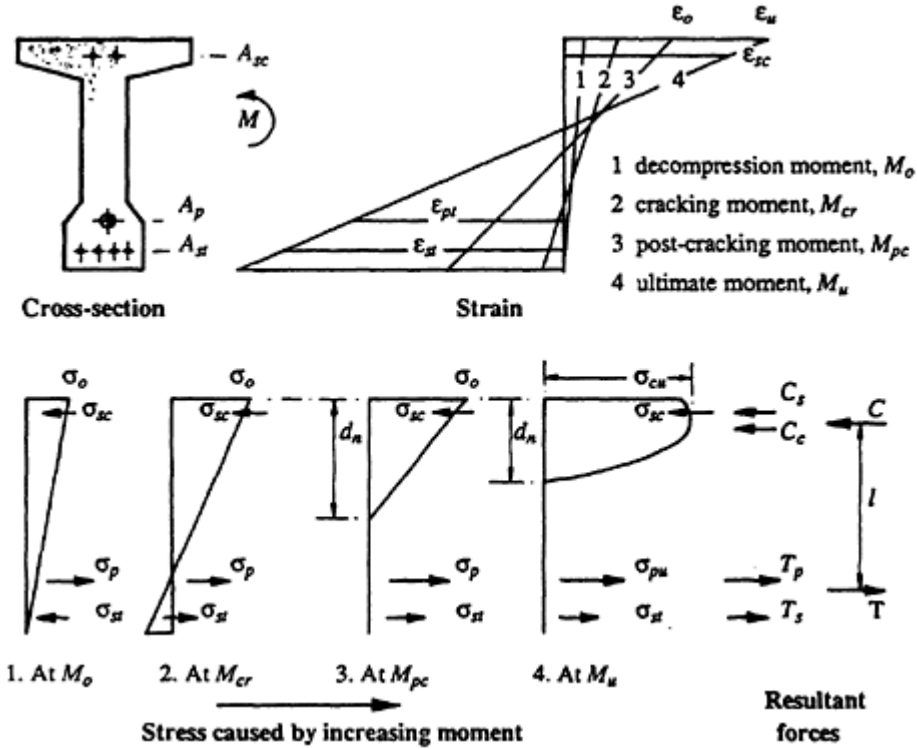


Figure 4.1 Stress and strain distributions caused by increasing moment.

moment. As the applied moment  $M$  increases from typical in-service levels into the overload range, the neutral axis gradually rises and eventually material behaviour becomes non-linear. The non-prestressed steel may yield if the strain  $\varepsilon_{st}$  exceeds the yield strain ( $\varepsilon_y = f_y/E_s$ ), the prestressed steel may enter the non-linear part of its stress-strain curve as  $\varepsilon_p$  increases, and the concrete compressive stress distribution becomes non-linear when the extreme fibre stress exceeds about  $0.5f'_c$ .

A flexural member which is designed to exhibit ductility at failure usually has failure of the critical section preceded by yielding of the bonded tensile steel, i.e. by effectively exhausting the capacity of the tensile steel to carry any additional force. Such a member is said to be under-reinforced. Because the stress-strain curve for the prestressing steel has no distinct yield point and the stress increases monotonically as the strain increases (see [Figure 2.13](#)), the capacity of the prestressing steel to carry additional force is never entirely used up until the steel actually fractures. However, when the steel strain  $\varepsilon_p$  exceeds about 0.01 (for wire or strand), the stress-strain curve becomes relatively flat and the rate of increase of stress with strain is small. After yielding, the resultant internal tensile force,  $T (=T_s + T_p)$  in [Figure 4.1](#), remains approximately constant (as does the resultant internal compressive force  $C$ , which is equal and opposite to  $T$ ). The moment capacity can be further increased by an increase in the lever arm between  $C$  and  $T$ . Under increasing deformation, the neutral axis rises, the compressive zone becomes smaller and smaller and the compressive concrete stress increases. Eventually, perhaps after considerable deformation, a compressive failure of the concrete above the neutral axis occurs and the section reaches its ultimate capacity. It is, however, the strength of the prestressing tendons and the non-prestressed reinforcement in the tensile zone that control the strength of a ductile section. In fact, the difference between the moment at first yielding of the tensile steel and the ultimate moment is usually small.

A flexural member which is over-reinforced, on the other hand, does not have significant ductility at failure and fails without the prestressed or non-prestressed tensile reinforcement reaching any form of yield. At the ultimate load condition, both the tensile strain at the steel level and the section curvature are relatively small and, consequently, there is little deformation or warning of failure.

Because it is the deformation at failure that defines ductility, it is both usual and reasonable in design to define a minimum ultimate curvature to ensure the ductility of a cross-section. This is often achieved by placing a maximum limit on the depth to the neutral axis at the ultimate load condition. Ductility can be increased by the inclusion of non-prestressed reinforcing steel in the compression zone of the beam. With compressive steel included, the internal compressive force  $C$  is shared between the concrete and the steel. The volume of the concrete stress block above the neutral axis

is therefore reduced and, consequently, the depth to the neutral axis is decreased. Some compressive reinforcement is normally included in beams to provide anchorage for transverse shear reinforcement.

Ductility is desirable in prestressed (and reinforced) concrete flexural members. In continuous or statically indeterminate members, ductility is particularly necessary. Large curvatures are required at the peak moment regions in order to permit the inelastic moment redistribution that must occur if the moment diagram assumed in design is to be realized in practice.

Consider the stress distribution caused by the ultimate moment on the section in [Figure 4.1](#). The resultant compressive force of magnitude  $C$  equals the resultant tensile force  $T$  and the ultimate moment capacity is calculated from the internal couple,

$$M_u = Cl = Tl \quad (4.1)$$

The lever arm  $l$  between the internal compressive and tensile resultants ( $C$  and  $T$ ) is usually about  $0.9d$ , where  $d$  is the *effective depth* of the section and may be defined as the distance from the extreme compressive fibre to the position of the resultant tensile force in all the steel on the tensile side of the neutral axis. To find the lever arm  $l$  more accurately, the location of the resultant compressive force in the concrete  $C_c$  needs to be determined. The shape of the actual stress-strain relationship for concrete in compression is required in order to determine the position of its centroid.

## 4.3 Flexural strength theory

### 4.3.1 Assumptions

In the analysis of a cross-section to determine its ultimate bending strength  $M_u$ , the following assumptions are usually made:

- (a) The variation of strain on the cross-section is linear, i.e. strains in the concrete and the bonded steel are calculated on the assumption that plane sections remain plane.
- (b) Concrete carries no tensile stress, i.e. the tensile strength of the concrete is ignored.
- (c) The stress in the compressive concrete and in the steel reinforcement (both prestressed and non-prestressed) are obtained from actual or idealized stress-strain relationships for the respective materials.

### 4.3.2 Idealized rectangular compressive stress blocks for concrete

In order to simplify numerical calculations for ultimate flexural strength, codes of practice usually specify idealized rectangular stress blocks for the

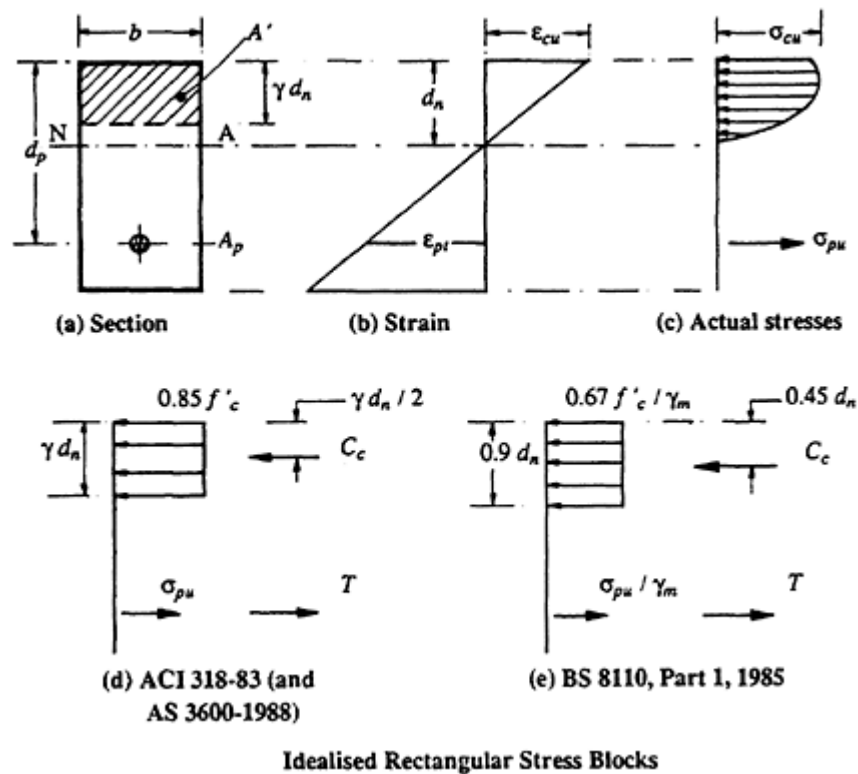


**Figure 4.2** Ultimate moment conditions and rectangular stress blocks.

compressive concrete above the neutral axis. The dimensions of the stress block are calibrated such that the volume of the stress block and the position of its centroid are approximately the same as in the real curvilinear stress block.

In [Figure 4.2a](#), an under-reinforced section at the ultimate moment is shown. The section has a single layer of bonded prestressing steel. The strain diagram and the actual concrete stress distribution at ultimate are illustrated in [Figures 4.2b](#) and [c](#), respectively. The idealized rectangular stress block for the compressive concrete at the ultimate flexural limit state specified in both ACI 318–83 and AS 3600–1988 is shown in [Figure 4.2d](#), and that specified in BS 8110: Part 1 (1985) is illustrated in [Figure 4.2e](#).

At the ultimate moment, the extreme fibre compressive strain  $\epsilon_{cu}$  is taken in ACI 318–83 (and in AS 3600–1988) to be

$$\epsilon_{cu} = 0.003$$

while in BS 8110: Part 1 (1985),  $\epsilon_{cu}$  is taken to be 0.0035. In fact, the actual extreme fibre strain at ultimate may not be close to either of these values. However, for under-reinforced members, with the flexural strength very much controlled by the strength of the tensile steel (both prestressed and



non-prestressed), variation in the assumed value of  $\varepsilon_{cu}$  does not have a significant effect on  $M_u$ .

The depth of the ACI 318–83's rectangular stress block (in [Figure 4.2d](#)) is  $\gamma d_n$  and the uniform stress intensity is  $0.85f'_c$ . The parameter  $\gamma$  depends on the concrete strength and may be taken as

$$\begin{aligned}\gamma &= 0.85 - 0.007(f'_c - 28) \\ 0.65 &\leq \gamma \leq 0.85\end{aligned}\quad (4.2)$$

$\gamma$  is given in [Table 4.1](#) for some standard concrete strength grades.

For the rectangular section of [Figure 4.2a](#), the hatched area  $A'$  ( $=\gamma d_n b$ ) is therefore assumed to be subjected to a uniform stress of  $0.85f'_c$  and the resultant compressive force  $C_c$  is the volume of the rectangular stress block.

Therefore,

$$C_c = 0.85f'_c b \gamma d_n \quad (4.3)$$

and the position of  $C_c$  is the centroid of the hatched area  $A'$ , i.e. at a depth of  $\gamma d_n/2$  below the extreme compressive fibre (provided, of course, that  $A'$  is rectangular).

The ultimate moment is obtained from Equation 4.1:

$$M_u = Tl = \sigma_{pu} A_p \left( d_p - \frac{\gamma d_n}{2} \right) \quad (4.4)$$

where  $\sigma_{pu}$  is the stress in the bonded tendons and is determined from considerations of strain compatibility and equilibrium.

In accordance with the design philosophy for the strength limit states outlined in [Section 1.7.6](#), the *design strength* is obtained by multiplying  $M_u$  from Equation 4.4 by a capacity reduction factor  $\phi$ . In ACI 318–83,  $\phi = 0.9$  for flexure (and  $\phi = 0.8$  in AS 3600–1988).

The ultimate curvature is the slope of the strain diagram at failure and is therefore given by

$$\kappa_u = \frac{\varepsilon_{cu}}{d_n} = \frac{0.003}{d_n} \quad (4.5)$$

**Table 4.1** Variation of  $\gamma$  with  $f'_c$ .

$f'_c$ (MPa)	20	25	30	35	40	50
$\gamma$	0.85	0.85	0.836	0.80	0.766	0.696

The ultimate curvature  $x_u$  is an indicator of ductility. Large deformations at ultimate are associated with ductile failures. To ensure ductility of a section at failure, codes of practice specify minimum limits for  $x_u$ . For example, ACI 318–83 limits curvature indirectly by limiting the quantity of tensile reinforcement, thereby placing a maximum limit of  $0.424d$  on the depth to the neutral axis at failure. The Australian code AS 3600–1988 suggests that  $d_n$  should not exceed  $0.4d_p$ . This is equivalent to suggesting that  $x_u$  should be greater than or equal to

$$(x_u)_{min} = \frac{0.003}{0.4d_p} = \frac{0.0075}{d_p} \quad (4.6)$$

For the cross-section shown in [Figure 4.2](#), the effective depth  $d$  equals the depth to the prestressing steel,  $d_p$ .

The rectangular stress block specified in BS 8110: Part 1 (1985) is shown in [Figure 4.2e](#). It has an overall depth of  $0.9d_n$  and a uniform stress intensity of  $0.67f_c'/\gamma_m$ . The parameter  $\gamma_n$  is the partial material safety factor for concrete and equals 1.5 (see [Section 1.7.6](#)). The stress in the bonded prestressing steel is  $\sigma_{pu}/\gamma_m$ , where  $\gamma_m=1.15$  for steel. The design strength of the member [designated  $M_u$  in BS 8110: Part 1 (1985) but equivalent to  $\phi M_u$  in ACI 318–83] is therefore given by

$$M_u = \frac{\sigma_{pu}}{1.15} A_p \left( d_p - \frac{0.45d_n}{2} \right) \quad (4.7)$$

In the remainder of this chapter, the idealized rectangular stress block and the design procedure specified in ACI 318–83 (and in AS 3600–1988) will be adopted for all numerical examples.

### 4.3.3 Prestressed steel strain components

For reinforced concrete sections, the strain in the non-prestressed steel and in the concrete at the steel level are the same at any stage of loading. For the prestressing tendons on a prestressed concrete section, this is not so. The strain in the bonded prestressing steel at any stage of loading is equal to the strain caused by the initial prestress plus the change in strain in the concrete at the steel level.

To calculate accurately the ultimate flexural strength of a section, an accurate estimate of the final strain in the prestressed and non-prestressed steel is required. The tensile strain in the prestressing steel at ultimate  $\varepsilon_{pu}$  is very much larger than the tensile strain in the concrete at the steel level, owing to the large initial prestress. For a bonded tendon,  $\varepsilon_{pu}$  is usually considered to be the sum of several sub-components. [Figure 4.3](#) indicates the strain distributions on a prestressed section at three stages of loading.

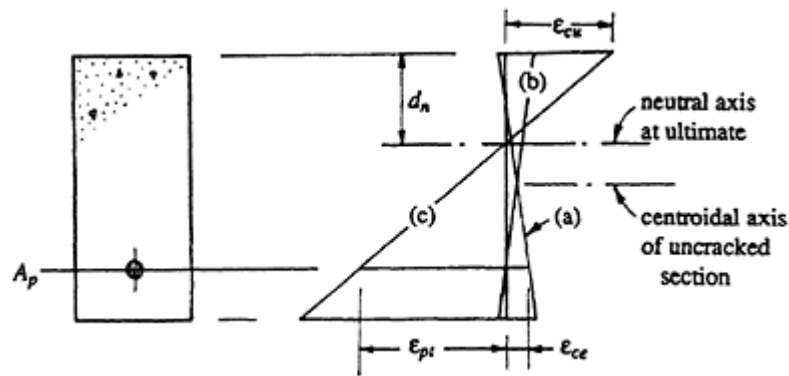


**Figure 4.3** Strain distributions at three stages of loading.

Stage (a) shows the elastic concrete strain caused by the effective prestress when the externally applied moment is zero. The strain in the concrete at the steel level is compressive, with magnitude equal to

$$\epsilon_{ce} = \frac{1}{E_c} \left( \frac{P_e}{A} + \frac{P_e e^2}{I} \right) \quad (4.8)$$

where  $A$  is the area of the section and  $I$  is the second moment of area of the section about its centroidal axis. The stress and strain in the prestressing steel are

$$\sigma_{pe} = \frac{P_e}{A_p} \quad \text{and} \quad \epsilon_{pe} = \frac{\sigma_{pe}}{E_p} \quad (4.9)$$

provided that the steel stress is within the elastic range.

Stage (b) is the concrete strain distribution when the applied moment is sufficient to decompress the concrete at the steel level. Provided that there is bond between the steel and the concrete, the change in strain in the prestressing steel is equal to the change in concrete strain at the steel level. The strain in the prestressing steel at stage (b) is therefore equal to the value at stage (a) plus a tensile increment of strain equal in magnitude to  $\epsilon_{ce}$  (from Equation 4.8).

Strain diagram (c) in [Figure 4.3](#) corresponds to the ultimate load condition. The concrete strain at the steel level  $\epsilon_{pt}$  can be expressed in terms of the extreme compressive fibre strain  $\epsilon_{cu}$  and the depth to the neutral axis at failure  $d_n$  as

$$\epsilon_{pt} = \epsilon_{cu} \left( \frac{d_p - d_n}{d_n} \right) \quad (4.10)$$

From the requirements of strain compatibility, the change in strain in the

prestressing steel between load stages (b) and (c) is also equal to  $\varepsilon_{pt}$ . Therefore, the strain in the prestressing tendon at the ultimate load condition may be obtained from

$$\varepsilon_{pu} = \varepsilon_{pe} + \varepsilon_{ce} + \varepsilon_{pt} \quad (4.11)$$

$\varepsilon_{pu}$  can therefore be determined in terms of the position of the neutral axis at failure  $d_n$  and the extreme compressive fibre strain  $\varepsilon_{cu}$ . If  $\varepsilon_{pu}$  is known, the stress in the prestressing steel at ultimate  $\sigma_{pu}$  can be determined from the stress-strain diagram for the prestressing steel. With the area of prestressing steel known, the tensile force at ultimate  $T_p$  can be calculated. In general, however, the steel stress is not known at failure and it is necessary to equate the tensile force in the steel tendon (plus the tensile force in any non-prestressed tensile steel) with the concrete compressive force (plus the compressive force in any non-prestressed compressive steel) in order to locate the neutral axis depth, and hence find  $\varepsilon_{pu}$ .

In general, the magnitude of  $\varepsilon_{ce}$  in Equation 4.11 is very much less than either  $\varepsilon_{pe}$  or  $\varepsilon_{pt}$ , and may usually be ignored without introducing serious errors.

#### 4.3.4 Determination of $M_u$ for a singly reinforced section with bonded tendons

Consider the section shown in [Figure 4.2a](#) and the idealized compressive stress block shown in [Figure 4.2d](#). In order to calculate the ultimate bending strength using Equation 4.4, the depth to the neutral axis  $d_n$  and the final stress in the prestressing steel  $\sigma_{pu}$  must first be determined.

An iterative trial and error procedure is usually used to determine the value of  $d_n$  for a given section. The depth to the neutral axis is adjusted until horizontal equilibrium is satisfied, i.e.  $C=T$ . Both  $C$  and  $T$  are functions of  $d_n$ . For this singly reinforced cross-section,  $C$  is the volume of the compressive stress block given by Equation 4.3 and  $T$  depends on the strain in the prestressing steel,  $\varepsilon_{pu}$ . For any value of  $d_n$ , the strain in the prestressing steel is calculated using Equation 4.11 (and Equations 4.8–4.10). The steel stress at ultimate  $\sigma_{pu}$  which corresponds to the calculated value of strain  $\varepsilon_{pu}$ , can be obtained from the stress-strain curve for the prestressing steel and the corresponding tensile force is  $T=\sigma_{pu}A_p$ .

When the correct value of  $d_n$  is found (i.e. when  $C=T$ ), the ultimate flexural strength  $M_u$  may be calculated from Equation 4.4.

A suitable iterative procedure is outlined below. About three iterations are usually required to determine a good estimate of  $d_n$  and hence  $M_u$ .

- (1) Select an *appropriate* trial value of  $d_n$  and determine  $\varepsilon_{pu}$  from Equation 4.11. By equating the tensile force in the steel to the compressive

force in the concrete, the stress in the tendon may be determined:

$$T = \sigma_{pu} A_p = C = 0.85 f'_c b \gamma d_n$$

$$\therefore \sigma_{pu} = \frac{0.85 f'_c b \gamma d_n}{A_p}$$

- (2) Plot the point  $\epsilon_{pu}$  and  $\sigma_{pu}$  on the graph containing the stress-strain curve for the prestressing steel. If the point falls on the curve, then the value of  $d_n$  selected in step 1 is the correct one. If the point is not on the curve, then the stress-strain relationship for the prestressing steel is not satisfied and the value of  $d_n$  is not correct.
- (3) If the point  $\epsilon_{pu}$  and  $\sigma_{pu}$  obtained in step 2 is not sufficiently close to the stress-strain curve for the steel, repeat steps 1 and 2 with a new estimate of  $d_n$ . A larger value for  $d_n$  is required if the point plotted in step 2 is below the stress-strain curve and a smaller value is required if the point is above the curve.
- (4) Interpolate between the plots from steps 2 and 3 to obtain a close estimate for  $\epsilon_{pu}$  and  $\sigma_{pu}$  and the corresponding value for  $d_n$ .
- (5) With the correct values of  $\sigma_{pu}$  and  $d_n$  determined in step 4, calculate the ultimate moment  $M_u$ . If the area above the neutral axis is rectangular,  $M_u$  is obtained from Equation 4.4. Non-rectangular-shaped cross-sections are discussed in more detail in [Section 4.6](#).

**Example 4.1**

The ultimate flexural strength  $M_u$  of the rectangular section of [Figure 4.4a](#) is to be calculated. The steel tendon consists of ten 12.7 mm diameter strands ( $A_p=1000 \text{ mm}^2$ ) with an effective prestress  $P_e=1200 \text{ kN}$ . The

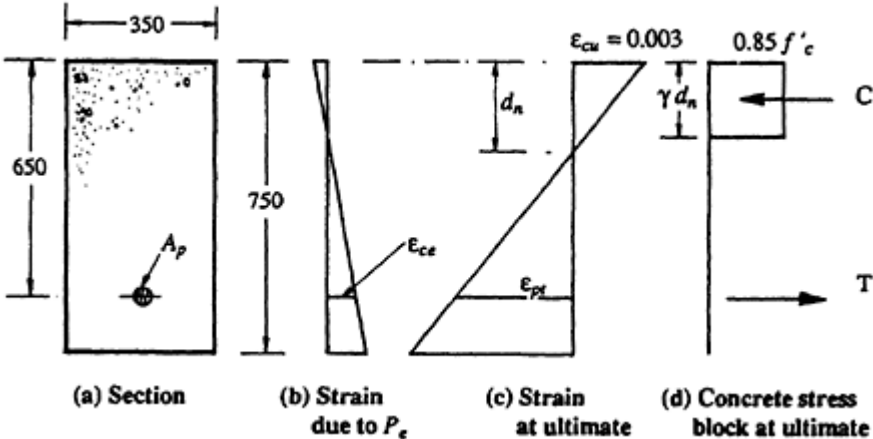


**Figure 4.4** Section details and stress and strain distributions at ultimate ([Example 4.1](#)).

stress–strain relationship for prestressing steel is as shown in [Figure 4.5](#) and the elastic modulus is  $E_p=195\times 10^3$  MPa. The concrete properties are  $f'_c = 35$ MPa,  $E_c=29800$  MPa, and from Equation 4.2,  $\gamma=0.801$ .

The initial strain in the tendons due to the effective prestress is given by Equation 4.9:

$$\varepsilon_{pe} = \frac{P_e}{E_p A_p} = \frac{1200 \times 10^3}{195 \times 10^3 \times 1000} = 0.00615$$

The strain in the concrete caused by the effective prestress at the level of the prestressing steel ( $\varepsilon_{ce}$  in [Figure 4.4b](#)) is calculated using Equation 4.8. Because  $\varepsilon_{ce}$  is very small compared with  $\varepsilon_{pe}$ , it is usually acceptable to use the properties of the gross cross-section for its determination. Therefore,

$$\varepsilon_{ce} = \frac{1}{29800} \left( \frac{1200 \times 10^3}{750 \times 350} + \frac{1200 \times 10^3 \times 275^2}{750^3 \times 350/12} \right) = 0.00040$$

The concrete strain at the prestressed steel level at failure is obtained from Equation 4.10:

$$\varepsilon_{pt} = 0.003 \left( \frac{650 - d_n}{d_n} \right)$$

and the final strain in the prestressing steel is given by Equation 4.11:

$$\varepsilon_{pu} = 0.00655 + 0.003 \left( \frac{650 - d_n}{d_n} \right)$$

The magnitude of resultant compressive force  $C$  carried by the concrete on the rectangular section is the volume of the idealized rectangular stress block in [Figure 4.4d](#) and is given by Equation 4.3:

$$C = 0.85 \times 35 \times 350 \times 0.801 \times d_n = 8340d_n$$

The resultant tensile force  $T$  is given by

$$T = A_p \sigma_{pu} = 1000 \sigma_{pu}$$

Horizontal equilibrium requires that  $C=T$  and hence

$$\sigma_{pu} = 8.34d_n$$

Trial values of  $d_n$  can now be selected and the corresponding values of  $\varepsilon_{pu}$  and  $\sigma_{pu}$  (calculated from the above two equations) are plotted on the

stress–strain curve for the steel, as shown in [Figure 4.5](#):

Trial $d_n$ (mm)	$\epsilon_{pu}$	$\sigma_{pu}$ (MPa)	Point plotted on <a href="#">Figure 4.5</a>
230	0.0120	1918	(1)
210	0.0128	1751	(2)
220	0.0124	1835	(3)

Point 3 lies sufficiently close to the stress–strain curve for the tendon and therefore the correct value for  $d_n$  is close to 220 mm ( $0.34 d_p$ ).

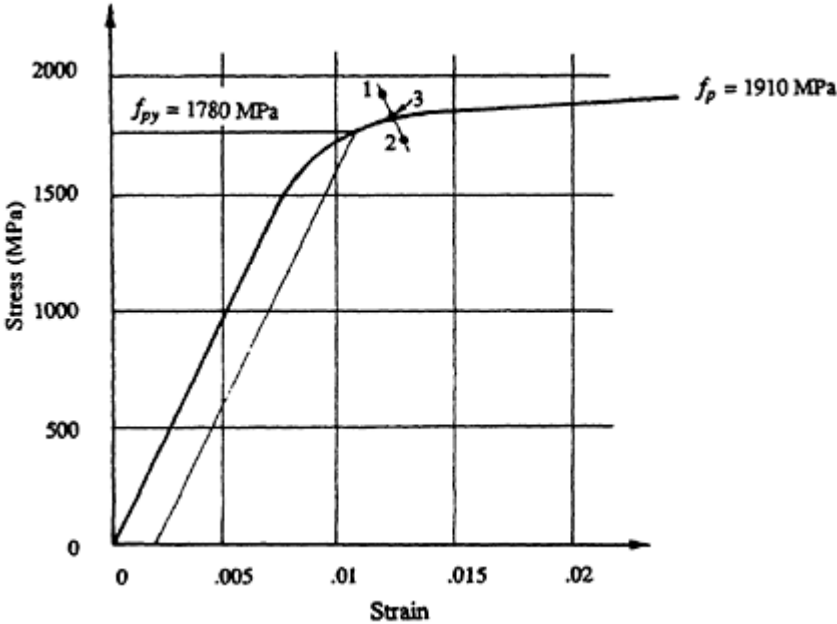


**Figure 4.5** Stress–strain curve for strand ([Example 4.1](#)).

From Equation 4.5, the curvature at ultimate is

$$x_u = \frac{0.003}{220} = 13.6 \times 10^{-6} \text{ mm}^{-1}$$

which is greater than the minimum value required for ductility given by Equation 4.6,

$$(x_u)_{min} = \frac{0.0075}{650} = 11.5 \times 10^{-6} \text{ mm}^{-1}$$

The ultimate moment is found using Equation 4.4:

$$M_u = 1835 \times 1000 \left( 650 - \frac{0.801 \times 220}{2} \right) \times 10^{-6} = 1030 \text{ kN m}$$

The design strength of the section in flexure is  $\phi M_u$ , where the value of  $\phi$  for bending can be obtained from [Table 1.1](#). In structural design, the moment  $M^*$  caused by the most severe factored load combination for strength (see [Section 1.7.3](#)) must be less than or equal to  $\phi M_u$ .

#### 4.3.5 Sections containing non-prestressed reinforcement and bonded tendons

Frequently, in addition to the prestressing reinforcement, prestressed concrete beams contain non-prestressed longitudinal reinforcement in both the compressive and tensile zones. This reinforcement may be included for a variety of reasons. For example, non-prestressed reinforcement is included in the tensile zone to provide additional flexural strength when the strength provided by the prestressing steel is not adequate. Non-prestressed tensile steel is also included to improve crack control when cracking is anticipated at service loads. Non-prestressed compressive reinforcement may be used to strengthen the compressive zone in beams that might otherwise be over-reinforced. In such beams, the inclusion of compression reinforcement not only increases the ultimate strength, but also causes increased curvature at failure and therefore improves ductility. The use of compressive reinforcement also reduces long-term deflections caused by creep and shrinkage and therefore improves serviceability. If for no other reason, compression reinforcement may be included to provide anchorage and bearing for the transverse reinforcement (stirrups) in beams.

When compressive reinforcement is included, closely spaced transverse ties should be used to brace laterally the highly stressed bars in compression and prevent them from buckling outward. In general, the spacing of these ties should not exceed about 16 times the diameter of the compressive bar.

Consider the *doubly reinforced* section shown in [Figure 4.6a](#). The resultant compressive force consists of a steel component  $C_s (= \sigma_{sc} A_{sc})$  and a concrete component  $C_c (= 0.85 f'_c b \gamma d_n)$ . The stress in the compressive reinforcement is determined from the geometry of the linear strain diagram shown in [Figure 4.6b](#). The magnitude of strain in the compressive steel is

$$\epsilon_{sc} = \frac{0.003(d_n - d_c)}{d_n} \quad (4.12)$$

If  $\epsilon_{sc}$  is less than or equal to the yield strain of the non-prestressed steel ( $\epsilon_y = f_y / E_s$ ), then  $\sigma_{sc} = \epsilon_{sc} E_s$ . If  $\epsilon_{sc}$  exceeds the yield strain, then  $\sigma_{sc} = f_y$ .



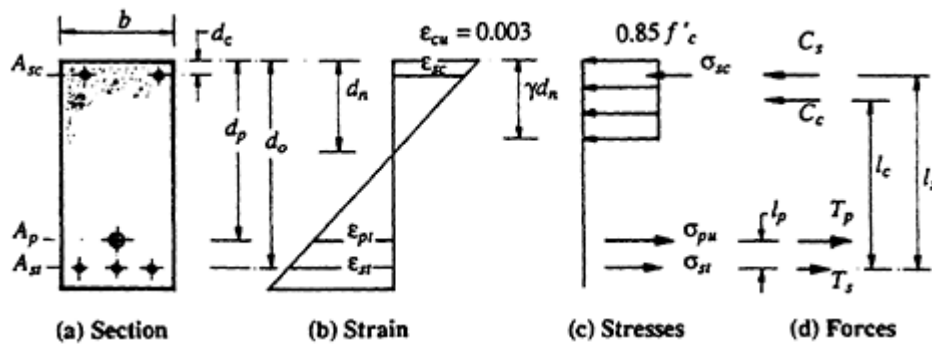


Figure 4.6 Doubly reinforced section at ultimate.

The resultant tensile force in [Figure 4.6d](#) consists of a prestressed component  $T_p (= \sigma_{pu} A_p)$  and a non-prestressed component  $T_s (= \sigma_{st} A_{st})$ . The stress in the non-prestressed steel is determined from the strain at ultimate,  $\epsilon_{st}$ , which is given by

$$\epsilon_{st} = \frac{0.003(d_o - d_n)}{d_n} \quad (4.13)$$

If  $\epsilon_{st} \leq \epsilon_y$ , then  $\sigma_{st} = \epsilon_{st} E_s$ . If  $\epsilon_{st} > \epsilon_y$ , then  $\sigma_{st} = f_y$ .

In order to calculate the depth to the neutral axis at ultimate,  $d_n$ , a trial and error procedure similar to that outlined in [Section 4.3.4](#) can be employed. Successive values of  $d_n$  are tried until the value which satisfies the horizontal equilibrium equation is determined:

$$T_p + T_s = C_c + C_s \quad (4.14)$$

Since one of the reasons for the inclusion of compressive reinforcement is to improve ductility, most doubly reinforced beams are, or should be, under-reinforced, i.e. the non-prestressed tensile steel is at yield at ultimate. Whether or not the compressive steel has yielded depends on its quantity  $A_{sc}$  and its depth from the top compressive surface of the section,  $d_c$ .

If it is assumed initially that both the compressive and the tensile non-prestressed steel are at yield, then

$$C_s = f_y A_{sc} \quad \text{and} \quad T_s = f_y A_{st}$$

From Equation 4.14:

$$C_c = T_p + T_s - C_s$$

$$0.85 f'_c b \gamma d_n = \sigma_{pu} A_p + f_y (A_{st} - A_{sc})$$

and therefore

$$\sigma_{pu} = \frac{0.85f'_c b \gamma d_n - f_y (A_{st} - A_{sc})}{A_p} \quad (4.15)$$

When the value of  $\sigma_{pu}$  (calculated from Equation 4.15) and the value of  $\varepsilon_{pu}$  (calculated from Equation 4.11) satisfy the stress–strain relationship of the prestressing steel, the correct value of  $d_n$  has been found. The non-prestressed steel strains should be checked to ensure that the steel has, in fact, yielded. If the compressive steel is not at yield, then the compressive force  $C_s$  has been overestimated and the correct value of  $d_n$  is slightly greater than the calculated value. The compressive steel stress in Equation 4.15 should be taken as  $\varepsilon_{sc} E_s$ , instead of  $f_y$ . Further iteration may be required to determine the correct value of  $d_n$  and the corresponding internal forces  $C_c$ ,  $C_s$ ,  $T_p$  and  $T_s$ .

With horizontal equilibrium satisfied, the ultimate moment of the section may be determined by taking moments of the internal forces about any convenient point on the section. Taking moments about the non-prestressed tensile reinforcement level gives

$$M_u = C_c l_c + C_s l_s - T_p l_p \quad (4.16)$$

For the rectangular section shown in [Figure 4.6a](#), the lever arms to each of the internal forces are

$$l_c = d_o - \frac{\gamma d_n}{2}, \quad l_s = d_o - d_c, \quad \text{and} \quad l_p = d_o - d_p$$

In the above equations,  $C_s$  and  $C_c$  are the magnitudes of the compressive forces in the steel and concrete, respectively, and are therefore considered to be positive.

The ultimate curvature is obtained from Equation 4.5 and the minimum curvature required for ductility is given by Equation 4.17, which is the same as Equation 4.6 except that the depth to the prestressing steel  $d_p$  is replaced by  $d$  (the depth to the resultant tensile force  $T$ ):

$$(\kappa_u)_{min} = \frac{0.0075}{d} \quad (4.17)$$

### Example 4.2

To the cross-section analysed in [Example 4.1](#) and shown in [Figure 4.4](#), three 24 mm diameter non-prestressed reinforcing bars ( $A_{st}=1350 \text{ mm}^2$ ) are added in the tensile zone at a depth  $d_o=690 \text{ mm}$ . The ultimate moment  $M_u$  for the section is to be calculated. The yield stress of the non-prestressed

steel is  $f_y=400$  MPa and all other material properties and cross-sectional details are as specified in [Example 4.1](#).

The strain in the prestressing steel at ultimate is as calculated in [Example 4.1](#):

$$\varepsilon_{pu} = 0.00655 + 0.003 \left( \frac{650 - d_n}{d_n} \right)$$

and the magnitude of the compressive force  $C_c$  carried by the concrete above the neutral axis is

$$C_c = 0.85 f'_c b \gamma d_n = 8340 d_n$$

From Equation 4.13, the non-prestressed steel is at yield (i.e.  $\varepsilon_{st} \geq \varepsilon_v = 0.002$ ), provided that the depth to the neutral axis  $d_n$  is less than or equal to  $0.6d_o (=414$  mm). If  $\sigma_{st}$  is assumed to equal  $f_y$ , the resultant tensile force  $T (=T_p + T_s)$  is given by

$$T = \sigma_{pu} A_p + f_y A_{st} = 1000 \sigma_{pu} + (400 \times 1350) = 1000(\sigma_{pu} + 540)$$

Horizontal equilibrium requires that  $C_c = T$  and hence

$$\sigma_{pu} = 8.34 d_n - 540$$

Trial values of  $d_n$  can now be selected and the respective values of  $\varepsilon_{pu}$  and  $\sigma_{pu}$  plotted on the stress–strain curve for the prestressing steel as shown in [Figure 4.7](#):

Trial $d_n$ (mm)	$\varepsilon_{pu}$	$\sigma_{pu}$ (MPa)	Point Plotted on <a href="#">Figure 4.7</a>
270	0.0108	1712	(4)
290	0.0103	1879	(5)
277	0.0106	1770	(6)

Since point 6 lies sufficiently close to the stress–strain curve for the tendon, the correct value for  $d_n$  is 277 mm.

From Equation 4.5, the ultimate curvature is

$$\kappa_u = \frac{0.003}{277} = 10.8 \times 10^{-6} \text{ mm}^{-1}$$

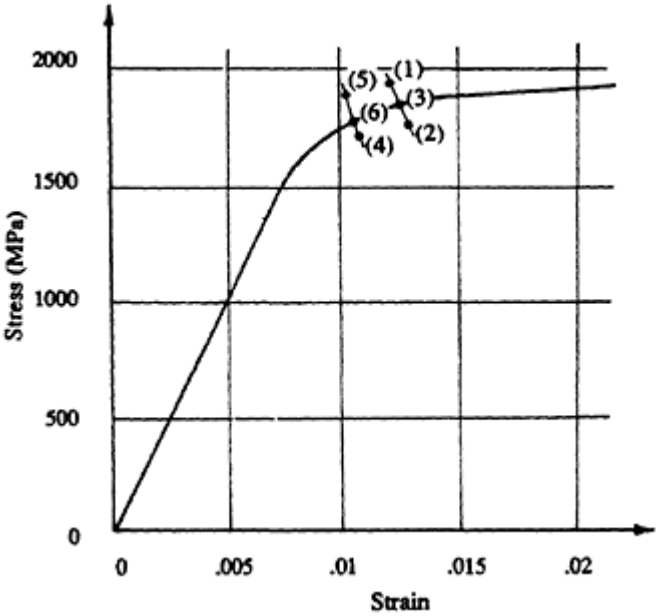


Figure 4.7 Stress-strain curve for strand (Example 4.2).

$d_n$  is much less than  $0.6d_o (=414 \text{ mm})$  and therefore the non-prestressed steel has yielded, as was assumed. The depth from the top surface to the resultant force in the tensile steel at ultimate is

$$d = \frac{\sigma_{pu} A_p d_p + f_y A_{st} d_o}{\sigma_{pu} A_p + f_y A_{st}} = 659 \text{ mm}$$

The minimum curvature required to ensure some measure of ductility is obtained from Equation 4.17:

$$(x_u)_{min} = \frac{0.0075}{659} = 11.4 \times 10^{-6} \text{ mm}^{-1}$$

which is greater than  $x_u$ . The section is therefore non-ductile and, in design, it would be prudent to insert some non-prestressed compressive reinforcement to increase the ultimate curvature and improve ductility (at least to the level required by Equation 4.17).

At ultimate, the compressive force in the concrete is  $C_c = 8340 d_n = 2310 \text{ kN}$  and the tensile force in the tendon is  $T_p = \sigma_{pu} A_p = 1770 \text{ kN}$ . The ultimate moment is calculated from Equation 4.15:

$$M_u = 2310 \times \left( 690 - \frac{0.801 \times 277}{2} \right) - 1770(690 - 650) = 1267 \text{ kN m}$$

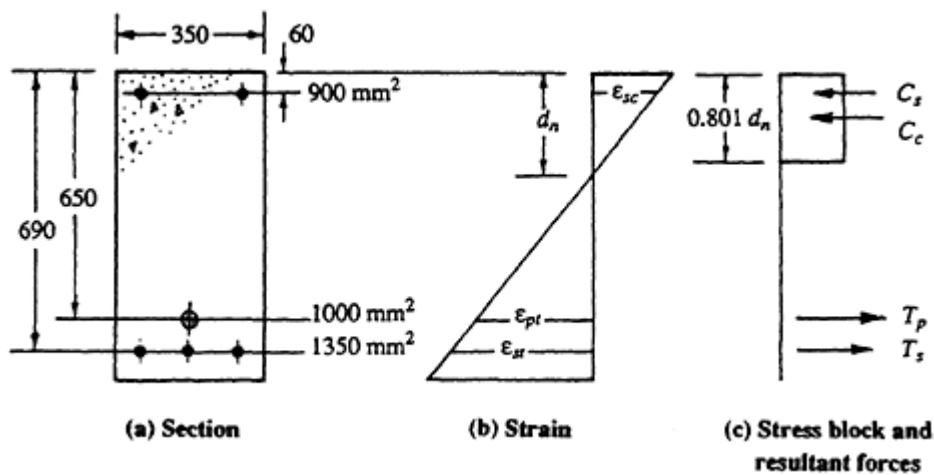


Figure 4.8 Section details and conditions at ultimate for [Example 4.3](#).

### Example 4.3

Consider the effect on both strength and ductility of the addition of two 24 mm diameter bars in the compression zone of the section in [Example 4.2](#). Details of the cross-section are shown in [Figure 4.8](#), together with the stress and strain distributions at ultimate. All data are as specified in [Examples 4.1](#) and [4.2](#).

From [Example 4.2](#), the ultimate strain in the tendons is

$$\epsilon_{pu} = 0.00655 + 0.003 \left( \frac{650 - d_n}{d_n} \right)$$

and the strain in the non-prestressed tensile reinforcement is greater than  $\epsilon_y$ . The magnitude of the compression steel strain at ultimate is given by Equation 4.12:

$$\epsilon_{sc} = \frac{0.003(d_n - 60)}{d_n}$$

The stress in the compression steel can be readily obtained from  $\epsilon_{sc}$  for any value of  $d_n$ . By equating  $C=T$ , an expression for  $\sigma_{pu}$  similar to Equation 4.15 is obtained. If the compression steel is assumed to be at yield, Equation 4.15 gives

$$\sigma_{pu} = \frac{(0.85 \times 35 \times 350 \times 0.801 d_n) - [400 \times (1350 - 900)]}{1000} = 8.34 d_n - 180$$

Values of  $\epsilon_{pu}$  and  $\sigma_{pu}$  for trial values of  $d_n$  are tabulated below and plotted as points (7)–(9) in [Figure 4.9](#).

Trial $d_n$	$\epsilon_{pu}$	$\epsilon_{sc}$	$\sigma_{pu}$ (MPa)	Point plotted on <a href="#">Figure 4.9</a>
250	0.0114	$>\epsilon_y$	1905	(7)
230	0.0120	$>\epsilon_y$	1738	(8)
239	0.0117	$>\epsilon_y$	1813	(9)

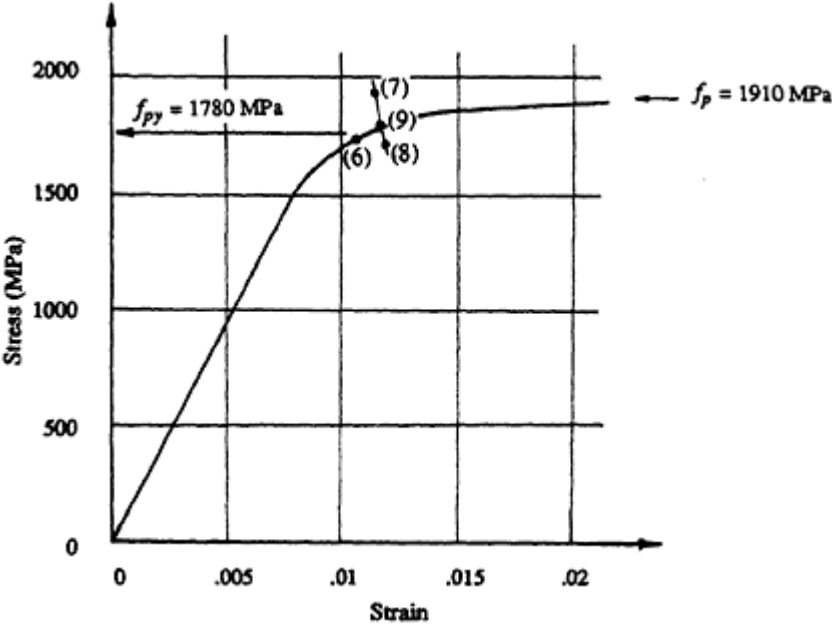


Figure 4.9 Stress–strain curve for strand ([Example 4.3](#)).

From [Figure 4.9](#), the point corresponding to  $d_n=239$  mm lies on the actual stress–strain curve and therefore represents the correct solution. It is also apparent in [Figure 4.9](#) that the strain in the prestressing steel at ultimate is increased by the introduction of compressive reinforcement [from point (6) to point (9)] and the depth to the neutral axis is decreased. The ultimate curvature is obtained from Equation 4.5:

$$\kappa_u = \frac{0.003}{239} = 12.6 \times 10^{-6} \text{ mm}^{-1}$$

which represents a 12% increase in final curvature caused by the introduction of the compressive reinforcement.

The depth  $d$  to the resultant tensile force ( $T=T_p+T_{st}$ ) remains at 659 mm and the magnitude of the resultant forces on the cross-section are

$C_c=1993$  kN,  $C_s=360$  kN,  $T_{st}=540$  kN, and  $T_p=1813$  kN. The ultimate moment is calculated using Equation 4.16:

$$M_u = 1993 \left( 690 - \frac{0.801 \times 239}{2} \right) + 360(690 - 60) - 1813(690 - 650) = 1339 \text{ kNm}$$

which is a 5.6% increase in strength. In general, for non-ductile sections, the addition of compressive reinforcement causes a significant increase in curvature at ultimate (i.e. a significant increase in ductility) and a less significant but nevertheless appreciable increase in strength.

## 4.4 Approximate code-oriented procedures

### 4.4.1 Bonded tendons

Approximate equations or procedures are specified in some codes of practice for the estimation of stress in a bonded tendon at the ultimate moment. These are generally conservative and may be used in lieu of the more accurate determination of  $\sigma_{pu}$  based on strain compatibility (as outlined in the previous sections). For example, when the effective prestress  $\sigma_{pe}$  ( $=P_e/A_p$ ) is not less than  $0.5 f_p$ , AS 3600–1988 specifies that the stress in the bonded steel at ultimate may be taken as

$$\sigma_{pu} = f_p \left( 1 - \frac{k_1 k_2}{\gamma} \right) \quad (4.18)$$

The same equation (with different notation) is also specified in ACI 318–83. The parameter  $\gamma$  is defined in Equation 4.2. The term  $k_1$  depends on the particular type of prestressing steel and may be taken as

$$k_1 = 0.40 \quad \text{if} \quad 0.85 \leq \frac{f_{py}}{f_p} < 0.9$$

$$= 0.28 \quad \text{if} \quad \frac{f_{py}}{f_p} \geq 0.9$$

where  $f_{py}$  is the specified yield strength of the prestressing tendon. The term  $k_2$  is given by

$$k_2 = \frac{A_p f_p + (A_{st} - A_{sc}) f_y}{b d_p f'_c} \quad (4.19)$$

where  $b$  is the width of the compressive face of the cross-section and  $d_p$  is the distance from the extreme compressive fibre to the centroid of the tendons. When compression reinforcement is present,  $k_2$  should be taken not less than 0.17. In addition, if the depth to the compressive steel  $d_c$  exceeds  $0.15 d_p$ , then  $A_{sc}$  should be set to zero in Equation 4.19. Other more accurate procedures are available for calculating  $\sigma_{pu}$  based on mathematical expressions for the shape of the stress-strain curve of the prestressing steel, such as that proposed recently by Loov (1988).

Consider a rectangular section such as that shown in [Figure 4.6](#) containing tensile prestressing steel, and both tensile and compressive non-prestressed reinforcement ( $A_p$ ,  $A_{st}$ , and  $A_{sc}$ , respectively). Assuming the non-prestressed tensile steel is at yield, the total tensile force in the steel at ultimate is

$$T = T_p + T_s = A_p \sigma_{pu} + A_{st} f_y$$

The magnitude of the total compressive force  $C$  consists of a concrete component  $C_c$  (given by Equation 4.3) and a steel component  $C_s = \sigma_{sc} A_{sc}$ . That is,

$$C = C_c + C_s = 0.85 f'_c b \gamma d_n + A_{sc} \sigma_{sc}$$

If the non-prestressed compressive steel is initially assumed to be at yield and the stress in the prestressing steel  $\sigma_{pu}$  is obtained from Equation 4.18, the depth to the neutral axis at ultimate may be obtained by equating  $C$  and  $T$ . Thus,

$$d_n = \frac{A_p \sigma_{pu} + A_{st} f_y - A_{sc} f_y}{0.85 f'_c b \gamma} \quad (4.20)$$

The calculated value of  $d_n$  can be used to check that the compressive steel has in fact yielded. If the steel has not yielded, a revised estimate of  $\sigma_{sc}$  ( $=E_s \varepsilon_{sc}$ ) may be made and used to calculate a new value of  $d_n$ . Relatively few iterations are required for convergence.

By taking moments about the level of the tensile steel, the ultimate moment  $M_u$  is given by

$$M_u = C_c \left( d_o - \frac{\gamma d_n}{2} \right) + C_s (d_o - d_c) - \sigma_{pu} A_p (d_o - d_p) \quad (4.21)$$

where  $d_o$  is the distance from the extreme compressive surface to the non-prestressed tensile reinforcement.

BS 8110: Part 1 (1985) tabulates approximate values for the tensile stress in the tendons and the depth to the neutral axis at the ultimate limit state.



**Table 4.2** Conditions at the ultimate limit state for rectangular beams with bonded tendons [BS 8110: Part 1 (1985)].

$\frac{f_p}{f'_c} \frac{A_p}{b d_p}$	$\lambda$			$\frac{d_n}{d_p}$		
	$\sigma_{pe}$			$\sigma_{pe}$		
	$0.4f_p$	$0.5f_p$	$0.6f_p$	$0.4f_p$	$0.5f_p$	$0.6f_p$
0.05	1.00	1.00	1.00	0.11	0.11	0.11
0.10	1.00	1.00	1.00	0.22	0.22	0.22
0.15	0.95	0.97	0.99	0.31	0.32	0.32
0.20	0.88	0.90	0.92	0.38	0.39	0.40
0.25	0.84	0.86	0.88	0.46	0.47	0.48
0.30	0.80	0.83	0.85	0.52	0.54	0.55
0.35	0.76	0.80	0.83	0.58	0.60	0.63
0.40	0.72	0.77	0.81	0.62	0.67	0.70
0.45	0.68	0.74	0.79	0.66	0.72	0.77
0.50	0.64	0.71	0.77	0.69	0.77	0.83

The tabulated values are based on the idealized rectangular stress block shown in [Figure 4.2e](#). Using the notation adopted in this chapter (and not that of BS 8110), the tensile stress in a bonded tendon may be taken as

$$\sigma_{pu} = \lambda \frac{f_p}{\gamma_m} \quad (4.22)$$

where  $\lambda$  may be interpolated from [Table 4.2](#) for any value of the effective prestress  $\sigma_{pe}$ ;  $\gamma_m$  is the partial material safety factor and equals 1.15. The depth to the neutral axis is also obtained from [Table 4.2](#). For a cross-section containing only bonded prestressing tendons at a depth  $d_p$ , BS 8110 specifies the design resistance moment (design strength) as

$$M_u = \sigma_{pu} A_p (d_p - 0.45 d_n) \quad (4.23)$$

#### Example 4.4

A comparison of the solution calculated in [Example 4.1](#) (using the actual stress–strain relationship of the prestressing steel) can be made with the

value obtained using the approximate estimate of  $\sigma_{pu}$  obtained from Equation 4.18. For this example,  $f_p=1910$  MPa and  $f_{py}=1780$  MPa (obtained from [Figure 4.5](#)) and the constants  $k_1$  and  $k_2$  are

$$k_1 = 0.28 \quad \text{and} \quad k_2 = \frac{1000 \times 1910}{350 \times 650 \times 35} = 0.24$$

From Equation 4.18, the stress in the tendon at ultimate is

$$\sigma_{pu} = 1910 \left( 1 - \frac{0.28 \times 0.24}{0.801} \right) = 1750 \text{ MPa}$$

which is 4.6% less than the more accurate value obtained by trial and error in [Example 4.1](#). From Equation 4.20,

$$d_n = \frac{1000 \times 1750}{0.85 \times 35 \times 350 \times 0.801} = 210 \text{ mm}$$

which compares with  $d_n=220$  mm in [Example 4.1](#). The ultimate strength is calculated using Equation 4.4 (or Equation 4.21):

$$M_u = 1750 \times 1000 \left( 650 - \frac{0.801 \times 210}{2} \right) \times 10^{-6} = 990 \text{ kN m}$$

This is about 4% more conservative than the value obtained in [Example 4.1](#). As expected, the simplified empirical procedure predicts a reasonable and conservative estimate of strength. However, the ultimate curvature is less conservative because the depth to the neutral axis is underestimated. The ultimate curvature is obtained from Equation 4.5:

$$x_u = \frac{0.003}{210} = 14.3 \times 10^{-6} \text{ mm}^{-1}$$

and is 4.6% greater than the previously predicted value. Nevertheless, for practical purposes, the simplified method is a useful design alternative.

The calculations are now repeated using the procedure specified in BS 8110: Part 1 (1985). In [Example 4.1](#),

$$\sigma_{pe} = 1200 \text{ MPa} = 0.63 f_p \quad \text{and} \quad \frac{f_p A_p}{f'_c b d_p} = \frac{1910 \times 1000}{35 \times 350 \times 650} = 0.24$$

and from [Table 4.2](#),  $\lambda=0.89$  and  $d_n=0.47d_p=305$  mm.

The stress in the bonded tendons is approximated using Equation 4.22:

$$\sigma_{pu} = \frac{0.89 \times 1910}{\gamma_m} = \frac{1700}{1.15} = 1478 \text{ MPa}$$

and Equation 4.23 gives

$$M_u = 1478 \times 1000 [650 - (0.45 \times 305)] \times 10^{-6} = 758 \text{ kN m}$$

and the ultimate curvature is

$$\kappa_u = \frac{\epsilon_{cu}}{d_n} = \frac{0.0035}{305} = 11.5 \times 10^{-6} \text{ mm}^{-1}$$

Direct comparison between the values for  $M_u$  predicted by the approach in AS 3600–1988 (and in ACI 318–83) and the BS 8110 approach is not possible, since the partial material safety factors are included in the latter and not in the former.

#### Example 4.5

In this example, [Example 4.3](#) is reworked using the approximate formula for  $\sigma_{pu}$  given in Equation 4.18:

$$k_1 = 0.28 \quad \text{and} \quad k_2 = \frac{(1000 \times 1910) + [(1350 - 900) \times 400]}{350 \times 650 \times 35} = 0.262$$

and

$$\sigma_{pu} = 1910 \left( 1 - \frac{0.28 \times 0.262}{0.801} \right) = 1735 \text{ MPa}$$

Assuming all non-prestressed steel is at yield, the depth to the neutral axis is obtained from Equation 4.20:

$$d_n = \frac{(1000 \times 1735) + [(1350 - 900) \times 400]}{0.85 \times 35 \times 350 \times 0.801} = 230 \text{ mm}$$

The non-prestressed steel strains are in fact much greater than the yield strain (=0.002) and the assumption to this effect is therefore correct. The resultant forces on the cross-section are  $C_c=1915$  kN,  $C_s=360$  kN,  $T_s=540$  kN, and  $T_p=1735$  kN, and the ultimate moment is obtained from Equation 4.6:

$$M_u = 1915 \left( 690 - \frac{0.801 \times 230}{2} \right) + 360(690 - 60) - 1735(690 - 650) = 1302 \text{ kN m}$$

This is about 3% less than the more accurate value calculated in [Example 4.3](#).

#### 4.4.2 Unbonded tendons

Where the prestressing steel is not bonded to the concrete, the stress in the tendon at ultimate,  $\sigma_{pu}$ , is significantly less than that predicted by Equation 4.18 and accurate determination of the ultimate flexural strength is more difficult than for a section containing bonded tendons. This is because the final strain in the tendon is more difficult to determine accurately. The ultimate strength of a section containing unbonded tendons may be as low as 75% of the strength of an equivalent section containing bonded tendons. Hence, from a strength point of view, bonded construction is to be preferred.

An unbonded tendon is not restrained by the concrete along its length and slip between the tendon and the duct takes place as the external loads are applied. The steel strain is more uniform along the length of the member and tends to be lower in regions of maximum moment than would be the case for a bonded tendon. The ultimate strength of the section may be reached before the stress in the unbonded tendon reaches the yield stress  $f_{py}$ . For members not containing any bonded reinforcement, crack control may be a problem if cracking occurs in the member for any reason. If flexural cracking occurs, the number of cracks in the tensile zone is fewer than in a beam containing bonded reinforcement, but the cracks are wider and less serviceable.

Approximate equations for the stress in an unbonded tendon at the ultimate limit state are also specified in codes of practice. AS 3600–1988 (and ACI 318–83), for example, specify the following equations for  $\sigma_{pu}$ :

(a) If the span to depth ratio of the member is 35 or less:

$$\sigma_{pu} = \sigma_{pe} + 70 + \frac{f'_c b d_p}{100 A_p} \quad (\text{MPa}) \quad (4.24a)$$

but  $\sigma_{pu}$  should not be taken greater than  $f_{py}$  or  $(\sigma_{pe}+400)$ .

(b) If the span to depth ratio of the member is greater than 35:

$$\sigma_{pu} = \sigma_{pe} + 70 + \frac{f'_c b d_p}{300 A_p} \quad (\text{MPa}) \quad (4.24b)$$

but not greater than  $f_{py}$  or  $(\sigma_{pe}+200)$ .

The approximate expressions specified in BS 8110: Part 1 (1985) for  $\sigma_{pu}$  and the depth to the neutral axis  $d_n$  for members containing unbonded

tendons are

$$\sigma_{pu} = \sigma_{pe} + \frac{7000}{L/d} \left( 1 - 1.7 \frac{f_p A_p}{f'_c b d_p} \right) \quad (4.25a)$$

and

$$d_n = \frac{2.47 A_p \sigma_{pu}}{f'_c b} \quad (4.25b)$$

To ensure ductility and some measure of crack control, it is good practice to include non-prestressed bonded tensile reinforcement in members with unbonded tendons. However, it is usual practice in most post-tensioning applications to grout the tendons within the duct after (or during) construction. Indeed, in Australia, for example, bonded construction is mandatory.

#### Example 4.6

The ultimate flexural strength of a simply supported post-tensioned beam is to be calculated. The beam spans 12 m and contains a single unbonded cable. The cross-section of the beam at mid-span is shown in [Figure 4.4a](#). Material properties are as specified in [Example 4.1](#).

The stress in the tendon caused by the effective prestressing force  $P_e=1200$  kN is

$$\sigma_{pe} = \frac{P_e}{A_p} = 1200 \text{ MPa}$$

With the span-to-depth ratio equal to 16, the stress in the unbonded tendon at ultimate, according to AS 3600–1988 and ACI 318–83, is given by Equation 4.24a:

$$\sigma_{pu} = 1200 + 70 + \frac{35 \times 350 \times 650}{100 \times 1000} = 1350 \text{ MPa}$$

and therefore the tensile force in the steel is  $T_p=1350$  kN ( $=C_d$ ). The depth to the neutral axis is calculated using Equation 4.20:

$$d_n = \frac{1350 \times 10^3}{0.85 \times 35 \times 350 \times 0.801} = 162 \text{ mm}$$

and Equation 4.4 gives

$$M_u = 1350 \times 1000 \left( 650 - \frac{0.801 \times 162}{2} \right) \times 10^{-6} = 790 \text{ kN m}$$

Using the alternative approach outlined in BS 8110: Part 1 (1985), estimates of  $\sigma_{pe}$  and  $d_n$  are made using Equations 4.25a and b, respectively:

$$\sigma_{pu} = 1200 + \frac{7000}{16} \left( 1 - 1.7 \frac{1910 \times 1000}{35 \times 350 \times 650} \right) = 1459 \text{ MPa}$$

and

$$d_n = \frac{2.47 \times 1000 \times 1459}{35 \times 350} = 294 \text{ mm}$$

and from Equation 4.23,

$$M_u = 1459 \times 1000 [650 - (0.45 \times 294)] \times 10^{-6} = 755 \text{ kNm}$$

## 4.5 Design calculations

### 4.5.1 Discussion

The magnitude of the prestressing force  $P_e$  and the quantity of the prestressing steel  $A_p$  are usually selected to satisfy the serviceability requirements of the member, i.e. to control deflection or to reduce or eliminate cracking. With serviceability satisfied, the member is then checked for adequate strength. The ultimate moment  $M_u$  for the section containing the prestressing steel (plus any non-prestressed steel added for crack control) is calculated and the *design strength* is compared with the *design action*, in accordance with the design requirements outlined in [Section 1.7.6](#). For example, in ACI 318–83 and in AS 3600–1988, the flexural strength is  $\phi M_u$ . The design action  $M^*$  is the moment caused by the most severe factored load combination specified for the strength limit state (see [Section 1.7.3](#)). The design requirement is that  $\phi M_u \geq M^*$ .

The prestressing steel needed for the satisfaction of serviceability requirements may not be enough to provide adequate strength. When this is the case, the ultimate moment capacity can be increased by the inclusion of additional non-prestressed tensile reinforcement. Additional compressive reinforcement may also be required to improve ductility.

### 4.5.2 Calculation of additional non-prestressed tensile reinforcement

Consider the singly reinforced cross-section shown in [Figure 4.10a](#). It is assumed that the effective prestress  $P_e$ , the area of the prestressing steel  $A_p$ , and the cross-sectional dimensions have been designed to satisfy the serviceability requirements of the member. The idealized strain and stress distributions specified by ACI 318–83 and AS 3600–1988 for the ultimate limit

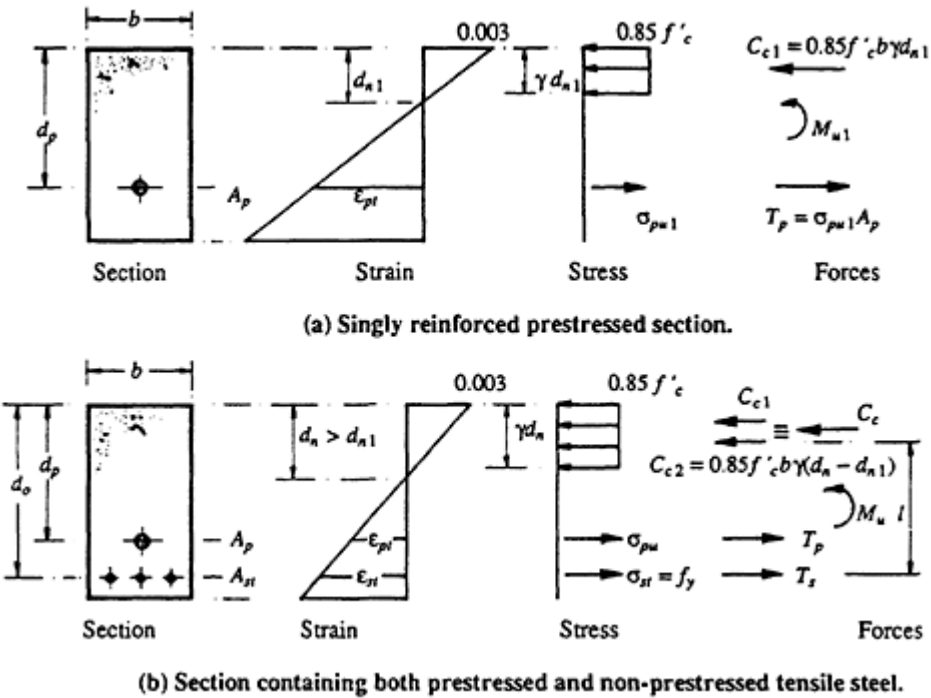


Figure 4.10 Cross-sections containing tensile reinforcement at the ultimate limit state (AS 3600–1988 and ACI 318–83).

state are also shown in Figure 4.10a. The ultimate moment for the section is denoted  $M_{u1}$ , where

$$M_{u1} = \sigma_{pu1} A_p \left( d_p - \frac{\gamma d_{n1}}{2} \right) \tag{4.26}$$

The tendon stress at ultimate  $\sigma_{pu1}$  may be calculated from the actual stress-strain curve for the steel (as illustrated in Example 4.1) or from the approximation of Equation 4.18 (as illustrated in Example 4.4).

If the design strength  $\phi M_{u1}$  is greater than or equal to  $M^*$ , then no additional steel is necessary. The cross-section has adequate strength. If  $\phi M_{u1}$  is less than  $M^*$ , the section is not adequate and additional tensile reinforcement is required.

In addition to providing adequate strength, it is important also to ensure that the section is ductile. In order that the curvature at ultimate  $x_u$  is large enough to impart ductility, an upper limit for the depth to the neutral axis of about  $0.4d_p$  is usually specified. However, to ensure ductility, a more satisfactory range for the depth to the neutral axis at failure is  $d_n \leq 0.3d_p$ . If the value of  $d_{n1}$  in Figure 4.10a is outside this range, some additional non-prestressed compressive reinforcement is required to relieve the concrete compressive zone and reduce  $d_n$ . The design procedure outlined in

[Section 4.5.3](#) for doubly reinforced cross-sections is recommended in such a situation.

For the cross-section shown in [Figure 4.10a](#), if  $\phi M_{u1}$  is less than  $M^*$  and if  $d_{n1}$  is small so that ductility is not a problem, the aim in design is to calculate the minimum area of non-prestressed tensile reinforcement  $A_{st}$  to be added to the section to satisfy strength requirements (i.e. the value of  $A_{st}$  such that  $\phi M_u = M^*$ ). In [Figure 4.10b](#), the new cross-section containing  $A_{st}$  is shown, together with the revised strain and stress distributions at ultimate. With  $d_n$  small enough to ensure ductility, the steel strain is greater than the yield strain  $\varepsilon_y (=f_y/E_s)$ , so that  $\sigma_{st} = f_y$ . The addition of  $A_{st}$  to the cross-section causes an increase in the resultant tension at ultimate ( $T_p + T_{st}$ ) and hence an increase in the resultant compression ( $C_c$ ). To accommodate this additional compression, the depth of the compressive stress block in [Figure 4.10b](#) must be greater than the depth of the stress block in [Figure 4.10a](#) (i.e.  $\gamma d_n > \gamma d_{n1}$ ). The increased value of  $d_n$  results in a reduction in the ultimate curvature (i.e. a decrease in ductility), a reduction in the strain in the prestressing steel, and a consequent decrease in  $\sigma_{pu}$ . The decrease in  $\sigma_{pu}$  is relatively small, however, provided that the section has adequate ductility (i.e. provided that the value of  $d_n$  remains less than about  $0.3d_p$ ).

If  $\sigma_{pu}$  is assumed to remain constant, a first estimate of the magnitude of the area of non-prestressed steel  $A_{st}$  required to increase the ultimate strength from  $M_{u1}$  (the strength of the section prior to the inclusion of the additional steel) to  $M_u$  (the required strength of the section) may be obtained from

$$A_{st} \approx \frac{M_u - M_{u1}}{f_y l} \quad (4.27)$$

where  $l$  is the lever arm between the tension force in the additional steel  $T_s$  and the equal and opposite compressive force  $C_c$  which results from the increase in the depth of the compressive stress block. The lever arm  $l$  may be approximated initially as

$$l = 0.9(d_o - \gamma d_{n1})$$

where  $d_{n1}$  is the depth to the neutral axis corresponding to  $M_{u1}$ .

#### Example 4.7

The ultimate strength of the singly reinforced section shown in [Figure 4.11](#) is  $M_{u1} = 1120$  kNm. The stress and strain distributions corresponding to  $M_{u1}$  are also shown in [Figure 4.11](#) and the material properties are  $f'_c = 35$  MPa ( $\gamma = 0.801$ ) and  $f_p = 1860$  MPa.

Calculate the additional amount of non-prestressed tensile reinforcement



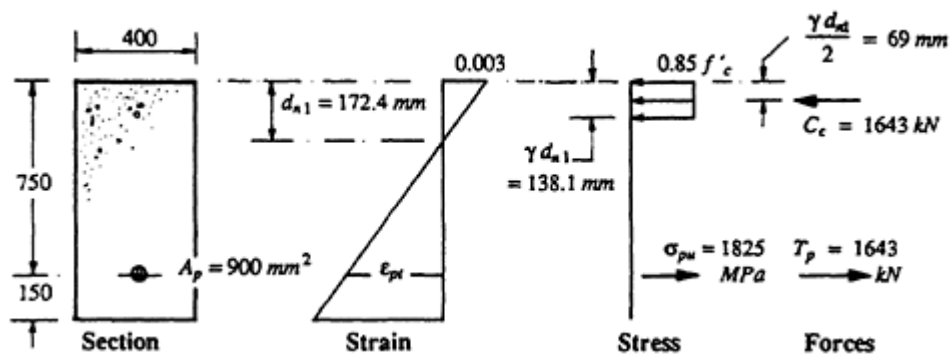


Figure 4.11 Singly reinforced cross-section at ultimate (Example 4.7).

( $f_y=400$  MPa) required to increase the ultimate strength of the section to  $M_u=1450$  kNm.

For the section in Figure 4.11,  $d_{n1}=172.4$  mm  $=0.23d_p$  and the section is ductile. If the additional tensile steel is to be added at  $d_o=840$  mm, then the lever arm  $l$  in Equation 4.27 may be approximated by

$$l = 0.9(d_o - \gamma d_{n1}) = 0.9(840 - 138.1) = 632 \text{ mm}$$

and the required area of non-prestressed steel is estimated using Equation 4.27:

$$A_{st} = \frac{(1450 - 1120) \times 10^6}{400 \times 632} = 1305 \text{ mm}^2$$

Choose three 24 mm diameter bars ( $A_{st}=1350$  mm<sup>2</sup>) located at a depth  $d_o=840$  mm.

A check of this section to verify that  $M_u \geq 1450$  kNm and that the section is ductile can next be made using the trial and error procedure illustrated in Example 4.2.

#### 4.5.3 Design of a doubly reinforced cross-section

For a singly reinforced section (such as that shown in Figure 4.12a) in which  $d_{n1}$  is greater than about  $0.3d_p$ , the inclusion of additional tensile reinforcement may cause ductility problems. In such cases, the ultimate strength may be increased by the inclusion of suitable quantities of both tensile and compressive non-prestressed steel without causing any reduction in curvature, i.e. without increasing  $d_n$ . If the depth to the neutral axis is held constant at  $d_{n1}$ , the values of both  $C_c$  (the compressive force carried by the concrete) and  $T_p$  (the tensile force in the prestressing steel) in Figures 4.12a and b are the same. In each figure,  $C_c$  is equal to  $T_p$ . With the strain diagram in

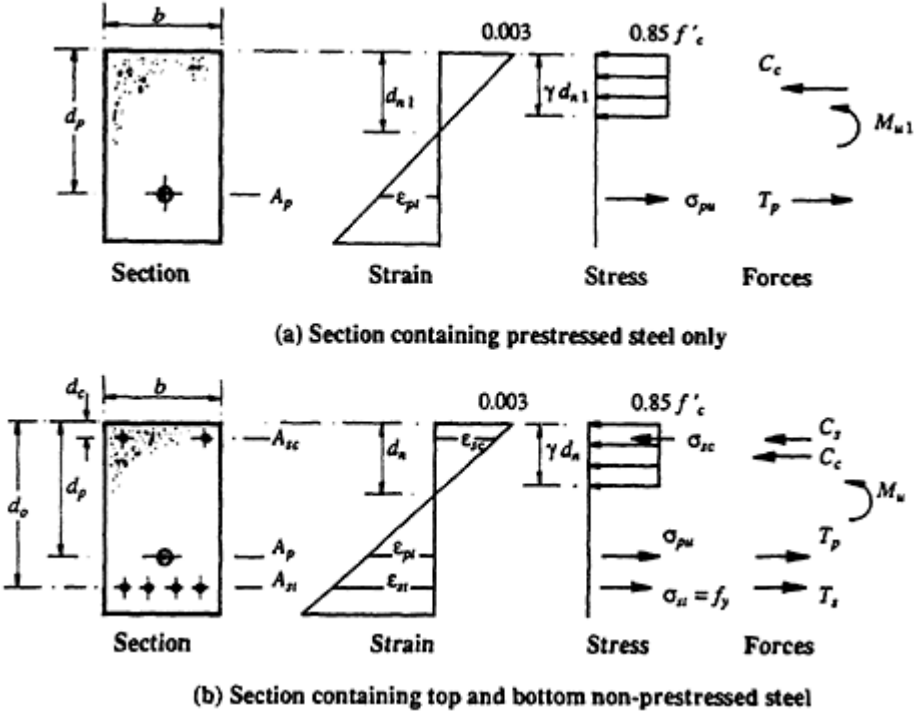


Figure 4.12 Doubly reinforced section at ultimate (AS 3600–1988 and ACI 318–83).

Figure 4.12b known, the strains at the levels of the non-prestressed steel may be calculated using Equations 4.12 and 4.13, and hence the non-prestressed steel stresses  $\sigma_{st}$  and  $\sigma_{sc}$  may be determined. The equal and opposite forces which result from the inclusion of the non-prestressed steel are

$$T_s = A_{st}\sigma_{st} \quad \text{and} \quad C_s = A_{sc}\sigma_{sc} \tag{4.28}$$

If  $M_{u1}$  is the strength of the singly reinforced section in Figure 4.12a (calculated using Equation 4.26) and  $M_u$  is the required strength of the doubly reinforced cross-section, the minimum area of the tensile reinforcement is given is

$$A_{st} = \frac{M_u - M_{u1}}{\sigma_{st}(d_o - d_c)}$$

(4.29)

For conventional non-prestressed steel,  $\sigma_{st}=f_y$  provided that the depth to the neutral axis  $d_n$  satisfies the stated ductility requirements. For equilibrium, the forces in the top and bottom non-prestressed steel are equal and opposite, i.e.  $C_s=T_s$  since  $C_c=T_p$ . From Equation 4.28,

$$A_{sc} = \frac{A_{st}\sigma_{st}}{\sigma_{sc}} \tag{4.30}$$

If the depth to the neutral axis in [Figure 4.12a](#) is greater than about  $0.4d_p$ , then the section is non-ductile and the value of  $d_n$  must be reduced. An appropriate value of  $d_n$  may be selected (say  $d_n=0.3d_p$ ). For this value of  $d_n$ , all the steel strains ( $\varepsilon_{sc}$ ,  $\varepsilon_{st}$ , and  $\varepsilon_{pt}$ ) and hence all the steel stresses at ultimate ( $\sigma_{sc}$ ,  $\sigma_{st}$ , and  $\sigma_{pu}$ ) may be determined. With  $\varepsilon_{pt}$  calculated from the assumed value for  $d_n$ , the total strain in the prestressing steel can be calculated using Equation 4.11 and the stress  $\sigma_{pu}$  can be read directly from the stress–strain curve. In this way, the magnitude of the tensile force in the tendon ( $T_p=A_p\sigma_{pu}$ ) and the compressive force in the concrete ( $C_c = 0.85f'_c b \gamma d_n$ ) may be evaluated. If the required strength of the section is  $M_u$ , the minimum area of compressive steel can be obtained by taking moments about the level of the non-prestressed reinforcement. That is,

$$A_{sc} = \frac{M_u + T_p(d_o - d_p) - C_c \left( d_o - \frac{\gamma d_n}{2} \right)}{\sigma_{sc}(d_o - d_c)} \quad (4.31)$$

Horizontal equilibrium requires that  $T_s=C_c+C_s-T_p$  and therefore the area of non-prestressed tensile steel is

$$A_{st} = \frac{0.85f'_c b \gamma d_n + A_{sc}\sigma_{sc} - A_p\sigma_{pu}}{\sigma_{st}} \quad (4.32)$$

### Example 4.8

Additional non-prestressed steel is required to increase the ultimate flexural strength of the section in [Figure 4.4](#) (and analysed in [Example 4.1](#)) to  $M_u=1300$  kNm.

From [Example 4.1](#),  $M_{u1}=1030$  kNm and  $d_{n1}=220$  mm. If only non-prestressed tensile steel were to be added, the lever arm  $l$  in Equation 4.27 would be

$$l = 0.9(d_o - \gamma d_{n1}) = 0.9[690 - (0.801 \times 220)] = 462 \text{ mm}$$

and from Equation 4.27,

$$A_{st} \approx \frac{(1300 - 1030) \times 10^6}{400 \times 462} = 1461 \text{ mm}^2$$

This corresponds to the addition of four 24 mm diameter bars in the bottom of the section shown in [Figure 4.4](#) at a depth  $d_o=690$  mm.

A check of the section to verify that  $M_u \geq 1300$  kN m can next be made using the trial and error procedure illustrated in [Example 4.1](#). In this example, however, the neutral axis depth increases above  $0.4d$  and the curvature at ultimate is less than the recommended minimum value. For this section,

it is appropriate to supply the additional moment capacity via both tensile and compressive non-prestressed reinforcement.

If the depth to the neutral axis is held constant at the value determined in [Example 4.1](#), i.e.  $d_n=220$  mm, then the stress and strain in the prestressed steel remain as previously calculated, i.e.

$$\epsilon_{pu} = 0.0124 \quad \text{and} \quad \sigma_{pu} = 1835 \text{ MPa}$$

If the depth to the compressive reinforcement is  $d_c=60$  mm, then from Equation 4.12,

$$\epsilon_{sc} = \frac{0.003(220 - 60)}{220} = 0.00218 > \epsilon_y \quad \text{and} \quad \therefore \sigma_{sc} = f_y = 400 \text{ MPa}$$

From Equation 4.13,

$$\epsilon_{st} = \frac{0.003(690 - 220)}{220} = 0.00641 > \epsilon_y \quad \text{and} \quad \therefore \sigma_{st} = f_y = 400 \text{ MPa}$$

The area of additional tensile steel is obtained using Equation 4.29:

$$A_{st} = \frac{(1300 - 1030) \times 10^6}{400(690 - 60)} = 1070 \text{ mm}^2$$

and from Equation 4.30,

$$A_{sc} = A_{st} = 1070 \text{ mm}^2$$

Use three 24 mm diameter non-prestressed tensile bars at  $d_o=690$  mm and three 24 mm diameter bars in the top of the section at  $d_c=60$  mm.

## 4.6 Flanged sections

Flanged sections such as those shown in [Figure 4.13a](#) are commonly used in prestressed concrete construction, where the bending efficiency of I-, T-, and box-shaped sections can be effectively utilized. Frequently, in the construction of prestressed floor systems, beams or wide bands are poured monolithically with the slabs. In such cases, a portion of slab acts as either a top or a bottom flange of the beam, as shown in [Figure 4.13b](#). Codes of practice generally specify the width of the slab which may be assumed to be part of the beam cross-section (i.e. the *effective width* of the flange,  $b_{ef}$ ).

Both AS 3600–1988 and BS 8110: Part 1 (1985) contain the following

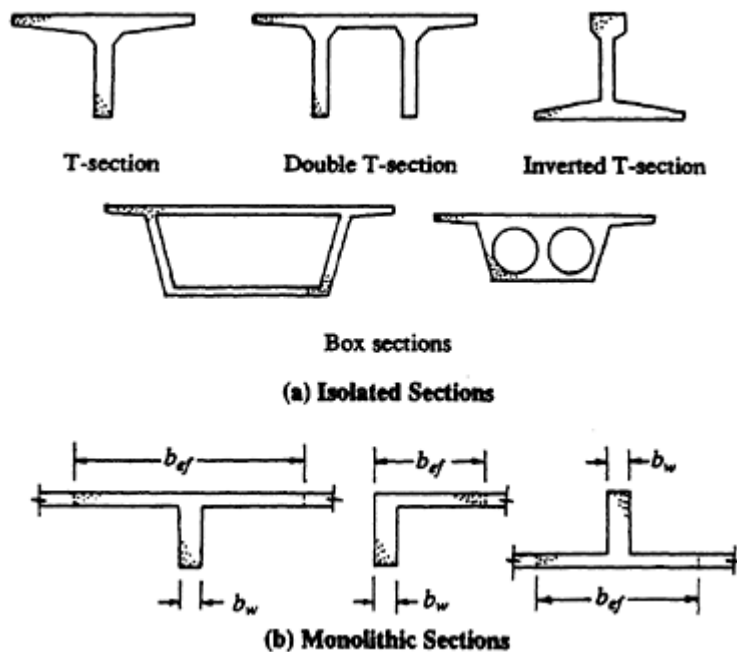


Figure 4.13 Typical flanged sections.

simple recommendations:

$$\begin{aligned} \text{For T-sections: } b_{ef} &= b_w + 0.2L_o \\ \text{For L-sections: } b_{ef} &= b_w + 0.1L_o \end{aligned} \quad (4.33)$$

except that the overhanging part of the effective flange should not exceed half the clear distance to the next parallel beam. The term  $b_w$  is the width of the web of the section.  $L_o$  is the distance along the beam between the points of zero bending moment and may be taken as the actual span for simply supported members and 0.7 times the actual span for a continuous member.

ACI 318–83 suggests that the effective width of the flange of a T-beam should not exceed one quarter of the span length of the beam, and the effective overhanging flange width on each side of the web should not exceed either eight times the slab thickness or one half the clear distance to the next web. For L-beams with a slab on one side only, the effective overhanging flange width should not exceed either one twelfth of the span of the beam, or six times the slab thickness, or half the clear distance to the next web.

The flexural strength theory discussed in [Section 4.3](#) can also be used to calculate the flexural strength of non-rectangular sections. The equations developed earlier for rectangular sections are directly applicable provided the depth of the idealized, rectangular stress block is less than the thickness

of the flange, i.e. provided the portion of the section subjected to the uniform compressive stress is rectangular ( $b_{ef}$  wide and  $\gamma d_n$  deep). The ultimate strength  $M_u$  is unaffected by the shape of the section below the compressive stress block. If the compressive stress block acts on a non-rectangular portion of the cross-section, some modifications to the formulae are necessary to calculate the resulting concrete compressive force and its line of action.

Consider the T-sections shown in Figure 4.14 and the idealized rectangular stress block defined in Figure 4.2d. If  $\gamma d_n \leq t$ , the area of the concrete in compression  $A'$  is rectangular, as shown in Figure 4.14a, and the strength of the section is identical with that of a rectangular section of width  $b_{ef}$  containing the same tensile steel at the same effective depth. Equation 4.21 may therefore be used to calculate the strength of such a section. The depth of the neutral axis  $d_n$  may be calculated using Equation 4.20, except that  $b_{ef}$  replaces  $b$  in the denominator.

If  $\gamma d_n > t$ , the area of concrete in compression  $A'$  is T-shaped, as shown in Figure 4.14b. Although not strictly applicable, the idealized stress block may still be used on this non-rectangular compressive zone. A uniform stress of  $0.85f'_c$  may therefore be considered to act over the area  $A'$ .

It is convenient to separate the resultant compressive force in the concrete

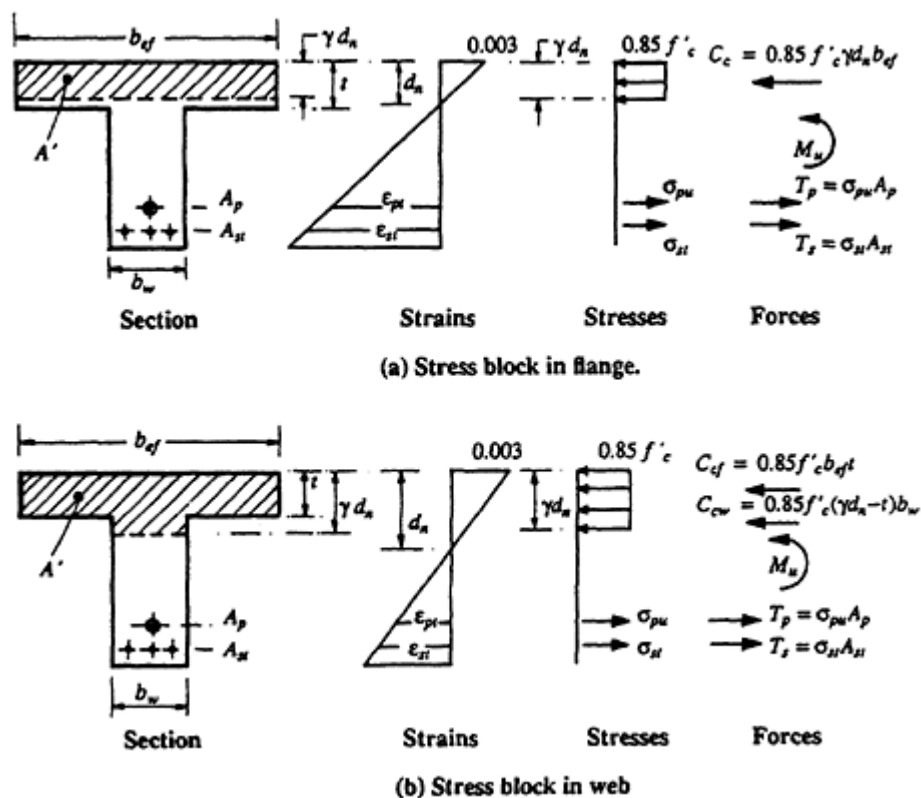


Figure 4.14 Flanged section subjected to the ultimate moment.

into a force in the flange  $C_{cf}$  and a force in the web  $C_{cw}$ , as shown:

$$C_{cf} = 0.85f'_c t b_{ef} \quad \text{and} \quad C_{cw} = 0.85f'_c (\gamma d_n - t) b_w \quad (4.34)$$

By equating the tensile and compressive forces on the section, the depth to the neutral axis  $d_n$  can be determined by trial and error and the ultimate moment  $M_u$  can be obtained by taking moments of the internal forces about any convenient point on the cross-section.

### Example 4.9

The ultimate flexural strength of the standardized double tee section shown in [Figure 4.15](#) is to be calculated. The section contains a total of 22 12.7 mm diameter strands (11 in each cable) placed at an eccentricity of 408 mm. The effective prestressing force  $P_e$  is 2640 kN. The stress–strain relationship for the prestressing steel is shown in [Figure 4.16](#) and the initial elastic modulus is  $E_p = 195000$  MPa. The properties of the section and other relevant material data are as follows:

$$A = 371 \times 10^3 \text{ mm}^2; \quad I = 22.8 \times 10^9 \text{ mm}^4; \quad A_p = 22 \times 100 = 2200 \text{ mm}^2;$$

$$f_p = 1880 \text{ MPa}; \quad Z_b = 43.7 \times 10^6 \text{ mm}^3; \quad Z_t = 82.5 \times 10^6 \text{ mm}^3;$$

$$E_c = 27800 \text{ MPa}; \quad f'_c = 35 \text{ MPa}; \quad \gamma = 0.801.$$

Using the same procedure as was illustrated in [Example 4.1](#), the strain components in the prestressing steel are obtained from Equations 4.8–4.10:

$$\epsilon_{pe} = \frac{2640 \times 10^3}{195000 \times 2200} = 0.00615$$

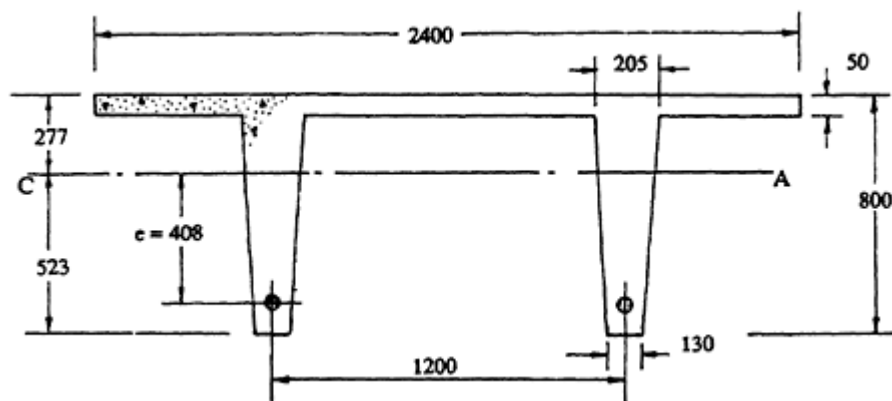


Figure 4.15 Standard 2400×800 double tee (CPCI 1982).

$$\varepsilon_{ce} = \frac{1}{27\,800} \left( \frac{2640 \times 10^3}{371 \times 10^3} + \frac{2640 \times 10^3 \times 408^2}{22.8 \times 10^9} \right) = 0.00095$$

$$\varepsilon_{pt} = 0.003 \left( \frac{685 - d_n}{d_n} \right)$$

and therefore from Equation 4.11,

$$\varepsilon_{pu} = 0.0071 + 0.003 \left( \frac{685 - d_n}{d_n} \right)$$

At this point, an assumption must be made regarding the depth of the equivalent stress block. If  $\gamma d_n$  is less than the flange thickness, the calculation would proceed as in previous examples. However, a simple check of horizontal equilibrium indicates that  $\gamma d_n$  is significantly greater than 50 mm. From Equation 4.34:

$$C_{cf} = 0.85 \times 35 \times 50 \times 2400 = 3570 \text{ kN}$$

In this example, the web is tapering and  $b_w$  varies with the depth. The width of the web at a depth of  $\gamma d_n$  is given by

$$b_{w1} = 210 - \frac{\gamma d_n}{10}$$

The compressive force in the web is therefore

$$\begin{aligned} C_{cw} &= 0.85 f'_c (\gamma d_n - 50) \left( \frac{205 + b_{w1}}{2} \right) \times 2 \\ &= 10\,000 d_n - 1.909 d_n^2 - 617\,300 \end{aligned}$$

The resultant compression force is

$$C = C_{cf} + C_{cw} = 2\,953\,000 + 10\,000 d_n - 1.909 d_n^2$$

and the resultant tension is

$$T = 2200 \sigma_{pu}$$

Equating  $C$  and  $T$  gives

$$\sigma_{pu} = 1342 + 4.549 d_n - 0.000868 d_n^2$$



Trial values of  $d_n$  may now be used to determine  $\varepsilon_{pu}$  and  $\sigma_{pu}$  from the above expressions and the resulting points plotted on the stress–strain diagram of [Figure 4.16](#):

Trial $d_n$	$\varepsilon_{pu}$	$\sigma_{pu}$	Point plotted on <a href="#">Figure 4.16</a>
130	0.0199	1919	(1)
110	0.0228	1832	(2)
115	0.0220	1854	(3)

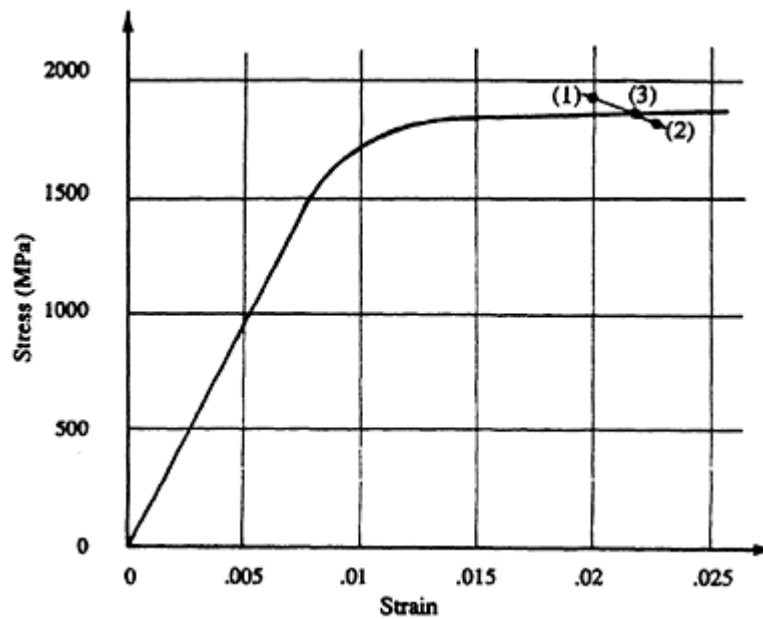


**Figure 4.16** Stress-strain for strands in [Example 4.9](#).

From [Figure 4.16](#), the neutral axis is close enough to  $d_n=115$  mm. The depth of the stress block is  $\gamma d_n=92.1$  mm, which is greater than the flange thickness (as was earlier assumed). The resultant forces on the cross-section are

$$T = 1854 \times 2200 = 4079 \text{ kN} = C$$

For this section,  $d_n=0.17d < 0.4d_p$  and therefore the failure is ductile. The compressive force in the flange  $C_{cf}=3570$  kN acts 25 mm below the top surface and the compressive force in the web  $C_{cw}=509$  kN acts at the centroid of the trapezoidal areas of the webs above  $\gamma d_n$ , i.e. 71.0 mm below the top surface.

By taking moments of these internal compressive forces about the level of the tendons,

$$M_u = 3570(685 - 25) + 509(685 - 71) = 2670 \text{ kN m}$$

## 4.7 References

- ACI 318–83 1983. *Building code requirements for reinforced concrete*. Detroit: American Concrete Institute.
- AS 3600–1988. *Australian standard for concrete structures*, Sydney: Standards Association of Australia.
- BS 8110: Part 1 1985. *Structural use of concrete, part 1, code of practice for design and construction*. London: British Standards Institution.
- Canadian Prestressed Concrete Institute (CPCI) 1982. *Metric design manual—precast and prestressed concrete*. Ottawa: Canadian Prestressed Concrete Institute.
- Loov, R.E. 1988. A general equation for the steel stress for bonded prestressed concrete members. *Journal of the Prestressed Concrete Institute*, **33**, 108–37.

## 5

# Design for shear and torsional strength

### 5.1 Introduction

In [Chapter 3](#), methods were presented for the determination of normal strains and stresses caused by the longitudinal prestress and the bending moment at a cross-section. Procedures for calculating the flexural strength of beams were discussed in [Chapter 4](#). In structural design, shear failure must also be guarded against. Shear failure is sudden and difficult to predict with accuracy. It results from diagonal tension in the web of a concrete member produced by shear stress in combination with the longitudinal normal stress. Torsion, or twisting of the member about its longitudinal axis, also causes shear stresses which lead to diagonal tension in the concrete and consequential inclined cracking.

Conventional reinforcement in the form of transverse stirrups is used to carry the tensile forces in the webs of prestressed concrete beams after the formation of diagonal cracks. This reinforcement should be provided in sufficient quantities to ensure that flexural failure, which can be predicted accurately and is usually preceded by extensive cracking and large deformation, will occur before diagonal tension failure.

In slabs and footings, a local shear failure at columns or under concentrated loads may also occur. This so-called *punching shear* type of failure often controls the thickness of flat slabs and plates in the regions above the supporting columns. In this chapter, the design for adequate strength of prestressed concrete beams in shear and in combined shear and torsion is described. Procedures for determining the punching shear strength of slabs and footings are also presented.

## SHEAR IN BEAMS

### 5.2 Inclined cracking

Cracking in prestressed concrete beams subjected to overloads depends on the local magnitudes of moment and shear, as shown in [Figure 5.1](#). In regions where the moment is large and the shear is small, vertical *flexural cracks* appear after the normal tensile stress in the extreme concrete fibres exceeds the tensile strength of concrete. These are the cracks referred to in [Section 3.5.2](#) and are shown in [Figure 5.1](#) as crack type A. Where both the moment and shear force are relatively large, flexural cracks which are vertical at the extreme fibres become inclined as they extend deeper into the beam owing to the presence of shear stresses in the beam web. These inclined cracks, which are often quite flat in a prestressed beam, are called *flexure-shear cracks* and are designated crack type B in [Figure 5.1](#). If adequate shear reinforcement is not provided, a flexure-shear crack may lead to a so-called *shear-compression failure*, in which the area of concrete in compression above the advancing inclined crack is so reduced as to be no longer adequate to carry the compression force resulting from flexure.

A second type of inclined crack sometimes occurs in the web of a prestressed beam in the regions where moment is small and shear is large, such as the cracks designated type C adjacent to the discontinuous support and near the point of contraflexure in [Figure 5.1](#). In such locations, high principal tensile stress may cause inclined cracking in the mid-depth region of the beam before flexural cracking occurs in the extreme fibres. These cracks are known as *web-shear cracks* and occur most often in beams with relatively thin webs.

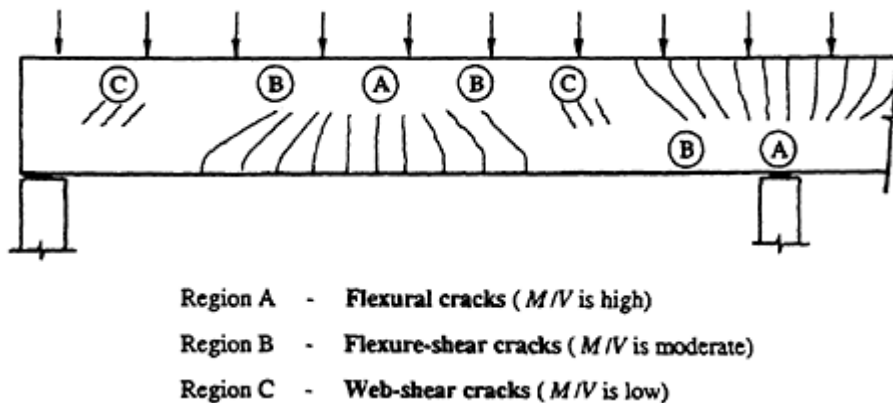


**Figure 5.1** Types of cracking at overload.

### 5.3 Effect of prestress

The longitudinal compression introduced by prestress delays the formation of each of the crack types shown in [Figure 5.1](#). The effect of prestress on the formation and direction of inclined cracks can be seen by examining the stresses acting on a small element located at the centroidal axis of the uncracked beam shown in [Figure 5.2](#). Using a simple Mohr's circle construction, the principal stresses and their directions are readily found. When the principal tensile stress  $\sigma_1$  reaches the tensile strength of concrete, cracking occurs and the cracks form in the direction perpendicular to the direction of  $\sigma_1$ .

When the prestress is zero,  $\sigma_1$  is equal to the shear stress  $\tau$  and acts at  $45^\circ$  to the beam axis, as shown in [Figure 5.2a](#). If diagonal cracking occurs, it will be perpendicular to the principal tensile stress, i.e. at  $45^\circ$  to the beam axis. When the prestress is not zero, the normal compressive stress  $\sigma (=P/A)$  reduces the principal tension  $\sigma_1$ , as illustrated in [Figure 5.2b](#). The angle between the principal stress direction and the beam axis increases, and consequently if cracking occurs, the inclined crack is flatter. Prestress therefore improves the effectiveness of any transverse reinforcement (stirrups) that may be used to increase the shear strength of a beam. With prestress

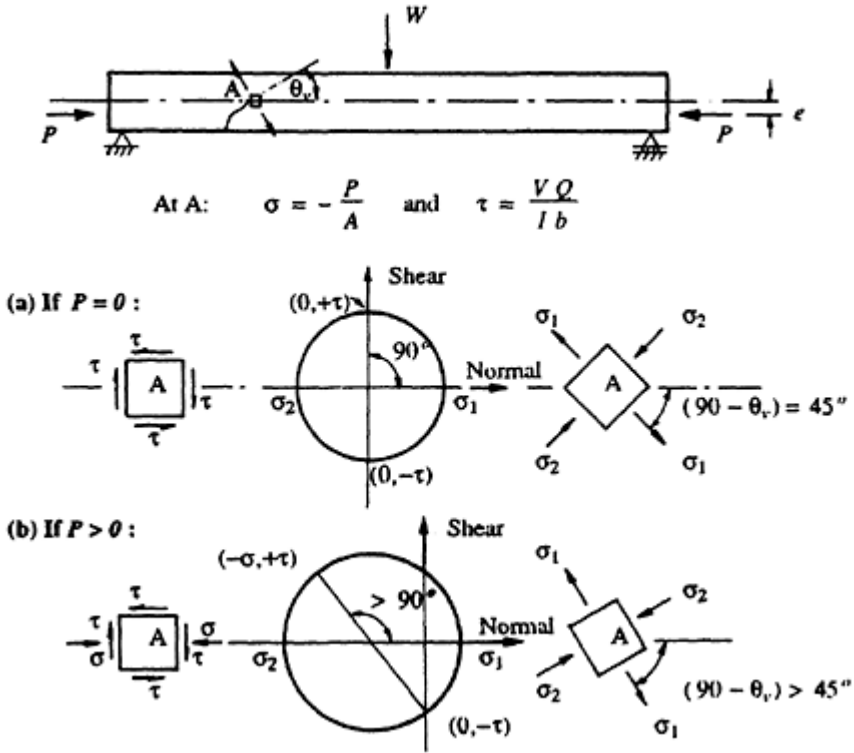


Figure 5.2 Effect of prestress on principal stresses in a beam web.

causing the inclined crack to be flatter, a larger number of the vertical stirrup legs are crossed by the crack and consequently a larger tensile force can be carried across the crack.

In the case of I-beams the maximum principal tension may not occur at the centroidal axis of the uncracked beam where the shear stress is greatest, but may occur at the flange–web junction where shear stresses are still high and the longitudinal compression is reduced by external bending.

If the prestressing tendon is inclined at an angle  $\theta_p$ , the vertical component of prestress  $P_v$  ( $=P \sin \theta_p \approx P\theta_p$ ) usually acts in the opposite direction to the load induced shear. The force  $P_v$  may therefore be included as a significant part of the shear strength of the cross-section. Alternatively,  $P_v$  may be treated as an applied load and the nett shear force,  $V$ , to be resisted by the section may be taken as

$$V = V_{\text{loads}} - P_v \quad (5.1)$$

In summary, the introduction of prestress increases the shear strength of reinforced concrete beams. Nevertheless, prestressed sections often have thin webs, the thickness of which may be governed by shear strength considerations.

## 5.4 Web reinforcement

In a beam containing no shear reinforcement, the shear strength is reached when inclined cracking occurs. The inclusion of shear reinforcement, usually in the form of vertical stirrups, increases the shear strength. After inclined cracking, the shear reinforcement carries tension across the cracks and resists widening of the cracks. Adjacent inclined cracks form in a regular pattern. The behaviour of the beam after cracking is explained conveniently in terms of an *analogous truss*, first described by Ritter (1899) and shown in [Figure 5.3b](#).

The web members of the analogous truss resist the applied shear and consist of vertical tension members (which represent the vertical legs of the closely spaced steel stirrups) and inclined compression members (which model the concrete segments between the inclined cracks). In reality, there exists a continuous field of diagonal compression in the concrete between the diagonal cracks. This is idealized in the analogous truss by the discrete diagonal compression struts. In a similar manner, the vertical members of the analogous truss may represent a number of more closely spaced vertical stirrups. The top compressive chord of the analogous truss represents the concrete compressive zone plus any longitudinal compressive reinforcement, and the bottom chord models the longitudinal prestressed and non-prestressed reinforcement in the tensile zone. At each panel point along the

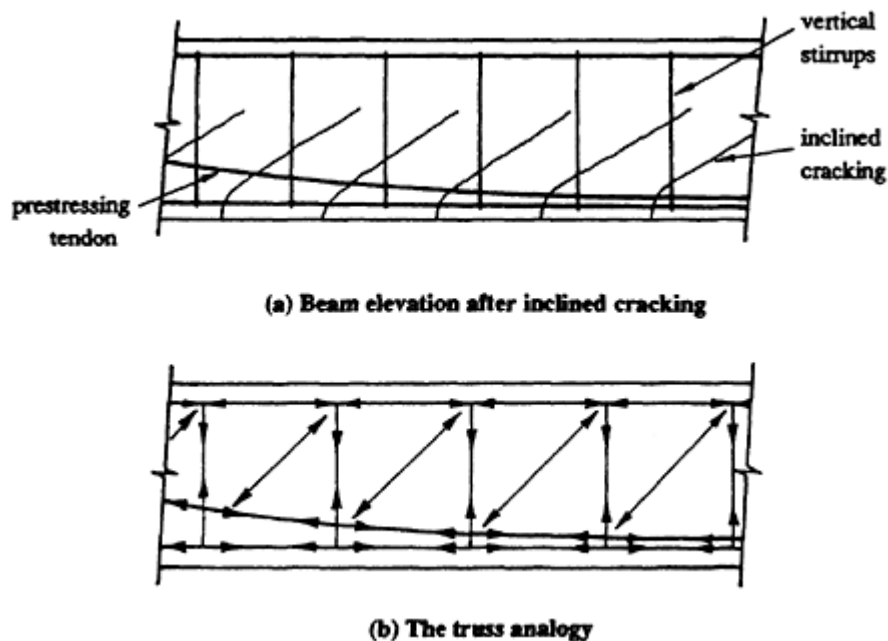


**Figure 5.3** Beam containing shear reinforcement.

bottom chord of the analogous truss, the vertical component of the compressive force in the inclined concrete strut must equal the tension in the vertical steel member, and the horizontal component must equal the change in the tensile force in the bottom chord (i.e. the change in force in the prestressing tendon and any other longitudinal non-prestressed reinforcement).

The analogous truss can be used to visualize the flow of forces in a beam after inclined cracking, but it is at best a simple model of a rather complex situation. The angle of the inclined compressive strut  $\theta_v$  has traditionally been taken as  $45^\circ$ , although in practical beams it is usually less. The stirrup stresses predicted by a  $45^\circ$  analogous truss are considerably higher than those measured in real beams (Hognestad 1952), because the truss is based on the assumption that the entire shear force is carried by the vertical stirrups. In fact, part of the shear is carried by dowel action of the longitudinal tensile steel and part by friction on the mating surfaces of the inclined cracks (known as aggregate interlock). Some shear may also be carried by the uncracked concrete compression zone. In addition, the truss model neglects the tension carried by the concrete between the inclined cracks. The stress in the vertical legs of the stirrups in a real beam is therefore a maximum at the inclined crack and significantly lower away from the crack.

At the ultimate limit state, shear failure may be initiated by yielding of the stirrups or, if large amounts of web reinforcement are present, crushing of the concrete compressive strut. The latter is known as *web-crushing* and is usually avoided by placing upper limits on the quantity of web reinforcement. Not infrequently, premature shear failure occurs because of inade-

quately anchored stirrups. The truss analogy shows that the stirrup needs to be able to carry the full tensile force from the bottom panel point (where the inclined compressive force is resolved both vertically and horizontally) to the top panel point. To achieve this, care must be taken to detail adequately the stirrup anchorages to ensure that the full tensile capacity of the stirrup can be developed at any point along the vertical leg. After all, an inclined crack may cross the vertical leg of the stirrup at any point.

Larger diameter longitudinal bars should be included in the corners of the stirrup to form a rigid cage and to improve the resistance to pull-out of the hooks at the stirrup anchorage. These longitudinal bars also disperse the concentrated force from the stirrup and reduce the likelihood of splitting in the plane of the stirrup anchorage. Stirrup hooks should be located on the compression side of the beam where anchorage conditions are most favourable and the clamping action of the transverse compression greatly increases the resistance to pull-out. If the stirrup hooks are located on the tensile side of the beam, anchorage may be lost if flexural cracks form in the plane of the stirrup. In current practice, stirrup anchorages are most often located at the top of a beam. In the negative moment regions of such beams, adjacent to the internal supports for example where shear and moment are relatively large, the shear capacity may be significantly reduced owing to loss of stirrup anchorages after flexural cracking.

## 5.5 Shear strength

### 5.5.1 Introductory remarks

From the point of view of structural design, the shear strength of a beam containing no shear reinforcement,  $V_w$  is the load required to cause the first inclined crack. In a beam containing web reinforcement, the ultimate strength in shear is usually calculated as the sum of the strength provided by the stirrups  $V_{us}$  and the strength provided by the concrete  $V_{uc}$ :

$$V_u = V_{uc} + V_{us} \quad (5.2)$$

In [Figure 5.4](#), the transfer of shear force across a diagonal crack is shown. The part of the shear force carried by shear stresses in the uncracked concrete compression zone is  $V_c$ , the part carried by bearing and friction between the two surfaces of the inclined crack is  $V_a$ , and the part carried by dowel action in the longitudinal steel crossing the crack is  $V_d$ . Because it is difficult to determine the magnitude of the force associated with each of these load-carrying mechanisms, they are usually lumped together and represented by a single empirical term for the shear strength contributed by the concrete,  $V_{uc}$ .



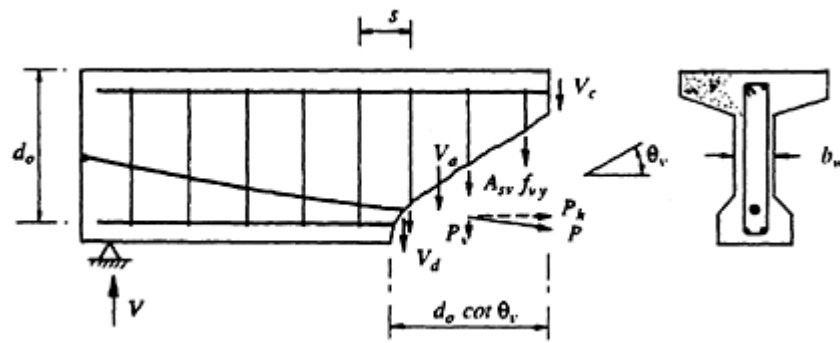


**Figure 5.4** Transfer of shear at an inclined crack.

From much research and many laboratory tests, it appears that the contribution of the concrete to the shear strength is not less than the shear force that initially caused the diagonal crack to form. For this reason,  $V_{uc}$  is conventionally taken as the shear force required to produce either flexure-shear or web-shear cracking, whichever is the smaller.

The contribution of stirrups to the shear strength of the beam,  $V_{us}$ , depends on the area of the vertical legs of each stirrup,  $A_{sv}$ , the yield stress of the steel,  $f_{vy}$ , and the number of stirrups which cross the inclined crack. As has already been stated, the longitudinal prestress causes the slope of the inclined crack,  $\theta_v$ , to be less than  $45^\circ$ . It is reasonable to take the length of the horizontal projection of the inclined crack to be  $d_o \cot \theta_v$ , where  $d_o$  is the distance from the extreme compressive fibre to the centroid of the outermost layer of tensile steel but need not be taken less than 0.8 times the overall depth of the member. The number of stirrups crossing the diagonal crack is therefore  $d_o \cot \theta_v / s$ , where  $s$  is the spacing of the stirrups in the direction of the member axis.

The total contribution of the stirrups to the shear strength of the section is the capacity of a stirrup times the number of stirrups crossing the inclined crack. An equation of the following form is contained in most codes of practice for the contribution of vertical stirrups to shear strength:

$$V_{us} = \frac{A_{sv} f_{vy} d_o \cot \theta_v}{s} \quad (5.3a)$$

If the shear reinforcement is inclined at an angle  $\alpha_v$  to the longitudinal tensile reinforcement (i.e. at an angle other than  $\alpha_v = 90^\circ$  for vertical stirrups),  $V_{us}$  may be calculated from

$$V_{us} = \frac{A_{sv} f_{vy} d_o}{s} (\sin \alpha_v \cot \theta_v + \cos \alpha_v) \quad (5.3b)$$

In many building codes [including ACI 318–83 and BS 8110 (1985)], the angle of the inclined crack  $\theta_v$  is taken to be constant and equal to  $45^\circ$

(i.e.  $\cot \theta_v = 1$  in Equation 5.3). However, in other codes (such as the CEB-FIP Model Code 1978 and AS 3600–1988),  $\theta_v$  is not constant and may be varied between specified limits. It is evident from Equations 5.3a and b that the contribution of stirrups to the shear strength of a beam depends on  $\theta_v$ . The flatter the inclined crack (i.e. the smaller the value of  $\theta_v$ ), the greater is the number of effective stirrups and the greater is the value of  $V_{us}$ . In order to achieve the desired shear strength in design, fewer stirrups are required as  $\theta_v$  is reduced. However, if the slope of the diagonal compression member in the analogous truss of [Figure 5.3b](#) is small, the change in force in the longitudinal tensile steel is relatively large. More longitudinal steel is required in the shear span near the support than would otherwise be the case and greater demand is placed on the anchorage requirements of these bars.

The empirical estimates for the contribution of the concrete to shear strength  $V_{uc}$  vary from code to code. In general, code expressions for  $V_{uc}$  are far more complicated than can be justified by their accuracy. In the following section, the procedures contained in the Australian code (AS 3600–1988) are discussed and compared with the provisions of ACI 318–83 and BS 8110 (1985). These provisions were selected because they represent a suitable compromise between accuracy, simplicity, and the current state of knowledge. However, other design approaches have been proposed and are used in practice. Some are based on more rational models of structural behaviour, but are considerably more complex. Such a method is the General Method contained in the Canadian Code (CSA Standard CAN3, 1984) which is based on *compression field theory* (Mitchell & Collins 1974, Collins 1978).

### 5.5.2 The AS 3600–1988 approach

AS 3600–1988 adopts a *limited variable angle truss model* in which  $\theta_v$  varies between  $30^\circ$  and  $45^\circ$ , depending on the magnitude of the factored design shear force  $V^*$ . The shear strength of a beam  $V_u$  is obtained from Equations 5.2 and 5.3.

In Equation 5.3,  $\theta_v$  may be assumed to vary linearly from  $30^\circ$ , when  $V^* = \phi V_{u,min}$ , to  $45^\circ$ , when  $V^* = \phi V_{u,max}$ . That is,

$$\theta_v = 30 + \frac{15(V^* - \phi V_{u,min})}{\phi V_{u,max} - \phi V_{u,min}} \quad (5.4)$$

$V_{u,min}$  is the shear strength of the beam containing the minimum amount of shear reinforcement,  $(A_{sv})_{min}$ , where

$$(A_{sv})_{min} = \frac{0.35b_v s}{f_{vy}} \quad (5.5)$$

The term  $b_v$  is the effective width of the web for shear and may be taken as  $b_v = b_w - 0.5 \sum d_d$ ,  $b_w$  is the width of the web minus the diameter of any ungrouted ducts across the web,  $\sum d_d$  is the sum of the diameter of the grouted ducts in a horizontal plane across the web, and  $\phi$  is the capacity reduction factor for shear (which is 0.7 in AS 3600–1988).  $V_{u,min}$  is obtained by substituting Equation 5.5 into Equation 5.3a and incorporating the resulting expression into Equation 5.2, as follows:

$$\begin{aligned} V_{u,min} &= V_{uc} + \left( \frac{0.35 b_v s}{f_{vy}} \right) f_{vy} \left( \frac{d_o}{s} \right) \cot 30 \\ &= V_{uc} + 0.6 b_v d_o \end{aligned} \quad (5.6)$$

$V_{u,max}$  is the maximum allowable shear strength for a section and is limited by web-crushing, i.e. failure of the diagonal concrete compression strut in the analogous truss. The maximum shear strength is given by

$$V_{u,max} = 0.2 f'_c b_v d_o + P_v \quad (5.7)$$

where  $P_v$  is the vertical component of the prestressing force at the section under consideration. The vertical force  $P_v$  is also included in Equation 5.6 as part of the “concrete” contribution  $V_{uc}$  (as indicated subsequently in Equations 5.8 and 5.10).

With  $\theta_v$  limited to a minimum value of  $30^\circ$ , the following requirements are imposed on the longitudinal reinforcement. At a simple support, sufficient positive moment reinforcement must be anchored past the face of the support, such that the anchored reinforcement can develop a tensile force of  $1.5 V^*$  at the face of the support (where  $V^*$  is the design shear force at a distance  $d$  from the support face). In addition, not less than 50% of the positive moment reinforcement required at mid-span should extend past the face of a simple support for a length of 12 bar diameters or an equivalent anchorage. At a support where the beam is continuous (or flexurally restrained), not less than 25% of the total positive reinforcement required at mid-span must continue past the near face of the support. AS 3600–1988 also requires that the steel necessary for flexure at any particular section must be provided and developed at a section a distance  $d$  along the beam in the direction of increasing shear.

Alternatively,  $\theta_v$  may be taken conservatively as constant and equal to  $45^\circ$  (as is the case in ACI 318–83), but this could result in considerably more transverse steel than is, in fact, necessary. The Canadian code (CAN3–A23.3–M84 1984) includes two alternative methods for shear design, a *simplified method* (similar to the ACI 318–83 approach) and a *general method*. In the general method, a variable-angle truss model based on compression field theory is used in which  $\theta_v$  may be selected to have any

value between  $15^\circ$  and  $75^\circ$ . The implications of selecting very low or very high values for  $\theta_o$  need to be carefully considered.

The contribution of the concrete to the shear strength of a section,  $V_{uc}$ , is taken to be the smaller of the shear forces required to produce either flexure-shear or web-shear cracking, as outlined below. However, if the cross-section under consideration is already cracked in flexure, only flexureshear cracking need be considered.

### Flexure-shear cracking

The shear force required to produce an inclined flexure-shear crack may be taken as the sum of the shear force that exists when the flexural crack first develops, the additional shear force required to produce the inclined portion of the crack (which extends a distance of about  $d_o$  along the beam in the direction of increasing moment), and the vertical component of the prestressing force. The first and third of these shear force components are easily calculated. The second is usually determined using empirical expressions developed from test data. AS 3600–1988 suggests that

$$V_{uc} = \beta_1 \beta_2 b_v d_o \left( \frac{A_{st} + A_{pt}}{b_v d_o} f'_c \right)^{1/3} + V_o + P_v \quad (5.8)$$

$\beta_1 = (1.4 - d_o/2000) \geq 1.1$  and is a *size effect* factor;

$\beta_2$  is a factor which accounts for the presence of any axial force  $N^*$  and

$\beta_2 = 1$  if no axial force is present;

$\beta_2 = 1 - (N^*/3.5A) \geq 0$  for axial tension;

$\beta_2 = 1 + (N^*/14A)$  for axial compression;

where  $N^*$  is the absolute value of the axial force.  $A_{st}$  and  $A_{pt}$  are the areas of the fully anchored longitudinal non-prestressed and prestressed steel, respectively, provided in the tension zone at the cross-section under consideration.

$V_o$  is the shear force (in Newtons) which exists at the section when the bending moment at that section equals the decompression moment  $M_o$  (i.e. the moment which causes zero stress in the extreme tensile fibre and may be taken as  $Z\sigma_{cp,f}$ , where  $Z$  is the section modulus and  $\sigma_{cp,f}$  is the compressive stress caused by prestress at the extreme fibre where cracking occurs). If  $M^*$  and  $V^*$  are the factored design moment and shear force at the section under consideration, then for statically determinate members,

$V_o$  may be taken as

$$V_o = M_o \frac{V^*}{M^*} \quad (5.9)$$

For statically indeterminate members, the shear and moment caused by the secondary effects of prestress should be taken into account when determining  $M_o$  and  $V_o$ .

### Web-shear cracking

If a cross-section is uncracked in flexure, the shear force required to produce web-shear cracking is given by

$$V_{uc} = V_t + P_v \quad (5.10)$$

$V_t$  is the shear force which when combined with the normal stresses caused by the prestress and the external loads would produce a principal tensile stress of  $0.33\sqrt{f'_c}$  at either the centroidal axis, the level of a prestressing duct, or at the intersection of the flange (if any) and the web, whichever is the more critical.  $V_t$  may be easily found analytically, or graphically using a Mohr's circle construction, by setting  $\sigma_1 = 0.33\sqrt{f'_c}$  in Equation 5.11:

$$\sigma_1 = \sqrt{\left(\frac{\sigma}{2}\right)^2 + \tau^2} + \frac{\sigma}{2} \quad (5.11)$$

The normal stress  $\sigma$  and the shear stress  $\tau$  are given by

$$\sigma = -\frac{P_e}{A} - \frac{P_e ey}{I} + \frac{My}{I} \quad \text{and} \quad \tau = \frac{V_t Q}{Ib} \quad (5.12)$$

where  $b$  is the appropriate width of the web and is equal to  $b_v$  at the level of any prestressing duct and  $b_w$  at points remote from the duct, and  $Q$  is the first moment about the centroidal axis of that part of the area of the cross-section between the level under consideration and the extreme fibre.

### Summary of design requirements

The following design requirements for shear are contained in AS 3600–1988 and are typical of those contained in most national building codes.

- (1) The design shear strength of a section is  $\phi V_u$ , where  $V_u = V_{uc} + V_{us}$  as stated in Equation 5.2.
- (2) The shear strength contributed by the concrete  $V_{uc}$  is the lesser of the values obtained from Equations 5.8 and 5.10.

- (3) The contribution of the shear reinforcement to the ultimate shear strength,  $V_{us}$ , is given by the equation

$$V_{us} = \frac{A_{sv} f_{vy} d_o}{s} (\sin \alpha_v \cot \theta_v + \cos \alpha_v) \quad (5.3b)$$

where  $s$  is the centre-to-centre spacing of the shear reinforcement measured parallel to the axis of the member;  $\theta_v$  is the angle of the concrete compression strut to the horizontal and may be conservatively taken as  $45^\circ$  or, more accurately, may be assumed to vary linearly from  $30^\circ$ , when  $V^* = \phi V_{u,min}$ , to  $45^\circ$ , when  $V^* = \phi V_{u,max}$ , in accordance with Equation 5.4;  $V^*$  is the factored design shear force;  $V_{u,min}$  and  $V_{u,max}$  are defined in Equations 5.6 and 5.7, respectively; and  $\alpha_v$  is the angle between the inclined shear reinforcement and the longitudinal tensile steel.

- (4) The critical section for maximum shear near to a support is at the distance  $d$  from the face of the support, where  $d$  is the depth to the position of the resultant tensile force at the ultimate strength condition in pure bending. Where diagonal cracking can take place at the support or extend into it, such as occurs if the support is above the beam, the critical section for shear is at the face of the support.
- (5) Where the factored design shear force  $V^*$  is less than  $0.5\phi V_{uc}$ , no shear reinforcement is required, except that when the overall depth of the beam exceeds 750 mm, minimum shear reinforcement should be provided. The minimum area of shear reinforcement is  $(A_{sv})_{min} = 0.35b_v s / f_{vy}$ .

Where  $0.5\phi V_{uc} < V^* \leq \phi V_{u,min}$ , minimum shear reinforcement shall be provided. If the total beam depth does not exceed 250 mm or half the width of the web, whichever is greater, and  $V^* \leq \phi V_{uc}$ , no shear reinforcement is required.

Where  $V^* > \phi V_{u,min}$ , shear reinforcement should be provided in accordance with Equation 5.3a (for vertical stirrups) or Equation 5.3b (for inclined stirrups).

- (6) In no case should the ultimate shear strength  $V_u$  exceed  $V_{u,max}$  (as defined in Equation 5.7).
- (7) The maximum spacing between stirrups measured in the direction of the beam axis should not exceed the lesser of  $0.5D$  or 300 mm, except that where  $V^* \leq \phi V_{u,min}$ , the spacing may be increased to  $0.75D$  or 500 mm, whichever is smaller. The maximum transverse spacing between the vertical legs of a stirrup measured across the web of a beam should not exceed the lesser of 600 mm and the overall depth of the cross-section,  $D$ .
- (8) The quantity of shear reinforcement calculated as being necessary at any section should be provided for a distance  $D$  from the section in the direction of decreasing shear.

- (9) Stirrups should be anchored on the compression side of the beam using standard hooks bent through an angle of at least  $135^\circ$  around a larger diameter longitudinal bar. As discussed in the last paragraph of [Section 5.4](#), it is important that the stirrup anchorage be located as close to the compression face of the beam as is permitted by concrete cover requirements and the proximity of other reinforcement and tendons.

### The design equation

The factored design shear force must be less than or equal to the design strength. That is,

$$V^* \leq \phi V_u = \phi (V_{uc} + V_{us}) \quad (5.13)$$

The capacity reduction factor  $\phi$  for shear is 0.7 in AS 3600–1988 (see [Table 1.1](#)). Substituting Equation 5.3a into Equation 5.13 gives

$$V^* \leq \phi V_{uc} + \frac{\phi A_{sv} f_{vy} d_o \cot \theta_v}{s}$$

and the design equation for vertical stirrups becomes

$$\frac{A_{sv}}{s} \geq \frac{1}{\phi} \left( \frac{V^* - \phi V_{uc}}{f_{vy} d_o \cot \theta_v} \right) \quad (5.14)$$

The use of Equation 5.14 for the design of web reinforcement is tedious

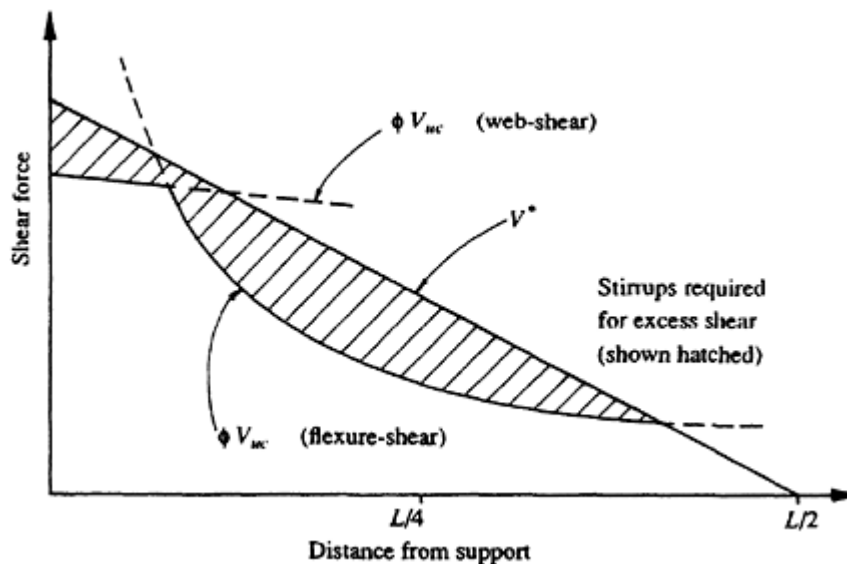


Figure 5.5 Web steel requirements for a uniformly loaded beam.

even for straightforward or ordinary cases. The critical value for  $V_{uc}$  (controlled by the onset of either flexure-shear or web-shear cracking) must be determined at each section along the beam and varies from section to section. However, the process is repetitive and may be easily performed using a small programmable calculator or desktop microcomputer.

The shear reinforcement requirements can be visualized by plotting the variation of both the applied shear ( $V^*$ ) and the shear strength provided by the concrete ( $\phi V_{uc}$ ) along the span of a uniformly loaded member, as shown in [Figure 5.5](#). The hatched area represents the design strength which must be supplied by the shear reinforcement ( $\phi V_{us}$ ).

### Example 5.1

The shear reinforcement for the post-tensioned beam shown in [Figure 5.6](#) is to be designed. The beam is simply supported over a 30 m span and carries a uniformly distributed live load of  $w_Q=25$  kN/m and dead load of  $w_G=30$  kN/m (which includes the beam self-weight). The beam is prestressed by a bonded parabolic cable ( $A_p=3800$  mm<sup>2</sup> and the duct diameter is 120 mm) with an eccentricity of 700 mm at mid-span and zero at each support. The prestress at each support is 4500 kN and at mid span 4200 kN and is assumed to vary linearly along the beam length.

The load combinations specified in AS 3600–1988 for the strength limit state are outlined in [Section 1.7.3](#). For this case of dead plus live load, the

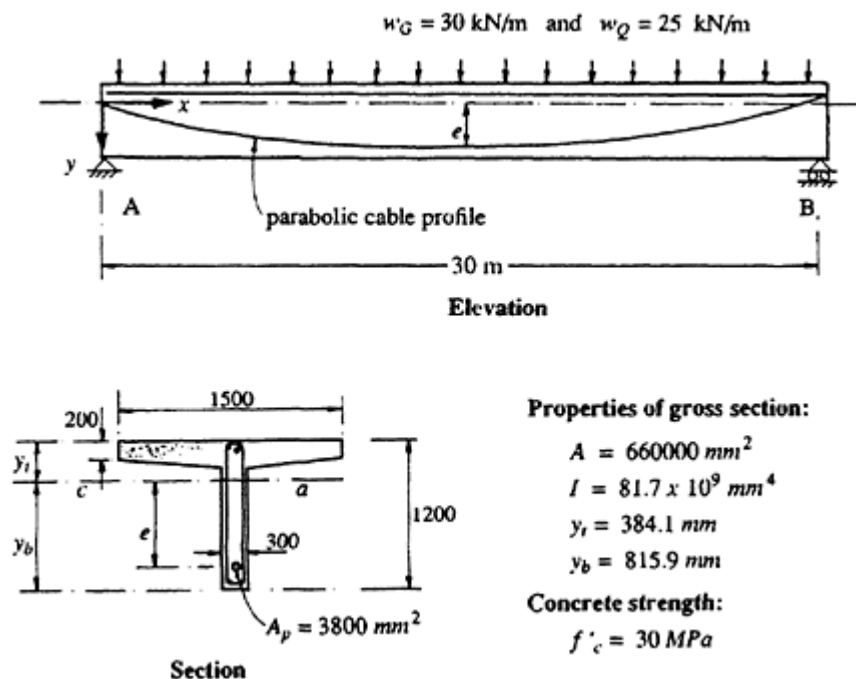


Figure 5.6 Beam details for [Example 5.1](#).



factored design load is

$$w^* = (1.25 \times 30) + (1.5 \times 25) = 75 \text{ kN/m}$$

At  $x$  m from support A:

$$V^* = 1125 - 75x \quad \text{and} \quad M^* = 1125x - 37.5x^2$$

The distance of the parabolic prestressing cable below the centroidal axis of the section at  $x$  m from A is obtained using Equation 1.3:

$$y = 2.8 \left[ \frac{x}{30} - \left( \frac{x}{30} \right)^2 \right]$$

and its slope is found from Equation 1.4:

$$y' = \frac{2.8}{30} \left( 1 - \frac{x}{15} \right)$$

Assuming 30 mm concrete cover, 12 mm diameter stirrups, and 24 mm diameter longitudinal bars in the corners of the stirrups, the depth  $d_o$  is

$$d_o = 1200 - 30 - 12 - 12 = 1146 \text{ mm}$$

In [Table 5.1](#), a summary of the calculations and reinforcement requirements at a number of sections along the beam is presented. The following

**Table 5.1** Summary of results—[Example 5.1](#).

$x$ (m)	$V^*$ (kN)	$M^*$ (kNm)	Web Shear $\phi V_{wc}$ (kNm)	Rezure Shear $\phi V_{wc}$ (kN)	$\phi V_{u,min}$ (kN)	$\theta_v$ (deg)	Spacing of 10 mm stirrups Eqn 5.14 (specified) (mm)
0.6	1080	662	897	1510	1013	32.4	271 (270)
1.0	1050	1090	932	1175	1047	30.1	460 (300)
2.0	975	2100	959	895	1011	30	467 (300)
3.0	900	3040	—	774	889	30.3	428 (300)
4.0	825	3900	—	692	808	30.5	402 (300)
5.0	750	4690	—	627	743	30.2	442 (300)
6.0	675	5400	—	571	687	30	467 (300)
7.0	600	6040	—	519	635	30	467 (300)
8.0	525	6600	—	471	586	30	467 (300)
9.0	450	7090	—	424	540	30	467 (300)
10.0	375	7500	—	380	495	30	467 (300)

sample calculations are provided for the sections at 0.6 m (0.5D) from the support and at 3 m from the support:

At  $x=0.6$  m From the above equations,  $V^*=1080$  kN,  $M^*=662$  kN m,  $y=0.0549$  m,  $y'=0.0896$  rad,  $P_e=4488$  kN, and the vertical component of prestress is  $P_v=P_e y'=402$  kN.

*Flexure-shear cracking* The decompression moment is

$$M_o = Z_b \left( \frac{P_e}{A} + \frac{P_e e}{Z_b} \right) = \frac{81.7 \times 10^9}{815.9} \left( \frac{4488 \times 10^3}{660 \times 10^3} + \frac{4488 \times 10^3 \times 54.9 \times 815.9}{81.7 \times 10^9} \right)$$

$$= 927 \text{ kNm}$$

and the corresponding shear force  $V_o$  is calculated using Equation 5.9:

$$V_o = 927 \times \frac{1080}{662} = 1512 \text{ kN}$$

Assuming a 24 mm diameter longitudinal bar in each bottom corner of the stirrups ( $A_{st}=900$  mm<sup>2</sup>), the shear force required to produce a flexure-shear crack is therefore obtained from Equation 5.8:

$$V_{uc} = 1.1 \times 1.0 \times 240 \times 1146 \left( \frac{3800 + 900}{240 \times 1146} \times 30 \right)^{1/3} \times 10^{-3} + 1512 + 402$$

$$= 2156 \text{ kN}$$

*Web-shear cracking* Since  $M^*$  is less than the decompression moment  $M_o$  (which is less than the cracking moment), web-shear cracking may be critical. Checks should be made at both the centroidal axis and at the tendon level.

At the centroidal axis, the first moment of the area below the centroidal axis is

$$Q = 0.5 \times 300 \times 815.9^2 = 99.9 \times 10^6 \text{ mm}^3$$

The effective width of the web at the centroidal axis is  $b=b_w=300$  mm, and from Equation 5.12,

$$\sigma = -\frac{P_e}{A} = -6.80 \text{ MPa} \quad \text{and} \quad \tau = \frac{V_t Q}{I b} = 4.07 \times 10^{-6} V_t \text{ MPa}$$

Setting  $\sigma_1 = 0.33 \sqrt{f'_c} = 1.81$  MPa in Equation 5.11 and solving gives  $V_t=969$  kN.

At the level of the prestressing tendon (i.e. 54.9 mm below the centroidal axis),

$$Q = 0.5 \times 300 \times (815.9 - 54.9)^2 = 86.9 \times 10^6 \text{ mm}^3$$

The effective width of the web for shear calculations at the level of the tendon is defined in the text immediately after Equation 5.5 and is given by

$$b_v = b_w - 0.5 \Sigma d_d = 300 - (0.5 \times 120) = 240 \text{ mm}$$

The moment at the section when the shear is  $V_t$  is

$$M_t = \frac{M^*}{V^*} V_t = 613 V_t$$

and from Equation 5.12,

$$\begin{aligned} \sigma &= -\frac{4488 \times 10^3}{660 \times 10^3} - \frac{4488 \times 10^3 \times 54.9^2}{81.7 \times 10^9} + \frac{613 V_t \times 54.9}{81.7 \times 10^9} \\ &= -6.97 + 0.412 \times 10^{-6} V_t \end{aligned}$$

and

$$\tau = \frac{86.9 \times 10^6 V_t}{81.7 \times 10^9 \times 240} = 4.43 \times 10^{-6} V_t$$

Solving Equation 5.11 with  $\sigma_1 = 0.33\sqrt{f'_c}$  gives  $V_t = 880$  kN, which is less than the value calculated at the centroidal axis. Therefore, from Equation 5.10,

$$V_{uc} = 880 + 402 = 1282 \text{ kN}$$

Clearly, at this section, web-shear cracking occurs at a lower load than flexure-shear cracking and is therefore critical. Thus,

$$\phi V_{uc} = 0.7 \times 1282 = 897 \text{ kN}$$

which is less than the design shear force  $V^*$ , and therefore shear reinforcement is required.

*Stirrup design* In this example, 10 mm diameter single stirrups (two vertical legs) with  $A_{sv} = 157 \text{ mm}^2$  and  $f_{vy} = 250 \text{ MPa}$  are to be used.

In order to find the inclination of the diagonal compressive strut,  $\theta_v$ , the

maximum and minimum shear strengths,  $V_{u,max}$  and  $V_{u,min}$ , must first be calculated. From Equation 5.7, the maximum shear strength (limited by web-crushing) is

$$V_{u,max} = (0.2 \times 30 \times 240 \times 1146) \times 10^{-3} + 402 = 2052 \text{ kN and}$$

$$\phi V_{u,max} = 1437 \text{ kN}$$

The design shear  $V^*$  is less than the maximum design strength  $\phi V_{u,max}$  and, therefore, the cross-section is suitable. The shear strength of the section containing the minimum shear reinforcement is obtained from Equation 5.6:

$$V_{u,min} = 1282 + (0.6 \times 240 \times 1146) \times 10^{-3} = 1447 \text{ kN and}$$

$$\phi V_{u,min} = 1013 \text{ kN}$$

which is less than  $V^*$ . For  $V^*=1080$  kN,  $\theta_v$  is obtained from Equation 5.4:

$$\theta_v = 30 + \frac{15(1080 - 1013)}{1437 - 1013} = 32.4^\circ$$

From the design equation for vertical stirrups (Equation 5.14):

$$s \leq \frac{\phi A_{sv} f_{yv} d_o \cot \theta_v}{V^* - \phi V_{uc}} = \frac{0.7 \times 157 \times 250 \times 1146 \times \cot 32.4}{(1080 - 897) \times 10^3} = 271 \text{ mm}$$

which satisfies both the minimum steel and maximum spacing requirements. At the critical section 0.6 m from the support, adopt

10 mm stirrups ( $f_{yv}=250$  MPa) at 270 mm centres

At  $x=3$  m From the equations given earlier,

$$V^* = 900 \text{ kN, } M^* = 3040 \text{ kN m, } y = 0.252 \text{ m, } y' = 0.0747 \text{ rad,}$$

$$P_e = 4440 \text{ kN, and } P_v = P_e y' = 332 \text{ kN.}$$

*Flexure-shear cracking* The decompression moment is

$$M_o = Z_b \left( \frac{P_e}{A} + \frac{P_e e}{Z_b} \right) = 1793 \text{ kN m}$$

and from Equation 5.9,

$$V_o = 1793 \times \frac{900}{3040} = 531 \text{ kN}$$

From Equation 5.8, the shear force required to produce a flexure-shear crack is

$$V_{uc} = 1.1 \times 1.0 \times 240 \times 1146 \left( \frac{3800 + 900}{240 \times 1146} \times 30 \right)^{1/3} \times 10^{-3} + 531 + 332$$

$$= 1105 \text{ kN}$$

Since  $M^*$  is greater than the cracking moment at this section, web-shear cracking need not be considered. Therefore, the contribution of the concrete to the design shear strength of the section is

$$\phi V_{uc} = 0.7 \times 1105 = 774 \text{ kN}$$

This is less than the design shear force  $V^*$ , and therefore shear reinforcement is required.

*Stirrup design* The minimum and maximum shear strengths,  $V_{u,min}$  and  $V_{u,max}$  are obtained from Equations 5.6 and 5.7, respectively:

$$V_{u,min} = 1105 + (0.6 \times 240 \times 1146) \times 10^{-3} = 1270 \text{ kN and}$$

$$\phi V_{u,min} = 889 \text{ kN}$$

$$V_{u,max} = (0.2 \times 30 \times 240 \times 1146) \times 10^{-3} + 332 = 1982 \text{ kN and}$$

$$\phi V_{u,max} = 1388 \text{ kN}$$

$V^*$  is only just greater than  $\phi V_{u,min}$ . Equation 5.4 gives

$$\theta_v = 30 + \frac{15(900 - 889)}{1388 - 889} = 30.3^\circ$$

and the stirrup spacing is

$$s \leq \frac{0.7 \times 157 \times 250 \times 1146 \times \cot 30.3}{(900 - 774) \times 10^3} = 428 \text{ mm}$$

This exceeds the maximum spacing requirement of  $0.5D$  or 300 mm, whichever is greater.

Therefore, at the section 3 m from the support, adopt

10 mm stirrups ( $f_{vy}=250$  MPa) at 300 mm centres

For other cross-sections, results are shown in [Table 5.1](#). When  $x \geq 6$  m, the design shear  $V^*$  is less than  $\phi V_{u,min}$  and the minimum amount of shear

reinforcement is required. However, for much of the span, the maximum spacing requirement of AS 3600–1988 governs the design.

### 5.5.3 The ACI 318–83 approach

The ultimate shear strength specified in ACI 318–83 is given by Equation 5.2 and the design requirement is

$$V^* \leq \phi V_u = \phi (V_{uc} + V_{us}) \quad (5.15)$$

The notation used here is consistent with that used elsewhere in this book and not necessarily with that used in ACI 318–83. The strength contributed by the stirrups  $V_{us}$  is given by either Equation 5.3a or b, except that  $\theta_v=45^\circ$  and  $\cot \theta_v=1$ . Therefore, for vertical stirrups,

$$V_{us} = \frac{A_{sv} f_{vy} d_p}{s} \quad (5.16a)$$

and for inclined stirrups,

$$V_{us} = \frac{A_{sv} f_{vy} d_p}{s} (\sin \alpha_v + \cos \alpha_v) \quad (5.16b)$$

where  $d_p$  is the depth from the extreme compressive fibre to the centroid of the prestressing steel, but should not be taken to be less than 0.8 times the overall depth of the member.

To avoid web crushing, the strength  $V_{us}$  should not be taken greater than  $0.66\sqrt{f'_c}$ . In addition, the code requires that whenever  $V^*$  exceeds  $0.5\phi V_{uc}$ , minimum shear reinforcement should be used. The minimum shear reinforcement is given by  $(A_{sv})_{min}=0.35b_w d_p / f_{vy}$ .

The concrete contribution to shear strength  $V_{uc}$  is the lesser of the shear required to cause web-shear or flexure-shear cracks. For web-shear cracking,  $V_{uc}$  is the shear force that results in a principal tensile stress of  $0.33\sqrt{f'_c}$  (in MPa) at the centroidal axis or, when the centroidal axis is in the flange, at the intersection of the flange and web. For web-shear cracking, therefore,  $V_{uc}$  may be calculated in the same way as in the AS 3600 approach using Equation 5.10 and solving Equation 5.11. Alternatively,  $V_{uc}$  for web-shear cracking may be approximated by

$$V_{uc} = (0.29\sqrt{f'_c} + 0.3\sigma_{cp})b_w d_p + V_p \quad (5.17)$$

where  $\sigma_{cp}$  is the concrete compressive stress at the centroid (or at the junction of the web and flange) after all prestress losses.

For flexure-shear cracking,  $V_{uc}$  is as shown in Equation 5.18 and is the sum of the shear force which exists when a flexure crack first develops and

an additional shear force required to produce inclined cracking:

$$V_{uc} = 0.05\sqrt{f'_c} b_w d_p + \frac{V^*}{M^*} M_{cr} \quad (5.18)$$

where  $M_{cr}$  is the cracking moment which occurs when the extreme fibre tensile stress reaches  $0.5\sqrt{f'_c}$ . However,  $V_{uc}$  for flexure-shear need not be taken less than  $0.141\sqrt{f'_c} b_w d_p$ .

For members with an effective prestressing force  $P_e$  greater than 40% of the tensile strength of all the flexural reinforcement, ACI 318–83 specifies the following approximate alternative expression for  $V_{uc}$ :

$$V_{uc} = \left( 0.05\sqrt{f'_c} + 4.83 \frac{V^*}{M^*} d_p \right) b_w d_p \quad (5.19)$$

but  $V_{uc}$  need not be taken less than  $0.166\sqrt{f'_c} b_w d_p$  nor greater than  $0.415\sqrt{f'_c} b_w d_p$ . This approximate expression should only be used when the critical section for shear does not occur within the transfer length near the end of a pretensioned member.

The most significant difference between the ACI approach and the AS 3600 approach, apart from the angle  $\theta_v$  being fixed at  $45^\circ$ , is the omission of the vertical component of the prestressing force in the equation for  $V_{uc}$  for flexure-shear (Equation 5.18). This may result in significant differences in the required amount of shear reinforcement. For example, at 3 m from the support of the beam shown in [Figure 5.6](#) and analysed in [Example 5.1](#), the AS 3600 approach predicted  $V_{uc}=1105$  kN and the required spacing of 10 mm diameter stirrups (two legs) was 428 mm. At the same section using the ACI approach,  $V_{uc}=691$  kN and the required stirrup spacing is only 75 mm. Using the ACI 318–83 load factors to calculate  $V^*$  and with  $\phi = 0.85$ , the force to be carried by the stirrups at this section is  $(V^* - \phi V_{uc})/\phi = 502$  kN. The corresponding force, calculated using the AS 3600 approach in [Example 5.1](#), is only 180 kN. This large difference is basically due to the omission of the vertical component of prestress ( $P_v=332$  kN) in the estimate of  $V_{uc}$  using the ACI approach. An examination of [Figure 5.4](#) indicates that  $P_v$  should be included in the estimate of the shear strength of the cross-section, provided the designer is confident that the slope of the tendon specified in design will in fact be realized in the real beam.

#### 5.5.4 The BS 8110 approach

The load combinations and design procedures for strength adopted in BS 8110 (1985) were outlined in Sections [1.7.3](#) and [1.7.6](#), respectively, and involve the use of partial safety factors for load and material strengths.

Using the notation adopted elsewhere in this book, the design shear stress is defined as

$$v = \frac{V^*}{b_w d} \quad (5.20)$$

where  $V^*$  is the design shear force at the section under consideration,  $b_w$  is the average web width, and  $d$  is the distance from the extreme compression fibre to the centroid of the steel area ( $A_p + A_{st}$ ) in the tensile zone. In no case should  $v$  exceed  $0.8\sqrt{f'_c}$  or 5 MPa, whichever is the smaller. Note that  $f'_c$  refers to the characteristic cube strength of the concrete.

The design ultimate shear resistance of the concrete alone,  $V_{uc}$ , is equal to  $V_{co}$  when the design moment  $M^*$  is less than  $M_o$ , and is the lesser of  $V_{co}$  and  $V_{cr}$  when  $M^* \geq M_o$ . The moment  $M_o$  produces zero stress in the concrete at the extreme tensile fibre. BS 8110 suggests that only 80% of the prestress should be taken into account when calculating  $M_o$ .

The shear resistance  $V_{co}$  produces a maximum tensile stress at the centroidal axis of  $\sigma_t = 0.24\sqrt{f'_c}$ . When calculating  $V_{co}$ , only 80% of the design compressive stress at the centroidal axis  $\sigma_{cp}$  (taken as +ve) should be considered.  $V_{co}$  may be calculated from

$$V_{co} = 0.67b_w D \sqrt{\sigma_t^2 + 0.8\sigma_{cp}\sigma_t} \quad (5.21)$$

where  $D$  is the overall depth of the member.

The design ultimate shear resistance when the section is cracked in flexure may be calculated from

$$\begin{aligned} V_{cr} &= \left(1 - 0.55 \frac{\sigma_{pe}}{f_p}\right) v_c b_w d + M_o \frac{V^*}{M^*} \\ &\geq 0.1\sqrt{f'_c} b_w d \end{aligned} \quad (5.22)$$

where  $\sigma_{pe}$  is the effective stress in the tendon after all losses have occurred (and should not be taken to be greater than  $0.6f_p$ );  $v_c$  is a design concrete shear stress given by

$$v_c = \frac{0.79}{\gamma_m} \left[ \frac{100(A_{st} + A_p)}{b_w d} \left( \frac{f'_c}{25} \right) \right]^{1/3} \left( \frac{400}{d} \right)^{1/4} \quad (5.23)$$

In this equation, the term  $100(A_{st} + A_p)/b_w d$  should not be taken as greater than 3, the term  $400/d$  should not be taken as less than 1.0,  $f'_c$  should not be taken as greater than 40 MPa, and  $\gamma_m$  is 1.25.

For sections cracked in flexure, the vertical component of the prestressing force (or the vertical component of the force in an inclined compressive



chord) should be combined with the external design load effects, wherever these effects are increased.

When  $V^* \leq V_{uc} + 0.4b_w d$ , the minimum quantity of shear reinforcement given by Equation 5.24 should be provided:

$$(A_{sv})_{min} = \frac{0.4b_w s}{0.87f_{vy}} \quad (5.25)$$

When  $V^* \geq V_{uc} + 0.4b_w d$ , then the required area of the stirrups is

$$A_{sv} = \frac{(V^* - V_{uc})s}{0.87f_{vy}d_o} \quad (5.25)$$

where  $d_o$  is the depth to the centroid of the bottom layer of longitudinal steel in the corners of the stirrups near the tensile face.

When  $V^* \leq 1.8V_{uc}$ , the spacing of stirrups along a member should not exceed  $0.75d_o$  or  $4b_w$  (in the case of flanged members). When  $V^* > 1.8V_{uc}$ , the maximum spacing is reduced to  $0.5d_o$ . The lateral spacing of individual stirrup legs across the width of a cross-section should not exceed  $d_o$ .

Like the ACI approach, the BS 8110 approach ignores the vertical component of prestress  $P_v$  whenever the effect is beneficial.

## TORSION IN BEAMS

### 5.6 Compatibility torsion and equilibrium torsion

In addition to bending and shear, some members are subjected to twisting about their longitudinal axes. A common example is a spandrel beam supporting the edge of a monolithic floor, as shown in [Figure 5.7a](#). The floor loading causes torsion to be applied along the length of the beam. A second example is a box girder bridge carrying a load in one eccentric traffic lane, as shown in [Figure 5.7b](#). Members which are curved in plan such as the beam in [Figure 5.7c](#) may also carry significant torsion.

For the design of spandrel beams, designers often disregard torsion and rely on redistribution of internal forces to find an alternative load path. This may or may not lead to a satisfactory design. When torsional cracking occurs in the spandrel, its torsional stiffness is reduced and, therefore, the restraint provided to the slab edge is reduced. Additional rotation of the slab edge occurs and the torsion in the spandrel decreases. Torsion such as this, which may be reduced by redistribution, is often called *compatibility torsion*. Whereas indeterminate structures generally tend to behave in

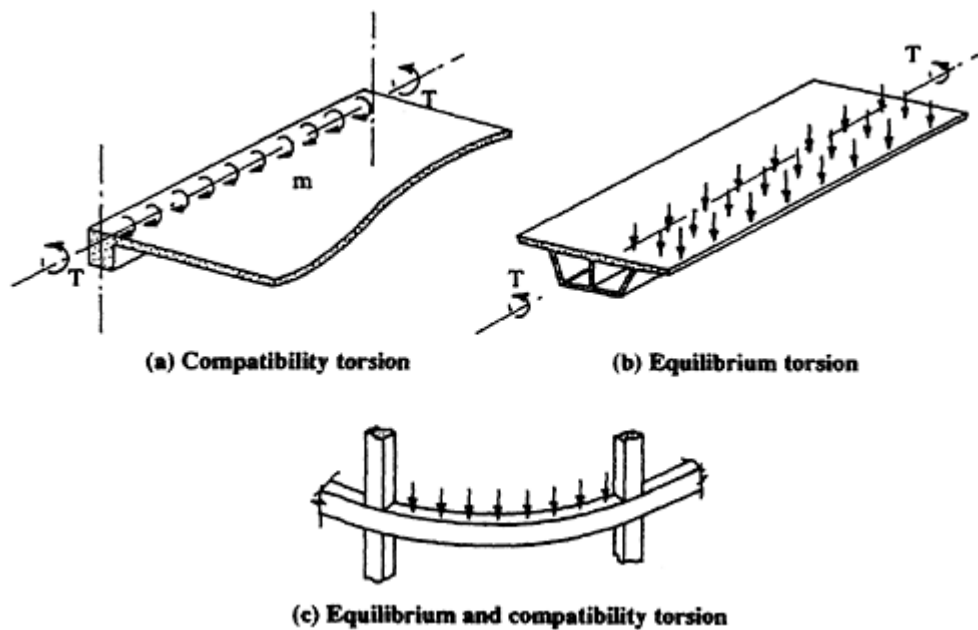


**Figure 5.7** Members subjected to torsion.

accordance with the design assumptions, full redistribution will occur only if the structure possesses adequate ductility, and may be accompanied by excessive cracking and large local deformations.

For some statically indeterminate members (and for statically determinate members) twisted about their longitudinal axes, some torsion is required for equilibrium and cannot be ignored. In the case of the box girder bridge of [Figure 5.7b](#), for example, torsion cannot be disregarded and will not be redistributed. There is no alternative load path. This is *equilibrium torsion* and must be considered in design.

Despite much research, the behaviour of beams carrying combined bending, shear, and torsion is not fully understood. Most current design recommendations rely heavily on gross simplifications and empirical estimates derived from experimental observations.

## 5.7 Effects of torsion

Prior to cracking, the torsional stiffness of a member may be calculated using elastic theory. The contribution of reinforcement to the torsional stiffness before cracking is insignificant and may be ignored. When cracking occurs, the torsional stiffness decreases significantly and is very dependent on the quantity of steel reinforcement. In addition to causing a large reduction of stiffness and a consequential increase in deformation (twisting), torsional cracks tend to propagate rapidly and are wider and more

unsightly than flexure cracks. A prudent designer will therefore endeavour to avoid torsional cracking at service loads.

Torsion causes additional longitudinal stresses in the concrete and the steel, and additional transverse shear stresses. If torsion is large, a significant reduction in load-carrying capacity results. To resist torsion after the formation of torsional cracks, additional longitudinal reinforcement and closely spaced, closed ties (stirrups) are required. Cracks caused by pure torsion form a spiral pattern around the beam (hence the need for closed ties). Many such cracks usually develop at close centres and failure eventually occurs on a warped failure surface owing to *skew bending*. The angles between the crack and the beam axis on each face of the beam are approximately the same and are here denoted  $\theta_t$ . After torsional cracking, the contribution of concrete to the torsional resistance of a reinforced or prestressed concrete member drops significantly. Any additional torque must be carried by the transverse reinforcement. Tests show that prestress increases significantly the torsional stiffness of a member, but does not greatly affect the strength. The introduction of prestress delays the onset of torsional cracking, thereby improving the member stiffness and increasing the cracking torque. The strength contribution of the concrete after cracking, however, is only marginally increased by prestress and the contribution of the transverse reinforcement remains unchanged.

For a beam in pure torsion, the behaviour after cracking can be described in terms of the three-dimensional analogous truss shown in [Figure 5.8](#). The closed stirrups act as transverse tensile web members (both vertical and horizontal); the longitudinal reinforcement in each corner of the stirrups act as the longitudinal chords of the truss; and the compressive web members inclined at an angle  $\theta_t$  on each face of the truss represent the concrete between the inclined cracks on each face of the beam and carry the inclined compressive forces.

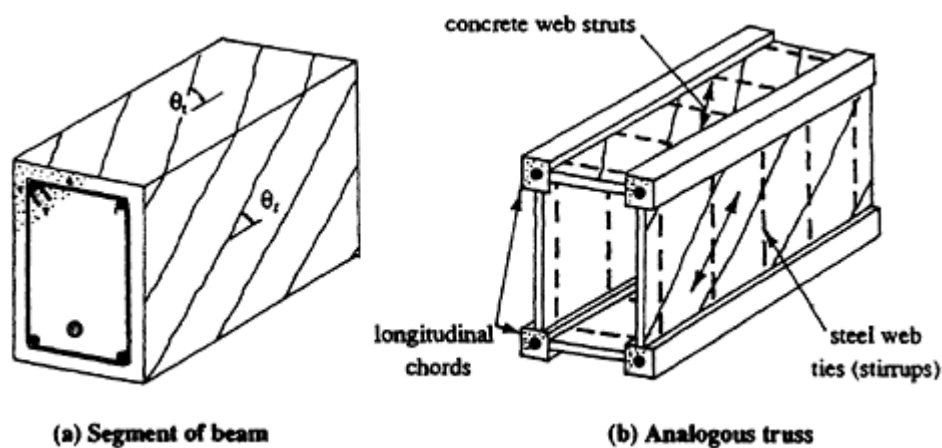


**Figure 5.8** A three-dimensional truss analogy for a beam in pure torsion.

The three-dimensional analogous truss ignores the contribution of the interior concrete to the post-cracking torsional strength of the member. The diagonal compressive struts are located on each face of the truss and, in the real beam, diagonal compressive stress is assumed to be located close to each surface of the member. The beam is therefore assumed to behave similarly to a hollow thin-walled section. Tests of members in pure torsion tend to support these assumptions.

Design models for reinforced and prestressed concrete beams in torsion are usually based on a simple model such as that described above.

## 5.8 Design provisions for torsion in AS 3600–1988

The provisions in the Australian Code (AS 3600–1988) for the design of beams subjected to torsion, and to torsion combined with flexure and shear, are outlined in this section and represent a simple and efficient design approach. Several conservative assumptions are combined with a variable angle truss model and the design procedure for shear presented in [Section 5.5.2](#).

### 5.8.1 Compatibility torsion

For a member subjected to compatibility torsion (such as the spandrel beam shown in [Figure 5.7a](#)), where torsional strength is not required for the equilibrium of the structure, the torsional stiffness of the member may be ignored in the analysis and torsion may be disregarded in design. However, the minimum torsion reinforcement provisions given in (a) and (b) below must be satisfied.

- (a) The cross-sectional area  $A_{sw}$  of the reinforcement bar used for the closed stirrup must be greater than the minimum value given by

$$(A_{sw})_{min} = 0.2y_1s/f_{vy} \quad (5.26)$$

where  $s$  is the stirrup spacing measured parallel to the axis of the member and  $y_1$  is the larger dimension of the closed rectangular stirrup.

- (b) An area of longitudinal reinforcement in addition to that required for flexure  $A_{s+}$  must also be provided and must be greater than the minimum value given by

$$(A_{s+})_{min} = 0.2y_1u_t/f_y \quad (5.27)$$

where  $u_t$  is the perimeter of the polygon with vertices at the centres of

the longitudinal bars at the corners of the closed stirrups and  $f_y$  is the yield stress of the additional non-prestressed reinforcement.

### 5.8.2 Equilibrium torsion

Where torsion is required for equilibrium, it must be considered in design and the ultimate torsional strength of each cross-section  $T_u$  must be calculated.

For a beam without torsional reinforcement,  $T_u$  is taken as the torsional strength of the concrete  $T_{uc}$  and is given by

$$T_{uc} = J_t(0.3\sqrt{f'_c})(\sqrt{1 + 10\sigma_{cp}/f'_c}) \quad (5.28)$$

In this equation,  $T_{uc}$  is an estimate of the pure torsion required to cause first cracking. The torsional constant  $J_t$  is taken as

$$\begin{aligned} J_t &= 0.4x^2y && \text{for solid sections;} \\ &= 0.4\Sigma x^2y && \text{for solid flanged sections;} \\ &= 2A_m b_w && \text{for hollow sections.} \end{aligned}$$

$x$  and  $y$  are the shorter and longer overall dimensions of the rectangular part(s) of the solid section, respectively;  $A_m$  is the area enclosed by the median lines of the walls of a hollow section;  $b_w$  is the minimum thickness of the walls of a hollow section; the term  $0.3\sqrt{f'_c}$  in Equation 5.28 represents the tensile strength of concrete; the term  $\sqrt{1 + 10\sigma_{cp}/f'_c}$  is the beneficial effect of the prestress; and  $\sigma_{cp}$  is the average effective prestress,  $P_e/A$ .

Torsional reinforcement is required in a member whenever the factored design twisting moment  $T^*$  exceeds  $0.5\phi T_{uc}$ .

For a beam with torsional reinforcement, the contribution of concrete to the torsional strength of a member after cracking is conservatively taken as zero (i.e.  $T_{uc}=0$ ). The torsional strength is therefore provided entirely by the stirrups ( $T_u=T_{us}$ ) and is given by

$$T_{us} = \frac{A_{sw}}{s} \times 2A_t f_{ly} \cot \theta_t \quad (5.29)$$

where  $A_t$  is the area of the polygon with vertices at the centres of the longitudinal bars at the corners of the closed stirrups;  $\theta_t$  is the angle between the axis of the concrete compressive strut and the longitudinal axis of the member and may be taken conservatively as  $45^\circ$  or, more accurately, to vary linearly from  $30^\circ$  when  $T^* = \phi T_{uc}$  to  $45^\circ$  when  $T^* = \phi T_{u,max}$ . That is,

$$\theta_t = 30 + \frac{15(T^* - \phi T_{uc})}{(\phi T_{u,max} - \phi T_{uc})} \quad (5.30)$$

where  $T_{uc}$  is given by Equation 5.28,  $\phi = 0.7$ , and  $T_{u,max}$  is the maximum ultimate torsional strength specified by AS 3600–1988 to avoid webcrushing and is given by

$$T_{u,max} = 0.2f'_c J_t \quad (5.31)$$

With the design requirement for a beam containing torsional reinforcement being  $T^* \leq \phi T_{us}$ , Equation 5.29 can be rearranged to form a design equation for the required quantity of transverse steel in a member subjected to pure torsion:

$$\frac{A_{sw}}{s} \geq \frac{T^*}{\phi f_{vy} \times 2A_t \cos \theta_t} \quad (5.32)$$

The torsional strength given by Equation 5.29 and the amount of transverse steel calculated using Equation 5.32 are only applicable provided that an additional area of longitudinal reinforcement  $A_{lt}^*$  (over and above that required for flexure) is included in the flexural tensile zone. This additional area of longitudinal reinforcement is specified as

$$A_{lt}^* = 0.5 \frac{A_{sw}}{s} u_t \cot^2 \theta_t \frac{f_{vy}}{f_y} \quad (5.33)$$

where  $f_{vy}$  and  $f_y$  are the characteristic strengths of the web steel and longitudinal steel, respectively. An additional area of longitudinal reinforcement  $A_{lc}^*$  is also required in the flexural compressive zone and is specified as

$$A_{lc}^* = 0.5 \frac{A_{sw}}{s} u_t \cot^2 \theta_t \frac{f_{vy}}{f_y} - \frac{F_c^*}{f_y} (\geq 0) \quad (5.34)$$

where  $F_c^*$  is the absolute value of the design force in the compressive zone caused by bending.

### 5.8.3 Torsion combined with bending and shear

For the design of members subjected to bending, shear, and torsion, the strengths in torsion and shear are determined separately, and the linear interaction equations presented below must be satisfied.

Transverse reinforcement is *not* required for shear plus torsion if

$$\frac{T^*}{\phi T_{uc}} + \frac{V^*}{\phi V_{uc}} \leq 0.5 \quad (5.35)$$

except that for a beam with overall depth not exceeding the greater of

250 mm or half the width of the web Equation 5.36 applies:

$$\frac{T^*}{\phi T_{uc}} + \frac{V^*}{\phi V_{uc}} \leq 1.0 \quad (5.36)$$

where  $T^*$  and  $V^*$  are the factored design torsion and shear,  $T_{uc}$  is determined from Equation 5.28, and  $V_{uc}$  is obtained from either Equation 5.8 or 5.10, whichever gives the smaller value.

When Equation 5.35 (or 5.36) is not satisfied and transverse reinforcement *is* required for shear and torsion, the concrete contribution to strength is ignored and Equation 5.37 must be satisfied:

$$\frac{T^*}{\phi T_{us}} + \frac{V^*}{\phi V_{us}} \leq 1.0 \quad (5.37)$$

provided that

$$\frac{T^*}{\phi T_{u,max}} + \frac{V^*}{\phi V_{u,max}} \leq 1.0 \quad (5.38)$$

$V_{us}$  is determined using Equations 5.3a and b, and  $T_{us}$  is given by Equation 5.29 (provided that the additional longitudinal steel indicated by Equations 5.33 and 5.34 is supplied). Equation 5.38 is aimed at preventing web-crushing under the combined effect of torsion and flexural shear, and  $V_{u,max}$  and  $T_{u,max}$  are obtained from Equations 5.7 and 5.31, respectively,

In all beams in which transverse steel is required for torsion and shear, the quantity of transverse and longitudinal reinforcement provided in the member should satisfy the minimum requirements specified in Equations 5.26 and 5.27.

When detailing the torsional reinforcement, the closed stirrups must be continuous around all sides of the section and be anchored so that the full strength of the bar can be developed at any point. The maximum spacing of the stirrups measured parallel to the longitudinal axis of the member is  $0.12u_t$  or 300 mm, whichever is smaller. The additional longitudinal reinforcement must be enclosed within the stirrup and as close to the corners of the section as possible. In all cases, at least one bar should be provided at each corner of the closed stirrup.

In [Section 5.7](#), the desirability of avoiding torsional cracking at service loads was discussed. Equation 5.28 provides an estimate of the pure torsion required to cause first cracking,  $T_{uc}$ . When torsion is combined with shear, the torque required to cause first cracking is reduced. An estimate of the torque necessary to cause torsional cracking at a section can be obtained

from the interaction equation

$$\frac{T_{cr}}{T_{uc}} + \frac{V_{cr}}{V_{uc}} = 1 \quad (5.39)$$

where  $T_{cr}$  and  $V_{cr}$  are the actual twisting moment and shear force, respectively, acting together at first cracking, and  $V_{uc}$  is the shear force required to cause inclined cracking when bending and shear are acting alone (and is the lesser of the values calculated using Equations 5.8 and 5.10).

If  $V_{cr}$  is expressed as  $T_{cr}/e$ , then Equation 5.39 can be rearranged to give

$$T_{cr} = \frac{T_{uc} e V_{uc}}{T_{uc} + e V_{uc}} \quad (5.40)$$

where  $e$  is the ratio of actual torsion to actual shear. In design, it is often advisable to check that the applied torque  $T$ , under in-service conditions, is less than  $T_{cr}$ .

#### 5.8.4 Design equation

Equations 5.37 and 5.38 are useful for checking the adequacy of a trial cross-section. When designing for combined torsion, bending, and shear, a more useful design equation is obtained by substituting Equations 5.3a and 5.29 into Equation 5.37. If vertical stirrups are to be used, Equation 5.37 becomes

$$\frac{T^*}{\phi(A_{sw}/s)2A_t f_{ly} \cot \theta_t} + \frac{V^*}{\phi(A_{sv}/s)f_{ly} d_o \cot \theta_v} \leq 1.0 \quad (5.41)$$

For closed stirrups with two vertical legs,  $A_{sv}=2A_{sw}$ , and Equation 5.41 may be rearranged to give

$$\frac{A_{sw}}{s} \geq \frac{T^*}{2\phi f_{ly} A_t \cot \theta_t} + \frac{V^*}{2\phi f_{ly} d_o \cot \theta_v} \quad (5.42)$$

The first term on the right-hand side of Equation 5.42 can be considered as the transverse steel required for torsion  $(A_{sw}/s)_t$  and the second term is the additional steel required for shear  $(A_{sw}/s)_v$ . When calculating the additional longitudinal steel required to carry torsion on the section, the quantity  $(A_{sw}/s)_t$  should be used in Equations 5.33 and 5.34.

Equation 5.42 and the theory outlined above were developed for the case of isolated beams subjected to torsion combined with bending and shear. When the beam forms part of a floor system and is integral with a slab, both its strength and stiffness are significantly greater than that of an isolated



beam of similar size and with similar reinforcement details. The slab prevents the longitudinal expansion of the beam in torsion and provides compressive restraint. The torque required to cause first cracking in such a beam is much greater than that predicted by Equation 5.28. The beneficial influence of the slab is not easily quantified. However, the procedure developed for an isolated beam provides a conservative and relatively simple design approach which can be used for a beam forming an integral part of a floor or deck system.

In cases where  $T^*$  and  $V^*$  are relatively small and only small amounts of transverse steel are required for torsion and shear, Equations 5.37 and 5.42 can lead to unduly conservative designs. This is because the concrete contribution to strength is entirely ignored. Rangan (1987b), in a commentary on AS 3600–1988's shear and torsion provisions, suggested that a less conservative and useful alternative in such cases is to adopt the following design requirement:

$$\frac{T^*}{\phi T_u} + \frac{V^*}{\phi V_u} \leq 1.0 \quad (5.43)$$

where  $T_u$  may be calculated using Equation 5.44, which is based on the work of Zia & Hsu (1978):

$$T_u = J_t(0.167\sqrt{f'_c})(2.5k - 1.5) + f_{vy}(A_{sw}/s)1.5x_1y_1 \quad (5.44)$$

and where  $x_1$  and  $y_1$  are the shorter and longer dimensions of the closed stirrups, respectively,  $J_t$  is as defined in Equation 5.28, and  $k = \sqrt{1 + 10\sigma_{cp}/f'_c}$ . In Equation 5.44, the angle  $\theta_t$  is assumed to be  $45^\circ$ . By taking  $\theta_v=45^\circ$ ,  $V_u$  may be obtained from Equations 5.2 and 5.3b:

$$V_u = V_{uc} + \frac{f_{vy}A_{sv}d_o}{s} \quad (5.45)$$

The contribution of the concrete to the shear strength  $V_{uc}$  is the lesser of the values obtained using Equations 5.8 and 5.10 and, as before, the additional areas of longitudinal steel required for torsion are calculated using Equations 5.33 and 5.34.

### Example 5.2 —torsion, bending and shear

A prestressed concrete beam has a rectangular cross-section 400 mm wide and 550 mm deep. At a particular cross-section, the beam must resist the following factored design actions:

$$M^* = 300 \text{ kN m}; \quad V^* = 150 \text{ kN}; \quad \text{and} \quad T^* = 60 \text{ kN m}$$

$$\begin{aligned}
 A &= 220 \times 10^3 \text{ mm}^2 \\
 I &= 5546 \times 10^6 \text{ mm}^4 \\
 Z &= 20.2 \times 10^6 \text{ mm}^3 \\
 y_1 &= 490 \text{ mm} \\
 x_1 &= 340 \text{ mm} \\
 d_\phi &= 500 \text{ mm} \\
 d &= 375 \text{ mm} \\
 A_t &= 450 \times 300 = 135 \times 10^3 \text{ mm}^2 \\
 u_t &= 2(450 + 300) = 1500 \text{ mm} \\
 P_e &= 700 \text{ kN} \\
 A_p &= 700 \text{ mm}^2
 \end{aligned}$$

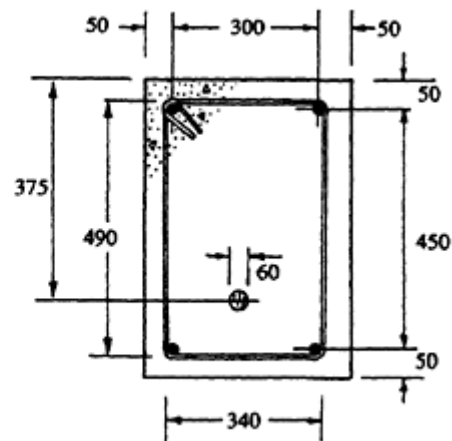


Figure 5.9 Cross-section details for [Example 5.2](#).

An effective prestress of 700 kN is applied at a depth of 375 mm by a single cable consisting of 7–12.5 mm diameter strands in a grouted duct of 60 mm diameter. The area of prestressing steel is  $A_p=700 \text{ mm}^2$  with an ultimate tensile strength of  $f_p=1840 \text{ MPa}$ . The vertical component of the prestressing force at the section under consideration is 50 kN and the concrete strength is  $f'_c = 30 \text{ MPa}$ . The dimensions and properties of the section are shown in [Figure 5.9](#). The longitudinal and transverse non-prestressed reinforcement requirements are to be determined.

- (1) Initially, the cross-section should be checked for web-crushing. The effective width of the web for shear is

$$b_v = b_w - 0.5 d_d = 400 - (0.5 \times 60) = 370 \text{ mm}$$

and from Equation 5.7,

$$V_{u,max} = (0.2 \times 30 \times 370 \times 500 \times 10^{-3}) + 50 = 1160 \text{ kN}$$

The torsional constant  $J_t$  is

$$J_t = 0.4 \times 400^2 \times 550 = 35.2 \times 10^6 \text{ mm}^3$$

and Equation 5.31 gives

$$T_{u,max} = (0.2 \times 30 \times 35.2 \times 10^6) \times 10^{-6} = 211 \text{ kN m}$$

The interaction equation for web-crushing (Equation 5.38) gives

$$\frac{60}{0.7 \times 211} + \frac{150}{0.7 \times 1160} = 0.59 < 1.0$$

- Therefore, web-crushing will not occur and the size of the cross-section is acceptable.
- (2) The longitudinal reinforcement required for bending must next be calculated. From the procedures outlined in [Chapter 4](#), the seven prestressing strands provide adequate ultimate flexural strength  $\phi M_u = 309 \text{ kN m} > M^* = 300 \text{ kN m}$ , where  $\phi = 0.8$  for bending as indicated in [Table 1.1](#)). No non-prestressed steel is therefore required for flexural strength.
- (3) To check whether torsional reinforcement is required,  $V_{uc}$  and  $T_{uc}$  must be calculated. Because bending is significant on this section, flexure-shear cracking will control and  $V_{uc}$  is obtained from Equation 5.8. The decompression moment  $M_o$  is given by

$$M_o = Z_b[(P_e/A) + (P_e e/Z_b)] = 134 \text{ kN m}$$

and the corresponding shear force is calculated using Equation 5.9:

$$V_o = 134 \times \frac{150}{300} = 67 \text{ kN}$$

From Equation 5.8,

$$V_{uc} = \left[ 1.15 \times 1.0 \times 370 \times 500 \left( \frac{700}{370 \times 500} \times 30 \right)^{1/3} \times 10^{-3} \right] + 67 + 50 = 220 \text{ kN}$$

The average effective prestress is  $\sigma_{cp} = P/A = 3.18 \text{ MPa}$  and from Equation 5.28,

$$T_{uc} = 35.2 \times 10^6 (0.3\sqrt{30}) [\sqrt{1 + (10 \times 3.18/30)}] \times 10^{-6} = 83 \text{ kN m}$$

The inequality of Equation 5.35 is not satisfied:

$$\frac{60 \times 10^6}{0.7 \times 83 \times 10^6} + \frac{150 \times 10^3}{0.7 \times 220 \times 10^3} \geq 0.5$$

Therefore, closed stirrups are required.

- (4) The shear strength of the section containing the minimum quantity of web reinforcement is calculated using Equation 5.6:

$$V_{u,min} = 220 + (0.6 \times 370 \times 500 \times 10^{-3}) = 331 \text{ kN}$$

Since  $V^* < \phi V_{u,min}$ , then  $\theta_o = 30^\circ$ , and since  $T^*$  is greater than

$\phi T_{uc}$  ( $=0.7 \times 83 = 58.1$  kNm), the angle  $\theta_t$  is calculated from Equation 5.30:

$$\theta_t = 30 + \frac{15(60 - 58.1)}{(0.7 \times 211) - 58.1} = 30.3^\circ$$

With  $A_t = 135 \times 10^3 \text{ mm}^2$  (see Figure 5.9) and  $f_{by} = 400$  MPa, the required amount of transverse steel may be determined from Equation 5.42:

$$\begin{aligned} \frac{A_{sw}}{s} &\geq \frac{60 \times 10^6}{0.7 \times 2 \times 400 \times 135 \times 10^3 \times \cot 30.3} \\ &+ \frac{150 \times 10^3}{0.7 \times 2 \times 400 \times 500 \times \cot 30} = 0.464 + 0.309 = 0.773 \end{aligned}$$

The steel required for torsion  $(A_{sw}/s)_t = 0.464$  is significantly more than the minimum steel requirements of Equation 5.26:

$$\frac{(A_{sw})_{min}}{s} = \frac{0.2 \times 490}{400} = 0.245$$

With 12 mm diameter stirrups,  $A_{sw} = 110 \text{ mm}^2$  and therefore

$$s \leq \frac{110}{0.773} = 142 \text{ mm}$$

which is less than the maximum permitted spacing of  $0.2u_t = 0.12 \times 1500 = 180$  mm

*Use 12 mm diameter stirrups at 140 mm centres ( $f_{vy} = 400$  MPa).*

- (5) Since the prestressing steel is required for flexural strength, the additional longitudinal steel required in the tension zone is to be supplied by non-prestressed reinforcement (with  $f_y = 400$  MPa) and is calculated using Equation 5.33. With  $(A_{sw}/s)_t = 0.464$ ,

$$A_t^* = 0.5 \times 0.464 \times 1500 \times \cot^2 30.3 \times \frac{400}{400} = 1020 \text{ mm}^2$$

*Use 4–20 mm diameter deformed longitudinal bars in the bottom of the section.*

The force in the compressive zone due to flexure,  $F_c^*$ , is approximately

$$F_c^* \approx \frac{M^*}{0.9d_p} = \frac{300 \times 10^3}{0.9 \times 375} = 889 \text{ kN}$$

and from Equation 5.34,

$$A_{lc}^* = 0.5 \times 0.464 \times 1500 \times \cot^2 30.3 - \frac{889 \times 10^3}{400} < 0$$

Therefore, no additional longitudinal reinforcement is theoretically required in the compressive zone.

*Use two 20 mm diameter top bars, one in each top corner of the stirrup.*

Checking this cross-section with the alternative procedure suggested by Rangan (1987b) (and outlined in Equations 5.43–5.45), the term

$$k = \sqrt{1 + 10\sigma_{cp}/f_c'} = \sqrt{1 + (10 \times 3.18/30)} = 1.44$$

and from Equation 5.44,

$$\begin{aligned} T_u &= \{35.2 \times 10^6 \times 0.167\sqrt{30}[(2.5 \times 1.44) - 1.5] \\ &\quad + (400 \times 0.773 \times 1.5 \times 490 \times 340)\} \times 10^{-6} = 67.6 + 77.3 = 145 \text{ kN m} \end{aligned}$$

From Equation 5.45,

$$V_u = 220 + \frac{400 \times 2 \times 110 \times 500}{142} = 530 \text{ kN}$$

and the interaction equation (Equation 5.43) gives

$$\frac{60}{0.7 \times 145} + \frac{150}{0.7 \times 530} = 0.996$$

For this example, the two procedures are in excellent agreement.

## SHEAR IN SLABS AND FOOTINGS

### 5.9 Punching shear

In the design of slabs and footings, strength in shear frequently controls the thickness of the member, particularly in the vicinity of a concentrated load or a column. Consider the pad footing shown in [Figure 5.10](#). Shear failure may occur on one of two critical sections. The footing may act essentially as a wide beam and shear failure may occur across the entire width of the member, as illustrated in [Figure 5.10a](#). This is *beam-type shear* (or one-way shear) and the shear strength of the critical section is calculated as for a beam. The critical section for this type of shear failure is usually assumed to be located at a distance  $d$  from the face of the column or concentrated load. Beam-type shear is often critical for footings but will rarely cause concern in the design of floor slabs.

An alternative type of shear failure may occur in the vicinity of a concentrated load or column and is illustrated in [Figure 5.10b](#). Failure may occur on a surface that forms a truncated cone or pyramid around the loaded area, as shown. This is known as *punching shear failure* (or two-way shear failure) and is often a critical consideration when determining the thickness of pad footings and flat slabs at the slab-column intersection. The critical section for punching shear is usually taken to be geometrically similar to the loaded area and located at a distance  $d/2$  from the face of the loaded area. The critical section (or surface) is assumed to be perpendicular to the plane of the footing or slab. The remainder of this chapter is concerned with this type of shear failure.

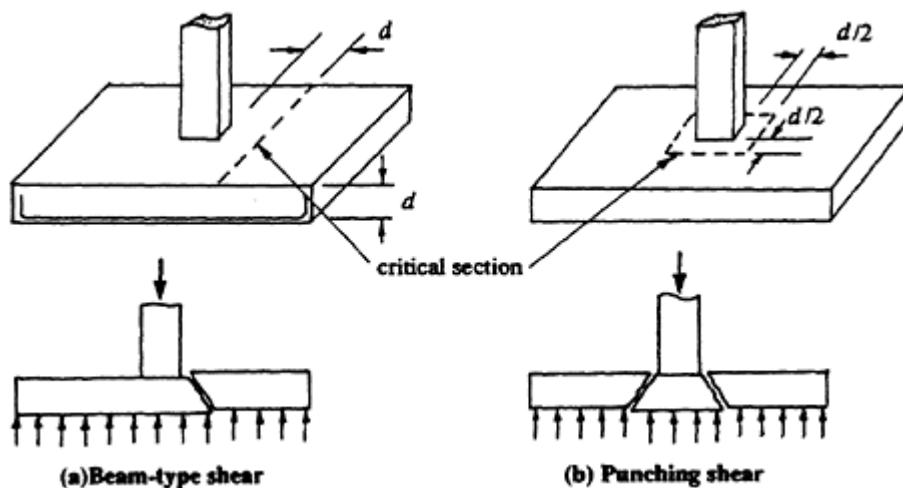


Figure 5.10 Shear failure surfaces in a footing or slab.

In ACI 318–83, the punching shear strength of a slab or footing not containing shear reinforcement,  $V_{uc}$ , is given by either Equation 5.46 or 5.47. For a non-prestressed slab or footing,

$$V_{uc} = \left(0.166 + \frac{0.33}{\beta_c}\right) \sqrt{f'_c} u d \quad (\leq 0.33 \sqrt{f'_c} u d) \quad (5.46)$$

where  $\beta_c$  is the ratio of the long side to the short side of the loaded area and  $u$  is the perimeter of the critical section. For a two-way prestressed slab, in which no portion of the column cross-section is closer to a discontinuous edge than four times the slab thickness,

$$V_{uc} = (0.29 \sqrt{f'_c} + 0.3 \sigma_{cp}) u d + V_p \quad (5.47)$$

where  $\sigma_{cp}$  is the average value of effective prestress ( $P/A$ ) for each direction and  $V_p$  is the vertical component of all effective prestressing forces crossing the critical section. In Equation 5.47,  $f'_c$  should not be taken greater than 35 MPa, and  $\sigma_{cp}$  in each direction should not be less than 1 MPa or greater than 3.5 MPa. The vertical component of prestress,  $V_p$ , in Equation 5.47 is generally small, since the tendons at the critical section are usually fairly flat and may be taken conservatively as zero.

For a critical section containing no shear reinforcement and carrying a factored design shear force  $V^*$ , the ACI 318–83 design requirement is that  $V^* \leq \phi V_{uc}$  where  $\phi = 0.85$  for shear. When both shear  $V^*$  and an unbalanced moment  $M_v^*$  are transferred from a slab to a column, ACI 318–83 suggests that the maximum shear stress on the critical section  $u_{max}^*$  may be calculated from

$$u_{max}^* = \frac{V^*}{A} + \frac{\gamma_v M_v^* y}{J} \quad (5.48)$$

where  $A$  is the area of the critical section,  $J$  is a property of the critical section analogous to the polar moment of inertia,  $\gamma_v M_v^*$  is the fraction of the unbalanced moment transferred to the column by eccentricity of shear about the centroid of the critical section (i.e. torsion), and  $y$  is the distance from the centroid of the critical section to the point where  $u_{max}^*$  acts. Shear stress resulting from  $V^*$  and  $M_v^*$  is thus assumed to vary linearly about the centroid of the critical section. The value of  $\gamma_v$  is given by the following empirical expression:

$$\gamma_v = 1 - \frac{1}{1 + \frac{2}{3} \sqrt{\frac{c_1 + d}{c_2 + d}}} \quad (5.49)$$

where  $c_1$  is the side dimension of the column in the direction of the span for which moments are determined and  $c_2$  is the side dimension of the column perpendicular to  $c_1$ .

The ACI 318–83 design requirement for a slab containing no shear reinforcement is that  $v_{max}^*$  does not exceed a permissible shear stress  $v_c$  carried by the concrete. For non-prestressed slabs,

$$v_c = \phi \left( 0.166 + \frac{0.33}{\beta_c} \right) \sqrt{f'_c} \quad (\leq \phi 0.33 \sqrt{f'_c}) \quad (5.50a)$$

and for two-way prestressed slabs that meet the requirements that apply for Equation 5.47,

$$v_c = \phi \left( 0.29 \sqrt{f'_c} + 0.3 \sigma_{cp} + \frac{V_p}{ud} \right) \quad (5.50b)$$

Although the ACI approach provides reasonable agreement with test results (Hawkins 1974), it is essentially a linear working stress design method. Such approaches for the determination of *ultimate strength* are not rational and have generally fallen from favour over the past 20 years. In addition, the approach is cumbersome and difficult to use, particularly in the case of edge and corner columns both with or without spandrel beams.

The provisions for punching shear in the Australian Code AS 3600–1988 have been developed from the results of a series of laboratory tests conducted by Rangan & Hall on large-scale reinforced concrete edge column-slab specimens (Rangan & Hall 1983a,b, Rangan 1987a). The extension of Rangan & Hall's proposals to cover prestressed concrete slabs is both logical and simple. The design rules proposed in AS 3600–1988 are outlined in [Section 5.10](#). The rules are based on a simple model of the slab-column connection. Rangan & Hall suggested that in order to determine the punching shear strength of a slab at a slab-column connection, the forces acting on the column and the capacity of the slab at each face of the column should be evaluated. Ideally in design, the column support should be large enough for the concrete to carry satisfactorily the moments and shears being transferred to the column without the need for any shear reinforcement. However, if this is not possible, procedures for the design of adequate, properly detailed reinforcement must be established.

In [Figure 5.11](#), the way in which the moments and shears are transferred to an edge column in a flat plate floor is illustrated. Some of these forces are transferred at the front face of the column ( $M_b$ ,  $V_b$ ) and the remainder through the side faces as bending, torsion and shear ( $M_s$ ,  $T_s$ ,  $V_s$ ). The front face must be able to carry  $M_b$  and  $V_b$  and the side faces must have enough strength to carry  $M_s$ ,  $T_s$ , and  $V_s$ . A punching shear failure is initiated by the failure of a slab strip at either of the side faces, in combined bending,



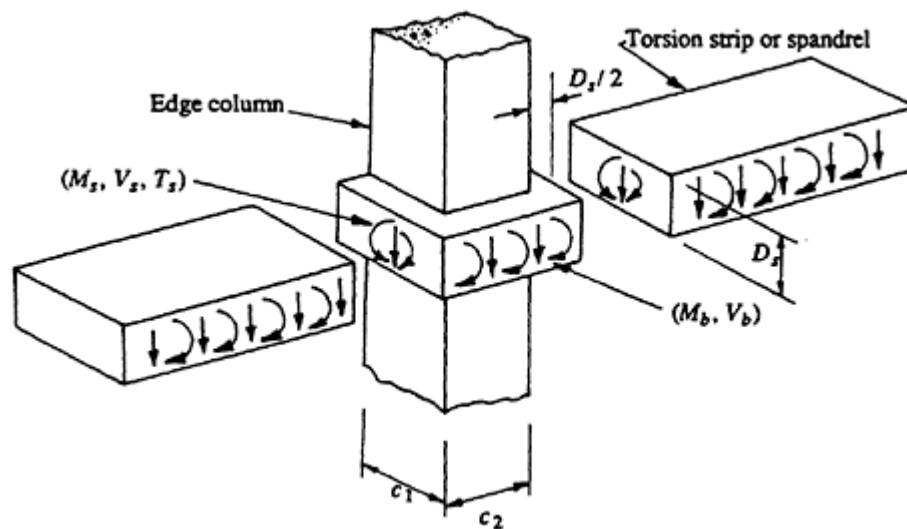


**Figure 5.11** Forces at an edge column of a flat plate floor (Rangan and Hall 1983a).

shear, and torsion, or at the front face (or back face, in the case of an interior column), in combined bending and shear. If the concrete alone is unable to carry the imposed torsion and shear in the side faces, then transverse reinforcement in the spandrels (or side strips) must be designed. The provisions for the design of beam sections in combined torsion, bending and shear (outlined in [Section 5.8](#)) may be used for the design of the spandrel strips. Account should be taken, however, of the longitudinal restraint offered by the floor slab which prevents longitudinal expansion of the strip and substantially increases torsional strength. In laboratory tests, Rangan (1987a) observed that the longitudinal restraint provided by the floor slab increased the torsional strength of the spandrels by a factor of between four and six.

## 5.10 Design procedures for punching shear in AS 3600–1988

### 5.10.1 Introduction and definitions

The *critical shear perimeter* is defined in AS 3600–1988 as being geometrically similar to the boundary of the effective area of a support, or concentrated, load and located at a distance  $d/2$  therefrom. The *effective area* of a support or concentrated load is the area totally enclosing the actual support or load, for which the perimeter is a minimum. Both the critical shear perimeter and the effective area of a support are illustrated in [Figure 5.12](#). Also shown in [Figure 5.12](#) is the reduction of the shear perimeter caused by an opening through the thickness of the slab and located

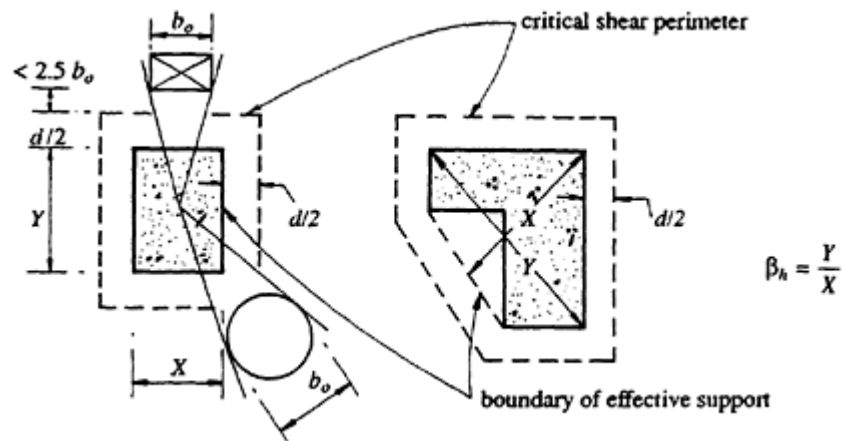


**Figure 5.12** The critical shear perimeter (from AS 3600–1988).

within a distance of  $2.5 b_o$  from the critical perimeter. The term  $b_o$  is the dimension of the critical opening, as illustrated.

The punching shear strength  $V_u$  of a slab depends on the magnitude of the bending moment ( $M_v^*$ ) being transferred from the slab to the support or loaded area. Accordingly, the design procedures with and without moment transfer are here considered separately.

### 5.10.2 Shear strength with no moment transfer

When no moment is transferred from the slab or footing to the column support or when the slab is subjected to a concentrated load, the punching shear strength of the slab is given by

$$V_{uo} = (f_{cv} + 0.3\sigma_{cp})ud \quad (5.51)$$

where  $u$  is the length of the critical shear perimeter (with account taken of the ineffective portions of the perimeter caused by adjacent openings),  $d$  is the average distance from the extreme compressive fibre to the tensile flexural reinforcement in the slab in each orthogonal direction,  $\sigma_{cp}$  is the average intensity of the effective prestress in the concrete ( $P_e/A$ ) in each direction, and  $f_{cv}$  is a limiting concrete shear stress on the critical section and is given by

$$f_{cv} = 0.17 \left( 1 + \frac{2}{\beta_h} \right) \sqrt{f'_c} \leq 0.34 \sqrt{f'_c} \quad (5.52)$$

The term  $\beta_h$  is the ratio of the longest overall dimension of the effective loaded area,  $Y$ , to the overall dimension,  $X$ , measured perpendicular to  $Y$ , as illustrated in [Figure 5.12](#). It is noted that  $f_{cv} = 0.34 \sqrt{f'_c}$  for all cases in which  $\beta_h \leq 2$ .

If a properly designed, fabricated shear head is used to increase the shear strength, an upper limit of

$$V_{uo} = (0.5\sqrt{f'_c} + 0.3\sigma_{cp})ud \leq 0.2f'_cud \tag{5.53}$$

is specified.

5.10.3 Shear strength with moment transfer

In the following, reference is made to the *torsion strips* associated with a particular slab-column connection. A torsion strip is a strip of slab of width  $a$  which frames into the side face of a column, as shown in Figure 5.13 (and also in Figure 5.11). In addition to the strip of slab, a torsion strip includes any beam that frames into the side face of the column. The longitudinal axis of a torsion strip is perpendicular to the direction of the spans used to calculate  $M_v^*$ .

Three cases are considered for the determination of the punching shear strength of slab-column connection where an unbalanced moment  $M_v^*$  is transferred from the slab to the column.

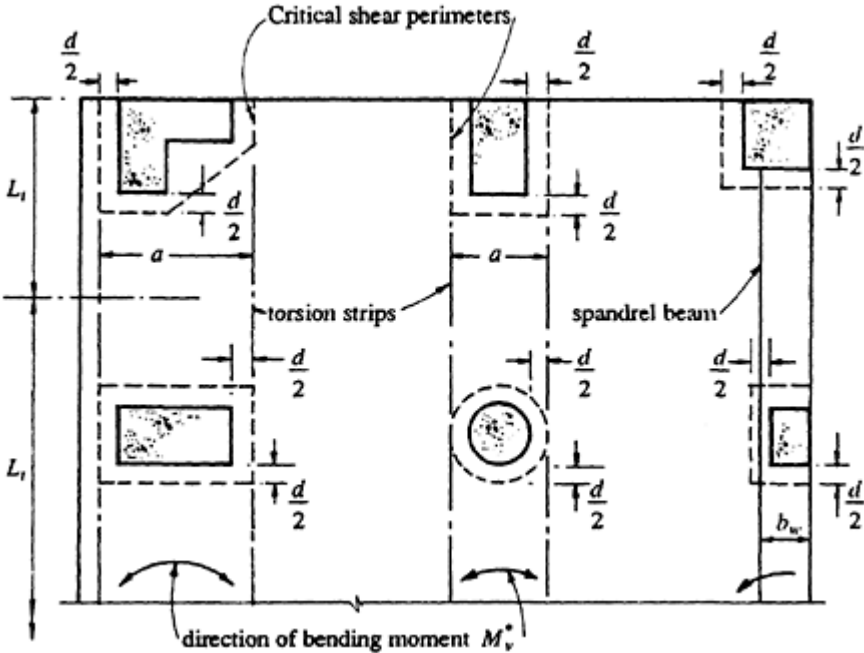


Figure 5.13 Torsion strips and spandrel beams (from AS 3600–1988).

(a) Where the torsion strip contains no beams and no closed ties

Consider a slab-column connection required to carry a factored design shear force  $V^*$  and an unbalanced moment  $M_v^*$ . The shear and torsion

carried by the torsional strip at each side face of a column may be conservatively taken to be  $V_1=(a/u)V^*$  and  $T_1=0.4M_v^*$  (Rangan 1987a). The design shear strength of the torsion strip is  $V_{uc}=(a/u)V_{uo}$  (where  $V_{uo}$  is given by Equation 5.51) and the torsional strength may be obtained using Equation 5.28. If the width of the torsion strip  $a$  is greater than the overall slab depth  $D_s$ , and if a factor  $\alpha$  is included to account for the restraint provided by the slab, then Equation 5.28 gives

$$T_{uc} = 0.4aD_s^2 \times 0.3\sqrt{f_c}k\alpha$$

where  $k = \sqrt{1 + (10\sigma_{cp}/f_c)}$ . By substituting these expressions into Equation 5.36 and by taking  $D_s=1.15d$  and  $k\alpha=6$  (as recommended by Rangan 1987a), the following expression can be derived:

$$M_v^* \leq 8d \frac{a}{u} (\phi V_{uo} - V^*) \quad (5.54)$$

i.e. the strength of the unreinforced torsion strip is adequate provided the combination of  $V^*$  and  $M_v^*$  satisfies the inequality of Equation 5.54. For design purposes, Equation 5.54 may be rearranged to give  $V^* \leq \phi V_u$ , where  $\phi = 0.7$  in AS 3600–1988.  $V_u$  is the strength of the critical section and is given by

$$V_u = \frac{V_{uo}}{1 + \frac{M_v^* u}{8V^* ad}} \quad (5.55)$$

According to AS 3600–1988, Equation 5.55 is applicable to both reinforced and prestressed concrete slab-column connections, the only difference being the inclusion of the average prestress,  $\sigma_{cp}$ , in the estimate of  $V_{uo}$  in Equation 5.51.

If  $V^*$  is not less than  $\phi V_u$ , then the critical section must be either increased in size or strengthened by the inclusion of closed stirrups in the torsion strips. In practice, it is prudent to ensure that  $M_v^*$  satisfies Equation 5.54 and hence that  $V^* \leq \phi V_u$  so that no shear reinforcement is required. The introduction of a drop panel to increase the slab depth locally over the column support or the introduction of a column capital to increase the effective support, and hence the critical shear perimeter, are measures that can often be taken to increase  $V_{uo}$ , and hence  $V_u$ , to its required value.

#### (b) Where the torsion strip contains the minimum quantity of closed stirrups

This section applies to slab-column connections that may or may not have a transverse spandrel beam within the torsion strip. AS 3600–1988 specifies that, if required, reinforcement for shear and torsion in the torsion strips

shall be in the form of closed stirrups that extend for a distance not less than  $L_t/4$  from the face of the support or concentrated load, where  $L_t$  is defined in [Figure 5.13](#). The minimum cross-section area of the closed stirrup  $(A_{sw})_{min}$  is given by Equation 5.26. The first stirrup should be located at not more than  $s/2$  from the face of the support and the stirrup spacing  $s$  should not exceed the greater of 300 mm and  $D_b$  or  $D_s$ , as applicable. At least one longitudinal bar should be provided at each corner of the stirrup. Reinforcement details and dimensions are illustrated in [Figure 5.14](#).

Using a similar derivation to that described for Equation 5.54 and with several conservative assumptions, Rangan (1987a) showed that, if a torsion strip contains the minimum quantity of closed stirrups (as specified in Equation 5.26), the strength is adequate provided that

$$M_v^* \leq 2b_w \frac{a}{u} \left[ \phi \times 1.2 \left( \frac{D_b}{D_s} \right) V_{uo} - V^* \right] \tag{5.56}$$

where  $b_w$  and  $D_b$  are the web width and overall depth of the beam in the torsion strip, as shown in [Figure 5.14](#). If the torsion strip contains no beam, then  $b_w=a$  and  $D_b=D_s$  (the slab thickness).

When  $M_v^*$  satisfies Equation 5.56, the shear strength of the critical section, with the minimum quantity of closed stirrups in the torsion strips, is given by

$$V_{u,min} = \frac{1.2(D_b/D_s)V_{uo}}{\left[ 1 + \frac{M_v^* u}{2V^* a b_w} \right]} \tag{5.57}$$

In the case of a slab-column connection without any beams framing into

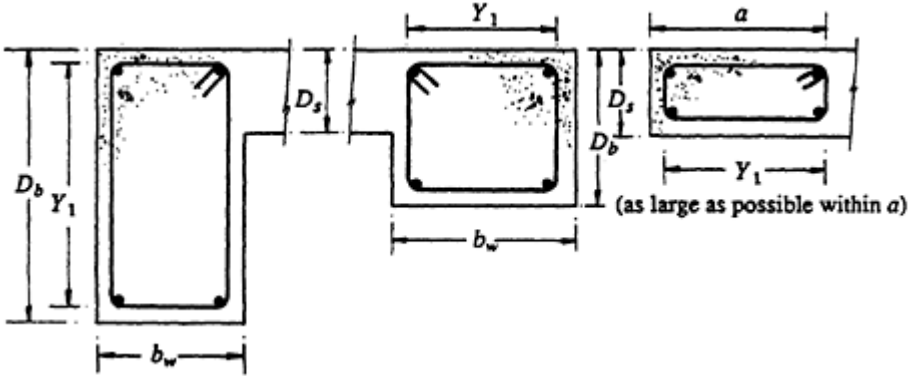


Figure 5.14 Shear reinforcement details and dimensions for slabs (from AS 3600–1988).

the side face of the column, Equation 5.57 becomes

$$V_{u,min} = \frac{1.2V_{u0}}{\left[1 + \frac{M_v^* u}{2V^* a^2}\right]} \quad (5.58)$$

When  $M_v^*$  does not satisfy Equation 5.56, i.e. when  $V^* \geq \phi V_{u,min}$  the critical section must be increased in size or the side faces must be reinforced with more than the minimum quantity of closed stirrups.

**(c) Where the torsion strips contain more than the minimum closed stirrups**

Frequently, architectural considerations prevent the introduction of spandrel beams, column capitals, drop panels (or other slab thickenings), or the use of larger columns. In such cases, when  $M_v^*$  is greater than the limits specified in Equation 5.54 or 5.56 (as applicable), it is necessary to design shear reinforcement to increase the shear strength of the critical section. This may be the case for some edge or corner columns where the moment transferred from the slab to the column is relatively large and restrictions are placed on the size of the spandrel beams.

When closed stirrups are included in the torsion strips at the side faces of the critical section, the punching shear strength is proportional to  $\sqrt{A_{sw}/s}$ , and the shear strength of the critical section containing more than the minimum amount of closed ties in the torsion strips is therefore given by (Rangan 1987a):

$$V_u = V_{u,min} \sqrt{\frac{A_{sw}}{(A_{sw})_{min}}}$$

or

$$V_u = V_{u,min} \sqrt{\frac{A_{sw} f_{ly}}{0.2 y_1 s}} \quad (5.59)$$

To avoid web-crushing of the side faces of the critical section, AS 3600–1988 requires that the maximum shear strength be limited to

$$V_{u,max} = 3V_{u,min} \sqrt{x/y} \quad (5.60)$$

where  $x$  and  $y$  are the smaller and larger dimensions, respectively, of the cross-section of the torsion strip or spandrel beam. By rearranging Equation 5.59, it can be shown that the amount of closed stirrups required in the torsion strip at the side face of the critical section must satisfy

$$\frac{A_{sw}}{s} \geq \frac{0.2 y_1}{f_{ly}} \left( \frac{V^*}{\phi V_{u,min}} \right)^2 \quad (5.61)$$



It is emphasized that Equation 5.61 should only be used where size restrictions are such that the slab thickness and support sizes are too small to satisfy Equation 5.54 or 5.56. In general, it is more efficient and economical to provide column capitals and/or drop panels to overcome punching shear than it is to try to design and detail stirrups within the slab thickness.

#### 5.10.4 Worked examples—punching shear

##### Example 5.3 —interior column (Case 1)

The punching shear strength of a prestressed concrete flat plate at an interior column is to be checked. The columns are 400 by 400 mm in section and are located on a regular rectangular grid at 8 m centres in one direction and 6 m centres in the other. The slab thickness  $D_s$  is 200 mm and the average effective depth of the tension steel is  $d=160$  mm. The following data are applicable:

$$\sigma_{cp} = 2.5 \text{ MPa}; f'_c = 30 \text{ MPa}; V^* = 520 \text{ kN}; \text{ and } M_v^* = 40 \text{ kN m.}$$

For a square interior column,  $\beta_h=1$ , and from Equation 5.52,

$$f_{cv} = 0.34\sqrt{30} = 1.86 \text{ MPa}$$

If no moment is transferred from slab to column, the shear strength of the critical section is calculated using Equation 5.51:

$$V_{uo} = 2240 \times 160 [1.86 + (0.3 \times 2.5)] \times 10^{-3} = 936 \text{ kN}$$

The critical shear perimeter  $u$  and the width of the torsion strip  $a$  are

$$u = 4(400 + 160) = 2240 \text{ mm} \quad \text{and} \quad a = 400 + 160 = 560 \text{ mm}$$

Provided that  $M_v^*$  satisfies Equation 5.54, the shear strength of the critical section is given by Equation 5.55 and no shear reinforcement is necessary.

$$8d \frac{a}{u} (\phi V_{uo} - V^*) = 8 \times 160 \times \frac{560}{2240} [(0.7 \times 936) - 520] \times 10^{-3} = 43 \text{ kN m}$$

which is greater than  $M_v^*$  and therefore the critical section is adequate without any shear reinforcement. The shear strength of the slab is obtained from Equation 5.55:

$$V_u = \frac{936}{1 + \frac{40 \times 10^6 \times 2240}{8 \times 520 \times 10^3 \times 560 \times 160}} = 755 \text{ kN}$$



and

$$\phi V_u = 528 \text{ kN} > V^*$$

∴ Punching shear strength is adequate

#### Example 5.4 —interior column (Case 2)

The slab–column connection analysed in [Example 5.3](#) is to be rechecked for the case when  $V^* = 720 \text{ kN}$  and  $M_v^* = 80 \text{ kN m}$  As in [Example 5.3](#),

$$V_{uo} = 936 \text{ kN} \quad \text{and} \quad \phi V_{uo} = 655 \text{ kN}$$

which is less than  $V^*$ , even without considering the unbalanced moment  $M_v^*$ . The critical shear perimeter is clearly not adequate. Shear and torsional reinforcement could be designed to increase the shear strength. However, successfully anchoring and locating stirrups within a 200 mm thick slab is difficult. An alternative solution is to use a fabricated steel shear head to improve resistance to punching shear. The most economical and structurally efficient solution, however, is to increase the size of the critical section. The slab thickness can often be increased locally by the introduction of a drop panel, or alternatively the critical shear perimeter may be increased by introducing a column capital or simply by increasing the column dimensions. In general, provided such dimensional changes are architecturally acceptable, they represent the best structural solution.

Let the slab thickness be increased to 250 mm by the introduction of a 50 mm thick drop panel over the column in question (i.e.  $d = 210 \text{ mm}$ ).

Now,

$$u = 4(400 + 210) = 2440 \text{ mm} \quad \text{and} \quad a = 400 + 210 = 610 \text{ mm}$$

From Equation 5.51,

$$V_{uo} = 2440 \times 210 [1.86 + (0.3 \times 2.50)] \times 10^{-3} = 1338 \text{ kN}$$

and checking Equation 5.54 gives

$$8d \frac{a}{u} (\phi V_{uo} - V^*) = 91.1 \text{ kN m} > M_v^*$$

∴ Shear strength will be adequate and no shear reinforcement is required.

Using Equation 5.55,  $\phi V_u = 741 \text{ kN}$ , which is greater than  $V^*$ , as expected.

### Example 5.5 —edge column

Consider the edge column–slab connection with critical perimeter as shown in [Figure 5.15](#). The design shear and unbalanced moment are  $V^* = 280$  kN and  $M_v^* = 160$  kN m. The slab thickness is constant at 220 mm, with *no* spandrel beams along the free slab edge. The average effective depth  $d$  to the flexural steel is 180 mm and  $f'_c = 30$  MPa.

When designing a slab for punching shear at an edge (or corner) column, the average prestress  $\sigma_{cp}$  perpendicular to the free edge across the critical section (i.e. across the width  $b_t$  in [Figure 5.15](#)) should be taken as zero, unless care is taken to ensure that the slab tendons are positioned so that this part of the critical section is subjected to prestress. Often this is not physically possible, as discussed in Section 10.2 and illustrated in [Figure 10.4](#). In this example, it is assumed that  $\sigma_{cp} = 0$  perpendicular to the free edge and  $\sigma_{cp} = 2.5$  MPa parallel to the edge.

As in [Example 5.3](#),  $f_{cv} = 1.86$  MPa and using Equation 5.51,

$$V_{uo} = \{ [1.86 + (0.3 \times 2.5)] \times 580 \times 180 + [1.86 \times (1560 - 580) \times 180] \} \times 10^{-3} = 601 \text{ kN}$$

Checking Equation 5.54 shows that

$$8 \times 180 \times \frac{490}{1560} [(0.7 \times 601) - 280] \times 10^{-3} = 63.7 \text{ kN m} < M_v^*$$

∴ The unreinforced section is *NOT* adequate.

As mentioned in the previous examples, a local increase in the slab thickness or the introduction of a spandrel beam or a column capital may prove to be the best solution. For the purposes of this example, however, shear

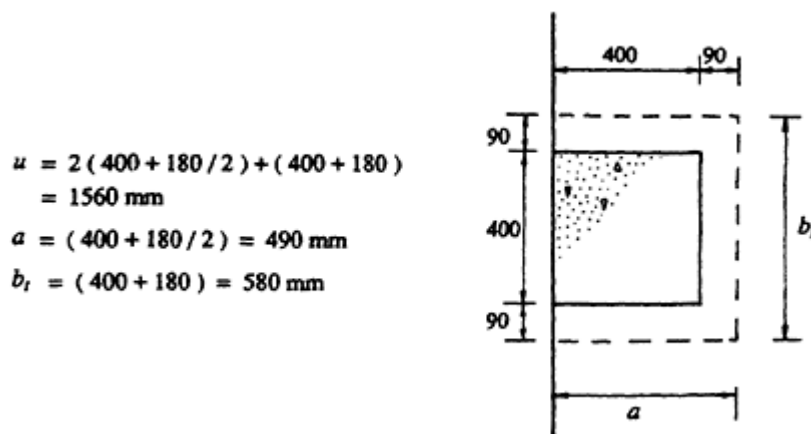


Figure 5.15 Plan view of critical section for [Example 5.5](#).

and torsional reinforcement will be designed in the slab strip of width  $a=490$  mm and depth  $D_s=220$  mm at the side faces of the critical section.

From Equation 5.58, the strength of the critical section when the side faces contain the specified minimum quantity of closed stirrups is

$$V_{u,min} = \frac{1.2 \times 601}{1 + \frac{160 \times 10^6 \times 1560}{2 \times 280 \times 10^3 \times 490 \times 490}} = 253 \text{ kN}$$

$\phi V_{u,min}$  is less than  $V^*$ , and therefore the torsion strips require more than the minimum quantity of closed stirrups. In this example, 10 mm diameter mild steel stirrups are to be used with 16 mm longitudinal bars in each corner, as shown in [Figure 5.16](#), and 25 mm clear concrete cover to the stirrups is assumed.

From Equation 5.61,

$$\frac{A_{sw}}{s} \geq \frac{0.2 \times 430}{250} \left( \frac{280}{0.7 \times 253} \right)^2 = 0.860$$

and therefore

$$s \leq 91 \text{ mm.}$$

Use 10 mm stirrups at 90 mm centres in the torsion strips.

The minimum area of longitudinal steel within the closed stirrups is obtained from Equation 5.27:

$$(A_{s+})_{min} \geq 0.2 \times 430 \times (1076/400) = 231 \text{ mm}^2$$

The 4–16 mm diameter longitudinal bars shown in [Figure 5.16](#) are more than adequate.

The shear strength of the critical section is given by Equation 5.59:

$$V_u = 253 \sqrt{\frac{78.5 \times 250}{0.2 \times 430 \times 90}} = 403 \text{ kN}$$

$$\begin{aligned} A_{sw} &= 78.5 \text{ mm}^2; f_{vy} = 250 \text{ MPa}; f_y = 400 \text{ MPa} \\ x_1 &= 220 - 2 \times 25 - 10 = 160 \text{ mm} \\ y_1 &= 490 - 2 \times 25 - 10 = 430 \text{ mm} \\ u_t &= 2 [ (430 - 26) + (160 - 26) ] \\ &= 1076 \text{ mm} \end{aligned}$$

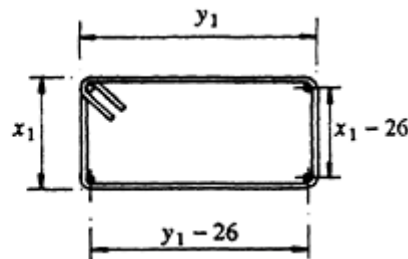


**Figure 5.16** Details of closed stirrups in the torsion strips of [Example 5.5](#).

and therefore

$$\phi V_u = 282 \text{ kN} > V^*$$

In addition, the shear strength  $V_u$  is less than the maximum strength controlled by web-crushing and given by Equation 5.60:

$$V_{u,max} = 3 \times 253 \times \sqrt{\frac{220}{490}} = 508 \text{ kN}$$

The cross-section of the proposed torsion strip is therefore adequate.

## 5.11 References

- ACI 318–83 1983. *Building code requirements for reinforced concrete*. Detroit: American Concrete Institute.
- AS 3600–1988. Australian standard for concrete structures. Sydney: Standards Association of Australia.
- BS 8110 1985. Structural use of concrete—parts 1 and 2. London: British Standards Institution.
- CAN3–A23.3–M84 1984. Design of concrete structures for buildings. Rexdale, Canada: Canadian Standards Association.
- CEB–FIP 1978. Model code for concrete structures. Paris: Comité Euro-International du Béton—Fédération Internationale de la Précontrainte.
- Collins, M.P. 1978. Towards a rational theory for RC members in shear. *Journal of the Structural Division, American Society of Civil Engineers* **104**, 649–66.
- Hawkins, N.M. 1974. Shear strength of slabs with moment transferred to columns. *Shear in Reinforced Concrete*, SP-42, Vol. 2. Detroit: American Concrete Institute.
- Hognestad, E. 1952. What do we know about diagonal tension and web reinforcement in concrete? *University of Illinois Engineering Experiment Station, Circular Series No. 64*. University of Illinois, Urbana.
- Mitchell, D. & M.P.Collins, 1974. Diagonal compression field theory—a rational model for structural concrete in pure torsion. *ACI Journal* **71**, 396–408.
- Rangan, B.V. 1987a. Punching shear strength of reinforced concrete slabs. *Civil Engineering Transactions, Institution of Engineers, Australia* **CE 29**, 71–8.
- Rangan, B.V. 1987b. Shear and torsion design in the new Australian standard for concrete structures. *Civil Engineering Transactions, Institution of Engineers, Australia*, **CE 29**, 148–56.
- Rangan, B.V. & A.S.Hall, 1983a. Forces in the vicinity of edge-columns in flat plate floors. *UNICIV Report No. R-203*. Sydney: School of Civil Engineering, University of New South Wales.
- Rangan, B.V. & A.S.Hall, 1983b. Moment and shear transfer between slab and edge column. *ACI Journal*, **80**, 183–91.
- Ritter, W. 1899. Die Bauweise Hennebique (construction methods of Hennebique). Zurich: Schweizerische Bauzeitung.
- Zia, P. & T.T.C.Hsu, 1978. Design for torsion and shear in prestressed concrete. *Preprints, ASCE Convention, Chicago*, No. 3424.

# 6

## Anchorage zones

### 6.1 Introduction

In prestressed concrete structural members, the prestressing force is usually transferred from the prestressing steel to the concrete in one of two different ways. In post-tensioned construction, relatively small anchorage plates transfer the force from the tendon to the concrete immediately behind the anchorage by bearing. For pretensioned members, the force is transferred by bond between the steel and the concrete. In either case, the prestressing force is transferred in a relatively concentrated fashion, usually at the end of the member, and involves high local pressures and forces. A finite length of the member is required for the concentrated forces to disperse to form the linear compressive stress distribution assumed in design.

The length of member over which this dispersion of stress takes place is called the *transfer length* (in the case of pretensioned members) and the *anchorage length* (for post-tensioned members). Within these so-called *anchorage zones*, a complex stress condition exists. Transverse tension is produced by the dispersion of the longitudinal compressive stress trajectories and may lead to longitudinal cracking within the anchorage zone. Similar zones of stress exist in the immediate vicinity of any concentrated force, including the concentrated reaction forces at the supports of a member.

The anchorage length in a post-tensioned member and the magnitude of the transverse forces (both tensile and compressive), that act perpendicular to the longitudinal prestressing force, depend on the magnitude of the prestressing force and on the size and position of the anchorage plate or plates. Both single and multiple anchorages are commonly used in post-tensioned construction. A careful selection of the number, size, and location of the anchorage plates can often minimize the transverse tension and hence minimize the transverse reinforcement requirements within the anchorage zone.

The stress concentrations within the anchorage zone in a pretensioned

member are not usually as severe as in a post-tensioned anchorage zone. There is a more gradual transfer of prestress. The prestress is transmitted by bond over a significant length of the tendon and there are usually numerous individual tendons that are well distributed throughout the anchorage zone. In addition, the high concrete bearing stresses behind the anchorage plates in post-tensioned members do not occur in pretensioned construction.

## 6.2 Pretensioned concrete—force transfer by bond

In pretensioned concrete, the tendons are usually tensioned within casting beds. The concrete is cast around the tendons and, after the concrete has gained sufficient strength, the pretensioning force is released. The subsequent behaviour of the member depends on the quality of bond between the tendon and the concrete. The transfer of prestress usually occurs only at the end of the member, with the steel stress varying from zero at the end of the tendon, to the prescribed amount (full prestress) at some distance in from the end. As mentioned in the previous section, the distance over which the transfer of force takes place is the *transfer length* (or the *transmission length*) and it is within this region that bond stresses are high. The better the quality of the steel–concrete bond, the more efficient is the force transfer and the shorter is the transfer length. Outside the transfer length, bond stresses at transfer are small and the prestressing force in the tendon is approximately constant. Bond stresses and localized bond failures may occur outside the transfer length after the development of flexural cracks and under overloads, but a bond failure of the entire member involves failure of the anchorage zone at the ends of the tendons.

The main mechanisms that contribute to the strength of the steel–concrete bond are chemical adhesion of steel to concrete, friction at the steel–concrete interface and mechanical interlocking of concrete and steel, which is associated primarily with deformed or twisted strands. When the tendon is released from its anchorage within the casting bed and the force is transferred to the concrete, there is a small amount of tendon slip at the end of the member. This slippage destroys the bond for a short distance into the member at the released end, after which adhesion, friction, and mechanical interlock combine to transfer the tendon force to the concrete.

During the stressing operation, there is a reduction in the diameter of the tendon due to the Poisson's ratio effect. The concrete is then cast around the highly tensioned tendon. When the tendon is released, the unstressed portion of the tendon at the end of the member returns to its original diameter, whilst at some distance into the member, where the tensile stress in the tendon is still high, the tendon remains at its reduced diameter. Within the transfer length, the tendon diameter varies as shown in [Figure 6.1](#) and there

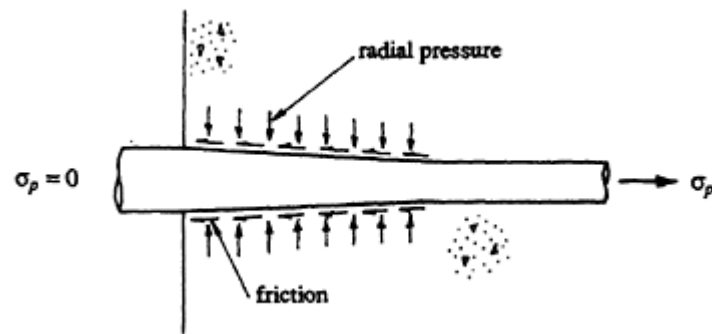


**Figure 6.1** The Hoyer effect (Hoyer 1939).

is a radial pressure exerted on the surrounding concrete. This pressure produces a frictional component which assists in the transferring of force from the steel to the concrete. The wedging action due to this radial strain is known as the *Hoyer effect* (after Hoyer 1939).

The transfer length and the rate of development of the steel stress along the tendon depend on many factors, including the size of the strand (i.e. the surface area in contact with the concrete), the surface conditions of the tendon, the type of tendon, the degree of concrete compaction within the anchorage zone, the degree of cracking in the concrete within the anchorage zone, the method of release of the prestressing force into the member, and, to a minor degree, the compressive strength of the concrete.

The factors of size and surface condition of a tendon affect bond capacity in the same way as they do for non-prestressed reinforcement. A light coating of rust on a tendon will provide greater bond than for steel that is clean and bright. The surface profile has a marked effect on transfer length. Stranded cables have a shorter transfer length than crimped or plain steel of equal area owing to the interlocking between the helices forming the strand. The strength of concrete, within the range of strengths used in prestressed concrete members, does not greatly affect the transfer length. However, with increased concrete strength, there is greater shear strength of the concrete embedded between the individual wires in the strand.

An important factor in force transfer is the quality and degree of concrete compaction. The transfer length in poorly compacted concrete is significantly longer than that in well compacted concrete. A prestressing tendon anchored at the top of a member generally has a greater transfer length than a tendon located near the bottom of the member. This is because the concrete at the top of a member is subject to increased sedimentation and is generally less well compacted than at the bottom of a member. When the tendon is released suddenly and the force is transferred to the concrete with impact, the transfer length is greater than for the case when the force in the steel is gradually imparted to the concrete.

Depending on the above factors, transfer lengths are generally within the

range 40–150 times the tendon diameter. The force transfer is not linear, with about 50% of the force transferred in the first quarter of the transfer length and about 80% within the first half of the length. For design purposes, however, it is reasonable and generally conservative to assume a linear variation of steel stress over the entire transfer length.

BS 8110 (1985) specifies that provided the initial prestressing force is not greater than 75% of the characteristic strength of the tendon and the concrete in the anchorage zone is well compacted, the transfer (transmission) length of a tendon that is gradually released at transfer, may be taken as

$$l_t = \frac{K_t d_b}{\sqrt{f'_{ci}}} \quad (6.1)$$

where  $d_b$  is the nominal diameter of the tendon and

$K_t$	=600	for plain or indented wire
	=400	for crimped wire
	=240	for 7-wire standard or super strands

A generally more conservative value of  $l_t=60d_b$  for regular, super, or compact strand is specified in AS 3600–1988.

Sudden release of the tendon at transfer may cause large increases in  $l_t$  above the value given by Equation 6.1. In addition, if the tendon is anchored in the top of a member, the value given by Equation 6.1 should be increased by at least 50%. Owing to the breakdown of bond at the end of a member and the consequent slip, a completely unstressed length of  $l_t/10$  should be assumed to develop at the end of the member (AS 3600–1988).

The value of stress in the tendon, in regions outside the transmission length, remains approximately constant under service loads or whilst the member remains uncracked, and hence the transfer length remains approximately constant. After cracking in a flexural member, however, the behaviour becomes more like that of a reinforced concrete member and the steel stress increases with increasing moment. If the critical moment location occurs at or near the end of a member, such as may occur in a short-span beam or a cantilever, the required development length for the tendon is much greater than the transfer length. In such cases, the bond capacity of the tendons needs to be carefully considered.

ACI 318–83 (1983) suggests that, at the ultimate load condition, in order to ensure the development of the final stress  $\sigma_{pu}$  in the prestressing steel at a section near the end of a member, a development length  $l_d$  is required. This development length is the sum of the transfer length  $l_t$ , which is the length required to develop the effective prestress in the steel,  $\sigma_{pe}$  (in MPa), and an additional length  $l'_d$  required to develop the additional steel stress  $\sigma_{pu}-\sigma_{pe}$ . For 7-wire strand, ACI 318–83 specifies the following empirical



estimates of these lengths (here converted to SI units):

$$l_t = \left(\frac{\sigma_{pe}}{20}\right) d_b \quad \text{and} \quad l'_t = (\sigma_{pu} - \sigma_{pe}) \frac{d_b}{7}$$

The total development length of  $l_d = (l_t + l'_t)$  is therefore given by

$$l_d = \left(\frac{\sigma_{pe}}{20}\right) d_b + \left(\frac{\sigma_{pu} - \sigma_{pe}}{7}\right) d_b \quad (6.2)$$

The ACI 318–83 requirements are based on tests of small diameter strands reported by Hanson & Kaar 1959. [Figure 6.2](#) illustrates the variation of steel stress with distance from the free end of the tendon.

ACI 318–83 further suggests that in the case of members where bond is terminated before the end of the member (i.e. a portion of the tendons at the member end is deliberately debonded), and where the design permits tension at service load in the pre-compressed tensile zone, the development length given by Equation 6.2 should be doubled.

From test results, Marshall and Mattock (1962) proposed the following simple equation for determining the amount of transverse reinforcement  $A_s$  (in the form of stirrups) in the end zone of a pretensioned member:

$$A_s = 0.021 \frac{D P}{l_t \sigma_s} \quad (6.3)$$

where  $D$  is the overall depth of the member,  $P$  is the prestressing force,

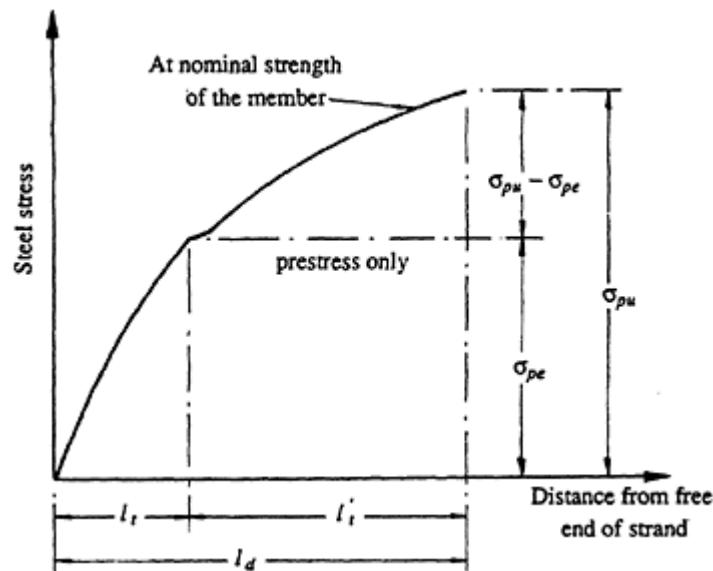


**Figure 6.2** Variation of steel stress near the free end of a tendon (ACI 318–83).

$l_t$  is the transfer length, and  $\sigma_s$  is the permissible steel stress which may be taken as 150 MPa. The transverse steel  $A_s$  should be equally spaced within  $0.2D$  from the end face of the member.

## 6.3 Post-tensioned concrete anchorage zones

### 6.3.1 Introduction

In post-tensioned concrete structures, failure of the anchorage zone is perhaps the most common cause of problems arising during construction. Such failures are difficult and expensive to repair and usually necessitate replacement of the entire structural member. Anchorage zones may fail owing to uncontrolled cracking or splitting of the concrete resulting from insufficient, well anchored, transverse reinforcement. Bearing failures immediately behind the anchorage plate are also common and may be caused by inadequately dimensioned bearing plates or poor quality concrete. Bearing failures are most often attributed to poor design and/or poor workmanship resulting in poorly compacted concrete in the heavily reinforced region behind the bearing plate. Great care should therefore be taken in both the design and construction of post-tensioned anchorage zones.

Consider the case shown in [Figure 6.3](#) of a single square anchorage plate centrally positioned at the end of a prismatic member of depth  $D$  and width  $B$ . In the *disturbed region* of length  $L_a$  immediately behind the anchorage plate (i.e. the anchorage zone), plane sections do not remain plane and simple beam theory does not apply. High bearing stresses at the anchorage plate disperse throughout the anchorage zone, creating high transverse stresses, until at a distance  $L_a$  from the anchorage plate the linear stress and strain distributions predicted by simple beam theory are produced. The dis-

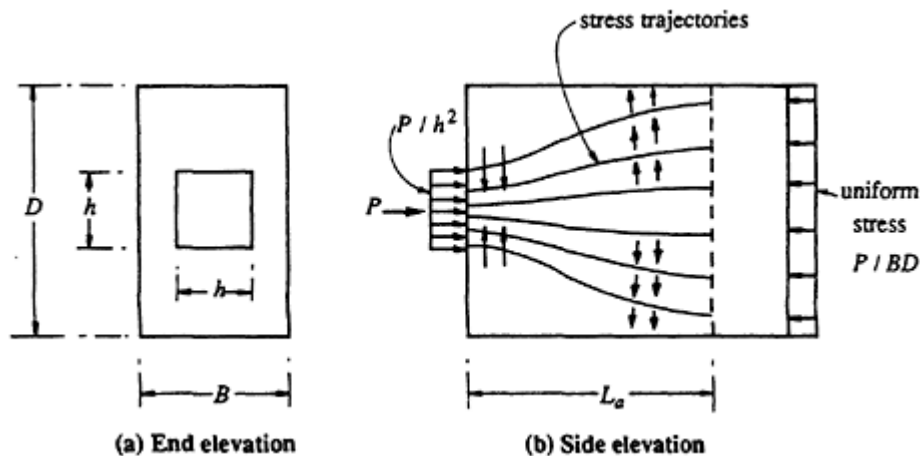


**Figure 6.3** Diagrammatic stress trajectories for a centrally placed anchorage.

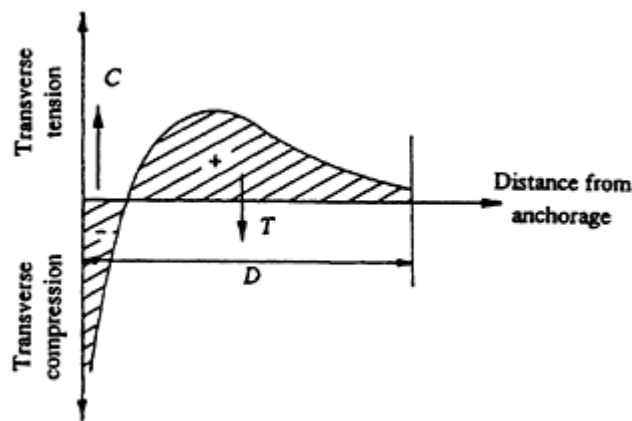


**Figure 6.4** Distribution of transverse stress behind single central anchorage.

persion of stress that occurs within the anchorage zone is illustrated in [Figure 6.3b](#). The stress trajectories directly behind the anchorage are convex to the centre-line of the member, as shown, and therefore produce a transverse component of compressive stress normal to the member axis. Further from the anchorage, the compressive stress trajectories become concave to the member axis and as a consequence produce transverse tensile stress components. The stress trajectories are closely spaced directly behind the bearing plate where compressive stress is high, and become more widely spaced as the distance from the anchorage plate increases. St Venant's principle suggests that the length of the disturbed region, for the single centrally located anchorage shown in [Figure 6.3](#), is approximately equal to the depth of the member,  $D$ . The variation of the transverse stresses along the centre-line of the member, and normal to it, are represented in [Figure 6.4](#).

The degree of curvature of the stress trajectories is dependent on the size of the bearing plate. The smaller the bearing plate, the larger are both the curvature and concentration of the stress trajectories, and hence the larger are the transverse tensile and compressive forces in the anchorage zone. The transverse tensile forces (often called *bursting* or *splitting forces*) need to be estimated accurately so that transverse reinforcement within the anchorage zone can be designed to resist them.

Elastic analysis can be used to analyse anchorage zones prior to the commencement of cracking. Early studies using photo-elastic methods (Tesar 1932, Guyon 1953) demonstrated the distribution of stresses within the anchorage zone. Analytical models were also proposed by Iyengar (1962), Iyengar and Yogananda (1966), Sargious (1960), and others. The results of these early elastic studies have been confirmed by more recent finite element investigations. [Figure 6.5a](#) shows stress isobars of  $\sigma_y/\sigma_x$  in an anchorage zone with a single centrally placed anchorage. These isobars are similar to those obtained in photo-elastic studies reported by Guyon (1953).  $\sigma_y$  is the

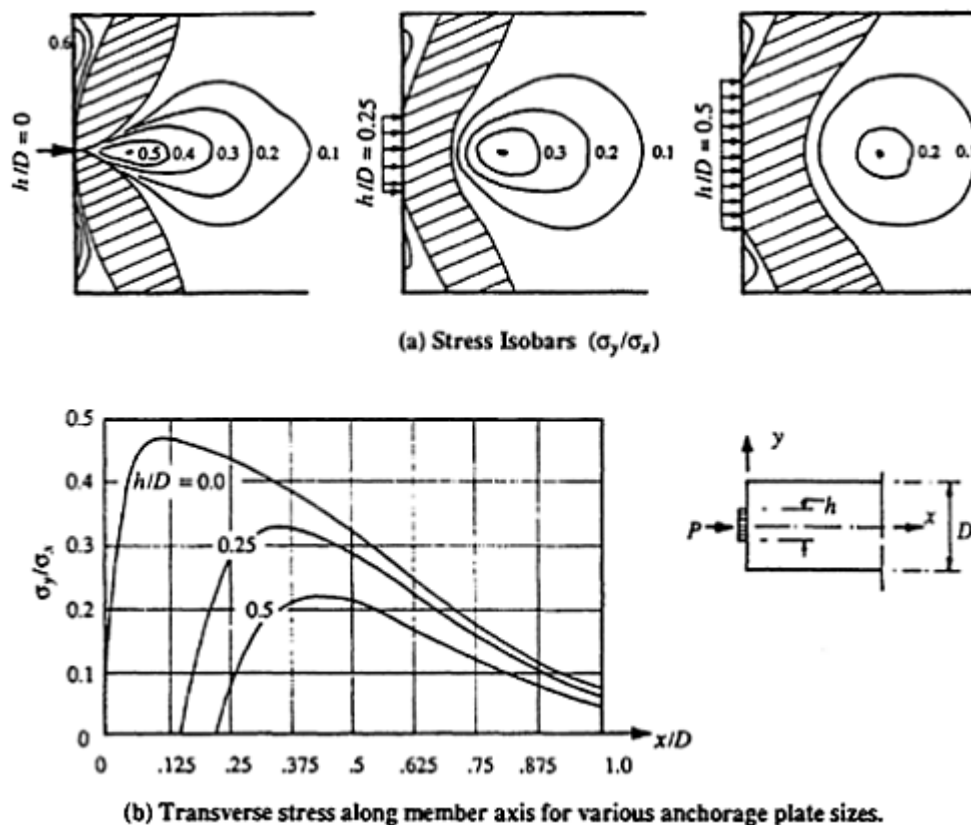


**Figure 6.5** Transverse stress distribution for central anchorage (after Guyon 1953).

transverse stress and  $\sigma_x$  is the average longitudinal compressive stress ( $P/BD$ ). The transverse compressive stress region is shaded.

The effect of varying the size of the anchor plate on both the magnitude and position of the transverse stress along the axis of the member can be also clearly seen in [Figure 6.5b](#). As the plate size increases, the magnitude of the maximum transverse tensile stress on the member axis decreases and its position moves further along the member (i.e. away from the anchorage plate). Tensile stresses also exist at the end surface of the anchorage zone in the corners adjacent to the bearing plate. Although these stresses are relatively high, they act over a small area and the resulting tensile force is small. Guyon (1953) suggested that a tensile force of about 3% of the longitudinal prestressing force is located near the end surface of a centrally loaded anchorage zone when  $h/D$  is greater than 0.10.

The position of the line of action of the prestressing force with respect to the member axis has a considerable influence on the magnitude and distribution of stress within the anchorage zone. As the distance of the applied force from the axis of the member increases, the tensile stress at the loaded face adjacent to the anchorage also increases. [Figure 6.6a](#) illustrates the

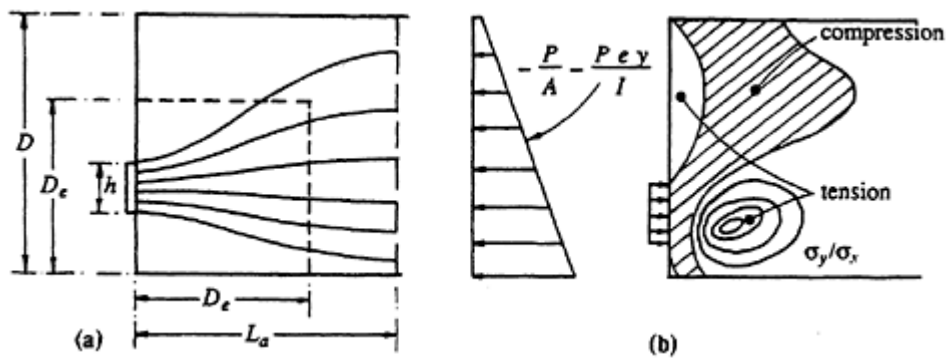


**Figure 6.6** Diagrammatic stress trajectories and isobars for an eccentric anchorage (Guyon 1953).

stress trajectories in the anchorage zone of a prismatic member containing an eccentrically positioned anchorage plate. At a length  $L_a$  from the loaded face, the concentrated bearing stresses disperse to the asymmetric stress distribution shown. The stress trajectories, which indicate the general flow of forces, are therefore unequally spaced, but will produce transverse tension and compression along the anchorage axis in a manner similar to that for the single centrally placed anchorage.

Isobars of  $\sigma_y/\sigma_o$  are shown in [Figure 6.6b](#). High bursting forces exist along the axis of the anchorage plate and, away from the axis of the anchorage, tensile stresses are induced on the end surface. These end tensile stresses, or spalling stresses, are typical of an eccentrically loaded anchorage zone.

Transverse stress isobars in the anchorage zones of members containing multiple anchorage plates are shown in [Figure 6.7](#). The length of the member over which significant transverse stress exists ( $L_a$ ) reduces with the number of symmetrically placed anchorages. The zone directly behind each

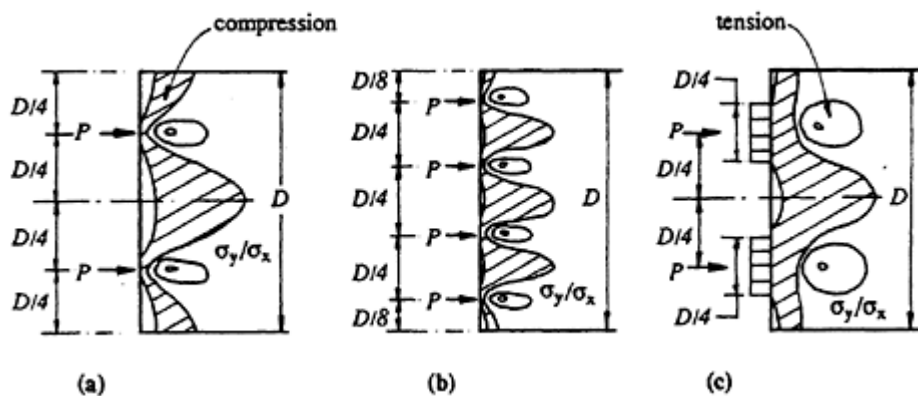


**Figure 6.7** Transverse stress isobars for end zones with multiple anchorages (Guyon 1953).

anchorage contains bursting stresses and the stress isobars resemble those in a single anchorage centrally placed in a much smaller end zone, as indicated. Tension also exists at the end face between adjacent anchorage plates. Guyon (1953) suggested that the tensile force near the end face between any two adjacent bearing plates is about 4% of the sum of the longitudinal prestressing forces at the two anchorages.

The isobars presented in this section are intended only as a means of visualizing behaviour. Concrete is not a linear-elastic material and a cracked prestressed concrete anchorage zone does not behave exactly as depicted by the isobars in [Figures 6.5–6.7](#). However, such linear-elastic analyses indicate the areas of high tension, both behind each anchorage plate and on the end face of the member, where cracking of the concrete can be expected during the stressing operation. The formation of such cracks reduces the stiffness in the transverse direction and leads to a significant redistribution of forces within the anchorage zone.

### 6.3.2 Methods of analysis

The design of the anchorage zone of a post-tensioned member involves both the arrangement of the anchorage plates, to minimize transverse stresses, and the determination of the amount and distribution of reinforcement to carry the transverse tension after cracking of the concrete. Relatively large amounts of transverse reinforcement, usually in the form of stirrups, are often required within the anchorage zone and careful detailing of the steel is essential to ensure the satisfactory placement and compaction of the concrete. In thin-webbed members, the anchorage zone is often enlarged to form an end-block which is sufficient to accommodate the anchorage devices. This also facilitates the detailing and fixing of the reinforcement and the subsequent placement of concrete.

The anchorages usually used in post-tensioned concrete are patented by the manufacturer and prestressing companies for each of the types and arrangements of tendons. In general, they are units which are recessed into the end of the member, and have bearing areas which are sufficient to prevent bearing problems in well-compacted concrete. Often the anchorages are manufactured with *fins* which are embedded in the concrete to assist in distributing the large concentrated force. Spiral reinforcement often forms part of the anchorage system and is located immediately behind the anchorage plate to confine the concrete and thus significantly improve its bearing capacity.

As discussed in [Section 6.3.1](#), the curvature of the stress trajectories determines the magnitude of the transverse stresses. In general, the dispersal of the prestressing forces occurs through both the depth and the width of the anchorage zone and therefore transverse reinforcement must be provided within the end zone in two orthogonal directions (usually, vertically

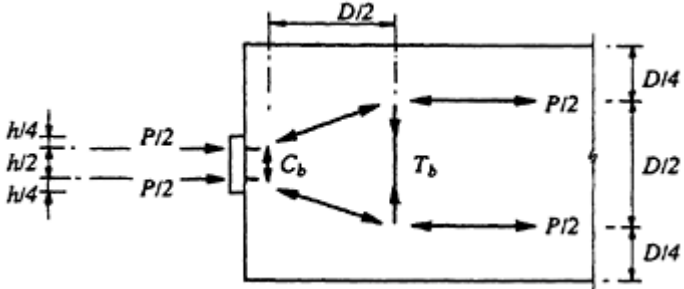


Figure 6.8 Truss analogy of anchorage zone.

and horizontally on sections through the anchorage zone). The reinforcement quantities required in each direction are obtained from separate two-dimensional analyses, i.e. the vertical transverse tension is calculated by considering the vertical dispersion of forces and the horizontal tension is obtained by considering the horizontal dispersion of forces.

The internal flow of forces in each direction can be visualized in several ways. A simple model is to consider truss action within the anchorage zone. For the anchorage zone of the beam of rectangular cross-section shown in Figure 6.8, the truss analogy shows that transverse compression exists directly behind the bearing plate, with transverse tension, often called the bursting force ( $T_b$ ), at some distance along the member.

Consider the anchorage zone of the T-beam shown in Figure 6.9. The truss analogy is recommended by the FIP (1984) for calculating both the vertical tension in the web and the horizontal tension across the flange.

An alternative model for estimating the internal tensile forces is to consider the anchorage zone as a deep beam loaded on one side by the bearing

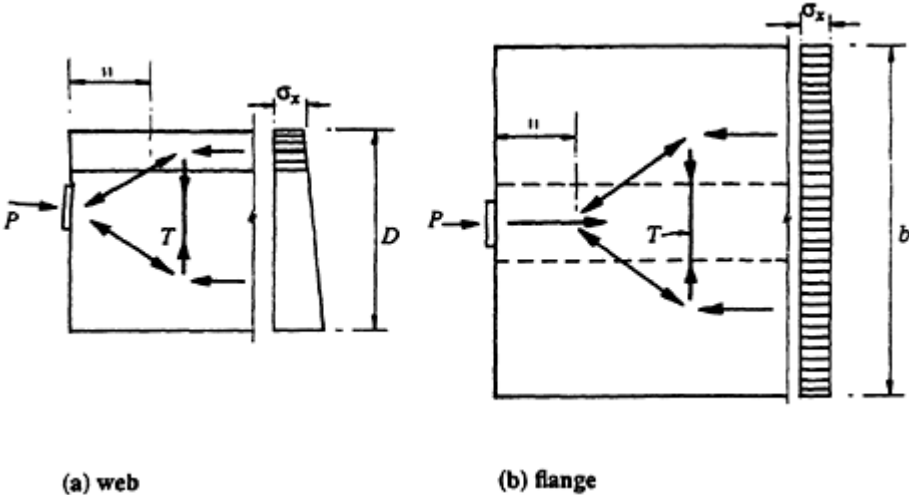


Figure 6.9 Vertical and horizontal tension in the anchorage zone of a post-tensioned T-beam (FIP 1984).

stresses immediately under the anchorage plate and resisted on the other side by the statically equivalent, linearly distributed stresses in the beam. The depth of the deep beam is taken as the anchorage length,  $L_a$ . This approach was proposed by Magnel (1954) and has been further developed by Gergely & Sozen (1967) and Warner & Faulkes (1979).

**A single central anchorage**

The beam analogy model is illustrated in [Figure 6.10](#) for a single central anchorage, together with the bending moment diagram for the idealized beam. Since the maximum moment tends to cause bursting along the axis of the anchorage, it is usually denoted by  $M_b$  and called the *bursting moment*.

By considering one half of the end-block as a free-body diagram, as shown in [Figure 6.11](#), the bursting moment  $M_b$  required for rotational equilibrium is obtained from statics. Taking moments about any point on the member axis gives

$$M_b = \frac{P}{2} \left( \frac{D}{4} - \frac{h}{4} \right) = \frac{P}{8} (D - h) \tag{6.4}$$

As has already been established, the position of the resulting transverse (vertical) tensile force  $T_b$  in [Figure 6.11](#) is located at some distance from the anchorage plate, as shown. For a linear-elastic anchorage zone, the exact position of  $T_b$  is the centroid of the area under the appropriate transverse tensile stress curve in [Figure 6.5b](#). For the single, centrally placed anchorage of [Figures 6.5, 6.10 and 6.11](#), the lever arm between  $C_b$  and  $T_b$  is approximately equal to  $D/2$ . This approximation also proves to be a reasonable one for a cracked concrete anchorage zone. Therefore, using Equation 6.4,

$$T_b \approx \frac{M_b}{D/2} = \frac{P}{4} \left( 1 - \frac{h}{D} \right) \tag{6.5}$$

Expressions for the bursting moment and the horizontal transverse tension

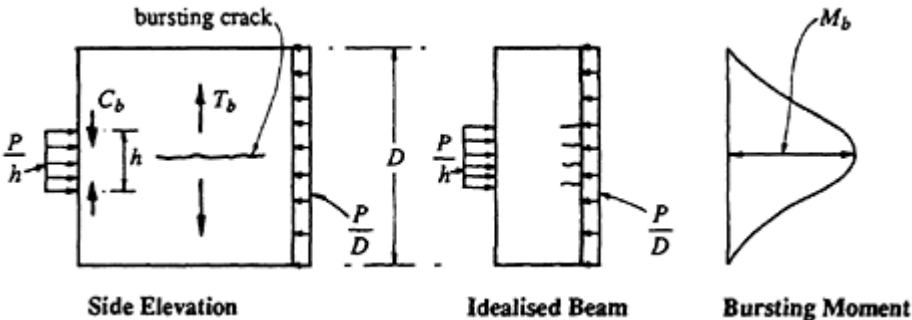


**Figure 6.10** Beam analogy for a single centrally placed anchorage.



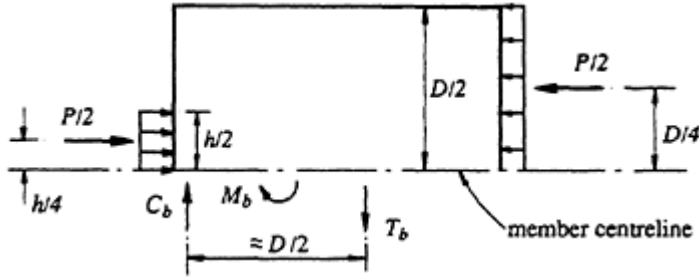


Figure 6.11 Free-body diagram of top half of the anchorage zone shown in Figure 6.10.

resulting from the lateral dispersion of bearing stresses across the width  $B$  of the section are obtained by replacing the depth  $D$  in Equations 6.4 and 6.5 with the width  $B$ .

**Two symmetrically placed anchorages**

Consider the anchorage zone shown in Figure 6.12a containing two anchorages each positioned equidistant from the member axis. The beam analogy of Figure 6.12b indicates bursting moments,  $M_b$ , on the axis of each anchorage and a spalling moment,  $M_s$  (of opposite sign to  $M_b$ ), on the member axis, as shown. Potential crack locations within the anchorage zone are also shown in Figure 6.12a. The bursting moments behind each anchorage plate produce tension at some distance into the member, while the spalling moments produce transverse tension at the end face of the member. This simple analysis agrees with the stress isobars for the linear-elastic end block of Figure 6.7c. Consider the free-body diagram shown in Figure 6.12c. The

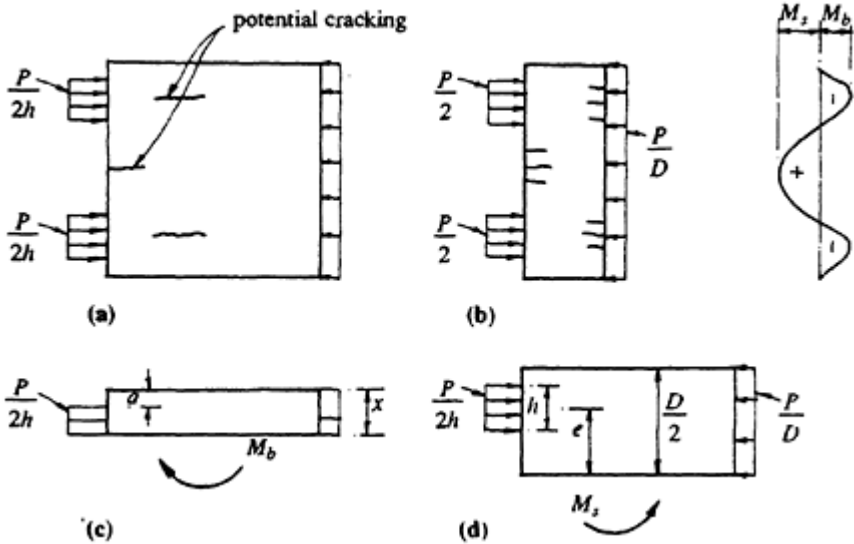


Figure 6.12 Beam analogy for an anchorage zone with two symmetric anchorages.

maximum bursting moment behind the top anchorage occurs at the distance  $x$  below the top fibre, where the shear force at the bottom edge of the free-body is zero. That is,

$$\frac{P}{D} x = \frac{P}{2h} (x - a) \quad \text{or} \quad x = \frac{aD}{D - 2h} \quad (6.6)$$

Summing moments about any point in [Figure 6.12c](#) gives

$$M_b = \frac{Px^2}{2D} - \frac{P(x - a)^2}{4h} \quad (6.7)$$

The maximum spalling moment  $M_s$  occurs at the member axis, where the shear is also zero, and may be obtained by taking moments about any point on the member axis in the free-body diagram of [Figure 6.12d](#):

$$M_s = \frac{P}{2} \left( e - \frac{D}{4} \right) \quad (6.8)$$

After the maximum bursting and spalling moments have been determined, the resultant internal compressive and tensile forces can be estimated provided that the lever arm between them is known. The internal tension  $T_b$  produced by the maximum bursting moment  $M_b$  behind each anchorage may be calculated from

$$T_b = \frac{M_b}{l_b} \quad (6.9)$$

By examining the stress contours in [Figure 6.7](#), the distance between the resultant transverse tensile and compressive forces behind each anchorage  $l_b$  depends on the size of the anchorage plate and the distance between the plate and the nearest adjacent plate or free edge of the section.

Guyon (1953) suggested an approximate method which involves the use of an *idealized symmetric prism* for computing the transverse tension behind an eccentrically positioned anchorage. The assumption is that the transverse stresses in the real anchorage zone are the same as those in a concentrically loaded idealized end block consisting of a prism that is symmetrical about the anchorage plate and with a depth  $D_e$  equal to twice the distance from the axis of the anchorage plate to the nearest concrete edge. If the internal lever arm  $l_b$  is assumed to be half the depth of the symmetrical prism (i.e.  $D_e/2$ ), then the resultant transverse tension induced along the line of action of the anchorage is obtained from an equation that is identical with Equation 6.5, except that the depth of the symmetric prism

$D_e$  replaces  $D$ . Thus

$$T_b = \frac{P}{4} \left( 1 - \frac{h}{D_e} \right) \quad (6.10)$$

where  $h$  and  $D_e$  are, respectively, the dimensions of the anchorage plate and the symmetric prism in the direction of the transverse tension  $T_b$ . For a single concentrically located anchorage plate  $D_e = D$  (for vertical tension) and Equations 6.5 and 6.10 are identical. Alternatively, the tension  $T_b$  can be calculated from the bursting moment obtained from the statics of the real anchorage zone using a lever arm  $l_b = D_e/2$ . Guyon's symmetric prism concept is now accepted as a useful design procedure and has been incorporated in a number of building codes, including AS 3600–1988.

For anchorage zones containing multiple bearing plates, the bursting tension behind each anchorage, for the case where all anchorages are stressed, may be calculated using Guyon's symmetric prisms. The depth of the symmetric prism  $D_e$  associated with a particular anchorage may be taken as the smaller of

- (a) the distance in the direction of the transverse tension from the centre of the anchorage to the centre of the nearest adjacent anchorage; and
- (b) twice the distance in the direction of the transverse tension from the centre of the anchorage to the nearest edge of the anchorage zone.

For each symmetric prism, the lever arm  $l_b$  between the resultant transverse tension and compression is  $D_e/2$ .

The anchorage zone shown in [Figure 6.13](#) contains two symmetrically placed anchorage plates located close together near the axis of the member. The stress contours show the bulb of tension immediately behind each anchorage plate. Also shown in [Figure 6.13](#) is the symmetric prism of depth

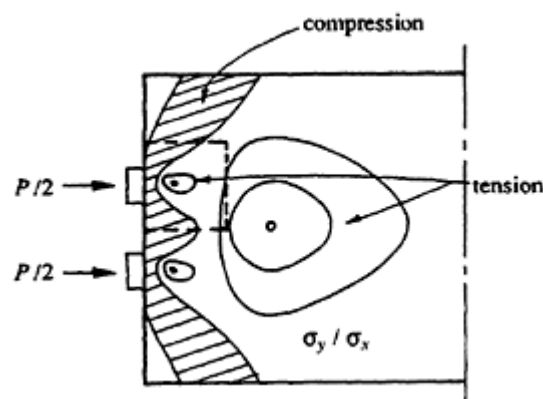


**Figure 6.13** Two closely spaced symmetric anchorage plates.

$D_e$  to be used to calculate the resultant tension and the transverse reinforcement required in this region. Tension also exists further along the axis of the member in a similar location to that which occurs behind a single concentrically placed anchorage. AS 3600–1988 suggests that where the distance between two anchorages is less than 0.3 times the total depth of a member, consideration must also be given to the effects of the pair of anchorages acting in a manner similar to a single anchorage subject to the combined forces.

### Reinforcement requirements

In general, reinforcement should be provided to carry all the transverse tension in an anchorage zone. It is unwise to assume that the concrete will be able to carry any tension or that the concrete in the anchorage zone will not crack. The quantity of transverse reinforcement  $A_{sb}$  required to carry the transverse tension caused by bursting can be obtained by dividing the appropriate tensile force, calculated using Equation 6.8 or 6.9, by the permissible steel stress:

$$A_{sb} = \frac{T_b}{\sigma_s} \quad (6.11)$$

AS 3600–1988 suggests that, for crack control, a steel stress of no more than 150 MPa should be used. Equation 6.11 may be used to calculate the quantity of bursting reinforcement in both the vertical and horizontal directions. The transverse steel so determined must be distributed over that portion of the anchorage zone in which the transverse tension associated with the bursting moment is likely to cause cracking of the concrete. Therefore, the steel area  $A_{sb}$  should be uniformly distributed over the portion of beam located from  $0.2D_e$  to  $1.0D_e$  from the loaded end face (AS 3600–1988). For the particular bursting moment being considered,  $D_e$  is the depth of the symmetric prism in the direction of the transverse tension and equals  $D$  for a single concentric anchorage. The stirrup size and spacing so determined should also be provided in the portion of the beam from  $0.2D_e$  to as near as practicable to the loaded face.

For spalling moments, the lever arm  $l_s$  between the resultant transverse tension  $T_s$  and compression  $C_s$  is usually larger than for bursting, as can be seen from the isobars in [Figure 6.7](#). AS 3600–1988 suggests that for a single eccentric anchorage, the transverse tension at the loaded face remote from the anchorage may be calculated by assuming that  $l_s$  is half the overall depth of the member. Between two widely spaced anchorages, the transverse tension at the loaded face may be obtained by taking  $l_s$  equal to 0.6 times the spacing of the anchorages. The reinforcement required to resist the

transverse tension at the loaded face  $A_{ss}$  is therefore obtained from

$$A_{ss} = \frac{T_s}{\sigma_s} = \frac{M_s}{\sigma_s l_s} \quad (6.12)$$

and should be placed within  $0.2D$  from the loaded face. In general,  $A_{ss}$  should be located as close to the loaded face as is permitted by concrete cover and compaction requirements.

### 6.3.3 Bearing stresses behind anchorages

Local concrete bearing failures can occur in post-tensioned members immediately behind the anchorage plates if the bearing area is inadequate and the concrete strength is too low. The design bearing strength for unconfined concrete may be taken as (ACI 318–83, AS 3600–1988, CAN3 1984):

$$F_b = \phi \times 0.85 f_{ci} \sqrt{\frac{A_2}{A_1}} \quad (\leq \phi \times 1.7 f_{ci}) \quad (6.13)$$

where  $f_{ci}$  is the compressive strength of the concrete at the time of first loading,  $A_1$  is the net bearing area and  $A_2$  is the largest area of the concrete supporting surface that is geometrically similar to and concentric with  $A_1$ .

For post-tensioned anchorages, provided the concrete behind the anchorage is well compacted, the bearing stress given by Equation 6.13 can usually be exceeded. The transverse reinforcement which is normally included behind the anchorage plate confines the concrete and generally improves the bearing capacity. Often spiral reinforcement, in addition to transverse stirrups, is provided with commercial anchorages. In addition, the transverse compression at the loaded face immediately behind the anchorage plate significantly improves the bearing capacity of such anchorages. Commercial anchorages are typically designed for bearing stresses of about 40 MPa and bearing strength is specified by the manufacturer and is usually based on satisfactory test performance. For post-tensioned anchorage zones containing transverse reinforcement, the design bearing stress given by Equation 6.13 can be increased by at least 50%, but a maximum value of  $\phi \times 2.5 f_{ci}$  is recommended.

### 6.3.4 Example 6.1—A single concentric anchorage on a rectangular section

The anchorage zone of a flexural member with the dimensions shown in [Figure 6.14](#) is to be designed. The size of the bearing plate is 315 mm square with a duct diameter of 106 mm, as shown. The jacking force is  $P_j=3000$  kN and the concrete strength at transfer is 35 MPa.

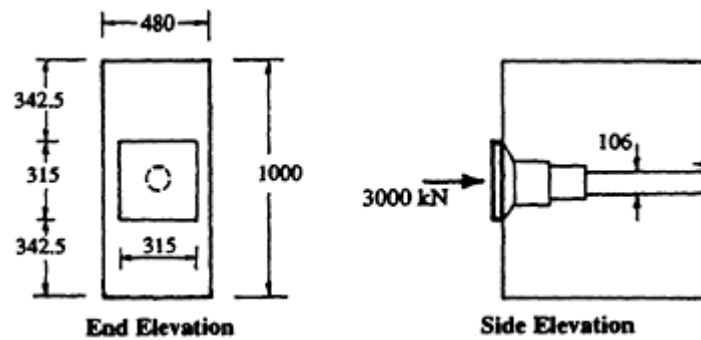


Figure 6.14 Anchorage zone arrangement in [Example 6.1](#)

Consider the bearing stress immediately behind the anchorage plate. For bearing strength calculations, the strength load factors and capacity reduction factors contained in AS 3600–1988 are adopted, i.e. the design load is  $1.15P_j$  and  $\phi = 0.6$  (see Sections [1.7.3](#) and [1.7.6](#)). The nett bearing area  $A_1$  is the area of the plate minus the area of the hollow duct. That is,

$$A_1 = 315 \times 315 - \frac{\pi \times 106^2}{4} = 90.4 \times 10^3 \text{ mm}^2$$

and for this anchorage

$$A_2 = 480 \times 480 = 230 \times 10^3 \text{ mm}^2$$

The design bearing stress is therefore

$$\sigma_b = \frac{1.15P_j}{A_1} = \frac{1.15 \times 3000 \times 10^3}{90.4 \times 10^3} = 38.2 \text{ MPa}$$

In accordance with the discussion in [Section 6.3.3](#), the design strength in bearing is taken as 50% greater than the value obtained using Equation 6.13. Therefore,

$$F_b = 1.5 \times 0.6 \times 0.85 \times 35 \sqrt{\frac{230 \times 10^3}{90.4 \times 10^3}} = 42.7 \text{ MPa}$$

which is acceptable.

**Consider moments in the vertical plane** (i.e. vertical bursting tension)

The forces and bursting moments in the vertical plane are illustrated in [Figure 6.15a](#). From Equations 6.4 and 6.5,

$$M_b = \frac{3000}{8} (1000 - 315) \times 10^{-3} = 257 \text{ kN m}$$

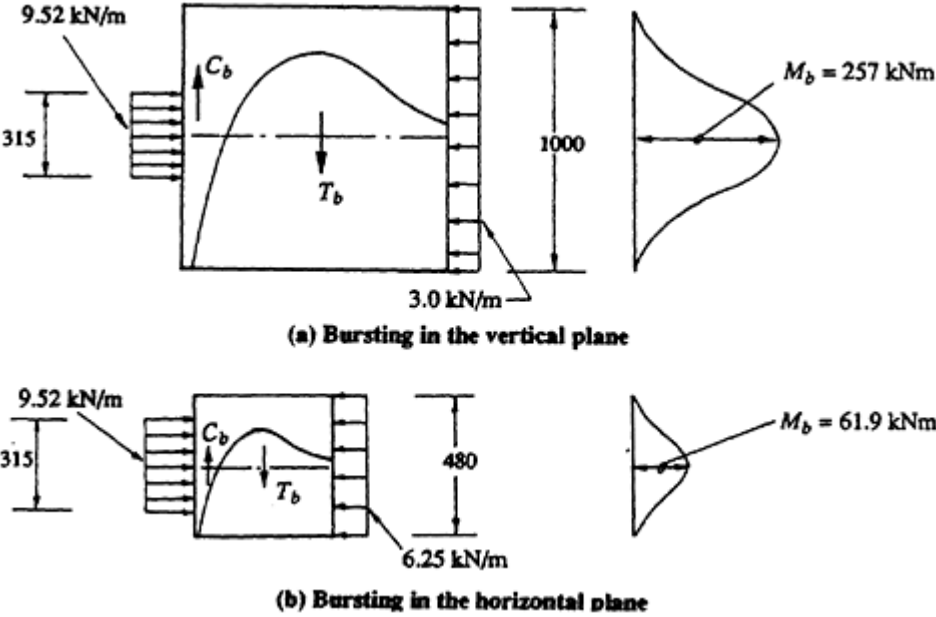


Figure 6.15 Force and moment diagrams for vertical and horizontal bursting.

and

$$T_b = \frac{257 \times 10^3}{500} = 514 \text{ kN}$$

The amount of vertical transverse reinforcement is calculated from Equation 6.11. Assuming that  $\sigma_s=150$  MPa:

$$A_{sb} = \frac{514 \times 10^3}{150} = 3430 \text{ mm}^2$$

This area of transverse steel must be provided within the length of beam located from  $0.2D$  to  $1.0D$  from the loaded end face, i.e. over a length of  $0.8D=800$  mm.

Two 12 mm diameter stirrups (four vertical legs) are required at 100 mm centres (i.e.  $A_{sb}=8 \times 4 \times 110=3520 \text{ mm}^2$  within the 800 mm length). This size and spacing of stirrups must be provided over the entire anchorage zone, i.e. for a distance of 1000 mm from the loaded face.

**Consider moments in the horizontal plane** (i.e., horizontal bursting tension)

The forces and bursting moments in the horizontal plane are illustrated in Figure 6.15b. With  $B=480$  mm replacing  $D$  in Equations 6.4 and 6.5, the bursting moment and horizontal tension are

$$M_b = \frac{3000}{8} (480 - 315) \times 10^{-3} = 61.9 \text{ kNm}$$

and

$$T_b = \frac{61.9 \times 10^3}{240} = 258 \text{ kN}$$

The amount of horizontal transverse steel is obtained from Equation 6.11 as

$$A_{sb} = \frac{258 \times 10^3}{150} = 1720 \text{ mm}^2$$

which is required within the length of beam located between 96 mm (0.2*B*) and 480 mm (1.0*B*) from the loaded face.

Four pairs of closed 12 mm stirrups (i.e. four horizontal legs per pair of stirrups) at 100 mm centres ( $A_{sb}=1760 \text{ mm}^2$ ) satisfies this requirement. To satisfy horizontal bursting requirements, this size and spacing of stirrups should be provided from the loaded face for a length of at least 480 mm.

To accommodate a tensile force at the loaded face of  $0.03P=90 \text{ kN}$ , an area of steel of  $90 \times 10^3 / 150 = 600 \text{ mm}^2$  must be placed as close to the loaded face as possible. This is in accordance with Guyon’s (1953) recommendation discussed in [Section 6.3.1](#). The first stirrup supplies  $440 \text{ mm}^2$  and, with two such stirrups located within 150 mm of the loaded face, the existing reinforcement is considered to be adequate.

The transverse steel details shown in [Figure 6.16](#) are adopted here. Within the first 480 mm, where horizontal transverse steel is required, the stirrups are closed at the top, as indicated, but for the remainder of the anchorage zone, between 480 and 1000 mm from the loaded face, open stirrups may be used to facilitate placement of the concrete. The first stirrup is placed as close as possible to the loaded face, as shown.

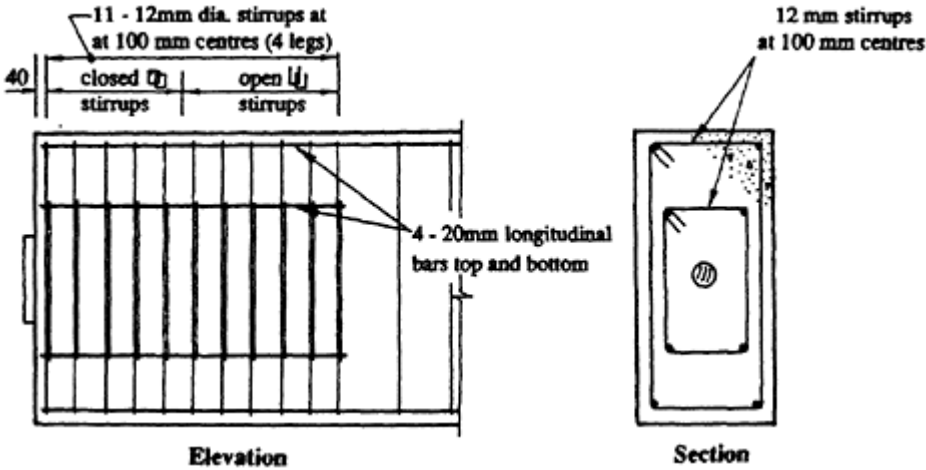
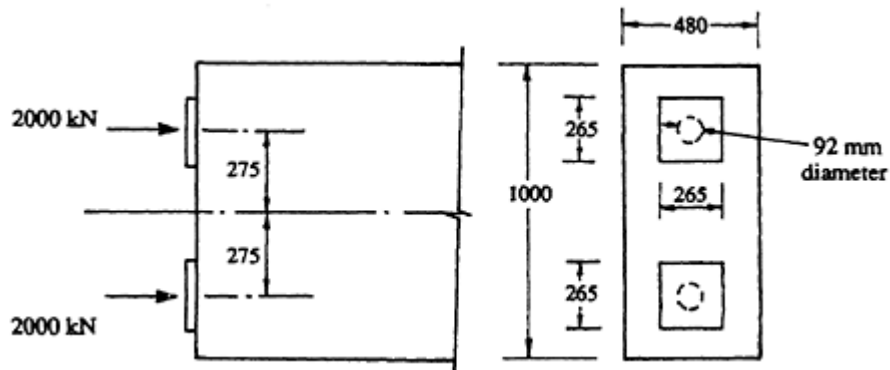


Figure 6.16 Reinforcement details, [Example 6.1](#).



### 6.3.5 Example 6.2—Twin eccentric anchorages on a rectangular section

The anchorage shown in [Figure 6.17](#) is to be designed. The jacking force at each of the two anchorages is  $P_j=2000$  kN and the concrete strength is  $f'_c = 35$  MPa.



**Figure 6.17** Twin anchorage arrangement, [Example 6.2](#).

#### Check on bearing stresses behind each anchorage

As in [Example 6.1](#), the design strength in bearing  $F_b$  is taken to be 50% greater than the value given by Equation 6.13. In this example,

$$A_1 = 265^2 - \frac{\pi \times 92^2}{4} = 63.6 \times 10^3 \text{ mm}^2; \quad A_2 = 450^2 = 202.5 \times 10^3 \text{ mm}^2$$

and

$$F_b = 1.5 \times 0.6 \times 0.85 \times 35 \sqrt{\frac{202.5 \times 10^3}{63.6 \times 10^3}} = 47.8 \text{ MPa}$$

Using a load factor of 1.15 for prestress (AS 3600–1988), the design bearing stress is

$$\sigma_b = \frac{1.15 \times 2000 \times 10^3}{63.6 \times 10^3} = 36.2 \text{ MPa}$$

which is less than  $F_b$  and is therefore satisfactory.

#### Case (a) Consider the lower cable only stressed

It is necessary first to examine the anchorage zone after just one of the tendons has been stressed. The stresses, forces, and corresponding moments acting on the eccentrically loaded anchorage zone are shown in [Figure 6.18](#).

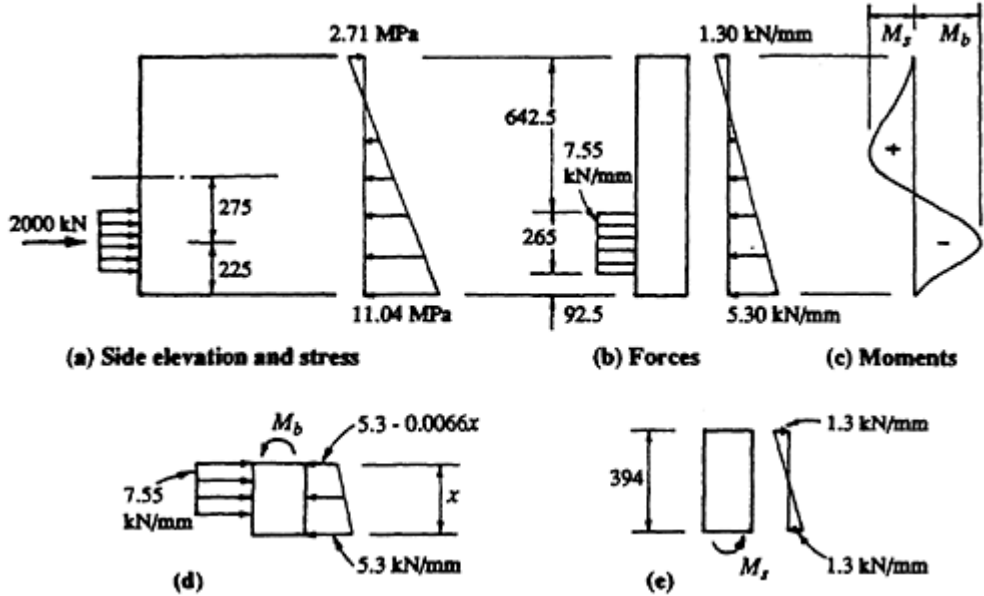


Figure 6.18 Actions on anchorage zone in Example 6.2 when the lower cable only is tensioned.

The maximum bursting moment  $M_b$  occurs at a distance  $x$  from the bottom surface at the point of zero shear in the free-body diagram of Figure 6.18d:

$$7.55(x - 92.5) = \frac{5.3 + (5.3 - 0.0066x)}{2} x$$

$$\therefore x = 231.8 \text{ mm}$$

and from statics

$$M_b = \left( 5.3 \frac{231.8^2}{2} - 1.53 \frac{231.8^2}{6} - 7.55 \frac{139.3^2}{2} \right) \times 10^{-3} = 55.5 \text{ kN m}$$

The maximum spalling moment  $M_s$  occurs at 394 mm below the top surface where the shear is also zero, as shown in Figure 6.18e:

$$M_s = 1.3 \frac{394^2}{6} \times 10^{-3} = 33.6 \text{ kN m}$$

**Design for  $M_b$**  The symmetric prism which is concentric with and directly behind the lower anchorage plate has a depth of  $D_e=450$  mm and is shown

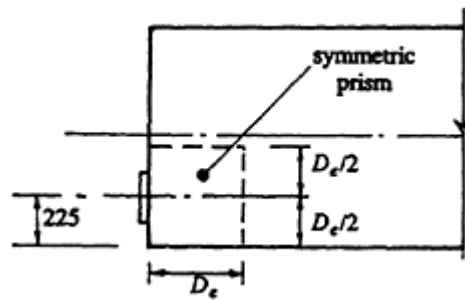


**Figure 6.19** Symmetric prism for one eccentric anchorage, [Example 6.2](#).

in [Figure 6.19](#). From Equation 6.9,

$$T_b = \frac{M_b}{l_b} = \frac{55.5 \times 10^3}{225} = 246.5 \text{ kN}$$

By contrast, Equation 6.10 gives

$$T_b = \frac{2000}{4} \left( 1 - \frac{265}{450} \right) = 206 \text{ kN}$$

which is considerably less conservative in this case. Adopting the value of  $T_b$  obtained from the actual bursting moment, Equation 6.11 gives

$$A_{sb} = \frac{246.5 \times 10^3}{150} = 1640 \text{ mm}^2$$

This area of steel must be distributed over a distance of  $0.8D_e=360$  mm.

For the steel arrangement illustrated in [Figure 6.21](#), 16 mm diameter and 12 mm diameter stirrups are used at the spacings indicated, i.e. a total of four vertical legs of area  $620 \text{ mm}^2$  per stirrup location are used behind each anchorage. The number of such stirrups required in the 360 mm length of the anchorage zone is  $1640/620=2.65$  and therefore the maximum spacing of the stirrups is  $360/2.65=135$  mm. This size and spacing of stirrups is required from the loaded face to 450 mm therefrom. The spacing of the stirrups in [Figure 6.21](#) is less than that calculated here because the horizontal bursting moment and spalling moment requirements are more severe. These are examined subsequently.

**Design for  $M_s$**  The lever arm  $l_s$  between the resultant transverse compression and tension forces which resist  $M_s$  is taken as  $0.5D=500$  mm. The area of transverse steel required within  $0.2D=200$  mm from the front face is

given by Equation 6.12:

$$A_{ss} = \frac{33.6 \times 10^6}{150 \times 500} = 448 \text{ mm}^2$$

The equivalent of about four vertical 12 mm diameter steel legs is required close to the loaded face of the member to carry the resultant tension caused by spalling. This requirement is easily met by the three full depth 16 mm diameter stirrups (six vertical legs) shown in [Figure 6.21](#) located within  $0.2D$  of the loaded face.

### Case (b) Consider both cables stressed

[Figure 6.20](#) shows the force and moment distribution for the end block when both cables are stressed.

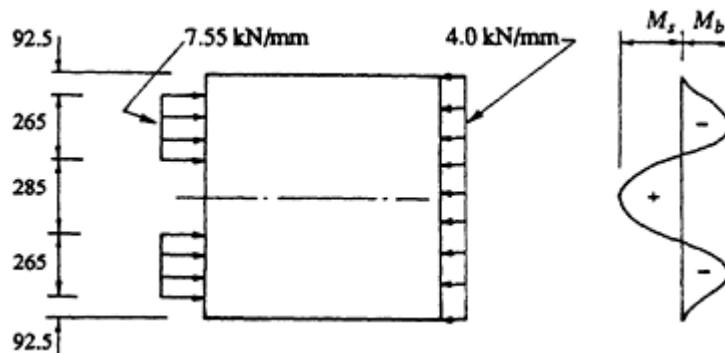


**Figure 6.20** Force and moment distribution when both cables are stressed.

**Design for  $M_b$**  The maximum bursting moment behind the anchorage occurs at the level of zero shear,  $x$  mm below the top surface and  $x$  mm above the bottom surface. From Equation 6.6:

$$x = \frac{92.5 \times 1000}{1000 - (2 \times 265)} = 196.8 \text{ mm}$$

and Equation 6.7 gives

$$M_b = \left( \frac{4000 \times 196.8^2}{2 \times 1000} - \frac{4000 \times 104.3^2}{4 \times 265} \right) \times 10^{-3} = 36.3 \text{ kN m}$$

which is less than the value for  $M_b$  when only the single anchorage was stressed. Since the same symmetric prism is applicable here, the reinforcement requirements for bursting determined in case (a) are more than sufficient.

**Design for  $M_s$**  The spalling moment at the mid-depth of the anchorage zone (on the member axis) is obtained from Equation 6.8:

$$M_s = \frac{4000}{2} \left( 275 - \frac{1000}{4} \right) \times 10^{-3} = 50 \text{ kNm}$$

With  $l_s$  taken as 0.6 times the spacing between the anchorages (see the discussion preceding Equation 6.12), i.e.  $l_s=330$  mm, the area of transverse steel required within 200 mm of the loaded face is found using Equation 6.12:

$$A_{ss} = \frac{50 \times 10^6}{150 \times 330} = 1010 \text{ mm}^2$$

To avoid steel congestion, 16 mm diameter stirrups will be used close to the loaded face, as shown in [Figure 6.21](#). Use six vertical legs of 16 mm diameter ( $1200 \text{ mm}^2$ ) across the member axis within 200 mm of the loaded face, as shown.

#### Case (c) Consider horizontal bursting

Horizontal transverse steel must also be provided to carry the transverse tension caused by the horizontal dispersion of the total prestressing force ( $P=400$  kN) from a 265 mm wide anchorage plate into a 480 mm wide section. With  $B=480$  mm used instead of  $D$ , Equations 6.4 and 6.5 give

$$M_b = 107.5 \text{ kNm} \quad \text{and} \quad T_b = 448 \text{ kN}$$

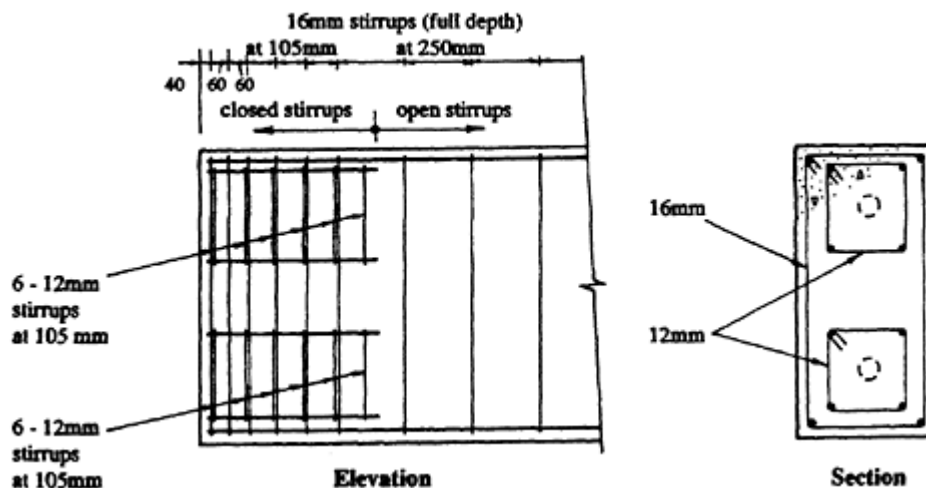


Figure 6.21 Reinforcement details for anchorage zone of [Example 6.2](#).

and the amount of horizontal steel is obtained from Equation 6.11:

$$A_{sb} = 2990 \text{ mm}^2$$

With the steel arrangement shown in [Figure 6.21](#), six horizontal bars exist at each stirrup location (2–16mm diameter bars and 4–12 mm diameter bars, i.e. 840 mm<sup>2</sup> at each stirrup location). The required stirrup spacing within the length  $0.8D(=384 \text{ mm})$  is 108 mm. Therefore, within 480 mm from the end face of the beam, all available horizontal stirrup legs are required and therefore all stirrups in this region must be closed.

The reinforcement details shown in [Figure 6.21](#) are adopted.

6.3.6 Example 6.3—Single concentric anchorage in a T-beam

The anchorage zone of the T-beam shown in [Figure 6.22a](#) is to be designed. The member is prestressed by a single cable with a 265 mm square anchorage plate located at the centroidal axis of the cross-section. The jacking force is  $P_j=2000 \text{ kN}$  and the concrete strength at transfer is 35 MPa. The distribution of forces on the anchorage zone in elevation and in plan are shown in [Figures 6.22b](#) and [c](#), respectively.

The design bearing stress and the design strength in bearing are calculated

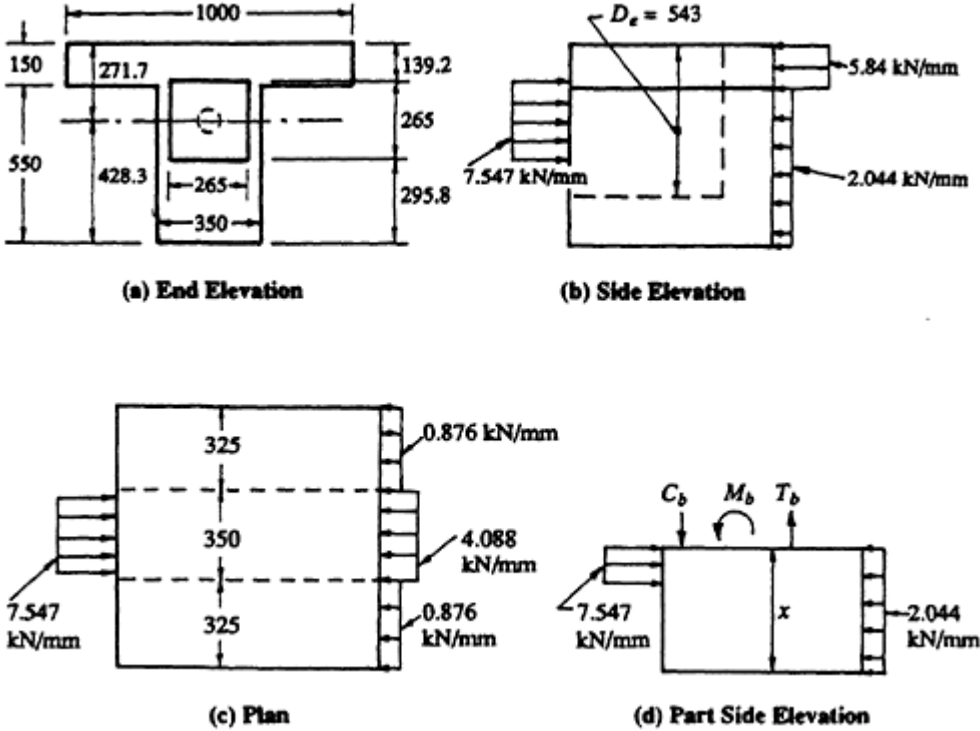


Figure 6.22 Details of the anchorage zone of the T-beam in [Example 6.3](#).

as for the previous examples:

$$\sigma_b = 36.2 \text{ MPa} \quad \text{and} \quad F_b = 37.2 \text{ MPa}$$

**Consider moments in the vertical plane**

The maximum bursting moment occurs at the level of zero shear at  $x$  mm above the bottom of the section. From [Figure 6.22d](#),

$$2.044x = 7.547(x - 295.8) \quad \text{and} \quad \therefore x = 405.7 \text{ mm}$$

and

$$M_b = \left( \frac{2.044 \times 405.7^2}{2} - \frac{7.547(405.7 - 295.8)^2}{2} \right) \times 10^{-3} = 123 \text{ kN m}$$

As indicated in [Figure 6.22b](#), the depth of the symmetric prism associated

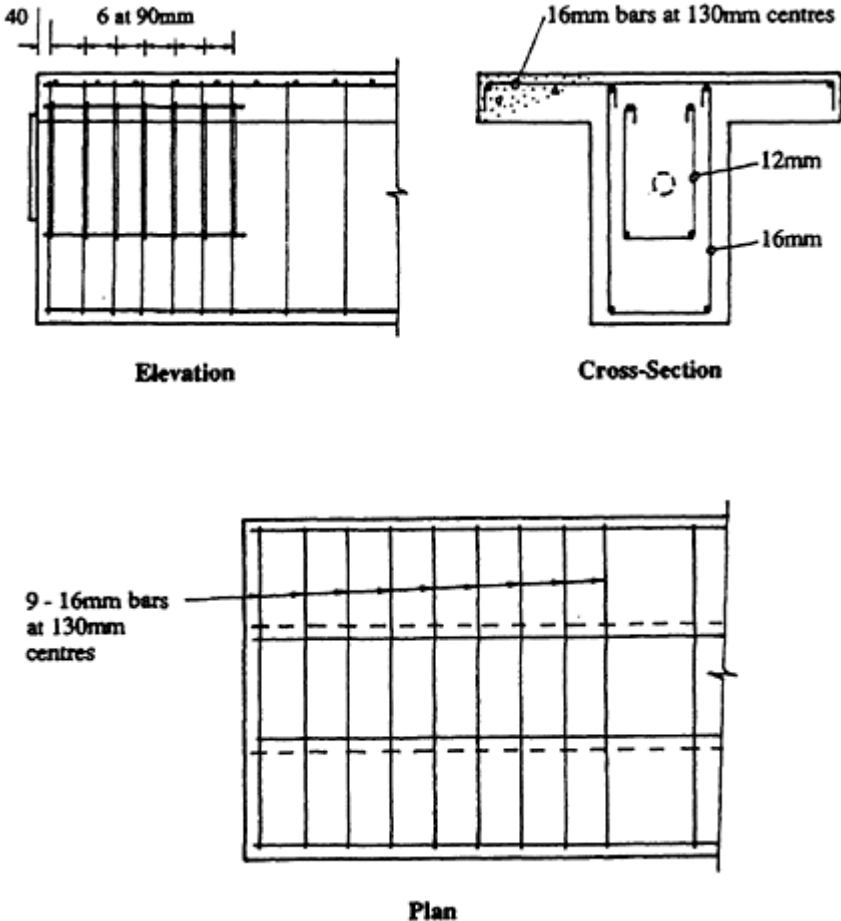


**Figure 6.23** Reinforcement details for anchorage zone of [Example 6.3](#).

with  $M_b$  is  $D_e=543$  mm and the vertical tension is

$$T_b = \frac{M_b}{D_e/2} = 451 \text{ kN}$$

The vertical transverse reinforcement required in the web is obtained from Equation 6.11:

$$A_{sb} = \frac{451 \times 10^3}{150} = 3010 \text{ mm}^2$$

This area of steel must be located within the length of the beam between  $0.2D_e=109$  mm and  $D_e=543$  mm from the loaded face.

By using 16 mm stirrups over the full depth of the web and 12 mm stirrups immediately behind the anchorage, as shown in [Figure 6.23](#) [i.e.  $A_{sb}=(2 \times 200)+(2 \times 110)=620 \text{ mm}^2$  per stirrup location], the number of double stirrups required is  $3010/620=4.85$  and the required spacing is  $(543-109)/4.85=90$  mm, as shown.

#### Consider moments in the horizontal plane

Significant lateral dispersion of prestress in plan occurs in the anchorage zone as the concentrated prestressing force finds its way out into the flange of the T-section. By taking moments of the forces shown in [Figure 6.22c](#) about a point on the axis of the anchorage, the horizontal bursting moment is

$$\begin{aligned} M_b &= [(0.876 \times 325 \times 337.5) + (4.088 \times 175 \times 87.5) \\ &\quad - (1000 \times 66.25)] \times 10^{-3} \\ &= 92.4 \text{ kN m} \end{aligned}$$

Much of this bursting moment must be resisted by horizontal transverse tension and compression in the flange. Taking  $D_e$  equal to the flange width, the lever arm between the transverse tension and compression is  $l_b=D_e/2=500$  mm and the transverse tension is calculated using Equation 6.9:

$$T_b = \frac{92.4 \times 10^3}{500} = 185 \text{ kN}$$

The area of horizontal transverse reinforcement required in the flange is therefore

$$A_{sb} = \frac{185 \times 10^3}{150} = 1235 \text{ mm}^2$$

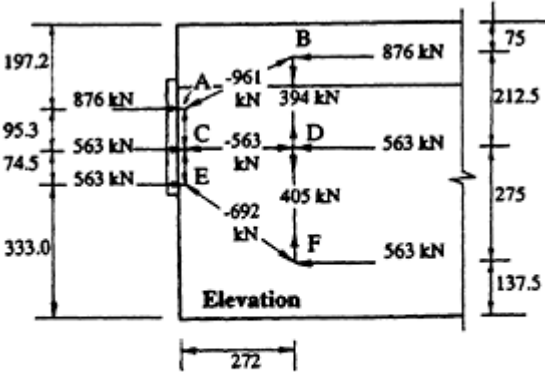


This quantity of steel should be provided within the flange and located between 200 and 1000 mm from the loaded face. Adopt 16 mm bars across the flange at 130 mm centres from the face of the support to 1000 mm therefrom, as shown in [Figure 6.23](#).

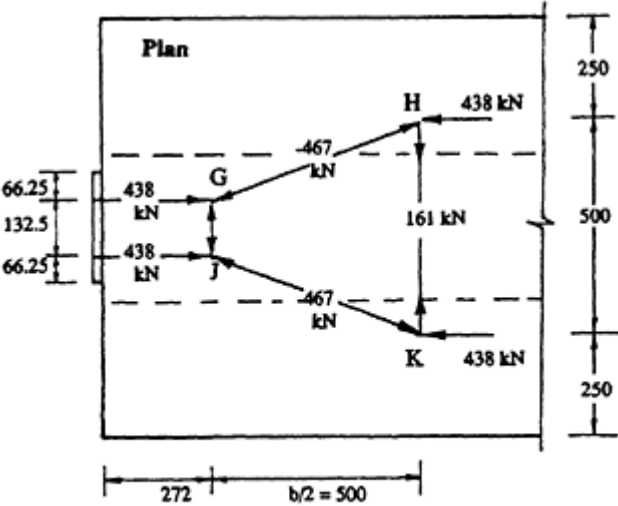
**The truss analogy**

An alternative approach to the design of the anchorage zone in a flanged member, and perhaps a more satisfactory approach, involves the truss analogy illustrated in [Figure 6.9](#).

The vertical dispersion of the prestress in the anchorage zone of [Example 6.3](#) may be visualized using the simple truss illustrated in [Figure 6.24a](#). The truss extends from the bearing plate into the beam for a length of about half the depth of Guyon's (1953) symmetric prism (i.e.  $D_e/2=272$  mm in this case). The total prestressing force carried in the flange is 876 kN and this



(a) Vertical dispersion of prestress



(b) Horizontal dispersion of prestress

Figure 6.24 Truss analogy of the anchorage zone in [Example 6.3](#).

force is assumed to be applied to the analogous truss at A and at B, as shown. The total prestressing force in the web of the beam is 1123 kN, which is assumed to be applied to the analogous truss at the quarter points of the web depth, i.e. at D and F, as shown. From statics, the tension force in the vertical tie DF is 405 kN, which is in reasonable agreement with the bursting tension (451 kN) calculated previously using the deep beam analogy. The area of steel required to carry the vertical tension in the analogous truss is

$$A_s = \frac{405 \times 10^3}{150} = 2700 \text{ mm}^2$$

and this should be located between  $0.2D_e$  and  $D_e$  from the loaded face. According to the truss analogy, therefore, the vertical steel spacing of 90 mm in [Figure 6.23](#) may be increased to 100 mm.

The horizontal dispersion of prestress into the flange is illustrated using the truss analogy of [Figure 6.24b](#). After the prestressing force has dispersed vertically to point B in [Figure 6.24a](#) (i.e. at 272 mm from the anchorage plate), the flange force then disperses horizontally. The total flange force (876 kN) is applied to the horizontal truss at the quarter points across the web, i.e. at points H and K in [Figure 6.24b](#). From statics, the horizontal tension in the tie HK is 161 kN (which is in reasonable agreement with the bursting tension of 185 kN calculated previously). The reinforcement required in the flange is

$$A_s = \frac{161 \times 10^3}{150} = 1070 \text{ mm}^2$$

This quantity of reinforcement is required over a length of beam equal to about 0.8 times the flange width and centred at the position of the tie HK in [Figure 6.24b](#). Reinforcement at the spacing thus calculated should be continued back to the free face of the anchorage zone. The reinforcement indicated in [Figure 6.23](#) meets these requirements.

## 6.4 References

- ACI 318–83 1983. *Building code requirements for reinforced concrete*. Detroit: American Concrete Institute.
- AS 3600–1988. *Australian standard for concrete structures*. Sydney: Standards Association of Australia.
- BS 8110 1985. *Structural use of concrete—parts 1 and 2*. London: British Standards Institution.
- CAN3–A23.3–M84 1984. *Design of concrete structures for buildings*. Rexdale, Canada: Canadian Standards Association.

- CEB–FIP 1978. *Model code for concrete structures*. Paris: Comité Euro-International du Béton—Fédération Internationale de la Précontrainte.
- FIP Recommendations 1984. *Practical design of reinforced and prestressed concrete structures based on the CEB–FIP model code*. London: Thomas Telford.
- Gergely, P. & M.A. Sozen 1967. Design of anchorage zone reinforcement in prestressed concrete beams. *Journal of the Prestressed Concrete Institute* **12**, No. 2, 63–75.
- Guyon, Y. 1953. *Prestressed concrete*, English edn. London: Contractors Record and Municipal Engineering.
- Hanson, N.W. & P.H. Kaar 1959. Flexural bond tests of pretensioned prestressed beams. *Journal of the American Concrete Institute* **30**, 783–802.
- Hoyer, E. 1939. *Der Stahlsaitenbeton*. Berlin, Leipzig: Elsner.
- Iyengar, K.T.S.R. 1962. Two-dimensional theories of anchorage zone stresses in post-tensioned concrete beams. *Journal of the American Concrete Institute* **59**, 1443–6.
- Iyengar, K.T.S.R. & C.V. Yogananda 1966. A three dimensional stress distribution problem in the end zones of prestressed beams. *Magazine of Concrete Research* **18**, 75–84.
- Leonhardt, F. 1964. *Prestressed concrete—design and construction*. Berlin, Munich: Wilhelm Ernst.
- Magnel, G. 1954. *Prestressed Concrete*, 3rd edn. New York: McGraw-Hill.
- Marshall, W.T., & A.H. Mattock 1962. Control of horizontal cracking in the ends of pretensioned prestressed concrete girders. *Journal of the Prestressed Concrete Institute* **7**, No. 5, 56–74.
- Sargious, M. 1960. *Beitrag zur Ermittlung der Hauptzugspannungen am Endauflager vorgespannter Betonbalken*. Dissertation, Stuttgart: Technische Hochschule.
- Tesar, M. 1932. Détermination expérimentale des tensions dans les extrémités des pièces prismatiques munies d'une semi-articulation. *International Vereinigung für Brückenbau und Hochbau*, Zurich, Abh. 1, 497–506.
- Warner, R.F. & K.A. Faulkes 1979. *Prestressed concrete*. 1st edn. Melbourne: Pitman Australia.

# 7

## Composite members

### 7.1 Types and advantages of composite construction

Composite construction in prestressed concrete usually consists of precast, prestressed members acting in combination with a cast *in situ* concrete component. The composite member is formed in at least two separate stages with some or all of the prestressing normally applied before the completion of the final stage. The precast and the cast *in situ* elements are mechanically bonded to each other to ensure that the separate components act together as a single composite member.

Composite members can take a variety of forms. In building construction, the precast elements are often pretensioned slabs (which may be either solid or voided), or single or double tee-beams. The cast *in situ* element is a thin, lightly reinforced topping slab placed on top of the precast units after the units have been erected to their final position in the structure. Single or double tee precast units are used extensively in building structures in the USA and elsewhere because of the economies afforded by this type of construction.

Composite prestressed concrete beams are widely used in the construction of highway bridges. For short- and medium-span bridges, standardized I-shaped or trough-shaped girders (which may be either pretensioned or post-tensioned) are erected between the piers and a reinforced concrete slab is cast onto the top flange of the girders. The precast girders and the *in situ* slab are bonded together to form a stiff and strong composite bridge deck.

The two concrete elements, which together form the composite structure, have different concrete strengths, different elastic moduli, and different creep and shrinkage characteristics. The concrete in the precast element is generally of better quality than the concrete in the cast *in situ* element because usually it has a higher specified target strength and is subject to better quality control and better curing conditions. With the concrete in the precast element being older and of better quality than the *in situ* concrete, restraining actions will develop in the composite structure with time owing

to differential creep and shrinkage movements. These effects should be carefully considered in design.

Prestressed concrete composite construction has many advantages over non-composite construction. In many situations, a significant reduction in construction costs can be achieved. The use of precast elements can greatly speed up construction time. When the precast elements are standardized and factory produced, the cost of long-line pretensioning may be considerably less than the cost of post-tensioning on site. Of course, the cost of transporting precast elements to the site must be included in these comparisons and it is often transportation difficulties that limit the size of the precast elements and the range of application of this type of construction. In addition, it is easier and more economical to manufacture concrete elements with high mechanical properties in a controlled prestressing plant rather than on a building or bridge site.

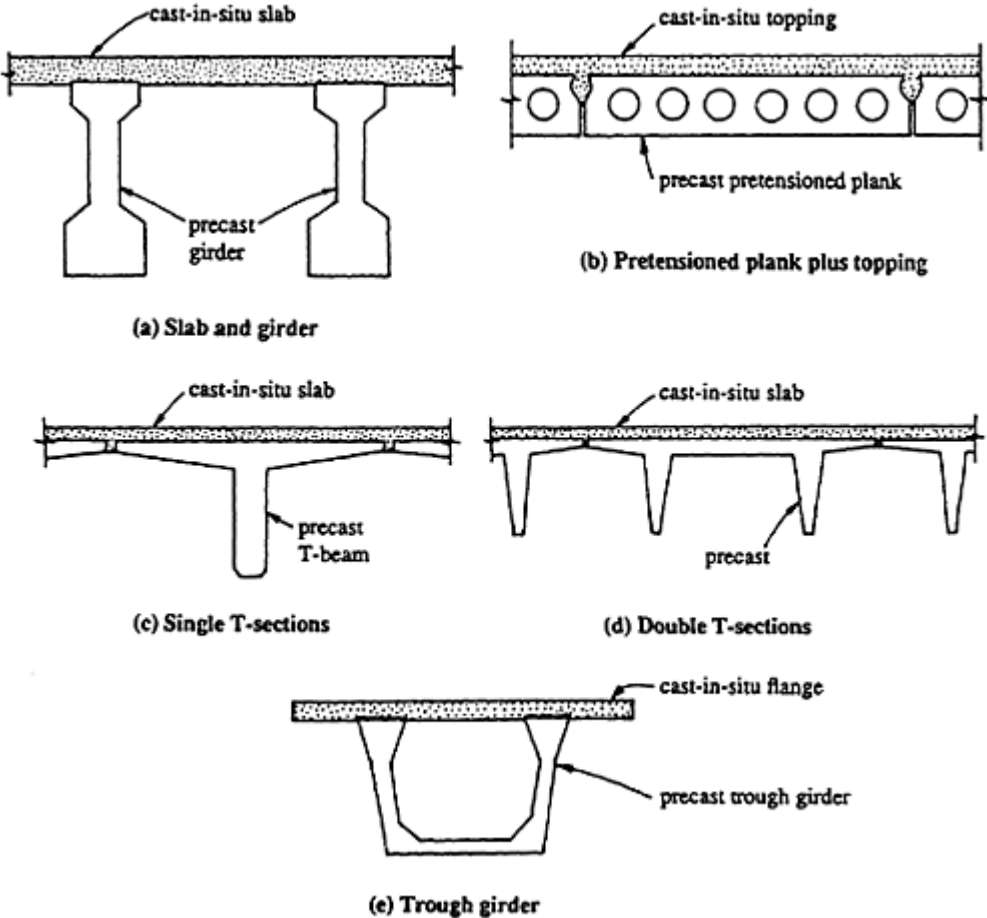


Figure 7.1 Typical composite cross-sections.

During construction, the precast elements can support the forms for the cast *in situ* concrete, thereby reducing falsework and shoring costs. The elimination of scaffolding and falsework is often a major advantage over other forms of construction, and permits the construction to proceed without interruption to the work or traffic beneath.

Apart from providing significant increases to both the strength and stiffness of the precast girders, the *in situ* concrete can perform other useful structural functions. It can provide continuity at the ends of precast elements over adjacent spans (as illustrated in [Figure 9.1d](#)). In addition, it provides lateral stability to the girders and also provides a means for carrying lateral loads back to the supports. Stage stressing can be used to advantage in some composite structures. A composite member consisting of a pretensioned, precast element and an *in situ* slab may be subsequently post-tensioned to achieve additional economies of section. This situation may arise, for example, when a relatively large load is to be applied at some time after composite action has been achieved.

Cross-sections of some typical composite prestressed concrete members commonly used in buildings and bridges are shown in [Figure 7.1](#).

## 7.2 Behaviour of composite members

The essential requirement for a composite member is that the precast and cast *in situ* elements act together as one unit. To achieve this, it is necessary to have a good bond between the two elements.

When a composite member is subjected to bending, a horizontal shear force develops at the interface between the precast and the *in situ* elements. This results in a tendency for horizontal slip on the mating surfaces if the bond is inadequate. Resistance to slip is provided by the naturally achieved adhesion and friction that occurs between the two elements. Often the top surface of the precast element is deliberately roughened during manufacture to improve its bonding characteristics and facilitate the transfer of horizontal shear through mechanical interlock. Where the contact surface between the two elements is broad (such as in [Figures 7.1b, c, and d](#)), natural adhesion and friction are usually sufficient to resist the horizontal shear. Where the contact area is small (such as between the slab and girders in [Figures 7.1a and e](#)), other provisions are necessary. Frequently, the web reinforcement in the precast girder is continued through the contact surface and anchored in the cast *in situ* slab. This reinforcement resists horizontal shear primarily by dowel action, but assistance is also gained by clamping the mating surfaces together and increasing the frictional resistance.

If the horizontal shear on the element interface is resisted without slip (or with small slip only), the response of the composite member can be determined in a similar manner to that of a monolithic member. Stresses and strains on the composite cross-section due to service loads applied after the

*in situ* slab has been placed (and has hardened) may be calculated using the properties of the combined cross-section calculated using the transformed area method. If the elastic modulus of the concrete in the *in situ* part of the cross-section,  $E_{c2}$ , is different to that in the precast element,  $E_{c1}$ , it is convenient to transform the cross-sectional area of the *in situ* element to an equivalent area of the precast concrete. This is achieved in much the same way as the areas of the bonded reinforcement are transformed into equivalent concrete areas in the analysis of a non-composite member. For a cross-section such as that shown in Figure 7.1a or e, for example, if the *in situ* concrete slab has an effective width  $b_{ef}$  and depth  $D_s$ , it is transformed into an equivalent area of precast concrete of depth  $D_s$  and width  $b_{tr}$ , where

$$b_{tr} = \frac{E_{c2}}{E_{c1}} b_{ef} = n_c b_{ef} \quad (7.1)$$

If the bonded steel areas are also replaced by equivalent areas of precast concrete (by multiplying by  $E_s/E_{c1}$  or  $E_p/E_{c1}$ ), the properties of the composite cross-section can be calculated by considering the fictitious transformed cross-section made up entirely of the precast concrete.

The width of the *in situ* slab that can be considered to be an effective part of the composite cross-section ( $b_{ef}$ ) depends on the span of the member and the distance between the adjacent precast elements. Maximum effective widths for flanged sections are generally specified in building codes, with the ACI 318–83, BS 8110 (1985), and AS 3600–1988 requirements previously outlined in Section 4.6. For composite members such as those shown in Figures 7.1a and e, the effective flange widths recommended by both BS 8110 and AS 3600 are given in Equation 4.33, except that the term  $b_w$  now refers to the width of the slab–girder interface.

The design of prestressed concrete composite members is essentially the same as that of non-composite members, provided that certain behavioural differences are recognized and taken into account. It is important to appreciate that part of the applied load is resisted by the precast element(s) prior to the establishment of composite action. Care must be taken, therefore, when designing for serviceability to ensure that behaviour of the cross-section and its response to various load stages are accurately modelled. It is also necessary in design to ensure adequate horizontal shear capacity at the element interface. The design for flexural, shear, and torsional strength is similar to that of a non-composite member.

### 7.3 Stages of loading

As mentioned in the previous section, the precast part of a composite member is required to carry loads prior to the establishment of composite action. When loads are applied during construction, before the cast *in situ*

slab has set, flexural stresses are produced about the centroidal axis of the precast element. After the *in situ* concrete has been placed and cured, the properties of the cross-section are substantially altered for all subsequent loadings. Flexural stresses due to service live loads, for example, act about the centroidal axis of the composite section, thereby modifying the stress distribution in the precast element and introducing stress into the cast *in situ* slab. Creep and shrinkage of the concrete also cause a substantial redistribution of stress with time between the precast and the *in situ* elements, and between the concrete and the bonded reinforcement in each element.

In the design of a prestressed concrete composite member, most of the following load stages will usually need to be considered:

- (1) The initial prestress at transfer in the precast element. This normally involves calculation of elastic stresses due to both the initial prestress  $P_i$  and the self-weight of the precast member. This load stage frequently occurs off-site in a precasting plant.
- (2) After the precast element has been erected prior to the application of any superimposed load. This involves a time analysis to determine the stress redistribution and change in curvature caused by creep and shrinkage of the concrete in the precast element between transfer and the time of erection. The only loads acting are the prestress ( $P_e$  after losses) and the self-weight of the precast element. A reasonably accurate time analysis can be performed using the analysis described in [Section 3.6.2](#). Concrete stresses at load stages 1 and 2 at the mid-span of the precast element are illustrated in [Figure 7.2a](#).
- (3) The effective prestress and the self-weight (determined in stage 2) plus any other superimposed dead loads applied prior to the establishment of composite action. If the precast element is unshored (i.e. not temporarily supported by props during construction), the superimposed dead load mentioned here includes the weight of the wet *in situ* concrete. This load stage involves a short-term analysis of the precast element to calculate the instantaneous effects of the additional dead

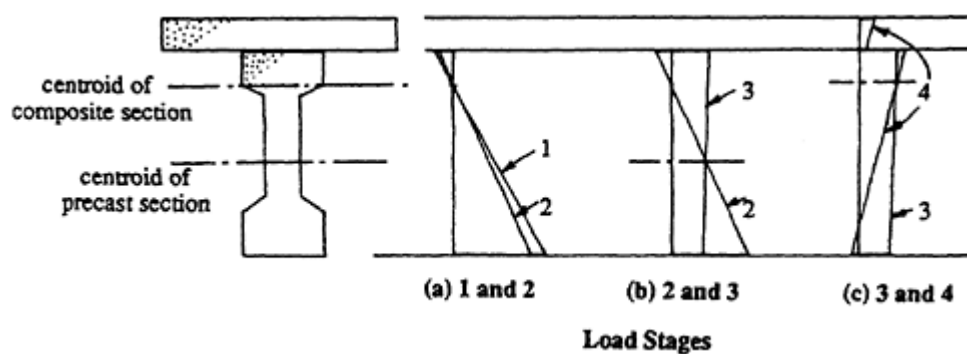


**Figure 7.2** Concrete stresses at the various load stages.



loads prior to composite action. The additional increments of stress and instantaneous strain in the precast element are added to the stresses and strains obtained at the end of stage 2. Concrete stresses at the critical section of an unshored member at load stage 3 are shown in [Figure 7.2b](#).

If the precast member is shored prior to placement of the cast *in situ* slab, the applied loads do not produce internal actions or deformations in the member and the imposed loads are carried by the shoring. Therefore, no additional stresses or strains occur in a fully shored precast element at this load stage. When curing of the cast *in situ* component has been completed, the shoring is removed and the self-weight of the cast *in situ* concrete, together with any other loading applied at this time, produce deformations and flexural stresses about the centroidal axis of the composite cross-section. This action is considered in the following load stage.

- (4) The instantaneous effect of any dead load or service live load and any additional prestressing not previously considered (i.e. not applied previously to the non-composite precast element). This involves a short-term analysis of the composite cross-section (see [Section 7.5.2](#)) to determine the change of stresses and deformations on the composite cross-section as all the remaining loads are applied. If cracking occurs, a cracked section analysis is required. Additional prestress may be applied to the composite member by re-stressing existing post-tensioned tendons or post-tensioning previously unstressed tendons. If the composite section remains uncracked, the increments of stress and strain calculated at this load stage on the precast part of the composite cross-section are added to the stresses and strains calculated in stage 3 prior to the establishment of composite action. The concrete stresses at the end of load stage 4 are shown in [Figure 7.2c](#).
- (5) The long-term effects of creep and shrinkage of concrete and relaxation of the prestressing steel on the behaviour of the composite section subjected to the sustained service loads. A time analysis of the composite cross-section is required (see [Section 7.5.3](#)) beginning at the time the sustained load is first applied (usually soon after the *in situ* concrete is poured).
- (6) The ultimate load condition for the composite section. Ultimate strength checks are required for flexure, shear, and torsion (if applicable) to ensure an adequate factor of safety. Under ultimate load conditions, the flexural strength of the composite section can be assumed to equal the strength of a monolithic cross-section of the same shape, with the same material properties, and containing the same amount and distribution of reinforcement, provided that slip at the element interface is small and full shear transfer is obtained (Hanson 1960, Saemann & Washa 1964). The stress discontinuity at the inter-

face at service loads and the inelastic effects of creep and shrinkage have an insignificant affect on the ultimate strength of the cross-section and can be ignored at the ultimate load condition.

## 7.4 Determination of prestress

In practice, the initial prestress  $P_i$  and the eccentricity of prestress  $e_{pc}$  at the critical section in the precast element are calculated to satisfy preselected stress limits at transfer. In general, cracking is avoided at transfer by limiting the tensile stress to about  $F_{ti} = 0.25\sqrt{f'_{ci}}$ . In addition, it is prudent to limit the initial compressive stresses to about  $F_{ci} = -0.5f'_{ci}$  in order to avoid unnecessarily large creep deformations. In the case of trough girders, as shown in [Figure 7.1e](#), the centroidal axis of the precast element is often not far above the bottom flange, so that loads applied to the precast element prior to or during placement of the *in situ* slab may cause unacceptably large compressive stresses in the top fibres of the precast girder.

Satisfaction of stress limits in the precast element at transfer and immediately prior to the establishment of composite action (at the end of load stage 3) can be achieved using the procedure discussed in [Section 3.3.1](#) and a Magnel design diagram, similar to that shown in [Figure 3.3](#). For the case of a precast girder, Equations 3.5–3.8 (which form the four limit lines on the Magnel diagram) become

$$\frac{1}{P_i} \geq \frac{\alpha_{t,pc} e_{pc} - 1}{A_{pc} F_{ti} + \alpha_{t,pc} M_1} \quad (7.2)$$

$$\frac{1}{P_i} \geq \frac{\alpha_{b,pc} e_{pc} + 1}{-A_{pc} F_{ci} + \alpha_{b,pc} M_1} \quad (7.3)$$

$$\frac{1}{P_i} \leq \frac{R_3(\alpha_{b,pc} e_{pc} + 1)}{-A_{pc} F_t + \alpha_{b,pc} M_3} \quad (7.4)$$

and

$$\frac{1}{P_i} \leq \frac{R_3(\alpha_{t,pc} e_{pc} - 1)}{A_{pc} F_c + \alpha_{t,pc} M_3} \quad (7.5)$$

where  $e_{pc}$  is the eccentricity of prestress from the centroidal axis of the precast section,  $\alpha_{t,pc} = A_{pc}/Z_{t,pc}$ ,  $\alpha_{b,pc} = A_{pc}/Z_{b,pc}$ ,  $A_{pc}$  is the cross-sectional area of the precast member,  $Z_{t,pc}$  and  $Z_{b,pc}$  are the top and bottom section moduli of the precast element, respectively,  $M_1$  is the moment applied at load stage 1 (usually resulting from the self-weight of the precast

member),  $M_3$  is the maximum in-service moment applied to the precast element prior to composite action (load stage 3), and  $R_3P_i$  is the prestressing force at load stage 3. An estimate of the losses of prestress between transfer and the placement of the *in situ* slab deck is required for the determination of  $R_3$ .

Equations 7.2 and 7.3 provide an upper limit to  $P_i$  and Equations 7.4 and 7.5 establish a minimum level of prestress in the precast element.

After the *in situ* slab has set, the composite cross-section resists all subsequent loading. There is a change both in the size and the properties of the cross-section and a stress discontinuity exists at the element interface. If cracking is to be avoided under the service loads, a limit  $F_t$  (say  $0.25\sqrt{f'_c}$ ) is placed on the magnitude of the extreme fibre tensile stress at the end of load stage 5, i.e. after all prestress losses and under full service loads. This requirement places another and more severe limit on the minimum amount of prestress than that imposed by Equation 7.4. Alternatively, this requirement may suggest that an additional prestressing force is required on the composite member, i.e. the member may need to be further post-tensioned after the *in situ* slab has developed its target strength.

The bottom fibre tensile stress immediately before the establishment of composite action may be approximated by

$$\sigma_{b3} = -\frac{R_3P_i}{A_{pc}} \left( 1 + \frac{A_{pc}e_{pc}}{Z_{b,pc}} \right) + \frac{M_3}{Z_{b,pc}} \quad (7.6)$$

If the maximum additional moment applied to the composite cross-section in load stage 4 is  $M_4$  and the prestressing force reduces to  $RP_i$  with time, then the final maximum bottom fibre stress at the end of load stage 5 may be approximated by

$$\sigma_{b5} = -\frac{RP_i}{A_{pc}} \left( 1 + \frac{A_{pc}e_{pc}}{Z_{b,pc}} \right) + \frac{M_3}{Z_{b,pc}} + \frac{M_4}{Z_{b,comp}} \quad (7.7)$$

where  $Z_{b,comp}$  is the section modulus for the bottom fibre of the composite cross-section. If  $\sigma_{b5}$  is to remain less than the stress limit  $F_t$ , then Equation 7.7 can be rearranged to give

$$\frac{1}{P_i} \leq \frac{R(\alpha_{b,pc}e_{pc} + 1)}{A_{pc} \left( \frac{M_3}{Z_{b,pc}} + \frac{M_4}{Z_{b,comp}} - F_t \right)} \quad (7.8)$$

Equation 7.8 can be plotted on a Magnel diagram together with Equations 7.2, 7.3, and 7.5 to establish a suitable combination of  $P_i$  and  $e_{pc}$ , as shown in [Figure 7.3](#). In some cases, the precast section may be proportioned

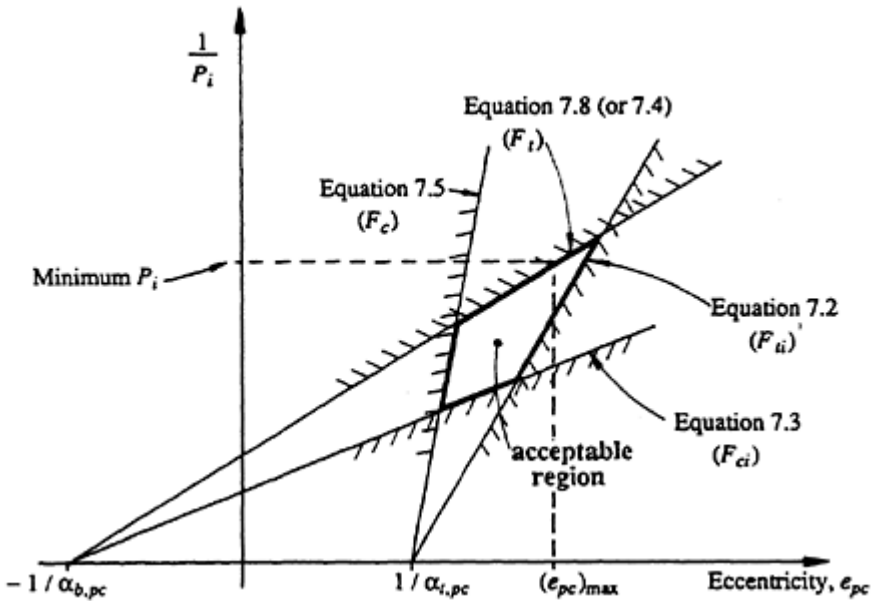


Figure 7.3 The Magnel diagram for a composite cross-section.

so that the prestress and eccentricity satisfy all stress limits prior to composite action (i.e. Equations 7.2–7.5 are all satisfied). However, when the additional requirement of Equation 7.8 is included, no combination of  $P_i$  and  $e_{pc}$  can be found to satisfy all the stress limits and no acceptable region exists on the Magnel diagram. In such cases, additional prestress may be applied to the composite member after the *in situ* slab is in place.

If cracking can be tolerated in the composite member under full service loads, a cracked section analysis is required to check for crack control and to determine the reduction of stiffness and its effect on deflection. Care must be taken in such an analysis to model accurately stresses in the various parts of the cross-section and the stress discontinuity at the slab-girder interface.

In many cases, cracking may be permitted under the full live load but not under the permanent sustained load. In such a case,  $M_4$  in Equation 7.8 can be replaced by the sustained part of the moment applied at load stage 4 ( $M_{4,sus}$ ). Therefore, Equation 7.8 becomes

$$\frac{1}{P_i} \leq \frac{R(\alpha_{b,pc} e_{pc} + 1)}{A_{pc} \left( \frac{M_3}{Z_{b,pc}} + \frac{M_{4,sus}}{Z_{b,comp}} - F_t \right)} \tag{7.9}$$

and Equation 7.9 can be used to determine the minimum level of prestress on a partially prestressed composite section.

## 7.5 Methods of analysis at service loads

### 7.5.1 Introductory remarks

After the size of the concrete elements and the quantity and disposition of prestressing steel have been determined, the behaviour of the composite member at service loads should be investigated in order to check deflection (and shortening) at the various load stages (and times), and also to check for the possibility of cracking. The short-term and time-dependent analyses of uncracked composite cross-sections can be carried out conveniently using procedures similar to those described in Sections 3.5.1 and 3.6.2 for non-composite cross-sections. The approaches described here were also presented by Gilbert (1988).

Consider a cross-section made up of a precast, prestressed girder (element 1) and a cast *in situ* reinforced concrete slab (element 2), as shown in Figure 7.4. The concrete in each element has different deformation characteristics. This particular cross-section contains four layers of non-prestressed reinforcement and two layers of prestressing steel, although any number of steel layers can be handled without added difficulty. As was demonstrated in Example 3.5, the presence of non-prestressed reinforcement may affect the time-dependent deformation of the section significantly and cause a reduction of the compressive stresses in the concrete. In the following analyses, no slip is assumed to occur between the two concrete elements or between the steel reinforcement and the concrete.

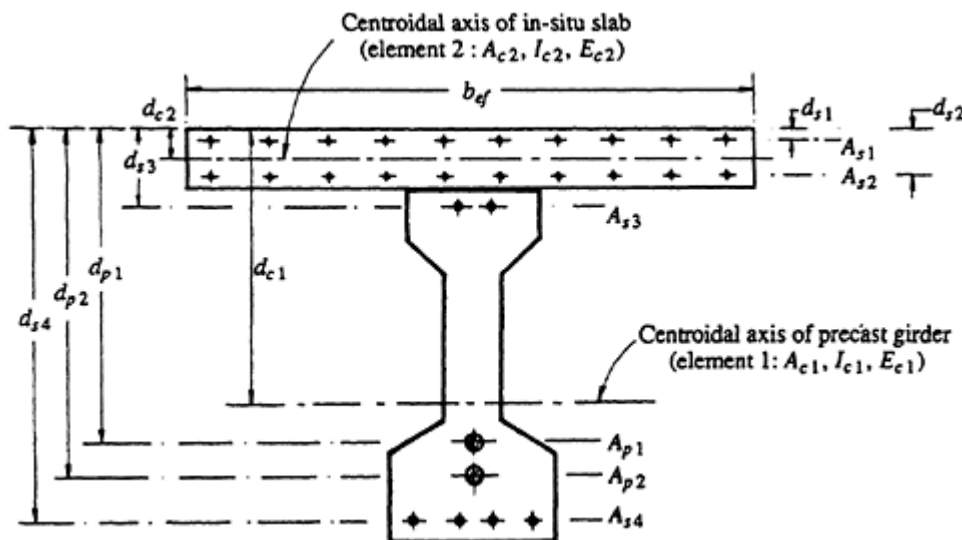


Figure 7.4 Typical prestressed concrete composite cross-section.

7.5.2 Short-term analysis

For the composite cross-section in [Figure 7.4](#), the elastic modulus of the concrete in one of the concrete elements is adopted as the modulus of the transformed section, say  $E_{c1}$  of element 1 (the precast girder). The area of the *in situ* slab and the areas of the bonded steel reinforcement are transformed into equivalent areas of the concrete of element 1. The transformed cross-section equivalent to the composite section of [Figure 7.4](#) is shown in [Figure 7.5](#).

The properties of this transformed section about the top surface of the precast slab are

$$\begin{aligned}
 A &= \sum_{j=1}^2 n_{cj} A_{cj} + \sum_{k=1}^4 n_{sk} A_{sk} + \sum_{m=1}^2 n_{pm} A_{pm} \tag{7.10} \\
 B &= \sum_{j=1}^2 n_{cj} A_{cj} d_{cj} + \sum_{k=1}^4 n_{sk} A_{sk} d_{sk} + \sum_{m=1}^2 n_{pm} A_{pm} d_{pm} \\
 \bar{I} &= \sum_{j=1}^2 (n_{cj} I_{cj} + n_{cj} A_{cj} d_{cj}^2) + \sum_{k=1}^4 n_{sk} A_{sk} d_{sk}^2 + \sum_{m=1}^2 n_{pm} A_{pm} d_{pm}^2
 \end{aligned}$$

where  $n_{cj}=E_{cj}/E_{c1}$ ,  $n_{sk}=E_{sk}/E_{c1}$ , and  $n_{pm}=E_{pm}/E_{c1}$ ;  $A$  is the area of the transformed section, and  $B$  and  $\bar{I}$  are the first and second moments of the transformed area about the top surface of the *in situ* slab. If the prestressed steel were post-tensioned and unbonded, it would not form part of the transformed section. By changing the summation limits, Equations 7.10 can be used no matter how many steel or concrete elements make up the composite cross-section.

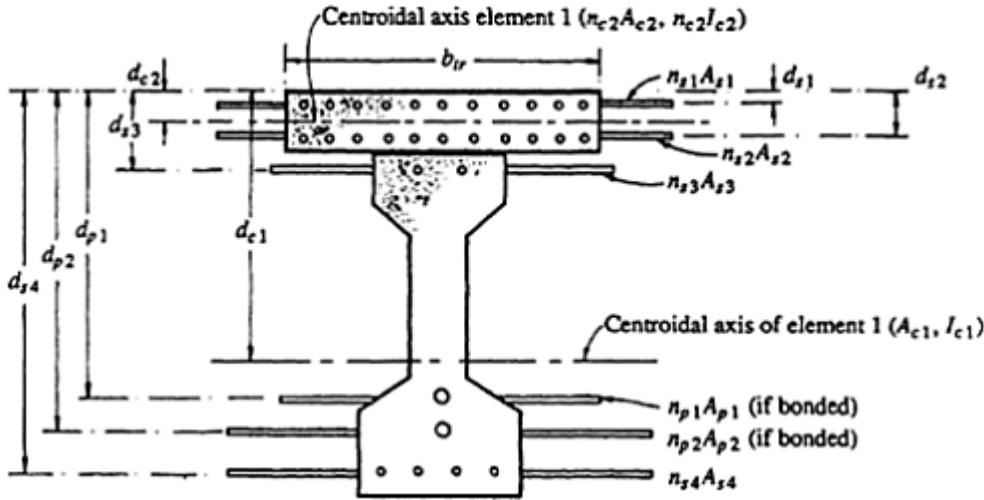


Figure 7.5 Transformed composite cross-section.

As outlined in [Section 3.5.1](#), the instantaneous change in the strain distribution caused by an increment of axial force  $\Delta N_i$  and an increment of moment  $\Delta M_i$  applied about the top surface of the *in situ* slab is obtained from Equations 3.20, 3.24 and 3.25, which are re-expressed here as follows:

$$\Delta \varepsilon_i = \Delta \varepsilon_{oi} + y \Delta \kappa_i \quad (7.11)$$

where

$$\Delta \varepsilon_{oi} = \frac{B \Delta M_i - \bar{I} \Delta N_i}{E_{c1}(B^2 - A\bar{I})} \quad (7.12)$$

$$\Delta \kappa_i = \frac{-A \Delta M_i + B \Delta N_i}{E_c(B^2 - A\bar{I})} \quad (7.13)$$

For a composite prestressed cross-section in pure bending, with no additional prestress applied after the establishment of composite action,  $\Delta N_i$  is zero. If a prestressing force  $\Delta P_i$  is applied through any unbonded tendons during load stage 4 (see [Section 7.3](#)),  $\Delta N_i$  is a compressive force equal in magnitude to  $\Delta P_i$ . The moment  $\Delta M_i$  is the sum of the moment caused by external loads applied to the composite section  $M_{comp}$  (which could be, for example, the total load applied in load stage 4 and designated  $M_4$  in Equation 7.7) and the moment about the top fibre caused by any additional prestress. Therefore,

$$\Delta N_i = -\Delta P_i \quad \text{and} \quad \Delta M_i = M_{comp} - \Delta P_i d_p \quad (7.14)$$

The force  $\Delta P_i$  is the prestress applied at load stage 4 after the *in situ* slab is in place. In many cases,  $\Delta P_i=0$  and Equation 7.14 reduces to  $\Delta N_i=0$  and  $\Delta M_i=M_{comp}$ . The stresses and strains caused by the initial prestress and other loads applied to the non-composite precast girder (in load stages 1–3) are calculated using the short-term and time-dependent analyses of [Sections 3.5.1](#) and [3.6.2](#). The strain distribution in the composite member at the end of load stage 4 are obtained by adding the instantaneous strains obtained from Equations 7.12 and 7.13 to the strains existing in the precast member at the end of load stage 3.

The change of concrete stress in the  $j$ th concrete element at  $y$  below the top fibre and the changes of stress in the bonded steel reinforcement caused by  $\Delta N_i$  and  $\Delta M_i$  may be calculated from

$$\Delta \sigma_i = E_{cj}(\Delta \varepsilon_{oi} + y \Delta \kappa_i) \quad (7.15)$$

$$\Delta \sigma_{sik} = E_{sk}(\Delta \varepsilon_{oi} + d_{sk} \Delta \kappa_i) \quad (7.16)$$

$$\Delta\sigma_{pim} = E_{pm}(\Delta\varepsilon_{oi} + d_{pm} \Delta x_i) \tag{7.17}$$



### 7.5.3 Time analysis

The age-adjusted effective modulus for each reinforced concrete element is calculated using Equation 2.14. In accordance with the analytical procedure outlined in [Section 3.6.2](#) for non-composite cross-sections, the restraining actions  $-\delta N$  and  $-\delta M$  required to prevent the development of creep and shrinkage in each concrete element and stress relaxation in the prestressing steel may be computed from expressions similar to Equations 3.47 and 3.48. For a cross-section containing  $n1$  concrete elements and  $n2$  levels of prestressing steel, Equations 3.47 and 3.48 become

$$-\delta N = - \sum_{j=1}^{n1} \bar{E}_{ej} [\Delta\phi_j (A_{cj}\epsilon_{oi} + B_{cj}\chi_i) + \epsilon_{shj} A_{cj}] + \sum_{m=1}^{n2} R_m \quad (7.18)$$

$$-\delta M = - \sum_{j=1}^{n1} \bar{E}_{ej} [\Delta\phi_j (B_{cj}\epsilon_{oi} + \bar{I}_{cj}\chi_i) + \epsilon_{shj} B_{cj}] + \sum_{m=1}^{n2} R_m d_{pm} \quad (7.19)$$

where  $A_{cj}$  is the area of the  $j$ th concrete element and  $B_{cj}$  and  $\bar{I}_{cj}$  are the first and second moments, respectively, of the area of the  $j$ th concrete element about the top of the *in situ* slab. In Equations 7.18 and 7.19, the terms  $\epsilon_{oi}$  and  $\chi_i$  are the top fibre *instantaneous* strain and *instantaneous* curvature (i.e. the slope of the instantaneous strain diagram), respectively, at the beginning of the current time interval caused by each previously applied load or time increment.

The change of top fibre strain and curvature with time are calculated using Equations 3.49 and 3.50 by applying  $\delta M$  and  $\delta N$  to the age-adjusted transformed section. The age-adjusted effective modulus of the precast element ( $\bar{E}_{e1}$ ) is selected as the modulus of the age-adjusted transformed section. The *in situ* slab is transformed into equivalent areas of the precast concrete by multiplying by the age-adjusted modular ratio  $\bar{n}_{c2} = \bar{E}_{e2}/\bar{E}_{e1}$ . The bonded steel area is transformed by multiplying by  $\bar{n}_{sk} = E_{sk}/\bar{E}_{e1}$  or  $\bar{n}_{pm} = E_{pm}/\bar{E}_{e1}$ .

For the cross-section shown in [Figure 7.4](#), the area of the age-adjusted transformed section  $\bar{A}_e$  and the first and second moments of the transformed area about the top surface  $\bar{B}_e$  and  $\bar{I}_e$  respectively, are

$$\bar{A}_e = \sum_{j=1}^2 \bar{n}_{cj} A_{cj} + \sum_{k=1}^4 \bar{n}_{sk} A_{sk} + \sum_{m=1}^2 \bar{n}_{pm} A_{pm} \quad (7.20)$$

$$\bar{B}_e = \sum_{j=1}^2 \bar{n}_{cj} A_{cj} d_{cj} + \sum_{k=1}^4 \bar{n}_{sk} A_{sk} d_{sk} + \sum_{m=1}^2 \bar{n}_{pm} A_{pm} d_{pm}$$

$$\bar{I}_e = \sum_{j=1}^2 (\bar{n}_{cj} I_{cj} + \bar{n}_{cj} A_{cj} d_{cj}^2) + \sum_{k=1}^4 \bar{n}_{sk} A_{sk} d_{sk}^2 + \sum_{m=1}^2 \bar{n}_{pm} A_{pm} d_{pm}^2$$

The time-dependent changes in top fibre strain and curvature are therefore

$$\Delta \epsilon_o = \frac{\bar{B}_e \delta M - \bar{I}_e \delta N}{\bar{E}_e (\bar{B}_e^2 - \bar{A}_e \bar{I}_e)} \tag{7.21}$$

and

$$\Delta \chi = \frac{-\bar{A}_e \delta M + \bar{B}_e \delta N}{\bar{E}_e (\bar{B}_e^2 - \bar{A}_e \bar{I}_e)} \tag{7.22}$$

The change of stress at a point in the *j*th concrete element at a depth *y* below the top fibre is calculated using Equations 3.51–3.53 and is given by

$$\Delta \sigma = -\bar{E}_{ej} [\Delta \phi_j (\epsilon_{oi} + y \chi_i) + \epsilon_{shj} - (\Delta \epsilon_o + y \Delta \chi)] \tag{7.23}$$

The change of stress with time in the *k*th layer of non-prestressed reinforcement is

$$\Delta \sigma_{sk} = E_{sk} (\Delta \epsilon_o + d_{sk} \Delta \chi) \tag{7.24}$$

and, in the *m*th layer of prestressed steel, it is

$$\Delta \sigma_{pm} = E_{pm} (\Delta \epsilon_o + d_{pm} \Delta \chi) + \frac{R_m}{A_{pm}} \tag{7.25}$$

**Example 7.1**

The cross-section of a composite footbridge consists of a precast, pretensioned trough girder and a *cast in situ* slab, as shown in Figure 7.6. The cross-section is subjected to the following load history. The precast section is cast and moist cured for 4 days. At *t*=4 days, the total prestressing force

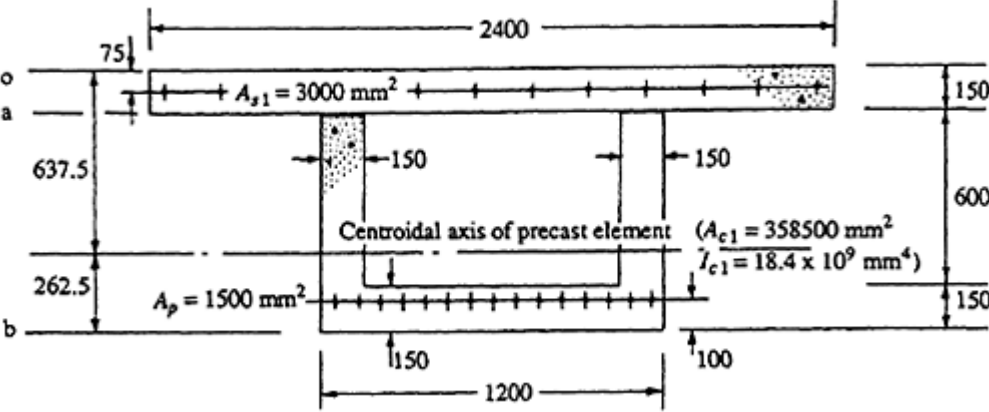


**Figure 7.6** Details of composite cross-section in [Example 7.1](#).

of 2000 kN is transferred to the girder. The centroid of all the pretensioned strands is located 100 mm above the bottom fibre of the precast girder, as shown. The moment on the section caused by the self-weight of the girder  $M_1=320$  kNm is introduced at transfer. Shrinkage of the concrete also begins to develop at this time. At  $t=40$  days, the *in situ* slab deck is cast and cured and the moment caused by the weight of the deck is applied to the precast section,  $M_3=300$  kNm. At  $t=60$  days, a wearing surface is placed and all other superimposed dead loads are applied to the bridge, thereby introducing an additional moment  $M_4=150$  kNm.

Composite action gradually begins to develop as soon as the concrete in the deck sets. Full composite action may not be achieved for several days. However, it is assumed here that the *in situ* deck and the precast section act compositely at all times after  $t=40$  days.

The stress and strain distributions on the composite cross-section are to be calculated immediately after the application of the prestress at  $t=4$  days, both before and after the slab deck is cast at  $t=40$  days, both before and after the road surface is placed at  $t=60$  days, and at time infinity.

For a precast section (element 1);  $f'_c = 40$  MPa:

$$\begin{aligned} E_{c1}(4) &= 25\,000 \text{ MPa}; E_{c1}(40) = 31\,500 \text{ MPa}; E_{c1}(60) = 33\,000 \text{ MPa}; \\ \varepsilon_{sh1}(40-4) &= -150 \times 10^{-6}; \varepsilon_{sh1}(60-4) = -200 \times 10^{-6}; \\ \varepsilon_{sh1}(\infty) &= -500 \times 10^{-6}; \\ \phi_1(40, 4) &= 0.9; \phi_1(60, 4) = 1.2; \phi_1(\infty, 4) = 2.4; \\ \phi_1(60, 40) &= 0.5; \phi_1(\infty, 40) = 1.6; \phi_1(\infty, 60) = 1.2; \\ \chi_1(40, 4) &= 0.88; \chi_1(60, 4) = 0.85; \chi_1(\infty, 4) = 0.8; \\ \chi_1(60, 40) &= 0.9; \chi_1(\infty, 40) = 0.8; \chi_1(\infty, 60) = 0.8. \end{aligned}$$

For the *in-situ* slab (element 2):  $f'_c = 25$  MPa:

$$\begin{aligned} E_{c2}(40) &= 18\,000 \text{ MPa}; E_{c2}(60) = 25\,000 \text{ MPa}; \\ \varepsilon_{sh2}(60-40) &= -120 \times 10^{-6}; \varepsilon_{sh2}(\infty) = -600 \times 10^{-6}; \\ \phi_2(60, 40) &= 0.8; \phi_2(\infty, 40) = 3.0; \phi_2(\infty, 60) = 2.0; \\ \chi_2(60, 40) &= 0.88; \chi_2(\infty, 40) = 0.8; \chi_2(\infty, 60) = 0.8. \end{aligned}$$

In the prestressing tendons, the relaxation  $R$  is equal to  $-24$  kN at  $t=40$  days,  $-32$  kN at  $t=60$  days, and  $-60$  kN at  $t=\infty$ . Take  $E_p=E_s=200\,000$  MPa.

(a) At  $t=4$  days The properties of the transformed precast section of

modulus  $E_{c1}(4)=25000$  MPa with respect to its top fibre are calculated as

$$A_1 = 370\,500 \text{ mm}^2; B_1 = 182.3 \times 10^6 \text{ mm}^3; \text{ and } \bar{I}_1 = 108.4 \times 10^9 \text{ mm}^4$$

The resultant initial axial force  $N_i$  and bending moment  $M_i$  applied at the top of the precast section are given by

$$N_i = -P_i = -2000 \text{ kN} \quad \text{and}$$

$$M_i = M_1 - P_i d_p = 320 - (2000 \times 0.65) = -980 \text{ kN m}$$

and the strain at the top of the precast section (level a in [Figure 7.6](#)) and the curvature are obtained from Equations 3.24 and 3.25:

$$\epsilon_{ai} = -220.2 \times 10^{-6} \quad \text{and} \quad \kappa_i = 0.0087 \times 10^{-6} \text{ mm}^{-1}$$

From Equation 3.21, the concrete stresses at the top and bottom of the precast section are

$$\sigma_{ai} = -5.51 \text{ MPa} \quad \text{and} \quad \sigma_{bi} = -5.34 \text{ MPa}$$

The stress and strain distributions at this time are shown in [Figure 7.7b](#) and the stress in the tendons is

$$\sigma_p = \frac{P_i}{A_p} + E_p(\epsilon_{ai} + d_p \kappa_i) = 1290 \text{ MPa}$$

(b) At  $t=40$  days. Prior to casting the *in situ* slab

The age-adjusted effective modulus at this time is (Equation 2.14)

$$\bar{E}_{c1}(40, 4) = \frac{25\,000}{1 + (0.88 \times 0.9)} = 13\,950 \text{ MPa}$$

and the properties of the concrete part of the precast section (with respect to level a) are

$$A_{c1} = 358\,500 \text{ mm}^2; B_{c1} = 174.5 \times 10^6 \text{ mm}^3; \text{ and } \bar{I}_{c1} = 103.3 \times 10^9 \text{ mm}^4$$

The restraining forces required to prevent creep and shrinkage of the concrete and relaxation of the prestressing steel between  $t=4$  and 40 days are determined using Equations 3.47 and 3.48. In this case,  $\Delta\phi = \phi_1(40, 4) = 0.9$ ,  $\epsilon_{sh} = \epsilon_{sh1}(40-4) = -150 \times 10^{-6}$ , and  $R = -24$  kN. Therefore,

$$-\delta N = 1698 \text{ kN} \quad \text{and} \quad -\delta M = 820.8 \text{ kN m}$$

The properties of the age-adjusted transformed section are calculated as

$$\bar{A}_{e1} = 380\,000 \text{ mm}^2; \bar{B}_{e1} = 188.5 \times 10^6 \text{ mm}^3; \text{ and } \bar{I}_{e1} = 112.4 \times 10^9 \text{ mm}^4$$

and the time-dependent change in the strain diagram between  $t=4$  and 40 days is found from Equations 3.49 and 3.50:

$$\Delta \varepsilon_a = -361.0 \times 10^{-6} \quad \text{and} \quad \Delta \kappa = 0.082 \times 10^{-6} \text{ mm}^{-1}$$

The changes of concrete stress at the top and bottom fibres are calculated using Equations 3.51 to 3.53 and are

$$\Delta \sigma_a = -0.18 \text{ MPa} \quad \text{and} \quad \Delta \sigma_b = 0.60 \text{ MPa}.$$

The change of the stress and strain distributions with time between  $t=4$  and 40 days are illustrated in [Figure 7.7c](#). The change of concrete stress with time is not great in this case because of the relatively small amount of bonded reinforcement and the small time interval under consideration. The change of stress in the tendons is obtained from Equation 3.55:

$$\Delta \sigma_p = 2 \times 10^5 [ -361 + (650 \times 0.082) ] \times 10^{-6} - \frac{24\,000}{1500} = -77.5 \text{ MPa}$$

**(c) At  $t=40$  days** After casting the *in situ* slab

The increments of stress and strain caused by  $M_3=300$  kN m applied to the precast section are calculated using the same procedure as was outlined in part (a) of this example. The properties of the transformed precast section with  $E_{c1}(40)=31500$  MPa are

$$A_1 = 368\,020 \text{ mm}^2; B_1 = 180.7 \times 10^6 \text{ mm}^3; \text{ and } \bar{I}_1 = 107.3 \times 10^9 \text{ mm}^4$$

With  $N_i=0$  and  $M_i=M_3=300$  kNm, the short-term increments of top fibre strain (at level a) and curvature are given by Equations 3.24 and 3.25 as

$$\Delta \varepsilon_{ai} = -251.4 \times 10^{-6} \quad \text{and} \quad \Delta \kappa_i = 0.512 \times 10^{-6} \text{ mm}^{-1}$$

From Equation 3.21,

$$\Delta \sigma_a = -7.92 \text{ MPa}; \Delta \sigma_b = 4.18 \text{ MPa}; \text{ and } \Delta \sigma_p = 16.3 \text{ MPa}$$

The increments of concrete stress and strain caused by  $M_3$  are shown in [Figure 7.7d](#). The extreme fibre concrete stresses in the precast girder

immediately after placing the *in situ* slab are obtained by summing the stress increments calculated in parts (a), (b), and (c):

$$\sigma_a = -5.51 - 0.18 - 7.92 = -13.61 \text{ MPa}$$

$$\sigma_b = -5.34 + 0.60 + 4.18 = -0.56 \text{ MPa}$$

Stress levels in the precast girder are satisfactory at all stages prior to and immediately after placing the *in situ* slab. Cracking will not occur and compressive stress in the top fibre is not excessive. However, with a sustained compressive stress of  $-13.61$  MPa in the top fibre, a large subsequent creep differential will exist between the precast and the *in situ* elements.

**(d) At  $t=60$  days** Prior to placement of the wearing surface

The change of stress and strain during the time interval from  $t=40$  to 60 days is to be calculated here. During this period, the precast section and the *in situ* slab are assumed to act compositely.

The concrete stress increments in the precast section, which were calculated in parts (a), (b), and (c) above, are applied at different times and are therefore associated with different creep coefficients. For the stresses applied at  $t=4$  days [(part (a))], the creep coefficient for this time interval is  $\phi_1(60, 4) - \phi_1(40, 4) = 0.3$ . The stress increment calculated in part (b), which is in fact gradually applied between  $t=4$  and 40 days, may be accounted for by assuming that it is suddenly applied at  $t=4$  days and using the reduced creep coefficient given by

$$\chi_1(40, 4)[\phi_1(60, 4) - \phi_1(40, 4)] = 0.26.$$

For the stress increment calculated in part (c) (and caused by  $M_3$ ), the appropriate creep coefficient is  $\phi_1(60, 40) = 0.5$ . The shrinkage strain which develops in the precast section during this time interval is  $\varepsilon_{sh1}(60-4) - \varepsilon_{sh1}(40-4) = -50 \times 10^{-6}$ .

For the *in situ* slab, the creep coefficient used in this time interval is  $\phi_2(60, 40) = 0.8$  and the shrinkage strain is  $\varepsilon_{sh2} = -120 \times 10^{-6}$ .

The loss of force in the prestressing tendons caused by relaxation is 8 kN.

The age-adjusted effective modulus for each concrete element is (Equation 2.14)

$$\bar{E}_{e1}(60, 40) = \frac{E_{c1}(40)}{1 + \chi_1(60, 40)\phi_1(60, 40)} = 21\,720 \text{ MPa}$$

$$\bar{E}_{e2}(60, 40) = \frac{E_{c2}(40)}{1 + \chi_2(60, 40)\phi_2(60, 40)} = 10\,560 \text{ MPa}$$

The section properties of the concrete part of the precast girder (element 1) and the *in situ* slab (element 2) with respect to the top surface of the composite section (level o of [Figure 7.6](#)) are

$$A_{c1} = 358\,500 \text{ mm}^2; B_{c1} = 228.3 \times 10^6 \text{ mm}^3; \bar{I}_{c1} = 163.7 \times 10^9 \text{ mm}^4$$

$$A_{c2} = 357\,000 \text{ mm}^2; B_{c2} = 26.78 \times 10^6 \text{ mm}^3; \bar{I}_{c2} = 2683 \times 10^6 \text{ mm}^4$$

and the properties of the transformed composite section with modulus  $\bar{E}_e=21720$  MPa are calculated using Equation 7.20:

$$\bar{A}_e = 572\,000 \text{ mm}^2; \bar{B}_e = 254.3 \times 10^6 \text{ mm}^3; \bar{I}_e = 174.0 \times 10^9 \text{ mm}^4$$

To determine the internal actions required to restrain creep, shrinkage, and relaxation (using Equations 7.18 and 7.19), the initial elastic strain distribution ( $\Delta\varepsilon_{oi}$  and  $\Delta x_i$ ) caused by each of the previously calculated stress increments in each concrete element must be determined.

In the *in situ* slab:  $\varepsilon_{oi}=0$  and  $x_i=0$  since the slab at  $t=40$  days is unloaded.

In the precast section:

Owing to the stresses applied at 4 days [calculated in part (a)],  $\varepsilon_{ai}=-220.2 \times 10^{-6}$ ,  $x_i=0.0087 \times 10^{-6} \text{ mm}^{-1}$ , and, therefore  $\varepsilon_{oi}=-221.5 \times 10^{-6}$ .

For the stress increment calculated in part (b) and assumed to be applied at 4 days,

$\Delta\varepsilon_{ai}=\Delta\sigma_a/E_{c1}(4)=-7.2 \times 10^{-6}$ ,  $\Delta\varepsilon_{bi}=\Delta\sigma_b/E_{c1}(4)=24.0 \times 10^{-6}$ , and therefore  $\Delta x_i=(24+7.2) \times 10^{-6}/750=0.0416 \times 10^{-6} \text{ mm}^{-1}$  and  $\Delta\varepsilon_{oi}=-13.4 \times 10^{-6}$ .

For the stresses applied at 40 days [part (c)],  $\Delta\varepsilon_{ai}=-215.4 \times 10^{-6}$ ,  $\Delta x_i=0.512 \times 10^{-6} \text{ mm}^{-1}$ , and therefore  $\Delta\varepsilon_{oi}=-328.2 \times 10^{-6}$ .

Hence, from Equations 7.18 and 7.19,

$$\begin{aligned} -\delta N &= -10\,560(-120 \times 10^{-6} \times 357\,000) - 21\,720\{0.3[(358\,500 \\ &\quad \times -221.5) + (228.3 \times 10^6 \times 0.0087)] + 0.26[(358\,500 \\ &\quad \times -13.4) + (228.3 \times 10^6 \times 0.0416)] + 0.5[(358\,500 \times -328.2) \\ &\quad + (228.3 \times 10^6 \times 0.512)] - (50 \times 358\,500)\} \times 10^{-6} - 8000 \\ &= +1320 \times 10^3 \text{ N} \end{aligned}$$



$$\begin{aligned}
-\delta M &= -10\,560(-120 \times 10^{-6} \times 26.78 \times 10^6) - 21\,720\{0.3[(228.3 \\
&\times 10^6 \times -221.5) + (163.7 \times 10^9 \times 0.0087)] + 0.26[(228.3 \times 10^6 \\
&\times -13.4) + (163.7 \times 10^9 \times 0.0416)] + 0.5[(228.3 \times 10^6 \times -328.2) \\
&+ (163.7 \times 10^9 \times 0.512)] - (50 \times 228.3 \times 10^6)\} \times 10^{-6} \\
&\quad - 8000 \times 800 \\
&= 477.8 \times 10^6 \text{ Nmm}
\end{aligned}$$

and the changes of top fibre strain and curvature between  $t=40$  and 60 days are calculated using Equations 7.21 and 7.22:

$$\Delta \epsilon_0 = -143.0 \times 10^{-6} \quad \text{and} \quad \Delta \kappa = 0.0825 \times 10^{-6} \text{ mm}^{-1}$$

The changes of concrete stress in both the slab deck and the precast section are calculated from Equation 7.23. In the *in situ* slab,

$$\begin{aligned}
\Delta \sigma_{o2} &= -10\,560(-120 + 143.0) \times 10^{-6} = -0.24 \text{ MPa} \\
\Delta \sigma_{a2} &= -10\,560\{-120 - [-143.0 + (150 \times 0.0825)]\} \times 10^{-6} \\
&= -0.11 \text{ MPa}
\end{aligned}$$

and in the precast section,

$$\begin{aligned}
\Delta \sigma_{a1} &= -21\,720\{0.3[-221.5 + (150 \times 0.0087)] + 0.26[-13.4 + (150 \\
&\times 0.0416)] + 0.5[-328.2 + (150 \times 0.512)] - 50 - [-143.0 \\
&+ (150 \times 0.0825)]\} \times 10^{-6} = 2.45 \text{ MPa} \\
\Delta \sigma_{b1} &= -21\,720\{0.3[-221.5 + (900 \times 0.0087)] + 0.26[-13.4 + (900 \\
&\times 0.0416)] + 0.5[-328.2 + (900 \times 0.512)] - 50 - [-143.0 + (900 \\
&\times 0.0825)]\} \times 10^{-6} = -0.59 \text{ MPa}
\end{aligned}$$

The changes in the concrete stress and strain distributions during this time period are shown in [Figure 7.7e](#). There is a complex interaction taking place between the two concrete elements. The *in situ* slab is shrinking at a faster rate than the precast element and, if this were the only effect, the *in situ* slab would suffer a tensile restraining force. Because of the high initial compressive stresses in the top fibres of the precast section, however, the precast concrete at the element interface is creeping more than the *in situ* concrete. A compressive restraining force is therefore imposed on the *in situ* slab and a significant reduction in compressive stress is observed in the top fibres of the precast element, even over this relatively short time period. At this

stage, the compressive restraining force in the *in situ* slab due to creep of the precast concrete is greater than the tensile force resulting from shrinkage, and the *in situ* concrete stresses are compressive.

The change of steel stresses are obtained from Equations 7.24 and 7.25 and are equal to

$$\Delta\sigma_{s1} = -27.4 \text{ MPa} \quad \text{and} \quad \Delta\sigma_p = -20.7 \text{ MPa}$$

(e) At  $t=60$  days After placement of the wearing surface

With  $E_{cl}(60)=33000$  MPa selected as the elastic modulus of the transformed composite section, the section properties are determined using expressions similar to Equations 7.10:

$$A = 655\,500 \text{ mm}^2; \quad B = 257.2 \times 10^6 \text{ mm}^3; \quad \text{and} \quad \bar{I} = 171.7 \times 10^9 \text{ mm}^4$$

The initial top fibre strain and curvature caused by  $\Delta M_i=M_4=150$  kNm and  $\Delta N_i=0$  are obtained from Equations 7.12 and 7.13:

$$\Delta\varepsilon_{oi} = \frac{257.2 \times 10^6 \times 150 \times 10^6}{33\,000[(257.2 \times 10^6)^2 - (655\,500 \times 171.7 \times 10^9)]} = -25.2 \times 10^{-6}$$

$$\begin{aligned} \Delta\kappa_i &= \frac{-655\,500 \times 150 \times 10^6}{33\,000[(257.2 \times 10^6)^2 - (655\,500 \times 171.7 \times 10^9)]} \\ &= 0.0642 \times 10^{-6} \text{ mm}^{-1} \end{aligned}$$

The increments of concrete stress at time  $\tau_0$  caused by  $M_4$  at the top and bottom of the *in situ* slab are obtained using Equation 7.15:

$$\Delta\sigma_{o2} = 25\,000(-25.2 \times 10^{-6}) = -0.63 \text{ MPa}$$

$$\Delta\sigma_{a2} = 25\,000[-25.2 + (150 \times 0.0642)] \times 10^{-6} = -0.39 \text{ MPa}$$

and at the top and bottom of the precast section,

$$\Delta\sigma_{a1} = 33\,000[-25.2 + (150 \times 0.0642)] \times 10^{-6} = -0.51 \text{ MPa}$$

$$\Delta\sigma_{b1} = 33\,000[-25.2 + (1300 \times 0.0642)] \times 10^{-6} = 1.08 \text{ MPa}$$

From Equations 7.16 and 7.17, the increments of stress in the bonded steel are

$$\Delta\sigma_{s1} = -4.12 \text{ MPa} \quad \text{and} \quad \Delta\sigma_p = +5.3 \text{ MPa}$$

The increments of concrete stress and instantaneous strain caused by the addition of the sustained load at  $t=60$  days are shown in [Figure 7.7f](#).

(f) At  $t=\infty$  For the time period from  $t=60$  days to  $t=\infty$ , the relevant creep coefficients for each of the previously calculated stress increments [determined in parts (a) to (e)] are as follows:

For the precast section:

- Part (a)  $\phi_1(\infty, 4) - \phi_1(60, 4) = 1.2$   
 Part (b)  $\chi_1(40, 4)[\phi_1(\infty, 4) - \phi_1(60, 4)] = 1.06$   
 Part (c)  $\phi_1(\infty, 40) - \phi_1(60, 40) = 1.1$   
 Part (d)  $\chi_1(60, 40)[\phi_1(\infty, 40) - \phi_1(60, 40)] = 0.99$   
 Part (e)  $\phi_1(\infty, 60) = 1.2$

For the *in situ* slab:

- Part (d)  $\chi_2(60, 40)[\phi_2(\infty, 40) - \phi_2(60, 40)] = 1.94$   
 Part (e)  $\phi_2(\infty, 60) = 2.0$

Note that the stress change calculated in part (d) is assumed to be suddenly applied at  $t=40$  days. The shrinkage strains which develop during this time period are, for the precast section,  $\varepsilon_{sh1}(\infty) - \varepsilon_{sh1}(60-4) = -300 \times 10^{-6}$ , and for the in situ slab,  $\varepsilon_{sh2}(\infty) - \varepsilon_{sh2}(60-40) = -480 \times 10^{-6}$ . The relaxation loss in the prestressing tendons after  $t=60$  days is 28 kN.

The age-adjusted effective moduli (from Equation 2.14) for the two elements are

$$\bar{E}_{e1}(\infty, 60) = 16840 \text{ MPa} \quad \text{and} \quad \bar{E}_{e2}(\infty, 60) = 9620 \text{ MPa}$$

and the properties of the concrete portions of each element and of the age-adjusted transformed section (with modulus  $\bar{E}_{e1}=16840$  MPa) are

$$\begin{aligned} A_{c1} &= 358\,500 \text{ mm}^2; B_{c1} = 228.3 \times 10^6 \text{ mm}^3; \bar{I}_{c1} = 163.7 \times 10^9 \text{ mm}^4 \\ A_{c2} &= 357\,000 \text{ mm}^2; B_{c2} = 26.78 \times 10^6 \text{ mm}^3; \bar{I}_{c2} = 2683 \times 10^6 \text{ mm}^4 \\ \bar{A}_e &= 614\,600 \text{ mm}^2; \bar{B}_e = 260.4 \times 10^6 \text{ mm}^3; \bar{I}_e = 176.9 \times 10^9 \text{ mm}^4 \end{aligned}$$

The initial elastic strain distributions associated with each of the previously calculated stress increments are determined as in part (d) and are as follows:

- Part (a)  $\Delta\varepsilon_{oi} = -221.5 \times 10^{-6}$  and  $\Delta x_i = 0.0087 \times 10^{-6} \text{ mm}^{-1}$   
 Part (b)  $\Delta\varepsilon_{oi} = -13.4 \times 10^{-6}$  and  $\Delta x_i = 0.0416 \times 10^{-6} \text{ mm}^{-1}$   
 Part (c)  $\Delta\varepsilon_{oi} = -328.4 \times 10^{-6}$  and  $\Delta x_i = 0.512 \times 10^{-6} \text{ mm}^{-1}$

Part (d) In Element 1:

$$\Delta \epsilon_{ai1} = \Delta \sigma_{ai1} / E_{c1}(40) = 77.8 \times 10^{-6}; \Delta \epsilon_{bi1} = -18.7 \times 10^{-6};$$

$$\Delta \epsilon_{oi1} = 97.1 \times 10^{-6}; \text{ and } \Delta x_{i1} = -0.1287 \times 10^{-6} \text{ mm}^{-1}$$

In Element 2:

$$\Delta \epsilon_{oi2} = \Delta \sigma_{oi2} / E_{c2}(40) = -13.3 \times 10^{-6}; \Delta \epsilon_{ai2} = -6.1 \times 10^{-6};$$

$$\text{and therefore } \Delta x_{i2} = 0.0481 \times 10^{-6} \text{ mm}^{-1}$$

Part (e) For both elements:

$$\Delta \epsilon_{oi} = -25.2 \times 10^{-6} \text{ and } \Delta x_i = 0.0642 \times 10^{-6} \text{ mm}^{-1}$$

The actions  $-\delta N$  and  $-\delta M$  required to restrain creep and shrinkage are calculated using Equations 7.18 and 7.19:

$$\begin{aligned} -\delta N &= -9620 \{ 1.94 [(357\,000 \times -13.3) + (26.78 \times 10^6 \times 0.0481)] \\ &\quad + 2.0 [(357\,000 \times -25.2) + (26.78 \times 10^6 \times 0.0642)] - (480 \\ &\quad \times 357\,000) \} \times 10^{-6} - 16\,840 \{ 1.2 [(358\,500 \times -221.5) + (228.3 \\ &\quad \times 10^6 \times 0.0087)] + 1.06 [(358\,500 \times -13.4) + (228.3 \times 10^6 \\ &\quad \times 0.0416)] + 1.1 [(358\,500 \times -328.2) + (228.3 \times 10^6 \times 0.512)] \\ &\quad + 0.99 [(358\,500 \times 97.1) + (228.3 \times 10^6 \times -0.1287)] \\ &\quad + 1.2 [(358\,500 \times -25.2) + (228.3 \times 10^6 \times 0.0642)] - (300 \\ &\quad \times 358\,500) \} \times 10^{-6} - 28\,000 = 4927 \times 10^3 \text{ N} \\ -\delta M &= -9620 \{ 1.94 [(26.78 \times 10^6 \times -13.3) + (2683 \times 10^6 \times 0.0481)] \\ &\quad + 2.0 [(26.78 \times 10^6 \times -25.2) + (2683 \times 10^6 \times 0.0642)] - (480 \\ &\quad \times 26.78 \times 10^6) \} \times 10^{-6} - 16\,840 \{ 1.2 [(228.3 \times 10^6 \\ &\quad \times -221.5) + (163.7 \times 10^9 \times 0.0087)] + 1.06 [(228.3 \times 10^6 \\ &\quad \times -13.4) + (163.7 \times 10^9 \times 0.0416)] + 1.1 [(228.3 \times 10^6 \times -328.2) \\ &\quad + (163.7 \times 10^9 \times 0.512)] + 0.99 [(228.3 \times 10^6 \times 97.1) + (163.7 \\ &\quad \times 10^9 \times -0.1287)] + 1.2 [(228.3 \times 10^6 \times -25.2) + (163.7 \times 10^9 \\ &\quad \times 0.0642)] - (300 \times 228.3 \times 10^6) \} \times 10^{-6} - 28\,000 \times 800 \\ &= 1919 \times 10^6 \text{ Nmm} \end{aligned}$$

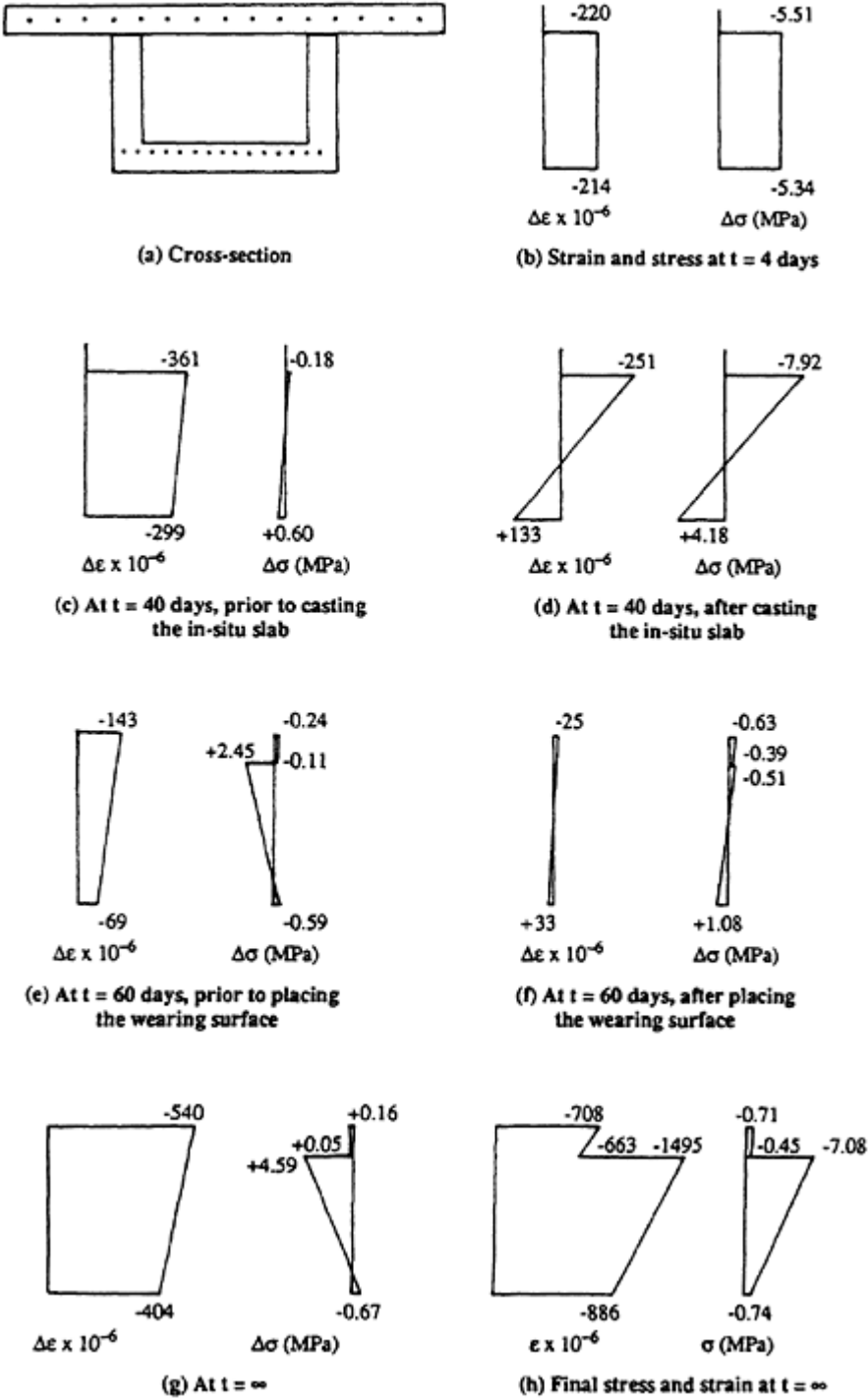


Figure 7.7 Stress and strain increments in [Example 7.1](#).

and from Equations 7.21 and 7.22,

$$\Delta \epsilon_0 = -540 \times 10^{-6} \quad \text{and} \quad \Delta \kappa = 0.151 \times 10^{-6} \text{ mm}^{-1}$$

The changes of concrete stress during this time period in both the slab and the precast section are obtained from Equation 7.23. In the *in situ* slab,

$$\begin{aligned} \Delta \sigma_{o2} &= -9620[(1.94 \times -13.3) + (2.0 \times -25.2) - 480 + 540] \times 10^{-6} \\ &= 0.16 \text{ MPa} \end{aligned}$$

$$\begin{aligned} \Delta \sigma_{a2} &= -9620\{1.94[-13.3 + (150 \times 0.0481)] + 2.0[-25.2 + (150 \\ &\quad \times 0.0642)] - 480 - [-540 + (150 \times 0.151)]\} \times 10^{-6} \\ &= 0.05 \text{ MPa} \end{aligned}$$

and, in the precast section,

$$\begin{aligned} \Delta \sigma_{a1} &= -16840\{1.2[-221.5 + (150 \times 0.0087)] + 1.06[-13.4 + (150 \\ &\quad \times 0.0416)] + 1.1[-328.2 + (150 \times 0.512)] + 0.99[97.1 \\ &\quad + (150 \times -0.1287)] + 1.2[-25.2 + (150 \times 0.0642)] - 300 \\ &\quad - [-540 + (150 \times 0.151)]\} \times 10^{-6} = 4.59 \text{ MPa} \end{aligned}$$

$$\begin{aligned} \Delta \sigma_{b1} &= -16840\{1.20[-221.5 + (900 \times 0.0087)] + 1.06[-13.4 + (900 \\ &\quad \times 0.0416)] + 1.1[-328.2 + (900 \times 0.512)] + 0.99[97.1 + (900 \\ &\quad \times -0.1287)] + 1.2[-25.2 + (900 \times 0.0642)] - 300 - [-540 \\ &\quad + (900 \times 0.151)]\} \times 10^{-6} = -0.67 \text{ MPa} \end{aligned}$$

The changes of stress and strain during this time interval are shown in [Figure 7.7g](#) and the final stress and strain distributions at time infinity (the sum of all the previously calculated increments) are shown in [Figure 7.7h](#). Note that the compressive stresses at the top of the precast member at the commencement of composite action are substantially reduced with time, much of the compression finding its way into the non-prestressed reinforcement in the *in situ* slab. The increments of steel stress from  $t=60$  days to  $t=\infty$  are calculated using Equations 7.24 and 7.25:

$$\Delta \sigma_{s1} = -105.7 \text{ MPa} \quad \text{and} \quad \Delta \sigma_p = -102.5 \text{ MPa}$$

## 7.6 Ultimate flexural strength

The ultimate flexural strength of a composite cross-section may be determined in accordance with the flexural strength theory outlined in [Chapter 4](#). If adequate provision is made to transfer the horizontal shear forces that exist on the interface between the *in situ* and precast components, the ultimate strength of a cross-section such as that shown in [Figure 7.6](#) may be calculated in the same way as for an identical monolithic cross-section with the same reinforcement quantities and material properties (see [Section 4.6](#)). The calculations are based on the full effective flange width and, in general, it is not necessary to account for variations in concrete strengths between the two components. In practice, owing to the typically wide effective compressive flange, the depth to the natural axis at ultimate is relatively small, usually less than the thickness of the *in situ* slab. It is therefore appropriate to consider an idealized rectangular stress block based on the properties of the *in situ* concrete rather than the precast concrete. Even in situations where the depth of the compressive zone exceeds the thickness of the slab, more complicated expressions for strength based on more accurate modelling of concrete compressive stresses are not generally necessary. As seen in [Chapter 4](#), the flexural strength of any ductile section is primarily dependent on the quantity and strength of the steel in the tensile zone and does not depend significantly on the concrete strength.

The strain discontinuity that exists at the element interface at service loads due to the construction sequence becomes less and less significant as the moment level increases. This discontinuity may be ignored in ultimate flexural strength calculations.

## 7.7 Horizontal shear transfer

### 7.7.1 Discussion

As has been emphasized in the previous section, the ability of the entire composite member to resist load depends on the ability to carry horizontal shear at the interface between the precast and *in situ* elements. If the two components are not effectively bonded together, slip occurs at the interface, as shown in [Figure 7.8a](#), and the two components act as separate beams each carrying its share of the external loads by bending about its own centroidal axis. To ensure full composite action, slip at the interface must be prevented. There must be an effective means for transferring horizontal shear across the interface. If slip is prevented, full composite action is assured (as shown in [Figure 7.8b](#)) and the advantages of composite construction are realized.

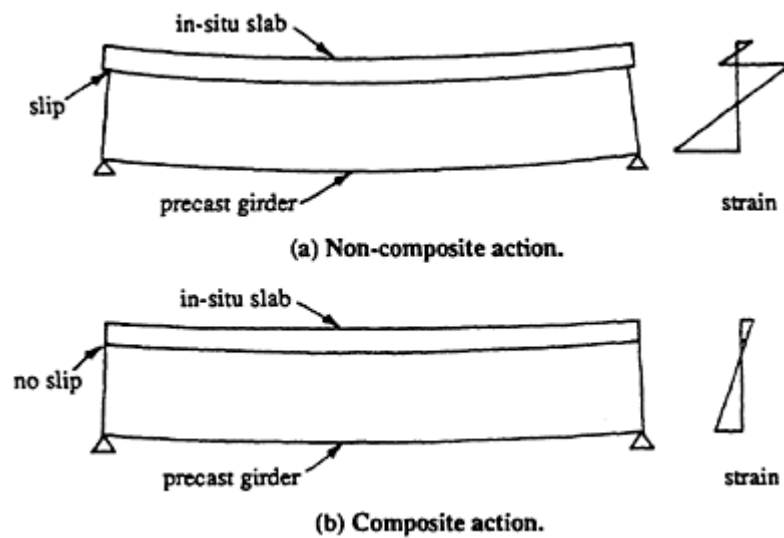


**Figure 7.8** Composite and non-composite action.

In [Section 7.2](#), various mechanisms for shear transfer were discussed. Natural adhesion and friction are usually sufficient to prevent slip in composite members with a wide interface between the components (such as the cross-sections shown in [Figures 7.1b, c and d](#)). The contact surface of the precast member is often roughened during manufacture to improve bond. Where the contact area is smaller (as on the cross-section of [Figures 7.1a and e and 7.6](#)), web reinforcement in the precast girder is carried through the interface and anchored in the *in situ* slab, thus providing increased frictional resistance (by clamping the contact surfaces together) and additional shear resistance through dowel action.

The theorem of complementary shear stress indicates that on the cross-section of an uncracked elastic composite member, the horizontal shear stress  $v_h$  at the interface between the two components is equal to the vertical shear stress at that point and is given by the well known expression

$$v_h = \frac{VQ}{Ib_f} \quad (7.26)$$

where  $V$  is that part of the shear force caused by loads applied after the establishment of composite action,  $Q$  is the first moment of the area of the *in situ* element about the centroidal axis of the composite cross-section,  $I$  is the moment of inertia of the gross composite cross-section, and  $b_f$  is the width of the contact surface (usually equal to the width of the top surface of the precast member). The distribution of shear stress and the direction of the horizontal shear at the interface are shown in [Figure 7.9](#).

At overloads, concrete members crack and material behaviour becomes non-linear and inelastic. In design, a simpler average or nominal shear stress



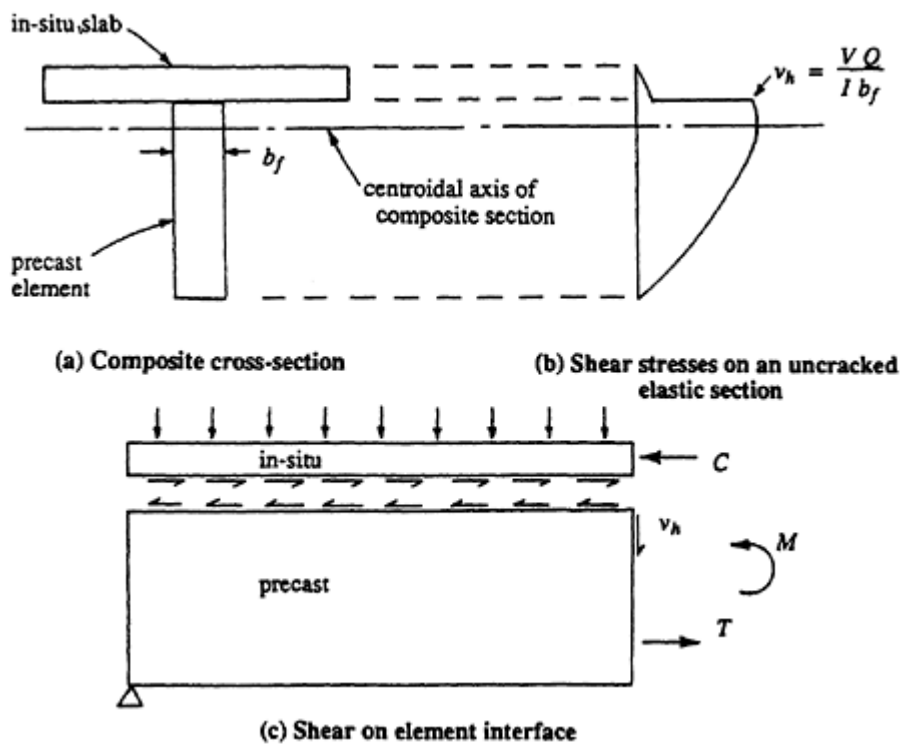


**Figure 7.9** Shear stresses in an elastic, uncracked composite beam.

is usually used for ultimate strength calculations and is given by

$$v_f^* = \frac{V^*}{b_f d} \quad (7.27)$$

where  $V^*$  is the total shear force obtained using the appropriate factored load combination for the strength limit state (see [Section 1.7.3](#)) and  $d$  is the effective depth to the tensile reinforcement in the composite beam. Note that in Equation 7.27,  $V^*$  is calculated from the total loads and not just the loads applied after the *in situ* slab has hardened. At ultimate loads, flexural cracking can actually cross the interface and horizontal shear resulting from all the applied load must be carried.

### 7.7.2 Code provisions for horizontal shear

#### AS 3600–1988

The design horizontal shear force  $V_f^*$  acting on the element interface depends on the position of the interface on the cross-section. For a shear plane through the compressive flange,

$$V_f^* = V^* \frac{A_1}{A_2} \quad (7.28)$$

where  $A_1/A_2$  is the ratio of the area of the flange outstanding beyond the shear plane to the total area of the flange. If the shear plane is through the web, or at the intersection of the *in situ* slab and a narrow flanged precast I-girder or trough girder,  $A_1/A_2$  is taken as unity and  $V_f^* = V^*$ .

For adequate strength,  $V_f^*$  must be less than the design strength,  $\phi V_{uf}$ . The design strength is made up of contributions from the concrete and from the steel reinforcement crossing the shear plane (if any) and is specified as

$$\phi V_{uf} = \phi \beta_4 A_s f_y \frac{d}{s} + \phi \beta_5 b_f d \times 0.4 \sqrt{f'_c} \leq 0.2 f'_c b_f d \quad (7.29)$$

where the strength reduction factor for shear is  $\phi = 0.7$ ,  $\beta_4$  and  $\beta_5$  are coefficients that depend on the surface condition of the shear plane and are given in [Table 7.1](#),  $A_s$  is the area of reinforcement (with yield stress  $f_y$ ) anchored on each side of the shear plane,  $d$  is the effective depth of the composite beam,  $s$  is the spacing of reinforcement crossing the shear plane, and  $b_f$  is the width of the shear interface.

If shear reinforcement ( $A_s$  in Equation 7.29) is required for strength (i.e. the concrete component in Equation 7.29 is insufficient on its own), the

**Table 7.1** Shear plane surface coefficients (AS 3600–1988).

Surface Conditions of the Shear Plane	Coefficients	
	$\beta_4$	$\beta_5$
A smooth surface, as obtained by casting against a form, or finished to a similar standard.	0.6	0.1
A surface trowelled or tamped, so that the fines have been brought to the top, but where some small ridges, indentations or undulations have been left; slip-formed and vibro-beam screeded; or produced by some form or extrusion technique.	0.6	0.2
A surface deliberately roughened	0.9	0.4
(a) by texturing the concrete to give a pronounced profile;		
(b) by compacting but leaving a rough surface with coarse aggregate protruding but firmly fixed in the matrix;		
(c) by spraying when wet, to expose the coarse aggregate without disturbing it; or		
(d) by providing mechanical shear keys		
Monolithic construction	0.9	0.5

minimum area of reinforcement crossing the shear plane is

$$(A_s)_{min} = \frac{0.35b_f s}{f_y} \quad (7.30)$$

### ACI 318–83

The ACI 318–83 design requirements are satisfied provided that

$$V^* \leq \phi V_{uf} = \phi v_{uf} b_f d \quad (7.31)$$

where  $v_{uf}$  is an ultimate shear stress related to the condition of the contact surfaces between the precast and cast *in situ* components and is equal to:

0.55 MPa when no reinforcement crosses the shear plane and the surface is clean, free from laitance, and deliberately roughened.

0.55 MPa when the surface is crossed by minimum reinforcement and the contact surface is clean, free from laitance, but not deliberately roughened.

2.4 MPa when the surface is crossed by minimum reinforcement and the contact surface is clean, free from laitance, and deliberately roughened to 6 mm amplitude.

The minimum reinforcement passing through the shear plane is given by

$$(A_s)_{min} = \frac{0.34b_f s}{f_y} \quad (7.32)$$

and the spacing  $s$  should not exceed four times the *in situ* slab thickness or 600 mm, whichever is less.

When the factored shear force  $V^*$  exceeds  $\phi V_{uf}$  (i.e. when  $V^* > \phi \times 2.4b_f d$ ), the shear friction method should be used to design for horizontal shear. In this method, a crack is assumed to occur along the shear plane (the interface between the *in situ* and precast components). As the jagged crack surfaces slide across each other, the crack opens and the reinforcement crossing the shear plane ( $A_s$ ) yields, thus inducing a clamping force across the crack and increasing the frictional resistance. Resistance to sliding is deemed to be provided by a friction force  $V_{un}$ , where

$$V_{un} = A_s f_y \mu \leq 0.2 f'_c A_c \quad (7.33)$$

In this expression,  $A_c$  is the area of the concrete section resisting shear transfer and  $\mu$  is an artificially high friction coefficient calibrated to account for the combined effects of friction, mechanical interlock, and dowel action. For normal-weight concrete,  $\mu=1.4$  for monolithic construction,

1.0 when the contact surface (i.e. the top of the precast element) is intentionally roughened, 0.6 when the contact surface is smooth concrete, and 0.7 when the contact is as rolled structural steel and is anchored to the concrete using headed studs or welded reinforcement. These values should be multiplied by 0.75 for lightweight concrete.

The design requirement when strength is provided by shear-friction is

$$V_n^* \leq \phi V_{un} \tag{7.34}$$

where  $V_n^*$  is the resultant horizontal shear force along the cracked interface over half the span of a simply supported beam (or about 0.35 of the span of a continuous member). The magnitude of  $V_n^*$  can be calculated from Figure 7.10 and depends on the depth of the idealized rectangular stress block at the region of maximum moment at mid-span. From Figure 7.10,

$$V_n^* = 0.85 f'_c a b_{ef} \quad \text{or} \quad V_n^* = 0.85 f'_c D_s b_{ef} \tag{7.35}$$

whichever is smaller, where  $a$  is the depth of the idealized rectangular stress block at the section of maximum moment and  $D_s$  is the depth of the *in situ* slab. By rearranging Equation 7.34, the area of reinforcement required across the shear plane must satisfy

$$A_s \geq \frac{V_n^*}{\phi f_y \mu} \tag{7.36}$$

and must be uniformly distributed over the length of the beam associated with  $V_n^*$ .

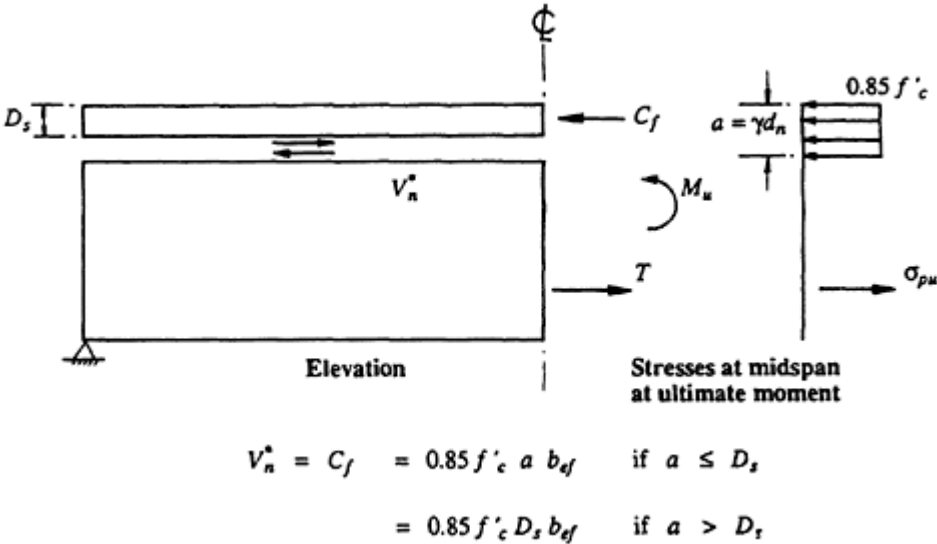


Figure 7.10 Total shear force on element interface.

### BS 8110 (1985)

According to the British Standard, the horizontal shear force caused by the factored design loads at the element interface  $V_h^*$  is calculated as for  $V_h^*$  in [Figure 7.10](#), except that the rectangular compressive stress block is different from that specified by ACI 318. The average horizontal shear stress at the interface is calculated by dividing  $V_h^*$  by the area of the contact surface, which is equal to  $b_f$  times the length of the beam between the point of maximum moment and the point of zero moment. The average calculated shear stress is then distributed in proportion to the vertical shear force diagram to give the design horizontal shear stress  $v_h^*$  at any point along the beam. The design shear stress at every point must be less than the value given in [Table 7.2](#).

When nominal reinforcement is provided and the appropriate design ultimate shear stress is taken from [Table 7.2](#), its cross-sectional area should be at least 0.15% of the contact area and it should be anchored on both sides of the interface. The spacing of the reinforcement should not exceed the lesser of four times the minimum thickness of *in situ* concrete or 600 mm. In regions where the design horizontal shear stress  $v_h^*$  exceeds the value given in [Table 7.2](#), the total horizontal shear force must be carried by adequately anchored reinforcement with an area given by the equation

$$A_s = \frac{1000b_f v_h^*}{0.87f_y} \text{ (mm}^2\text{/m)} \quad (7.37)$$

**Table 7.2** Design ultimate horizontal shear stresses at interface (MPa) [BS 8110 (1985)].

Precast unit	Surface type	Grade of in-situ concrete		
		25	30	40 and over
Without links	As-cast or as-extruded	0.4	0.55	0.65
	Brushed, screeded, or rough-tamped (deliberately roughened)	0.6	0.65	0.75
	Washed to remove laitance or treated with retarder and cleaned	0.7	0.75	0.8
With nominal links projecting into in-situ concrete	As-cast or as-extruded	1.2	1.8	2.0
	Brush, screeded or rough-tamped (deliberately roughened)	1.8	2.0	2.2
	Washed to remove laitance or treated with retarder and cleaned	2.1	2.2	2.5

### Example 7.2

The horizontal shear transfer requirements for the beam with cross-section shown in [Figure 7.6](#) are to be determined. The beam is simply supported over a span of 17.2 m and is subjected to the following loads:

Self-weight of precast trough-girder:	8.64 kN/m
Self-weight of <i>in situ</i> slab:	8.10 kN/m
Superimposed dead load:	4.05 kN/m
Transient live load:	9.60 kN/m

The behaviour of the cross-section at mid-span at service loads is calculated in [Example 7.1](#). The effective prestressing force calculated in [Example 7.1](#) is 1670 kN and is assumed here to be constant along the beam. Take  $f_p=1840$  MPa.

### AS 3600–1988

The factored load combination for the strength limit state (see [Section 1.7.3](#)) is

$$w^* = 1.25(8.64 + 8.10 + 4.05) + (1.5 \times 9.60) = 40.4 \text{ kN/m}$$

The maximum shear force adjacent to each support is

$$V^* = \frac{40.4 \times 17.2}{2} = 347 \text{ kN}$$

and, from Equation 7.28,

$$V_f^* = V^* = 347 \text{ kN}$$

The design strength  $\phi V_{wf}$  is obtained from Equation 7.29. If the top surface of the precast trough has been deliberately roughened to facilitate shear transfer, from [Table 7.1](#),  $\beta_4=0.9$ ,  $\beta_5=0.4$ , and with  $f'_c = 25$  MPa for the *in situ* slab, Equation 7.29 gives

$$\begin{aligned} \phi V_{wf} &= \left( 0.7 \times 0.9 \times \frac{A_s}{s} \times 400 \times 800 \right) + (0.7 \times 0.4 \times 300 \times 800 \times 0.4 \sqrt{25}) \\ &= \left( 201.6 \frac{A_s}{s} \right) + 134.4 \text{ (kN)} \geq V_f^* \end{aligned}$$

Therefore,

$$\frac{A_s}{s} \geq \frac{347 - 134.4}{201.6} = 1.05 \text{ mm}^2/\text{mm}$$

If 2–12 mm bars ( $f_y=400$  MPa) cross the shear perimeter, one in each web,  $A_s=220$  mm<sup>2</sup>, the required spacing near each support is

$$s \leq \frac{220}{1.05} = 209 \text{ mm}$$

The spacing can be increased further into the span, as the shear force  $V^*$  decreases. It is important to ensure adequate anchorage of these bars on each side of the shear plane.

If the contact surface were not deliberately roughened, but screeded and trowelled,  $\beta_4=0.6$ ,  $\beta_5=0.2$ , and Equation 7.29 gives

$$\phi V_{uf} = \left( 134.4 \frac{A_s}{s} \right) + 67.2 \text{ (kN)}$$

and with  $A_s=220$  mm<sup>2</sup>,

$$\frac{A_s}{s} \geq 2.08 \quad \text{and} \quad s \leq 106 \text{ mm}$$

At the quarter-span point, where  $V_f^* = 174$  kN,  $A_s/s \geq 0.79$  and  $s \leq 277$  mm.

The maximum spacing between the reinforcement crossing the shear plane (if  $A_s=220$  mm<sup>2</sup>) is obtained from Equation 7.30:

$$s_{max} = \frac{A_s f_y}{0.35 b_f} = \frac{220 \times 400}{0.35 \times 300} = 838 \text{ mm}$$

which is greater than the maximum recommended spacing of four times the slab thickness or 600 mm.

### AS 318–83

The factored load combination for the strength limit state (see [Section 1.7.3](#)) is

$$w^* = 1.4(8.64 + 8.10 + 4.05) + (1.7 \times 9.60) = 45.4 \text{ kN/m}$$

The maximum shear force adjacent to each support is

$$V^* = \frac{45.4 \times 17.2}{2} = 391 \text{ kN}$$

With minimum reinforcement crossing the shear plane and a deliberately

roughened contact surface, Equation 7.31 gives

$$\phi V_{wf} = 0.85 \times 2.4 \times 300 \times 800 = 490 \text{ kN} > V^*$$

According to ACI 318–83, minimum steel reinforcement given by Equation 7.32 (with a maximum spacing of 600 mm) is all that is required here. If, however, the contact surface is not deliberately roughened, Equation 7.31 gives

$$\phi V_{wf} = 0.85 \times 0.55 \times 300 \times 800 = 112 \text{ kN} < V^*$$

and additional reinforcement must be designed using the shear-friction concept. The horizontal shear force along the cracked contact surface over half the span of the simply supported beam is calculated using Equation 7.35. From an ultimate flexural strength analysis at midspan, the depth of the idealized rectangular stress block at ultimate is  $a=53$  mm and Equation 7.35 gives

$$V_n^* = 0.85 \times 25 \times 53 \times 2400 = 2703 \text{ kN}$$

With the coefficient of friction  $\mu=0.6$ , the total amount of shear reinforcement crossing the shear plane is given by Equation 7.36:

$$A_s \geq \frac{2703 \times 10^3}{0.85 \times 400 \times 0.6} = 13\,250 \text{ mm}^2$$

which must be uniformly distributed across the contact surface over half the length of the beam (8.6 m). This amounts to 2–12 mm reinforcing bars (one in each web) at 143 mm centres throughout.

According to ACI 318–83, the difference between the steel requirements when the contact surface is smooth and when it is rough is very large indeed.

### BS 8110:1985

In this example, when the cross-section at midspan is subjected to the ultimate moment, the shear plane between the two concrete elements is in the tension zone. The total horizontal shear force  $V_h^*$  at the interface, between mid-span and the support, is equal to the resultant tension in the prestressing steel at mid-span. The magnitude of  $V_h^*$  is equal to  $V_n^*$  as calculated previously for the ACI 318 shear-friction approach, i.e.  $V_h^* = 2703$  kN. With a triangular shear force diagram, the maximum horizontal shear stress on the shear plane occurs adjacent to the support and is double the average value. Therefore,

$$(v_h^*)_{max} = \frac{2 \times 2703 \times 10^3}{300 \times 8600} = 2.10 \text{ MPa}$$



which exceeds the maximum allowable values given in [Table 7.2](#) for a shear plane containing nominal ties (i.e. 1.2 MPa if the contact surface is not deliberately roughened, and 1.8 MPa if the contact surface is deliberately roughened). The total amount of steel required to cross the shear plane in this region is given by Equation 7.37:

$$A_s = \frac{1000 \times 300 \times 2.10}{0.87 \times 400} = 1810 \text{ mm}^2/\text{m}$$

which corresponds to 2–12 mm bars at 122 mm centres. In regions where  $v_h^*$  is less than the limiting value given in [Table 7.2](#), nominal ties only are required. The area of nominal ties is 0.15% of the contact area and is equal to

$$A_s = 0.0015 \times 300 \times 1000 = 450 \text{ mm}^2/\text{m}$$

or 2–12 mm bars at 489 mm centres.

## 7.8 Ultimate shear strength

### 7.8.1 Introductory remarks

The design procedures for composite members in shear and torsion are similar to those outlined in [Chapter 5](#) for non-composite members. An additional complication arises, however, in the estimation of the diagonal cracking load for a composite member, and hence in the estimation of the contribution of the concrete to the shear strength,  $V_{uc}$  (in Equation 5.2).

Before cracking, part of the applied load is resisted exclusively by the precast element (i.e. the load applied in load stages 1–3, as defined in [Section 7.3](#)) and part by the composite section (in load stages 4 and 5). In theory, these loads need to be considered separately, using the precast section properties and the composite section properties as appropriate, in order to determine the shear force existing at the onset of diagonal cracking. As discussed in [Section 5.5.1](#), the concrete contribution to shear strength,  $V_{uc}$ , is usually taken as the smaller of the shear force required to produce a flexure-shear crack and the shear force required to cause a web-shear crack.

The design approach described in [Section 5.5.2](#) may be used for the determination of the shear strength of a composite member, provided the stress conditions existing in the precast element are taken into account in the determination of  $V_{uc}$ .

### 7.8.2 Web-shear cracking

The shear force required to produce web-shear cracking at a section may be calculated from the following modification to Equation 5.10:

$$V_{uc} = V_{t,comp} + V_{pc} + P_v \quad (7.38)$$

where  $V_{pc}$  is the shear force applied to the precast member only,  $P_v$  is the vertical component of prestress, and  $V_{t,comp}$  is the shear force applied to the composite section which, when combined with the normal stresses caused by loads applied to the composite section and normal and shear stresses caused by the prestress and the external loads applied to the precast section, produces a principal tensile stress of  $0.33\sqrt{f'_c}$  at either the centroidal axis of the precast section, the centroidal axis of the composite section, the level of the prestressing duct, or the intersection of the flange and the web, whichever is critical.

At a particular point on the cross-section,  $V_{t,comp}$  is calculated by setting  $\sigma_1 = 0.33\sqrt{f'_c}$  in Equation 5.11. The normal stress,  $\sigma$  in Equation 5.11, is the sum of the normal stresses on the precast element (caused by the initial prestress and moments arising from loads applied directly to the precast member in load stages 1 and 3,  $M_{1,3}$ ), and the bending stress due to moments caused by the loads producing  $V_{t,comp}$  applied to the composite section (in load state 4,  $M_{t,comp}$ ). Therefore,

$$\sigma = \left( -\frac{P_e}{A} - \frac{P_e ey}{I} + \frac{M_{1,3}y}{I} \right)_{\text{precast}} + \left( \frac{M_{t,comp}y}{I} \right)_{\text{composite}} \quad (7.39)$$

The shear stress  $\tau$  in Equation 5.11 is the sum of the shear stress existing on the precast section (due to  $V_{pc}$  and  $P_v$ ) and that arising from  $V_{t,comp}$  on the composite section. That is,

$$\tau = \left[ \frac{(V_{pc} - P_v)Q}{Ib_w} \right]_{\text{precast}} + \left( \frac{V_{t,comp}Q}{Ib_w} \right)_{\text{composite}} \quad (7.40)$$

On the right-hand sides of Equations 7.39 and 7.40, the section properties used inside each bracket are those relating to either the precast or the composite cross-sections as indicated.

### 7.8.3 Flexure-shear cracking

The shear force  $V_{uc}$  required to produce a flexure-shear crack is given by Equation 5.8 and is made up of the shear force that exists at decompression of the extreme tensile fibre at the section under consideration,  $V_o$ , an empirical term representing the additional shear force required to produce an

inclined crack, and the vertical component of prestress:

$$V_{uc} = \beta_1 \beta_2 b_v d_o \left( \frac{A_{sr} + A_{pt}}{b_v d_o} f'_c \right)^{1/3} + V_o + P_v \quad (5.8)$$

When applying Equation 5.8 to composite members, consideration must be given to the loading sequence and the stresses existing in the precast element prior to composite action. Decompression may occur with the addition of dead load to the precast section in load stage 3, i.e. decompression occurs on the precast section even before the *in situ* slab is cast and composite action begins. Alternatively, and more commonly, decompression occurs after the composite section is formed in load stage 4 or under overloads.

If decompression occurs on the precast section,  $V_o$  must be calculated using the properties of the precast section. Some portion of the additional shear force required to produce the inclined crack (represented by the first term of Equation 5.8) will be acting on the precast section, with the remaining shear acting on the composite section. Because this term is empirical, it is not sensible to try to separate the precast and composite components. If decompression occurs in the precast section prior to composite action with the cast *in situ* slab,  $V_{uc}$  should be calculated using the properties of the precast section for the determination of each term in Equation 5.8.

When decompression and cracking of the tension zone do not occur until after the section is composite,  $V_o$  is the sum of the shear force caused by the loads on the precast section (at the end of load stage 3) and the additional shear force added to the composite cross-section when the extreme tensile fibre is decompressed. In this case, the empirical term in Equation 5.8 should be calculated using the properties of the full composite section (i.e.  $d_o$  in Equation 5.8 should be the depth of the tensile reinforcement from the top surface of the *in situ* slab).

### Example 7.3

In this example, the beam described in [Example 7.2](#), with cross-section shown in [Figure 7.6](#), is checked for shear at the cross-section 2 m from the support. In accordance with AS 3600–1988, the factored design load for strength was determined in [Example 7.2](#) as  $w^* = 40.4$  kN/m. At 2 m from the support

$$V^* = 267 \text{ kN} \quad \text{and} \quad M^* = 614 \text{ kN m}$$

For this member with straight tendons,  $P_1 = 0$ .

**Web-shear cracking** The load applied to the precast member in load stages 1 and 3 is  $8.64 + 8.10 = 16.74$  kN/m and the corresponding shear force and

bending moment at the section 2 m from the support are

$$V_{pc} = \frac{16.74}{40.4} \times 267 = 110 \text{ kN} \quad \text{and} \quad M_{1,3} = \frac{16.74}{40.4} \times 614 = 255 \text{ kN m}$$

The centroidal axis of the precast section is located 262.5 mm above the bottom fibre (as shown in [Figure 7.6](#)) and the centroidal axis of the composite section is 543.8 mm from the bottom fibre. The properties of both the precast and composite sections about their centroidal axes are

Precast:  $I=18390 \times 10^6 \text{ mm}^4$ ;  $A=360000 \text{ mm}^2$ ;  
 $Q=35.65 \times 10^6 \text{ mm}^3$  at centroid of precast section;  
 $Q=23.78 \times 10^6 \text{ mm}^3$  at level of composite centroid.

Composite:  $I=76020 \times 10^6 \text{ mm}^4$ ;  
 $Q=107.6 \times 10^6 \text{ mm}^3$  at centroid of composite section;  
 $Q=85.8 \times 10^6 \text{ mm}^3$  at level of precast centroid.

The moment caused by the loads producing  $V_{t,comp}$  is

$$M_{t,comp} = \frac{M^*}{V^*} V_{t,comp} = 2300 V_{t,comp}$$

The normal stresses at the centroid of the composite section,  $\sigma_{comp}$ , and at the level of the centroid of the precast section,  $\sigma_{pc}$ , are obtained from Equation 7.39:

$$\begin{aligned} \sigma_{comp} &= -\frac{1670 \times 10^3}{360000} + \frac{1670 \times 10^3 \times 162.5 \times 281.3}{18390 \times 10^6} - \frac{255 \times 10^6 \times 281.3}{18390 \times 10^6} \\ &= -4.39 \text{ MPa} \end{aligned}$$

and

$$\begin{aligned} \sigma_{pc} &= -\frac{1670 \times 10^3}{360000} + \frac{2300 V_{t,comp} \times 10^3 \times 281.3}{76020 \times 10^6} \\ &= -4.64 + 8.51 \times 10^{-3} V_{t,comp} \end{aligned}$$

The shear stress at the level of both centroids are found using Equation 7.40,

$$\begin{aligned}\tau_{comp} &= \frac{110 \times 10^3 \times 23.78 \times 10^6}{18\,390 \times 10^6 \times 300} + \frac{V_{t,comp} \times 10^3 \times 107.6 \times 10^6}{76\,020 \times 10^6 \times 300} \\ &= 0.474 + 4.72 \times 10^{-3} V_{t,comp}\end{aligned}$$

and

$$\begin{aligned}\tau_{pc} &= \frac{110 \times 10^3 \times 35.65 \times 10^6}{18\,390 \times 10^6 \times 300} + \frac{V_{t,comp} \times 10^3 \times 95.8 \times 10^6}{76\,020 \times 10^6 \times 300} \\ &= 0.711 + 4.20 \times 10^{-3} V_{t,comp}\end{aligned}$$

By substituting the above expressions into Equation 5.11 and solving, with  $\sigma_1 = 0.33\sqrt{f'_c} = 0.33\sqrt{40} = 2.09$  MPa, the shear forces needed to be applied to the composite section to produce web-shear cracking at each critical location are obtained:

At the centroid of the composite section:  $V_{t,comp} = 679$  kN.

At the centroid of the precast section:  $V_{t,comp} = 434$  kN.

The latter value clearly governs and the total shear force required to cause web-shear cracking is obtained from Equation 7.38:

$$V_{uc} = 434 + 110 = 544 \text{ kN}$$

**Flexure-shear cracking** Decompression occurs when the moment applied to the composite section  $M_{o,comp}$  just causes the bottom fibre stress to be zero. That is,

$$\left( -\frac{P_e}{A} - \frac{P_e e y_b}{I} + \frac{M_{1,3} y_b}{I} \right)_{\text{precast}} + \left( \frac{M_{o,comp} y_b}{I} \right)_{\text{composite}} = 0$$

and

$$\begin{aligned}M_{o,comp} &= \left( +\frac{1670 \times 10^3}{360\,000} + \frac{1670 \times 10^3 \times 162.5 \times 262.5}{18\,390 \times 10^6} \right. \\ &\quad \left. - \frac{255 \times 10^6 \times 262.5}{18\,390 \times 10^6} \right) \frac{76\,020}{543.8} = 681 \text{ kNm}\end{aligned}$$

The shear force at decompression is therefore

$$V_o = V_{pc} + \frac{V^*}{M^*} M_{o,comp} = 110 + 296 = 406 \text{ kN}$$

The shear force required to produce flexure-shear cracking is obtained from Equation 5.8:

$$V_{uc} = 1.1 \times 300 \times 800 \left( \frac{1500 \times 40}{300 \times 800} \right)^{1/3} \times 10^{-3} + 406 = 572 \text{ kN}$$

Evidently,  $V_{uc}$  is governed by web-shear cracking at this cross-section and is equal to 544 kN. The design strength is

$$\phi V_{uc} = 0.7 \times 544 = 381 \text{ kN}$$

which is greater than the design action  $V^*$  and only minimum shear reinforcement is required.

## 7.9 References

- ACI 318–83 1983. *Building code requirements for reinforced concrete*. Detroit: American Concrete Institute.
- AS 3600 1988. *Australian standard for concrete structures*. Sydney: Standards Association of Australia.
- BS 8110 1985. *Structural use of concrete—part I*. London: British Standards Institution.
- Gilbert, R.I. 1988. *Time effects in concrete structures*. Amsterdam: Elsevier.
- Hanson, N.W. 1960. Precast-prestressed concrete bridges: (2) horizontal shear connections. *Journal of the Research and Development Laboratory, Portland Cement Association* **2**, No. 2, 35–58.
- Saemann, J.C. & G.W. Washa, 1964. Horizontal shear connections between precast beams and cast-in-place slabs. *ACI Journal* **61**, 1383–1409.

# 8

## Design procedures for determinate beams

### 8.1 Introduction

The variables which must be established in the design of a statically determinate prestressed concrete beam are the shape and size of the section, the amount and location of both the prestressed steel and the non-prestressed reinforcement, and the magnitude of the prestressing force. The designer is constrained by the various design requirements for the strength, serviceability, stability, and durability limit states.

The optimal design is the particular combination of design variables which satisfies all the design constraints at a minimum cost. The cost of a particular design depends on local conditions at the time of construction, and variations in the costs of materials, formwork, construction expertise, labour, plant hire, etc., can change the optimal design from one site to another and also from one time to another.

It is difficult, therefore, to fix hard and fast rules to achieve the optimal design. It is difficult even to determine confidently when prestressed concrete becomes more economic than reinforced concrete or when partially prestressed concrete is the best solution. However, it is possible to give some broad guidelines to achieve feasible design solutions for both fully and partially prestressed members. In this chapter, such guidelines are presented and illustrated by examples.

### 8.2 Types of section

Many types of cross-section are commonly used for prestressed girders. The choice depends on the nature of the applied loads, the function of the member, the availability and cost of formwork, aesthetic considerations, and ease of construction. Some commonly used cross-sections are shown in [Figure 8.1](#).

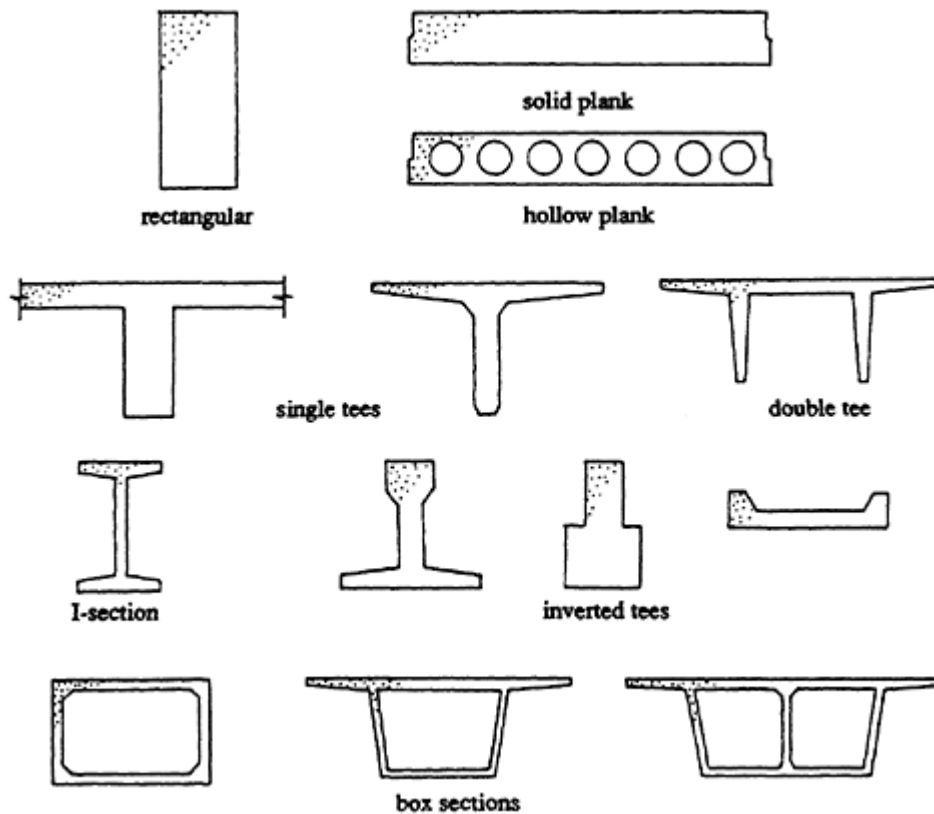


**Figure 8.1** Some common prestressed concrete beam cross-sections.

Most *in situ* prestressed concrete beam sections are rectangular (or slab and beam tee-sections with rectangular webs). Rectangular sections are not particularly efficient in bending. The self-weight of a rectangular section is larger than for an I- or T-section of equivalent stiffness, and the prestress required to resist an external moment also tends to be larger. The formwork costs for a rectangular section, however, are generally lower and steel fixing is usually easier.

For precast prestressed concrete, where re-usable formwork is available, the more efficient flanged sections are commonly used. T-sections and double T-sections are ideal for simply supported members in situations where the self-weight of the beam is a significant part of the total load. If the moment at transfer due to self-weight (plus any other external load) is not significant, excessive compressive stresses may occur in the bottom fibres at transfer in T-shaped sections.

Inverted T-sections can accommodate large initial compressive forces in the lower fibres at transfer and, whilst being unsuitable by themselves for resisting positive moment, they are usually used with a cast *in situ* composite concrete deck. The resulting composite section is very efficient in positive bending.



For continuous members, where both positive and negative moments exist, I-sections and closed box sections are appropriate. Box-shaped sections are laterally stable and have found wide application as medium-and long-span bridge girders. In addition, box sections can carry efficiently the torsional moments caused by eccentric traffic loading.

### 8.3 Initial trial section

#### 8.3.1 Based on serviceability requirements

A reliable initial trial cross-section is required at the beginning of a design in order to estimate accurately self-weight and to avoid too many design iterations.

For a fully prestressed member, Equation 3.9 provides an estimate of the minimum section modulus required to satisfy the selected stress limits at the critical section both at transfer and under the full service loads. If the time-dependent loss of prestress is assumed to be 25%, Equation 3.9 may be simplified to

$$Z_b \geq \frac{M_T - 0.75M_o}{F_t - 0.75F_{ci}} \quad (8.1)$$

The compressive stress limit at transfer  $F_{ci}$  in this expression is a negative number.

For a member containing a parabolic cable profile, a further guide to the selection of an initial trial section may be obtained by considering the deflection requirements for the member. The deflection of an uncracked prestressed beam under a uniformly distributed unbalanced load  $w_u$  may be expressed as

$$v = \beta \frac{w_u L^4}{E_c I} + \lambda \beta \frac{w_{us} L^4}{E_c I} \quad (8.2)$$

where  $w_{us}$  is the sustained part of the unbalanced load,  $\beta$  is a deflection coefficient,  $L$  is the span of the beam,  $E_c$  is the elastic modulus of concrete,  $I$  is the moment of inertia of the gross cross-section, and  $\lambda$  is a long-term deflection multiplication factor, which should not be taken to be less than 3.0 for an uncracked prestressed member. The deflection coefficient  $\beta$  is equal to  $5/384$  for a uniformly loaded simply supported member. For a continuous member,  $\beta$  depends on the support conditions, the relative lengths of the adjacent spans, and the load pattern. When the variable part of the unbalanced load is not greater than the sustained part, the deflection coefficients for a continuous beam with equal adjacent spans may be taken as  $\beta=2.75/384$  for an end span and  $\beta=1.8/384$  for an interior span.

Equation 8.2 can be re-expressed as

$$v = \beta \frac{w_t L^4}{E_c I} \quad (8.3)$$

where

$$w_t = w_u + \lambda w_{us} \quad (8.4)$$

If  $v_{max}$  is the maximum permissible total deflection, then from Equation 8.3 the initial gross moment of inertia must satisfy the following:

$$I \geq \beta \frac{w_t L^4}{E_c v_{max}} \quad (8.5)$$

All the terms in Equation 8.5 are generally known at the start of a design, except for an estimate of  $\lambda$  (in Equation 8.4), which may be taken initially to equal 3 for an uncracked member. Since self-weight is usually part of the load being balanced by prestress, it does not form part of  $w_t$ .

For a cracked partially prestressed member,  $\lambda$  should be taken as not more than 2, for the reasons discussed in [Section 3.8.3](#). After cracking the effective moment of inertia  $I_e$  depends on the quantity of tensile steel and the level of maximum moment. If  $I_e$  is taken to be  $0.5I$ , which is usually conservative, an initial estimate of the gross moment of inertia of the partially-prestressed section can be obtained from

$$I \geq 2\beta \frac{w_t L^4}{E_c v_{max}} \quad (8.6)$$

### 8.3.2 Based on strength requirements

An estimate of the section size for a partially prestressed member can be obtained from the flexural strength requirements of the critical section. The ultimate moment of a ductile rectangular section containing both non-prestressed and prestressed tensile steel may be found using Equation 4.21. By taking moments of the internal tensile forces in the steel about the level of the resultant compressive force in the concrete, the ultimate moment may be expressed as

$$M_u = \sigma_{pu} A_p \left( d_p - \frac{\gamma d_n}{2} \right) + f_y A_{st} \left( d_o - \frac{\gamma d_n}{2} \right) \quad (8.7)$$

For preliminary design purposes, this expression can be simplified if the stress in the prestressing steel at ultimate  $\sigma_{pu}$  is assumed (say  $\sigma_{pu} = 0.9f_p$ ) and the internal lever arm between the resultant tension and compression

forces is estimated (say  $0.85d$ , where  $d$  is the effective depth to the resultant tensile force at the ultimate limit state). Equation 8.7 becomes

$$M_u = 0.85d(0.9f_p A_p + f_y A_{st}) \quad (8.8)$$

Dividing both sides by  $f'_c b d^2$  gives

$$\frac{M_u}{f'_c b d^2} = 0.85 \left[ \left( \frac{0.9f_p}{f'_c} \frac{A_p}{bd} \right) + \left( \frac{f_y}{f'_c} \frac{A_{st}}{bd} \right) \right]$$

and therefore

$$bd^2 = \frac{M_u}{0.85f'_c(q_p + q_s)} \quad (8.9)$$

where

$$q_p = \frac{0.9f_p}{f'_c} \frac{A_p}{bd} \quad \text{and} \quad q_s = \frac{f_y}{f'_c} \frac{A_{st}}{bd}$$

Knowing that the design strength  $\phi M_u$  must exceed the factored design moment  $M^*$ , Equation 8.9 becomes

$$bd^2 \geq \frac{M^*}{0.85\phi f'_c(q_p + q_s)} \quad (8.10)$$

The quantity  $q_p + q_s$  is the combined steel index. A value of  $q_p + q_s$  of about 0.2 will usually provide a ductile section and, with this approximation, Equation 8.10 may be simplified to

$$bd^2 \geq \frac{M^*}{0.17\phi f'_c} \quad (8.11)$$

Equation 8.11 can be used to obtain preliminary dimensions for an initial trial section.  $M^*$  must include an initial estimate of self-weight.

With the cross-sectional dimensions so determined, the initial prestress and the area of prestressing steel can then be selected based on serviceability requirements. Various criteria can be adopted. For example, the prestress required to cause decompression (i.e. zero bottom fibre stress) at the section of maximum moment under full dead load could be selected. Alternatively, load balancing could be used to calculate the prestress required to produce zero deflection under a selected portion of the external load. With the level of prestress determined and the serviceability requirements for the member satisfied, the amount of non-prestressed steel required for strength is calculated.

The size of the web of a beam is frequently determined from shear strength calculations. In arriving at a preliminary cross-section for a thin-webbed member, preliminary checks in accordance with the procedures outlined in [Chapter 5](#) should be carried out to ensure that adequate shear strength can be provided. In addition, the arrangement of the tendon anchorages at the ends of the beam often determines the shape of the section in these regions. Consideration must be given therefore to the anchorage zone requirements (in accordance with the principles discussed in [Chapter 6](#)) even in the initial stages of design.

## 8.4 Design procedures—fully prestressed beams

For the design of a fully prestressed member, stress limits both at transfer and under full loads must be selected to ensure that cracking does not occur at any time. There are relatively few situations that specifically require *no cracking* as a design requirement. Depending on the span and load combinations, however, a fully prestressed design may well prove to be the most economic solution.

For long-span members, where self-weight is a major part of the design load, relatively large prestressing forces are required to produce an economic design and fully prestressed members frequently result. Fully prestressed construction is also desirable if a crack-free or water-tight structure is required or if the structure needs to possess high fatigue strength. In building structures, however, where the spans are generally small to medium, full prestressing may lead to excessive camber and partial prestressing is often a better solution.

When the critical sections have been proportioned so that the stress limits are satisfied at all stages of loading, checks must be made on the magnitude of the losses of prestress, the deflection, and the flexural, shear, and torsional strengths. In addition, the anchorage zone must be designed.

### 8.4.1 Beams with varying eccentricity

The following steps will usually lead to the satisfactory design of a statically determinate, fully prestressed beam with a draped tendon profile:

- (1) Determine the loads on the beam both at transfer and under the most severe load combination for the serviceability limit states. Hence determine the moments at the critical section(s) both at transfer and under the full service loads ( $M_o$  and  $M_T$ , respectively) (an initial estimate of self-weight is required here).
- (2) Using Equation 8.1, choose an initial trial cross-section,
- (3) Select the maximum permissible total deflection  $v_{max}$  caused by the

- estimated unbalanced loads (this is a second serviceability requirement in addition to the no cracking requirement that prompted the fully prestressed design) and use Equation 8.5 to check that the gross moment of inertia of the section selected in step 2 is adequate.
- (4) Estimate the time-dependent losses of prestress (see [Section 3.7.5](#)) and, using the procedure outlined in [Section 3.3.1](#), determine the prestressing force and eccentricity at the critical section(s). With due consideration of the anchorage zone and other construction requirements, select the size and number of prestressing tendons.
  - (5) Establish suitable cable profile(s) by assuming the friction losses and obtaining bounds to the cable eccentricity using Equations 3.16–3.19.
  - (6) Calculate both the immediate and time-dependent losses of prestress. Ensure that the calculated losses are less than those assumed in steps 4 and 5. Repeat steps 4 and 5, if necessary.
  - (7) Check the deflection at transfer and the final long-term deflection under maximum and minimum loads. If necessary, consider the inclusion of non-prestressed steel to reduce time-dependent deformations (top steel to reduce downward deflection, bottom steel to reduce time-dependent camber). Adjust the section size or the prestress level (or both), if the calculated deflection is excessive.
  - (8) Check the ultimate strength in bending at each critical section. If necessary, additional non-prestressed tensile reinforcement may be used to increase strength. Add compressive reinforcement to improve ductility, as required.
  - (9) Check the shear strength of the beam (and torsional strength if applicable) in accordance with the provisions outlined in [Chapter 5](#). Design suitable shear reinforcement where required.
  - (10) Design the anchorage zone using the procedures presented in [Chapter 6](#).

*Note:* Durability and fire protection requirements are usually satisfied by an appropriate choice of concrete quality and cover to the tendons in step 4.

#### 8.4.2 Example 8.1—Fully-prestressed design (draped tendon)

A slab and beam floor system consists of post-tensioned, simply supported T-beams spanning 18.5 m and spaced at 4 m centres. A 140 mm thick, continuous, reinforced concrete, one-way slab spans from beam to beam. An elevation and a cross-section of a typical T-beam are shown in [Figure 8.2](#). The beam is to be designed as a fully prestressed member. The floor supports a superimposed permanent dead load of 2 kPa and a variable live load of 3 kPa. Material properties are  $f'_c = 32$  MPa,  $f'_{ci} = 25$  MPa,  $f_p = 1840$  MPa,  $E_c = 28600$  MPa, and  $E_p = 195000$  MPa.

For this fully prestressed design, the following stress limits have been

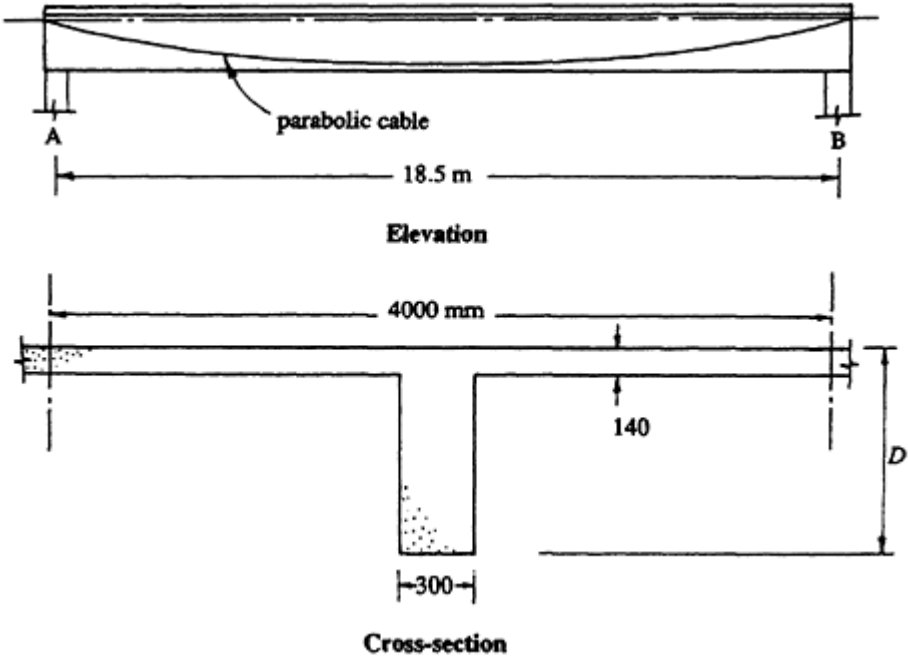


Figure 8.2 Beam details for [Example 8.1](#)

selected:

$$F_{ti} = 1.25 \text{ MPa}; \quad F_{ci} = -12.5 \text{ MPa}; \quad F_t = 1.5 \text{ MPa}; \quad F_c = -16.0 \text{ MPa}.$$

(1) Mid-span moments

Due to self-weight:

To estimate the self-weight of the floor  $w_{sw}$ , an initial trial depth  $D=1100$  mm is assumed (about span/17). If the concrete floor weighs  $24 \text{ kN/m}^3$ ,

$$w_{sw} = 24 [4 \times 0.14 + 0.3(1.1 - 0.14)] = 20.4 \text{ kN/m}$$

Therefore,

$$M_{sw} = \frac{20.4 \times 18.5^2}{8} = 871 \text{ kN m}$$

Due to 2.0 kPa superimposed dead load:

$$w_G = 2 \times 4 = 8 \text{ kN/m} \quad \text{and} \quad M_G = \frac{8 \times 18.5^2}{8} = 342 \text{ kN m}$$

Due to the 3.0 kPa live load:

$$w_Q = 3 \times 4 = 12 \text{ kN/m} \quad \text{and} \quad M_Q = \frac{12 \times 18.5^2}{8} = 513 \text{ kN m}$$

At transfer:

$$M_o = M_{sw} = 871 \text{ kN m}$$

Under full loads:

$$M_T = M_{sw} + M_G + M_Q = 1726 \text{ kN m}$$

## (2) Trial section size

From Equation 8.1:

$$Z_b \geq \frac{[1726 - (0.75 \times 871)] \times 10^6}{1.5 - (0.75 \times -12.5)} = 98.6 \times 10^6 \text{ mm}^3$$

Choose the trial cross-section shown in [Figure 8.3](#).

*Notes:*

- The revised estimate of self-weight is 20.7 kN/m and therefore the revised design moments are  $M_o=886$  kNm and  $M_T=1741$  kNm.
- This section just satisfies the requirement for the effective width of T-beam flanges in AS 3600–1988, namely that the flange width does not exceed the web width plus 0.2 times the span. However, the section fails to satisfy the ACI 318–83 requirement that the overhanging portion of the flange is less than eight times the flange thickness. The latter requirement is unreasonable for both prestressed and reinforced concrete T-sections, particularly for sections where the edge of the effective flange is continuously supported, as is the case here.

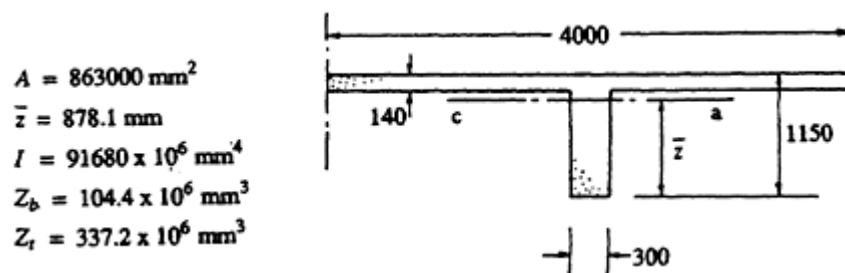


Figure 8.3 Trial cross-section for [Example 8.1](#).

### (3) Check deflection requirements

For this particular floor, the maximum deflection,  $v_{max}$  is taken to be span/500=37 mm. If it is assumed that only the self-weight of the floor is balanced by prestress, the unbalanced load is

$$w_u = w_G + w_Q = 20 \text{ kN/m}$$

and therefore

$$w_{us} = w_G = 8 \text{ kN/m}$$

With the long-term deflection multiplier  $\lambda$  taken as 3, Equation 8.4 gives

$$w_t = 20 + (3 \times 8) = 44 \text{ kN/m}$$

and from Equation 8.5:

$$I \geq \frac{5}{384} \times \frac{44 \times 18\,500^4}{28\,600 \times 37} = 63\,400 \times 10^6 \text{ mm}^4$$

The trial cross-section satisfies this requirement and deflection does not appear to be a critical consideration in this T-beam.

### (4) Determine the prestressing force and eccentricity at mid-span

The procedure outlined in [Section 3.3.1](#) is used for the satisfaction of the selected stress limits. The section properties  $\alpha_t$  and  $\alpha_b$  are given by

$$\alpha_t = \frac{A}{Z_t} = 0.00256 \quad \text{and} \quad \alpha_b = \frac{A}{Z_b} = 0.00827$$

and Equations 3.5 and 3.6 provide upper limits on the magnitude of prestress at transfer:

$$\frac{1}{P_i} \geq \frac{0.00256e - 1}{(863 \times 10^3 \times 1.25) + (0.00256 \times 886 \times 10^6)} = \frac{0.00256e - 1}{3.35 \times 10^6} \quad (3.5)$$

$$\frac{1}{P_i} \geq \frac{0.00827e + 1}{(-863 \times 10^3 \times -12.5) + (0.00827 \times 886 \times 10^6)} = \frac{0.00827e + 1}{18.11 \times 10^6} \quad (3.6)$$

Equations 3.7 and 3.8 provide lower limits on the prestress under full service loads. If the time-dependent loss of prestress is assumed to be 20% ( $R=0.80$ ), then

$$\frac{1}{P_i} \leq \frac{0.80(0.00827e + 1)}{(-863 \times 10^3 \times 1.5) + (0.00827 \times 1741 \times 10^6)} = \frac{0.00827e + 1}{16.38 \times 10^6} \quad (3.7)$$



$$\frac{1}{P_i} \leq \frac{0.80(0.00256e - 1)}{(863 \times 10^3 \times -16.0) + (0.00256 \times 1741 \times 10^6)} = \frac{0.00256e - 1}{-11.69 \times 10^6} \tag{3.8}$$

Each of these equations is plotted on the design diagram in [Figure 8.4](#).

Two cables are assumed with duct diameters of 80 mm and with 40 mm minimum cover to the ducts. The position of the ducts at mid-span and the location of the resultant prestressing force are illustrated in [Figure 8.5](#). The maximum eccentricity to the resultant prestressing force is therefore

$$e_{max} = 878 - 155 = 723 \text{ mm}$$

The resultant force in each tendon is assumed to be located at one quarter

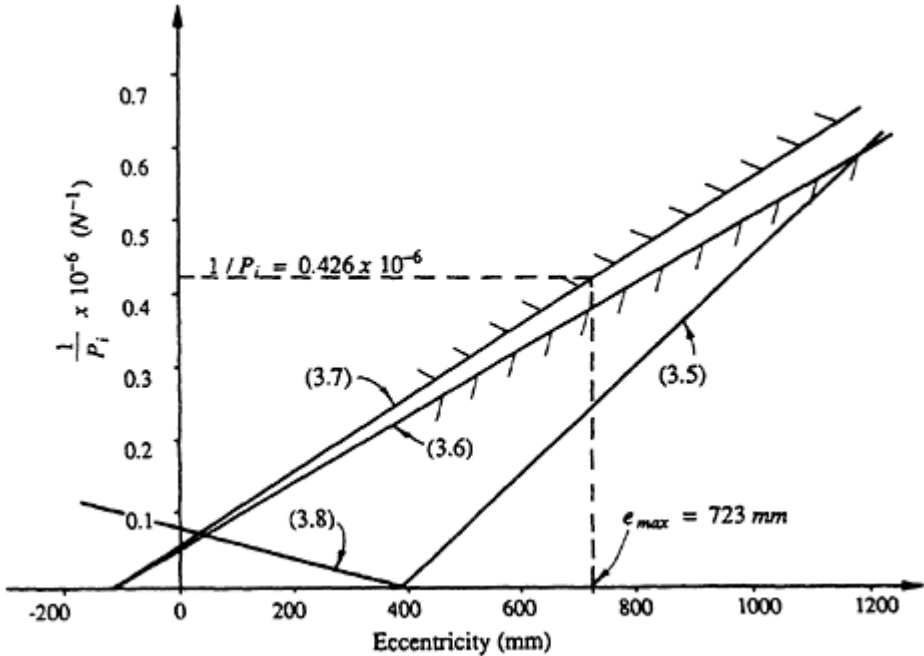


Figure 8.4 Magnel's design diagram for [Example 8.1](#).

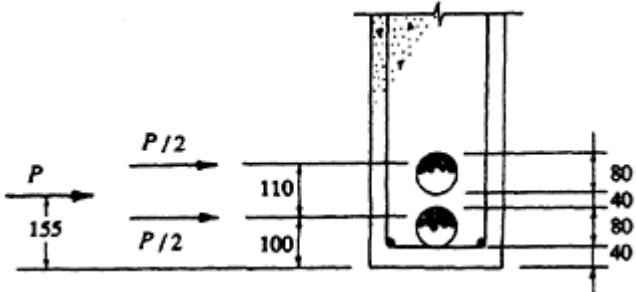


Figure 8.5 Cable locations and relevant dimensions at mid-span.

of the duct diameter below the top of the duct. From [Figure 8.4](#), for  $e=723$  mm the minimum required prestressing force at mid-span is

$$P_i = 2350 \text{ kN}$$

If the immediate losses at mid-span are assumed to be 10%, then the required jacking force is

$$P_j = \frac{P_i}{0.9} = 2610 \text{ kN}$$

From [Table 2.1](#), the cross-sectional area of a 12.7 mm diameter 7-wire super strand is  $A_p=100$  mm<sup>2</sup>, the minimum breaking load is 184 kN, and therefore the maximum jacking force is  $0.85 \times 184 = 156.4$  kN. The minimum number of 7-wire strands is therefore  $2610/156.4 = 16.7$ .

Try two cables each containing 9 strands, i.e.  $A_p=900$  mm<sup>2</sup>/cable.

### (5) Establish cable profiles

Since the member is simply supported and uniformly loaded, and because the friction losses are only small, parabolic cable profiles with a sufficiently small resultant eccentricity at each end and an eccentricity of 723 mm at mid-span will satisfy the stress limits at every section along the beam. In order to determine the zone in which the resultant prestressing force must be located (see [Figure 3.5](#)), it is first necessary to estimate the prestress losses. The cables are to be stressed from one end only. From preliminary calculations the friction losses between the jack and mid-span are assumed to be 6% (i.e. 12% from jack to dead end anchorage), the anchorage losses

**Table 8.1** Bounds on the eccentricity of prestress in [Example 8.1](#).

Distance from jack (mm)	0	4625	9250	13875	18500
Estimated short-term losses (%)	15	12.5	10	10.5	13
$P_i$ (kN)	2220	2280	2350	2335	2270
$P_e$ (kN)	1775	1830	1880	1870	1820
$M_o$ (kN m)	0	664	886	664	0
$M_T$ (kN m)	0	1306	1741	1306	0
$e_{max}$ (mm)	467	743	811	722	454
$e_{min}$ (mm)	-209	507	722	494	-207

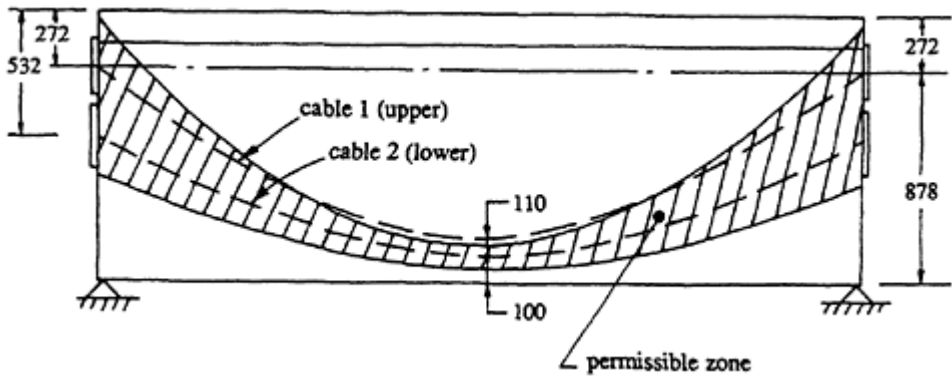


Figure 8.6 Parabolic cable profiles for Example 8.1.

resulting from slip at the anchorages are assumed to be 14% at the jack and 2% at mid-span, and the elastic deformation losses are taken to be 1% at each end and 2% at mid-span. These assumptions will be checked subsequently. If the time-dependent losses are assumed to be 20%, the prestressing forces  $P_i$  and  $P_e$  at the ends, quarter-span and mid-span are as shown in Table 8.1. Also tabulated are the moments at each section at transfer and under full loads, the maximum eccentricity (determined in this case from Equation 3.17), and the minimum eccentricity (determined from Equation 3.18 in this example).

The permissible zone, in which the resultant force in the prestressing steel must be located, is shown in Figure 8.6. The individual cable profiles are also shown. The cables are separated sufficiently at the ends of the beam to accommodate easily the anchorages for the two cables.

**(6) Check losses of prestress**

**Immediate losses**

*Elastic deformation* At mid-span, the initial prestress in each cable is  $P_i=2350/2=1175$  kN/cable. The upper cable is the first to be stressed and therefore suffers elastic deformation losses when the second (lower) cable is subsequently stressed. The prestressing force in the lower cable causes a concrete stress at the level of the upper tendon of

$$\sigma_{cp} = - \frac{1175 \times 10^3}{863 \times 10^3} - \frac{1175 \times 10^3 \times 778 \times 668}{91\,680 \times 10^6} = - 8.02 \text{ MPa}$$

and the loss of steel stress in the upper cable is obtained from Equation 3.58:

$$\Delta\sigma_p = \frac{195\,000}{28\,600} \times - 8.02 = - 55 \text{ MPa}$$

The loss of force in the upper cable, that occurs as the lower cable is stressed, is therefore  $\Delta\sigma_p A_p = 55 \times 900 = 49$  kN (about 1.9% of the total jacking force). The loss of force in the lower cable due to elastic shortening is zero.

*Friction losses* The change in slope of the tendon between the support and midspan is obtained using Equation 1.6. For the upper cable, the drape is 668 mm and therefore

$$\alpha_{tot} = \frac{4 \times 668}{18\,500} = 0.144$$

With  $\mu = 0.2$  and  $\beta_p = 0.013$ , the friction loss at mid-span is calculated using Equation 3.60:

$$P_a = P_j e^{-0.2(0.144 + 0.013 \times 9.25)} = 0.948 P_j$$

Therefore, the friction loss at mid-span in the upper cable is 5.2%. In the lower cable, where the drape is only 518 mm, the friction loss at mid-span is 4.6%. The average loss of the prestressing force at mid-span due to friction is therefore  $0.049 \times 2610 = 128$  kN. This loss is slightly less than that assumed in step 5.

*Anchorage losses* The loss of prestress caused by a 6 mm slip at the wedges at the jacking end is calculated in accordance with the discussion in [Section 3.7.4](#). With the average friction loss at midspan of 4.9%, the slope of the prestressing line is

$$\frac{\alpha}{2} = \frac{0.049 P_j}{L/2} = \frac{0.049 \times 2610 \times 10^3}{9250} = 13.8 \text{ N/mm}$$

The length of beam  $L_{di}$  over which the anchorage slip affects the prestress is found using Equation 3.61:

$$L_{di} = \sqrt{\frac{195\,000 \times 1800 \times 6}{13.8}} = 12\,340 \text{ mm}$$

The loss of force at the jack due to slip at the anchorage is

$$\delta P = \alpha L_{di} = 2 \times 13.8 \times 12\,340 \times 10^{-3} = 341 \text{ kN} \quad (\approx 13\%)$$

and at mid-span

$$\delta P = \alpha (L_{di} - L/2) = 2 \times 13.8 \times (12\,340 - 9250) \times 10^{-3} = 85 \text{ kN} \quad (\approx 3.3\%)$$

*Jacking force* From step 4, the required prestress at mid-span immediately after transfer is  $P_f=2350$  kN. Adding the elastic shortening, friction, and anchorage losses, the force required at the jack is

$$P_j = 2350 + 49 + 128 + 85 = 2612 \text{ kN} = 1306 \text{ kN/cable}$$

which is very close to the value assumed in steps 4 and 5. The tendon stress at the jack is

$$\sigma_{pj} = \frac{1306 \times 10^3}{900} = 1451 \text{ MPa} = 0.79f_p$$

which is less than  $0.85f_p$  and is therefore acceptable.

**Time-dependent losses** An accurate time analysis of the cross-section at mid-span can be carried out using the procedure outlined in [Section 3.6.2](#) (and illustrated in [Example 3.5](#)). In this example, the more approximate procedures discussed in [Section 3.7.5](#) are used to check time-dependent losses.

*Shrinkage losses* The hypothetical thickness of the web of this beam is defined in [Section 2.5.3](#) and is taken as

$$t_h = \frac{2 \times 300 \times 1150}{2 \times (300 + 1150)} = 238 \text{ mm}$$

(It would be conservative in this case to include the slender flange in the determination of the hypothetical thickness.) Using the predictive model in AS 3600–1988 and assuming an air-conditioned (arid) environment, the shrinkage coefficient  $k_1=0.80$  is obtained from [Figure 2.11](#) and the final shrinkage strain may be estimated using Equation 2.21:

$$\varepsilon_{sh}^* = 0.0007 \times 0.80 = 0.00056$$

As mentioned in [Section 2.5.1](#), shrinkage strain is difficult to predict accurately and a high coefficient of variation must be expected. It is pointless to strive for undue accuracy here. From Equation 3.62, the loss of steel stress due to shrinkage may be taken as

$$\Delta\sigma_p = 0.00056 \times 195\,000 = 109 \text{ MPa}$$

*Creep losses* The final creep coefficient is determined from Equation 2.20, taking  $\phi_{cc.b} = 3.4$ ,  $k_2=0.8$ , and  $k_3=1.2$

$$\phi^* = 0.80 \times 1.2 \times 3.4 = 3.3$$

The concrete stress at the centroid of the prestressing steel at mid-span ( $e=723$  mm) immediately after the application of the full sustained load is

$$\sigma_c = -\frac{P_i}{A} - \frac{P_i e^2}{I} + \frac{M_{sus} e}{I} = -6.44 \text{ MPa}$$

From Equations 3.63 and 3.64, a conservative estimate of the loss of steel stress at midspan due to creep is

$$\Delta\sigma_p = \frac{6.44}{28\,600} \times 3.3 \times 195\,000 = 145 \text{ MPa}$$

*Relaxation losses* For low relaxation strand,  $R_{1000}=0.025$  (see [Table 2.2](#)). From Equation 2.22, the final relaxation (at  $t=10000$  days) is

$$R = 1.1 \times 1.0 \times 0.025 \times 1.4 = 0.0385$$

The stress in the tendons at mid-span immediately after transfer is  $\sigma_{pi}=P_i/A_p=1306$  MPa= $0.71f_p$ . The loss of steel stress due to relaxation may be approximated using Equation 3.65:

$$(\Delta\sigma_p)_{relax} = \sigma_{pi} R \left( 1 - \frac{2\Delta\sigma_p}{\sigma_{pi}} \right) = 1306 \times 0.0385 \left[ 1 - \frac{2(109 + 145)}{1306} \right] = 31 \text{ MPa}$$

*Total time-dependent losses* The total loss of steel stress with time at mid-span is  $\Delta\sigma_p=109+145+31=285$  MPa (which is 21.8% of the prestress immediately after transfer). This is slightly higher than the time-dependent losses assumed in steps 3, 4 and 5 (20%). However, the above procedures are conservative and the original estimate of  $P_i$  is considered satisfactory. (A more accurate time analysis, in accordance with the procedure outlined in [Section 3.6.2](#), reveals that the total time-dependent loss at midspan is only 15.9%.)

### (7) Deflection check

**At transfer** The average drupe for the two cables is 593 mm and the transverse force exerted on the beam by the draped tendons at transfer may be taken as

$$w_{bi} = \frac{P_i e \times 8}{L^2} = \frac{2350 \times 0.593 \times 8}{18.5^2} = 32.6 \text{ kN/m} \uparrow$$

This overestimates the upward load on the member by a small amount, since the prestressing force at mid-span is taken as an average for the span.

The self-weight of the floor was calculated in step 2 and is  $w_{sw}=20.7$  kN/m↓. Immediately after transfer,  $f_{cp} = 25$  MPa and, from Equation 2.7,  $E_c=25\ 300$  MPa. The mid-span deflection at transfer is

$$v_i = \frac{5}{384} \frac{(32.6 - 20.7) \times 18\ 500^4}{25\ 300 \times 91\ 680 \times 10^6} = 7.8 \text{ mm } \uparrow = \frac{\text{span}}{2360}$$

which is clearly satisfactory.

**Under full loads** The effective prestress at mid-span after all losses is here assumed to be  $P_e=0.841 P_i=1976$  kN (15.9% losses). The transverse load exerted on the beam by the tendons is therefore

$$w_b = \frac{P_e e \times 8}{L^2} = \frac{1976 \times 0.593 \times 8}{18.5^2} = 27.4 \text{ kN/m } \uparrow$$

The sustained gravity loads are  $w_{sw}+w_G=28.7$  kN/m and the short-term deflection at mid-span caused by all the sustained loads is

$$v_{sus} = \frac{5}{384} \frac{(28.7 - 27.4) \times 18\ 500^4}{28\ 600 \times 91\ 680 \times 10^6} = 0.8 \text{ mm } \downarrow$$

Under the sustained loads, the initial curvature is small on all sections and the short-term and long-term deflections are also small. The creep induced deflection may be approximated using Equation 3.76. Because the member is uncracked and contains only small quantities of bonded reinforcement, the factor  $\alpha$  in Equation 3.76 is taken as 1.1:

$$v_{cr} = \frac{\phi^*}{\alpha} v_{sus} = \frac{3.3}{1.1} \times 0.8 = 2.4 \text{ mm } \downarrow$$

From Equation 3.78, an estimate of the average shrinkage induced curvature is

$$\kappa_{sh}^* = \frac{0.5 \epsilon_{sh}^*}{D} = \frac{0.5 \times 0.00056}{1150} = 0.243 \times 10^{-6} \text{ mm}^{-1}$$

This positive load-independent curvature causes a downward deflection that may be calculated using Equation 3.77:

$$v_{sh} = 0.125 \times 0.243 \times 10^{-6} \times 18\ 500^2 = 10.4 \text{ mm } \downarrow$$

The final deflection due to the sustained load and shrinkage is therefore

$$v = v_{sus} + v_{cr} + v_{sh} = 13.6 \text{ mm } \downarrow$$

The deflection that occurs on application of the variable live load ( $w_Q=12$  kN/m) is

$$u_{var} = \frac{5}{384} \frac{12 \times 18\,500^4}{28\,600 \times 91\,680 \times 10^6} = 7.0 \text{ mm} \downarrow$$

It is evident that the beam performs satisfactorily at service loads with a maximum deflection of  $13.6+7.0=20.6$  mm=span/900. This conclusion was foreshadowed in the preliminary deflection check in step 3.

### (8) Check ultimate strength in bending at mid-span

Strength checks in this example are undertaken using the load factors and capacity reduction factors specified in AS 3600–1988 (see Sections [1.7.3](#) and [1.7.6](#)). The design load is

$$w^* = 1.25(w_{sw} + w_G) + 1.5w_Q = 53.9 \text{ kN/m}$$

and the design moment at mid-span is

$$M^* = \frac{53.9 \times 18.5^2}{8} = 2310 \text{ kN m}$$

The cross-section at mid-span contains a total area of prestressing steel  $A_p=1800$  mm<sup>2</sup> at an effective depth  $d_p=995$  mm. The ultimate moment is calculated using the approximate procedure outlined in [Section 4.4.1](#). With  $f'_c = 32$  MPa, Equation 4.2 gives  $\gamma=0.822$ . From Equation 4.19,  $k_1=0.28$  and

$$k_2 = \frac{1800 \times 1840}{4000 \times 995 \times 32} = 0.026$$

The steel stress at ultimate is given by Equation 4.18:

$$\sigma_{pu} = 1840 \left( 1 - \frac{0.28 \times 0.026}{0.822} \right) = 1824 \text{ MPa}$$

The resultant tensile force is  $T=\sigma_{pu}A_p=3280$  kN and, assuming the neutral axis lies within the slab flange, the depth to the neutral axis is given by Equation 4.20:

$$d_n = \frac{3280 \times 10^3}{0.85 \times 32 \times 4000 \times 0.822} = 36.7 \text{ mm}$$

which is in fact within the flange. For this section, the quantity of tensile steel is only small and the member will be very ductile ( $d_n=$



$0.04d_p \ll 0.4d$ ). By taking moments of the internal forces about any point on the cross-section (for example, the level of the resultant compressive force  $\gamma d_n/2$  below the top surface), the ultimate moment is found:

$$M_u = \sigma_{pu} A_p \left( d_p - \frac{\gamma d_n}{2} \right) = 3280 \left( 995 - \frac{0.822 \times 36.7}{2} \right) \times 10^{-3}$$

$$= 3210 \text{ kN m}$$

With the capacity reduction factor for bending  $\phi = 0.8$ , the design strength is

$$\phi M_u = 2570 \text{ kN m} > M^*$$

and, therefore, the cross-section at mid-span has adequate flexural strength and no non-prestressed longitudinal steel is required. At least two non-prestressed longitudinal reinforcement bars will be located in the top and bottom of the web of the beam in the corners of the transverse stirrups that are required for shear.

### (9) Check shear strength

As in step 8,  $w^* = 53.9 \text{ kNm}$ . Shear strength is here checked at the section 1 m from the support, where  $V^* = 445 \text{ kN}$  and  $M^* = 472 \text{ kN m}$ . At this section, the average depth of the prestressing steel below the centroidal axis of the cross-section is  $y = e = 251 \text{ mm}$  and its slope is  $y' = 0.114 \text{ rad}$ . The effective prestress is  $P_e = 1790 \text{ kN}$  and the vertical component of prestress is  $P_v = P_e y' = 204 \text{ kN}$ .

Flexure-shear cracking:

The decompression moment at this section is

$$M_o = Z_b \left( \frac{P_e}{A} + \frac{P_e e}{Z_b} \right) = 666 \text{ kN m}$$

and the corresponding shear force is found using Equation 5.9:

$$V_o = 666 \times \frac{445}{472} = 628 \text{ kN}$$

If two 20 mm diameter reinforcing bars are located in each bottom corner of the stirrups ( $A_{st} = 620 \text{ mm}^2$ ), then from Equation 5.8

$$V_{uc} = 1.1 \times 1.0 \times 260 \times 1100 \left[ \frac{(620 \times 1800)}{260 \times 1100} \times 32 \right]^{1/3} \times 10^{-3} + 628 + 204$$

$$= 1036 \text{ kN}$$

in which the effective width for shear (defined after Equation 5.5) is taken as  $b_v = 300 - (0.5 \times 80) = 260$  mm and the depth to the centroid of  $A_{st}$  is  $d_o = 1100$  mm.

Web-shear cracking:

At the centroidal axis,  $Q = 0.5 \times 300 \times 878.1^2 = 116 \times 10^6$  mm<sup>3</sup>,  $\sigma = -P_e/A = -2.07$  MPa and  $\tau = V_t Q / (I b) = 4.21 \times 10^{-6} V_t$ . With  $\sigma_1 = 0.33 \sqrt{f'_c} = 1.87$  MPa, solving Equation 5.11 gives  $V_t = 645$  kN and, therefore, from Equation 5.10,  $V_{uc} = 645 + 204 = 849$  kN.

At this section, the concrete contribution to the design strength of the section in shear is governed by web-shear cracking and is equal to

$$\phi V_{uc} = 0.7 \times 849 = 594 \text{ kN}$$

This is greater than the design shear force  $V^*$  and minimum shear reinforcement only is required. Checks at other sections along the span indicate that the minimum reinforcement requirements are sufficient throughout the length of the member. If 10 mm closed stirrups are used (two vertical legs with  $A_{sv} = 157$  mm<sup>2</sup> and  $f_{vy} = 250$  MPa), then the required spacing of stirrups is found using Equation 5.5:

$$s \leq \frac{157 \times 250}{0.35 \times 260} = 431 \text{ mm}$$

Use 10 mm closed stirrups at 430 mm maximum centres throughout.

#### (10) Design anchorage zone

The bearing plates at the end of each cable are 220 mm square as shown in Figure 8.7. The centroid of each plate lies on the vertical axis of symmetry, the upper plate being located on the centroidal axis of the cross-section and the lower plate centred 260 mm below the centroidal axis, as shown.

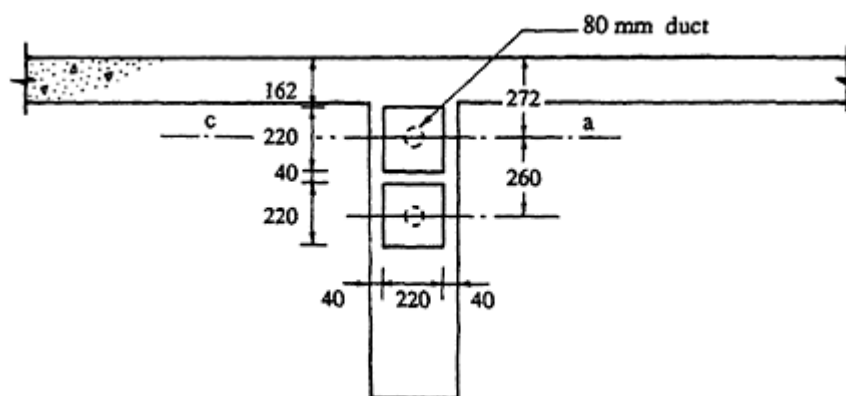


Figure 8.7 End elevation showing size and location of bearing plates.

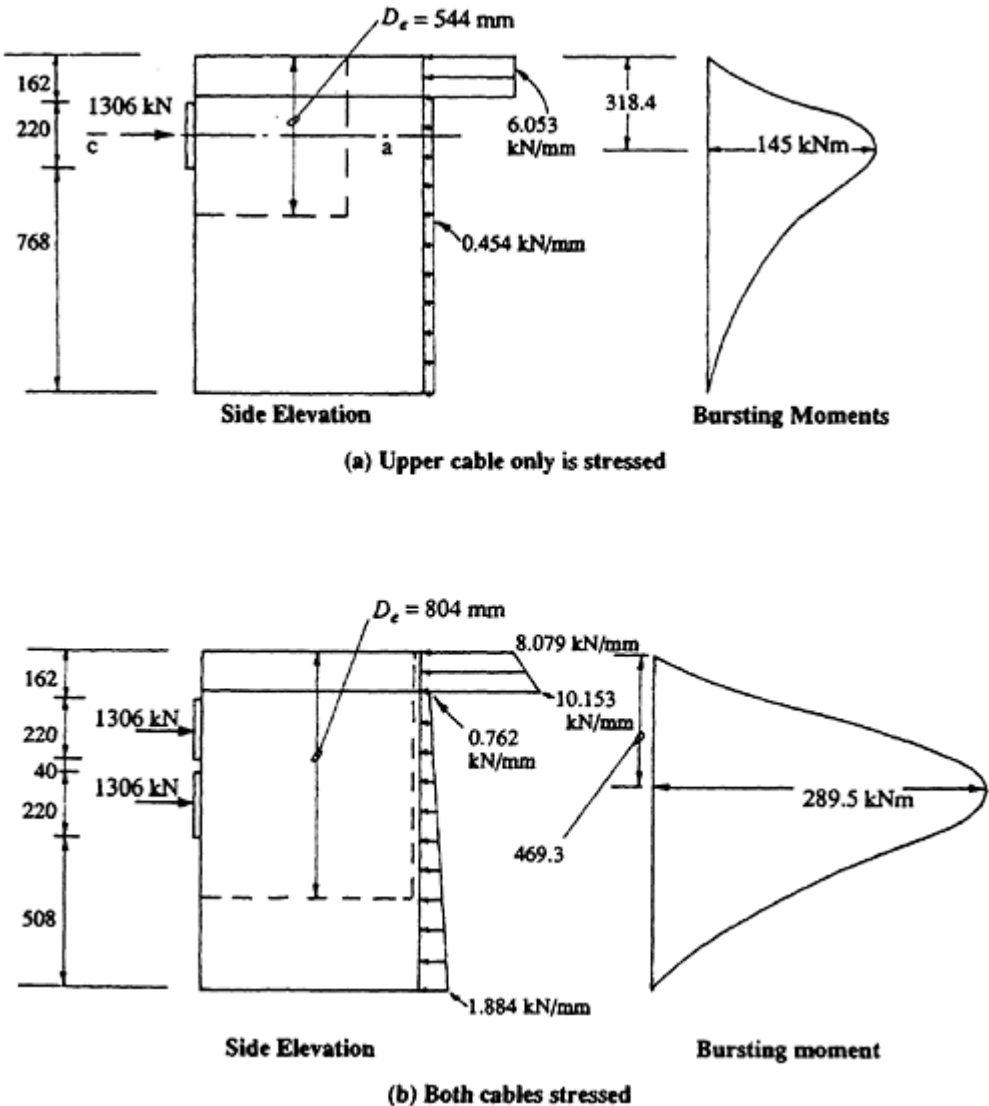


Figure 8.8 Forces and moments in anchorage zone.

The distribution of forces on the anchorage zone after the upper cable is stressed is shown in Figure 8.8a, together with the bursting moments induced within the anchorage zone. The depth of the symmetrical prism behind the upper anchorage plate is 544 mm as shown. The transverse tension within the symmetrical prism caused by the bursting moment behind the anchorage plate ( $M_b=145$  kNm) is

$$T_b = \frac{M_b}{D_e/2} = \frac{145}{0.544/2} = 533 \text{ kN}$$

and the area of transverse steel required within a length of beam equal to

$0.8D_e=435$  mm is

$$A_{sb} = \frac{533 \times 10^3}{150} = 3550 \text{ mm}^2.$$

Using 4–16mm diameter vertical stirrup legs at each stirrup location ( $800 \text{ mm}^2$ ), the required spacing is  $(435 \times 800)/3550=98$  mm.

The distribution of forces on the anchorage zone when both cables are stressed is shown in [Figure 8.8b](#). The maximum bursting moment is 289 kN m and the depth of the symmetrical prism behind the combined anchorage plates is 804 mm. The vertical tension and the required area of transverse steel (needed within a length of beam equal to  $0.8D_e=643$  mm) are

$$T_b = \frac{289.5}{0.804/2} = 720 \text{ kN} \quad \text{and} \quad A_{sb} = \frac{720 \times 10^3}{150} = 4800 \text{ mm}^2$$

The maximum spacing of the vertical stirrups ( $800 \text{ mm}^2/\text{stirrup location}$ ) is  $(643 \times 800)/4800=107$  mm. Use two 16 mm diameter stirrups every 100 mm from the end face of the beam to 800 mm therefrom.

The horizontal dispersion of prestress into the slab flange creates transverse tension in the slab, as indicated in the plan in [Figure 8.9](#). From the truss analogy shown, the transverse tension is 319 kN and the required area of steel is  $A_s=(319 \times 10^3)/150=2130 \text{ mm}^2$ . This steel must be placed horizontally in the slab within a length of  $0.8 \times 4000=3200$  mm. Use

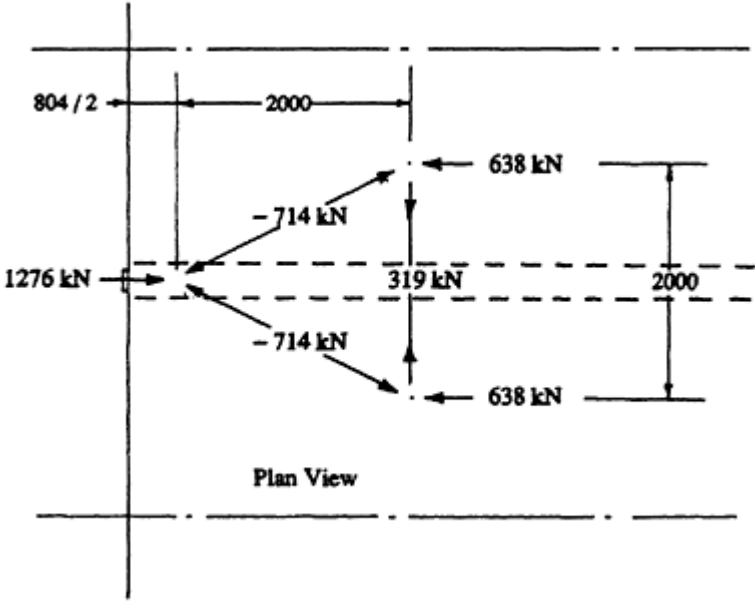


**Figure 8.9** Idealized horizontal truss within slab flange.

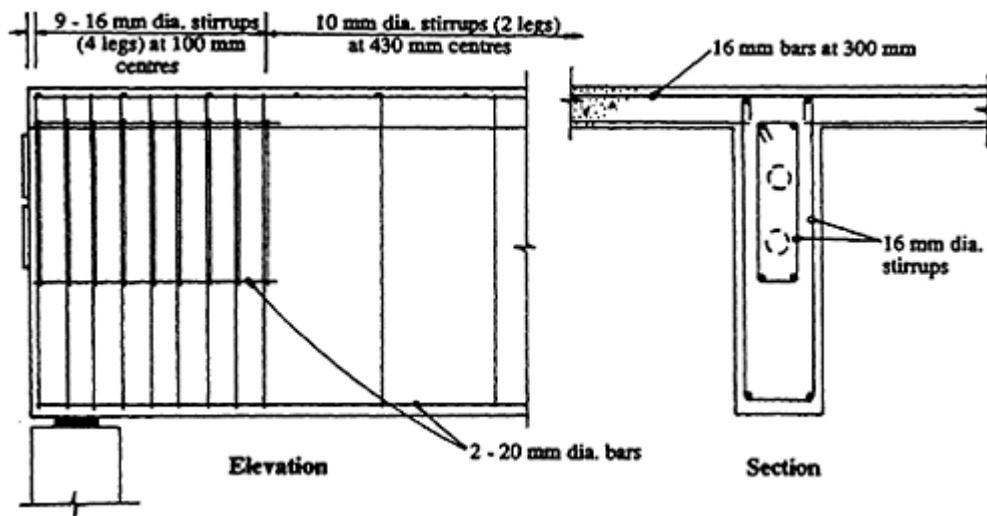


Figure 8.10 Reinforcement details in anchorage zone.

16 mm diameter bars at  $(3200 \times 200 / 2130) = 300$  mm centres within 4 m of the free edge of the slab.

The reinforcement details within the anchorage zone are shown in the elevation and cross-section in [Figure 8.10](#).

#### 8.4.3 Beams with constant eccentricity

The graphical procedure described in [Section 3.3.1](#) is a convenient technique for the satisfaction of concrete stress limits at any section at any stage of loading. However, the satisfaction of stress limits at one section does not guarantee satisfaction at other sections. If  $P_i$  and  $e$  are determined at the section of maximum moment  $M_o$ , and if  $e$  is constant over the full length of the beam, the stress limits  $F_{ci}$  and  $F_{ti}$  may be exceeded in regions where the moment is less than the maximum value.

In pretensioned construction, where it is most convenient to use straight tendons at a constant eccentricity throughout the length of the member, the maximum constant eccentricity is usually determined from conditions at the support of a simply supported member where the moment is zero. In a simple pretensioned beam of constant cross-section, the stress distributions at the support and at the section of maximum moment ( $M_o$  at transfer and  $M_T$  under the maximum in-service loads) are shown in [Figure 8.11](#).

At transfer, the maximum concrete tensile and compressive stresses both occur at the support. The tensile top fibre stress must be less than the tensile stress limit  $F_{ti}$  and the compressive bottom fibre stress must be numerically less than the compressive stress limit  $F_{ci}$ :

$$\sigma_{ti} = -\frac{P_i}{A} + \frac{P_i e}{Z_t} \leq F_{ti} \quad (8.12)$$

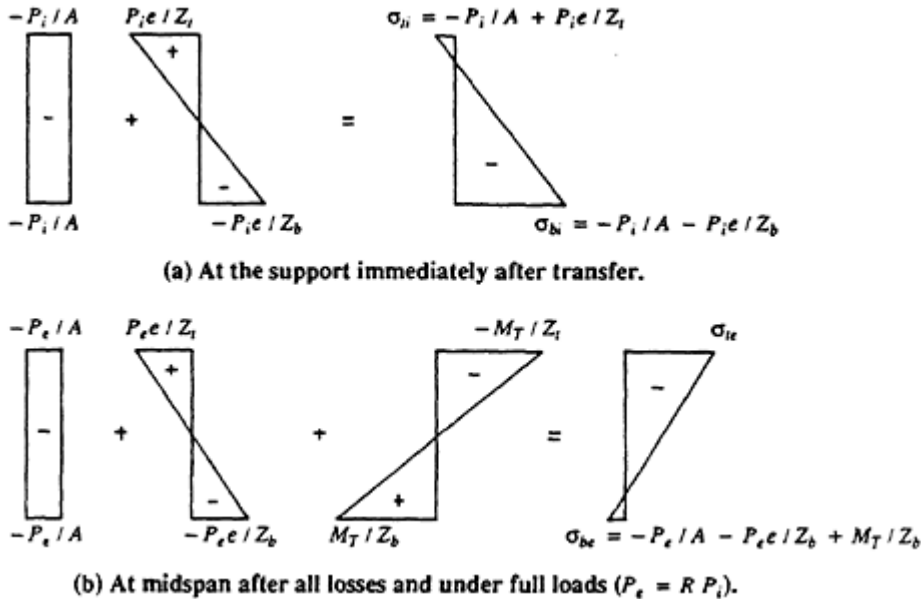


Figure 8.11 Concrete stresses in member with constant eccentricity.

and

$$\sigma_{bi} = -\frac{P_i}{A} - \frac{P_i e}{Z_b} \geq F_{ci} \tag{8.13}$$

By rearranging Equations 8.12 and 8.13 to express  $1/P_i$  as a linear function of  $e$ , the following design equations similar to Equations 3.5 and 3.6 (with  $M_0=0$ ) are obtained:

$$\frac{1}{P_i} \geq \frac{\alpha_t e - 1}{A F_{ti}} \tag{8.14}$$

$$\frac{1}{P_i} \geq \frac{\alpha_b e + 1}{-A F_{ci}} \tag{8.15}$$

where  $\alpha_t=A/Z_t$ ,  $\alpha_b=A/Z_b$ , and the compressive stress limit  $F_{ci}$  is a negative quantity.

After all the time-dependent losses have taken place, the maximum tensile stress occurs in the bottom concrete fibre at mid-span ( $\sigma_{be}$  in Figure 8.11) and must be less than the tensile stress limit  $F_t$ :

$$\sigma_{be} = -\frac{R P_i}{A} - \frac{R P_i e}{Z_b} + \frac{M_T}{Z_b} \leq F_t \tag{8.16}$$

This is identical with Equation 3.3 and may be rearranged to give the design

Equation 3.7:

$$\frac{1}{P_i} \leq \frac{R(\alpha_b e + 1)}{-AF_t + \alpha_b M_T} \quad (3.7)$$

Equations 8.14, 8.15, and 3.7 may be plotted on a graph of  $1/P_i$  versus  $e$  (similar to [Figure 3.3](#)) and a design diagram constructed that ensures satisfaction of the selected stress limits both at the support at transfer and at the critical section of maximum moment under the full service loads. If required, Equation 3.8 may also be plotted on the design diagram, but the compressive stress limit  $F_c$  at the critical section is rarely of concern in a pretensioned member of constant cross-section.

To find the minimum sized section required to satisfy the selected stress limits both at the support and at mid-span at all stages of loading, Equation 8.13 may be substituted into Equation 8.16 to give

$$RF_{ci} + \frac{M_T}{Z_b} \leq F_t$$

and therefore

$$Z_b \geq \frac{M_T}{F_t - RF_{ci}} \quad (8.17)$$

Equation 8.17 can be used to select an initial trial, and then the required prestressing force and the maximum permissible eccentricity can be determined using Equations 8.14, 8.15, and 3.7.

Note the difference between Equation 8.1 (where  $R=0.75$ ) and Equation 8.17. The minimum section modulus obtained from Equation 8.1 is controlled by the *incremental moment* ( $M_T - RM_o$ ) since the satisfaction of stress limits are considered only at the critical section. The stress limits on all other sections are automatically satisfied by suitably varying the eccentricity along the span. If the eccentricity varies such that  $P_i e$  is numerically equal to the moment at transfer  $M_o$  at all sections, then only the change in moment  $M_T - RM_o$  places demands on the flexural rigidity of the member.  $RM_o$  is balanced by the eccentricity of prestress. However, for a beam with constant eccentricity,  $e$  is controlled by the stress limits at the support (where  $M_o$  is zero). It is therefore the total moment at the critical section  $M_T$  which controls the minimum section modulus, as indicated in Equation 8.17.

In order to avoid excessive concrete stresses at the supports at transfer, tendons are often *debonded* near the ends of pretensioned members. In this way, a constant eccentricity greater than that given by Equations 8.14 and 8.15 is possible.

For a simply supported member containing straight tendons at a constant eccentricity, the following design steps are appropriate:

- (1) Determine the loads on the beam both at transfer and under the most severe load combination for the serviceability limit states. Hence determine the moments  $M_o$  and  $M_T$  at the critical section (an initial estimate of self-weight is required here).
- (2) Using Equation 8.17, choose an initial trial cross-section.
- (3) Estimate the time-dependent losses and use Equations 8.14, 8.15, and 3.7 to determine the prestressing force and eccentricity at the critical section.
- (4) Calculate both the immediate and time-dependent losses. Ensure that the calculated losses are less than those assumed in step 3. Repeat step 3, if necessary.
- (5) Check the deflection at transfer and the final long-term deflection under maximum and minimum loads. Consider the inclusion of non-prestressed steel to reduce the long-term deformation, if necessary. Adjust section size and/or prestress level, if necessary.
- (6) Check the ultimate flexural strength at the critical sections. Calculate the quantities of non-prestressed reinforcement required for strength and ductility.
- (7) Check shear strength of beam (and torsional strength if applicable) in accordance with the provisions outlined in [Chapter 5](#). Design suitable stirrups where required.
- (8) Design the anchorage zone using the procedures presented in [Chapter 6](#).

#### 8.4.4. Example 8.2—Fully prestressed design (straight tendons)

Simply supported fully prestressed planks, with a typical cross-section shown in [Figure 8.12](#), are to be designed to span 6.5 m. The planks are to be placed side by side to form a precast floor and are to be pretensioned with straight tendons at a constant eccentricity. The planks are assumed to be long enough for the full prestress to develop at each support (although this is frequently not the case in practice). The floor is to be subjected to a superimposed dead load of 1.2 kPa and a live load of 3.0 kPa (of which

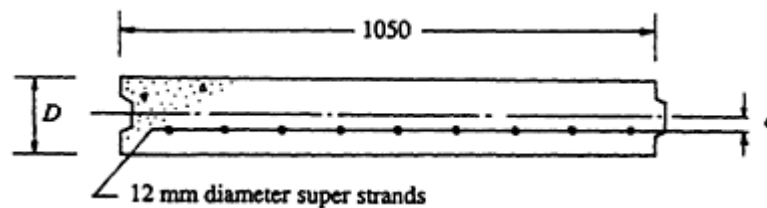


**Figure 8.12** Cross-section of typical pretensioned plank ([Example 8.2](#)).



0.7 kPa may be considered to be permanent and the remainder transitory). As in [Example 8.1](#), material properties are  $f'_c = 32$  MPa,  $f'_{ci} = 25$  MPa,  $f'_p = 1840$  MPa,  $E_c = 28600$  MPa, and  $E_p = 195000$  MPa and the selected stress limits are  $F_{ti} = 1.25$  MPa,  $F_{ci} = -12.5$  MPa,  $F_t = 1.5$  MPa, and  $F_c = -16.0$  MPa.

### (1) Mid-span moments

Due to self-weight:

If the initial depth of the plank is assumed to be  $D \approx \text{span}/40 \approx 160$  mm, and the plank is assumed to weigh  $24 \text{ kN/m}^3$ , then  $w_{sw} = 24 \times 0.16 \times 1.05 = 4.03 \text{ kN/m}$  and at mid-span

$$M_{sw} = \frac{4.03 \times 6.5^2}{8} = 21.3 \text{ kN m}$$

Due to the superimposed dead and live loads:

$w_G = 1.2 \times 1.05 = 1.26 \text{ kN/m}$  and  $w_Q = 3.0 \times 1.05 = 3.15 \text{ kN/m}$ . Therefore,

$$M_G = \frac{1.26 \times 6.5^2}{8} = 6.7 \text{ kN m} \quad \text{and} \quad M_Q = \frac{3.15 \times 6.5^2}{8} = 16.6 \text{ kN m}$$

At transfer,  $M_o = M_{sw} = 21.3 \text{ kNm}$  and under the full loads  $M_T = 21.3 + 6.7 + 16.6 = 44.6 \text{ kNm}$ .

### (2) Trial section size

From Equation 8.17,

$$Z_b \geq \frac{44.6 \times 10^6}{1.5 - (0.75 \times -12.5)} = 4.10 \times 10^6 \text{ mm}^3$$

and therefore

$$D \geq \sqrt{\frac{4.10 \times 10^6 \times 6}{1050}} = 153 \text{ mm}$$

Try  $D = 160$  mm as originally assumed.

### (3) Determine the prestressing force and eccentricity

With  $D = 160$  mm, the section properties are  $A = 168 \times 10^3 \text{ mm}^2$ ,  $I = 358.4 \times 10^6 \text{ mm}^4$ ,  $Z_t = Z_b = 4.48 \times 10^6 \text{ mm}^3$ , and  $\alpha_t = \alpha_b = 0.0375$ . Substituting into Equations 8.14 and 8.15 gives

$$\frac{1}{P_i} \geq \frac{0.0375e - 1}{210 \times 10^3} \quad \text{and} \quad \frac{1}{P_i} \geq \frac{0.0375e + 1}{2100 \times 10^3}$$

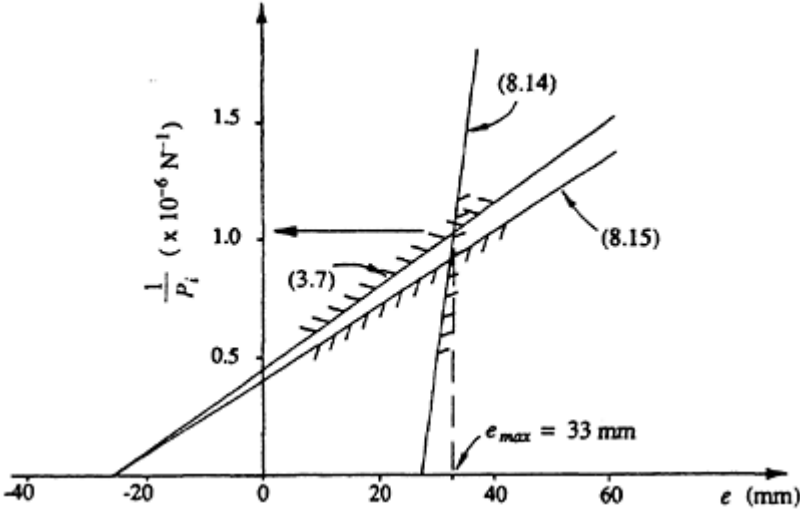


Figure 8.13 Design diagram for Example 8.2.

respectively. If  $R$  is assumed to be 0.75, Equation 3.7 becomes

$$\frac{1}{P_i} \leq \frac{0.0375e + 1}{1894 \times 10^3}$$

The plot of these three straight lines is shown in Figure 8.13.

The maximum eccentricity occurs at the intersection of Equations 8.14 and 3.7 and is  $e=33$  mm. The corresponding minimum prestress  $P_i$  is obtained from Equation 3.7:

$$P_i = \frac{1894 \times 10^3}{(0.0375 \times 33) + 1} = 846.5 \text{ kN}$$

Assuming 5% immediate losses at mid-span, the minimum jacking force is  $P_j = P_i / 0.95 = 891$  kN. The minimum number of 12.7 mm diameter 7-wire super strand (each with breaking load=184 kN) is  $891 / (0.85 \times 184) = 5.7$ .

Use six 12.7 mm diameter strands at  $e=33$  mm  
 i.e.  $A_p = 600 \text{ mm}^2$  at  $d_p = 113$  mm.

**(4) Calculate losses of prestress at mid-span**

**Immediate losses** For this pretensioned member, the immediate losses of prestress are due to elastic shortening. The concrete stress at the steel level

immediately after transfer is

$$\begin{aligned}\sigma_{cp} &= -\frac{846.5 \times 10^3}{168 \times 10^3} - \frac{846.5 \times 10^3 \times 33 \times 33}{358.4 \times 10^6} + \frac{21.3 \times 10^6 \times 33}{358.4 \times 10^6} \\ &= -5.65 \text{ MPa}\end{aligned}$$

and from Equation 3.58,

$$\Delta\sigma_p = \frac{195\,000}{28\,600} \times -5.65 = -38.5 \text{ MPa}$$

The loss of prestress at mid-span due to elastic shortening is  $\Delta\sigma_p A_p = 38.5 \times 600 = 23.1 \text{ kN}$  ( $\approx 2.7\%$  of  $P_i$ ).

### Time-dependent losses

*Shrinkage losses* The hypothetical thickness of the plank is  $t_h = 160 \text{ mm}$  and from [Figure 2.11](#), for an arid environment,  $k_1 = 1.00$  and  $\epsilon_{sh}^* = 0.0007 \times 1.0 = 0.0007$ . From Equation 3.62,  $\Delta\sigma_p = 0.0007 \times 195\,000 = 137 \text{ MPa}$ .

*Creep losses* In Equation 2.20,  $\phi_{cc.b} = 3.4$ ,  $k_2 = 0.9$ , and  $k_3 = 1.3$ , and therefore  $\phi^* = 0.90 \times 1.3 \times 3.4 = 4.0$ . The sustained load is  $w_{sus} = 6.03 \text{ kN/m}$  and the sustained moment at mid-span is therefore  $M_{sus} = 31.8 \text{ kNm}$ . The concrete stress at the centroid of the prestressing steel at mid-span ( $e = 33 \text{ mm}$ ) immediately after the application of the full sustained load is

$$\sigma_c = -\frac{P_i}{A} - \frac{P_i e^2}{I} + \frac{M_{sus} e}{I} = -4.68 \text{ MPa}$$

and from Equations 3.63 and 3.64,

$$\Delta\sigma_p = \frac{4.68}{28\,600} \times 4.0 \times 195\,000 = 128 \text{ MPa}$$

*Relaxation losses* The stress in the steel immediately after transfer is  $\sigma_{pi} = P_i / A_p = 1411 \text{ MPa}$  ( $= 0.77f_p$ ) and from Equation 2.22, for low-relaxation strand, the final relaxation ( $t = 10\,000$  days) is  $R = 1.4 \times 1.0 \times 0.025 \times 1.4 = 0.049$ . Equation 3.65 gives

$$\Delta\sigma_p = 1411 \times 0.049 \left[ 1 - \frac{2(137 + 128)}{1411} \right] = 43 \text{ MPa}$$

*Total time-dependent losses* At mid-span,  $\Delta\sigma_p=137+128+43=308$  MPa, which is less than the assumed value of  $0.25\sigma_{pi}=353$  MPa and is therefore acceptable.

### (5) Deflection check

**At transfer** The curvature immediately after transfer at each support is

$$\chi_{i,s} = \frac{-P_i e}{E_c I} = \frac{-846.5 \times 10^3 \times 33}{28\,600 \times 358.4 \times 10^6} = -2.73 \times 10^{-6} \text{ mm}^{-1}$$

and at mid-span

$$\begin{aligned} \chi_{i,m} &= \frac{M_o - P_i e}{E_c I} = \frac{(21.3 \times 10^6) - (846.5 \times 10^3 \times 33)}{28\,600 \times 358.4 \times 10^6} \\ &= -0.65 \times 10^{-6} \text{ mm}^{-1} \end{aligned}$$

The corresponding deflection at mid-span may be calculated using Equation 3.68c:

$$v_{im} = \frac{6500^2}{96} [-2.73 + (10 \times -0.65) - 2.73] \times 10^{-6} = 5.3 \text{ mm} \uparrow$$

which is satisfactory.

**Under full loads** If the effective prestress after all losses is taken to be  $P_e=0.8P_i=678$  kN, the final *load-dependent* curvature at the supports may be approximated by

$$\chi_{sus,s} = -\frac{P_e e}{E_c I} \left(1 + \frac{\phi^*}{\alpha}\right).$$

With  $\phi^* = 4.0$  and  $\alpha$  taken to be 1.5 for this uncracked section (in accordance with the discussion in [Section 3.8.3](#)), then,

$$\chi_{sus,s} = -\frac{678 \times 10^3 \times 33}{28\,600 \times 358.4 \times 10^6} \left(1 + \frac{4.0}{1.5}\right) = -8.00 \times 10^{-6} \text{ mm}^{-1}$$

The moment at mid-span caused by the sustained loads is  $M_{sus}=M_{sw}+ M_G+(0.7/3.0)M_Q=31.9$  kNm and the final curvature caused by  $M_{sus}$  is

$$\chi_{sus,m} = \frac{M_{sus} - P_e e}{E_c I} \left(1 + \frac{\phi^*}{\alpha}\right) = 3.41 \times 10^{-6} \text{ mm}^{-1}$$

The moment at mid-span due to the variable part of the live load is  $(2.3/3.0)M_Q=12.7$  kNm and the corresponding curvature at mid-span is  $\kappa_{var,m}=1.24\times 10^{-6}$  mm<sup>-1</sup>.

The shrinkage-induced curvature is constant along the span (since the bonded steel is at a constant eccentricity) and may be approximated by Equation 3.78:

$$\kappa_{sh}^* = \frac{0.5 \times 0.0007}{160} = 2.19 \times 10^{-6} \text{ mm}^{-1}$$

The final curvatures at each end and at mid-span are the sum of the load-dependent and shrinkage curvatures:

$$\kappa_s = \kappa_{sus,s} + \kappa_{sh}^* = -5.81 \times 10^{-6} \text{ mm}^{-1}$$

and

$$\kappa_m = \kappa_{sus,m} + \kappa_{var,m} + \kappa_{sh}^* = 6.84 \times 10^{-6} \text{ mm}^{-1}$$

From Equation 3.68c, the final maximum mid-span deflection is

$$v_m = \frac{6500^2}{96} [-5.81 + (10 \times 6.84) - 5.81] \times 10^{-6} = 25.0 \text{ mm} \downarrow \left( = \frac{\text{span}}{260} \right)$$

which is probably satisfactory, provided that the floor does not support brittle partitions or finishes.

### (6) Check ultimate strength in bending at midspan

Using the same procedure as outlined in step 8 of [Example 8.1](#), the design strength in bending of the cross-section containing  $A_p=600$  mm<sup>2</sup> at  $d_p=113$  mm is

$$\phi M_u = 76.1 \text{ kNm} \quad (\text{with } d_n = 42.4 \text{ mm} = 0.37 d_p)$$

which is greater than the design moment  $M^*=59.9$  kN m. Flexural strength and ductility are therefore adequate.

### (7) Check shear strength

For this wide shallow plank, the design shear force  $V^*$  is much less than the design strength  $\phi V_u$  on each cross-section and no transverse steel is required.

## 8.5 Design procedures—partially prestressed beams

### 8.5.1 Discussion

In the design of a partially prestressed member, concrete stresses at transfer must satisfy the selected stress limits, but cracking is permitted under full service loads. It is often convenient to approach the design from an ultimate strength point of view in much the same way as for a conventionally reinforced member. Equations 8.6 and 8.11 can both be used to select an initial section size in which tensile reinforcement (both prestressed and non-prestressed) may be added to provide adequate strength and ductility. The various serviceability requirements can then be used to determine the level of prestress. The designer may choose to limit tension under the sustained load or some portion of it. Alternatively, the designer may select a part of the total load that is balanced by the prestress, under which the deflection is zero. Losses are calculated and the area of prestressing steel is determined.

It should be remembered that the cross-section obtained using Equation 8.11 is a trial section only. Serviceability requirements may indicate that a larger section is needed or that a smaller section would be satisfactory. If the latter is the case, the strength and ductility requirements can usually still be met by the inclusion of either compressive or tensile non-prestressed reinforcement, or both.

After consideration of the serviceability design requirements, and after the magnitude of the prestressing force and the size and location of prestressed steel has been determined, the non-prestressed steel required to provide the necessary additional strength and ductility is calculated. Checks for serviceability are performed and the shear reinforcement and anchorage zones are designed.

The following steps usually lead to a satisfactory design:

- (1) Determine the loads on the beam including an initial estimate of self-weight. Hence determine the in-service moments at the critical section, both at transfer  $M_o$  and under the full loads  $M_T$ . Also calculate the design ultimate moment  $M^*$  at the critical section.
- (2) Using Equation 8.11, determine suitable section dimensions. (Care should be taken when using Equation 8.11 if the neutral axis at ultimate is likely to be outside the flange in a T-beam or I-beam and the approximation of a rectangular compression zone is not acceptable.) For long-span, lightly loaded members, deflection and not strength will usually control the size of the section.
- (3) By selecting a suitable load to be balanced, the unbalanced load can be calculated and Equation 8.6 can be used to check the initial trial section selected in step 2. Adjust section dimensions, if necessary.

- (4) Determine the prestressing force and cable profile to suit the serviceability requirements. For example, no tension may be required under a portion of the service load, such as the dead load. Alternatively, the load at which deflection is zero may be the design criterion.
- (5) Calculate the immediate and time-dependent losses of prestress and ensure that the serviceability requirements adopted in step 4 and the stress limits at transfer are satisfied.
- (6) Calculate the non-prestressed reinforcement (if any) required in addition to the prestressing steel to provide adequate flexural strength.
- (7) Check crack control and deflections both at transfer and under full loads. A cracked section analysis is usually required to determine  $I_e$  and to check the increment of steel stress after cracking.
- (8) Design for shear (and torsion) at the critical sections in accordance with the design provisions in [Chapter 5](#).
- (9) Design the anchorage zone using the procedures outlined in [Chapter 6](#).

### 8.5.2 Example 8.3—Partially prestressed beam (draped tendon)

The fully-prestressed T-beam designed in [Example 8.1](#) is redesigned as a partially prestressed beam. A section and an elevation of the beam are shown in [Figure 8.2](#) and the material properties and floor loadings are as described in [Section 8.4.2](#). At transfer, the stress limits are  $F_{ti}=1.25$  MPa and  $F_{ci}=-12.5$  MPa.

#### (1) Midspan moments

As in Step 1 of [Example 8.1](#),  $w_G=8.0$  kN/m,  $w_Q=12$  kN/m,  $M_G=342$  kNm, and  $M_Q=513$  kN m.

Since the deflection of the fully prestressed beam designed in [Example 8.1](#) is only small, a section of similar size may be acceptable even after cracking. The same section will be assumed here in the estimate of self-weight. Therefore,  $w_{sw}=20.7$  kN/m,  $M_{sw}=886$  kNm, and the moments at mid-span at transfer and under full loads are as calculated previously:

$$M_o = 886 \text{ kNm} \quad \text{and} \quad M_T = 1741 \text{ kNm}$$

The design ultimate moment at mid-span is calculated as in step 8 of [Example 8.1](#), i.e.  $M^*=2310$  kNm.

#### (2) Trial section size based on strength considerations

From Equation 8.11,

$$bd^2 \geq \frac{2310 \times 10^6}{0.17 \times 0.8 \times 32} = 531 \times 10^6$$

For  $b=4000$  mm, the required effective depth is  $d>364$  mm.

Clearly, strength and ductility are easily satisfied (as is evident in step 8 of [Example 8.1](#)). Deflection requirements will control the beam depth.

### (3) Choose trial section based on acceptable deflection

In [Example 8.1](#), the balanced load was  $w_b=27.4$  kN/m (see step 7). For this cracked, partially prestressed member, it is initially assumed that  $w_b=20$  kN/m. Therefore, the maximum unbalanced load is  $w_u=w_{sw}+w_G+w_Q-20=20.7$  kN/m and the sustained unbalanced load is  $w_{us}=w_u-w_Q=8.7$  kN/m. From Equation 8.4,

$$w_t = 20.7 + (2 \times 8.7) = 38.1 \text{ kN/m}$$

If a total deflection limit of span/400=46 mm is assumed, then from Equation 8.6,

$$I \geq 2 \times \frac{5}{384} \times \frac{38.1 \times 18\,500^4}{28\,600 \times 46} = 88\,300 \times 10^6 \text{ mm}^4$$

Choose the same trial section as was used for the fully prestressed design (as shown in [Figure 8.3](#)).

### (4) Determine the prestressing force and cable profile

A single prestressing cable is to be used, with sufficient prestress to balance a load of 20 kN/m. The cable is to have a parabolic profile with zero eccentricity at each support and  $e=778$  mm at mid-span (i.e. the cable is to be located in the same position at mid-span as the lower cable shown in [Figure 8.5](#)). The duct diameter is therefore taken to be 80 mm with 40 mm concrete cover to the duct.

The effective prestress required at mid-span to balance  $w_b=20$  kN/m may be calculated using Equation 1.7:

$$P_e = \frac{w_b L^2}{8e} = \frac{20 \times 18.5^2}{8 \times 0.778} = 1100 \text{ kN}$$

Since the initial stress in the concrete at the steel level is lower than that in [Example 8.1](#), the creep losses will be lower. The time-dependent losses are here assumed to be 15%. Therefore,

$$P_i = \frac{P_e}{0.85} = 1294 \text{ kN}$$

If the immediate losses at mid-span (friction plus anchorage draw-in) are



assumed to be 10%, the required jacking force is

$$P_j = \frac{P_i}{0.9} = 1438 \text{ kN}$$

and the number of 12.7 mm diameter strands  $n$  is

$$n = \frac{1438}{0.85 \times 184} = 9.2$$

Try ten 12.7 mm diameter super grade 7-wire strands ( $A_p=1000 \text{ mm}^2$ ).

### (5) Calculate losses of prestress

**Immediate losses** With only one prestressing cable, elastic deformation losses are zero. Using the same procedures as demonstrated in [Example 8.1](#), the friction loss between the jack and mid-span is 5.6% and the anchorage (draw-in) loss at mid-span is 2.8%. The total immediate loss is therefore 8.4%.

**Time-dependent losses** As in [Example 8.1](#), the loss of prestress due to shrinkage is 109 MPa. Under the action of  $P_i$  and the sustained load, the concrete stress at the steel level is  $\sigma_c=0.4$  MPa (tensile), and therefore tensile creep will cause a small (insignificant) gain in stress in the steel. In this beam, it is conservative to ignore creep in the estimation of losses. With  $\sigma_{pi}=1294$  MPa and with  $R=0.0385$  (from [Example 8.1](#)), the relaxation loss is 41 MPa. The total time-dependent loss is therefore  $\Delta\sigma_p=150 \text{ MPa}=0.116\sigma_{pi}$  (11.6%).

With  $P_e=1100$  kN as calculated in step 5, the revised estimates of  $P_i$  and  $P_j$  are

$$P_i = \frac{1100}{0.884} = 1244 \text{ kN} \quad \text{and} \quad P_j = \frac{1244}{0.916} = 1358 \text{ kN}$$

and the required minimum number of strands is

$$n = \frac{1358}{0.85 \times 184} = 8.7$$

Use nine 12.7 mm diameter super grade 7-wire strands ( $A_p=900 \text{ mm}^2$ ).

By comparison with the beam in Equation 8.1 with almost double the jacking force, the concrete stress limits at transfer are clearly satisfied.

### (6) Design for flexural strength

As given in Step 1, the design moment at mid-span is  $M^* = 2310$  kNm and the minimum required ultimate strength is  $M_u = M^*/\phi = 2890$  kNm ( $\phi = 0.8$  as specified in AS 3600–1988). Using the approximate procedure described in [Section 4.4.1](#), the ultimate strength of the cross-section containing  $A_p = 900$  mm<sup>2</sup> at  $d_p = 1050$  mm is  $M_{u1} = 1710$  kNm (with  $d_n = 23$  mm). Clearly, additional non-prestressed tensile steel is required to ensure adequate strength. If the depth of the non-prestressed tensile reinforcement is  $d_o = 1080$  mm, then the required steel area may be obtained from Equation 4.27:

$$A_{st} = \frac{M_u - M_{u1}}{f_{yt}} \approx \frac{(2890 - 1710) \times 10^6}{400 \times 0.9 (1080 - 0.822 \times 23)} = 3090 \text{ mm}^2$$

Try four 32 mm diameter bottom reinforcing bars in two layers, as shown in [Figure 8.14](#).

Checking the strength of this proposed cross-section gives  $T_p = 1640$  kN,  $T_s = 1280$  kN,  $d_n = 33$  mm, and  $M_u = 3020$  kNm, and therefore  $\phi M_u = 2420$  kNm  $> M^*$ . The proposed section at mid-span has adequate strength and ductility.

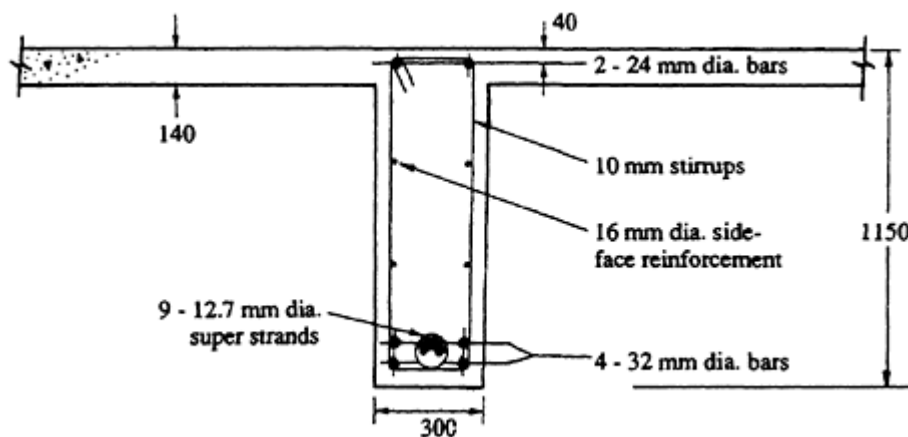


**Figure 8.14** Proposed steel layout at mid-span ([Example 8.3](#)).

### (7) Check for deflection and crack control

The maximum moment at mid-span due to the full service load is  $M_T = 1741$  kNm and the moment at mid-span caused by the sustained load is  $M_{sus} = 1228$  kNm. With  $P_e = 1100$  kN and the tensile strength of concrete taken to be  $0.6\sqrt{f'_c} = 3.4$  MPa, the cracking moment can be approximated by

$$M_c = Z_b \left( \frac{P_e}{A} + \frac{P_e e}{Z_b} + 0.6\sqrt{f'_c} \right) = 1340 \text{ kNm}$$

Cracking occurs at mid-span when the full variable live load is applied. However, the moment caused by the sustained load is less than the cracking moment.

Using the cracked section analysis described in [Section 3.5.2](#), the response of the cracked section at mid-span to the full service moment (1741 kNm) is as follows:

The extreme fibre stress and strain:

$$\sigma_{oi} = 4.81 \text{ MPa and } \epsilon_{oi} = 168 \times 10^{-6}.$$

The depth to the neutral axis:

$$d_n = 198 \text{ mm.}$$

The stress in the non-prestressed steel:

$$\sigma_{st} = 147 \text{ MPa.}$$

The stress in the prestressed steel:

$$\sigma_p = 1422 \text{ MPa.}$$

The average moment of inertia:

$$I_{av} = 37\,700 \times 10^6 \text{ mm}^4$$

The effective moment of inertia (using Equation 3.72 to account for tension stiffening):

$$I_e = 62\,500 \times 10^6 \text{ mm}^4.$$

Since the maximum stress in the non-prestressed steel is less than 200 MPa, flexural crack control should not be a problem. Side-face reinforcement as shown in [Figure 8.14](#) should be included to control flexural cracking in the web of the beam above the bottom steel.

The upward transverse force exerted by the prestress on the member is

$$w_b = \frac{8P_e e}{L^2} = 20.0 \text{ kN/m}$$

and the maximum gravity load is 40.7 kN/m. An estimate of the maximum short-term deflection  $v_i$  caused by the full service load is

$$v_i = \frac{5}{384} \times \frac{(40.7 - 20) \times 18\,500^4}{28\,600 \times 62\,500 \times 10^6} = 17.7 \text{ mm} \downarrow$$

Under the sustained loads, the loss of stiffness due to cracking will not be as great. The cracks will partially close and the depth of the compression zone will increase as the variable live load is removed. For the calculation of the short-term deflection due to the sustained loads (28.7 kN/m), the magnitude of  $I_e$  is higher than that used above. However, using  $I_e = 62\,500 \times 10^6 \text{ mm}^4$  will result in a conservative overestimate of deflection:

$$v_{sus} = \frac{5}{384} \times \frac{(28.7 - 20) \times 18\,500^4}{28\,600 \times 62\,500 \times 10^6} = 7.4 \text{ mm} \downarrow$$

The creep-induced deflection is estimated using Equation 3.76. If two 24 mm diameter bars are included in the compression zone ( $A_{sc}=900 \text{ mm}^2$ ), the coefficient  $\alpha$  is taken to be 3.0 and

$$v_{cr} \approx \frac{\phi^*}{\alpha} v_{sus} = \frac{3.3}{3} \times 7.4 = 8.1 \text{ mm.}$$

From Equation 3.79,

$$\kappa_{sh}^* = \frac{\epsilon_{sh}^*}{D} \left(1 - \frac{A_{sc}}{A_s}\right) = \frac{0.00056}{1150} \left(1 - \frac{900}{4100}\right) = 0.38 \times 10^{-6} \text{ mm}^{-1}$$

and Equation 3.77 gives

$$v_{sh} = 0.125 \times 0.38 \times 10^{-6} \times 18\,500^2 = 16.2 \text{ mm}$$

The maximum final deflection is therefore

$$v_{max} = v_i + v_{cr} + v_{sh} = 42 \text{ mm} = \frac{\text{span}}{440}$$

Deflections of this order may be acceptable for most floor types and occupancies.

The design for shear strength and the design of the anchorage zone for this beam are similar to the procedures illustrated in steps 9 and 10 of [Example 8.1](#).

It should be noted that the same cross-sectional dimensions are required for both the partially prestressed and the fully prestressed solutions in Examples [8.1](#) and [8.3](#). Both satisfy strength and serviceability requirements. In Australia, at present, the partially prestressed beam would be the more economic solution.

## 9

# Statically indeterminate members

### 9.1 Introduction

The previous chapters have been concerned with the behaviour of individual cross-sections and the analysis and design of statically determinate members. In such members, the deformation of individual cross-sections can take place without restraint being introduced at the supports, and internal actions can be determined using only the principles of statics. In this chapter, attention is turned towards the analysis and design of statically indeterminate or continuous members. The internal actions in a continuous member depend on the relative stiffness of the individual regions and, in structural analysis, consideration must be given to geometric compatibility in addition to equilibrium. Imposed deformations cause internal actions in statically indeterminate members and methods for determining the internal actions caused by both imposed loads and imposed deformations must be established.

By comparison with simply-supported members, continuous members enjoy certain structural and aesthetic advantages. Maximum bending moments are significantly smaller and deflections are substantially reduced. The reduced demand on strength and the increase in overall stiffness permit a shallower member cross-section for any given serviceability requirement, and this leads to greater flexibility in sizing members for aesthetic considerations.

In reinforced concrete structures, these advantages are often achieved without an additional cost premium, since continuity is an easily achieved consequence of *in situ* construction. Prestressed concrete, on the other hand, is very often not cast *in situ*, but is precast, and continuity is not a naturally achieved consequence. In precast construction, continuity is obtained with extra expense and care in construction. When prestressed concrete is cast *in situ*, or when continuity can be achieved by stressing

precast units together over several supports, continuity can result in significant cost savings. By using each cable for several spans, a significant reduction in the number of anchorages and in the labour involved in the stressing operation can be achieved.

Continuity provides increased resistance to transient loads and also to progressive collapse resulting from wind, explosion, or earthquake. In continuous structures, failure of one member or cross-section does not necessarily jeopardize the entire structure, and a redistribution of internal actions may occur. When overload of the structure or member in one area occurs, a redistribution of forces may take place, provided that the structure is sufficiently ductile and an alternative load path is available.

In addition to the obvious advantages of continuous construction, there are several notable disadvantages. Some of the disadvantages are common to all continuous structures, and others are specific to the characteristics of prestressed concrete. Among the disadvantages common to all continuous structures are the occurrence of regions of both high shear and high moment adjacent to the internal supports, the high localized moment peaks over the internal supports of continuous beams, and the possibility of high moments and shears resulting from imposed deformations caused by foundation or support settlement, temperature changes, and restrained shrinkage.

In continuous beams of prestressed concrete, the quantity of prestressed reinforcement can often be determined from conditions at mid-span, with additional non-prestressed reinforcement included at each interior support to provide the additional strength required in these regions. The length of beam associated with the high local moment at each interior support is relatively small, so that only short lengths of non-prestressed reinforcement are usually required. In this way, economical partially prestressed concrete continuous structures can be proportioned.

When cables are stressed over several spans in a continuous member, the loss of prestress caused by friction along the duct may be large. The tendon profile usually follows the moment diagram and relatively large angular changes occur as the sign of the moment changes along the member from span to span and the distance from the jacking end of the tendon increases. In the design of long continuous members, the loss of prestress that occurs during the stressing operation must therefore be carefully checked. Attention must also be given to the accommodation of the axial deformation that takes place as the member is stressed. Prestressed concrete members shorten as a result of the longitudinal prestress and this can require special structural details at the supports of continuous members in order to allow for this movement.

There are other disadvantages or potential problems that may arise as a result of continuous construction. Often beams are built into columns or walls in order to obtain continuity, thereby introducing large additional lateral forces and moments in these supporting elements.

Perhaps the most significant difference between the behaviour of statically indeterminate and statically determinate prestressed concrete structures is the restraining actions that develop in continuous structures as a result of imposed deformations. As a statically indeterminate structure is prestressed, reactions are usually introduced at the supports. The supports provide restraint to the deformations caused by prestress (both axial shortening and curvature). The supports also provide restraint to volume changes of the concrete caused by temperature variations and shrinkage. The reactions induced at the supports during the prestressing operation cause so-called *secondary moments and shears* in a continuous member, and these actions may or may not be significant in design. Methods for determining the magnitudes of the secondary effects and their implications in the design for both strength and serviceability are discussed in this chapter.

## 9.2 Tendon profiles

The tendon profile used in a continuous structure is selected primarily to maximize the beneficial effects of prestress and to minimize the disadvantages discussed in [Section 9.1](#). The shape of the profile may be influenced by the techniques adopted for construction. Construction techniques for prestressed concrete structures have changed considerably over the past 40 years with many outstanding and innovative developments. Continuity can be achieved in many ways. Some of the more common construction techniques and the associated tendon profiles are briefly discussed here. The methods presented later in the chapter for the analysis of continuous structures are not dependent, however, on the method of construction.

[Figure 9.1a](#) represents the most basic tendon configuration for continuous members and is used extensively in slabs and relatively short, lightly loaded beams. Because of the straight soffit, simplicity of formwork is the main advantage of this type of construction. The main disadvantage is the high immediate loss of prestress caused by friction between the tendon and the duct. With the tendon profile following the shape of the moment diagram, the tendon undergoes large angular changes over the length of the member. Tensioning from both ends can be used to reduce the maximum friction loss in long continuous members.

[Figure 9.1b](#) indicates an arrangement that has considerable use in longer span structures subjected to heavy applied loads. By haunching the beam as shown, large eccentricities of prestress can be obtained in the regions of high negative moment. This arrangement permits the use of shallower cross-sections in the mid-span region and the reduced cable drape can lead to smaller friction losses.

Techniques for overlapping tendons or providing cap cables are numerous. [Figure 9.1c](#) shows a tendon layout where the regions of high negative



moment are provided with extra prestressing. Continuity of the structure is maintained even though there may be considerable variation of prestress along the member. This general technique can eliminate some of the disadvantages associated with the profiles shown in Figures 9.1a and b where the prestressing force is essentially constant throughout the structure. However, any structural benefits are gained at the expense of extra prestressing and additional anchorages.

Many types of segmental construction are available and a typical case is

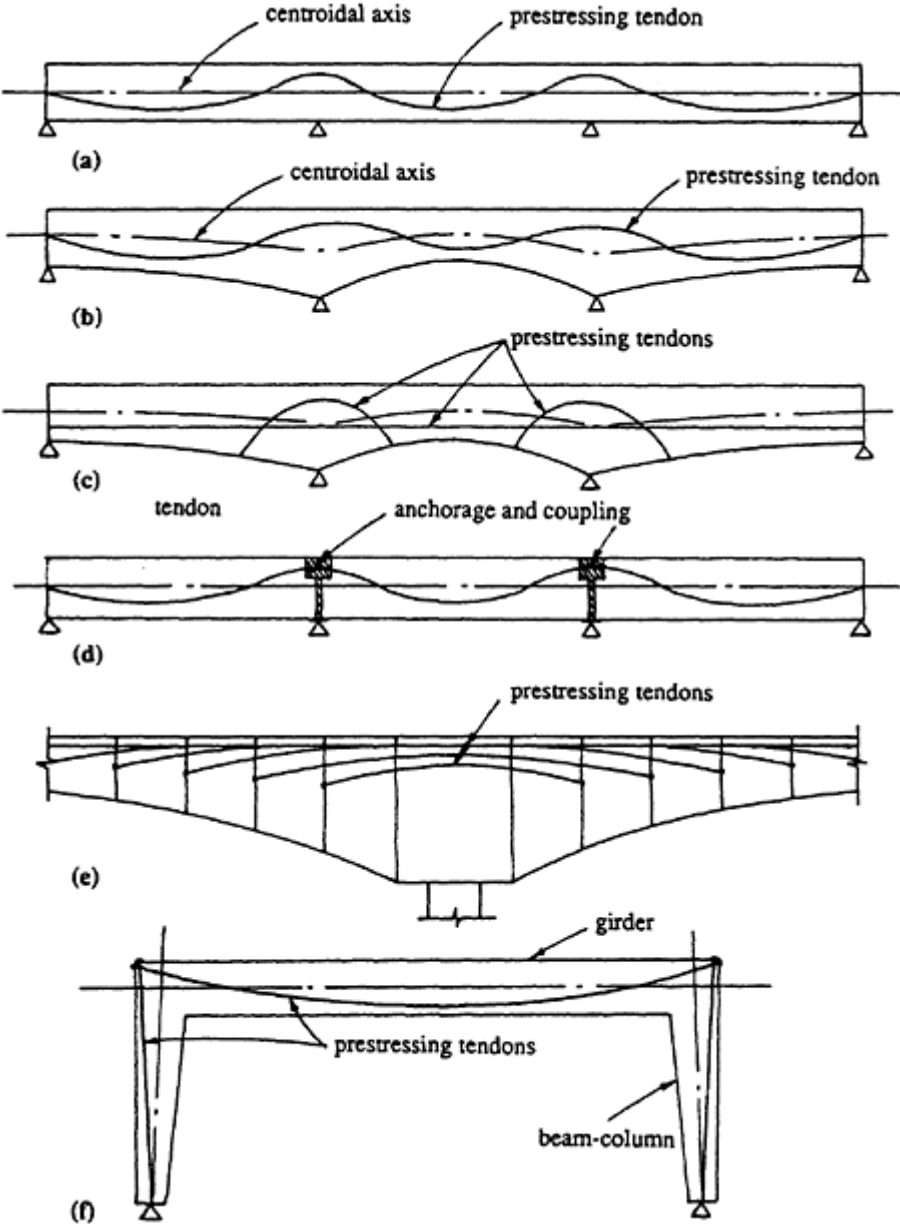


Figure 9.1 Representative tendon profiles.

represented in [Figure 9.1d](#). Precast or cast *in situ* segments are stressed together using prestress couplers to achieve continuity. The couplers and hydraulic jacks are accommodated during the stressing operation within cavities located in the end surface of the individual segments. The cavities can later be filled with concrete, cement grout, or other suitable compounds, as necessary.

In large-span structures, such as bridges spanning highways, rivers, and valleys, construction techniques are required where falsework is restricted to a minimum. The cantilever construction method permits the erection of prestressed concrete segments without the need for major falsework systems. [Figure 9.1e](#) illustrates diagrammatically the tendon profiles for a method of construction where precast elements are positioned alternatively on either side of the pier and stressed against the previously placed elements, as shown. The structure is designed initially to sustain the erection forces and construction loads as simple balanced cantilevers on each side of the pier. When the structure is completed and the cantilevers from adjacent piers are joined, the design service loads are resisted by the resulting continuous haunched girders. Construction and erection techniques, such as cantilevered construction, are continually evolving and considerable ingenuity is evident in the development of these applications.

[Figure 9.1f](#) shows a typical tendon profile for a prestressed concrete portal frame. Prestressed concrete portal frames have generally not had widespread use. With the sudden change of direction of the member axis at each corner of the frame, it is difficult to prestress the columns and beams in a continuous fashion. The horizontal beam and vertical columns are therefore usually stressed separately, with the beam and column tendons crossing at the frame corners and the anchorages positioned on the end and top outside faces of the frame, as shown.

## 9.3 Continuous beams

### 9.3.1 The effects of prestress

As mentioned in [Section 9.1](#), the deformation caused by prestress in a statically determinate member is free to take place without any restraint from the supports. In statically indeterminate members, however, this is not necessarily the case. The redundant supports impose additional geometric constraints, such as zero deflection at intermediate supports (or some prescribed non-zero settlement) or zero slope at a built-in end. During the stressing operation, the geometric constraints may cause additional reactions to develop at the supports, which in turn change the distribution and magnitude of the moments and shears in the member. The magnitudes of these additional reactions (usually called *hyperstatic reactions*) depend

on the magnitude of the prestressing force, the support configuration, and the tendon profile. For a particular structure, a prestressing tendon with a profile that does not cause hyperstatic reactions is called a *concordant tendon*. Concordant tendons are discussed further in [Section 9.3.2](#).

The moment induced by prestress on a particular cross-section in a statically indeterminate structure may be considered to be made up of two components:

- (a) The first component is the product of the prestressing force  $P$ , and its eccentricity from the centroidal axis,  $e$ . This is the moment that acts on the concrete part of the cross-section when the geometric constraints imposed by the redundant supports are removed. The moment  $Pe$  is known as the *primary moment*.
- (b) The second component is the moment caused by the hyperstatic reactions, i.e. the additional moment required to achieve deformations that are compatible with the support conditions of the indeterminate structure. The moments caused by the hyperstatic reactions are the *secondary moments*.

In a similar way, the shear force caused by prestress on a cross-section in a statically indeterminate member can be divided into primary and secondary components. The primary shear force in the concrete is equal to the prestressing force,  $P$ , times the slope  $\theta$ , of the tendon at the cross-section under consideration. For a member containing only horizontal tendons ( $\theta=0$ ), the primary shear force on each cross-section is zero. The secondary shear force at cross-section is caused by the hyperstatic reactions.

The resultant internal actions at any section caused by prestress are the algebraic sums of the primary and secondary effects.

Since the secondary effects are caused by hyperstatic reactions at each support, it follows that the secondary moments always vary linearly between the supports in a continuous prestressed concrete member and the secondary shear forces are constant in each span.

### 9.3.2 Determination of secondary effects using virtual work

In the design and analysis of continuous prestressed concrete members, it is usual to make the following simplifying assumptions (none of which introduce significant errors for normal applications):

- (a) The concrete behaves in a linear elastic manner within the range of stresses considered.
- (b) Plane sections remain plane throughout the range of loading considered.
- (c) The effects of external loading and prestress on the member can be

calculated separately and added to obtain the final conditions, i.e. the principle of superposition is valid.

- (d) The magnitude of the eccentricity of prestress is small in comparison with the member length, and hence the horizontal component of the prestressing force is assumed to be equal to the prestressing force at every cross-section.

Consider the two-span beam shown in [Figure 9.2a](#) with straight prestressing tendons at a constant eccentricity  $e$  below the centroidal axis. Prior to prestressing, the beam rests on the three supports at A, B, and C. On each cross-section, prestress causes an axial force  $P$  on the concrete and a negative primary moment,  $Pe$ . If the support at B were removed, the hogging curvature associated with the primary moment would cause the beam to deflect upward at B, as shown in [Figure 9.2b](#). In the real beam, the deflection at B is zero, as indicated in [Figure 9.2c](#). To satisfy this geometric constraint, a downward reaction is induced at support B, together with equilibrating upward reactions at supports A and C.

To determine the magnitude of these hyperstatic reactions, one of a number of different methods of structural analysis can be used. For one or two-fold indeterminate structures, the force method (or flexibility method) is a convenient approach. For multiply redundant structures, a displacement method (such as moment distribution, for example) is more appropriate.

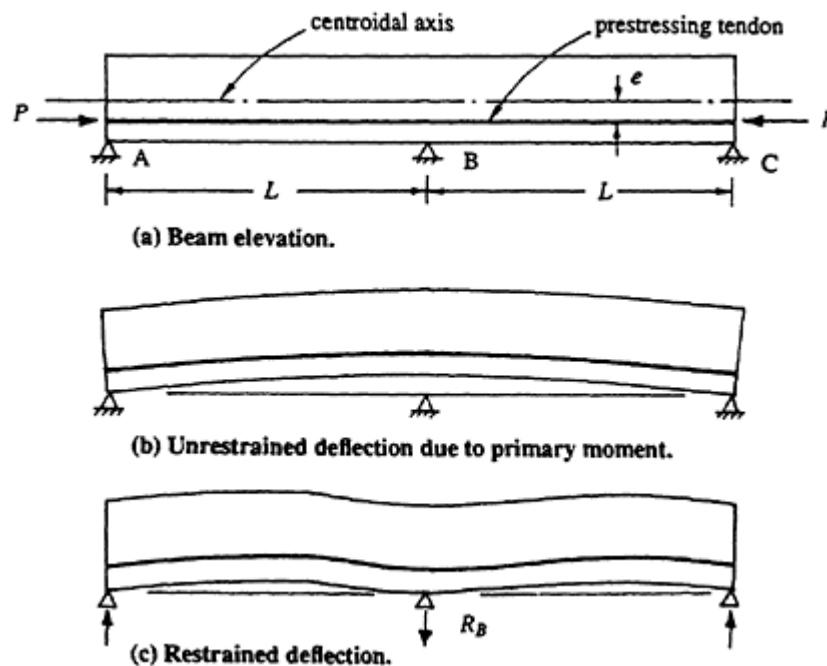


**Figure 9.2** Two-span prestressed beam with constant eccentricity.

Moment–area methods can be used for estimating the deflection of beams from known curvatures. The principle of virtual work can also be used and is often more convenient. The principle is briefly outlined below. For a more comprehensive discussion of virtual work, the reader is referred to a structural analysis text, such as Hall & Kabaila (1977) or Ghali & Neville (1978).

The principle of virtual work states that if a structure is subjected to an equilibrium force field (i.e. a force field in which the external forces are in equilibrium with the internal actions) and a geometrically consistent displacement field (i.e. a displacement field in which the external displacements are compatible with the internal deformations), then the external work product,  $W$ , of the two fields is equal to the internal work product of the two fields,  $U$ . The force field may be entirely independent of the compatible displacement field.

In the applications discussed here, the compatible displacement field is the actual strain and curvature on each cross-section caused by the external loads and prestress, together with the corresponding external displacements. The equilibrium force field consists of a unit external force (or couple) applied to the structure at the point and in the direction of the displacement being determined, together with any convenient set of internal actions that are in equilibrium with this unit force (or couple). The unit force is called a *virtual force* and is introduced at a particular point in the structure to enable the rapid determination of the real displacement at that point. The bending moments caused by the virtual force are designated  $\bar{M}$ .

To illustrate the principle of virtual work, consider again the beam of [Figure 9.2](#). In order to determine the hyperstatic reaction at B, it is first necessary to determine the upward deflection  $v_B$  caused by the primary moment when the support at B is removed (as illustrated in [Figure 9.3a](#)). If the prestress is assumed constant throughout the length of the beam, the curvature caused by the primary moment is as shown in [Figure 9.3b](#). A unit virtual force is introduced at B in the direction of  $v_B$ , as indicated in [Figure 9.3c](#), and the corresponding virtual moments are illustrated in [Figure 9.3d](#).

The external work is the product of the virtual forces and their corresponding displacements:

$$W = 1 \times v_B = v_B \quad (9.1)$$

In this example, the internal work is the integral over the length of the beam of the product of the virtual moments,  $\bar{M}$ , and the real deformations,  $(-Pe/EI)$ . That is,

$$U = \int_0^{2L} \bar{M} \frac{-Pe}{EI} dx \quad (9.2)$$

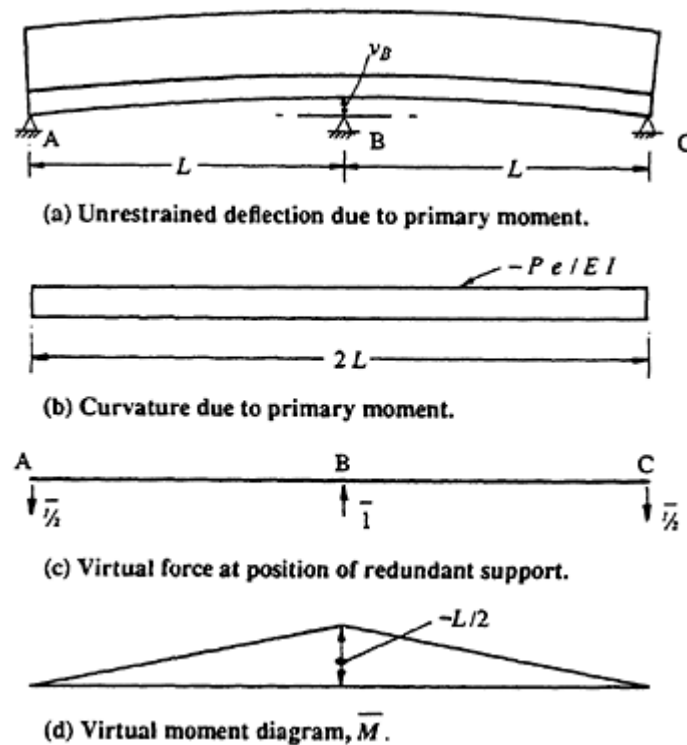


**Figure 9.3** The principle of virtual work applied to a two-span beam.

If the virtual force applied to a structure produces virtual axial forces  $\bar{N}$ , in addition to virtual bending, then internal work is also done by the virtual axial forces and the real axial deformation. For any length of beam,  $\Delta L$ , a more general expression for internal work is

$$U = \int_0^{\Delta L} \bar{M} \frac{M}{EI} dx + \int_0^{\Delta L} \bar{N} \frac{N}{EA} dx \quad (9.3)$$

where  $M/EI$  and  $N/EA$  are the real curvature and axial strain, respectively, and  $\bar{M}$  and  $\bar{N}$  are the virtual internal actions.

An integral of the form

$$U = \int_0^{\Delta L} \bar{F}(x) F(x) dx \quad (9.4)$$

may be considered as the volume of a solid of length  $\Delta L$  whose plan is the function  $F(x)$  and whose elevation is the function  $\bar{F}(x)$ . Consider the two functions  $F(x)$  and  $\bar{F}(x)$  illustrated in [Figure 9.4](#) and the notation also shown. The volume integral (Equation 9.4) can be evaluated exactly using Simpson's rule if the shape of the function  $F(x)$  is linear or parabolic and

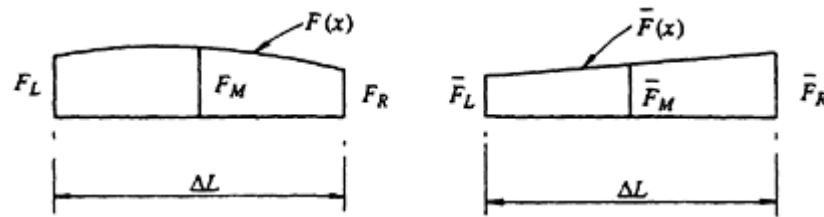


**Figure 9.4** Notation for volume integration.

the shape of  $\bar{F}(x)$  is linear. Thus,

$$\int_0^{\Delta L} \bar{F}(x)F(x) dx = \frac{\Delta L}{6} (\bar{F}_L F_L + 4\bar{F}_M F_M + \bar{F}_R F_R) \quad (9.5)$$

In the example considered here, the function  $F(x)$  is constant and equal to  $-Pe/EI$  (i.e.  $F_L = F_M = F_R = -Pe/EI$ ) and the function  $\bar{F}(x)$  is the virtual moment diagram  $\bar{M}$ , which is also negative and varies linearly from A to B and from B to C, as shown in [Figure 9.3d](#). Evaluating the internal work in the spans AB and BC, Equation 9.2 gives

$$U_{AB} = U_{BC} = \int_0^L \bar{M} \frac{-Pe}{EI} dx$$

Therefore,

$$U = 2 \int_0^L \bar{M} \frac{-Pe}{EI} dx \quad (9.6a)$$

With  $\bar{F}_L = 0$ ,  $\bar{F}_M = -L/4$ , and  $\bar{F}_R = -L/2$ , Equation 9.5 gives

$$U = 2 \times \frac{L}{6} \left[ \left(0 \times \frac{-Pe}{EI}\right) + \left(4 \times \frac{L}{4} \times \frac{Pe}{EI}\right) + \left(\frac{L}{2} \times \frac{Pe}{EI}\right) \right] = \frac{PeL^2}{2EI} \quad (9.6b)$$

The principle of virtual work states that

$$W = U \quad (9.7)$$

and substituting Equations 9.1 and 9.6b into Equation 9.7 gives

$$v_B = \frac{PeL^2}{2EI} \quad (9.8)$$

It is next necessary to calculate the magnitude of the redundant reaction,  $R_B$ , required to restore compatibility at B, i.e. the value of  $R_B$  required to produce a downward deflection at B equal in magnitude to the upward

deflection given in Equation 9.8. It is convenient to calculate the *flexibility coefficient*,  $f_B$ , associated with the released structure. The flexibility coefficient  $f_B$  is the deflection at B caused by a unit value of the redundant reaction at B. The curvature diagram caused by a unit vertical force at B has the same shape as the moment diagram shown in [Figure 9.3d](#). That is, the curvature diagram caused by a unit force at B,  $(M/EI)$ , and the virtual moment diagram,  $\bar{M}$ , have the same shape and the same sign. Using the principle of virtual work and Equation 9.5 to evaluate the volume integral,

$$f_B = \int_0^{2L} \bar{M} \frac{M}{EI} dx = 2 \times \frac{L}{6EI} \left[ \left( 4 \times \frac{L}{4} \times \frac{L}{4} \right) + \left( \frac{L}{2} \times \frac{L}{2} \right) \right] = \frac{L^3}{6EI} \quad (9.9)$$

Compatibility requires that the deflection of the real beam at B is zero, i.e.

$$v_B + f_B R_B = 0 \quad (9.10)$$

and therefore

$$R_B = -\frac{v_B}{f_B} = -\frac{PeL^2}{2EI} \times \frac{6EI}{L^3} = -\frac{3Pe}{L} \quad (9.11)$$

The negative sign indicates that the hyperstatic reaction is downward (or opposite in direction to the unit virtual force at B). With the hyperstatic reactions thus calculated, the secondary moments and shears are determined readily. The effects of prestress on the two-span beam under consideration are shown in [Figure 9.5](#).

In a statically determinate beam under the action of prestress only, the resultant force on the concrete at a particular cross-section is a compressive force  $C$  equal in magnitude to the prestressing force and located at the position of the tendon. The distance of the force  $C$  from the centroidal axis is therefore equal to the primary moment divided by the prestressing force,  $Pe/P=e$ . In a statically indeterminate member, if secondary moments exist at a section, the location of  $C$  does not coincide with the position of the tendon. The distance of  $C$  from the centroidal axis is the total moment due to prestress (primary plus secondary) divided by the prestressing force.

For the beam shown in [Figure 9.5a](#), the total moment due to prestress is illustrated in [Figure 9.5e](#). The position of the stress resultant  $C$  varies as the total moment varies along the beam. At the two exterior supports (ends A and C),  $C$  is located at the tendon level (i.e. a distance  $e$  below the centroidal axis), since the secondary moment at each end is zero. At the interior support B, the secondary moment is  $3Pe/2$ , and  $C$  is located at  $e/2$  above the centroidal axis (or  $3e/2$  above the tendon level). In general, at any section of a continuous beam, the distance of  $C$  from the level of the



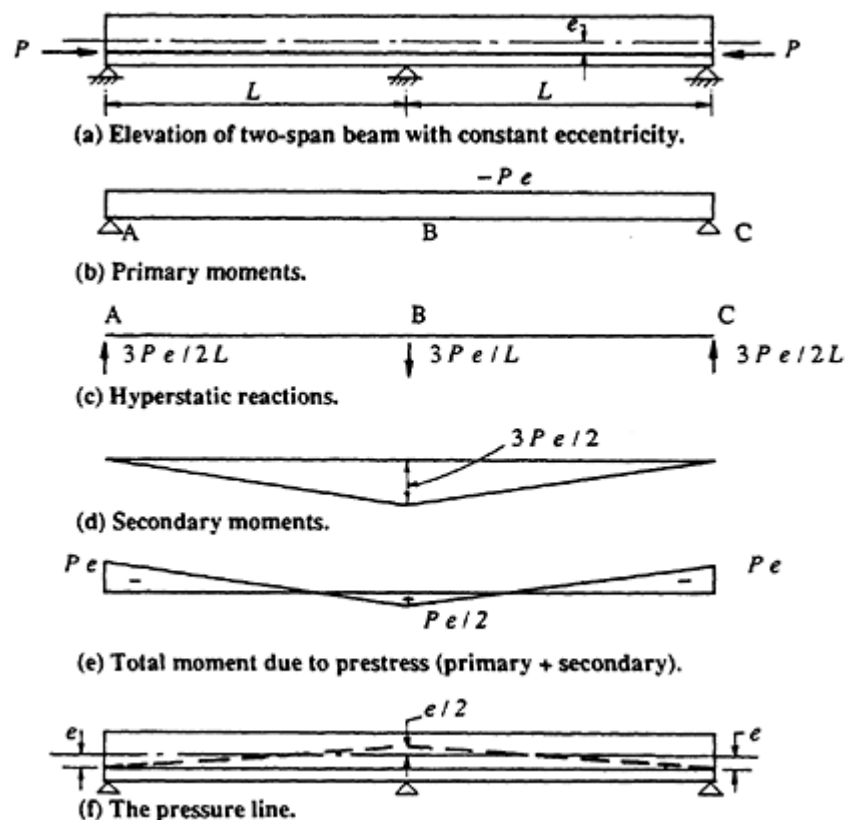


Figure 9.5 Effects of prestress.

tendon is equal to the secondary moment divided by the prestressing force.

If the position of  $C$  at each section is plotted along the beam, a line known as the *pressure line* is obtained. The pressure line for the beam of Figure 9.5a is shown in Figure 9.5f.

If the prestressing force produces hyperstatic reactions, and hence secondary moments, the pressure line does not coincide with the tendon profile. If, however, the pressure line and the tendon profile do coincide at every section along a beam, there are no secondary moments and the tendon profile is said to be *concordant*. In a statically determinate member, of course, the pressure line and the tendon profile always coincide.

### Linear transformation of a tendon profile

The two-span beam shown in Figure 9.6 is similar to the beam in Figure 9.2a (and Figure 9.5a), except the eccentricity of the tendon is not constant but varies linearly in each span. At the exterior supports, the eccentricity is  $e$  (as in the previous examples) and at the interior support the eccentricity is  $ke$ , where  $k$  is arbitrary. If the tendon is above the centroidal axis at  $B$ , as shown,  $k$  is negative.

The primary moment at a section is the product of the prestressing force

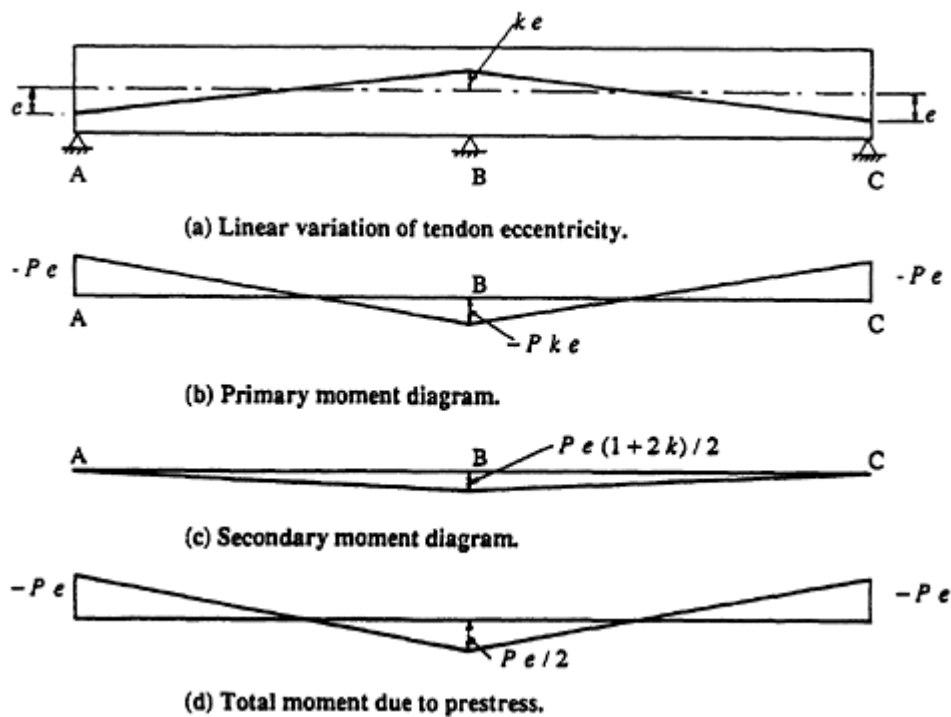


**Figure 9.6** Moments induced by prestress in a two-span beam with a linearly-varying tendon profile.

and the tendon eccentricity and is shown in [Figure 9.6b](#). If the support at B is removed, the deflection at B ( $v_B$ ) caused by the primary moment may be calculated using the principle of virtual work. The virtual moment diagram,  $\bar{M}$ , is shown in [Figure 9.3d](#). Using Equation 9.5 to perform the required volume integration.

$$v_B = 2 \frac{L}{6EI} \left[ 4 \frac{L}{4} \left( \frac{Pe + Pke}{2} \right) + \frac{L}{2} Pke \right] = \frac{PeL^2}{EI} \left( \frac{1 + 2k}{6} \right) \quad (9.12)$$

The flexibility coefficient associated with a release at support B is given by Equation 9.9 and the compatibility condition of zero deflection at the interior support is expressed by Equation 9.10. Substituting Equations 9.9 and 9.12 into Equation 9.10 gives the hyperstatic reaction at B:

$$R_B = - \frac{Pe}{L} (1 + 2k) \quad (9.13)$$

The secondary moments produced by this downward reaction at B are shown in [Figure 9.6c](#). The secondary moment at the interior support is  $(R_B \times 2L)/4 = Pe(1+2k)/2$ . Adding the primary and secondary moment

diagrams gives the total moment diagram produced by prestress and is shown in [Figure 9.6d](#). This is identical with the total moment diagram shown in [Figure 9.5e](#) for the beam with a constant eccentricity  $e$  throughout.

The total moments induced by prestress are unaffected by variations in the eccentricity at the interior support. The moments due to prestress are produced entirely by the eccentricity of the prestress at each end of the beam. If the tendon profile remains straight, variation of the eccentricity at the interior support does not impose transverse loads on the beam (except directly over the supports) and therefore does not change the moments caused by prestress. It does change the magnitudes of both the primary and secondary moments, however, but not their sum. If the value of  $k$  in [Figure 9.6](#) is  $-0.5$  (i.e. the eccentricity of the tendon at support B is  $e/2$  above the centroidal axis), the secondary moments in [Figure 9.6c](#) disappear. The tendon profile is concordant and follows the pressure line shown in [Figure 9.5f](#).

A change in the tendon profile in any beam that does not involve a change in the eccentricities at the free ends and does not change the tendon curvature within each span will not affect the total moments due to prestress. Such a change in the tendon profile is known as *linear transformation*, since it involves a change in the tendon eccentricity at each cross-section by an amount that is linearly proportional to the distance of the cross-section from the end of each span.

Linear transformation can be used in any beam to reduce or eliminate secondary moments. For any statically indeterminate beam, the tendon profile in each span can be made concordant by linearly transforming the profile so that the total moment diagram and the primary moment diagram are the same. The tendon profile and the pressure line for the beam will then coincide.

The calculation of stresses at any section in an uncracked structure due to the prestressing force can be made using the following equation:

$$\sigma = -\frac{P}{A} \pm \frac{Pe^*y}{I} \quad (9.14)$$

The term  $e^*$  is the eccentricity of the pressure line from the centroidal axis of the member, and not the actual eccentricity of the tendon (unless the tendon is concordant and the pressure line and tendon profile coincide). The significance of the pressure line is now apparent. It is the location of the concrete stress resultant caused by the axial prestress, the moment caused by the tendon eccentricity, and the moment caused by the hyperstatic support reactions.

9.3.3 Analysis using equivalent loads

In the previous section, the force method was used to determine the hyperstatic reaction in a one-fold indeterminate structure. This method is useful for simple structures, but is not practical for manual solution when the number of redundants becomes large (more than about three).

A procedure more suited to determining the effects of prestress in highly indeterminate structures is the *equivalent load method*. In this method, the forces imposed on the concrete by the prestressing tendons are considered as externally applied loads. The structure is then analysed under the action of these *equivalent loads* using moment distribution or an equivalent method of structural analysis. The equivalent loads include the loads imposed on the concrete at the tendon anchorage (which may include the axial prestress, the shear force resulting from a sloping tendon, and moment due to an eccentrically placed anchorage) and the transverse forces exerted on the member wherever the tendon changes direction. Commonly occurring tendon profiles and their equivalent loads are illustrated in [Figure 9.7](#).

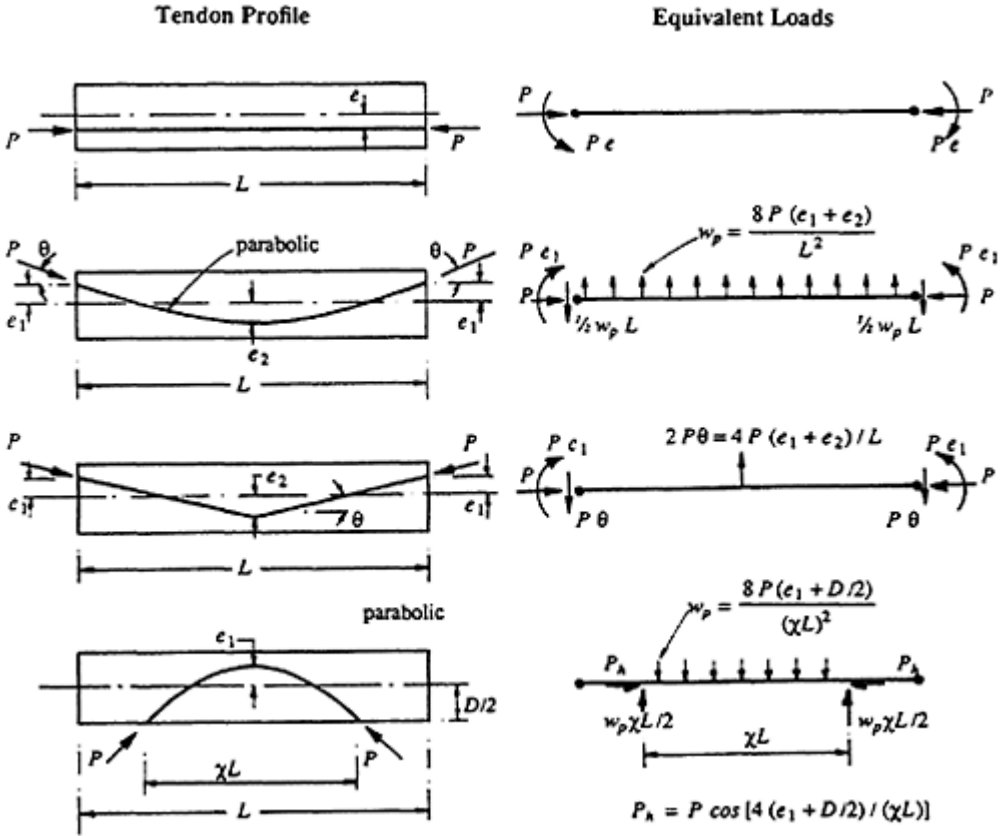


Figure 9.7 Tendon profiles and equivalent loads.

The total moment caused by prestress at any cross-section is obtained by analysing the structure under the action of the equivalent loads in each span. The moment due to prestress is caused only by moments applied at each end of a member (due to an eccentrically located tendon anchorage) and by transverse loads resulting from changes in the direction of the tendon anywhere between the supports. Changes in tendon direction at a support (such as at support B in [Figure 9.6a](#)) do not affect the moment caused by prestress, since the transverse load passes directly into the support. This is why the total moments caused by prestress in the beams of [Figures 9.5](#) and [9.6](#) are identical.

The primary moment at any section is the product of the prestress and its eccentricity,  $Pe$ . The secondary moment may therefore be calculated by subtracting the primary moment from the total moment caused by the equivalent loads.

### Moment distribution

Moment distribution is a relaxation procedure developed by Hardy Cross (1930) for the analysis of statically indeterminate beams and frames. It is a displacement method of analysis that is ideally suited to manual calculation. Although the method has been replaced in many applications by more computer-oriented displacement methods, it remains a valuable tool for practising engineers because it is simple, easy to use, and provides an insight into the physical behaviour of the structure.

Initially, the rotational stiffness of each member framing into each joint in the structure is calculated. Joints in the structure are then *locked* against rotation by the introduction of imaginary restraints. With the joints locked, *fixed-end moments* (F.E.M.) develop at the ends of each loaded member. At a locked joint, the imaginary restraint exerts a moment on the structure equal to the *unbalanced moment*, which is the resultant of all the fixed-end moments at the joint. The joints are then released, one at a time, by applying a moment to the joint equal and opposite to the unbalanced moment. This balancing moment is distributed to the members framing into the joint in proportion to their rotational stiffnesses. After the unbalanced moment at a joint has been balanced, the joint is relocked. The moment distributed to each member at a released joint induces a *carry-over moment* at the far end of the member. These carry-over moments are the source of new unbalanced moments at adjacent locked joints. Each joint is unlocked, balanced, and then relocked, in turn, and the process is repeated until the unbalanced moments at every joint are insignificant. The final moment in a particular member at a joint is obtained by summing the initial fixed-end moment and all the increments of distributed and carryover moments. With the moment at each end of a member thus calculated, the moments and shears at any point along the member can be obtained from statics.

Consider the member AB shown in [Figure 9.8a](#). When the couple  $M_{AB}$  is applied to the rotationally released end at A, the member deforms as shown and a moment  $M_{BA}$  is induced at the fixed support B at the far end of the member. The relationships between the applied couple  $M_{AB}$  and the rotation at A ( $\theta_A$ ) and between the couples at A and B may be expressed as

$$M_{AB} = k_{AB}\theta_A \quad \text{and} \quad M_{BA} = CM_{AB} \tag{9.15}$$

where  $k_{AB}$  is the *stiffness coefficient* for the member AB and the term  $C$  is the *carry-over factor*. For a prismatic member, it is a simple matter (using

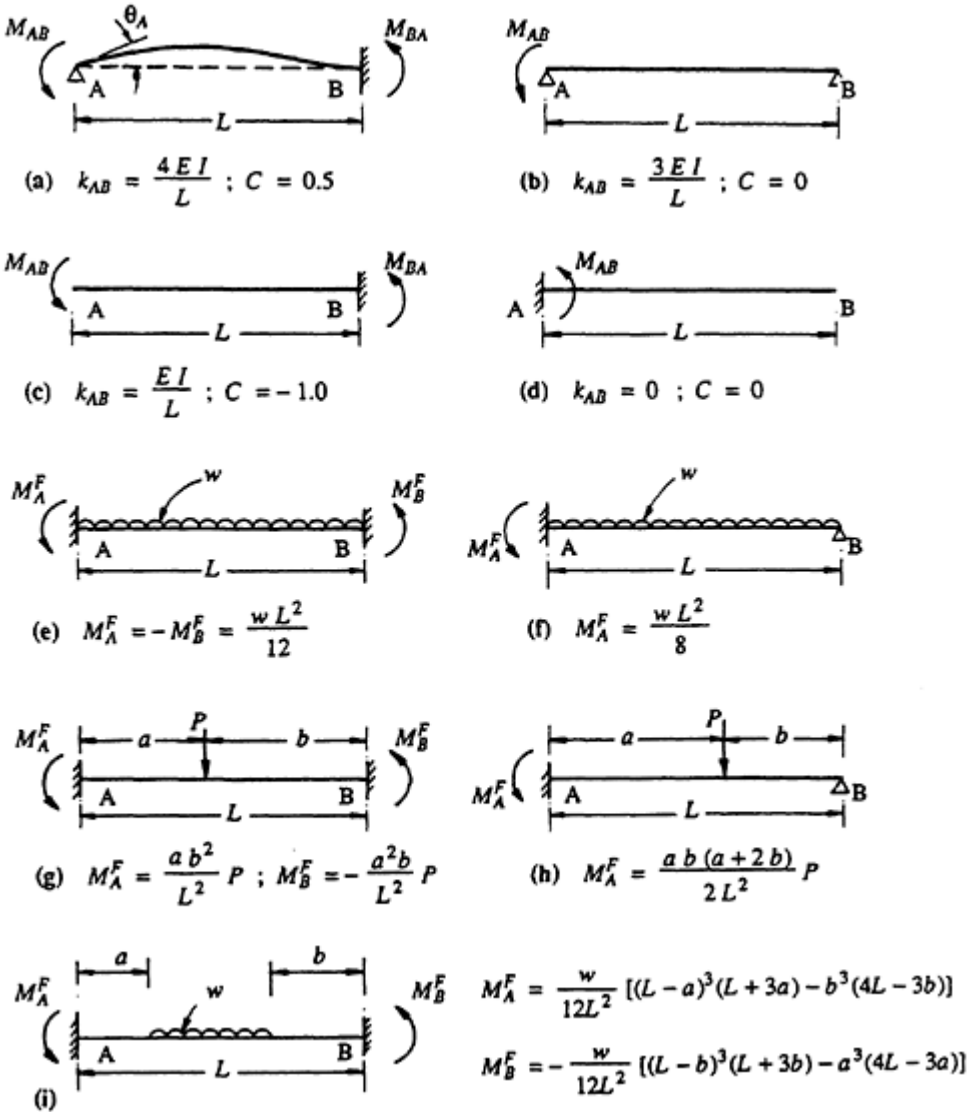


Figure 9.8 Stiffness coefficients, carry-over factors and fixed-end moments for prismatic members.

virtual work) to show that for the beam in [Figure 9.8a](#),

$$k_{AB} = \frac{4EI}{L} \quad \text{and} \quad C = 0.5 \quad (9.16)$$

Expressions for the stiffness coefficient and carry-over factor for members with other support conditions are shown in [Figures 9.8b–d](#). Fixed-end moments for members carrying distributed and concentrated loads are shown in [Figures 9.8e–i](#).

The stiffness coefficient for each member framing into a joint in a continuous beam or frame is calculated and summed to obtain the total rotational stiffness of the joint,  $\Sigma k$ . The *distribution factor* for a member at the joint is the fraction of the total balancing moment distributed to that particular member each time the joint is released. Since each member meeting at a joint rotates by the same amount, the distribution factor for member AB is  $k_{AB}/\Sigma k$ . The sum of the distribution factors for each member at a joint is therefore unity.

An example of moment distribution applied to a continuous beam is given in the following example. For a more detailed description of moment distribution, the reader is referred to Hall & Kabaila (1977) or Ghali & Neville (1978), or other standard texts on structural analysis.

#### Example 9.1 —Continuous beam

The continuous beam shown in [Figure 9.9a](#) has a rectangular cross-section 400 mm wide and 900 mm deep. The prestressing force is assumed to be constant along the length of the beam and equal to 1800 kN. The tendon profile shown in [Figure 9.9a](#) is adopted for illustrative purposes only. In practice, a post-tensioned tendon profile with sharp kinks or sudden changes in direction would not be used. Relatively short lengths of more gradually curved tendons would be used instead of the kinks shown at B, C, and D. The results of an analysis using the idealized tendon profile do, however, provide a reasonable approximation of the behaviour of a more practical beam with continuous curved profiles at B, C, and D.

In span AB, the shape of the parabolic tendon is  $y = -0.00575x^2 + 0.1025x - 0.1$  and its slope is  $dy/dx = 0.1025 - 0.0115x$ , where  $x$  is the distance (in metres) along the beam from support A and  $y$  is the depth (in metres) of the tendon below the centroidal axis. At support A ( $x=0$ ), the tendon is 100 mm above the centroidal axis ( $y=-0.1$ ) and the corresponding moment applied at the support is 180 kNm, as shown in [Figure 9.9b](#). The slope of the tendon at A is  $dy/dx = 0.1025$  rads and the vertical component of prestress is therefore  $1800 \times 0.1025 = 184.5$  kN. The parabolic tendon exerts an upward uniformly distributed load on span AB. With the cable drape being  $h = 350 + [(100 + 350)/2] = 575$  mm = 0.575 m, the

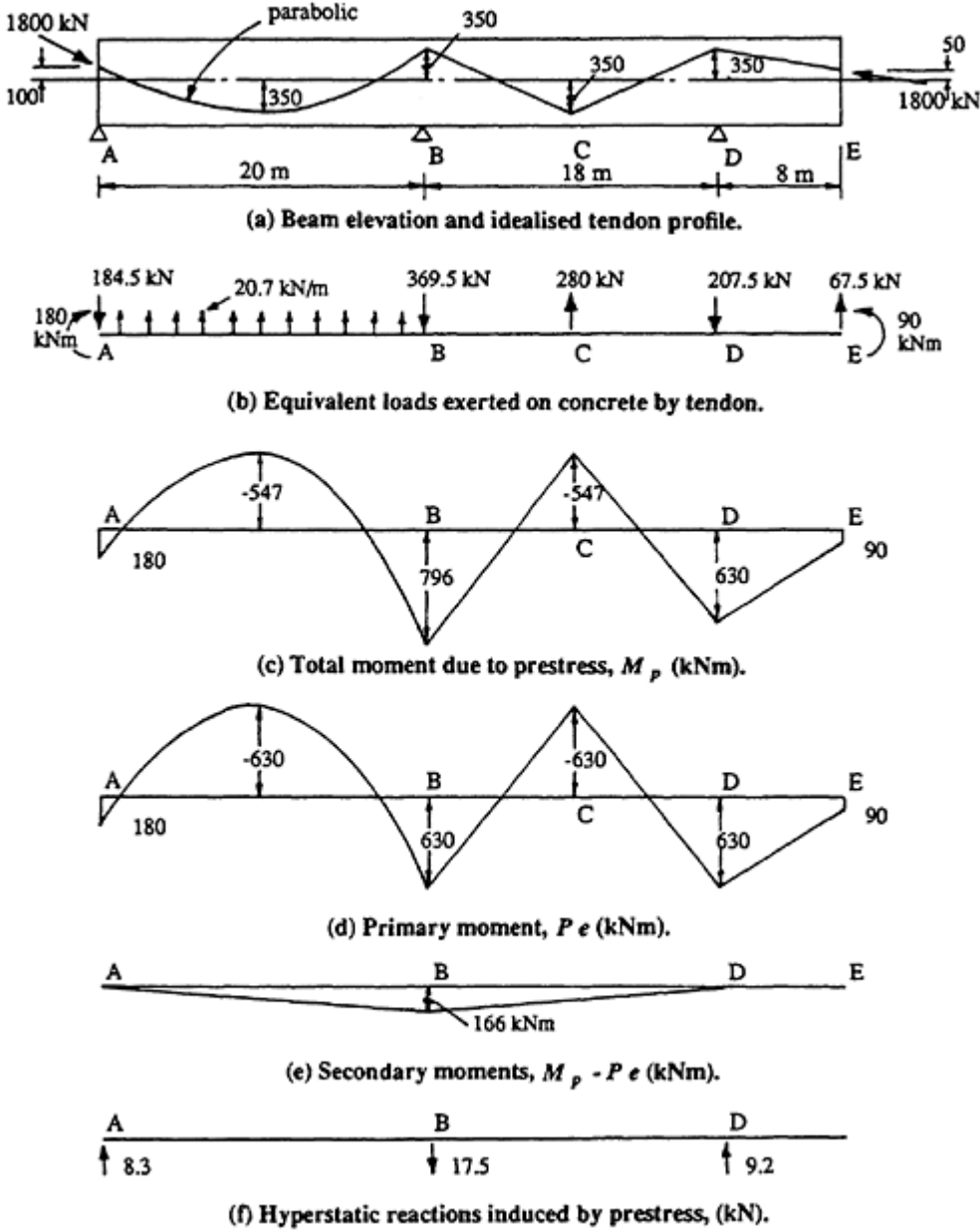


Figure 9.9 Equivalent loads and actions induced by prestress in Example 9.1.

equivalent load  $w_p$  is

$$w_p = \frac{8Ph}{L^2} = \frac{8 \times 1800 \times 0.575}{20^2} = 20.7 \text{ kN/m}$$

The slope of the parabolic tendon at B is  $\theta_{BA} = dy/dx = -0.1275$  rad and, in span BD, the slope of the straight tendon at B is  $\theta_{BC} = (0.35 + 0.35)/$



$\theta = 0.0778$  rad. The change of slope at B is therefore  $\theta_{BC} - \theta_{BA} = 0.205$  rad, and therefore the vertical downward force at B is  $1800 \times 0.205 = 369.5$  kN.

The angular change at C is  $\theta_C = 2 \times 0.0778 = 0.1556$  rad and the upward equivalent point load at C is therefore  $1800 \times 0.1556 = 280$  kN. The slope of the tendon in CD is  $\theta_{DC} = -0.0778$  rad, and in DE,  $\theta_{DE} = 0.3/8 = 0.0375$  rad. The change in tendon direction at D is therefore  $\theta_{DE} - \theta_{DC} = 0.115$  rad and the transverse equivalent point load at D is 207.5 kN (downward). At the free end E, the equivalent couple is  $1800 \times 0.05 = 90$  kNm and the vertical component of the prestressing force is upward and equal to  $P\theta_{ED} = 1800 \times 0.0375 = 67.5$  kN.


All these equivalent loads are shown in [Figure 9.9b](#). Note that the equivalent loads are self-equilibrating. The vertical equivalent loads at A, B, and D pass directly into the supports and do not affect the moment induced in the member by prestress.

The continuous beam is analysed under the action of the equivalent loads using moment distribution as outlined in [Table 9.1](#).

The total moment diagram caused by prestress (as calculated in [Table 9.1](#)) and the primary moments are illustrated in [Figures 9.9c](#) and [d](#), respectively. The secondary moment diagram in [Figure 9.9e](#) is obtained by subtracting the primary moments from the total moments and the hyperstatic reactions shown in [Figure 9.9f](#) are deduced from the secondary moment diagram.

The secondary shear force diagram corresponding to the hyperstatic

**Table 9.1** Moment distribution table for [Example 9.1](#).



	AB	BA	BD	DB	DE	ED
Stiffness Coefficient		$\frac{3EI}{20}$	$\frac{4EI}{18}$	$\frac{4EI}{18}$	0	-
Carry-over factor	0.5	0	0.5	0.5	0	-1.0
Distribution factor	0	0.403	0.597	1.0	0	0
F.E.M. (kN m)	180	-1035 90 127	630 188 -47 28 -7 4	-630 94 -94 14 -14	630	-90
Final moments (kN m)	180	-796	796	-630	630	-90

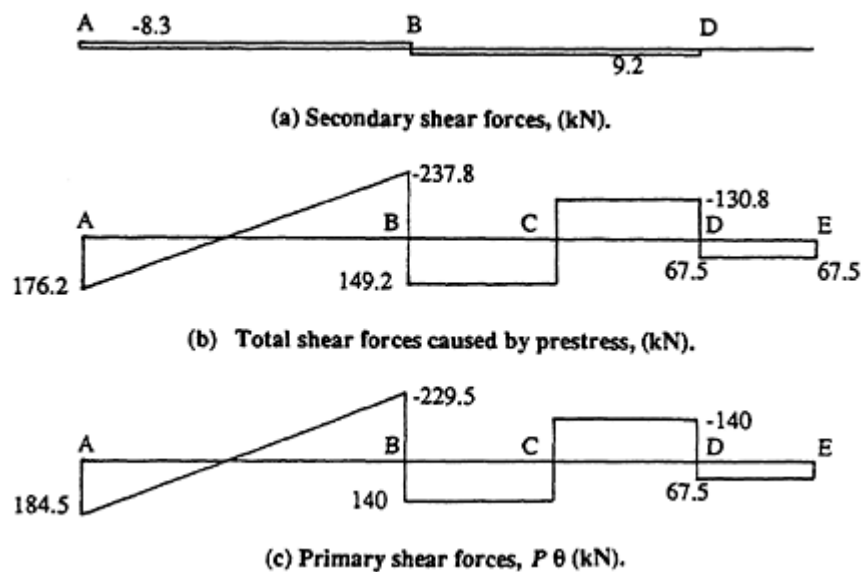


**Figure 9.10** Shear force components caused by prestress in [Example 9.1](#).

reactions is illustrated in [Figure 9.10a](#). The total shear force diagram is obtained from statics using the total moments calculated by moment distribution and is given in [Figure 9.10b](#). By subtracting the secondary shear force from the total shear force at each section, the primary shear force diagram shown in [Figure 9.10c](#) is obtained. Note that the primary shear force at any section is the vertical component of prestress,  $P\theta$ . The reader may verify the results given in [Figures 9.9](#) and [9.10](#) by calculating the hyperstatic reactions at B using the force method and the principle of virtual work.

### Example 9.2 —Fixed-end beams

The beams shown in [Figures 9.11a](#), [9.12](#), and [9.13a](#) are rotationally restrained at each end but are not restrained axially. The moments induced by prestress in each member are required. Assume that the prestressing force is constant throughout and the member has a constant  $EI$ .

**Case (a)** The beam shown in [Figure 9.11a](#) is prestressed with a parabolic tendon profile with unequal end eccentricities. The equivalent loads on the structure are illustrated in [Figure 9.11b](#), with end moments of  $Pe_A$  and  $Pe_B$ , as shown, and an equivalent uniformly distributed upward load of  $w_p = 8Ph/L^2$ .

If the rotational restraints at each end of the beam are released, the curvature is due entirely to the primary moment and is directly proportional to the tendon eccentricity, as shown in [Figure 9.11c](#). The final curvature diagram is obtained by adding the curvature caused by the primary moments to the curvature caused by the restraining secondary moments at

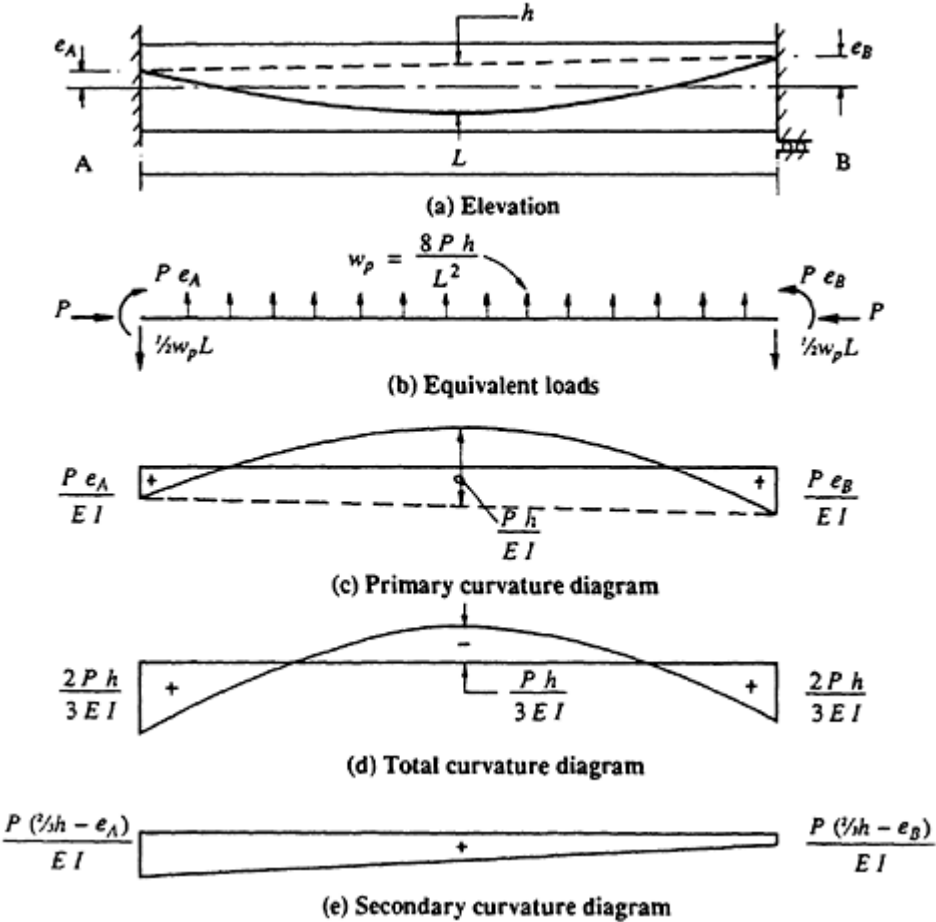


Figure 9.11 Moments induced by a parabolic tendon in a fixed-end member.

each end of the beam,  $M_A^s$  and  $M_B^s$ , respectively. The secondary curvature caused by these secondary moments varies linearly over the length of the beam, so that the final curvature involves a linear shift in the base line of the primary curvature diagram (see Figure 9.11c).

It is straightforward, using virtual work, to calculate the restraining moments  $M_A^s$  and  $M_B^s$  required to produce zero slope at each end of the beam, i.e.  $\theta_A = \theta_B = 0$ . However, because the beam is fixed-ended, the moment-area theorems reduce the problem to one that can be solved by inspection. Since the slopes at each end are identical, the net area under the total curvature diagram must be zero, i.e. the base line in Figure 9.11c must be translated and rotated until the area under the curvature diagram is zero. In addition, because support A lies on the tangent to the beam axis at B, the first moment of the final curvature diagram about support A must also be zero. With these two requirements, the total curvature diagram is as shown in Figure 9.11d.

Note that this is the only solution in which the net area under the curv-

ature diagram is zero and the centroids of the areas above and below the base line are the same distance from A. It should also be noted that the fixed-end moment at each end of the beam is  $\frac{2}{3}Ph = w_p L^2/12$ , which is independent of the initial eccentricities at each end,  $e_A$  and  $e_B$ . Evidently, the moment induced by prestress depends only on the prestressing force and the cable drupe, and not on the end eccentricities. This conclusion was foreshadowed in the discussion of linear transformation in [Section 9.3.2](#). The secondary moment diagram is obtained by subtracting the primary moment diagram from the total moment diagram. From [Figures 9.11c](#) and [d](#), it can be seen that

$$M_A^s = P(\frac{2}{3}h - e_A) \quad \text{and} \quad M_B^s = P(\frac{2}{3}h - e_B) \quad (9.17)$$

The secondary curvature diagram caused by the linearly varying secondary moments is shown in [Figure 9.11e](#).

**Case (b)** The beam in [Figure 9.12](#) is prestressed with a single straight tendon with arbitrary end eccentricities. This beam is essentially the same as that in the previous example, except that the tendon drupe is zero. To satisfy the moment–area theorems in this case, the base line of the total curvature diagram coincides with the primary curvature diagram, i.e. the total moment induced by prestress is everywhere zero, and the primary and secondary moments at each cross-section are equal in magnitude and opposite in sign. By substituting  $h=0$  in Equations 9.17, the secondary moments at each end of the beam of [Figure 9.12](#) are

$$M_A^s = -Pe_A \quad \text{and} \quad M_B^s = -M_B^p = -Pe_B.$$

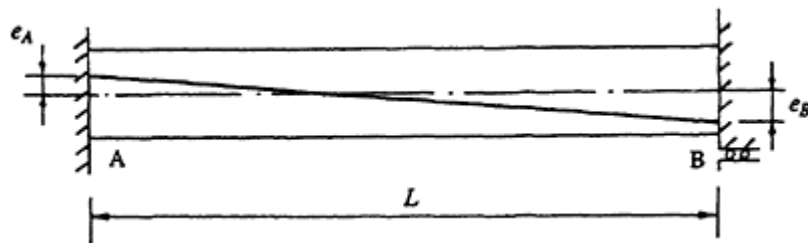


**Figure 9.12** Fixed-end beam with straight tendon.

**Case (c)** The beam in [Figure 9.13a](#) is prestressed with the harped tendon shown. The primary curvature diagram is shown in [Figure 9.13b](#) and the total curvature diagram, established by satisfaction of the moment–area theorems, is illustrated in [Figure 9.13c](#). As for the previous case, the total curvature (moment) induced by prestress is independent of the end eccentricities  $e_A$  and  $e_B$ . The curvature induced by the secondary moments is

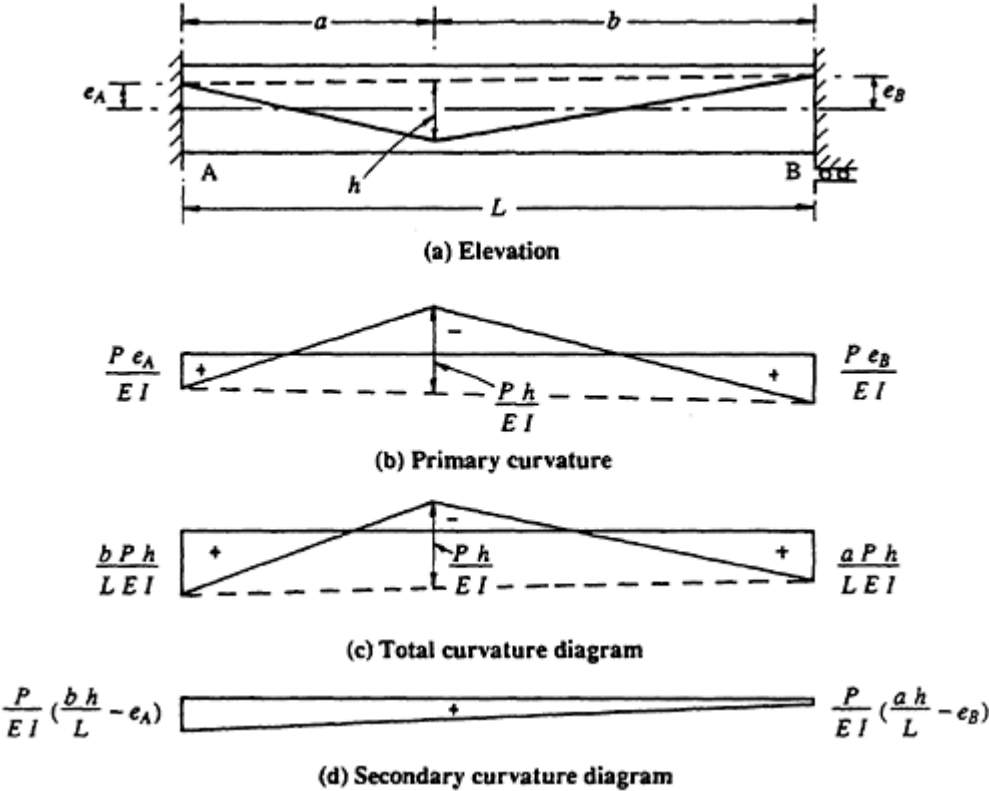


Figure 9.13 Moments induced by a harped tendon in a fixed-end beam.

given in Figure 9.13d, and the secondary moments at each support are

$$M_A^s = P \left( \frac{b}{L} h - e_A \right) \quad \text{and} \quad M_B^s = P \left( \frac{a}{L} h - e_B \right)$$

9.3.4 Practical tendon profiles

In a span of a continuous beam, it is rarely possible to use a tendon profile that consists of a single parabola, as shown in Figure 9.11a. A more realistic tendon profile consists of a series of segments each with a different shape. Frequently, the tendon profile is a series of parabolic segments, concave in the spans and convex over the interior supports, as illustrated in Figure 9.1a. The convex segments are required to avoid sharp kinks in the tendon at the supports.

Consider the span shown in Figure 9.14, with a tendon profile consisting of three parabolic segments. Adjacent segments are said to be compatible at the points of intersection if the slope of each segment is the same. Compatible segments are desirable to avoid kinks in the tendon profile.

In Figure 9.14, B is the point of maximum eccentricity,  $e_1$ , and is located a distance of  $\alpha_1 L$  from the interior support. Both parabolas 1 and 2 have

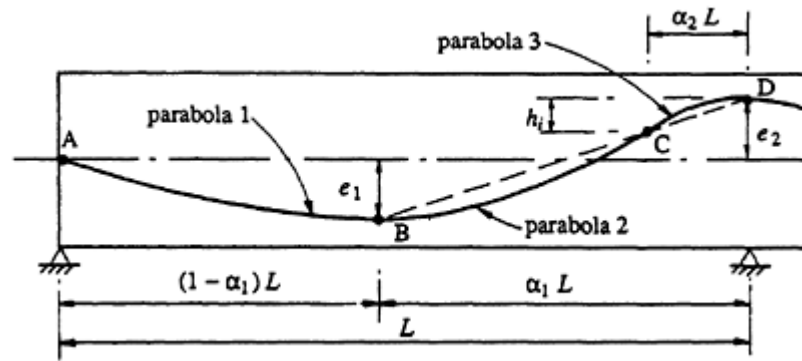


Figure 9.14 Tendon profile with parabolic segments.

zero slope at B. The point of inflection at C between the concave parabola 2 and the convex parabola 3 is located a distance  $\alpha_2 L$  from the interior support. Parabolas 2 and 3 have the same slope at C. Over the internal support at D, the eccentricity is  $e_2$  and the slope of parabola 3 is zero. By equating the slopes of parabolas 2 and 3 at C, it is simple, using geometry, to show that

$$h_i = \frac{\alpha_2}{\alpha_1} (e_1 + e_2) \quad (9.18)$$

and the point C lies on the straight line joining the points of maximum eccentricity, B and D. The slope of parabolas 2 and 3 at C is

$$\theta_C = \frac{2(e_1 + e_2)}{\alpha_1 L} \quad (9.19)$$

The curvature of each of the three parabolic segments ( $x_{p1}$ ,  $x_{p2}$ , and  $x_{p3}$ , respectively) are given by

$$x_{p1} = \frac{1}{R_1} = \frac{2e_1}{L^2(1 - \alpha_1)^2} \quad (\text{concave}) \quad (9.20a)$$

$$x_{p2} = \frac{1}{R_2} = \frac{2(e_1 + e_2 - h_i)}{L^2(\alpha_1 - \alpha_2)^2} \quad (\text{concave}) \quad (9.20b)$$

$$x_{p3} = \frac{1}{R_3} = \frac{2(e_1 + e_2)}{\alpha_1 \alpha_2 L^2} \quad (\text{convex}) \quad (9.20c)$$

where  $R_1$ ,  $R_2$ , and  $R_3$  are the radius of curvature of parabolas 1, 2 and 3, respectively.

The length of the convex parabola,  $\alpha_2 L$ , should be selected so that the

radius of curvature of the tendon is not less than the minimum value recommended by the appropriate building code. For a multi-strand system,  $R$  should be greater than about  $75 d_d$ , where  $d_d$  is the inside diameter of the duct.

Equations 9.18 and 9.20 are useful for the calculation of the equivalent loads imposed by a realistic draped tendon profile and the determination of the effects of these loads on the behaviour of a continuous structure.

**Example 9.3**

The fixed-end beam shown in [Figure 9.15a](#) is to be analysed. The tendon profile ACDEB consists of three parabolic segments and the prestressing force is 2500 kN throughout the 16 m span. The convex segments of the tendon at each end of the beam are identical, with zero slope at A and B and a radius of curvature  $R_3=8$  m. The tendon eccentricity at mid-span and at each support is 300 mm, i.e.  $e_1=e_2=0.3$  m, and  $\alpha_1$  (as defined in

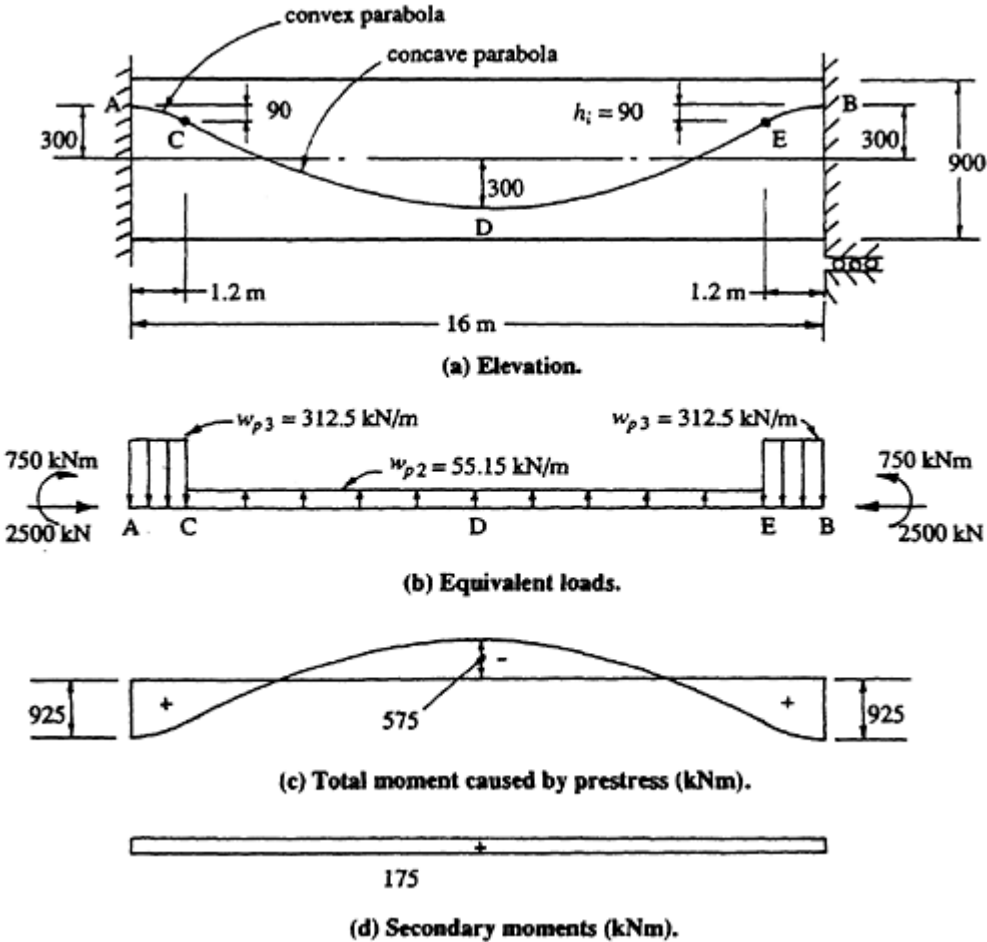


Figure 9.15 Fixed-end beam with a realistic tendon profile ([Example 9.3](#)).

[Figure 9.14](#)) equals 0.5. From Equation 9.20c,

$$\alpha_2 = \frac{2R_3(e_1 + e_2)}{\alpha_1 L^2} = \frac{2 \times 8 \times (0.3 + 0.3)}{0.5 \times 16^2} = 0.075$$

The convex parabolic segments therefore extend for a distance  $\alpha_2 L = 1.2$  m at each end of the span, as shown.

The depth of the points of inflection (points C and E) below the tendon level at each support is obtained using Equation 9.18:

$$h_i = \frac{0.075}{0.5} (0.3 + 0.3) = 0.09 \text{ m}$$

The curvature of the concave parabolic segment CDE extending over the middle  $16 - (2 \times 1.2) = 13.6$  m of the span is given by Equation 9.20b:

$$\kappa_{p2} = \frac{2 \times (0.3 + 0.3 - 0.09)}{16^2 \times (0.5 - 0.075)^2} = 0.022 \text{ m}^{-1}$$

and the equivalent uniformly distributed *upward* load exerted by the concrete tendon is

$$w_{p2} = P \kappa_{p2} = 55.15 \text{ kN/m } \uparrow$$

The equivalent load  $w_{p2}$  acts over the middle 13.6 m of the span. The equivalent downward uniformly distributed load imposed at each end of the beam by the convex tendons AC and EB is

$$w_{p3} = P \kappa_{p3} = \frac{P}{R_3} = \frac{2500}{8} = 312.5 \text{ kN/m } \downarrow$$

The equivalent loads on the beam imposed by the tendon are shown in [Figure 9.15b](#). For this beam, the vertical component of prestress at each support is zero (since the slope of the tendon is zero) and the uniformly distributed loads are self-equilibrating.

The total moment diagram caused by prestress for this prismatic beam may be obtained by using the moment-area principles discussed in Equation 9.2, i.e. by translating the base line of the primary moment diagram ( $Pe$ ) so that the net area under the moment diagram is zero. Alternatively, the total moment diagram may be obtained by calculating the fixed-end moments caused by the equivalent distributed loads in [Figure 9.15b](#). The total moment diagram caused by prestress is shown in [Figure 9.15c](#). By subtracting the primary moments from the total moments, the linear secondary moment diagram shown in [Figure 9.15d](#) is obtained.



If an idealized tendon such as that shown in [Figure 9.11a](#) was used to model this more realistic profile (with  $e_A=e_B=0.3$  m and  $h=0.6$  m), the total moment at each end (see [Figure 9.11d](#)) is

$$\frac{2Ph}{3} = \frac{2 \times 2500 \times 0.6}{3} = 1000 \text{ kN m}$$

which is about 8% higher than the value shown in [Figure 9.15c](#).

9.3.5 Members with varying cross-sectional properties

The techniques presented for the analysis of continuous structures hold equally well for members with non-uniform section properties. Section properties may vary owing to haunching or changes in member depth (as illustrated in [Figures 9.1b, c, and e](#)), from varying web and flange thicknesses, or simply from cracking in regions of high moment.

Increasing the member depth by haunching is frequently used to increase

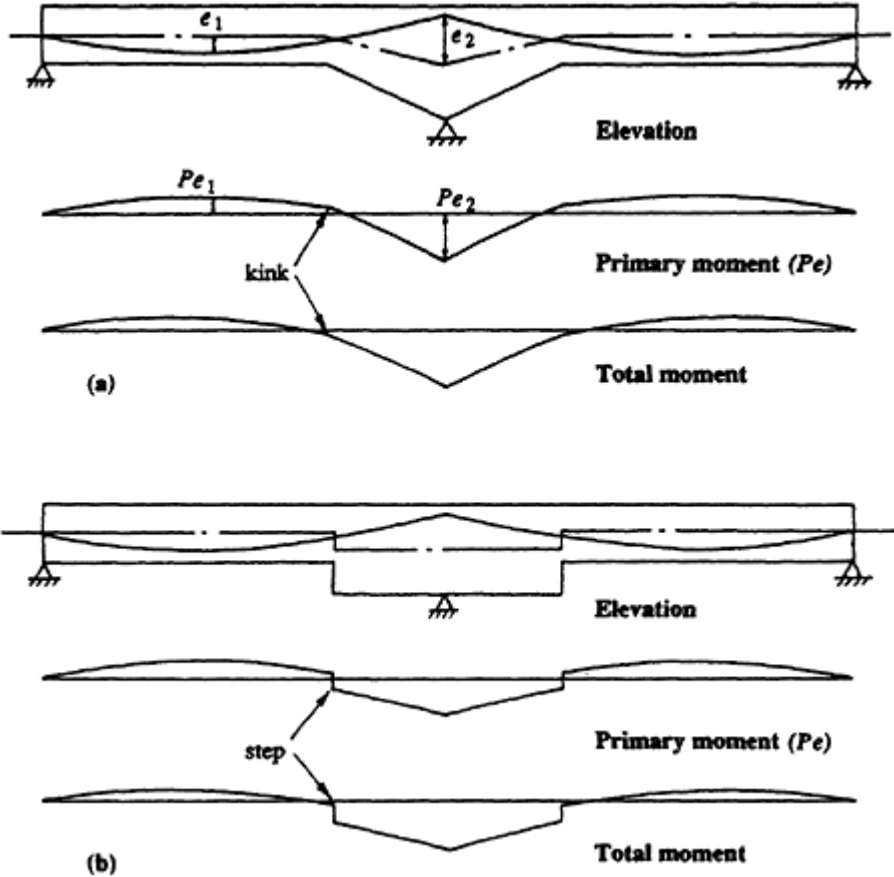


Figure 9.16 Moments induced by prestress in haunched members.

the tendon eccentricity in the peak moment regions at the interior supports. In such members, the position of the centroidal axis varies along the member. If the tendon profile is a smooth curve, and the centroidal axis suffers sharp changes in direction or abrupt steps (where the member depth changes suddenly), the total moment diagram caused by prestress also exhibits corresponding kinks or steps, as shown in [Figure 9.16](#).

To determine the fixed-end moments and carry-over factors for members with varying section properties and to calculate the member displacements, the principle of virtual work may be used. The internal work is readily calculated using Equation 9.3 by expressing the section properties ( $EI$  and  $EA$ ) as functions of position  $x$ . By dividing the structure into small segments, Equation 9.5 can be used in many practical problems to provide a close approximation of the volume integral for internal work in a non-prismatic member.

### 9.3.6 Effects of creep

When a statically indeterminate member is subjected to an imposed deformation, the resulting internal actions are proportional to the member stiffness. Since creep gradually reduces stiffness, the internal actions caused by an imposed deformation in a concrete structure decrease with time. Imposed deformations are caused by volume changes, such as shrinkage and temperature changes, and by support settlements or rotations. Under these deformations, the time-dependent restraining actions can be estimated using a reduced or effective modulus for concrete. The age-adjusted effective modulus defined in Equation 2.14 may be used to model adequately the effects of creep.

Provided the creep characteristics are uniform throughout a structure, creep does not cause redistribution of internal actions caused by imposed loads. The effect of creep in this case is similar to a gradual and uniform change in the elastic modulus. Deformations increase significantly, but internal actions are unaffected. When the creep characteristics are not uniform, redistribution of internal actions does occur with time. In real structures, the creep characteristics are rarely uniform throughout. Portions of a structure may be made of different materials or of concrete with different composition or age. The rate of change of curvature due to creep is dependent on the extent of cracking and the size and position of the bonded reinforcement. The creep characteristics are therefore not uniform if part of the structure has cracked or when the bonded reinforcement layout varies along the member. In general, internal actions are redistributed from the regions with the higher creep rate to the regions with the lower creep rate. Nevertheless, the creep induced redistribution of internal actions in indeterminate structures is generally relatively small.

Since prestress imposes equivalent loads on structures rather than fixed

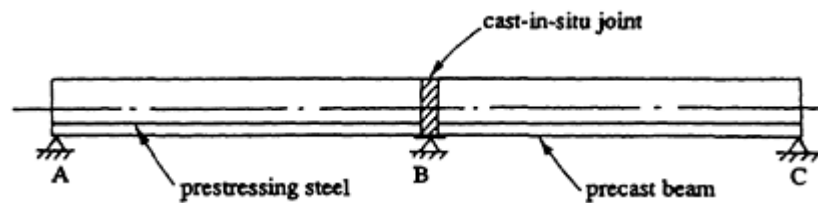


**Figure 9.17** Providing continuity at an internal support.

deformations, the internal actions caused by prestress are not significantly affected by creep. The internal actions are affected in so far as creep causes a reduction of the prestressing force of the order of 5–15%. Hyperstatic reactions induced by prestress in indeterminate structures are not therefore significantly relieved by creep.

If the structural system changes after the application of some of the prestress, creep may cause a change in the hyperstatic reactions. For example, the two-span beam shown in [Figure 9.17](#) is fabricated as two precast units of length  $L$  and joined together at the interior support by a cast *in situ* joint. Creep causes the gradual development of hyperstatic reactions with time and the resulting secondary moments and shears. After the *in situ* joint is constructed, the structure is essentially the same as that shown in [Figure 9.5a](#).

Before the joint in [Figure 9.17](#) is cast, the two precast units are simply supported, with zero deflection but some non-zero slope at the interior support. Immediately after the joint is made and continuity is established, the primary moment in the structure is the same as that shown in [Figure 9.5b](#), but the secondary moment at B (and elsewhere) is zero. With time, creep causes a gradual change in the curvature on each cross-section. If the support at B was released, the member would gradually deflect upward due to the creep induced hogging curvature associated with the primary moment,  $Pe$ . If it is assumed that the creep characteristics are uniform and that the prestressing force is constant throughout, the time-dependent upward deflection caused by prestress is obtained by multiplying the deflection given in Equation 9.8 by the creep coefficient:

$$v_B(t) = \frac{PeL^2}{2E_c I} \phi(t, \tau) \quad (9.21)$$

It is assumed here that the restraint offered to creep by the bonded reinforcement is insignificant (i.e. the parameter  $\alpha$  used in Equation 3.76 and defined in [Section 3.8.3](#) is taken as unity).

The short-term deflection at B caused by a unit value of the redundant force applied at the release B is given in Equation 9.9. Owing to creep, however, the redundant at B is gradually applied to the structure. It is therefore appropriate to use the age-adjusted effective modulus ( $\bar{E}_e$  given

in Equation 2.14) to determine the corresponding time-dependent deformations (elastic plus creep). Substituting  $\bar{E}_e$  for  $E$  in Equation 9.9 gives

$$f_B(t) = \frac{L^3 [1 + \chi\phi(t, \tau)]}{6E_e I} \quad (9.22)$$

To enforce the compatibility condition that the deflection at B is zero, Equation 9.10 gives

$$R_B(t) = -\frac{v_B(t)}{f_B(t)} = -\frac{3Pe}{L} \frac{\phi(t, \tau)}{1 + \chi\phi(t, \tau)} = R_B \frac{\phi(t, \tau)}{1 + \chi\phi(t, \tau)} \quad (9.23)$$

where  $R_B(t)$  is the creep induced hyperstatic reaction at B, and  $R_B$  is the hyperstatic reaction that would have developed at B if the structure was initially continuous and later prestressed with a straight tendon. The reaction  $R_B$  is shown in [Figure 9.5](#) and given in Equation 9.11. For typical long-term values of the creep and aging coefficient, say  $\phi(t, \tau) = 2.5$  and  $\chi=0.8$ , Equation 9.23 gives

$$R_B(t) = \frac{2.5}{1 + (0.8 \times 2.5)} = 0.833R_B$$

In general, if  $R$  is any hyperstatic reaction or the restrained internal action that would occur at a point due to prestress in a continuous member, and  $R(t)$  is the corresponding creep induced value if the member is made continuous only after the application of the prestress, then

$$R(t) = \frac{\phi(t, \tau)}{1 + \chi\phi(t, \tau)} R \quad (9.24)$$

If the creep characteristics are uniform throughout the structure, then Equation 9.24 may be applied to systems with any number of redundants.

Providing continuity at the interior supports of a series of simple precast beams not only restrains the time-dependent deformation caused by prestress, but also restrains the deformation due to the external loads. For all external loads applied after continuity has been established, the effects can be calculated by moment distribution or an equivalent method of analysis. Under the loads applied prior to casting the joints when the precast units are simply supported (such as self-weight), the moments at each interior support are initially zero. However, after the joint has been cast, the creep-induced deformation resulting from the self-weight moments in the spans is restrained and moments develop at the supports. For the beam shown in [Figure 9.5a](#), the moment at B due to self-weight is  $M_B = w_{sw}L^2/8$ . For the segmental beam shown in [Figure 9.17](#), it can be easily shown that the

restraining moment that develops at support B due to creep and self-weight is

$$M_B(t) = \frac{\phi(t, \tau)}{1 + \chi\phi(t, \tau)} M_B$$

### 9.4 Statically indeterminate frames

The procedures discussed for the analysis of continuous beams can be applied equally well to indeterminate frames. The equivalent load method is a convenient approach for the determination of primary and secondary moments in framed structures. In the treatment of continuous beams in the previous section, it was assumed that all members were free to undergo axial shortening. This is often not the case in real structures. When the horizontal member of a portal frame, for example, is prestressed, significant restraint to axial shortening may be provided by the flexural stiffness of the vertical columns. Moment distribution can be used to determine the internal actions that develop in the structure as a result of the axial restraint.

Consider the single-bay portal frame shown in [Figure 9.18a](#). Owing to the axial shortening of the girder BC, the top of each column moves laterally by an amount  $\Delta$ . The fixed-end moments induced in the structure are shown in [Figure 9.18b](#). If the girder BC was free to shorten (i.e. was unrestrained by the columns), the displacement  $\Delta$  that would occur immediately after the application of a prestressing force  $P$  to the girder is

$$\Delta = \frac{P}{E_c A_b} \frac{L_b}{2} \quad (9.25)$$

This value of  $\Delta$  is usually used as a starting point in the analysis. The fixed-end moments in the supporting columns due to a relative lateral end

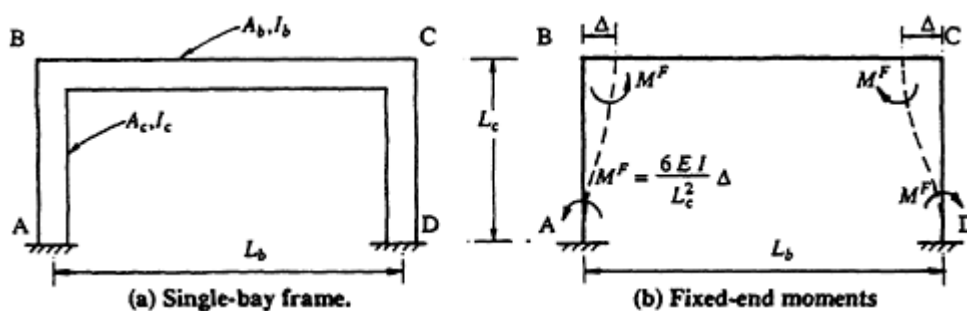


**Figure 9.18** Fixed-end moments in a fixed-base frame due to axial shortening of the girder.

displacement of  $\Delta$  are given by

$$M^F = \frac{6E_c I_c}{L_c^2} \Delta \quad (9.26)$$

and a moment distribution is performed to calculate the restraining actions produced by the fixed-end moments. If the base of the frame at A was pinned rather than fixed, the fixed end moment at B due to the displacement  $\Delta$  would be  $(3E_c I_c / L_c^2) \Delta$ . In addition to bending in the beam and in the columns, an outward horizontal reaction is induced at the base of each column and the girder BC is therefore subjected to tension. The tension in BC will reduce the assumed axial shortening, usually by a small amount. If the reduction in  $\Delta$  is significant, a second iteration could be performed using the reduced value for  $\Delta$  to obtain a revised estimate of the fixed-end moments and, hence, a more accurate estimate of the axial restraint.

The magnitude of the axial restraining actions depends on the relative stiffness of the columns and girder. The stiffer the columns, the greater is the restraint to axial shortening of the girder, and hence the larger is the reduction in prestress in the girder. On the other hand, slender columns offer less resistance to deformation and less restraint to the girder.

Axial shortening of the girder BC can also occur due to creep and shrinkage. A time analysis to include these effects can be made by using the age-adjusted effective modulus for concrete, instead of the elastic modulus, to model the gradually applied restraining actions caused by creep and shrinkage.

The internal actions that arise in a prestressed structure as a result of the restraint of axial deformation are sometimes called *tertiary effects*. These effects are added to the primary and secondary effects (calculated using the equivalent load method) to obtain the total effect of prestress in a framed structure.

#### Example 9.4

Consider the single bay, fixed-base portal frame shown in [Figure 9.19a](#). The vertical columns AB and ED are prestressed with a straight tendon profile, while the horizontal girder BD is post-tensioned with a parabolic profile, as shown. The girder BD has a rectangular cross-section 1200 mm by 450 mm and the column dimensions are 900 mm by 450 mm. The girder carries a uniformly distributed live load of 10 kN/m, a superimposed dead load of 5 kN/m, and the self-weight of the girder is 13 kN/m. If  $E_c = 30\,000$  MPa, the moments caused by the total uniformly distributed load on the girder (live load+dead load+self-weight=28 kN/m) are calculated using moment distribution and are shown in [Figure 9.19b](#).

By satisfying the serviceability requirements (as discussed in [Chapter 3](#)),

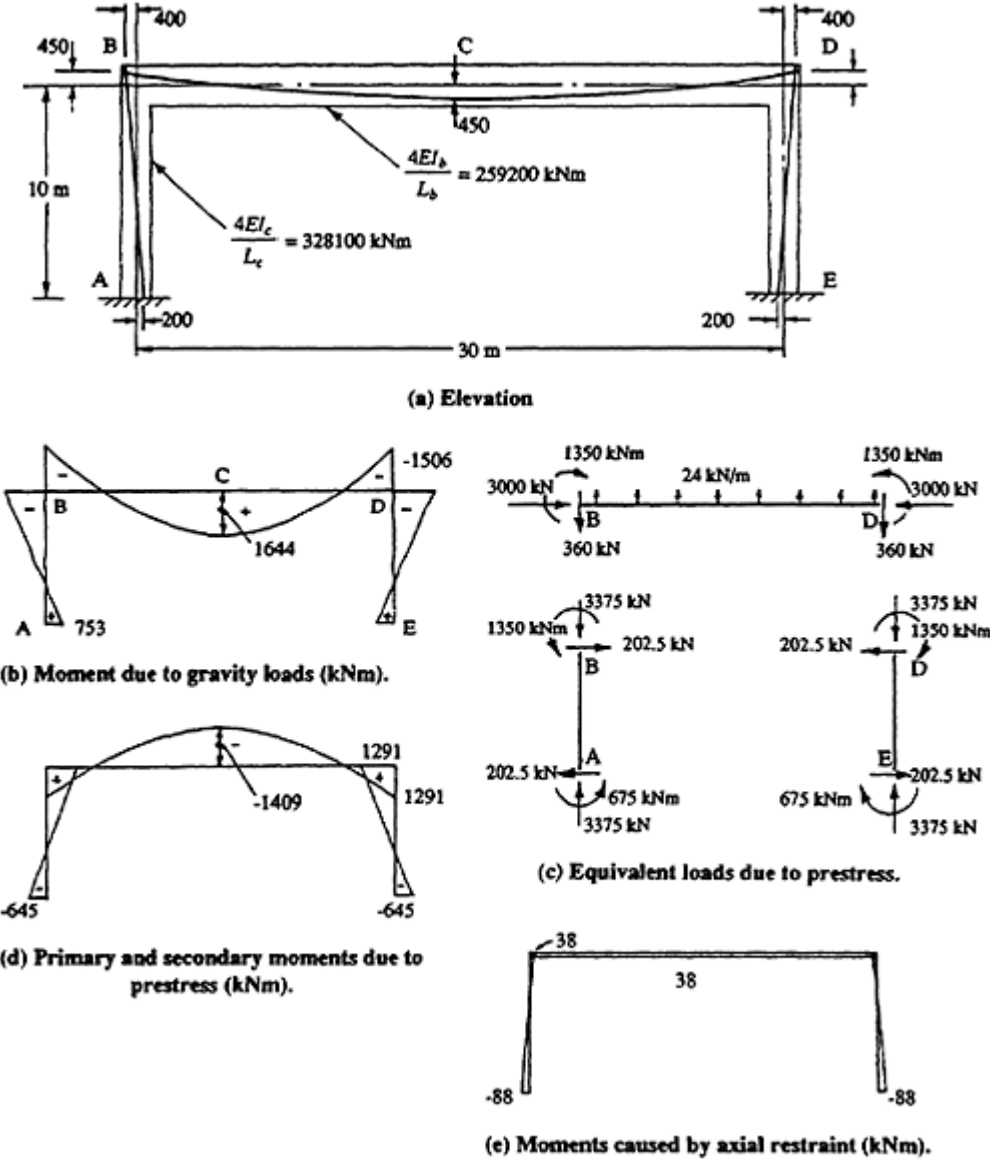


Figure 9.19 Actions in fixed-base portal frame of Example 9.4.

an estimate of the prestressing force and the tendon profile can be made for both the girder BD and the columns. For the girder, the tendon profile shown in Figure 9.19a is selected and the effective prestress  $P_{e,BD}$  required to balance the self-weight plus dead load is determined:

$$P_{e,BD} = \frac{18 \times 30^2}{8 \times 0.9} = 2250 \text{ kN}$$

If the time-dependent losses are taken as 25%, the average prestressing force in the girder immediately after transfer is  $P_{i,BD}=3000$  kN.

To determine the effective prestress in the columns, the primary moments in the girder and in the columns at the corner connections B and D are taken to be the same. If the eccentricity in the column at B (at the centroidal axis of the girder) is 400 mm, as shown in [Figure 9.19a](#), then

$$0.4P_{e,AB} = 0.45P_{e,BD}$$

Therefore

$$P_{e,AB} = \frac{2250 \times 0.45}{0.4} = 2531 \text{ kN}$$

The time-dependent losses in the columns are also taken as 25% and the prestressing force immediately after transfer is therefore  $P_{i,AB}=3375$  kN.

The equivalent load method and moment distribution are used here to calculate the primary and secondary moments caused by prestress. The equivalent loads imposed by the tendon on the concrete members immediately after prestressing are shown in [Figure 9.19c](#). The fixed-end moment caused by prestress at each end of span BD is obtained using the results of the fixed-end beam analysed in [Example 9.2](#), case (a) (and illustrated in [Figure 9.11](#)) and is given by

$$M_{BD}^F = \frac{2}{3} P_{i,BD} h_{BD} = \frac{2}{3} \times 3000 \times 0.9 = 1800 \text{ kN}$$

The fixed-end moments in the vertical columns due to the straight tendon profile are zero, as was determined for the fixed-end beam analysed in [Example 9.2](#), case (b). From a moment distribution, the primary and secondary moments caused by prestress are calculated and are illustrated in [Figure 9.19d](#).

To calculate the tertiary effect of axial restraint, the axial shortening of BD immediately after prestressing is estimated using Equation 9.25:

$$\Delta = \frac{3000 \times 10^3}{30\,000 \times 1200 \times 450} \times \frac{30\,000}{2} = 2.78 \text{ mm}$$

The fixed-end moment in the columns is obtained from Equation 9.26 and is given by

$$M^F = \frac{6 \times 30\,000 \times 900^3 \times 450}{10\,000^2 \times 12} \times 2.78 \times 10^{-6} = 137 \text{ kNm}$$

Moment distribution produces the tertiary moments shown in [Figure 9.19e](#). The restraining tensile axial force induced in the girder BD is only 12.6 kN and, compared with the initial prestress, is insignificant in this case.



## 9.5 Design of continuous beams

### 9.5.1 General

The design procedures outlined in [Chapter 8](#) for statically determinate beams can be extended readily to cover the design of indeterminate beams. The selection of tendon profile and magnitude of prestress in a continuous beam is based on serviceability considerations, as is the case for determinate beams. Load balancing is a commonly used technique for making an initial estimate of the level of prestress required to control deflections. The design of individual cross-sections for bending and shear strength, the estimation of losses of prestress, and the design of the anchorage zones are the same for all types of beams, irrespective of the number of redundants.

In continuous beams, the satisfaction of concrete stress limits for crack control must involve consideration of both the primary and secondary moments caused by prestress. Concrete stresses resulting from prestress should be calculated using the pressure line, rather than the tendon profile, as the position of the resultant prestress in the concrete.

Because of the relatively large number of dependent and related variables, the design of continuous beams tends to be more iterative than the design of simple beams, and more dependent on the experience and engineering judgement of the designer. A thorough understanding of the behaviour of continuous prestressed beams and a knowledge of the implications of each design decision is of great benefit.

### 9.5.2 The service load range—before cracking

Prior to cracking, the behaviour of a continuous beam is essentially linear and the principle of superposition can be used in the analysis. This means that the internal actions and deformations caused by prestress and those caused by the external loads can be calculated separately using linear analyses and the combined effects obtained by simple summation.

Just as for simple beams, a designer must ensure that a continuous beam is serviceable at the two critical loading stages, immediately after transfer (when the prestress is at its maximum and the applied service loads are small) and under the full loads after all losses have taken place (when the prestress is at a minimum and the applied loads are at a maximum).

In order to obtain a good estimate of the in-service behaviour, the prestressing force must be accurately known at each cross-section. This involves a reliable estimate of losses, both short and long-term. It is also important to know the load at which flexural cracking is likely to occur. In [Section 3.6.2](#), it was observed that creep and shrinkage gradually relieve the concrete of prestress and transfer the resultant compression from the concrete to the bonded reinforcement. To make reliable estimates of the

cracking moment at a particular cross-section, therefore, involves consideration of the time-dependent effects of creep and shrinkage.

Prior to cracking, load balancing can be used in design to establish a suitable effective prestressing force and tendon profile. The concept of load balancing was introduced in [Section 1.5.3](#) and involves balancing a preselected portion of the applied load (and self-weight) with the transverse equivalent load imposed on the beam by the draped tendons. Under the balanced load,  $w_b$ , the curvature on each cross-section is zero, the beam does not therefore deflect, and each cross-section is subjected only to the longitudinal axial prestress applied at the anchorages.

By selecting a parabolic tendon profile with the drape,  $h$ , as large as cover requirements permit, the minimum prestressing force required to balance  $w_b$  is calculated from

$$P = \frac{w_b L^2}{8h} \quad (9.27)$$

This equation is a rearrangement of Equation 1.7. In order to control the final deflection of a continuous beam, the balanced load  $w_b$  is often taken to be the sustained or permanent load (or some large percentage of it).

Because of its simplicity, load balancing is probably the most popular approach for determining the prestressing force in a continuous member. Control of deflection is an obvious attraction. However, load balancing does not guard against cracking caused by the unbalanced loads and it does not ensure that individual cross-sections possess adequate strength. If the balanced load is small, and hence the prestressing force and prestressing steel quantities are also small, significant quantities of non-prestressed steel may be required to increase the strength of the critical cross-sections and to limit crack widths under the full service loads.

At service loads prior to cracking, the concrete stresses on any cross-section of a continuous beam can be calculated easily by considering only the unbalanced load and the longitudinal prestress. The transverse loads imposed on the beam by the draped tendons have been effectively cancelled by  $w_b$ . The total moment diagram due to prestress (primary+secondary moments) is equal and opposite to the moment diagram caused by  $w_b$ . The primary and secondary moments induced by prestress need not, therefore, enter into the calculations and there is no need to calculate the hyperstatic reactions at this stage (at least for the determination of concrete stresses). In [Example 9.5](#), the load balancing approach is applied to a two-span continuous member.

In the discussion to this point, the prestressing force has been assumed to be constant throughout the member. In long members, friction losses may be significant and the assumption of constant prestress may lead to serious errors. To account for variations in the prestressing force with

distance from the anchorage, a continuous member may be divided into segments. Within each segment, the prestressing force may be assumed constant and equal to its value at the mid-point of the segment. In many cases, it may be acceptable to adopt each individual span as a segment of constant prestress. In other cases, it may be necessary to choose smaller segments to model the effects of prestress more accurately.

It is possible, although rarely necessary, to calculate the equivalent loads due to a continuously varying prestressing force. With the shape of the tendon profile throughout the member and the variation of prestress due to friction and draw-in determined previously, the transverse equivalent load at any point is equal to the curvature of the tendon (obtained by differentiating the equation for the tendon shape twice) times the prestressing force at that point. The effect of prestress due to these non-uniform equivalent transverse loads can then be determined using the same procedures as for uniform loads.

### Example 9.5 — Load balancing

The idealized parabolic tendons in the two-span beam shown in [Figure 9.20](#) are required to balance a uniformly distributed gravity load of 20 kN/m. The beam cross-section is rectangular, 800 mm deep and 300 mm wide. The concrete stress distribution on the cross-section at B over the interior support when the total uniformly distributed gravity load is 25 kN/m is required. Assume that the prestressing force is constant throughout.

In span AB, the tendon sag is  $h_{AB}=325+(0.5\times 325)=487.5$  mm and the required prestressing force is obtained from Equation 9.27:

$$P = \frac{20 \times 16^2}{8 \times 0.4875} = 1313 \text{ kN}$$

If  $P$  is constant throughout, the required sag in BC may also be obtained from Equation 9.27:

$$h_{BC} = \frac{20 \times 14^2}{8 \times 1313} = 0.373 \text{ m} = 373 \text{ mm}$$

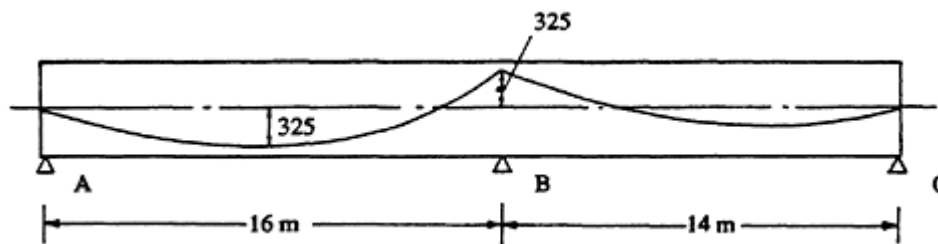


Figure 9.20 Two-span beam of [Example 9.5](#).

and the eccentricity of the tendon at the mid-point of the span BC is equal to  $373 - (0.5 \times 325) = 210.5$  mm (below the centroidal axis).

Under the balanced load of 20 kN/m, the beam is subjected only to the axial prestress applied at each anchorage. The concrete stress on every cross-section is uniform and equal to

$$\sigma = -\frac{P}{A} = -\frac{1313 \times 10^3}{800 \times 300} = -5.47 \text{ MPa}$$

Owing to the uniformly distributed unbalanced load of 5 kN/m, the moment at B is  $-142.5$  kNm (obtained by moment distribution or an equivalent method of analysis). The extreme fibre concrete stresses at B caused by the unbalanced moment are

$$\sigma = \frac{M}{Z} = \pm \frac{142.5 \times 10^6 \times 6}{800^2 \times 300} = \pm 4.45 \text{ MPa}$$

The resultant extreme fibre stresses at B caused by prestress and the applied load of 25 kN/m are therefore:

in the top:  $\sigma_t = -5.47 + 4.45 = -1.02 \text{ MPa}$

in the bottom:  $\sigma_b = -5.47 - 4.45 = -9.92 \text{ MPa}$

The reader may wish to check that the same result is obtained if the total stresses caused by the equivalent loads (longitudinal plus transverse forces imposed by prestress) are added to the stresses caused by a uniformly distributed gravity load of 25 kN/m.

### 9.5.3 The service load range—after cracking

When the balanced load is relatively small, the unbalanced load may cause cracking in the peak moment regions over the interior supports and at mid-span. When cracking occurs, the stiffness of the member is reduced in the vicinity of the cracks. The change in relative stiffness between the positive and negative moment regions causes a redistribution of bending moments. In prestressed members, the reduction of stiffness caused by cracking in a particular region is not as great as in an equivalent reinforced concrete member and the redistribution of bending moments at service loads can usually be ignored. It is therefore usual to calculate beam moments using a linear analysis both before and after cracking.

The effect of cracking should not be ignored, however, when calculating the deflection of the member. A cracked section analysis (see [Section 3.5.2](#)) can be used to determine the effective moment of inertia of the cracked

section (see [Section 3.8.2](#)) and the corresponding initial curvature. After calculating the initial curvature at each end and at the mid-point of a span, the short-term deflection may be obtained using Equation 3.68c.

Under the sustained loads, the extent of cracking is usually not great. In many partially prestressed members, the cracks over the interior supports (caused by the peak loads) are completely closed for most of the life of the member. The time-dependent change in curvature caused by creep, shrinkage, and relaxation at each support and at mid-span can be calculated using the time analysis of [Section 3.6.2](#) (or [Section 3.6.3](#) if the cracks remain open under the permanent loads). With the final curvature determined at the critical sections, the long-term deflection can also be calculated using Equation 3.68c.

Alternatively, long-term deflections may be estimated from the short-term deflections using the approximate expressions outlined in [Section 3.8.3](#).

The control of flexural cracking in partially prestressed beams is easily achieved by suitably detailing the bonded reinforcement in the cracked region. According to AS 3600–1988, crack widths may be considered to be satisfactory for interior exposure conditions provided the change in stress in the bonded tensile steel is less than 200 MPa as the load is increased from its value when the extreme concrete tensile fibre is at zero stress to the full service load. The change in tensile steel stress may be calculated in a cracked section analysis. In addition, the centre-to-centre spacing of the bonded steel should be less than 200 mm.

#### *9.5.4 The overload range and ultimate strength in bending*

##### **Behaviour**

The behaviour of a continuous beam in the overload range depends on the ductility of the cross-sections in the regions of maximum moment. If the cross-sections are ductile, the moment curvature relationships are similar to that shown in [Figure 9.21](#).

Consider the propped cantilever shown in [Figure 9.22a](#). Each cross-section is assumed to possess a ductile moment–curvature relationship. At service loads, bending moments in the beam, even in the post-cracking range, may be approximated reasonably using elastic analysis. The negative elastic moment at A caused by the uniformly distributed load  $w$  is  $wL^2/8$ . When the load  $w$  causes yielding of the reinforcement on the cross-section at A, a sudden loss of stiffness occurs (as illustrated by the kinks in the moment–curvature relationship in [Figure 9.21](#)). Any further increase in load will cause large increases in curvature at A, but only small increases in moment. A constant-moment (plastic) hinge develops at A as the moment capacity is all but exhausted and the curvature becomes large. In

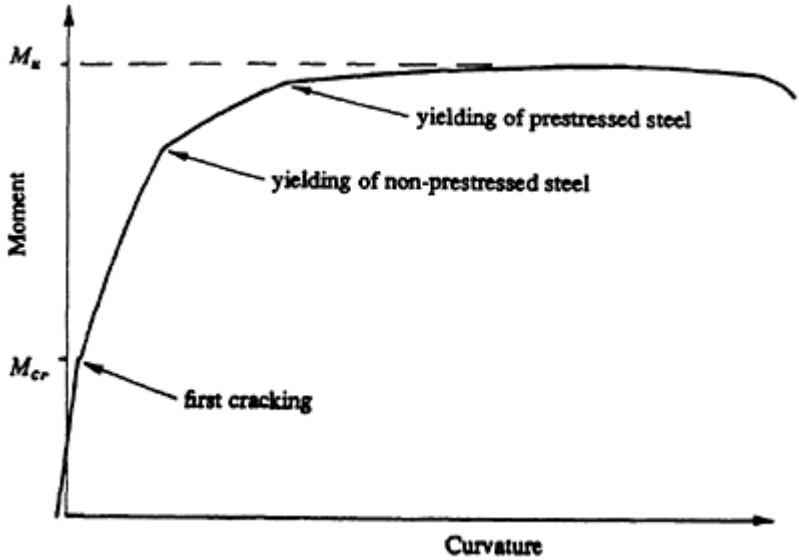


Figure 9.21 Moment-curvature relationship for a ductile partially prestressed cross-section.

reality, the moment at the hinge is not constant, but the rate of increase in moment with curvature in the post-yield range is very small. As loading increases and the moment at the support A remains constant or nearly so, the moment at mid-span increases until it too reaches its ultimate value,  $M_u$ , and a second plastic hinge develops. The formation of two constant-moment hinges reduces a one-fold indeterminate structure to a mechanism and collapse occurs. If an elastic-perfectly plastic moment-curvature relationship is assumed with the same moment capacity  $M_u$  at both hinge locations, the moment diagrams associated with the formation of the first and second hinges are as shown in Figure 9.22b. The ductility at A results in an increase in load-carrying capacity of 46% above the load required to cause the first hinge to form.

Plastic analysis techniques can therefore be used to estimate the collapse

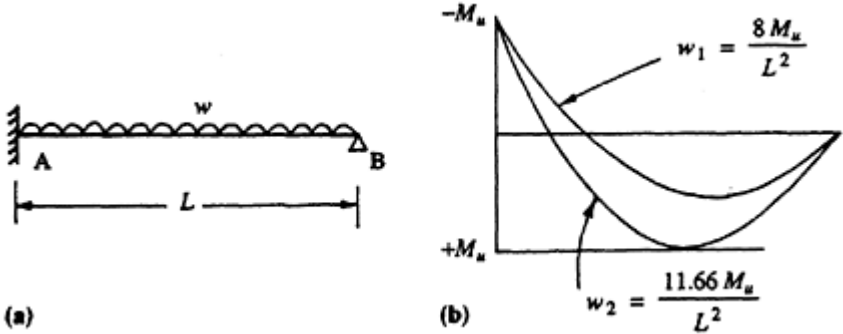


Figure 9.22 Moment redistribution in a propped cantilever.

load of a continuous prestressed beam, provided the critical cross-sections are ductile, i.e. provided the moment–curvature relationships can be assumed to be elastic–plastic and the critical cross-sections possess the necessary rotational capacity.

By subdividing a member into small segments and calculating the moment–curvature relationship for each segment, an incremental analysis may be used to calculate the collapse load more accurately.

### Permissible moment redistribution at ultimate

For the design of prestressed concrete continuous structures, collapse load methods are either not recommended or not mentioned in many building codes. In general, a lower bound ultimate strength approach is specified in which the design moment,  $M^*$ , on every cross-section must be less than the design strength,  $\phi M_u$ . Design moments are calculated using elastic analysis and gross member stiffnesses (and are therefore very approximate). To account for the beneficial effects of moment redistribution, building codes generally permit the peak elastic moments at the supports of a continuous beam to be reduced provided the cross-section is ductile. A reduction in the magnitudes of the negative moments at the ends of a span must be associated with an increase in the positive span moment in order to maintain equilibrium. AS 3600–1988, for example, allows the negative moment at an interior support to be modified by a maximum amount ( $\lambda_m$  in percent) which depends on the neutral axis parameter  $k_u = d_n/d$ :

$\lambda_m = 30$	when	$k_u \leq 0.2$
$\lambda_m = 75(0.4 - k_u)$	when	$0.2 < k_u \leq 0.4$
$\lambda_m = 0$	when	$k_u > 0.4$

With a different rectangular compressive stress block at ultimate, BS 8110 (1985) permits

$\lambda_m = 20$	when	$k_u \leq 0.3$
$\lambda_m = 50 - 100k_u$	when	$0.3 < k_u \leq 0.5$

The redistribution permitted by ACI 318–83 depends on the reinforcement index,  $q$ , where

$$q = \frac{A_p f_p}{b d_p f'_c} + \frac{A_s f_y}{b d f'_c} - \frac{A_{sc} f_y}{b d f'_c}$$

As  $q$  increases, the ductility of the cross-section decreases. According to

ACI 318–83,

$$\lambda_m = 20 \left( 1 - \frac{q}{0.36\gamma} \right) \quad \text{provided } q \leq 0.24\gamma$$

where  $\gamma$  is defined in Equation 4.2 (and given the symbol  $\beta_1$  in ACI 318–83).

### Secondary effects at ultimate

Both AS 3600–1988 and ACI 318–83 require that the design moment,  $M^*$ , be calculated as the sum of the moments caused by the factored design load combination (dead, live, etc., as outlined in [Section 1.7.3](#)) and the moments resulting from the hyperstatic reactions caused by prestress (with a load factor of 1.0).

Earlier in this chapter, the hyperstatic reactions and the resulting secondary moments were calculated using linear-elastic analysis. Primary moments, secondary moments, and the moments caused by the applied loads were calculated separately and summed to obtain the combined effect. Superposition is only applicable, however, when the member behaviour is linear. At overloads, behaviour is highly non-linear and it is not possible to distinguish between the moments caused by the applied loads and those caused by the hyperstatic reactions. Consider the ductile propped cantilever in [Figure 9.22](#). After the formation of the first plastic hinge at A, the beam becomes determinate for all subsequent load increments. With no rotational restraint at A, the magnitude of the secondary moment is not at all clear. The total moment and shears can only be determined using a refined analysis that accurately takes into account the various sources of material non-linearity. It is meaningless to try to subdivide the total moments into individual components. The treatment of secondary moments at ultimate has been studied by Lin & Thornton (1972), Mattock (1972), Nilson (1978), Warner & Faulkes (1983), and others.

Provided that the structure is ductile and moment redistribution occurs as the collapse load is approached, secondary moments can be ignored in ultimate strength calculations. After all, the inclusion of an uncertain estimate of the secondary moment generally amounts to nothing more than an increase in the support moments and a decrease in the span moment or vice versa, i.e. a redistribution of moments. Since the moments due to the factored loads at ultimate are calculated using elastic analysis, there is no guarantee that the inclusion of the secondary moments (also calculated using gross stiffnesses) will provide better agreement with the actual moments in the structure after moment redistribution (as may be calculated using a refined non-linear analysis).

On the other hand, if the critical section at an interior support is non-ductile, the situation is not so cut and dried. It is usually possible to avoid



non-ductile sections by the inclusion of sufficient quantities of compressive reinforcement. If non-ductile sections cannot be avoided, it is recommended that secondary moments (calculated using linear elastic analysis and gross stiffnesses) be considered at ultimate. Where the secondary moment at an interior support has the same sign as the moment caused by the applied loads, it is conservative to include the secondary moment (with a load factor of 1.0) in the calculation of the design moment  $M^*$ . Where the secondary moment is of opposite sign to the moment caused by the applied loads, it is conservative to ignore its effect.

9.5.5 Steps in design

A suitable design sequence for a continuous prestressed concrete member is as follows:

- (1) Determine the loads on the beam both at transfer and under the most severe load combination for the serviceability limit states. Using approximate analysis techniques, estimate the maximum design moments at the critical sections in order to make an initial selection of cross-section size and self-weight. The moment and deflection coefficients given in [Figure 9.23](#) may prove useful.

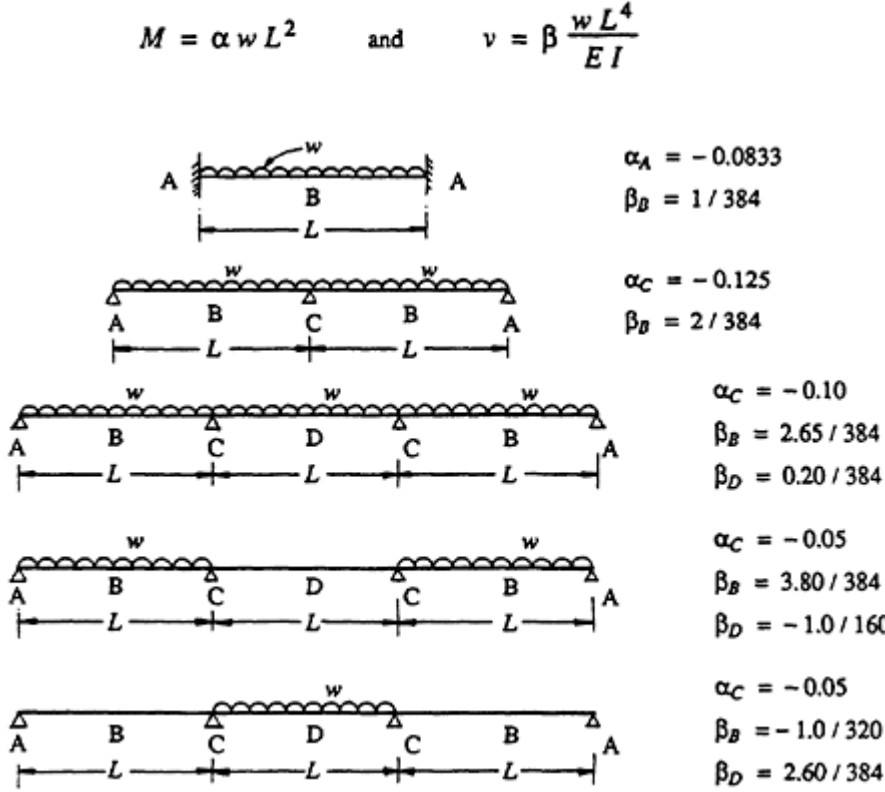


Figure 9.23 Moment and deflection coefficients for equal span elastic beams.

Determine appropriate cross-section sizes at the critical sections. The discussion in [Section 8.3](#) is relevant here. Equation 8.11 may be used to obtain cross-sectional dimensions that are suitable from the point of view of flexural strength and ductility. By estimating the maximum unbalanced load, the sustained part of the unbalanced load and by specifying a maximum deflection limit for the structure, a minimum moment of inertia may be selected from Equation 8.5 (if the member is to be crack free) or Equation 8.6 (if cracking is permitted). If a fully prestressed beam is required, Equation 8.1 can be used to determine the minimum section modulus at each critical section. For continuous beams in *normal* situations, the span to depth ratio is usually in the range 24–30, but this depends on the load level and the type of cross-section.

- (2) Determine the bending moment and shear force envelopes both at transfer and under the full service loads. These envelopes should include the effects of self-weight, superimposed permanent dead and live loads, and the maximum and minimum values caused by transient loads. Where they are significant, pattern loadings such as those shown in [Figure 9.23](#) should be considered. For example, the minimum moment at the mid-point of a particular span may not be due to dead load only, but may result when the transient live load occurs only on adjacent spans. Consideration of pattern loading is most important in structures supporting large transient live loads.
- (3) Determine trial values for the prestressing force and tendon profile. Use idealized tendon profiles that follow the shape of the bending moment diagram caused by the anticipated balanced loads (or as near to it as is practical). In each span, make the tendon drape as large as possible in order to minimize the required prestress.

If a fully prestressed beam is required, the trial prestress and eccentricity at each critical section can be determined using a Magnel diagram and the procedure outlined in [Section 3.3.1](#). At this stage, it is necessary to assume that the tendon profile is concordant. If load balancing is used, the maximum available eccentricity is generally selected at mid-span and over each interior support and the prestress required to balance a selected portion of the applied load ( $w_b$ ) is calculated using Equation 9.27. The balanced load selected in the initial stages of design may need to be adjusted later when serviceability and strength checks are made.

Determine the number and size of tendons and the appropriate duct diameter(s).

- (4) Replace the kink in the idealized tendon profile at each interior support with a short convex parabolic segment as discussed in [Section 9.3.4](#). Determine the equivalent loads due to prestress and using

moment distribution (or an equivalent method of analysis) determine the total moment caused by prestress at transfer and after the assumed time-dependent losses. By subtracting the primary moments from the total moments, calculate the secondary moment diagram and, from statics, determine the hyperstatic reactions at each support.

- (5) Concrete stresses at any cross-section caused by prestress (including both primary and secondary effects) and the applied loads may now be checked at transfer and after all losses. If the beam is fully prestressed, the trial estimate of prestress made in step 3 was based on the assumption of a concordant tendon profile and secondary moments were ignored. If secondary moments are significant, stresses calculated here may not be within acceptable limits and a variation of either the prestressing force or the eccentricity may be required.
- (6) Calculate the losses of prestress and check the assumptions made earlier.
- (7) Check the ultimate strength in bending at each critical section. If necessary, additional non-prestressed tensile reinforcement may be used to increase strength. Add compressive reinforcement to improve ductility, if required. Some moment redistribution at ultimate may be permissible to reduce peak negative moments at interior supports, provided that the cross-sections at the supports have adequate ductility.
- (8) Check the deflection at transfer and the final long-term deflection. For partially prestressed designs, check crack control in regions of peak moment. Consider the inclusion of non-prestressed steel to reduce time-dependent deformations, if necessary. Adjust the section size or the prestress level (or both), if the calculated deflection is excessive.
- (9) Check shear strength of beam (and torsional strength if applicable) in accordance with the provisions outlined in [Chapter 5](#). Design suitable shear reinforcement where required.
- (10) Design the anchorage zone using the procedures presented in [Chapter 6](#).

*Note:* Durability and fire protection requirements are usually satisfied by an appropriate choice of concrete strength and cover to the tendons in step 3.

### Example 9.6

The four-span beam shown in [Figure 9.24](#) is to be designed. The beam has a uniform I-shaped cross-section and carries a uniformly distributed dead load of 25 kN/m (not including self-weight) and a transient live load

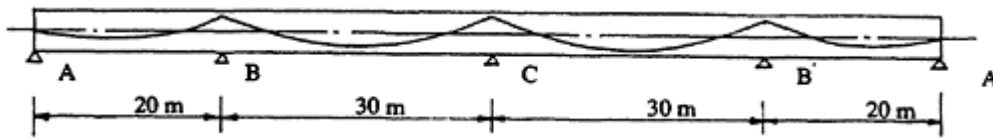


Figure 9.24 Elevation of beam of [Example 9.6](#).

of 20 kN/m. Controlled cracking is to be permitted at peak loads. The beam is prestressed by jacking simultaneously from each end, thereby maintaining symmetry of the prestressing force about the central support C and avoiding excessive friction losses. Take  $f'_c = 40$  MPa and  $f'_{ci} = 30$  MPa.

- (1) (and 2) The bending moments caused by the applied loads must first be determined. Because the beam is symmetrical about the central support at C, the bending moment envelopes can be constructed from the moment diagrams shown in [Figure 9.25](#) caused by the distributed load patterns shown. These moment diagrams were calculated for a unit distributed load (1 kN/m) using moment distribution.

If the self-weight is estimated at 15 kN/m, the total dead load is 40 kN/m, and the AS 3600–1988 load factors for the strength limit state ([Section 1.7.3](#)) are adopted, the factored design loads are

$$w_G^* = 1.25 \times 40 = 50 \text{ kN/m} \quad \text{and} \quad w_Q^* = 1.5 \times 20 = 30 \text{ kN/m}$$

The maximum design moment  $M^*$  occurs over the support C, when the transient live load is on only the adjacent spans BC and CB'. Therefore, using the moment coefficients in [Figure 9.25](#),

$$M^* = 80.9 \times 50 + [(46.3 + 46.3) \times 30] = 6823 \text{ kN m}$$

The overall dimensions of the cross-section are estimated using Equation 8.11 (which is valid provided the compressive stress block at ultimate is within the flange of the I-section):

$$bd^2 \geq \frac{6823 \times 10^6}{0.17 \times 0.8 \times 40} = 1254 \times 10^6 \text{ mm}^3$$

Try  $b=750$  mm,  $d=1290$  mm and  $D=1400$  mm.

The span-to-depth ratio for the interior span is 21.4 which should prove acceptable from a serviceability point of view.

To obtain a trial flange thickness, find the depth of the compressive stress block at ultimate. If the volume of the stress block is  $C = 0.85f'_c\gamma dnb$  and the lever arm between C and the resultant tension

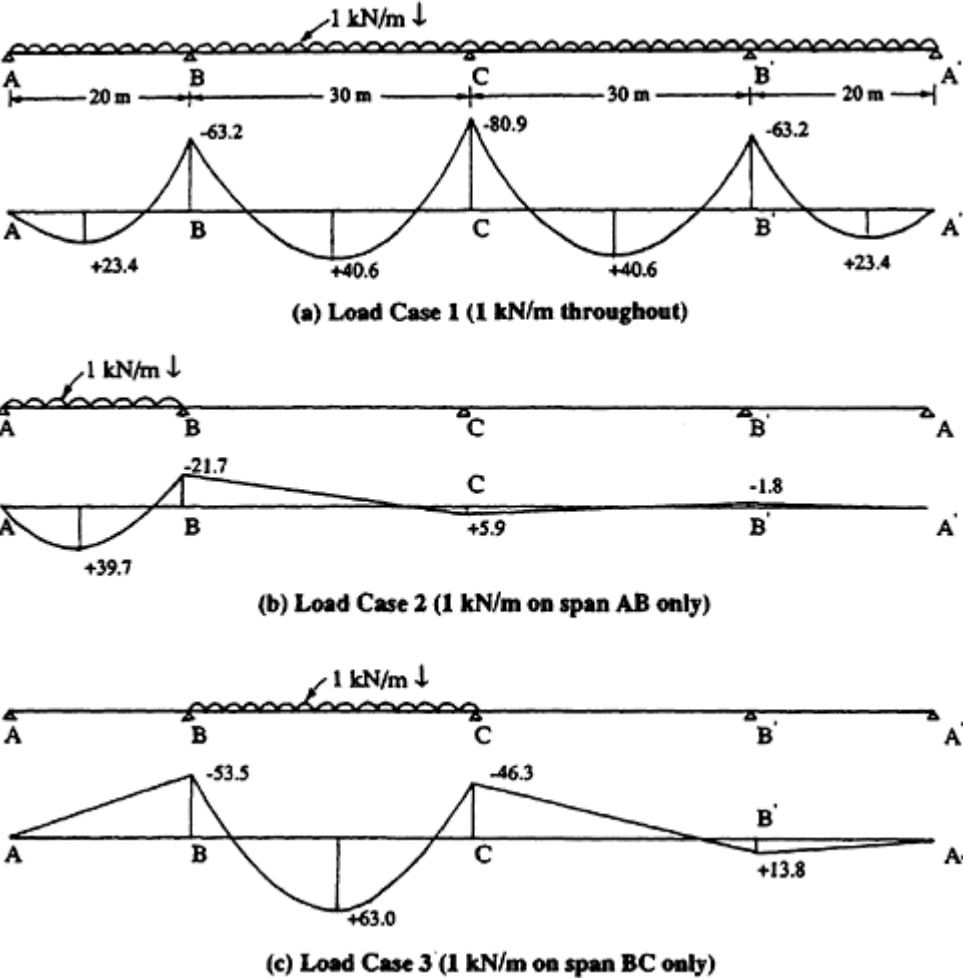


Figure 9.25 Bending moment diagrams due to unit distributed loads (Example 9.6).

is taken to be  $0.85d$ , then

$$\gamma d_n = \frac{M^*}{\phi \times 0.85 \times d \times 0.85 \times f'_c b} = \frac{6823 \times 10^6}{0.8 \times 0.85 \times 1290 \times 0.85 \times 40 \times 750}$$

$$= 305 \text{ mm}$$

Adopt a tapering flange 250 mm thick at the tip and 350 mm thick at the web. To ensure that the web width is adequate for shear, it is necessary to ensure that web crushing does not occur. If the vertical component of the prestressing force,  $P_v$ , is ignored, then Equation 5.7 gives

$$V^* \leq \phi V_{u,max} = \phi \times 0.2 f'_c b_v d_o$$

and therefore

$$b_v \geq \frac{7.2V^*}{f'_c d_o}$$

The maximum shear force  $V^*$  also occurs adjacent to support C when live load is applied to span BC and CB' and is equal to 1180 kN. Therefore,

$$b_v \geq \frac{7.2 \times 1180 \times 10^3}{40 \times 1340} = 158 \text{ mm}$$

It is advisable to select a web width significantly greater than this minimum value in order to avoid unnecessarily large quantities of transverse steel and the resulting steel congestion. Duct widths of about 100 mm are anticipated, with only one duct in any horizontal plane through the web. With these considerations, the web width is taken to be

$$b_w = b_v + \frac{1}{2} d_d = 300 \text{ mm}$$

The trial cross-section and section properties are shown in [Figure 9.26](#). The self-weight is actually  $24 \times 0.69 = 16.6 \text{ kN/m}$ , which is 10% higher than originally assumed. The revised value of  $M^*$  is 6985 kNm.

- (3) If 100 mm ducts are assumed (side by side in the flanges) and 40 mm cover to the reinforcement, the maximum eccentricity over an interior

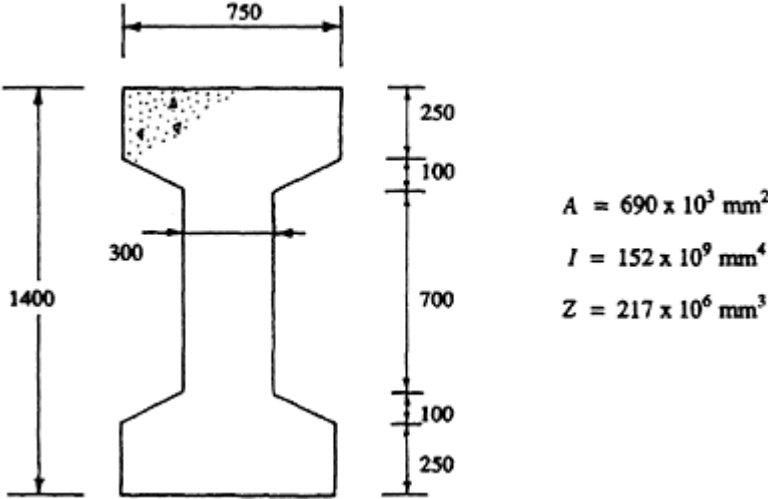


Figure 9.26 Trial section dimensions and properties.

support and at mid-span is

$$e_{max} = 700 - 40 - 12 - \left(\frac{2}{3} \times 100\right) = 580 \text{ mm}$$

The maximum drape in the spans BC and CB' is therefore

$$(h_{BC})_{max} = 2e_{max} = 1160 \text{ mm}$$

The balanced load is taken to be 32 kN/m (which is equal to self-weight plus about 60% of the additional dead load). From Equation 9.27, the required average effective prestress in span BC is

$$(P_e)_{BC} = \frac{32 \times 30^2}{8 \times 1.16} = 3103 \text{ kN}$$

If the friction loss between the mid-point of span BC and the mid-point of AB is guessed at 15%, then

$$(P_e)_{AB} = \frac{3103}{0.85} = 3650 \text{ kN}$$

and the required drape in span AB is

$$h_{AB} = \frac{32 \times 20^2}{8 \times 3650} = 0.438 \text{ m} = 438 \text{ mm}$$

The required eccentricity at mid-span is therefore

$$e_{AB} = 438 - \frac{580}{2} = 148 \text{ mm}$$

The idealized tendon profiles for spans AB and BC are shown in [Figure 9.27](#), together with the corresponding tendon slopes and friction losses (calculated from Equation 3.60, with  $\mu=0.2$  and  $\beta_p=0.01$ ). The friction losses at the midspan of BC are 17.3%, and if the time-dependent losses in BC are assumed to be 20%, then the required jacking force is

$$P_j = \frac{3103}{0.827 \times 0.8} = 4690 \text{ kN}$$

The maximum jacking force for a 12.7 mm diameter strand is  $0.85 \times 184 = 156.4$  kN (see [Table 2.1](#)). The minimum number of strands is therefore  $4690/156.4=30$ .

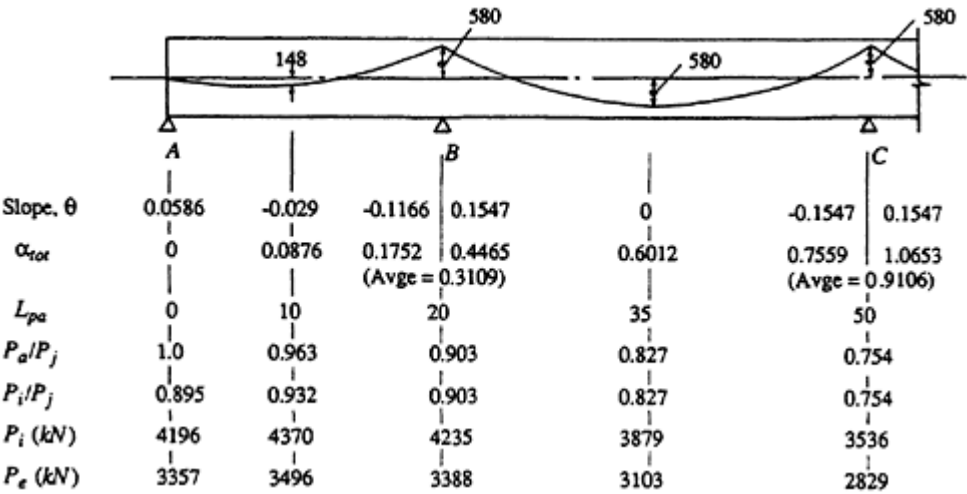


Figure 9.27 Friction losses and tendon forces.

Try two cables each containing 15 strands ( $A_p=1500 \text{ mm}^2/\text{strand}$ ). The two cables are to be positioned so that they are located side by side in the top flange over the interior supports and in the bottom flange at mid-span of BC, but are located one above the other in the web. The position of the resultant tension in the tendons should follow the desired tendon profile. The loss of prestress due to a 6 mm draw-in at the anchorage is calculated as outlined in Section 3.7.2. The slope of the prestress line adjacent to the anchorage at A is

$$\frac{\alpha}{2} = \frac{0.037 \times P_j}{L_{AB}/2} = \frac{0.037 \times 4690}{20/2} = 17.35 \text{ N/mm}$$

and, from Equation 3.61, the length of beam associated with the draw-in losses is

$$L_{di} = \sqrt{\frac{195\,000 \times 3000 \times 6}{17.35}} = 14\,220 \text{ mm}$$

The loss of force at the jack due to slip at the anchorage is

$$\delta P = \alpha L_{di} = 2 \times 17.35 \times 14\,220 \times 10^{-3} = 494 \text{ kN} (= 0.105 P_j)$$

and at mid-span

$$\begin{aligned} \delta P &= \alpha(L_{di} - L_{AB}/2) = 2 \times 17.35 \times (14\,220 - 10\,000) \times 10^{-3} \\ &= 146 \text{ kN} (= 0.031 P_j) \end{aligned}$$



The initial prestressing force  $P_i$  (after friction and anchorage losses) is shown in [Figure 9.27](#), together with the effective prestress assuming 20% time-dependent losses. The average effective prestress in span AB is 3434 kN (and not 3650 kN as previously assumed). The revised drupe in AB and eccentricity at mid-span are

$$h_{AB} = \frac{32 \times 20^2}{8 \times 3434} \times 10^3 = 466 \text{ mm} \quad \text{and} \quad e_{AB} = 176 \text{ mm}$$

This minor adjustment to the tendon profile will not cause significant changes in the friction losses.

- (4) The beam is next analysed under the equivalent transverse loads caused by the effective prestress. The sharp kinks in the tendons over the supports B and C are replaced by short lengths with a convex parabolic shape, as illustrated and analysed in [Example 9.3](#). In this example, it is assumed that the idealized tendons provide a close enough estimate of moments due to prestress.

The equivalent uniformly distributed transverse load due to the effective prestress is approximately 32 kN/m (upward). Using the moment diagram in [Figure 9.25a](#), the total moments due to prestress at B and C are

$$(M_{pt})_B = +63.2 \times 32 = 2022 \text{ kN m} \quad \text{and}$$

$$(M_{pt})_C = +80.9 \times 32 = 2589 \text{ kN m.}$$

The secondary moments at B and C are obtained by subtracting the primary moments corresponding to the average prestress in each span (as was used for the calculation of total moments):

$$\begin{aligned} (M_{ps})_B &= (M_{pt})_B - (P_e e)_B = 2022 - [(3103 + 3434)/2] \times 0.58 \\ &= 126 \text{ kN m} \end{aligned}$$

$$\begin{aligned} (M_{ps})_C &= (M_{pt})_C - (P_e e)_C = 2589 - (3103 \times 0.58) \\ &= 789 \text{ kN m} \end{aligned}$$

The total and secondary moment diagrams are shown in [Figure 9.28](#), together with the corresponding hyperstatic reactions. It should be noted that, in fact, the equivalent transverse load varies along the beam as the prestressing force varies and the moment diagrams shown in [Figure 9.28](#) are only approximate. A more accurate estimate of the

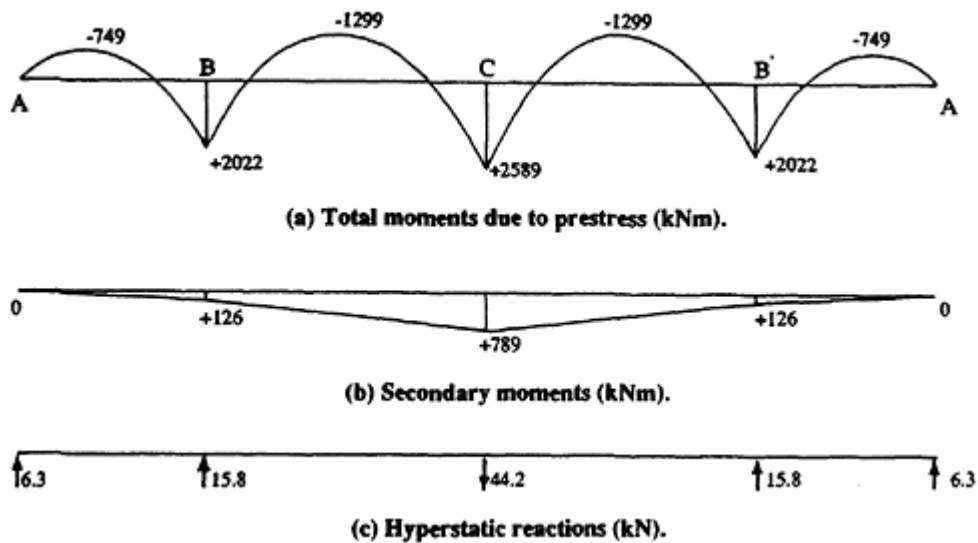


**Figure 9.28** Moments and reactions caused by the average effective prestress.

moments due to prestress and the hyperstatic reactions can be made by dividing each span into smaller segments (say four per span) and assuming constant prestress in each of these segments.

- (5) It is prudent to check the concrete stresses at transfer. The equivalent transverse load at transfer is  $32/0.8=40$  kN/m  $\uparrow$  and the self-weight is  $16.6$  kN/m  $\downarrow$ . Therefore, the unbalanced load is  $23.4$  kN/m  $\uparrow$ . At support C, the moment caused by the uniformly distributed unbalanced load is (see [Figure 9.25a](#))

$$(M_{ub})_C = 80.9 \times 23.4 = 1893 \text{ kN m}$$

and the initial prestressing force at C is  $3536$  kN. The extreme fibre concrete stresses immediately after transfer are

$$\sigma_t = -\frac{3536 \times 10^3}{690 \times 10^3} - \frac{1893 \times 10^6}{217 \times 10^6} = -5.1 - 8.7 = -13.8 \text{ MPa}$$

and

$$\sigma_b = -\frac{3536 \times 10^3}{690 \times 10^3} + \frac{1893 \times 10^6}{217 \times 10^6} = -5.1 + 8.7 = +3.6 \text{ MPa}$$

The flexural tensile strength at transfer is  $0.6\sqrt{f'_c} = 3.3$  MPa and, therefore, cracking at support C is likely to occur at transfer. Bonded reinforcement should therefore be provided in the bottom of the member over support C to control cracking at transfer. For this level

of tension, it is reasonable to calculate the resultant tensile force on the concrete (assuming no cracking) and supply enough non-prestressed steel to carry this tension with a steel stress of 150 MPa. In this case, the resultant tension near the bottom of the cross-section (determined from the calculated stress distribution) is 390 kN and therefore

$$A_{sr} = \frac{390 \times 10^3}{150} = 2600 \text{ mm}^2$$

Use four 28 mm diameter reinforcing bars or equivalent.

As an alternative to the inclusion of this non-prestressed reinforcement, the member might be *stage stressed*. Only part of the prestress is transferred under self-weight conditions (perhaps just one of the cables is fully stressed) and the remaining prestress applied when the sustained dead load (or part of it) is in place.

Similar calculations are required to check for cracking at other sections at transfer. At support B,  $(M_{ub})_B = 63.2 \times 23.4 = 1479 \text{ kN m}$ ;  $P_t = 4235 \text{ kN}$  and  $\sigma_b = +0.67 \text{ MPa}$ . Cracking will not occur at B at transfer. Evidently, support C is the only location where cracking is likely to occur at transfer.

For this partially prestressed beam, before conditions under full loads can be checked (using cracked section analyses in the cracked regions), it is necessary to determine the amount of non-prestressed steel required for strength.

- (6) In this example, the time-dependent losses estimated earlier are assumed to be satisfactory. In practice, of course, losses should be calculated.
- (7) The strength of each cross-section should now be checked. For the purpose of this example, calculations are provided for the critical section at support C only. From steps 1 and 2,  $M^* = -6985 \text{ kNm}$  (due to the factored dead plus live loads). The secondary moment can be included with a load factor of 1.0. Therefore,

$$M^* = -6985 + 789 = -6196 \text{ kNm}$$

The inclusion of the secondary moment here is equivalent to a redistribution of moment at C of 11.3%. The secondary moment will cause a corresponding increase in the positive moments in the adjacent spans. If the cross-section at C is ductile, a further redistribution of moment is permissible (as outlined in [Section 9.5.4](#)). The design moment at C is here redistributed by an additional 3.2% to  $M^* = 6000 \text{ kN m}$ . When checking the strength in positive bending in

the adjacent spans, the design moment must be increased above the elastically determined value in order to maintain equilibrium.

The minimum required ultimate strength at C is  $M_u = M^*/\phi = 7500$  kN m. Using the procedure outlined in [Section 4.4.1](#), the strength of a cross-section with flange width  $b=750$  mm and containing  $A_p=3000$  mm<sup>2</sup> at  $d_p=1280$  mm is

$$M_{u1} = 6156 \text{ kN m (with } d_n = 268 \text{ mm)}$$

Additional non-prestressed tensile reinforcement  $A_{st}$  is required in the top of the cross-section at C. If the depth from the tensile steel to the compressive face is  $d_o=1330$  mm, then  $A_{st}$  can be calculated using Equation 4.27:

$$A_{st} = \frac{M_u - M_{u1}}{f_{yl}} = \frac{(7500 - 6156) \times 10^6}{400 \times 0.9[1280 - (0.766 \times 268)]} = 3474 \text{ mm}^2$$

Use six 28 mm diameter bars in the top over support C. This is in addition to the four 28 mm bars required for crack control at transfer in the bottom of the section. The bottom bars in the compressive zone at the ultimate limit state will improve ductility. From an ultimate strength analysis of the proposed cross-section, with reinforcement details shown in [Figure 9.29](#), the section satisfies strength requirements ( $M_u=7940$  kN m) and with  $d_n=292$  mm  $=0.23d$  the section is ductile enough to justify the moment redistribution assumed at C.

Similar calculations show that four 28 mm diameter bars are required in the negative moment region over the first interior support

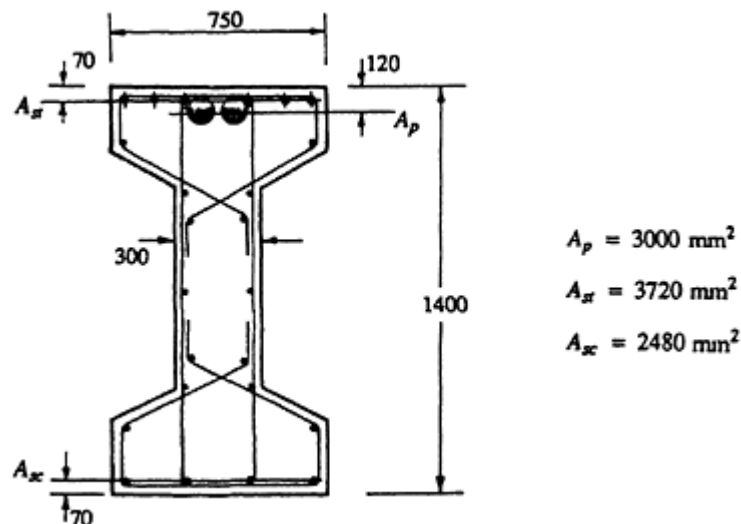


Figure 9.29 Reinforcement details on section over support C in [Example 9.6](#).

at B and B', but at the mid-span regions the prestressing steel provides adequate moment capacity.

- (8) It is necessary to check crack control under full service loads. Results are provided for the cross-section at support C. With the effective prestress balancing 32 kN/m, the unbalanced sustained load is  $w_{us}=25+16.6-32=9.6$  kN/m and the unbalanced transient load is 20 kN/m. The maximum unbalanced moment at support C is

$$(M_{ub})_C = (9.6 \times -80.9) + (20 \times -92.6) = -2629 \text{ kN m}$$

and the corresponding extreme fibre stresses are

$$\sigma_{t,b} = \pm \frac{2629 \times 10^6}{217 \times 10^6} = \pm 12.1 \text{ MPa}$$

The effective prestress at C is  $P_e=2629$  kN and the average stress is

$$\sigma = -\frac{P_e}{A} = -\frac{2629 \times 10^3}{690 \times 10^3} = -4.1 \text{ MPa}$$

The tensile stress in the top fibre is

$$\sigma_t = -4.1 + 12.1 = 8.0 \text{ MPa}$$

and, with the tensile strength taken as  $0.6\sqrt{40} = 3.8$  MPa, cracking will occur under the full unbalanced moment. The error associated with estimates of the cracking moment based on elastic stress calculation may be significantly large. As seen in [Section 3.6.2](#) and [Example 3.5](#), creep and shrinkage cause large redistributions of stress on the cross-section with time, particularly in this case where the cross-section contains significant quantities of non-prestressed reinforcement. If a more accurate estimate of stresses is required, a time analysis is recommended (see [Section 3.6.2](#)).

A cracked section analysis, similar to that outlined in [Section 3.5.2](#), is required to calculate the loss of stiffness due to cracking and the increment of tensile steel stress, in order to check crack control. The maximum in-service moment at C is equal to the sum of the moment caused by the full external service loads and the secondary moment. Owing to the external loads,

$$M_c = -[80.9 \times (25 + 16.6)] - (92.6 \times 20) = -5217 \text{ kN m}$$

and adding the secondary moment gives

$$M_C = -5217 + 789 = 4428 \text{ kN m}$$

A cracked section analysis reveals that the tensile stress in the non-prestressed top steel at this moment is only 110 MPa, which is much less than the increment of 200 MPa permitted in AS 3600–1988. Crack widths should therefore be acceptably small. This design example is taken no further here. Deflections are unlikely to be excessive, but should be checked using the procedures outlined in [Section 3.8](#). The design for shear and the design of the anchorage zones are in accordance with the discussions in Chapters [5](#) and [6](#), respectively, and follow the same steps as outlined in the examples of [Chapter 8](#).

## 9.6 References

- ACI 318–83 1983. *Building code requirements for reinforced concrete*. Detroit: American Concrete Institute.
- AS 3600–1988. *Australian standard for concrete structures*. Sydney: Standards Association of Australia.
- BS 8110 1985. *Structural use of concrete—part I*. London: British Standards Institution.
- Cross, H. 1930. Analysis of continuous frames by distributing fixed-end moments. *Transactions of the American Society of Civil Engineers* Paper No. 1793, 10 pp.
- Ghali, A. & A.M.Neville 1978. *Structural analysis—a unified classical and matrix approach*. London: Chapman and Hall.
- Gilbert, R.I. 1988. *Time effects in concrete structures*. Amsterdam: Elsevier.
- Hall, A.S. & A.P.Kabaila 1977. *Basic concepts of structural analysis*, London: Pitman.
- Lin, T.Y. & K.Thornton 1972. Secondary moments and moment redistribution in continuous prestressed concrete beams. *Journal of the Prestressed Concrete Institute* **17**, No. 1, 1–20.
- Mattock, A.H. 1972, *Secondary moments and moment redistribution in continuous prestressed concrete beams*. Discussion of Lin and Thornton 1972. *Journal of the Prestressed Concrete Institute*, **17**, No. 4, 86–8.
- Nilson, A.H. 1978. *Design of prestressed concrete*. New York: Wiley.
- Warner, R.F. & K.A.Faulkes 1983. *Overload behaviour and design of continuous prestressed concrete beams*. Presented at the International Symposium on Non-Linearity and Continuity in Prestressed Concrete, University of Waterloo, Ontario.

# 10

## Two-way slabs—behaviour and design

### 10.1 Introduction

Post-tensioned concrete floors form a large proportion of all prestressed concrete construction and are economically competitive with reinforced concrete slabs in most practical medium- to long-span situations.

Prestressing overcomes many of the disadvantages associated with reinforced concrete slabs. Deflection, which is almost always the governing design consideration, is better controlled in post-tension slabs. A designer is better able to reduce or even eliminate deflection by a careful choice of prestress. More slender slab systems are therefore possible, and this may result in increased head room or reduced floor to floor heights. Prestress also inhibits cracking and may be used to produce crack-free and watertight floors. Prestressed slabs generally have simple, uncluttered steel layouts. Steel fixing and concrete placing are therefore quicker and easier. In addition, prestress improves punching shear (see [Chapter 5](#)) and reduces formwork stripping times and formwork costs. On the other hand, prestressing often produces significant axial shortening of slabs and careful attention to the detailing of movement joints is frequently necessary.

In this chapter, the analysis and design of the following common types of prestressed concrete slab systems are discussed. Each type is illustrated in [Figure 10.1](#).

- (a) One-way slabs.
- (b) Edge-supported two-way slabs: rectangular slab panels supported on all four edges by either walls or beams. Each panel edge may be either continuous or discontinuous.
- (c) Flat plate slabs: continuous slab of constant thickness supported by a rectangular grid of columns.
- (d) Flat slab with drop panels: as for a flat plate but with a local increase in slab thickness (drop panel) over each supporting column.

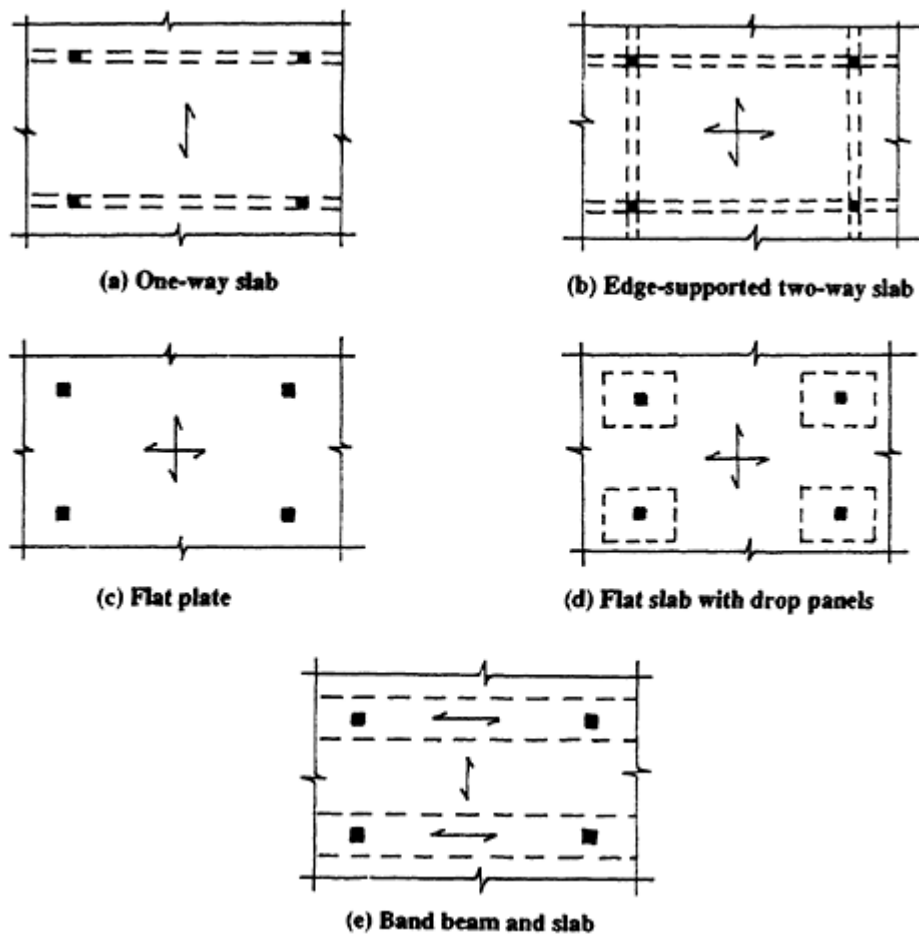


**Figure 10.1** Types of slab systems.

(e) Band-beam and slab system: wide, shallow, continuous, prestressed beams in one direction (the longer span) with one-way prestressed or reinforced slabs in the transverse direction (the shorter span).

Almost all prestressed slabs are post-tensioned using draped tendons. In Australia and elsewhere, use is made of flat-ducted tendons, consisting of five or less super-grade strands in a flat sheath, and fan-shaped anchorages, as shown in [Figure 10.2](#). Individual strands are usually stressed one at a time using light hydraulic jacks. The flat ducts are structurally efficient and allow maximum tendon eccentricity and drape. These ducts are almost always grouted after stressing to provide bond between the steel and the concrete.

In North America, unbonded construction is often used for slabs. Single, plastic-coated, greased tendons are generally used, resulting in slightly lower costs, small increases in available tendon drape, the elimination of the grouting operation (therefore reducing cycle times), and reduced



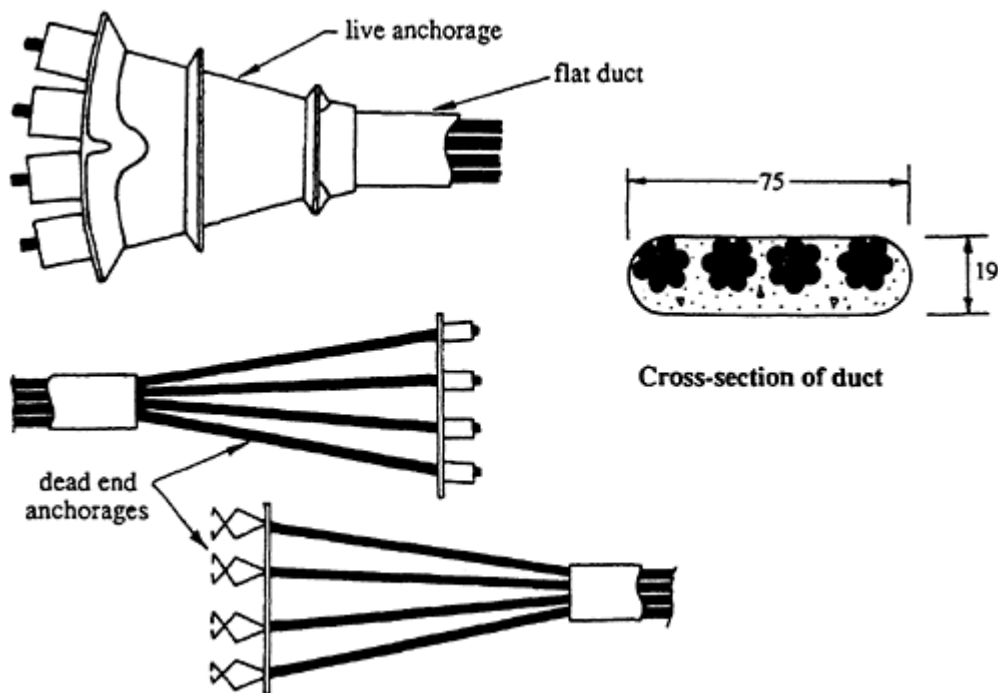


**Figure 10.2** Details of typical flat-ducted tendons.

friction losses. However, unbonded construction also leads to reduced flexural strength, reduced crack control (additional bonded reinforcement is often required), possible safety problems if a tendon is lost or damaged (by corrosion, fire, accident), and increased demolition problems. Single strands are also more difficult to fix to profile.

## 10.2 Effects of prestress

As discussed previously, the prestressing operation results in the imposition of both longitudinal and transverse forces on post-tensioned members. The concentrated longitudinal prestress  $P$  produces a complex stress distribution immediately behind the anchorage and the design of this anchorage zone requires careful attention (see [Chapter 6](#)). At sections further away from the anchorage, the longitudinal prestress applied at the anchorage causes a linearly varying compressive stress over the depth of the slab. If the longitudinal prestress is applied at the centroidal axis (which is generally the slab mid-depth), this compressive stress is uniform over the slab thickness and equal to  $P/A$ .

It has been shown that wherever a change in direction of the prestressing tendon occurs, a transverse force is imposed on the member. For a parabolic tendon profile such as that shown in [Figure 10.3a](#), the curvature is

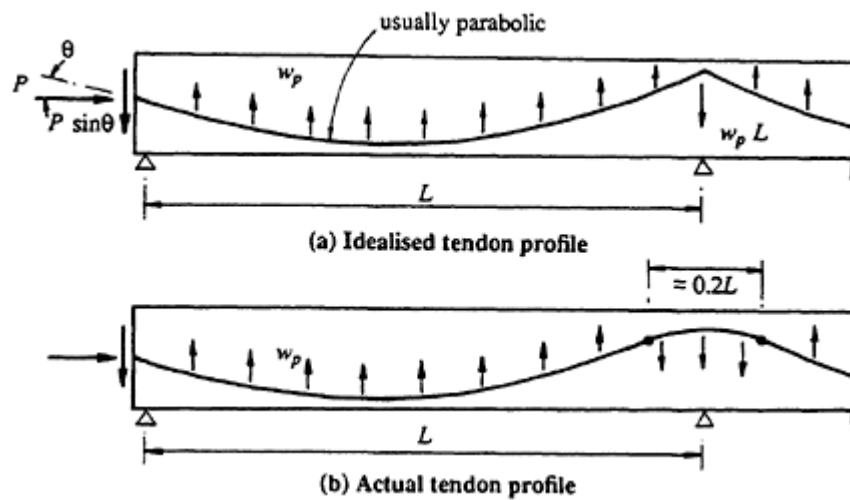


**Figure 10.3** Idealized and actual tendon profiles in a continuous slab.

constant along the tendon and hence the transverse force imposed on the member is uniform along its length. From Equation 1.7, the uniformly distributed transverse force caused by the prestress is

$$w_p = \frac{8Ph}{L^2} \quad (10.1)$$

where  $h$  is the sag of the parabolic tendon and  $L$  is the span. If the cable spacing is uniform across the width of a slab and  $P$  is the prestressing force per unit width of slab, then  $w_p$  is the uniform upward load per unit area.

The cable profile shown in [Figure 10.3a](#), with the sharp kink located over the internal support, is an approximation of the more realistic and practical profile shown in [Figure 10.3b](#). The difference between the effects of the idealized and practical profiles was discussed in [Section 9.3.4](#) for continuous beams. The idealized profile is more convenient for the analysis and design of continuous slabs and the error introduced by the idealization is usually not great.

The transverse load  $w_p$  causes moments and shear which usually tend to be opposite in sign to those produced by the external loads. In [Figure 10.4](#), the elevation of a prestressing tendon in a continuous slab is shown. The transverse load imposed on the slab by the tendon in each span is indicated. If the slab is a two-way slab, with prestressing tendons placed in two orthogonal directions, the total transverse load caused by the prestress is the sum of  $w_p$  for the tendons in each direction.

The longitudinal prestress applied at the anchorage may also induce moments and shears in a slab. At changes of slab thickness, such as occur in a flat slab with drop panels, the anchorage force  $P$  becomes eccentric with respect to the centroidal axis of the section, as shown in [Figure 10.5a](#).

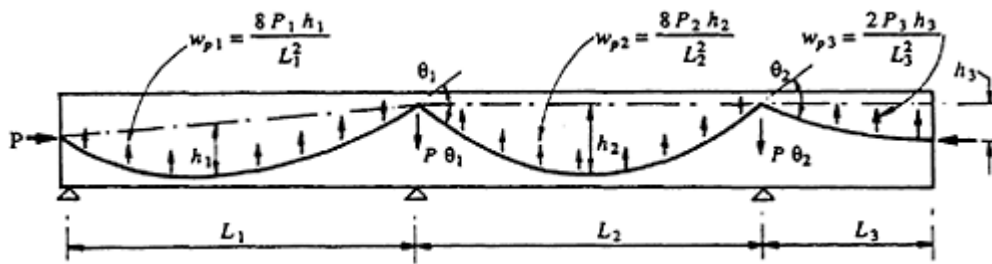


Figure 10.4 Transverse loads imposed by tendons in one direction.

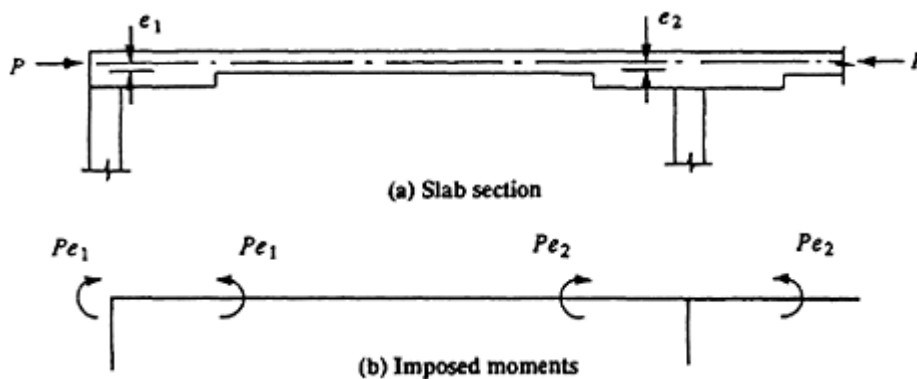
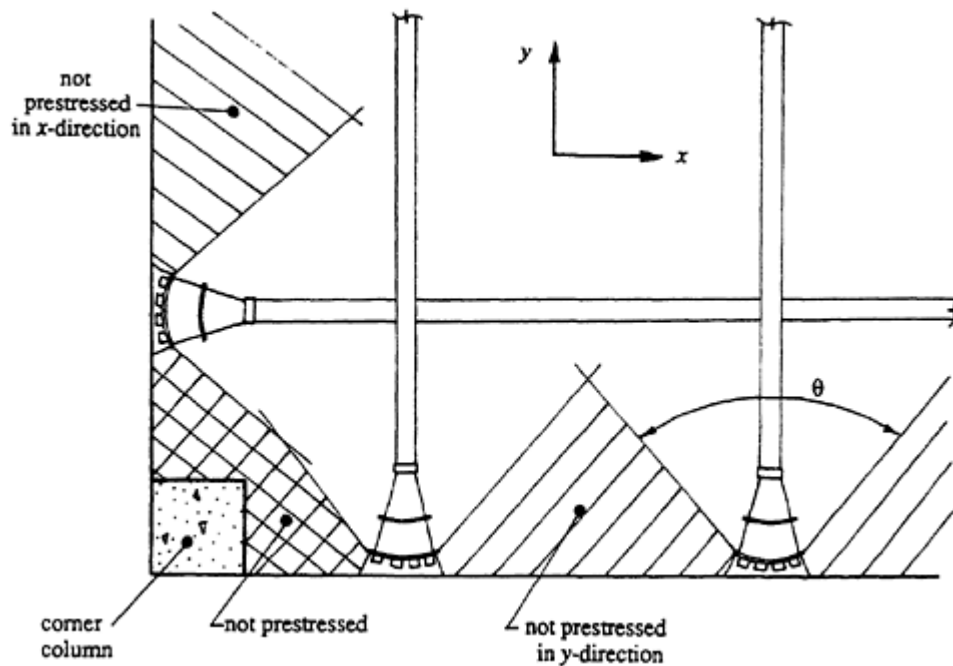


Figure 10.5 Effect of changes in slab thickness.

The moments caused by this eccentricity are indicated in [Figure 10.5b](#) and should also be considered in analysis. However, the moments produced by relatively small changes in slab thickness tend to be small compared with those caused by cable curvature and, if the thickening is below the slab, it is conservative to ignore them.

At some distance from the slab edge, the concentrated anchorage forces have dispersed and the slab is uniformly stressed. The so-called *angle of dispersion*,  $\theta$ , as shown in [Figure 10.6](#), determines the extent of slab in which the prestress is not effective. Specifications for  $\theta$  vary considerably. It is claimed in some trade literature (VSL 1988) that tests have shown  $\theta$  to be  $120^\circ$ . In AS 3600–1988,  $\theta$  is taken as low as  $60^\circ$ . A value of  $\theta=90^\circ$  is usually satisfactory for design purposes.

Care must be taken in the design of the hatched areas of slab shown in [Figure 10.6](#), where the prestress in one or both directions is not effective. It is good practice to include a small quantity of bonded non-prestressed reinforcement in the bottom of the slab perpendicular to the free edge in all exterior spans. An area of non-prestressed steel of about  $0.0015bd_o$  is usually sufficient, where  $d_o$  is the effective depth to the non-prestressed steel. In addition, when checking the punching shear strength at the corner column in [Figure 10.6](#), the beneficial effect of prestress is not available. At



**Figure 10.6** Areas of ineffective prestressing at slab edges.

sections remote from the slab edge, the average  $P/A$  stresses are uniform across the entire slab width and do not depend on changes of  $\theta$  and variations of cable spacing from one region of the slab to another.

### 10.3 Design approach—general

The first step in the design of a post-tensioned slab is the selection of an initial slab thickness. Guidelines for this selection are discussed in [Chapter 11](#). Serviceability considerations usually dictate the required slab thickness, and in [Section 11.3.2](#), an approach for the sizing of slabs is presented which should ensure satisfactory service-load behaviour.

The second step in slab design is to determine the amount and distribution of prestress. Load balancing is generally used to this end. A portion of the load on a slab is balanced by the transverse forces imposed by the draped tendons in each direction. To minimize serviceability problems, a substantial portion of the sustained load should usually be balanced. Under the balanced load, the slab remains plane (without curvature) and is subjected only to the resultant, longitudinal, compressive,  $P/A$  stresses. It is the remaining unbalanced load that enters into the calculation of service-load behaviour, particularly for the estimation of load-dependent deflections and for checking the extent of cracking and crack control. Calculations of deflection and checks for crack control are discussed in detail in [Chapter 11](#).

At ultimate conditions, when the slab behaviour is non-linear and superposition is no longer valid, the full factored design load must be considered. No part of the external load is balanced by the prestress and the transverse force exerted by the cable should not enter into the calculations. The factored design moments and shears at each critical section must be calculated and compared with the design strength of the section, as discussed in Chapters [4](#) (for flexure) and [5](#) (for shear). Slabs are usually very ductile and redistribution of moment occurs as the collapse load of the slab is approached. In these conditions, secondary moments can usually be ignored.

In the following sections, procedures for the calculation of design moments and shears at the critical sections in the various slab types are presented. In addition, techniques and recommendations are also presented for the determination of the magnitude of the prestressing force required in each direction to balance the desired load.

## 10.4 One-way slabs

A one-way slab is generally designed as a beam with cables running in the direction of the span at uniform centres. A slab strip of unit width is analysed using simple beam theory. In any span, the maximum cable sag  $h$  depends on the concrete cover requirements and the tendon dimensions. When  $h$  is determined, the prestressing force required to balance an external load  $w_b$  is calculated from Equation 9.27, which for convenience is restated and renumbered here:

$$P = \frac{w_b L^2}{8h} \quad (10.2)$$

In the transverse direction, conventional reinforcement may be used to control shrinkage and temperature cracking and to distribute local load concentrations. Minimum quantities of conventional steel for the control of shrinkage and temperature induced cracking in a variety of situations are outlined in [Section 11.5.2](#). Not infrequently, the slab is prestressed in the transverse direction to eliminate the possibility of shrinkage cracking parallel to the span and to ensure a watertight and crack-free slab.

## 10.5 Two-way edge-supported slabs

### 10.5.1 Load balancing

Consider the interior panel of the two-way edge-supported slab shown in [Figure 10.7](#). The panel is supported on all sides by walls or beams and

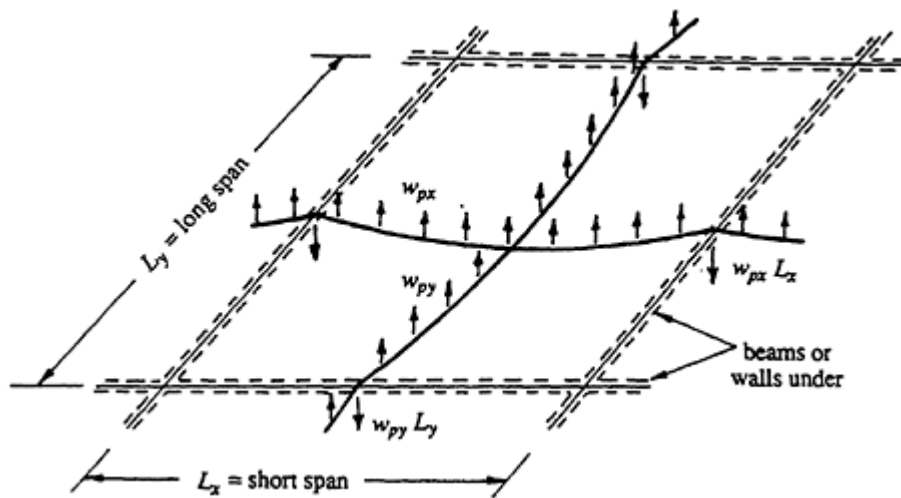


**Figure 10.7** Edge-supported slab panel.

contains parabolic tendons in both the  $x$  and  $y$  directions. If the cables in each direction are uniformly spaced, then the upward forces per unit area exerted by the tendons are

$$w_{px} = \frac{8P_x h_x}{L_x^2} \quad \text{and} \quad w_{py} = \frac{8P_y h_y}{L_y^2} \quad (10.3)$$

where  $P_x$  and  $P_y$  are the prestressing forces per unit width in each direction and  $h_x$  and  $h_y$  are the cable drapes in each direction.

If  $w_b$  is the uniformly distributed downward load to be balanced, then

$$w_b = w_{px} + w_{py}. \quad (10.4)$$

In practice, perfect load balancing is not possible, since external loads are rarely perfectly uniformly distributed. However, for practical purposes, adequate load balancing can be achieved.

Any combination of  $w_{px}$  and  $w_{py}$  that satisfies Equation 10.4 can be used to make up the balanced load. The smallest quantity of prestressing steel will result if all the load is balanced by cables in the short span direction, i.e.  $w_{px} = w_b$ . However, under unbalanced loads, serviceability problems and unsatisfactory behaviour would almost certainly result. It is often preferable to distribute the prestress in much the same way as the load is distributed to the supports, i.e. more prestress in the short-span direction than in the long-span direction. The balanced load resisted by tendons in the short direction may be approximated by

$$w_{px} = \frac{L_y^4}{\alpha L_x^4 + L_y^4} w_b \quad (10.5)$$

where  $\alpha$  depends on the support conditions and is given by

$\alpha = 1.0$	for 4 edges continuous or discontinuous
$= 1.0$	for 2 adjacent edges discontinuous
$= 2.0$	for 1 long edge discontinuous
$= 0.5$	for 1 short edge discontinuous
$= 2.5$	for 2 long and 1 short edges discontinuous
$= 0.4$	for 2 short and 1 long edges discontinuous
$= 5.0$	for 2 long edges discontinuous
$= 0.2$	for 2 short edges discontinuous

Equation 10.5 is the expression obtained for that portion of any external load which is carried in the short-span direction if twisting moments are ignored and the mid-span deflections of the two orthogonal unit wide strips through the slab centre are equated.

With  $w_{px}$  and  $w_{py}$  selected, the prestressing force per unit width in each direction is calculated from Equation 10.3:

$$P_x = \frac{w_{px}L_x^2}{8h_x} \quad \text{and} \quad P_y = \frac{w_{py}L_y^2}{8h_y} \quad (10.6)$$

Equilibrium dictates that the downward forces per unit length exerted over each edge support by the reversal of cable curvature (as shown in [Figure 10.7](#)) are

$w_{py}L_y$  (kN/m) carried by the short span supporting beams or walls per unit length  
and

$w_{px}L_x$  (kN/m) carried by the long span supporting beams or walls per unit length.

The total force imposed by the slab tendons that must be carried by the edge beams is

$$w_{px}L_xL_y + w_{py}L_yL_x = w_bL_xL_y$$

which is equal to the total upward force exerted by the slab cables. Therefore, for this two-way slab system, in order to carry the balanced load to the supporting columns, resistance must be provided for twice the total load to be balanced (i.e. in both the slab and in the beams). This requirement is true for all two-way slab systems irrespective of construction type or material.

At the balanced load condition, when the transverse forces imposed by the cables exactly balance the applied external loads, the slab is subjected only to the compressive stresses imposed by the longitudinal prestress in each direction:

$$\sigma_x = \frac{P_x}{t} \quad \text{and} \quad \sigma_y = \frac{P_y}{t}$$

where  $t$  is the slab thickness.

### 10.5.2 Methods of analysis

For any service load above (or below) the balanced load, moments are induced in the slab which may lead to cracking or excessive deflection. A reliable technique for estimating slab moments is therefore required in order to check in-service behaviour under the unbalanced loads. In addition, reliable estimates of the maximum moments and shears caused by the full factored dead and live loads must be made in order to check the flexural and shear strength of a slab.

In AS 3600–1988, a simplified method is proposed for the analysis of reinforced, two-way, edge-supported slabs subjected to uniformly distributed design ultimate loads. Moment coefficients derived from yield line theory are specified. Despite inherent difficulties in applying yield line analysis to prestressed edge-supported slabs, the collapse load moment coefficients specified in the code may be used reliably to calculate design ultimate moments.

The positive design moments per unit width at the mid-span of the slab in each direction are

$$M_x^* = \beta_x w^* L_x^2 \quad \text{and} \quad M_y^* = \beta_y w^* L_x^2 \quad (10.7)$$

where  $w^*$  is the factored design load per unit area,  $L_x$  is the short span, and  $\beta_x$  and  $\beta_y$  are moment coefficients which depend on the support conditions and the aspect ratio of the panel (i.e.  $L_y/L_x$ ). Values for  $\beta_x$  and  $\beta_y$  are given in [Table 10.1](#) or may be obtained from the following equations:

$$\beta_y = \frac{2[\sqrt{3 + (\gamma_x/\gamma_y)^2} - \gamma_x/\gamma_y]^2}{9\gamma_y^2} \quad (10.8a)$$

$$\beta_x = (L_x/L_y)\beta_y + \frac{2[1 - (L_x/L_y)]}{3\gamma_y^2} \quad (10.8b)$$



**Table 10.1** Ultimate moment coefficients for rectangular edge-supported slabs (AS 3600–1988).

Support Conditions	Short-Span Coefficient $\beta_x$								Long span Coefficient $\beta_y$ for all values of $L_y/L_x$
	Aspect Ratio, $L_y/L_x$								
	1.0	1.1	1.2	1.3	1.4	1.5	1.75	2.0	
1 Four edges continuous	0.024	0.028	0.032	0.035	0.037	0.040	0.044	0.048	0.024
2 One short edge discontinuous	0.028	0.032	0.036	0.038	0.041	0.043	0.047	0.050	0.028
3 One long edge discontinuous	0.028	0.035	0.041	0.046	0.050	0.054	0.061	0.066	0.028
4 Two adjacent edges discontinuous	0.035	0.041	0.046	0.051	0.055	0.058	0.065	0.070	0.035
5 Two short edges discontinuous	0.034	0.038	0.040	0.043	0.045	0.047	0.050	0.053	0.034
6 Two long edges discontinuous	0.034	0.046	0.056	0.065	0.072	0.079	0.091	0.100	0.034
7 Three edges discontinuous (one long edge continuous)	0.043	0.049	0.053	0.057	0.061	0.064	0.069	0.074	0.043
8 Three edges discontinuous (one short edge continuous)	0.043	0.054	0.064	0.072	0.078	0.084	0.096	0.105	0.043
9 Four edges discontinuous	0.056	0.066	0.074	0.081	0.087	0.093	0.103	0.111	0.056

where

$\gamma_x$	=2	if both short edges are discontinuous
	=2.5	if one short edge is discontinuous
	=3.0	if both short edges are continuous

and  $\gamma_y$  is as for  $\gamma_x$  applied to the long edges.

The negative design moments at a continuous edge are taken to be 1.33 times the mid-span value in the direction considered and, at a discontinuous edge, the negative design moment is taken as 0.5 times the mid-span value.

For the purposes of calculating the shear forces in a slab or the forces applied to the supporting walls or beams, AS 3600–1988 suggests that the uniformly distributed load on the slab is allocated to the supports as shown in [Figure 10.8](#).

It is recommended that the moment coefficients given by Equations 10.8a and b and shown in [Table 10.1](#) are used for ultimate strength calculations. However, for service load calculations, moment coefficients based on elastic behaviour are perhaps more appropriate. It is therefore suggested that the moment coefficients reproduced in [Table 10.2](#) be used for serviceability calculations. These coefficients are based on the study of elastic slabs by Westergaard & Slater (1921) and are contained in a number of building codes. The coefficients in [Table 10.2](#) may be used to predict both the



-ve Moment at continuous edge	0.058	0.065	0.071	0.077	0.081	0.085	0.092	0.098	0.058
-ve Moment at discontinuous edge	0.029	0.033	0.036	0.038	0.040	0.042	0.046	0.049	0.029
+ve Moment at midspan	0.044	0.049	0.054	0.058	0.061	0.064	0.069	0.074	0.044
<hr/>									
7. Four edges discontinuous									
-ve Moment at discontinuous edge	0.033	0.038	0.041	0.044	0.046	0.049	0.053	0.055	0.033
+ve Moment at midspan	0.050	0.057	0.062	0.067	0.071	0.075	0.081	0.083	0.050

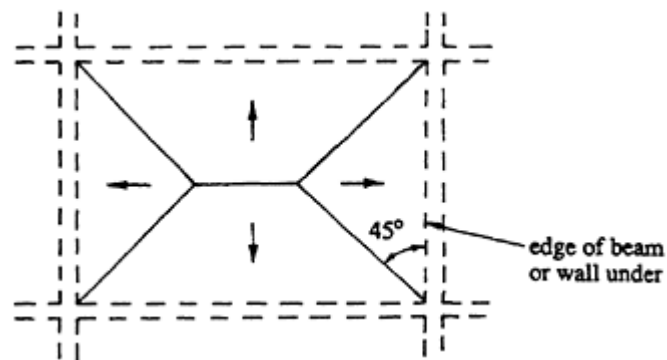


**Figure 10.8** Distribution of shear forces in an edge-supported slab.

positive and negative moments at the critical sections using

$$M_x = \beta_x w L_x^2 \quad \text{and} \quad M_y = \beta_y w L_x^2 \quad (10.9)$$

where  $w$  is the unbalanced service load and  $\beta_x$  and  $\beta_y$  are obtained from [Table 10.2](#).

### 10.5.3 Example 10.1

An exterior panel of a 180 mm thick two-way floor slab for a retail store is to be designed. The rectangular panel is supported on four edges by stiff beams and is discontinuous on one long edge as shown in [Figure 10.9a](#). The slab is post-tensioned in both directions using the draped parabolic cable profiles shown in [Figures 10.9c](#) and [d](#). The slab supports a dead load of 1.5 kPa in addition to its own self-weight and the live load is 5.0 kPa. The level of prestress required to balance a uniformly distributed load of 5.0 kPa is required. Relevant material properties are as follows:

Concrete compressive strength:	$f'_c = 35 \text{ MPa}$
Concrete tensile strength:	$f'_t = 3.5 \text{ MPa}$
Elastic modulus of concrete:	$E_c = 30000 \text{ MPa}$
Characteristic strength of steel:	$f_p = 1840 \text{ MPa}$
Elastic modulus of prestressing steel:	$E_p = 195000 \text{ MPa}$

### Load balancing

Flat ducted tendons containing four 12.5 mm strands are to be used with duct size 75 mm × 19 mm, as shown in [Figure 10.9b](#). With 25 mm concrete cover to the duct, the maximum depth to the centre of gravity of the short-span tendons is

$$d_x = 180 - 25 - (19 - 7) = 143 \text{ mm (as indicated in Figure 10.9c)}$$

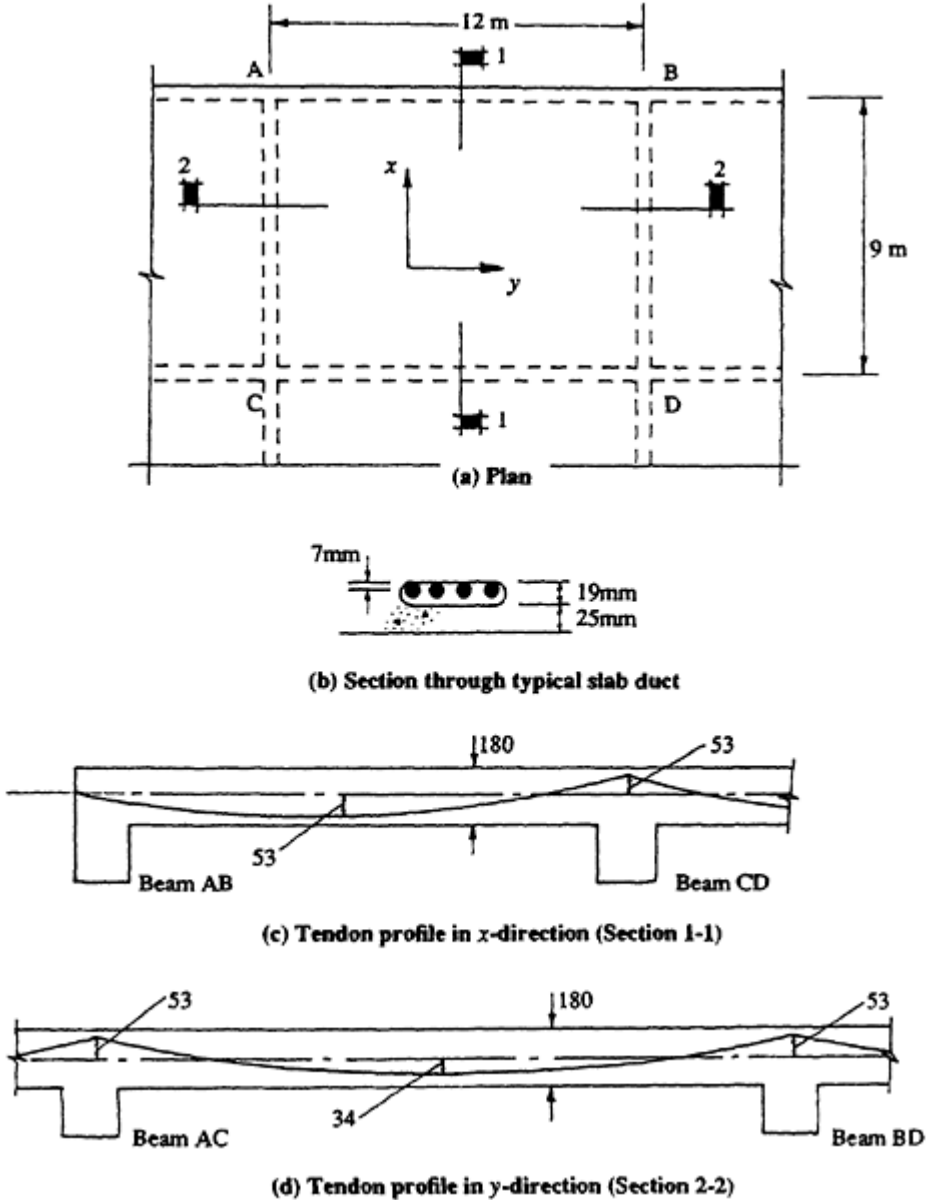


Figure 10.9 Details of edge-supported slab of Example 10.1.

The cable drape in the short-span direction is therefore

$$h_x = \frac{53 + 0}{2} + 53 = 79.5 \text{ mm}$$

The depth  $d_y$  of the long-span tendons at mid-span is less than  $d_x$  by the thickness of the duct running in the short-direction, i.e.  $d_y = 143 - 19 = 124 \text{ mm}$ . The cable drape in the long-span direction is shown in

Figure 10.9d and is given by

$$h_y = \frac{53 + 53}{2} + 34 = 87 \text{ mm}$$

The self-weight of the slab is  $24 \times 0.18 = 4.3$  kPa and if 30% of the live load is assumed to be sustained, then the total sustained load is

$$w_{sus} = 4.3 + 1.5 + (0.3 \times 5.0) = 7.3 \text{ kPa}$$

In this example, the effective prestress in the tendons in both directions balances an external load of  $w_b = 5.0$  kPa. From Equation 10.5, the transverse load exerted by the tendons in the short-span direction is

$$w_{px} = \frac{12^4}{2 \times 9^4 + 12^4} \times 5.0 = 3.06 \text{ kPa}$$

and the transverse load imposed by the tendons in the long-span direction is calculated using Equation 10.4:

$$w_{py} = 5.0 - 3.06 = 1.94 \text{ kPa}$$

The effective prestress in each direction is obtained from Equation 10.6:

$$P_x = \frac{3.06 \times 9000^2}{8 \times 79.5} = 390 \text{ kN/m} \quad \text{and} \quad P_y = \frac{1.94 \times 12000^2}{8 \times 87} = 401 \text{ kN/m}$$

To determine the jacking forces and cable spacing in each direction, both the deferred losses and friction losses must be calculated. For the purpose of this example, it is assumed that the time-dependent losses in each direction are 15% and the immediate losses (friction, anchorage, etc.) in the  $x$ -direction are 8% and in the  $y$ -direction are 12%. Immediately after transfer, before the time-dependent losses have taken place, the prestressing forces at mid-span in each direction are

$$P_{xi} = \frac{390}{0.85} = 459 \text{ kN/m} \quad \text{and} \quad P_{yi} = \frac{401}{0.85} = 472 \text{ kN/m}$$

and, at the jack,

$$P_{xj} = \frac{459}{0.92} = 499 \text{ kN/m} \quad \text{and} \quad P_{yj} = \frac{472}{0.88} = 536 \text{ kN/m}$$

Using four 12.7 mm strands/tendon,  $A_p=400 \text{ mm}^2$ /tendon and the breaking load per tendon is  $4 \times 184=736 \text{ kN}$  (see [Table 2.1](#)).

If a limit of  $0.85f_p A_p$  is placed on the maximum force to be applied to a stress-relieved post-tensioned tendon during the stressing operation, the maximum jacking force/tendon is  $0.85f_p A_p=0.85 \times 736=626 \text{ kN}$  and the required tendon spacing in each direction is therefore

$$s_x = \frac{1000 \times 626}{499} = 1250 \text{ mm} \quad \text{and} \quad s_y = \frac{1000 \times 626}{536} = 1160 \text{ mm}$$

Select a tendon spacing of 1200 mm in each direction

With each tendon stressed to 626 kN, the revised prestressing forces at the jack per metre width are

$$P_{xj} = P_{yj} = \frac{626}{1.2} = 522 \text{ kN/m}$$

and at mid-span, after all losses,

$$P_x = 0.85 \times 0.92 \times 522 = 408 \text{ kN} \quad \text{and} \quad P_y = 0.85 \times 0.88 \times 522 = 390 \text{ kN}$$

The load to be balanced is revised using Equation 10.3:

$$w_{px} = \frac{8 \times 408 \times 10^3 \times 79.5}{9000^2} = 3.2 \text{ kPa}$$

and

$$w_{py} = \frac{8 \times 390 \times 10^3 \times 87}{12000^2} = 1.9 \text{ kPa}$$

and therefore

$$w_b = 3.2 + 1.9 = 5.1 \text{ kPa}$$

In [Example 11.3](#), the service-load behaviour of this slab is calculated. Checks are made for cracking using moment coefficients from [Table 10.2](#) and deflections are calculated. No cracking is detected and total deflections are acceptable.

### Flexural strength check

It is necessary to check the ultimate strength of the slab. As previously calculated, the dead load is  $1.5+4.3=5.8 \text{ kPa}$  and the live load is  $5.0 \text{ kPa}$ .

The factored design load (using the load factors specified in AS 3600–1988 and outlined in [Section 1.7.3](#)) is

$$w^* = (1.25 \times 5.8) + (1.5 \times 5.0) = 14.75 \text{ kPa}$$

The design moments at mid-span in each direction are obtained from Equation 10.7 with values of  $\beta_x=0.047$  and  $\beta_y=0.028$  taken from [Table 10.1](#):

$$M_x^* = 0.047 \times 14.75 \times 9^2 = 56.5 \text{ kN m/m}$$

$$M_y^* = 0.028 \times 14.75 \times 9^2 = 33.8 \text{ kN m/m}$$

The maximum design moment occurs over the beam support CD (the long continuous edge) and is

$$M_x^* = 1.33 \times 56.5 = 75.1 \text{ kN m/m}$$

A safe, lower bound solution to the problem of adequate ultimate strength will be obtained if the design strength of the slab at this section exceeds the design moment.

The ultimate strength per metre width of the 180 mm thick slab containing tendons at 1200 mm centres (i.e.  $A_p=400/1.2=333 \text{ mm}^2/\text{m}$ ) at an effective depth of 143 mm is obtained using the procedures discussed in [Chapter 4](#). Such an analysis indicates that the cross-section is ductile, with the depth to the neutral axis at ultimate equal to 24.5 mm (or  $0.17d$ ), which is much less than the maximum limiting value of  $0.4d$ . The tensile force in the steel is 583 kN/m ( $\sigma_{pu}=1750 \text{ MPa}$ ) and the strength is

$$M_u = 583 \left( 143 - \frac{0.8 \times 24.5}{2} \right) = 77.7 \text{ kN m/m}$$

$$\phi M_u = 62.2 \text{ kN m/m} < M_x^*$$

Conventional reinforcement is required to supplement the prestressed steel over the beam support CD. From Equation 4.27, with the internal lever arm  $l$  taken to be  $0.9d$ , the required area of additional non-prestressed steel is approximated by

$$A_{st} \approx \frac{M_x^* - \phi M_u}{\phi f_y \times 0.9d} = \frac{(75.1 - 62.2) \times 10^6}{0.8 \times 400 \times 0.9 \times 143} = 313 \text{ mm}^2/\text{m}$$

Try 12 mm diameter bars ( $f_y=400 \text{ MPa}$ ) at 300 mm centres as additional steel in the top of the slab over beam support CD. With this additional steel



in place, an ultimate strength analysis of the cross-section indicates that the depth to the neutral axis increases to 30.7 mm ( $0.21d$ ) and  $M_u=95.4$  kN m/m. Therefore,

$$\phi M_u = 76.3 \text{ kN m/m} > M_x^*$$

which is acceptable.

Checking strength at other critical sections indicates that:

(a) at mid-span in the  $x$ -direction:

$$M_x^* = 56.5 \text{ kN m/m}; \phi M_u = 62.2 \text{ kN m/m} (d = 143 \text{ mm})$$

∴ No additional reinforcement is required at mid-span in the  $x$ -direction.

(b) At mid-span in the  $y$ -direction:

$$M_y^* = 33.8 \text{ kN m/m}; \phi M_u = 53.3 \text{ kN m/m} (d = 124 \text{ mm})$$

∴ No additional reinforcement required at mid-span in the  $y$ -direction.

(c) At the short continuous supports:

$$M_y^* = 33.8 \times 1.33 = 45.0 \text{ kN m/m}; \phi M_u = 62.2 \text{ kN m/m} \\ (d = 143 \text{ mm})$$

∴ No additional reinforcement is required at the short continuous support.

### Summary of reinforcement requirements

Tendons consisting of four 12.7 mm strands at 1200 mm centres in each direction are used with the profiles shown in Figures [10.9c](#) and [d](#). In addition, 12mm diameter non-prestressed reinforcing bars in the  $x$ -direction at 300 mm centres are also placed in the top of the slab over the long support CD.

### Check shear strength

In accordance with [Figure 10.8](#), the maximum shear in the slab occurs at the face of the long support near its mid-length:

$$V^* \approx \frac{L_x}{2} w^* = 4.5 \times 14.75 = 66 \text{ kN/m}$$

The contribution of the concrete to the shear strength in the region of low moment at the face of the discontinuous support is given by Equation 5.10

as follows:

$$V_{uc} = V_t + P_v$$

where  $V_t$  is the shear force required to cause web-shear cracking. From Equation 5.12,

$$\sigma = -\frac{408 \times 10^3}{180 \times 10^3} = -2.267 \text{ MPa} \quad \text{and} \quad \tau = \frac{V_t Q}{Ib} = (8.33 \times 10^{-6}) V_t$$

and solving Equation 5.11 gives

$$V_t = 344 \text{ kN/m}$$

Clearly,  $V^*$  is much less than  $\phi V_{uc}$  and the shear strength is ample here. Shear strengths at all other sections are also satisfactory. Shear is rarely a problem in edge-supported slabs.

## 10.6 Flat plate slabs

### 10.6.1 Load balancing

Flat plates behave in a similar manner to edge-supported slabs except that the *edge beams* are strips of slab located on the column lines, as shown in [Figure 10.10](#). The edge beams have the same depth as the remainder of the slab panel and therefore the system tends to be less stiff and more prone to serviceability problems. The load paths for both the flat plate and the edge-supported slab are, however, essentially the same (compare [Figures 10.7](#) and [10.10](#)).

In the flat plate panel of [Figure 10.10](#), the total load to be balanced is  $w_b L_x L_y$ . The upward forces per unit area exerted by the slab tendons in each direction are given by Equation 10.3 and the slab tendons impose a total upward force of

$$w_{px} L_x L_y + w_{py} L_y L_x = w_b L_x L_y$$

Just as for edge-supported slabs, the slab tendons may be distributed arbitrarily between the  $x$ - and  $y$ -directions provided that adequate additional tendons are placed in the slab strips to balance the line loads  $w_{py} L_y$  and  $w_{px} L_x$  shown on the column lines in [Figure 10.10](#). These additional *column line* tendons correspond to the *beam* tendons in an edge-supported slab system. For perfect load balancing, the column line tendons would have to be placed within the width of slab in which the slab tendons exert down-

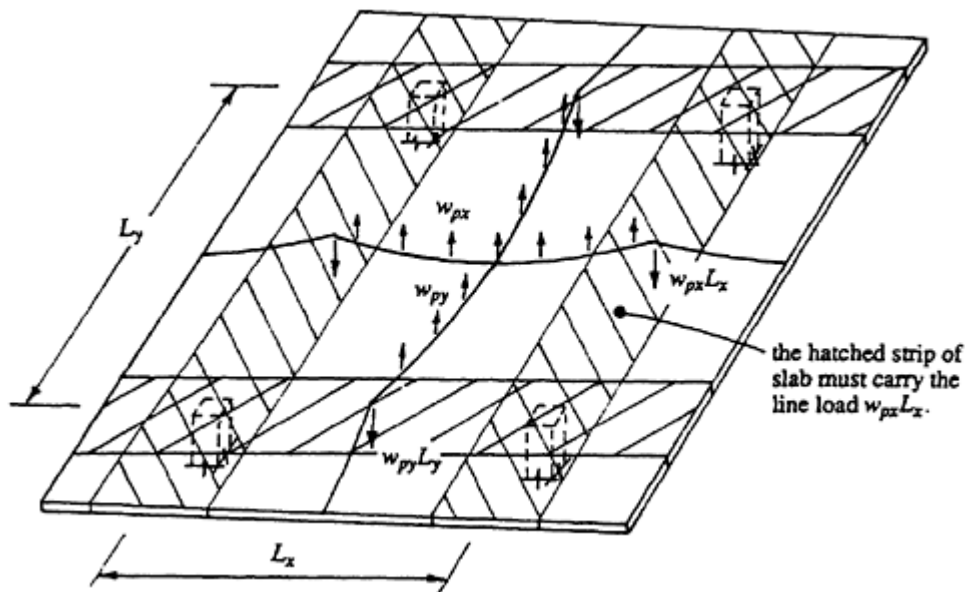


**Figure 10.10** Flat plate panel.

ward load due to reverse curvature. However, this is not a strict requirement and considerable variation in tendon spacing can occur without noticeably affecting slab behaviour. Column line tendons are frequently spread out over a width of slab as large as one half the shorter span, as indicated in [Figure 10.11c](#).

The total upward force which must be provided in the slab along the column lines is

$$w_{px}L_xL_y + w_{py}L_yL_x = w_bL_xL_y$$

Therefore, prestressing tendons (slab tendons plus column line tendons) must be provided in each panel to give a total upward force of  $2w_bL_xL_y$ . The slab tendons and column line tendons *in each direction* must provide between them an upward force equal to the load to be balanced,  $w_bL_xL_y$ . For example, in the slab system shown in [Figure 10.11a](#), the entire load to be balanced is carried by slab tendons in the  $x$ -direction, i.e.  $w_{px}=w_b$  and  $w_{py}=0$ . This entire load is deposited as a line load on the column lines in the  $y$ -direction and must be balanced by column line tendons in this vicinity. This slab is in effect treated as a one-way slab spanning in the  $x$ -direction and being supported by shallow, heavily stressed, slab strips on the  $y$ -direction column lines. The two-way system shown in [Figure 10.11b](#) is more likely to perform better under unbalanced loads, particularly when the orthogonal spans  $L_x$  and  $L_y$  are similar and the panel is roughly square. In practice, steel congestion over the supporting columns and minimum spacing requirements (often determined by the size of the anchorages)

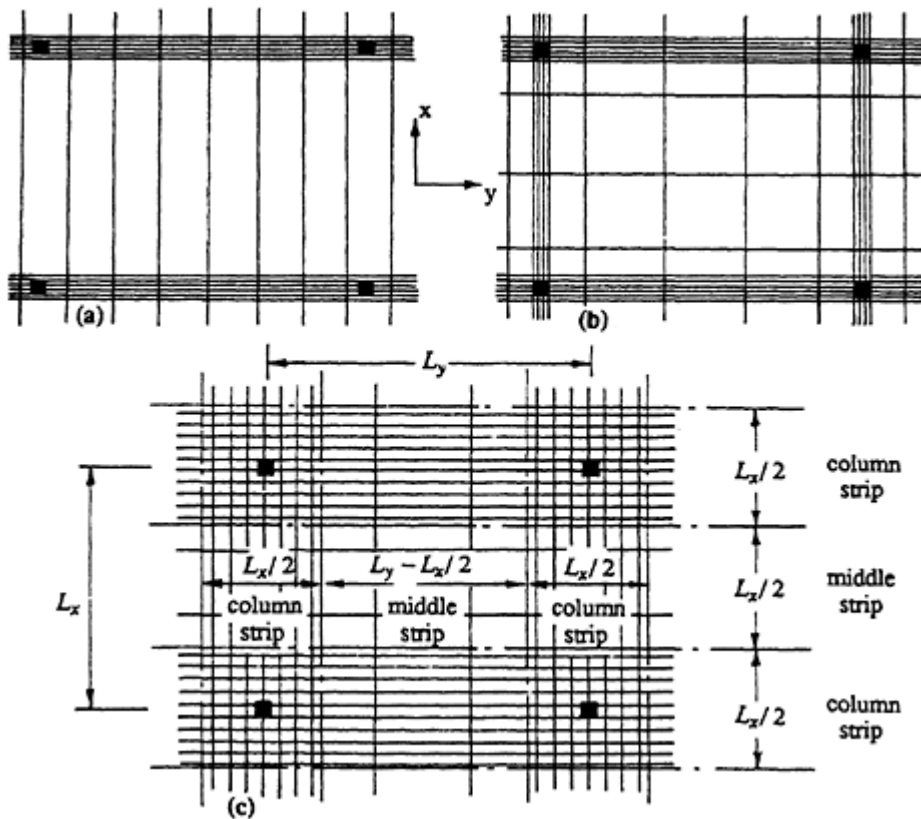


**Figure 10.11** Alternative tendon layouts.

make the concentration of tendons on the column lines impossible. [Figure 10.11c](#) shows a more practical and generally acceptable layout. Approximately 75% of the tendons in each direction are located in the column strips, as shown, the remainder being uniformly spread across the middle strip regions.

If the tendon layout is such that the upward force on the slab is approximately uniform, then at the balanced load the slab has zero deflection and is subjected only to uniform compression caused by the longitudinal prestress in each direction applied at the anchorages. Under unbalanced loads, moments and shears are induced in the slab. To calculate the moments and stresses due to unbalanced service loads and to calculate the factored design moments and shears in the slab (in order to check ultimate strength), one of the methods described in the following sections may be adopted.

### 10.6.2 Behaviour under unbalanced load

[Figure 10.12](#) illustrates the distribution of moments caused by an unbalanced uniformly distributed load  $w$  on an internal panel of a flat plate. The moment diagram in the direction of span  $L_y$  is shown in [Figure 10.12b](#).

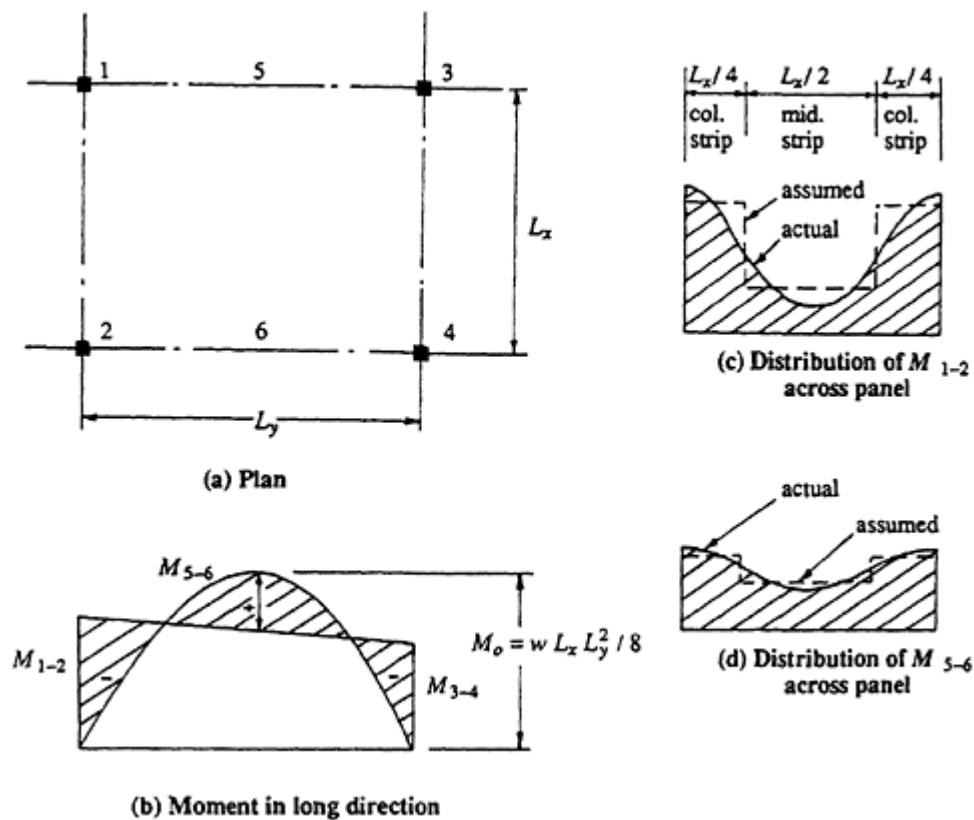


Figure 10.12 Moment distribution in flat plates.

The slab in this direction is considered as a wide, shallow beam of width  $L_x$ , span  $L_y$ , and carrying a load  $wL_x$  per unit length. The relative magnitudes of the negative moments ( $M_{1-2}$  and  $M_{3-4}$ ) and positive moment  $M_{5-6}$  are found by elastic frame analysis (see [Section 10.6.3](#)) or by more approximate recommendations (see [Section 10.6.4](#)). Whichever method is used, the total static moment  $M_o$  is fixed by statics and is given by

$$M_o = \frac{wL_x L_y^2}{8} \quad (10.10)$$

In Figures [10.12c](#) and [d](#), variations in elastic moments across the panel at the column lines and at mid-span are shown. At the column lines, where curvature is a maximum, the moment is also a maximum. On panel centreline where curvature is a minimum, so too is moment. In design, it is convenient to divide the panel into column and middle strips and to assume that the moment is constant in each strip as shown. The column strips in the  $L_y$  direction are defined as strips of width  $0.25L_x$ , but not greater than  $0.25L_y$ , on each side of the column centreline. The middle strips are the slab strips between the column strips.

It may appear from the moment diagrams that at ultimate loads, the best distribution of tendons (and hence strength) is one in which tendons are widely spaced in the middle strips and closer together in the column strips, as shown in [Figure 10.11c](#). However, at ultimate loads, provided that the slab is ductile, redistribution of moments takes place as the ultimate condition is approached and the final distribution of moments depends very much on the layout of the bonded steel.

After the slab cracks and throughout the overload range, superposition is no longer applicable and the concepts of balanced and unbalanced loads are not meaningful. As discussed in [Section 9.5.4](#), at ultimate conditions, when the load factors are applied to the dead and live load moments, codes of practice usually insist that secondary moments are considered with a load factor of 1.0. However, provided that the slab is ductile, and slabs most often are very ductile, secondary moments may be ignored in ultimate strength calculations. The difficulty in accurately estimating slab moments, particularly in the overload range, is rendered relatively unimportant by the ductile nature of slabs.

### 10.6.3 Frame analysis

Perhaps the most commonly used technique for the analysis of flat plates is the *equivalent frame method*. The structure is idealized into a set of parallel two-dimensional frames running in two orthogonal directions through the building. Each frame consists of a series of vertical columns spanned by horizontal *beams*. These beams are an idealization of the strip of slab of width on each side of the column line equal to half the distance to the adjacent parallel row of columns and includes any floor beams forming part of the floor system. The member stiffnesses are determined and the frames are analysed under any desired gravity loading using a linear-elastic frame analysis. For a flat plate building in which shear walls or some other bracing system is provided to resist all lateral loads, it is usually permissible to analyse each floor of the building separately with the columns above and below the slab assumed to be fixed at their remote ends.

In the equivalent frame method, as specified in ACI 318–83, the stiffness of each supporting column is modified to account for the twisting of the slab spandrel strips. These so-called spandrel strips are transverse to the frame and adjacent to each supporting column, and are similar to the torsion strips discussed in [Section 5.10.3](#) and illustrated in [Figure 5.13](#). For a flat slab structure, the torsional stiffness of a spandrel strip is relatively low and this causes a reduction of the stiffness of the *equivalent column* in the idealized frame. The modification of the stiffness of the columns to account for twisting of the spandrel strips complicates the analysis and may not necessarily improve the accuracy. The equivalent frame method provides at best a crude model of structural behaviour, with inaccuracies being associ-

ated with each of the following assumptions: (a) a two-way plate is idealized by orthogonal one-way strips; (b) the stiffness of a cracked slab is usually based on gross section properties; and (c) a linear-elastic analysis is applied to a structure that is non-linear and inelastic both at service loads and at overloads. A simpler estimate of member stiffness, based for example on gross section properties only, will lead to an estimate of frame moments which is no less valid.

AS 3600–1988 suggests that the stiffness of the frame members should be chosen “to represent conditions at the limit state under consideration. All such assumptions shall be applied consistently throughout the analysis.” If an idealized frame analysis is adopted, a procedure based on gross member stiffnesses is recommended here and will usually provide an acceptable solution that is as accurate as is possible using an approximate frame analysis. When such a frame analysis is used to check bending strength, an equilibrium load path is established that will prove to be a satisfactory basis for design, provided that the slab is ductile and the moment distribution in the real slab can redistribute towards that established in the analysis.

The following live loading patterns are usually considered for the determination of the design moments at each critical section of the frame (ACI 318–83, AS 3600–1988):

- (a) Where the loading pattern is known, the frame should be analysed under that loading.
- (b) Where the live load  $Q$  is not greater than three quarters of the dead load  $G$ , or when the nature of the loading is such that all panels will be loaded simultaneously, the frame should be analysed with the full factored live load on all spans.
- (c) Where loads are other than specified in (b) (e.g. when  $Q > \frac{3}{4}G$ ), the maximum factored positive moment near mid-span of a panel may be assumed to occur with three quarters of the full factored live load on the panel and on alternate panels. The maximum factored negative moment at a support may be assumed to occur with three quarters of the full factored live load on adjacent panels only.

The frame moments calculated at the critical sections of the idealized horizontal members are distributed across the floor slab into the column and middle strips (as defined in the previous Section). In ACI 318–83, the fraction of the total frame moment to be carried by the column strip at each critical section is specified. The fraction depends on the aspect ratio of the slab panel and the relative stiffnesses of the various frame elements (beams, slabs, and columns) in both the longitudinal and transverse directions. Studies have shown that the performance of reinforced concrete flat slabs both at service loads and at overloads is little affected by variations in the fraction of the total frame moment that is assigned to the column

**Table 10.3** Fraction of frame moment distributed to column strip (AS 3600–1988).

Bending Moment Under Consideration	Column Strip Moment Factor
Negative Moment at an Interior Support	0.60 to 1.00
Negative Moment at an Exterior Support	0.75 to 1.00
Positive Moment at all Spans	0.50 to 0.70

strip (Gilbert 1984), provided that the slab is ductile and capable of the necessary moment redistribution.

AS 3600–1988 specifies that the column strip shall be designed to resist the total negative or positive frame bending moment at each section multiplied by a *column strip moment factor* taken within the ranges given in [Table 10.3](#).

An idealized frame analysis may be used to examine the serviceability of a floor slab. With the in-service moments caused by the unbalanced loads determined at all critical regions, checks for cracking and crack control and calculations of deflection may be undertaken in accordance with the procedures outlined in [Chapter 11](#).

When the ultimate strengths of the column and middle strips are being checked, it is advisable to ensure that the depth to the neutral axis at ultimate at any section does not exceed  $0.25d$ . This will ensure sufficient ductility for the slab to establish the moment distribution assumed in design (i.e. the moment pattern predicted by the idealized frame analysis) and also allows the designer safely to ignore the secondary moments. There are obvious advantages in allocating a large fraction of the negative moment at the supports to the column strip. The increased steel quantities that result stiffen and strengthen this critical region thereby improving punching shear and crack control. In prestressed flat slabs, it is usually only the column strip region over the interior columns that is likely to experience significant cracking. In Australia, in recent years, the use of uniform steel in the bottom of the slab (i.e. 50% of the positive frame moments assigned to the column strip) with all the top steel confined to the column strip (i.e. 100% of the negative frame moments assigned to the column strip) has become fairly common for reinforced concrete slabs which are not exposed to the weather. The in-service performance of such slabs is at least as good as that of the more traditionally reinforced slabs and significant cost savings usually result. Steel fixing is greatly simplified and, with large portions of the slab free from top steel, concrete placing is much easier.



### 10.6.4 Direct design method

A simple, semi-empirical approach for the analysis of flat plates is the *direct design method*. The method is outlined specifically for reinforced concrete slabs in a number of codes, including ACI 318–83 and AS 3600–1988. Within certain limitations, the direct design method can be applied equally well to prestressed slabs and the results obtained are just as reliable as those obtained from a frame analysis.

Limitations are usually imposed on the use of the direct design method, such as the following requirements imposed by AS 3600–1988. A similar set of requirements is contained in ACI 318–83.

- (a) There are at least two continuous spans in each direction (ACI 318–83 requires at least three continuous spans in each direction).
- (b) The support grid is rectangular, or nearly so.
- (c) The ratio of the longer to shorter span measured centre-to-centre of supports within any panel is not greater than 2.0.
- (d) In each direction, successive span lengths do not differ by more than one third of the longer span and in no case should an end span be longer than the adjacent interior span.
- (e) Gravity loads are essentially uniformly distributed. Lateral loads are resisted by shear walls or braced vertical elements and do not enter into the analysis.
- (f) The live load  $Q$  does not exceed twice the dead load  $G$  (in ACI 318–83,  $Q$  must not exceed  $3G$ ).

The slab is analysed one panel at a time. The total static moment,  $M_o$ , in each direction in each panel is calculated. For a particular span,

$$M_o = \frac{wL_t L_e^2}{8} \quad (10.11)$$

where  $w$  is the design load per unit area,  $L_t$  is the width, measured transverse to the direction of bending, equal to the average of the centre-to-centre distance between the supports of the adjacent transverse spans,  $L_e$  is the effective span, which is the lesser of the centre-to-centre distance between supports and  $(L_n + D)$ ,  $L_n$  is the clear span, and  $D$  is the overall slab thickness.

The static moment  $M_o$  is shared between the supports (negative moments) and the mid-span (positive moment). At any critical section, the design moment is determined by multiplying  $M_o$  by the relevant factor given in either Table 10.4 or 10.5. It is permissible to modify these design moments by up to 10% provided that the total static design moment  $M_o$  for the span is not reduced. At any interior support, the floor slab should

**Table 10.4** Design moment factors for an end span (AS 3600–1988).

Type of Slab System	Negative Moment at Exterior Support	Positive Moment	Negative Moment at Interior Support
<b>Flat Slabs</b>			
Exterior edge unrestrained	0.0	0.60	0.80
Exterior edges restrained by columns only	0.25	0.50	0.75
Exterior edges restrained by spandrel beams & columns	0.30	0.50	0.70
Exterior edge fully restrained	0.65	0.35	0.60
<b>Beam and Slab</b>	0.15	0.55	0.75

**Table 10.5** Design moment factor for an interior span (AS 3600–1988).

Type of Slab System	Negative Moment at Support	Positive Moment
ALL	0.65	0.35

be designed to resist the larger of the two negative design moments determined for the two adjacent spans unless the unbalanced moment is distributed to the adjoining members in accordance with their relative stiffnesses.

The positive and negative design moments are next distributed to the column and middle strips using the column strip moment factor from [Table 10.3](#).

#### 10.6.5 Shear strength

Punching shear strength requirements often control the thickness of a flat slab at the supporting columns and must always be checked. The shear strength of the slabs was discussed in [Chapter 5](#) (Sections [5.9](#) and [5.10](#)) and methods for designing the slab–column intersection were presented.

If frame analyses are performed in order to check the flexural strength of a slab, the design moment  $M_v^*$  transferred from the slab to a column and the design shear  $V^*$  are obtained from the relevant analyses. If the

direct design method is used for the slab design,  $M_v^*$  and  $V^*$  must be calculated separately. The shear force crossing the critical shear perimeter around a column support may be taken as the product of the factored design load  $w^*$  and the plan area of slab supported by the column and located outside the critical section. Equations for determining minimum values of  $M_v^*$  are specified in some codes of practice. AS 3600–1988 suggests that at an interior support,  $M_v^*$  should not be taken to be less than the value given by

$$M_v^* = 0.06[(1.25g + 0.75q)L_t(L_e)^2 - 1.25gL_t(L_e')^2] \quad (10.12)$$

where  $L_e$  and  $L_e'$  are, respectively, the longer and shorter of the two adjacent effective spans on either side of the column and  $L_t$  is the transverse width of slab defined in the text under Equation 10.11. The terms  $g$  and  $q$  are the dead and live loads on the slab per unit area, respectively. For an edge column,  $M_v^*$  is equal to the design moment at the exterior edge of the slab and may be taken as  $0.25M_o$  (where  $M_o$  is the static moment for the end span of the slab calculated using Equation 10.11).

When detailing the slab–column connection, it is advisable to have at least two prestressing tendons crossing the critical shear perimeter in each direction. Additional well anchored non-prestressed reinforcement crossing the critical perimeter will also prove beneficial (both in terms of crack control and ductility) in the advent of unexpected overloads.

### 10.6.6 Example 10.2

The tendons required in the 220 mm thick flat plate shown in [Figure 10.13](#) are to be calculated. The live load on the slab is 3.0 kPa and the dead load is 1.0 kPa plus the slab self-weight. All columns are 600 mm by 600 mm and are 4 m long above and below the slab. At the top of each column, a 300 mm column capital is used to increase the supported area, as shown. In this example, the dead load  $g$  is to be effectively balanced by prestress and is given by

$$g = 1 \text{ kPa} + \text{self-weight} = 1 + (24 \times 0.22) = 6.3 \text{ kPa}$$

#### 1 Checking punching shear

Before proceeding too far into the design, it is prudent to make a preliminary check of punching shear at typical interior and exterior columns. Consider the interior column B in [Figure 10.13](#). The area of slab supported by the column is  $10 \times (8.5 + 10) / 2 = 92.5 \text{ m}^2$ . Using the strength load factors specified in AS 3600–1988 (see [Section 1.7.3](#)), the factored design load is

$$w^* = 1.25g + 1.5q = (1.25 \times 6.3) + (1.5 \times 3.0) = 12.4 \text{ kN/m}^2$$

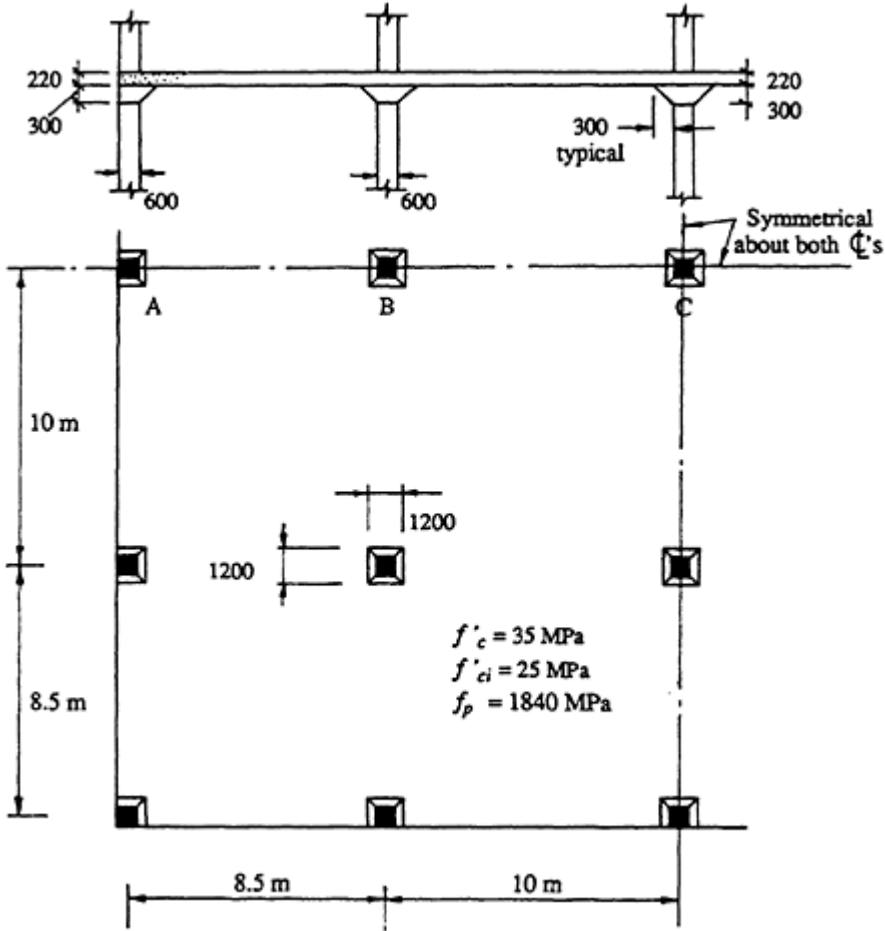


Figure 10.13 Plan and section of flat plate in Example 10.2.

and therefore the shear force crossing the critical section may be approximated by

$$V^* \doteq 12.4 \times 92.5 = 1140 \text{ kN}$$

From Equation 10.12, the design moment transferred to the column may be taken as

$$M_v^* = 0.06\{ [(1.25 \times 6.3) + (0.75 \times 3.0)] \times (10 \times 9.02^2) - (1.25 \times 6.3 \times 10 \times 7.52^2) \} = 227 \text{ kNm}$$

In this case, the effective spans  $L_e$  and  $L'_e$  are equal to the clear span on either side of the column capital plus the slab thickness. The average effective depth is taken to be  $d=220-50=170 \text{ mm}$  and the critical shear

perimeter is therefore

$$u = 4(1200 + 170) = 5480 \text{ mm}$$

The average prestress in the concrete is assumed to be  $\sigma_{cp}=2.75$  MPa and the concrete shear stress  $f_{cv}$  is given by Equation 5.52:

$$f_{cv} = 0.34\sqrt{35} = 2.01 \text{ MPa}$$

From Equation 5.51,

$$V_{uo} = [2.01 + (0.3 \times 2.75)] \times 5480 \times 170 \times 10^{-3} = 2640 \text{ kN}$$

The critical section possesses adequate shear strength if the design shear  $V^*$  is less than  $\phi V_u$ , where  $V_u$  is given by Equation 5.55:

$$\phi V_u = \frac{0.7 \times 2640}{1 + \frac{227 \times 10^6 \times 5480}{8 \times 1140 \times 10^3 \times 1200 \times 170}} = 1104 \text{ kN}$$

which is close enough to  $V^*$  to be considered acceptable at this preliminary stage. Punching shear at typical exterior columns should similarly be checked.

## 2 Establish cable profiles

Using four 12.7 mm strands in a flat duct and with 25 mm concrete cover to the duct (as shown in [Figure 10.9b](#)), the maximum depth to the centre of gravity of the strand is

$$d = 220 - (25 + 19 - 7) = 183 \text{ mm}$$

and the corresponding eccentricity is  $e=73$  mm. The maximum cable drape in an exterior span is therefore

$$h = \frac{73}{2} + 73 = 109.5 \text{ mm}$$

and in an interior span is

$$h = \frac{73 + 73}{2} + 73 = 146 \text{ mm}$$

Consider the trial cable profile shown in [Figure 10.14](#). For the purposes of this example, it is assumed that jacking occurs simultaneously from both

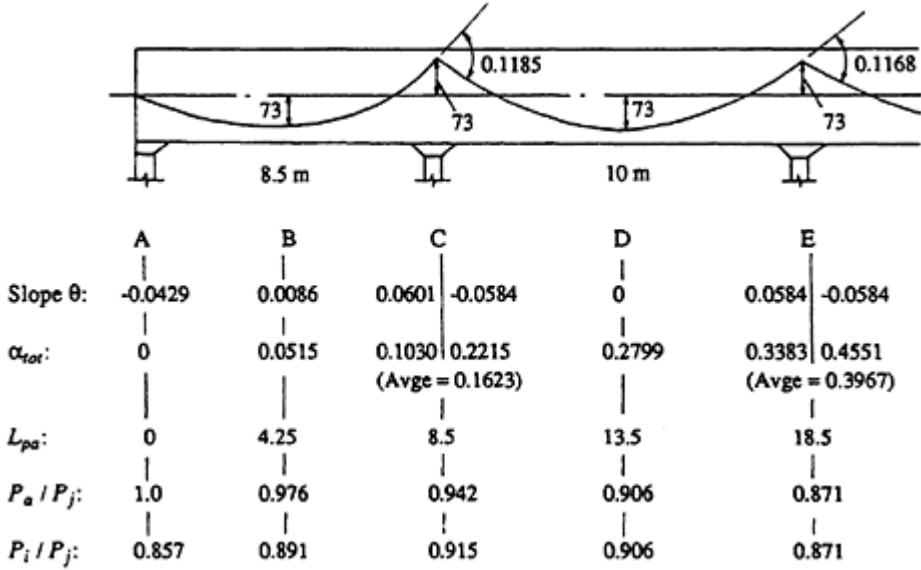


Figure 10.14 Friction loss details in Example 10.2

ends of a tendon, so that the prestressing force in a tendon is symmetrical with respect to the centreline of the structure shown in Figure 10.13. The friction losses are calculated from the exponential expression

$$\frac{P_a}{P_j} = \exp[-\mu(\alpha_t + \beta_p L_{pa})] \tag{3.60}$$

and the results are also shown in Figure 10.14. In this case,  $\mu=0.2$  and  $\beta=0.016$  for flat ducts.

The loss of prestress due to a 6 mm draw-in at the anchorage and the length of tendon affected should also be calculated. If the jacking force in a strand is assumed to be  $0.85f_p A_p = 0.85 \times 1840 \times 100 \times 10^{-3} = 156.4$  kN, the slope of the prestressing line in the exterior span is

$$\alpha/2 = (0.058 \times 156.4)/8.5 = 1.07 \text{ N/mm}$$

The length of beam affected by draw-in is given by Equation 3.61:

$$L_{di} = \sqrt{\frac{195\,000 \times 100 \times 6}{1.07}} = 10\,470 \text{ mm}$$

and the loss of force at the jack due to slip at the anchorage is

$$\delta P = \alpha L_{di} = 2 \times 1.07 \times 10\,470 \times 10^{-3} = 22.4 \text{ kN} = 0.143 P_j$$

The corresponding draw-in losses at B (the mid-point of the exterior

span) and at C (the first interior support) are

$$(\delta P)_B = 13.3 \text{ kN} = 0.085 P_j \quad \text{and} \quad (\delta P)_C = 4.4 \text{ kN} = 0.027 P_j$$

The ratio of the prestressing force after all short-term losses to the jacking force  $P_i/P_j$  is also shown in [Figure 10.14](#).

### 3 Calculate tendon layout

It is assumed here that the average time-dependent loss of prestress in each low relaxation tendon is 15%. Of course, this assumption should be subsequently checked.

The effective prestress per metre width required to balance 6.3 kPa using the full available drap is found using Equation 10.2:

$$P_e = \frac{6.3 \times 8.5^2}{8 \times 0.1095} = 520 \text{ kN/m in an exterior span}$$

and

$$P_e = \frac{6.3 \times 10^2}{8 \times 0.146} = 540 \text{ kN/m in an interior span}$$

and the corresponding forces required at the jack prior to the time-dependent and the short-term losses are

$$P_j = \frac{520}{0.85 \times 0.891} = 687 \text{ kN/m (exterior span)}$$

$$P_j = \frac{540}{0.85 \times 0.906} = 701 \text{ kN/m (interior span)}$$

The jacking force is therefore governed by the requirements for the interior span.

For the 8.5 m wide panel, the total jacking force required is  $701 \times 8.5 = 5960$  kN. If the maximum stress in the tendon is  $0.85f_p$ , the total area of prestressing steel is therefore

$$A_p \geq \frac{5960 \times 10^3}{0.85 \times 1840} = 3810 \text{ mm}^2$$

At least ten flat ducted cables are required in each 8.5 m wide panel ( $A_p = 400 \text{ mm}^2/\text{cable}$ ) with an initial jacking force of  $5960/10 = 596$  kN per cable ( $\sigma_{pj} = 0.81f_p$ ).

The required jacking force in the 10 m wide panel is  $701 \times 10 = 7010$  kN

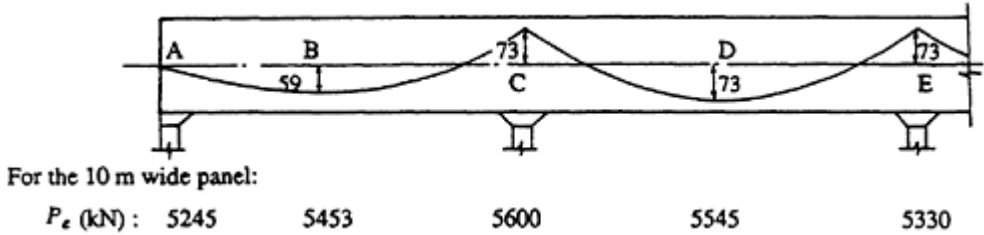


Figure 10.15 Cable profile and effective prestress in Example 10.2.

and therefore

$$A_p \geq \frac{7010 \times 10^3}{0.85 \times 1840} = 4482 \text{ mm}^2$$

At least twelve flat ducted cables are needed in each 10 m wide panel ( $A_p=4800 \text{ mm}^2$ ) with an initial jacking force of  $7010/12=584 \text{ kN}$  per cable ( $\sigma_{pj}=0.794f_p$ ).

In the interests of uniformity, all tendons will be initially stressed with a jacking force of  $600 \text{ kN}$  ( $\sigma_{pj}=0.82f_p$ ). This means that a slightly higher load than  $6.3 \text{ kPa}$  will be balanced in each span. The average prestress at the jack is  $(22 \times 600)/(8.5+10)=714 \text{ kN/m}$  and the revised drape in the

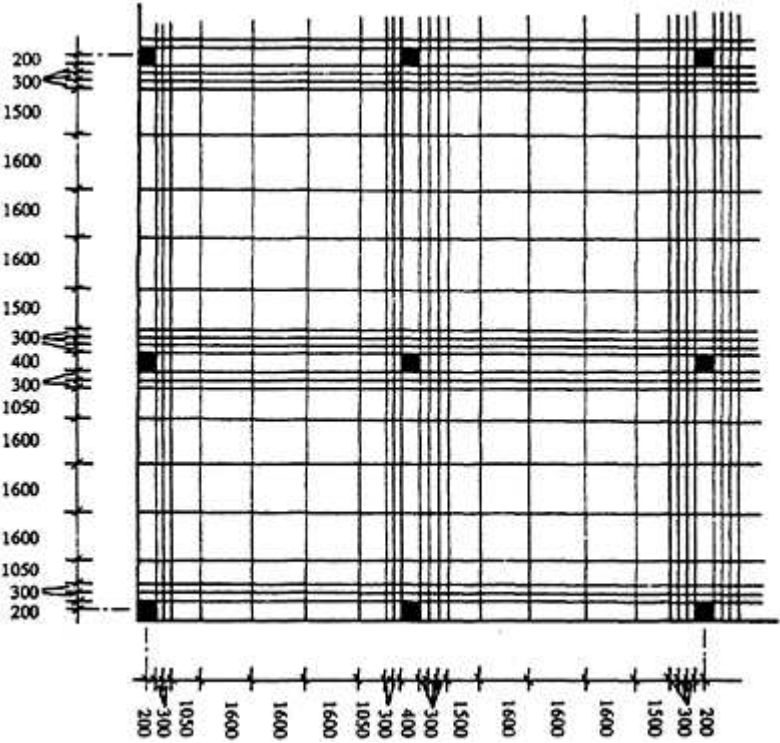


Figure 10.16 Tendon layout in Example 10.2.



exterior span is

$$h = \frac{6.3 \times 8.5^2}{8 \times 714 \times 0.891 \times 0.85} = 105 \text{ mm}$$

The final cable profile and effective prestress per panel after all losses are shown in [Figure 10.15](#).

The maximum average stress in the concrete due to the longitudinal anchorage force after the deferred losses is

$$\frac{P}{A} = \frac{5600 \times 10^3}{10000 \times 220} = 2.55 \text{ MPa}$$

which is within the recommended range for serviceability (see [Section 11.2](#)).

The cable layout for the slab is shown on the plan in [Figure 10.16](#). For effective load balancing, about 75% of the cables are located in the column strips. The minimum spacing of tendons is usually governed by the size of the anchorage and is taken here as 300 mm, while a maximum spacing of 1600 mm has also been adopted.

#### 4 Serviceability considerations

In practice, the deferred losses should now be checked and the slab analysed under the unbalanced loads to determine the extent of cracking and to calculate the slab deflections. Such serviceability considerations are examined in detail in [Chapter 11](#). A mat of conventional steel is often required over the columns to improve both crack control and strength. In addition, bonded non-prestressed steel of area  $0.0015bd_o = 0.0015 \times 1000 \times 195 = 293 \text{ mm}^2/\text{m}$  (12 mm diameter bars at 375 mm centres) is to be placed in the bottom of the slab perpendicular to the free edge in all exterior panels (in accordance with the discussion in the last paragraph of [Section 10.2](#)).

#### 5 Check shear and flexural strength

With the level of prestress determined, punching shear should also be checked at both exterior and interior columns in accordance with the procedure outlined in [Chapter 5](#) (see Sections [5.9](#) and [5.10](#)). The dimensions of the column capitals may need to be modified and shear reinforcement may be required in the spandrel strips along each free edge.

The ultimate flexural strength of the slab must also be checked. For the purposes of this example, the flexural strength of the interior panel will be compared with the design moments determined from the direct design method. As calculated in step 1,  $w^* = 12.4 \text{ kPa}$ , the panel width is  $L_t = 10 \text{ m}$  and the effective span of an interior panel is  $L_e = L_n + D =$

$10 - 1.2 + 0.22 = 9.02$  m. From Equation 10.11, the total static moment is

$$M_o = \frac{12.4 \times 10 \times 9.02^2}{8} = 1261 \text{ kN m}$$

From [Table 10.5](#), the negative support moment is

$$0.65M_o = 820 \text{ kN m}$$

Because both the positive and negative moment capacities are similar (each having the same quantity of prestressed steel at the same effective depth), it is appropriate to take advantage of the 10% permissible redistribution (reduction) in the negative support moment (as discussed in [Section 10.6.4](#)). The negative support moment is therefore taken as  $0.9 \times 820 = 738$  kNm and therefore the positive design moment at mid-span is  $1261 - 738 = 523$  kNm. From [Table 10.3](#), the design negative moment in the column strip at the support is taken as

$$M^* = 0.75 \times 738 = 554 \text{ kN m}$$

The 5 m wide column strip contains eight cables ( $A_p = 3200 \text{ mm}^2$ ) at an effective depth of 183 mm. The following results are obtained for the column strip at the column support in accordance with the ultimate strength procedures outlined in [Chapter 4](#):

$$\sigma_{pu} = 1750 \text{ MPa}; T_p = 5600 \text{ kN}; d_n = 47.0 \text{ mm} = 0.257 d;$$

$$M_u = 5600 \times 10^3 \left( 183 - \frac{0.801 \times 47.0}{2} \right) \times 10^{-6} = 919 \text{ kN m}; \text{ and}$$

$$\phi M_u = 736 \text{ kN m}$$

which is substantially greater than  $M^*$  and therefore the slab possesses adequate strength at this location. The strength is also adequate at all other regions in the slab. With the maximum value of  $d_n/d = 0.257$ , ductility is also acceptable.

### 10.6.7 Yield line analysis of flat plates

Yield line analysis is a convenient tool for calculating the collapse load required to cause flexural failure in reinforced concrete slabs. The procedure was described in detail by Johansen (1962, 1972) and is, in effect, a plastic method for the analysis of a two-way slab, with *yield lines* (or plastic hinge lines) developing in the slab and reducing the slab to a mechanism.

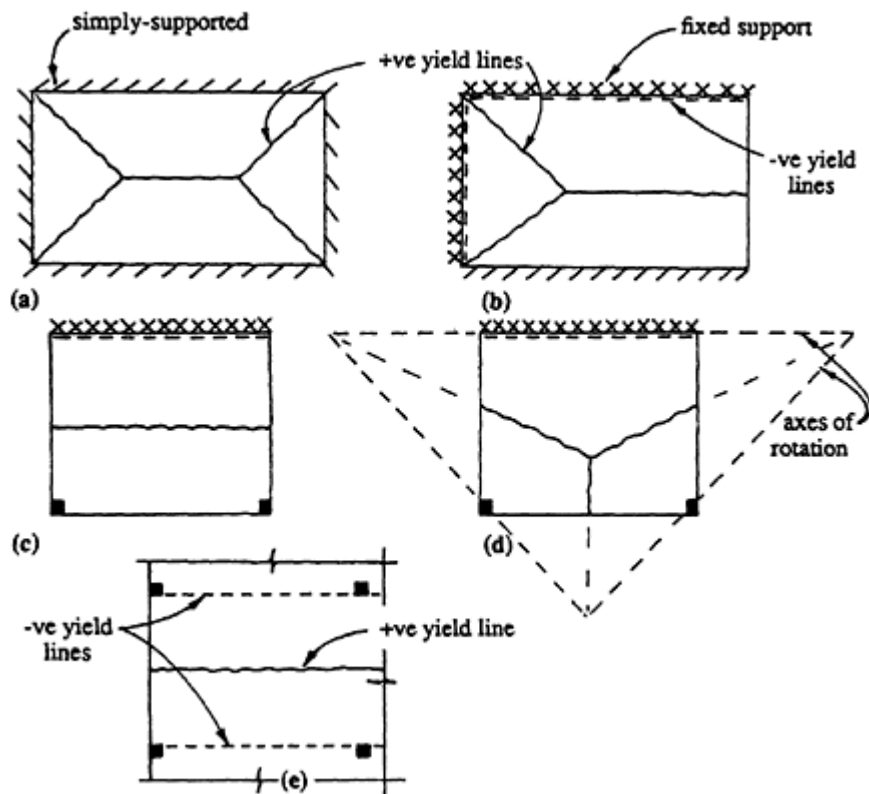


**Figure 10.17** Typical yield line patterns.

Typical yield line patterns for a variety of slab types subjected to uniformly distributed loads are shown in [Figure 10.17](#). The yield lines divide the slab into rigid segments. At collapse, each segment rotates about an axis of rotation that is either a fully supported edge or a straight line through one or more point supports, as shown. All deformation is assumed to take place on the yield lines between the rigid segments or on the axes of rotation. The yield line pattern (or the collapse mechanism) for a particular slab must be compatible with the support conditions.

The principle of virtual work is used to determine the collapse load corresponding to any possible yield line pattern. For a particular layout of yield lines, a compatible virtual displacement system is postulated. Symmetry in the slab and yield line pattern should be reflected in the virtual displacement system. The *external work*,  $U_e$  done by all the external forces as the slab undergoes its virtual displacement is equal to the *internal work*,  $U_i$ . The internal work associated with a particular yield line is the product of the total bending moment on the yield line and the angular rotation that takes place at the line. Since all internal deformation takes place on the yield lines, the internal work  $U_i$  is the sum of the work done on all yield lines.

In reinforced concrete slabs with isotropic reinforcement, the ultimate moment of resistance or plastic moment  $m_u$  (per unit length) is constant along any yield line and the internal work associated with any of the collapse mechanisms shown in [Figure 10.17](#) is easily calculated. In prestressed concrete slabs, the depth of the orthogonal prestressing tendons may vary from point to point along a particular yield line and the calculation of  $U_i$  is more difficult.

For flat plate structures, however, with the yield line patterns shown in [Figures 10.17e](#) and [10.18](#), the prestressing tendons crossing a particular yield line do so at the same effective depth, the plastic moment per unit length of the yield line is constant and the collapse load is readily calculated.

Consider the interior span of [Figure 10.18a](#). It is assumed conservatively that the columns are point supports and that the negative yield lines pass through the support centrelines. The slab strip shown is given a unit vertical displacement at the position of the positive yield line. The work done by the collapse loads  $w_u$  (in  $\text{kN/m}^2$ ) acting on the slab strip in the span under consideration is the total load on the strip times its average virtual displacement (which in this case is 0.5). That is,

$$U_e = \frac{w_u L_t L}{2} \tag{10.13}$$

The internal work done at the negative yield line at each end of the span is the total moment  $m_u L_t$  times the angular change at the yield line  $\theta$  ( $=1/(L/2)=2/L$ ). At the positive yield line, the angular change is  $2\theta$

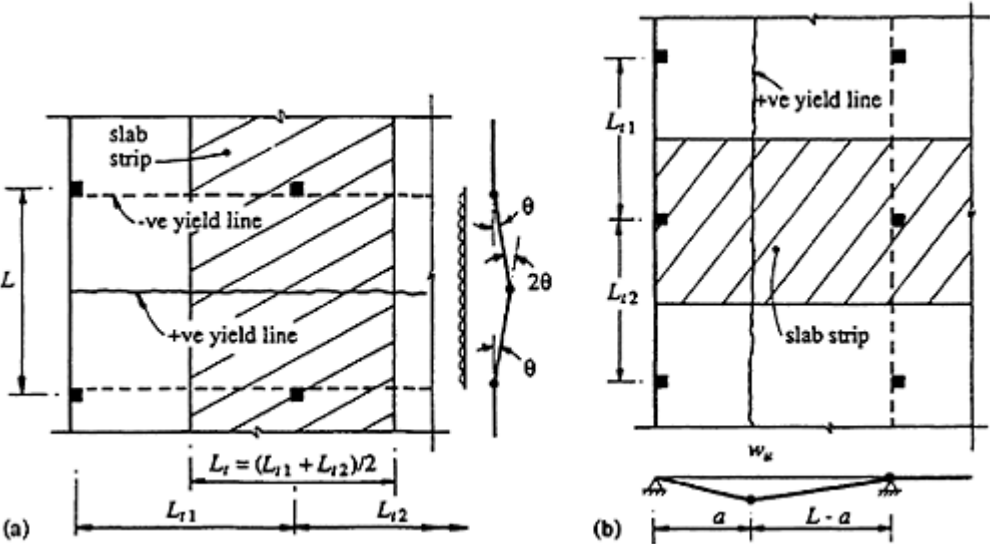


Figure 10.18 Yield line analysis of a flat plate.

( $=4/L$ ) and the internal work is  $m_u L_t \times 4/L$ . The total internal work on all yield lines is

$$U_i = m_u L_t \frac{4}{L} + 2m'_u L_t \frac{2}{L} = \frac{4L_t(m_u + m'_u)}{L} \quad (10.14)$$

The principle of virtual forces states that  $U_e = U_i$  and therefore

$$w_u = \frac{8}{L^2} (m_u + m'_u) \quad (10.15)$$

where  $m_u$  and  $m'_u$  are the ultimate moments of resistance per unit length along the positive and negative yield lines, respectively.

When calculating  $m_u$  and  $m'_u$ , it is reasonable to assume that the total quantity of prestressed and non-prestressed steel crossing the yield line is uniformly distributed across the slab strip, even though this is unlikely to be the case.

The amount of non-prestressed steel and the depth of the prestressed tendons may be different at each end of an interior span, and hence the value of  $m'_u$  at each negative yield line may be different. When this is the case, the positive yield line will not be located at mid-span. The correct position is the one that corresponds to the smallest collapse load  $w_u$ .

Consider the exterior span in [Figure 10.18b](#). If the positive yield line is assumed to occur at mid-span, the collapse load is given by an expression similar to Equation 10.15, except that only one negative yield line contributes to the internal work and therefore

$$w_u = \frac{8}{L^2} (m_u + 0.5m'_u) \quad (10.16)$$

For the case when  $m_u$  and  $m'_u$  have the same magnitude, the value of  $w_u$  given by Equation 10.16 is

$$w_u = \frac{12m_u}{L^2} \quad (10.17)$$

However, a smaller collapse load can be obtained by moving the position of the positive yield line a little closer to the exterior edge of the slab strip. The minimum collapse load for the mechanism shown in [Figure 10.18b](#) occurs when  $a=0.414L$ , and the internal work is

$$U_i = L_t m_u \left( \frac{1}{0.414L} + \frac{1}{0.586L} \right) + L_t m'_u \frac{1}{0.586L} = \frac{5.83 L_t m_u}{L}$$

The external work is still given by Equation 10.13. Equating the internal and external work gives

$$w_u = \frac{11.66m_u}{L^2} \quad (10.18)$$

The collapse loads predicted by both Equations 10.17 and 10.18 are close enough to suggest that, for practical purposes, the positive yield line in this mechanism may be assumed to be at mid-span.

Yield line analysis is therefore an *upper bound approach* and predicts a collapse load that is equal to or greater than the theoretically correct value. It is important to check that another yield line pattern corresponding to a lower collapse load does not exist. In flat plates, a fan-shaped yield line pattern may occur locally in the slab around a column (or in the vicinity of any concentrated load), as shown in [Figure 10.19](#).

The concentrated load  $P_u$  at which the fan mode shown in [Figure 10.19c](#) occurs is

$$P_u = 2\pi(m_u + m'_u) \quad (10.19)$$

The loads required to cause the fan mechanisms around the columns in [Figures 10.19a](#) and [b](#) increase as the column dimensions increase. Fan mechanisms may be critical in cases where the column dimensions are both less than about 6% of the span in each direction (see Ritz *et al.* 1981).

Although yield analysis theoretically provides an upper bound to the collapse load, slabs tested to failure frequently (almost invariably) carry very much more load than that predicted. When slab deflections become large, in-plane forces develop in the slab and the applied load is resisted by *membrane action* in addition to bending. The collapse load predicted by yield line analysis is therefore usually rendered conservative by membrane action.

Although yield line analysis provides a useful measure of flexural strength, it does not provide any information regarding serviceability. Service-load behaviour must be examined separately.

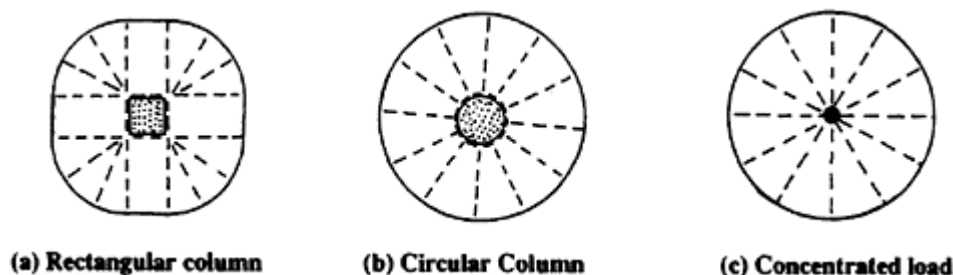


**Figure 10.19** Fan mechanisms at columns or under concentrated loads.

## 10.7 Flat slabs with drop panels

Flat slabs with drop panels behave and are analysed similarly to flat plates. The addition of drop panels improves the structural behaviour both at service loads and at overloads. Drop panels stiffen the slab, thereby reducing deflection. Drop panels also increase the flexural and shear strength of the slab by providing additional depth at the slab-column intersection. The extent of cracking in the negative moment region over the column is also reduced. The slab thickness outside the drop panel may be significantly reduced from that required for a flat plate. Drop panels, however, interrupt ceiling lines and are often undesirable from an architectural point of view.

Drop panels increase the slab stiffness in the regions over the columns and therefore affect the distribution of slab moments caused by unbalanced loads. The negative or hogging moments over the columns tend to be larger and the span moments tend to be smaller than the corresponding moments in a flat plate.

Building codes usually place minimum limits on the dimensions of drop panels. For example, on each side of the column centreline, drop panels should extend a distance equal to at least one sixth of the span in that direction (measured centre to centre of supports) (ACI 318–83). The projection of the drop below the slab should be at least one quarter of the slab thickness beyond the drop (ACI 318–83).

In [Figure 10.5](#), the moments introduced into a slab by the change in eccentricity of the horizontal prestressing force at the drop panels were illustrated. These may be readily included in the slab analysis. The fixed

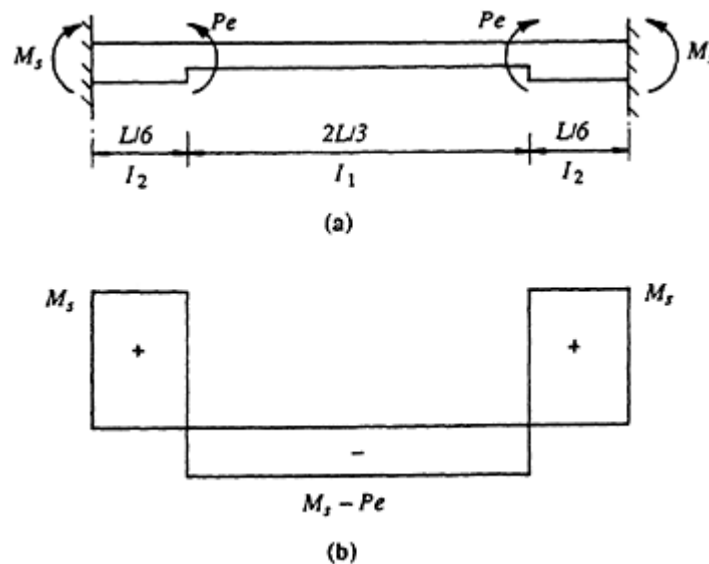


**Figure 10.20** Bending moments due to eccentricity of longitudinal prestress.

end moment at each support of the span shown in [Figure 10.20a](#) is given by

$$M_s = \frac{2P_e}{(I_1/I_2) + 2} \quad (10.20)$$

and the resultant bending moment diagram is shown in [Figure 10.20b](#). The moments of inertia of the various slab regions  $I_1$  and  $I_2$  are defined in [Figure 10.20a](#). The moments in the drop panel due to this effect are positive and those in the span are negative, as shown, and although usually relatively small, tend to reduce the moments caused by the unbalanced loads.

### 10.8 Band-beam and slab systems

Band-beam floors have become an increasingly popular form of prestressed concrete construction over the past decade or so. A one-way prestressed or reinforced concrete slab is supported by wide, shallow beams (slab-bands or band-beams) spanning in the transverse direction. The system is particularly appropriate when the spans in one direction are significantly larger than those in the other direction.

The slab-bands, which usually span in the long direction, have a depth commonly about two to three times the slab thickness and a width that may be as wide as the drop panels in a flat slab. A section through a typical band-beam floor is shown in [Figure 10.21](#). The one-way slab is normally considered to have an effective span equal to the clear span (from band edge to band edge) plus the slab depth. If the slab is prestressed, the tendons are usually designed using a load balancing approach and have a constant eccentricity over the slab bands with a parabolic drape through the effective span as shown in [Figure 10.21](#). The depth and width of the band beams should be carefully checked to ensure that the reaction from the slab, deposited near the edge of the band, can be safely carried back to the column line.

The prestressing forces at the slab tendon anchorages will also induce moments at the change of depth from slab to slab-band in the same way as was discussed for drop panels.



**Figure 10.21** Band-beam and slab floor system.



The slab-band is normally designed to carry the full load in the transverse direction (usually the long-span direction). The prestressing tendons in this direction are concentrated in the slab-bands and are also designed by load balancing. Because the prestress disperses out into the slab over the full panel width, the prestress anchorage should be located at the centroid of the T-section comprising the slab-band and a slab flange equal in width to the full panel.

When checking serviceability and strength of the slab-band, the effective flange width of the T-section is usually assumed to be equal to the width of the column strip as defined for a flat plate in [Section 10.6.2](#).

## 10.9 References

- ACI 318–83 1983. *Building code requirements for reinforced concrete*. Detroit: American Concrete Institute.
- AS 3600–1988. *Australian standard for concrete structures*. Sydney: Standards Association of Australia.
- AS 1480–1982. *Concrete structures code*. Sydney: Standards Association of Australia.
- Gilbert, R.I. 1984. Effect of reinforcement distribution on the serviceability of reinforced concrete flat slabs. *Proceedings of the 9th Australasian Conference on the Mechanics of Structures and Materials, University of Sydney, Sydney*, 210–214.
- Johansen, K.W. 1962. *Yield-line theory*. London: Cement and Concrete Association.
- Johansen, K.W. 1972. *Yield-line formulae for slabs*. London: Cement and Concrete Association.
- Ritz, P., P.Matt, Ch.Tellenbach, P.Schlub & H.U.Aeberhard, 1981. *Post-tensioned concrete in building construction—post-tensioned slabs*. Berne: Losinger.
- VSL Prestressing (Aust.) Pty. Ltd 1988. *Slab Systems*, 2nd edn. Sydney: V.S.L.
- Westergaard, H.M. & W.A.Slater 1921. Moments and stresses in slabs, *ACI Journal* **17**, 415–538.

# 11

## Two-way slabs—serviceability

### 11.1 Introduction

Prestressed concrete slabs are typically thin in relation to their spans and, although possessing adequate strength, may not possess adequate stiffness. If a slab is too thin, it may suffer excessively large deflections when fully loaded or exhibit excessive camber after transfer.

The initial selection of the thickness of a slab is usually governed by the serviceability requirements for the member. The selection is often based on personal experience or on recommended maximum span to depth ratios. Whilst providing a useful starting point in design, such a selection of slab thickness does not necessarily ensure serviceability. Deflections at all critical stages in the slab's history must be calculated and limited to acceptable design values. Failure to predict deflections adequately has frequently resulted in serviceability problems. In slab design, *excessive deflection* is a relatively common type of failure. This is particularly true for slabs supporting relatively large transitory live loads or for slabs not subjected to their full service loads until some considerable time after transfer. Codes of practice require that the camber, deflection, and vibration frequency and amplitude of slabs must be within acceptable limits at service loads. In general, however, little guidance is given as to how this is to be done and methods for computing camber or deflection are not prescribed.

The service load behaviour of a concrete structure is far less reliably known than its strength. Strength depends primarily on the properties of the reinforcing steel, whilst serviceability is most affected by the properties of concrete. The non-linear and inelastic nature of concrete complicates the calculation of deflection, even for line members such as beams. For two-way slab systems, the three-dimensional nature of the structure, the less well defined influence of cracking and tension stiffening, and the development of biaxial creep and shrinkage strains create additional difficulties. A more general discussion of the design of prestressed struc-

tures for serviceability, including types of deflection problems and criteria for deflection control, was given in [Section 1.7.7](#). Methods for determining the instantaneous and time-dependent behaviour of cross-sections at service loads were outlined in [Sections 3.5](#) and [3.6](#), and techniques for calculating beam deflections were presented in [Section 3.8](#).

Classical methods for calculating the deflection of elastic plates with ideal boundary conditions are of limited use in the design of practical concrete slabs. The edges of a concrete slab panel are never fully fixed or perfectly hinged, but have some intermediate degree of fixity which depends on the relative stiffnesses of the slab panel, the adjacent slab panels, and the supporting columns, beams, or walls. Numerical techniques, such as finite elements, are capable of closely modelling the non-linear and inelastic behaviour of slabs. However, for most slabs, the expense of such an analysis cannot be justified.

Nevertheless, various approximate methods are available which may be used economically and reliably to predict ball-park estimates of the deflection of two-way slabs. Several of these approximate methods are reviewed in [Section 11.4](#) and design recommendations are also made.

## 11.2 The balanced load stage

Under transverse loads, two-way panels deform into dish-shaped surfaces, as shown in [Figure 11.1](#). The slab is curved in both principal directions and therefore bending moments exist in both directions. In addition, part of the applied load is resisted by twisting moments which develop in the slab at all locations except the lines of symmetry.

As has already been discussed in [Chapter 10](#), prestressing tendons are usually placed in two directions parallel to the panel edges, each tendon providing resistance for its share of the applied load. The transverse load on the slab produced by the tendons in one direction adds to (or subtracts from) the transverse load imparted by the tendons in the perpendicular direction. For edge-supported slabs, the portion of the load to be carried

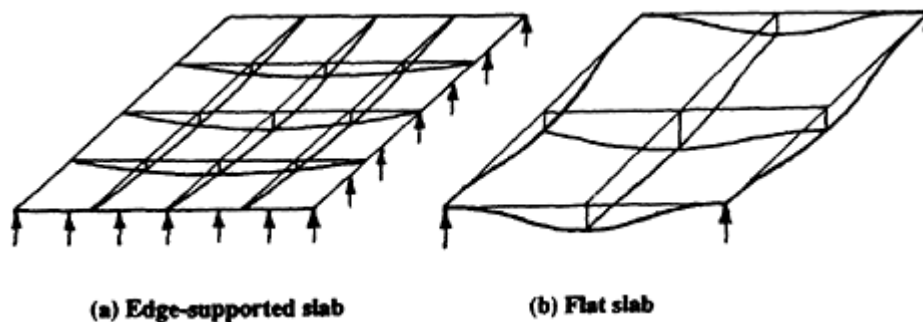


**Figure 11.1** Deformation of two-way slabs.

by tendons in each direction is more or less arbitrary, the only strict requirement is the satisfaction of statics (i.e. the satisfaction of Equation 10.4). For flat slabs the total load must be carried by tendons in each direction from column line to column line.

The concept of utilizing the transverse forces, resulting from the curvature of the draped tendons, to balance a selected portion of the applied load is useful from the point of view of controlling deflections. In addition to providing the basis for establishing a suitable tendon profile, load balancing allows the determination of the prestressing force required to produce zero deflection in a slab panel under the selected balanced load.

At the balanced load, the slab is essentially flat (no curvature) and is subjected only to the effects of the prestressing forces applied at the anchorages. A slab of uniform thickness is subjected only to uniform compression ( $P/A$ ) in the directions of the orthogonal tendons. With the state of the slab under the balanced load confidently known, the deflection due to the unbalanced portion of the load may be calculated by one of the approximate techniques discussed in [Section 11.4](#). The techniques are usually more reliable for prestressed slabs than for conventionally reinforced slabs, because only a portion of the total service load needs to be considered (the unbalanced portion) and, unlike reinforced concrete slabs, prestressed slabs are often uncracked at service loads.

To minimize deflection problems, the external load to be balanced is usually a significant portion of the sustained or permanent service load. If all the permanent load is balanced, the sustained concrete stress ( $P/A$ ) is uniform over the slab depth. A uniform compressive stress distribution produces uniform creep strain and, hence, little long-term load-dependent curvature or deflection. Bonded reinforcement does, of course, provide restraint to both creep and shrinkage and causes a change of curvature with time if the steel is eccentric to the slab centroid. However, the quantity of bonded steel in prestressed slabs is generally small and the time-dependent curvature caused by this restraint does not usually cause significant deflection.

Problems can arise if a relatively heavy dead load is to be applied at some time after stressing. Excessive camber after transfer, which will continue to increase with time owing to creep, may cause problems prior to the application of the full balanced load. In such a case, the designer may consider *stage stressing* as a viable solution.

The magnitude of the average concrete compressive stress after all losses can indicate potential serviceability problems. If  $P/A$  is too low, the prestress may not be sufficient to prevent or control cracking due to shrinkage, temperature changes, and the unbalanced loads. Some codes of practice specify minimum limits on the average concrete compressive stress after all losses. ACI 318–83 requires that  $P/A$  is greater than 125 psi (0.9 MPa). In Australia, where flat-ducted tendons containing four or more strands are

used, considerably more prestress is usually specified, with average compressive stress levels typically within the range 2.0–3.0 MPa in each direction of a two-way slab.

If the average prestress is high, axial deformation of the slab may be large and may result in distress in the supporting structure. The remainder of the structure must be capable of withstanding and accommodating the shortening of the slab, irrespective of the average concrete stress, but when  $P/A$  is large, the problem is exacerbated. Movement joints may be necessary to isolate the slab from stiff supports.

The FIP (1980) recommendation for the maximum spacing of tendons is six times the slab thickness. However, provided that cracking is unlikely (e.g. in the middle strips of a flat slab), a tendon spacing of eight times the slab thickness should prove acceptable (ACI 318–83).

## 11.3 Initial sizing of slabs

### 11.3.1 Existing guidelines

At the beginning of the design of a post-tensioned floor, the designer must select an appropriate floor thickness. The floor must be stiff enough to avoid excessive deflection or camber, and it must have adequate fire resistance and durability.

In its recommendations for the design of post-tensioned slabs, the Post-Tensioning Institute (1977) suggested typical span-to-depth ratios that had proved acceptable, in terms of both performance and economy, for a variety of slab types. These recommendations are summarized in [Table 11.1](#). Note that for flat plates and flat slabs with drop panels, the longer of the two orthogonal spans is used in the determination of the span-to-depth ratio, while for edge-supported slabs, the shorter span is used.

For flat slabs continuous over two or more spans in each direction, the

**Table 11.1** Span-to-depth ratios (Post-Tensioning Institute 1977).

Floor System	Span-to-Depth Ratio
Flat plate	45
Flat slab with drop panels	50
One-way slab	48
Edge-supported slab	55
Waffleslab	35
Band-beams ( $b \approx 3D$ )	30

**Table 11.2** Minimum slab thickness for insulation (AS 3600–1988).

Fire resistance period (minutes)	Minimum effective Minimum effective slab thickness (mm)
30	60
60	80
90	100
120	120
180	150
240	170

FIP (1980) recommends that the span-to-depth ratio should not generally exceed 42 for floors and 48 for roofs. These limits may be increased to 48 and 52, respectively, if the calculated deflections, camber and vibration frequency and amplitude are acceptable. Of course, strength requirements, such as punching shear, and fire resistance and durability requirements must also be considered.

A slab exposed to fire must retain its structural adequacy and its integrity for a particular *fire resistance period*. It must also be sufficiently thick to limit the temperature on one side when exposed to fire on the other side, i.e. it must provide a suitable fire resistance period for insulation. The fire resistance period required for a particular structure is generally specified by the local building authority and depends on the type of structure and its occupancy. The Australian code AS 3600–1988 specifies the minimum effective thickness of a slab required to provide a particular fire resistance

**Table 11.3** Minimum concrete cover for fire resistance of slabs (AS 3600–1988).

Fire resistance period (minutes)	Minimum concrete cover to bottom reinforcement (mm)			
	For simply-supported slabs		For continuous slabs	
	reinforcement	tendons	reinforcement	tendons
30	15	20	10	15
60	20	25	15	20
90	25	35	15	25
120	30	40	15	25
180	45	55	25	35
240	55	65	35	45

period for insulation and the minimum concrete cover to the bottom reinforcement in a slab in order to maintain structural adequacy. These requirements are given in Tables [11.2](#) and [11.3](#).

The span-to-depth ratios recommended by both the Post-Tensioning Institute and the FIP are usually conservative, but do not always guarantee serviceability. No consideration is made of the magnitude of the applied load, the level of prestress or the material properties, all of which greatly affect in-service behaviour. At best, these limits provide a useful starting point for design.

### *11.3.2 A serviceability approach for the calculation of slab thickness*

For uniformly loaded slabs, a better initial estimate of slab thickness which should ensure adequate stiffness and satisfactory service load behaviour can be made using a procedure originally developed for reinforced concrete slabs (Gilbert 1985) and recently extended to cover post-tensioned floor systems (Gilbert 1989). By rearranging the expression for the deflection of a span, a simple equation is developed for the span-to-depth ratio that is required to satisfy any specified deflection limit. The method forms the basis of the deemed to comply span-to-depth ratios for reinforced concrete slabs in the Australian code (AS 3600–1988).

If it is assumed that a prestressed concrete slab is essentially uncracked at service loads, which is most often the case, the procedure for estimating the overall depth of the slab is relatively simple. [Figure 11.2](#) shows a typical interior panel of a one-way slab, a flat-slab, and an edge-supported slab. *Equivalent one-way slab strips* are also defined for each slab type. For a one-way slab, the mid-span deflection is found by analysing a strip of unit width as shown in [Figure 11.2a](#). For the flat slab, the deflection at the midpoint of the long-span on the column line is found by analysing a unit wide strip located on the column line, as shown in [Figure 11.2b](#). For the edge-supported slab, the deflection at the centre of the panel may be calculated from an equivalent slab strip through the centre of the panel in the short direction, as shown in [Figure 11.2c](#).

By rearranging the equation for the mid-span deflection of the equivalent strip, an expression can be obtained for the minimum slab thickness required to satisfy any specified deflection limit. The stiffness of the equivalent strip must be adjusted for each slab type, so that the deflection of the strip is similar to the deflection of the two-way slab. For a flat slab, for example, the stiffness of the slab strip must be reduced significantly, if the maximum deflection at the centre of the panel is to be controlled rather than the deflection on the column line. This stiffness adjustment has been made in the following procedure by means of a *slab system factor*,  $K$ , which was originally calibrated using a non-linear, finite element model

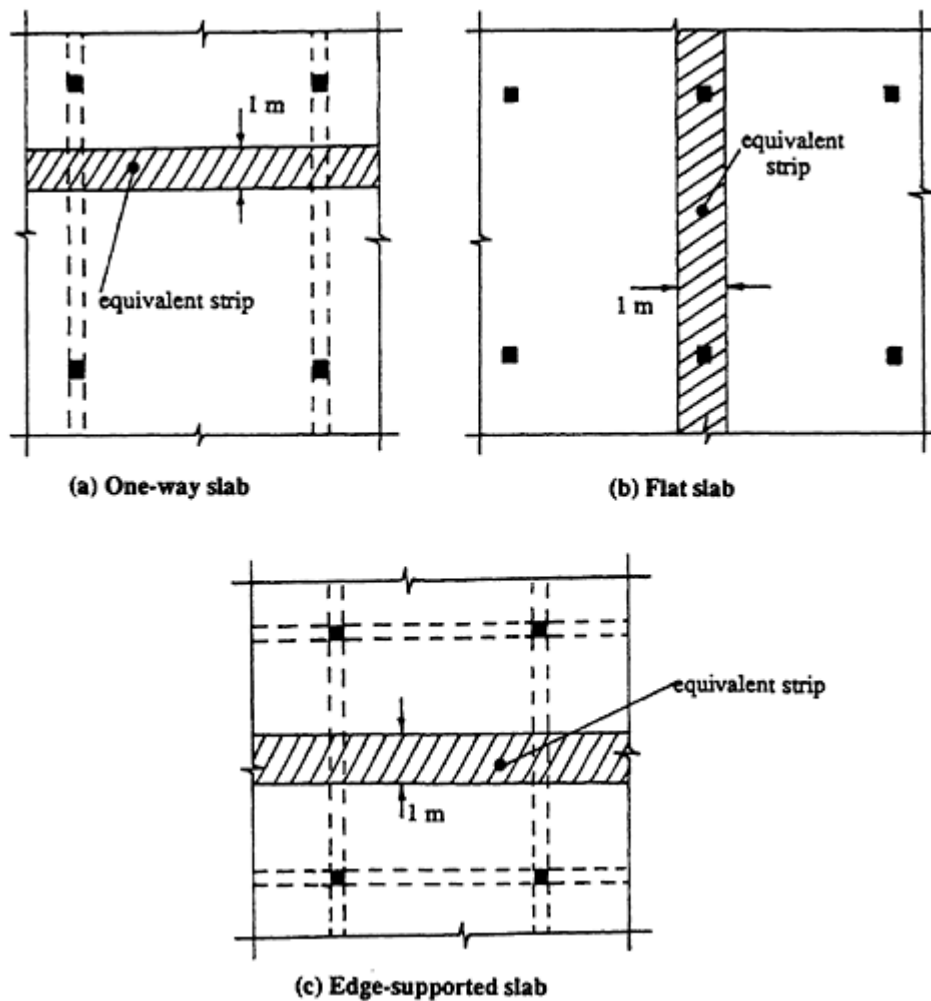


**Figure 11.2** Slab types and equivalent slab strips.

(Gilbert 1979a,b). A brief description of the finite element model is presented in [Section 11.4.7](#).

The maximum deflection caused by the unbalanced uniformly distributed service loads on an uncracked prestressed slab strip may be estimated using Equation 8.2, which is reproduced and renumbered here:

$$v = \beta \frac{w_u L e^4}{E_c I} + \beta \frac{\lambda w_{us} L e^4}{E_c I} \quad (11.1)$$

where  $w_u$  is the unbalanced service load per unit length and  $w_{us}$  is the sustained portion of the unbalanced load per unit length. In the design of a slab,  $w_{us}$  should not be taken less than 25% of the self-weight of the member. This is to ensure that at least a small long-term deflection is predicted by Equation 11.1. A small long-term deflection is inevitable, even



for the case when an attempt is made to balance the entire sustained load by prestress. The term  $\beta$  is a deflection coefficient that depends on the support conditions and the type of load. The effective span of the slab strip  $L_e$  may be taken to be the centre to centre distance between supports or the clear span plus the depth of the member, whichever is the smaller (AS 3600–1988).  $E_c$  is the elastic modulus of concrete and  $I$  is the gross moment of inertia of the cross-section. As discussed in [Section 8.3.1](#), the long-term deflection multiplier  $\lambda$  for an uncracked prestressed member is significantly higher than for a cracked reinforced concrete member. The ratio of the time-dependent creep-induced curvature and the initial curvature on an uncracked cross-section containing only small amounts of bonded reinforcement is similar in magnitude to the creep coefficient, and is therefore significantly greater than the corresponding ratio for a cracked cross-section. For uncracked, prestressed members, the value of  $\lambda$  in Equation 11.1 should not be less than 3.

By substituting  $bD^3/12$  for  $I$  and rearranging Equation 11.1, the following expression may be obtained for an uncracked beam of rectangular section (with width  $b$  and overall depth  $D$ ):

$$\frac{L_e}{D} = \left[ \frac{(v/L_e)bE_c}{12\beta(w_u + \lambda w_{us})} \right]^{1/3} \quad (11.2)$$

If  $v$  is the deflection limit selected in design, the maximum span to depth ratio for the beam is obtained from Equation 11.2.

To avoid dynamic problems, a maximum limit should be placed on the span-to-depth ratio. For concrete floors subjected to normal in-service loading conditions and not possessing any special vibration requirements, a lower limit to the frequency of the fundamental mode of the slab of about 5 cycles per second is sufficient to avoid excessive vertical acceleration which may cause discomfort to occupants. In a previous investigation, upper limits of the span-to-depth ratio for slabs were recommended to avoid vibration problems due to pedestrian traffic (Mickleborough & Gilbert 1986). This work forms the basis of the upper limits on  $L/D$  specified below in Equation 11.3.

For prestressed concrete slabs, an estimate of the minimum slab thickness may be obtained by applying Equation 11.2 to the slab strips in [Figure 11.2](#). Equation 11.2 can be re-expressed as follows:

$$\begin{aligned} \frac{L_e}{D} &\leq K \left[ \frac{(v/L_e)1000E_c}{w_u + 3w_{us}} \right]^{1/3} & (11.3) \\ &\leq 50 \quad \text{for one-way slabs and flat slabs} \\ &\leq 55 \quad \text{for two-way edge-supported slabs} \end{aligned}$$

The width of the equivalent slab strip  $b$  and the long-term deflection multiplier  $\lambda$  are taken as 1000 mm and 3, respectively. The loads  $w_u$  and  $w_{us}$  are in kPa and  $E_c$  is in MPa. The term  $K$  is the slab system factor, which accounts for the support conditions of the slab panel, the aspect ratio of the panel, the load dispersion, and the torsional stiffness of the slab. For each slab type, values for  $K$  are presented and discussed below.

### The slab system factor, $K$

**One-way slabs** For a one-way slab,  $K$  depends only on the support conditions and the most critical pattern of unbalanced load. From Equation 11.2,

$$K = (1/12\beta)^{1/3} \quad (11.4)$$

For a continuous slab,  $\beta$  should be determined for the distribution of unbalanced load which causes the largest deflection in each span. For most slabs, a large percentage of the sustained load (including self-weight) is balanced by the prestress and much of the unbalanced load is transitory. Pattern loading must therefore be considered in the determination of  $\beta$ .

For a *simply supported span*,  $\beta=5/384$  and from Equation 11.4,  $K=1.85$ . For a fully-loaded *end span* of a one-way slab that is continuous over three or more equal spans and with the adjacent interior span unloaded,  $\beta$  may be determined from an elastic analysis and taken to be  $3.5/384$  and therefore  $K=2.1$ . For an *interior span* of a continuous member, with adjacent spans unloaded,  $\beta$  may be taken to be  $2.6/384$  and  $K=2.3$ .

**Flat slabs** For flat slabs, the values of  $K$  given above must be modified to account for the variation of curvature across the panel width. The moments, and hence curvatures, in the uncracked slab are greater close to the column line than near the mid-panel of the slab in the middle strip region. For this reason, the deflection of the slab on the column line will be greater than the deflection of a one-way slab of similar span and continuity. If the deflection of the equivalent slab strip in [Figure 11.2b](#) is to represent accurately the deflection of the real slab on the column-line, a greater than average share of the total load on the slab must be assigned to the column strip (of which the equivalent strip forms a part). If it is assumed that 65% of the total load on the slab is carried by the column strips, then the value for  $K$  for a flat slab becomes

$$K = (1/15.6\beta)^{1/3} \quad (11.5)$$

For an end span, with  $\beta=3.5/384$ , Equation 11.5 gives  $K=1.90$ . For an interior span with  $\beta=2.6/384$ , the slab system factor  $K=2.1$ .

For a slab containing drop panels that extend at least  $L/6$  in each direction on each side of the support centreline and that have an overall depth not less than 1.3 times the slab thickness beyond the drops, the above values for  $K$  may be increased by 10%. If the maximum deflection at the centre of the panel is to be limited (rather than the deflection on the long-span column line), the values of  $K$  for an end span and for an interior span should be reduced to 1.75 and 1.90, respectively.

**Edge-supported two-way slabs** For an edge-supported slab, values for  $K$  must be modified to account for the fact that only a portion of the total load is carried in the short span direction and the fact that torsional stiffness and even compressive membrane action increase the overall slab stiffness. In a previous investigation of span-to-depth limits for reinforced concrete slabs, a non-linear finite element model was used to quantify these effects (Gilbert 1985). Values of  $K$  depend on the aspect ratio of the rectangular edge-supported panel and the support conditions of all edges, and are given in [Table 11.4](#).

**Table 11.4** Values of  $K$  for an uncracked two-way edge-supported slab (Gilbert 1989).

	Values of $K$			
	Ratio of Long Span to Short Span			
	1.0	1.25	1.5	2.0
4 edges continuous	3.0	2.6	2.4	2.3
1 short edge discontinuous	2.8	2.5	2.4	2.3
1 long edge discontinuous	2.8	2.4	2.3	2.2
2 short edge discontinuous	2.6	2.4	2.3	2.3
2 long edge discontinuous	2.6	2.2	2.0	1.9
2 adjacent edges discontinuous	2.5	2.3	2.2	2.1
2 short+1 long edge discontinuous	2.4	2.3	2.2	2.1
2 long+1 short edge discontinuous	2.4	2.2	2.1	1.9
4 edges discontinuous	2.3	2.1	2.0	1.9

### 11.3.3 Discussion

Equation 11.3 forms the basis of a useful approach to the design of prestressed concrete slabs. When the load to be balanced and the deflection limit have been selected, an estimate of slab depth can readily be made. All parameters required for input into Equation 11.3 are usually known at the beginning of the design. No estimate of self-weight is needed since, almost always, self-weight is part of the balanced load.

Deflections at various stages in the slab history may still have to be calculated, particularly if the unbalanced load causes significant cracking or if an unusual load history is expected. Serviceability problems, however, can be minimized by a careful choice of slab depth  $D$  using Equation 11.3. This involves an understanding of the derivation of the equation and its limitations. If, for example, a designer decides to minimize deflection by balancing the entire sustained load, it would be unwise to set the sustained part of the unbalanced load  $w_{us}$  to zero in Equation 11.3. In the real slab, of course, the magnitude of the sustained unbalanced load varies as the prestressing force varies with time and cannot remain zero. Restraint to creep and shrinkage caused by the eccentric bonded steel will inevitably cause some time-dependent deflection (or camber). In such cases, selection of a slab depth greater than that indicated by Equation 11.3 would be prudent. It is suggested that in no case should  $w_{us}$  be taken as less than 0.25 times the self-weight of the slab. As with the rest of the design process, sound engineering judgement is required.

### Example 11.1

A preliminary estimate is required of the thickness of a post-tensioned, flat slab floor for an office building. The supporting columns are 400 mm by 400 mm in section and are regularly spaced at 9.8 m centres in one direction and 7.8 m centres in the orthogonal direction. Drop panels extending span/6 in each direction are located over each interior column. The slab supports a dead load of 1 kPa (in addition to self-weight) and a service live load of 2.5 kPa (of which 0.75 kPa is sustained or permanent). The self-weight of the slab only is to be balanced by prestress. Therefore, the unbalanced loads are

$$w_u = 3.5 \text{ kPa} \quad \text{and} \quad w_{us} = 1.75 \text{ kPa}$$

In this example, the longer effective span is calculated as  $clear\ span + D$ . If  $D$  is initially assumed to be about 200 mm, then

$$L_e = 9800 - 400 + 200 = 9600 \text{ mm}$$

The elastic modulus for concrete is  $E_c = 28000 \text{ MPa}$ .

**Case (a)** The maximum deflection on the column line in the long-span direction is to be limited to span/250.

The deflection in an exterior or edge panel of the slab will control the thickness. From Equation 11.5,  $K = 1.90$  for an end span and may be increased by 10% to account for the stiffening effect of the drop panels.

Equation 11.3 gives

$$\frac{9600}{D} \leq 1.9 \times 1.1 \times \left[ \frac{(1/250) \times 1000 \times 28\,000}{3.5 + (3 \times 175)} \right]^{1/3} = 48.9$$

$$\therefore D \geq 196 \text{ mm plus drop panels}$$

**Case (b)** If the slab supports brittle partitions and the deflection limit is taken to be span/500, Equation 11.3 gives

$$\frac{9600}{D} \leq 1.9 \times 1.1 \times \left[ \frac{(1/500) \times 1000 \times 28\,000}{3.5 + (3 \times 1.75)} \right]^{1/3} = 38.8$$

$$\therefore D \geq 247 \text{ mm plus drop panels}$$

### Example 11.2

The slab thickness is required for an edge-panel of a two-way slab with short and long effective spans of 8.5 and 11 m, respectively. The slab is continuously supported on all four edges by stiff beams and is discontinuous on one long edge only. The slab must carry a dead load of 1.25 kPa (plus self-weight) and a service live load of 3 kPa (of which 1 kPa is sustained). As in the previous example, only the self-weight is to be balanced by prestress, and therefore,

$$w_u = 4.25 \text{ kPa} \quad \text{and} \quad w_{us} = 2.25 \text{ kPa}$$

The maximum midpanel deflection is limited to  $v=25$  mm. Take  $E_c=28\,000$  MPa.

With an aspect ratio of  $11.0/8.5=1.29$ , the slab system factor is obtained from [Table 11.4](#), i.e.  $K=2.4$ . From Equation 11.3,

$$\frac{8500}{D} \leq 2.4 \times \left[ \frac{(25/8500) \times 1000 \times 28\,000}{4.25 + (3 \times 2.25)} \right]^{1/3} = 47.0$$

$$\therefore D \geq 181 \text{ mm}$$

## 11.4 A review of simplified slab deflection models

### 11.4.1 Introduction

In view of the complexities and uncertainties involved in the calculation of the service load behaviour of two-way slab systems, great accuracy in the calculation of deflection is neither possible nor warranted. The procedures

briefly reviewed here for calculating initial and time-dependent slab deflections vary from simple estimates to reasonably sophisticated research models. A review of many of these approaches has been presented in a state-of-the-art report by ACI Committee 435 (1974).

#### 11.4.2 Classical methods

Small deflection theory of elastic plates can be used to predict slab deflections. Deflection coefficients for elastic slabs with ideal boundary conditions and subjected to full panel loading have been presented by Timoshenko & Woinowsky-Krieger (1959). The deflection of an elastic uniformly loaded slab panel may be expressed as

$$v = \beta \frac{wL^4}{C} \quad (11.6)$$

where  $\beta$  is the slab deflection coefficient,  $w$  is the uniformly distributed load,  $L$  is the longer span;  $C$  is the flexural rigidity, which is given by

$$C = \frac{E_c D^3}{12(1 - \nu^2)} \quad (11.7)$$

$D$  is the slab thickness; and  $\nu$  is Poisson's ratio for concrete (usually taken as about 0.2). For an uncracked concrete slab, the Poisson's ratio effect is small and Equation 11.6 can be approximated by

$$v = \beta \frac{wL^4}{E_c I_e} \quad (11.8)$$

**Table 11.5** Slab deflection coefficients,  $\beta$  (for  $\nu=0.2$ ).

<u>Long Span</u> <u>Short Span</u> $L/S$	Simply-supported on four edges $\beta$ for maximum $v$ in Equation 11.8	Fully fixed on four edges $\beta$ for maximum $v$ in Equation 11.8	Flat plate, $\beta$ for mid-span deflection in Equation 11.8	
			Single Isolated Panel	Interior Panel
1.0	0.00406	0.00126	0.0263	0.00581
1.2	0.00279	0.00085	0.0189	0.00428
1.4	0.00184	0.00059	0.0162	0.00358
1.6	0.00127	0.00035	0.0150	0.00321
1.8	0.00089	0.00023	0.0144	0.00302
2.0	0.00063	0.00016	0.0140	0.00292

where  $I_e$  is the moment of inertia per unit width, and may be taken as the gross moment of inertia for an uncracked slab.

Theoretical slab deflection coefficients ( $\beta$ ) for some uniformly loaded slab panels with ideal boundary conditions are given in [Table 11.5](#).

#### 11.4.3 Crossing beam analogy

The crossing beam analogy for *two-way edge-supported slabs* involves the consideration of a pair of orthogonal beams through the centre of the panel. By equating the deflection of each beam (calculated using gross stiffnesses), the fraction of the unbalanced load carried in each direction is readily determined. If  $L_y$  is the long span and  $L_x$  is the short span, the fraction of the unbalanced load carried in the short-span direction may be calculated using an expression similar to Equation 10.5, i.e.

$$w_{ux} = \frac{L_y^4}{\alpha L_x^4 + L_y^4} w_u \quad (11.9)$$

where  $\alpha$  depends on the support conditions of each orthogonal beam, with numerical values given under Equation 10.5. The slab deflection is calculated as the deflection of the shorter span beam strip subjected to the uniformly distributed load,  $w_{ux}$ . This method was first proposed by Marsh (1904) and is recommended for deflection calculation for two-way slabs in AS 3600–1988. The method ignores the torsional stiffness of the slab (which is a conservative assumption) and also assumes that the supports are unyielding (which may be an unconservative assumption).

The method has been modified by a number of investigators to account for the torsional moments in the slab. In fact, the approach described in [Section 11.3.2](#) for estimating the depth of a two-way edge-supported prestressed slab is based on the crossing beam analogy with the slab system factor  $K$  in [Table 11.4](#) calibrated to account for torsional moments.

For estimating the deflection at the centre of a uniformly loaded interior panel of a flat slab, the Portland Cement Association (1965) proposed the analysis of a fixed ended beam of unit width having a span equal to the diagonal length of the panel. The beam carries a load per unit length equal to the load per unit area of the slab. Although simple, this method has little to recommend it.

#### 11.4.4 Analogous gridwork and statics ratio methods

The analogous gridwork method (Ewell *et al.* 1952) is similar to the crossing beam method except that the effects of torsional moments are included. The slab is modelled by a set of orthogonal intersecting beams (say three or four in each direction) having the same flexural and torsional stiffness

as the slab. A stiffness analysis is then performed to obtain the deflection of the grid system. The number of calculations required is considerable and the number of simultaneous equations usually is too large for manual solution. However, the procedure is suitable for use with a small microcomputer or programmable calculator.

The statics ratio method (Furr 1959) is another variation on the crossing beam analogy. The slab is again divided into strips in each direction. The distributed slab load is replaced by statically equivalent concentrated loads acting at the beam strip intersections. An initial grid deflection is assumed and the vertical shears at each joint are found. The assumed grid deflection is successively modified until the vertical shear at each joint balances the applied load and the requirements of statics are met. Once again, the solution procedure is laborious. Since the advent of more accurate numerical techniques, such as finite difference and finite element methods, both the analogous gridwork method and the statics ratio method have fallen from favour.

#### 11.4.5 The Illinois method

The method proposed for the calculation of the mid-panel deflection of a flat slab by Vanderbilt *et al.* (1963) at the University of Illinois is well known. In [Figure 11.3](#), an interior panel of a flat slab is shown. Lines of contraflexure are assumed at one fifth of the span from the centrelines of the supporting columns, as indicated.

The deflection at the centre of the panel  $v_E$  is assumed to be the sum of three components:

$$v_E = v_1 + v_2 + v_3 \quad (11.10)$$

where  $v_1$  is the deflection at the mid-point C of the slab strip AB located on the column line in the longer span direction and bounded by the points of contraflexure (see [Figure 11.3](#)). The load assumed to act on the slab strip is the unbalanced load applied directly onto its surface plus the reaction off the central portion of the slab which may be treated as a two-way slab simply supported at the lines of contraflexure. In general,  $v_1$  is usually about three quarters of the value of  $v_E$ . The deflection increment  $v_2$  is the relative deflection between points D and C and is calculated by treating DC as a uniformly loaded, fixed ended cantilever with a concentrated load at the tip (the reaction from the central panel).  $v_3$  is the relative deflection between D and E and is found by treating the central portion of the slab as a simply supported two-way slab.

In general, good agreement has been found between results obtained by this method and those obtained by finite difference and finite element



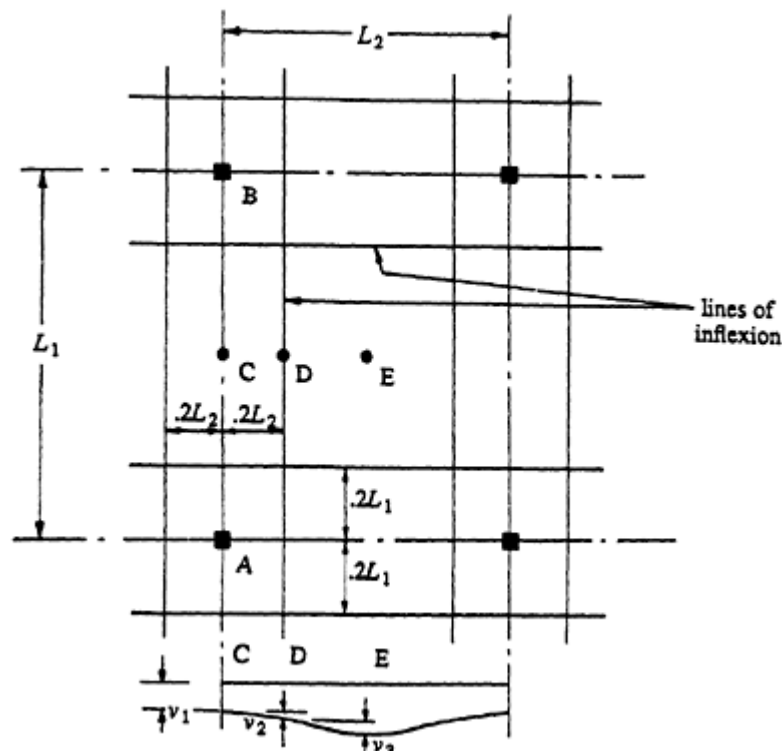


**Figure 11.3** The Illinois model for flat slab deflection (Vanderbilt *et al.* 1963).

analysis. However, the method involves many calculations and is not as convenient for manual solution as the following alternative approach.

#### 11.4.6 The wide beam method

The deflection of a uniformly loaded flat slab may be estimated using a wide beam method (often called the equivalent frame method) which was formalized by Nilson & Walters (1975). Originally developed for reinforced concrete slabs, the method is particularly appropriate for prestressed flat slabs which are usually uncracked at service loads (Nawy & Chakrabarti 1976). The basis of the method is illustrated in [Figure 11.4](#). Deflections of the two-way slab are calculated by considering separately the slab deformations in each direction. The contributions in each direction are then added to obtain the total deflection.

In [Figure 11.4a](#), the slab is considered to act as a wide, shallow beam of width equal to the panel dimension  $L_y$  and span equal to  $L_x$ . This wide beam is assumed to rest on unyielding supports. Because of variations in the unbalanced moments and flexural rigidity across the width of the slab, all unit strips in the  $x$ -direction will not deform identically. Unbalanced moments and hence curvatures in the regions near the column lines (the column strip) are greater than in the middle strips. This is particularly so for

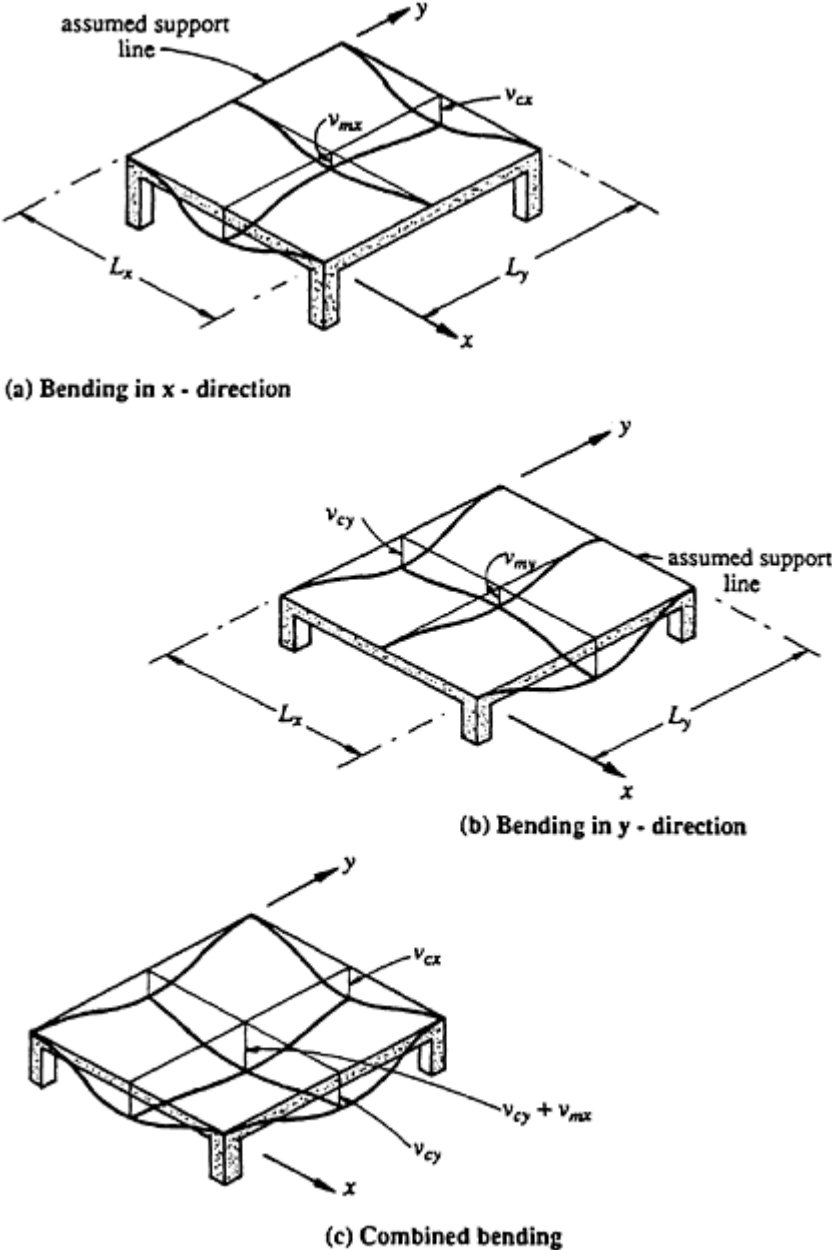


Figure 11.4 The basis of the wide beam method (Nilson & Walters 1975).

uncracked prestressed concrete slabs or in prestressed slabs that are cracked only in the column strips. The deflection on the column line is therefore greater than that at the panel centre. The slab is next considered to act as a wide shallow beam in the y-direction, as shown in Figure 11.4b. Once again, the effect of variation of moment across the wide beam is shown.

The mid-panel deflection is the sum of the mid-span deflection of the column strip in the long direction and that of the middle strip in the short

direction, as shown in [Figure 11.4c](#):

$$v_{max} = v_{cy} + v_{mx} \quad (11.11)$$

The method can be used irrespective of whether the moments in each direction are determined by the equivalent frame method, frame analysis based on gross stiffnesses, or the direct design method (see Sections [10.6.3](#) and [10.6.4](#)). The definition of column and middle strips, the longitudinal moments in the slab, the lateral moment distribution coefficients, and other details are the same as for the moment analysis, so that most of the information required for the calculation of deflection is already available.

The actual deflection calculations are more easily performed for strips of floor in either direction bounded by the panel centrelines, as is used for the moment analysis. In each direction, an average deflection  $v_{avge}$  at mid-span of the wide beam is calculated from the previously determined moment diagram and the moment of inertia of the entire wide beam,  $I_{beam}$ . This may be accomplished using the deflection calculation procedures outlined in [Section 3.8](#). The effect of the moment variation across the wide beam, as well as possible differences in column and middle strip sizes and rigidities, is accounted for by multiplying the average deflection by the ratio of the curvature of the relevant strip to the curvature of the beam. For example, for the wide beam in the  $x$ -direction, the column strip deflection is

$$v_{cx} = v_{avge.x} \frac{M_{col}}{M_{beam}} \frac{E_c I_{beam}}{E_c I_{col}} \quad (11.12)$$

and the middle strip deflection is

$$v_{mx} = v_{avge.x} \frac{M_{mid}}{M_{beam}} \frac{E_c I_{beam}}{E_c I_{mid}} \quad (11.13)$$

It is usual to assume  $M_{col}/M_{beam}$  to be about 0.7 and therefore  $M_{mid}/M_{beam}$  is about 0.3. If cracking is detected in the column strip, the effective moment of inertia of the cracked cross-section can be calculated using the analysis described in [Section 3.5.2](#). The average moment of inertia of the column strip is obtained by averaging the effective moments of inertia at each support and at mid-span. The moment of inertia of the wide beam is, of course, always the sum of  $I_{col}$  and  $I_{mid}$ . Long-term deflections due to sustained unbalanced loads can also be calculated in each direction using the procedure outlined in [Section 3.8.3](#).

Nilson & Walters (1975) originally proposed to analyse a fixed ended beam and then calculate the deflection produced by rotation at the supports. This does not significantly improve the accuracy of the model and the additional complication is not warranted.

11.4.7 Finite element methods

The finite element method is a powerful tool for the analysis of concrete slabs. The basic method is now well established and has been described in many text books. In this section, a brief description only is presented of a non-linear plate bending finite element model that was developed for the service-load analysis of both reinforced and prestressed concrete slabs.

Since the early 1970s, many investigators have developed finite element models to study the short-term service load behaviour of reinforced concrete slabs. A number of researchers have extended their models to handle the time-dependent effects of creep and shrinkage, including Scanlon & Murray (1974) and Gilbert (1979a,b). However, relatively few attempts have been made to model prestressed concrete slabs using finite elements.

The model briefly described here is presented in detail elsewhere (Gilbert 1979a). The elements used are rectangular, compatible, 16 degrees of freedom, plate-bending elements having four generalized displacements at each corner node of each element, namely the deflection, the slope about each orthogonal axis, and the twist. Each element is sub-divided into horizontal layers, as shown in [Figure 11.5](#), and idealized biaxial constitutive relation-

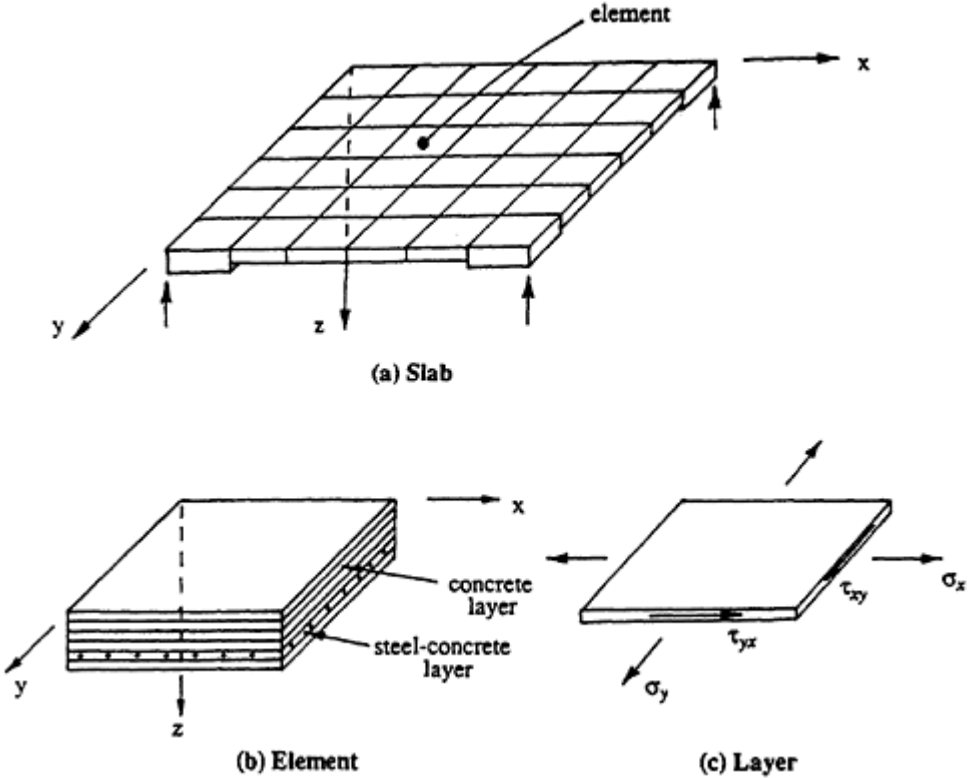


Figure 11.5 Finite element discretization (Gilbert 1979a).

ships are used to model the various stages of material behaviour in each layer. Non-linearities due to progressive cracking, tension stiffening, creep, and shrinkage are considered. Steel reinforcement is represented by an equivalent composite steel–concrete layer, in which the steel area is considered to be uniformly distributed throughout the layer and to contribute to the layer stiffness only in the direction of the bars. A draped post-tensioned tendon can be modelled by locating the tendon in different layers from element to element as required.

By layering each element, changes in material behaviour through the thickness of a slab can be accounted for, as either the external load or the time after first loading is increased, while retaining the limited number of degrees of freedom of a two-dimensional plate analysis. A close study of the internal state of stress and strain in the various regions of a slab is possible and an accurate model of the behaviour of slabs under service loads is obtained.

An incremental, piece-wise linear calculation procedure, involving geometric, load, and temporal discretization, is used. Structural response is calculated only at discrete instants along the time scale. At the first time instant (time zero), the initial prestress is transferred from the steel into the concrete using an initial-stress approach. The transverse external service load is then applied in small increments. Material non-linearity is also treated using a tangent stiffness, initial-stress procedure. At each subsequent time instant, the vectors of creep and shrinkage strain, which develop during the previous time increment in each concrete layer, are calculated. A direct relaxation approach is used to convert the time-dependent strain increments into stress decrements. Equilibrium is restored using a stress transfer procedure and structural response is calculated.

The model has been shown to predict accurately both the instantaneous and time-dependent behaviour of a variety of reinforced and prestressed concrete slabs and beams. However, the model places heavy demands on the computer, in terms of both storage requirements and solution times, and is entirely unsuitable for routine use in design. However, as a research tool the model is extremely useful. The effect of various parameters on slab behaviour can be examined. Factors which in practice are coupled and confounded may be uncoupled and examined separately in order to gain a better qualitative understanding of the mechanism of structural behaviour. Such parametric studies have been reported elsewhere (Gilbert 1979a).

The model also provides a rapid and relatively inexpensive means of generating the extensive test data which are required for deriving and calibrating simplified, design-oriented methods for estimating slab behaviour. In fact, the finite element model was used for the calibration of the values of  $K$  (in [Table 11.4](#)) which are used for the initial estimate of slab depth as discussed in [Section 11.3.2](#).

### 11.4.8 Recommendations

It can be seen that for estimating the deflection of prestressed concrete slab panels the designer has a reasonably wide choice of options. Considering both accuracy and ease of solution, it is recommended that for two-way edge-supported slabs, either the deflection coefficients based on classical methods ([Section 11.4.2](#)) or the crossing beam analogy ([Section 11.4.3](#)) is used. For flat slabs and plates, the wide beam method ([Section 11.4.6](#)) is recommended. These approaches have, in fact, been used in the calibration of the coefficients used in Equation 11.3. For uncracked slabs, Equation 11.3 may also be used to obtain a ball-park estimate of deflection.

## 11.5 Cracking in prestressed slabs

### 11.5.1 Loss of stiffness

The effect of cracking in slabs is to reduce the flexural stiffness of the highly stressed regions and thus to increase the deflection. Prior to cracking, deflection calculations are usually based on the moment of inertia of the gross concrete section,  $I_g$ , neglecting the contributions of the reinforcement. After cracking, an effective moment of inertia,  $I_e$ , which is less than  $I_g$  is used. In [Chapter 3](#), the analysis of a cracked prestressed section was presented and procedures for calculating the cracked moment of inertia and for including the tension stiffening effect were discussed. Using these procedures, the effective moment of inertia of a cracked region of the slab can be calculated.

For edge-supported prestressed concrete slabs, cracking is unlikely at service loads. Even reinforced concrete slabs continuously supported on all edges are often uncracked at service loads. However, if cracking is detected, then an average effective moment of inertia,  $I_e$ , should be used for the analysis of the equivalent slab strip or when using the slab deflection coefficients in [Table 11.5](#). Branson (1977) recommended that the value used for  $I_e$  should be the average of the moments of inertia of the positive and negative moment regions in the shorter span analogous beam. If a particular region is uncracked,  $I_e$  for this region should be taken to be equal to the gross moment of inertia  $I_g$ .

For prestressed concrete flat slabs, cracking at service loads is usually confined to the negative moment column strip region above the supports. A mat of non-prestressed reinforcement is often placed in the top of the slab over the column supports for crack control and to increase both the stiffness and the strength of this highly stressed region (see [Table 11.6](#)).

In the wide beam method, the effective moment of inertia of the column strip  $I_{col}$  is calculated as the average of  $I_e$  at the negative moment region

**Table 11.6** Minimum amount of non-prestressed reinforcement in slabs (CAN3 1984).

Type of Member	Tendon Type	
	bonded	unbonded
Beams and one-way slabs	0.003 $A$	0.005 $A$
Flat slabs		
–ve moment regions	0.00045 $h L_n$	0.00075 $h L_n$
+ve moment regions	0.003 $A$	0.005 $A$

Note:  $A$ =area of cross-section between tensile face and centroid;

$h$ =slab thickness;

$L_n$ =clear span in direction of reinforcement; and

$\lambda=1.0$  for normal-weight concrete

= 0.7 for light-weight concrete.

at each end of the strip, which may include the loss of stiffness due to cracking and/or the stiffening effect of a drop panel, and the positive moment region, which is usually uncracked.  $I_{col}$  is then added to the moment of inertia of the middle strip  $I_{mid}$  (which is also usually uncracked and therefore based on gross section properties) to form the moment of inertia of the wide beam,  $I_{beam}$ . These quantities are then used in the calculation of the column and middle strip deflections in each direction using Equations 11.12 and 11.13. The Commentary to ACI 318–83 recommends that the weighted average effective moment of inertia of an interior span of a continuous member is taken as 0.7 times the value at mid-span plus 0.3 times the average of the values at each end of the span. For an exterior span, the weighted average is 0.85 times the mid-span value plus 0.15 times the value at the continuous end. This recommendation may be used for the calculation of  $I_{col}$  for a cracked column strip.

### 11.5.2 Crack control

The mechanism of flexural cracking in a statically indeterminate two-way concrete slab is complex. The direction of flexural cracking is affected to some extent by the spacing and type of bonded reinforcement, the level of prestress in each direction, the support conditions, and the level and distribution of the applied loads. However, for slabs containing conventionally tied, bonded reinforcement at practical spacings in both directions,

flexural cracks occur in the direction perpendicular to the direction of principal tension.

If the level of prestress in a slab is sufficient to overcome the tension induced by bending, flexural cracking will not occur. If the level of prestress is not sufficient, cracking occurs and bonded reinforcement at reasonable centres is necessary to control the cracks adequately. Because slabs tend to be very lightly reinforced, the maximum moments at service loads are rarely very much larger than the cracking moment. However, when cracking occurs, the stress in the bonded reinforcement increases suddenly and crack widths may become excessive if too little bonded steel is present or the steel spacing is too wide. If the maximum flexural tensile stress in normal-weight concrete (calculated assuming linear-elastic material behaviour) does not exceed about  $0.5 \sqrt{f_c}$  (in MPa), flexural cracking will not be a problem in prestressed slabs containing bonded tendons (AS 3600–1988). If the calculated maximum tensile stress exceeds about  $0.5 \sqrt{f_c}$ , then cracking is likely to occur. To ensure crack control in such a region, the calculated increment of tensile steel stress, which occurs as the load is increased from its value when the extreme fibre concrete stress is zero up to the maximum service load, should be less than about 150 MPa (AS 3600–1988). In addition, the centre-to-centre spacing of bonded reinforcement should not exceed twice the slab thickness or 500 mm, whichever is smaller. Compare this with the requirements for beams, viz. a maximum tensile steel stress increment of 200 MPa and a maximum steel spacing of only 200 mm. In the Canadian code (CAN3 1984), the minimum amount of bonded non-prestressed reinforcement required for crack control in prestressed slabs in regions where the maximum calculated tensile stress exceeds  $0.5 \lambda \sqrt{f_c}$  is given in [Table 11.6](#).

As has already been mentioned, flexural cracking in practical prestressed slabs containing the minimum quantities of bonded reinforcement is rarely a problem. In contrast, *direct tension cracking* due to restrained shrinkage and temperature changes frequently leads to serviceability problems. This is particularly so for slabs that are prestressed in one direction only and slabs that are very lightly stressed in one or both directions. Shrinkage and temperature induced cracks in regions of low moment or, in the case of one-way slabs, in the direction of no moment, usually extend completely through the slab and tend to be more parallel sided than flexural cracks. To control such cracks, several options are available to the designer. Sufficient prestress may be introduced to overcome the load-independent tension, adequate quantities of non-prestressed steel may be included to limit the crack width to some acceptably small value, or a sufficient number of control joints (contraction joints) may be specified to ensure that all cracking is confined to predefined weakened planes across the slab. If direct tension cracks are uncontrolled and become excessively wide, waterproofing and corrosion problems may result, in addition to the obvious aesthetic problems.



Evidence of direct tension cracking is common in both reinforced and prestressed concrete slab systems. As an example, consider a one-way slab system with prestress only in the direction of the span. The applied load is carried across the span to the supporting beams or walls, while in the orthogonal direction the bending moment in the slab is small. Shrinkage occurs in both directions and restraint to shrinkage usually exists in both directions. In the span direction, shrinkage-induced tension may not be sufficient to overcome the prestress. If cracking does occur, it will be caused by tension induced by both shrinkage and flexure. Such cracks usually do not extend completely through the slab, but behave like flexural cracks and are controlled by the bonded flexural reinforcement. In summary, shrinkage in the direction of the span causes small increases in the widths of the existing flexural cracks and may cause additional flexure-type cracks in the previously uncracked regions. In the direction at right-angles to the span, there is no prestress and little moment. Restraint to shrinkage may cause tension over the entire slab thickness and result in a few widely spaced cracks which penetrate completely through the slab. If it is decided not to prestress in this direction or not to introduce control joints, a significant quantity of non-prestressed reinforcement is required to ensure that the cracks do not become unserviceable.

If the amount of reinforcement which crosses a direct tension crack is too small, yielding of the steel will occur and a wide, unserviceable crack will result. AS 3600–1988 specifies the minimum quantity of non-prestressed steel required to control cracking in a direct tension situation, i.e. when shrinkage and temperature effects are unaccompanied by bending. These requirements are summarized below.

Where the ends of a slab are unrestrained and the slab is free to expand or contract in the secondary direction (i.e. little or no induced tension), the minimum area of non-prestressed reinforcement in this direction is

$$(A_s)_{min} = \frac{(0.7 - \sigma_{cp})bD}{f_y} \quad (11.14)$$

where  $\sigma_{cp}$  is the average prestress ( $P/A$ ) in the direction under consideration. For a slab that is not prestressed in this direction (i.e.  $\sigma_{cp}=0$ ) and with reinforcement of yield stress  $f_y=400$  MPa, Equation 11.14 indicates a minimum reinforcement ratio ( $A_s/bD$ ) of 0.0018.

Where the ends of a slab are restrained and the slab is not free to expand or contract (as is usually the case in most practical situations), the minimum area of reinforcement in the restrained direction depends on the exposure conditions. For severe exposure conditions (such as a marine or aggressive industrial environment),

$$(A_s)_{min} = \frac{(2.5 - \sigma_{cp})bD}{f_y} \quad (11.15)$$

which corresponds to a reinforcement ratio of 0.0063 for 400 MPa steel, when the prestress is zero. For moderate exposure conditions, in situations where a strong degree of control over cracking is required,  $(A_s)_{min}$  is given by Equation 11.15. This would apply for example in the case of an exposed roof slab (not located in a marine or industrial environment), where water tightness is a design requirement, or any other slab in which visible cracking must be avoided. For moderate exposure conditions, where a moderate degree of control over cracking is required,

$$(A_s)_{min} = \frac{(1.4 - \sigma_{cp})bD}{f_y} \quad (11.16)$$

which corresponds to a reinforcement ratio of 0.0035 for 400 MPa steel when  $\sigma_{cp}=0$ . This would apply for example in the case of an interior slab in which visible cracking could be tolerated or an interior slab which was later to be covered by a floor covering or ceiling.

## 11.6 Long-term deflections

As discussed in [Chapter 3](#), long-term deflections due to creep and shrinkage are influenced by many variables, including load intensity, mix proportions, slab thickness, age of slab at first loading, curing conditions, quantity of compressive steel, relative humidity, and temperature.

In most prestressed slabs, the majority of the sustained load is balanced by the transverse force exerted by the tendons on the slab. Under this balanced load, the time-dependent deflection will not be zero because of the restraint to both creep and shrinkage offered by eccentrically located bonded reinforcement. The use of a simple deflection multiplier to calculate long-term deflection is not, therefore, always satisfactory.

In [Section 2.5](#), guidelines for determining both the final creep coefficient for concrete,  $\phi^*$ , and the final shrinkage strain,  $\epsilon_{sh}^*$ , were presented and a procedure for the determination of the long-term behaviour of a partially prestressed section in bending was outlined in [Section 3.6.3](#). Alternative and more approximate expressions for estimating the creep and shrinkage components of the long-term deflection of beams were given in [Section 3.8.3](#). Similar equations for slab deflection are presented below.

For uncracked, prestressed concrete slabs, which usually have low quantities of steel, the increase in curvature due to creep is nearly proportional to the increase in strain due to creep. This is in contrast with the behaviour of a cracked, reinforced section. The final creep induced deflection  $v_{cr}$  may therefore be approximated by setting  $\alpha=1.0$  in Equation 3.76. That is,

$$v_{cr} = \phi^* v_{sus} \quad (11.17)$$

where  $v_{sus}$  is the short-term deflection produced by the sustained portion of the unbalanced load. Typical values for the final creep coefficient for concrete in post-tensioned slabs are  $\phi^* = 2.5-3.0$ .

The average deflection due to shrinkage of an equivalent slab strip (in the case of edge-supported slabs) or the wide beam (as discussed in [Section 11.4.6](#) for the case of flat slabs) may be obtained from Equation 3.77 as

$$v_{sh} = \beta \kappa_{sh}^* L_e^2 \quad (11.18)$$

where  $\kappa_{sh}^*$  is the average shrinkage-induced curvature,  $L_e$  is the effective span of the slab strip under consideration, and  $\beta$  depends on the support conditions and equals 0.125 for a simply supported span, 0.090 for an end span of a continuous member, and 0.065 for an interior span of a continuous member.

The shrinkage curvature  $\kappa_{sh}^*$  is non-zero wherever the eccentricity of the steel area is non-zero and varies along the span as the eccentricity of the draped tendons varies. A simple and very approximate estimate of the average shrinkage curvature for a fully prestressed slab, which will usually produce reasonable results is

$$\kappa_{sh}^* = \frac{0.3 \epsilon_{sh}^*}{D} \quad (11.19)$$

For a cracked partially prestressed slab, with significant quantities of conventional reinforcement, the value of  $\kappa_{sh}^*$  is usually at least 100% higher than that indicated above.

## 11.7 Worked examples

### 11.7.1 Example 11.3—edge-supported slab

The deflection at the mid-span of the exterior panel of the 180 mm thick floor slab shown in [Figure 10.9](#) and analysed in [Example 10.1](#) is to be calculated. The slab forms the floor of a retail store and is post-tensioned in both directions using the draped parabolic cable profiles shown in [Figure 10.9c](#) and 10.9d. For the purpose of this example, the average effective prestress after losses in each direction is assumed to be 400 kN/m. The slab supports a dead load of 1.5 kPa in addition to its own self-weight and the live load  $Q$  is 5.0 kPa. As in [Example 10.1](#),  $f_c^i = 35 \text{ MPa}$ ,  $E_c = 30000 \text{ MPa}$ ,  $\phi^* = 2.5$ ,  $\epsilon_{sh}^* = 0.0005$ , and  $E_p = 195\,000 \text{ MPa}$ .

#### Calculate slab loads

$$\text{Dead load, } G = (24 \times 0.18) + 1.5 = 5.8 \text{ kPa}$$

In accordance with the discussion in [Section 1.7.5](#) concerning *load combinations* for the serviceability limit states, the fraction of the live load which is considered to be appropriate for short-term service load calculations for a retail store is taken to be  $\psi_s = 0.6$  (AS 3600–1988). The fraction of the live load which is considered to be sustained or permanent is taken to be  $\psi_l = 0.3$  (AS 3600–1988).

### Calculate the balanced load

In the  $x$ -direction, the tendon drupe is  $h_x=79.5$  mm (as calculated in [Example 10.1](#)), and the transverse force exerted by the  $x$ -direction tendons on the slab is obtained from Equation 10.3:

$$w_{bx} = \frac{8h_x P_x}{L^2} = \frac{8 \times 0.0795 \times 400}{9^2} = 3.14 \text{ kN/m}^2$$

In the  $y$ -direction, the drupe is  $h_y=87$  mm and the associated transverse force is

$$w_{by} = \frac{8h_y P_y}{L^2} = \frac{8 \times 0.087 \times 400}{12^2} = 1.93 \text{ kN/m}^2$$

The total transverse force due to the curvature of the tendons in each direction (the balanced load) is therefore

$$w_b = w_{bx} + w_{by} = 5.1 \text{ kPa}$$

### Estimate maximum moment due to unbalanced load

The maximum unbalanced transverse load to be considered for short-term serviceability calculations is

$$w_u = G + w_b + \psi_s Q = 5.8 - 5.1 + (0.6 \times 5.0) = 3.7 \text{ kPa}$$

Under this unbalanced load, the maximum moment occurs over the beam support CD. Using the moment coefficients for edge-supported slabs in [Table 10.2](#), the maximum moment is

$$M_{CD} = -0.058 \times 3.7 \times 9^2 = -17.4 \text{ kNm/m}$$

### Check for cracking

In the  $x$ -direction over support CD, the concrete stresses in the top and bottom fibres are

$$\sigma_t = -\frac{P_x}{A} - \frac{M_{CD}}{Z} = -2.22 + 3.22 = +1.00 \text{ MPa (tension)}$$

$$\sigma_b = -\frac{P_x}{A} + \frac{M_{CD}}{Z} = -2.22 - 3.22 = -5.44 \text{ MPa (compression)}$$

where  $A$  is the area of the gross cross-section per metre width ( $=180 \times 10^3 \text{ mm}^2/\text{m}$ ) and  $Z$  is the section modulus per metre width ( $=5.4 \times 10^6 \text{ mm}^3/\text{m}$ ).

As can be seen, both tensile and compressive stresses are low. Even though the moment used in these calculations is an average and not a peak moment, cracking is unlikely and deflection calculations may be based on the gross moment of inertia,  $I_g$ :

$$I_g = \frac{180^3 \times 1000}{12} = 486 \times 10^6 \text{ mm}^4/\text{m}$$

### Estimate maximum total deflection

Using the crossing beam analogy of [Section 11.4.3](#), the unbalanced load carried by the analogous beam in the  $x$ -direction is obtained from Equation 11.9:

$$w_{ux} = \frac{12^4}{2.0 \times 9^4 + 12^4} \times 3.7 = 0.61 \times 3.7 = 2.27 \text{ kN/m}$$

and the corresponding short-term deflection at mid-span of this 1 m wide propped cantilever is approximated by

$$v = \frac{2w_{ux}L_x^4}{384E_cI_g} = \frac{2}{384} \times \frac{2.27 \times 9000^4}{30\,000 \times 486 \times 10^6} = 5.3 \text{ mm}$$

The sustained portion of the unbalanced load on the analogous beam is  $0.61(G_u + \psi_l Q_u) = 0.61[(5.8 - 5.1) + (0.3 \times 5.0)] = 1.34 \text{ kN/m}$  and the corresponding short-term deflection is

$$v_{sus} = \frac{1.34}{2.27} \times 5.3 = 3.1 \text{ mm}$$

Assuming a creep coefficient of  $\phi^* = 2.5$ , the creep-induced deflection may be estimated using Equation 11.17:

$$v_{cr} = 2.5 \times 3.1 = 7.7 \text{ mm}$$

If the final shrinkage strain is assumed to be  $\epsilon_{sh}^* = 0.0005$ , the average shrinkage-induced curvature is estimated using Equation 11.19:

$$\kappa_{sh}^* = \frac{0.3 \times 0.0005}{180} = 0.83 \times 10^{-6} \text{ mm}^{-1}$$

and the shrinkage-induced deflection is approximated using Equation 11.18:

$$v_{sh} = 0.090 \times 0.83 \times 10^{-6} \times 9000^2 = 6.1 \text{ mm}$$

The maximum total deflection of the analogous beam is therefore

$$v_{tot} = v + v_{cr} + v_{sh} = 19.1 \text{ mm}$$

The deflection at the centre of the slab panel will be approximately 30% less than this owing to the torsional stiffness of the slab which has been ignored in the above analysis. The maximum panel deflection is therefore approximated by

$$v_{tot} = \frac{19.1}{1.3} = 14.7 \text{ mm}$$

It is of value to examine the slab thickness predicted by Equation 11.3 if the limiting deflection is taken to be 14.7 mm. For this edge-supported slab panel, the slab system factor is obtained from [Table 11.4](#) as  $K=3.07$ , the unbalanced load  $w_u=3.7$  kPa, and the sustained part of the unbalanced load is  $w_{us}=0.7+1.5=2.2$  kPa. The minimum slab thickness required to limit the total deflection to 14.7 mm is obtained from Equation 11.3:

$$\frac{9000}{D} \leq 3.07 \left[ \frac{(14.7/9000) \times 1000 \times 30\,000}{3.7 + (3 \times 2.2)} \right]^{1/3} = 51.6$$

$$\therefore D \geq 174 \text{ mm}$$

In this example, Equation 11.3 is slightly unconservative because the unbalanced sustained load is small and the creep and shrinkage deflections are not completely accounted for by the assumed deflection multiplier. Nevertheless, it can be seen that a very useful initial estimate of slab thickness can be obtained by using Equation 11.3 and heeding the discussion in [Section 11.3.3](#).

### 11.7.2 Example 11.4—flat slab

The deflection of an interior panel of a 200 mm thick flat slab in a library is to be checked. A plan of the slab panel is shown in [Figure 11.6](#). Drop panels 3400×2700×100 mm thick are located above each column support, as shown. All columns are 400×400 mm in plan. The slab supports a dead load of 0.5 kPa, in addition to self-weight, and a live load of 8.0 kPa. The average effective prestress in the  $y$ -direction is 640 kN/m and in the

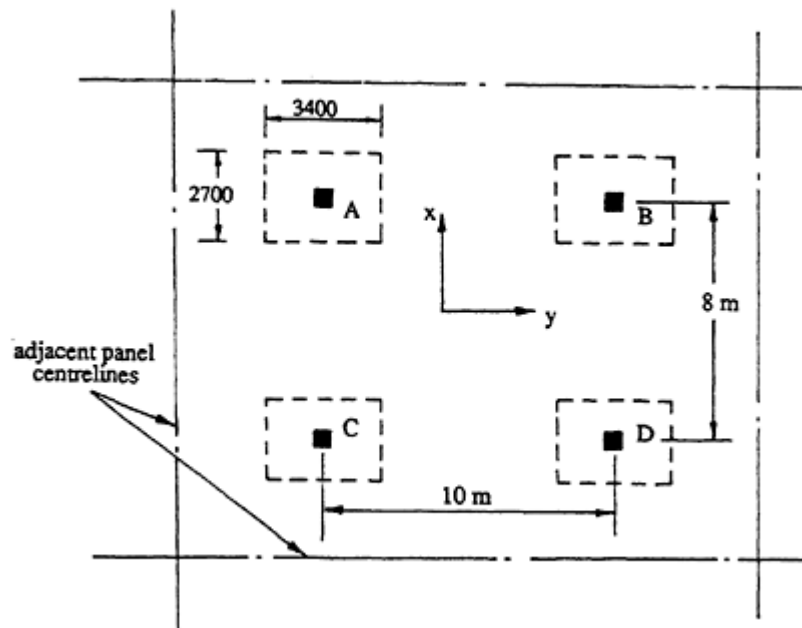


Figure 11.6 Plan of flat slab of [Example 11.4](#).

$x$ -direction 410 kN/m. The post-tensioned tendons in each direction are bonded to the surrounding concrete and have been designed to balance a total load of 6.0 kPa. The concrete and steel properties are as for Example 11.3.

### Calculate slab loads

The dead load is

$$G = (24 \times 0.2) + 0.5 = 5.3 \text{ kPa}$$

For a library, the service load factors specified in AS 3600–1988 are  $\psi_s = 0.8$  and  $\psi_l = 0.5$ , and live loads for short- and long-term serviceability calculations are therefore  $\psi_s Q = 6.4$  kPa and  $\psi_l Q = 4.0$  kPa, respectively.

### Estimate unbalanced load

The maximum short-term transverse load to be considered is

$$w_u = G + w_b + \psi_s Q = 5.3 - 6.0 + (0.8 \times 8.0) = 5.7 \text{ kPa}$$

The wide beam method ([Section 11.4.6](#)) is used here to calculate slab deflection. The wide beams in each direction are bounded by the panel centreline and the centreline of the adjacent panel. Under the unbalanced load, the moment diagrams for the wide beams in each direction were calculated using the direct design method (see [Section 10.6.4](#)) and are shown in

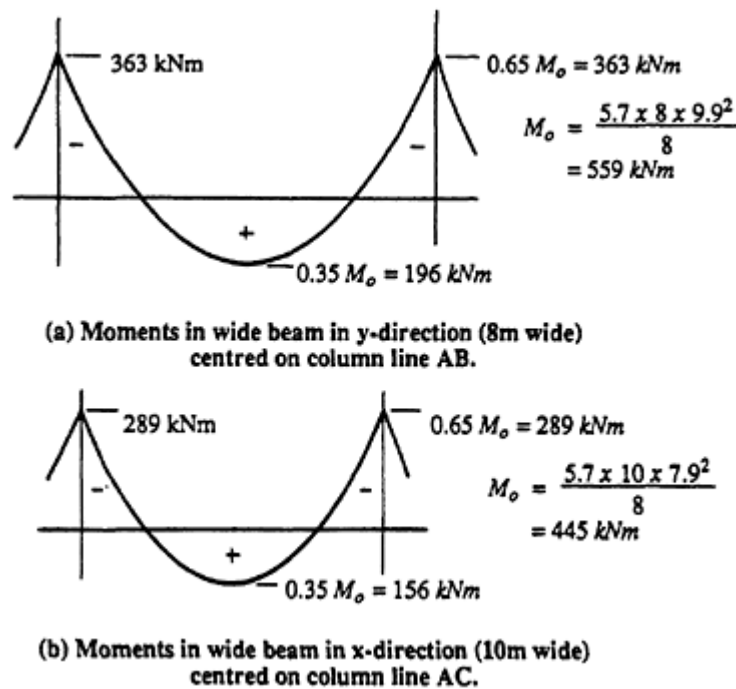


Figure 11.7 Moment diagrams for flat slab panel of [Example 11.4](#).

Figures [11.7a](#) and [b](#). The effective spans in the short and long directions are 7.9 and 9.9 m, respectively (i.e. clear span plus depth).

### Check for cracking

**(a) Negative moment in column strip in y-direction** The cross-section of the column strip in the y-direction is shown in [Figure 11.8a](#), together with the section properties. The longitudinal prestress in the column strip is  $P_y = 4 \times 640 = 2560$  kN. Taking 75% of negative moment in column strip gives

$$M_y = -0.75 \times 363 = -272 \text{ kNm}$$

and the tensile stress in the top fibre is

$$\begin{aligned} \sigma_t &= -\frac{P_y}{A} - \frac{M_y z}{I_g} = -\frac{2560 \times 10^3}{1070 \times 10^3} - \frac{-272 \times 10^6 \times 137.9}{7.43 \times 10^9} \\ &= +2.66 \text{ MPa} < 0.5\sqrt{f'_c} \end{aligned}$$

**(b) Negative moment in column strip in x-direction** The longitudinal prestress in the column strip shown in [Figure 11.8b](#) is  $P_x = 4 \times 410 = 1640$  kN. The



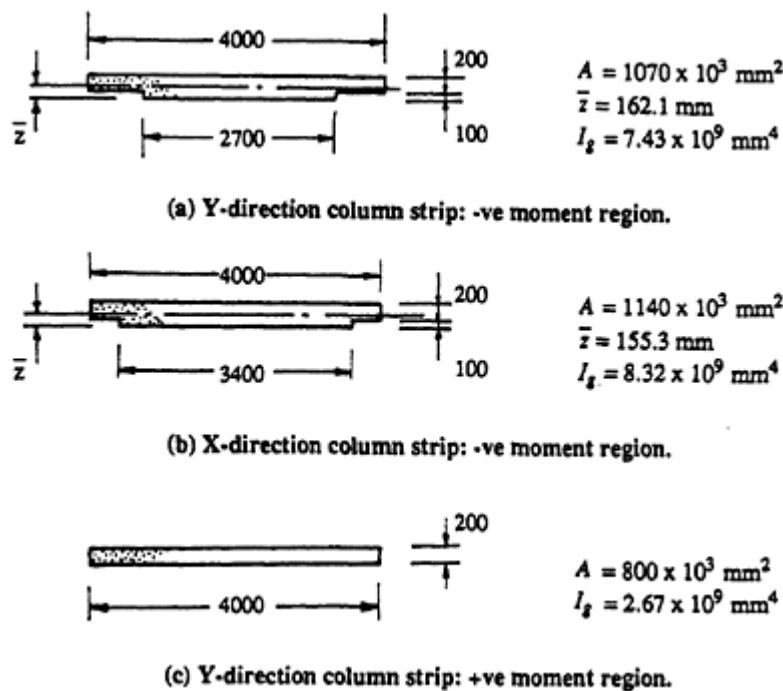


Figure 11.8 Cross-sectional properties of column strips in [Example 11.4](#).

column strip moment is

$$M_x = -0.75 \times 289 = -217 \text{ kN m}$$

and the top fibre tensile stress is given by

$$\begin{aligned} \sigma_t &= -\frac{P_x}{A} - \frac{M_x z}{I_g} = -\frac{1640 \times 10^3}{1140 \times 10^3} - \frac{-217 \times 10^6 \times 144.7}{8.32 \times 10^9} \\ &= +2.33 \text{ MPa} < 0.5\sqrt{f'_c} \end{aligned}$$

Although the average tensile stresses in the column strips are less than the tensile strength of concrete, some local cracking over the column support is likely since peak moments are much higher than average values. A mesh of non-prestressed reinforcement should be provided over the drop panel to ensure crack control. However, the calculated top fibre tensile stresses indicate that cracking will not be extensive and is not likely to reduce the stiffness of the column strip significantly. The area of non-prestressed steel in each direction may be obtained from [Table 11.6](#):

$$A_{sty} = 0.00045 \times 300 \times 9600 = 1296 \text{ mm}^2$$

$$A_{stx} = 0.00045 \times 300 \times 7600 = 1026 \text{ mm}^2$$

(c) **Positive moment in column strip in y-direction** If 60% of the positive moment in the y-direction is assigned to the column strip, then

$$M_y = 0.6 \times 196 = 118 \text{ kNm}$$

and the tensile stress in the bottom fibre of the cross-section shown in [Figure 11.8c](#) is

$$\begin{aligned}\sigma_b &= -\frac{P_y}{A} + \frac{M_y z}{I_g} = -\frac{2560 \times 10^3}{800 \times 10^3} + \frac{118 \times 10^6 \times 100}{2.67 \times 10^9} \\ &= +1.22 \text{ MPa} < 0.5\sqrt{f'_c}\end{aligned}$$

By inspection, the maximum tensile stress at mid-span in the column strip in the x-direction is also small. Cracking is therefore unlikely to reduce the slab stiffness significantly and deflections may be calculated using gross section properties.

### Short-term deflections

The small upward deflection caused by eccentricity of prestress at the drops is not included in the following calculations. Consider a wide beam in the y-direction (similar to that described in [Section 11.4.6](#)). The average moment of inertia of the column strip  $I_{col}$  is taken as the weighted average of  $I$  at the supports ( $7.43 \times 10^9 \text{ mm}^4$ ) and at mid-span ( $2.67 \times 10^9 \text{ mm}^4$ ). In accordance with the weighting procedure outlined in the Commentary to ACI 318–83,

$$I_{col} = (0.7 \times 2.67 \times 10^9) + (0.3 \times 7.43 \times 10^9) = 4.10 \times 10^9 \text{ mm}^4$$

The middle strip is 4000 mm wide and 200 mm deep, and therefore  $I_{mid} = 2.67 \times 10^9 \text{ mm}^4$ . The moment of inertia of the wide beam is thus

$$I_{beam} = I_{col} + I_{mid} = 6.77 \times 10^9 \text{ mm}^4$$

The maximum average deflection  $v_{avge}$  at mid-span of the wide beam occurs when adjacent spans are unloaded. In accordance with the discussion in [Section 11.3.2](#) concerning pattern loading, the appropriate deflection coefficient is  $\beta = 2.6/384$  and the average deflection of the wide beam may be taken as

$$v_{avge,y} = \frac{2.6}{384} \times \frac{w_u L_e^4}{E_c I_{beam}} = \frac{2.6 \times 8 \times 5.7 \times 9900^4}{384 \times 30\,000 \times 6.77 \times 10^9} = 14.6 \text{ mm}$$

Taking 70% of moment in the column strip, the deflection of the column

strip is obtained from Equation 11.12:

$$v_{cy} = 0.7 v_{avg,y} \frac{I_{beam}}{I_{col}} = 0.7 \times 14.6 \times \frac{6.77}{4.10} = 16.9 \text{ mm}$$

From Equation 11.13, the middle strip deflection in the  $y$ -direction is

$$v_{my} = 0.3 \times 14.6 \times \frac{6.77}{2.67} = 11.1 \text{ mm}$$

Similarly, considerations of the wide beam in the  $x$ -direction give  $I_{col}=4.37 \times 10^9 \text{ mm}^4$ ,  $I_{mid}=4.00 \times 10^9 \text{ mm}^4$ ,  $I_{beam}=8.37 \times 10^9 \text{ mm}^4$ , and

$$v_{cx} = 8.0 \text{ mm} \quad \text{and} \quad v_{mx} = 3.8 \text{ mm}$$

The maximum short-term deflection at the mid-point of the panel due to the unbalanced load is obtained by adding the  $y$ -direction column strip deflection to the  $x$ -direction middle strip deflection (Equation 11.11):

$$v_{max} = v_{cy} + v_{mx} = 16.9 + 3.8 = 20.7 \text{ mm}$$

### Long-term deflections

The sustained portion of the unbalanced load is

$$w_{us} = -0.7 + (0.5 \times 8) = 3.3 \text{ kPa}$$

The short-term mid-panel deflection produced by the sustained unbalanced load is therefore

$$v_{sus} = \frac{3.3}{5.7} \times 20.7 = 12.0 \text{ mm}$$

With a creep factor of  $\phi^* = 2.5$ , the creep-induced deflection is obtained from Equation 11.17:

$$v_{cr} = 2.5 \times 12.0 = 30.0 \text{ mm}$$

If the final shrinkage strain is  $\epsilon_{sh}^* = 0.0005$ , then from Equation 11.19, the shrinkage curvature in each direction is

$$\kappa_{sh} = \frac{0.3 \times 0.0005}{200} = 0.75 \times 10^{-6} \text{ mm}^{-1}$$

and using Equation 11.18, the shrinkage-induced deflection at mid-panel is the sum of the shrinkage deflection in each direction:

$$v_{sh} = 0.065 \times 0.75 \times 10^{-6} \times (10\,000^2 + 8000^2) = 8.0 \text{ mm}$$

Therefore, the maximum total deflection at the mid-panel is given by

$$v_{tot} = v_{max} + v_{cr} + v_{sh} = 20.7 \times 30.0 + 8.0 = 58.7 \text{ mm}$$

which is probably unserviceable for this relatively heavily loaded floor system.

If the total deflection limit for this slab was taken to be 58.7 mm, the slab thickness predicted by Equation 11.3 is

$$\frac{9900}{D} \leq 1.1 \times 1.9 \left[ \frac{(58.7/9900) \times 1000 \times 30\,000}{5.7 + (3 \times 3.3)} \right]^{1/3} = 47.0$$

which gives

$$D \geq 210 \text{ mm}$$

For this case, the prediction made by Equation 11.3 is slightly conservative in comparison with the deflection calculation procedure.

## 11.8 References

- ACI 318–83 1983. *Building code requirements for reinforced concrete*. Detroit: American Concrete Institute.
- ACI 318R–83 1983. *Commentary on building code requirements for reinforced concrete (ACI 318–83)*. Detroit: American Concrete Institute.
- ACI Committee 435 1974. *State-of-the-art report deflection of two-way reinforced concrete floor systems*. Publication SP-43, Deflections of Concrete Structures, Paper No. 3, 55–81. Detroit: American Concrete Institute.
- AS 1480–1982. *SAA concrete structures code*. Sydney: Standards Association of Australia.
- AS 1481–1981, *SAA prestressed concrete code*. Sydney: Standards Association of Australia.
- AS 3600–1988, *Australian standard for concrete structures*. Sydney: Standards Association of Australia.
- Branson, D.E. 1977. *Deformation of concrete structures*. New York: McGraw-Hill.
- CAN3–A23.3–M84 1984. *Design of concrete structures for buildings*. Rexdale, Canada: Canadian Standards Association.
- CEB–FIP 1978. *Model code for concrete structures*. Paris: Comité Euro-International du Béton—Fédération Internationale de la Précontrainte.
- Ewell, W.W., S.Okuba & J.I.Abrams 1952. Deflections in gridworks and slabs. *Transactions of the American Society of Civil Engineers (ASCE)* **117**, 869–90.

- FIP (Fédération Internationale de la Précontrainte) 1980. *Recommendations for the design of flat slabs in post-tensioned concrete (using unbonded tendons)*. London: Cement and Concrete Association. English translation.
- Furr, W.L. 1959. Numerical method for approximate analysis of building slabs. *ACI Journal* **31**, 511–41.
- Gilbert, R.I. 1979a. Time-dependent behaviour of structural concrete slabs. *PhD Thesis*. Sydney: School of Civil Engineering, University of New South Wales.
- Gilbert, R.I. 1979b. Time-dependent analysis of reinforced and prestressed concrete slabs. *Proceedings of the Third International Conference in Australia on Finite Elements Methods*. Sydney: University of New South Wales, Unisearch Ltd, 215–30.
- Gilbert, R.I. 1985. Deflection control of slabs using allowable span to depth ratios. *ACI Journal, Proceedings* **82**, 67–72.
- Gilbert, R.I. 1989. Determination of slab thickness in suspended post-tensioned floor systems. *ACI Journal, Proceedings* **86**, 607–7.
- Marsh, C.F. 1904. *Reinforced concrete*. New York: Van Nostrand.
- Mickleborough, N.C. & R.I.Gilbert 1986. Control of concrete floor slab vibration by L/D limits. *Proceedings of the 10th Australian Conference on the Mechanics of Structures and Materials, Adelaide, University of Adelaide*, 51–6.
- Nawy, E.G. & P.Chakrabarti 1976. Deflection of prestressed concrete flat plates. *Journal of the PCI* **21**, 86–102.
- Nilson, A.H. & D.B.Walters 1975. Deflection of two-way floor systems by the equivalent frame method. *ACI Journal* **72**, 210–8.
- Portland Cement Association 1965. *Deflection of flat plate floors*. PCA Concrete Report XS6504, 1–3. Skokie, IL.: Portland Cement Association.
- Post-Tensioning Institute 1977. *Design of post-tensioned slabs*, Glenview, IL: Post-Tensioning Institute.
- Rangan, B.V. 1982. Control of beam deflections by allowable span–depth ratios. *ACI Journal*, **79**, 372–7.
- Scanlon, A. & D.W.Murray 1974, Time-dependent reinforced concrete slab deflections, *Journal of the Structural Division, ASCE* **100**, 1911–24.
- Timoshenko, S. & S.Woinowsky-Krieger 1959, *Theory of plates and shells*. New York: McGraw-Hill.
- Vanderbilt, M.D., M.A.Sozen & C.P.Siess 1963. *Deflections of reinforced concrete floor slabs*. Structural Research Series, No. 263. Urbana, Department of Civil Engineering, University of Illinois.

# 12

## Compression and tension members

### 12.1 Types of compression members

Many structural members are subjected to longitudinal compression, including columns and walls in buildings, bridge piers, foundation piles, poles, towers, shafts, and web and chord members in trusses. The idea of applying prestress to a compression member may at first seem unnecessary or even unwise. In addition to axial compression, however, these members are often subjected to significant bending moments. Bending in compression members can result from a variety of load types. Gravity loads on floor systems induce moments in columns by frame action. Lateral loads on buildings and bridges cause bending in columns and piers and lateral earth pressures bend foundation piles. Even members that are intended to be axially loaded may be subjected to unintentional bending caused by eccentric external loading or by initial crookedness of the member itself. Most codes of practice specify a minimum eccentricity for use in design. All compression members must therefore be designed for combined bending and compression.

Prestress can be used to overcome the tension caused by bending and therefore reduce or eliminate cracking at service loads. By eliminating cracking, prestress can be used to reduce the lateral deflection of columns and piles and greatly improve the durability of these elements. Prestress also improves the handling of slender precast members and is used to overcome the tension due to rebound in driven piles. The strength of compression members is dependent on the strength of the concrete and considerable advantage can be gained by using concrete with high mechanical properties. Prestressed columns and piles are therefore commonly precast, in an environment where quality control and supervision are of a high standard.

If a structural member is subjected primarily to axial compression, with little or no bending, prestress causes a small reduction in the load-carrying capacity. For most prestressed concrete columns, the level of prestress is

usually between 1.5 and 5 MPa, which is low enough not to cause significant reductions in strength. When the eccentricity of the applied load is large and bending is significant, however, prestress results in an increase in the moment capacity, in addition to improved behaviour at service loads.

## 12.2 Classification and behaviour of compression members

Consider the pin-ended column shown in [Figure 12.1](#). The column is subjected to an external compressive force  $P$  applied at an initial eccentricity  $e_o$ . When  $P$  is first applied, the column shortens and deflects laterally by an amount  $\delta_i$ . The bending moment at each end of the column is  $Pe_o$ , but at the column mid-length the moment is  $P(e_o + \delta_i)$ . The moment at any section away from the column ends depends on the lateral deflection of the column, which in turn depends on the column's length and flexural stiffness. The initial moment  $Pe_o$  is called the *primary moment* and the moment caused by the lateral displacement of the column  $P\delta_i$  is the *secondary moment*. As the applied load  $P$  increases, so too does the lateral displacement  $\delta_i$ . The rate of increase of the secondary moment  $P\delta_i$  is therefore faster than the rate of increase of  $P$ . This non-linear increase in the internal actions is brought about by the change in geometry of the column and is referred to as *geometric non-linearity*.

For a reinforced or prestressed concrete column under sustained loads,

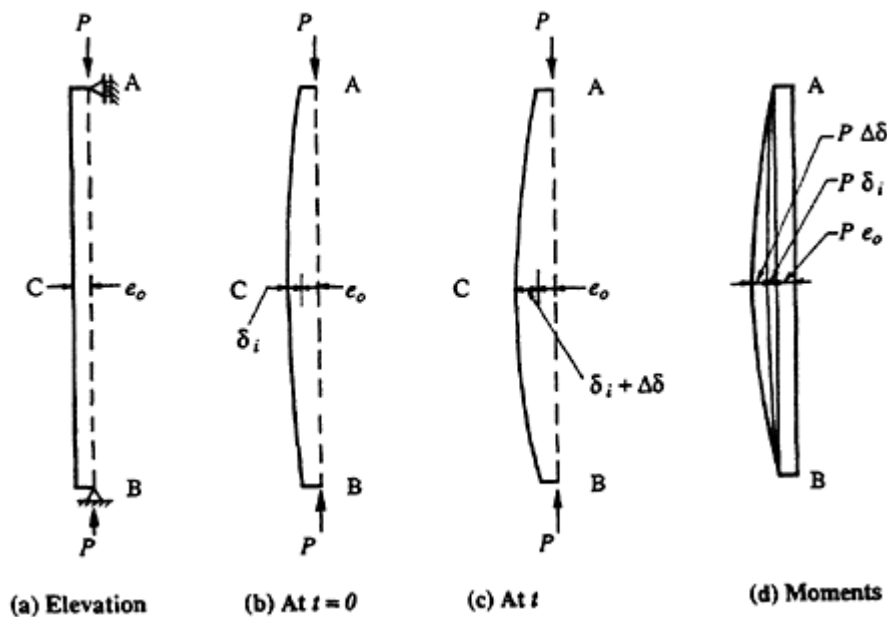


**Figure 12.1** Deformation and moments in a slender, pin-ended column.

the member suffers additional lateral deflection due to creep. This time-dependent deformation leads to additional bending in the member, which in turn causes the column to deflect still further. During a period of sustained loading, an additional deflection  $\Delta\delta$  develops and the resulting gradual increase in secondary moment with time  $P(\delta_i+\Delta\delta)$  reduces the factor of safety.

Columns are usually classified in two categories according to their length or slenderness. Short (or stocky) columns are compression members in which the secondary moments are insignificant, i.e. columns that are geometrically linear. Long (or slender) columns are geometrically nonlinear and the secondary moment is significant, i.e. the lateral deflection of the column is enough to cause a significant increase in the bending moment at the critical section and, hence, a reduction in strength. For given cross-section and material properties, the magnitude of the secondary moment depends on the length of the column and its support conditions. The secondary moment in a long column may be as great as or greater than the primary moment, and the load-carrying capacity is much less than that of a short column with the same cross-section.

The strength of a stocky column is equal to the strength of its cross-section when a compressive load is applied at an eccentricity  $e_o$ . Strength depends only on the cross-sectional dimensions, the quantity and distribution of the steel reinforcement (both prestressed and non-prestressed), and the compressive strengths of the concrete and the steel. Many practical concrete columns in buildings are, in fact, stocky columns. Ultimate strength analysis of a prestressed concrete column cross-section is presented in [Section 12.3](#).

The strength of a slender column is also determined from the strength of the critical cross-section subjected to an applied compressive load at an eccentricity  $(e_o+\delta)$ . The calculation of secondary moments  $(P\delta)$  at the ultimate limit state and the treatment of slenderness effects in design are discussed in [Section 12.4](#). Many precast, prestressed compression members, as well as some *in situ* columns and piers, fall into the category of slender columns.

For very long columns, an instability or buckling failure may take place before the strength of any cross-section is reached. The strength of a very slender member is not dependent on the cross-sectional strength and must be determined from a non-linear stability analysis (which is outside the scope of this book). A very slender member may buckle under a relatively small applied load, either when the load is first applied or after a period of sustained loading. The latter type of instability is caused by excessive lateral deformation due to creep and is known as creep buckling. Upper limits on the slenderness of columns are usually specified by codes of practice in order to avoid buckling failures.



### 12.3 Cross-sectional analysis—compression and bending

#### 12.3.1 The strength interaction diagram

The ultimate strength of a prestressed concrete column cross-section in combined bending and uniaxial compression is calculated as for a conventionally reinforced concrete cross-section. Strength is conveniently represented by a plot of the axial load capacity  $N_u$  versus the moment on the section at ultimate. This plot is called the *strength interaction curve*.

A typical strength interaction curve is shown in [Figure 12.2](#) and represents the failure line or strength line. Any combination of axial force and bending moment applied to the column cross-section that falls inside the

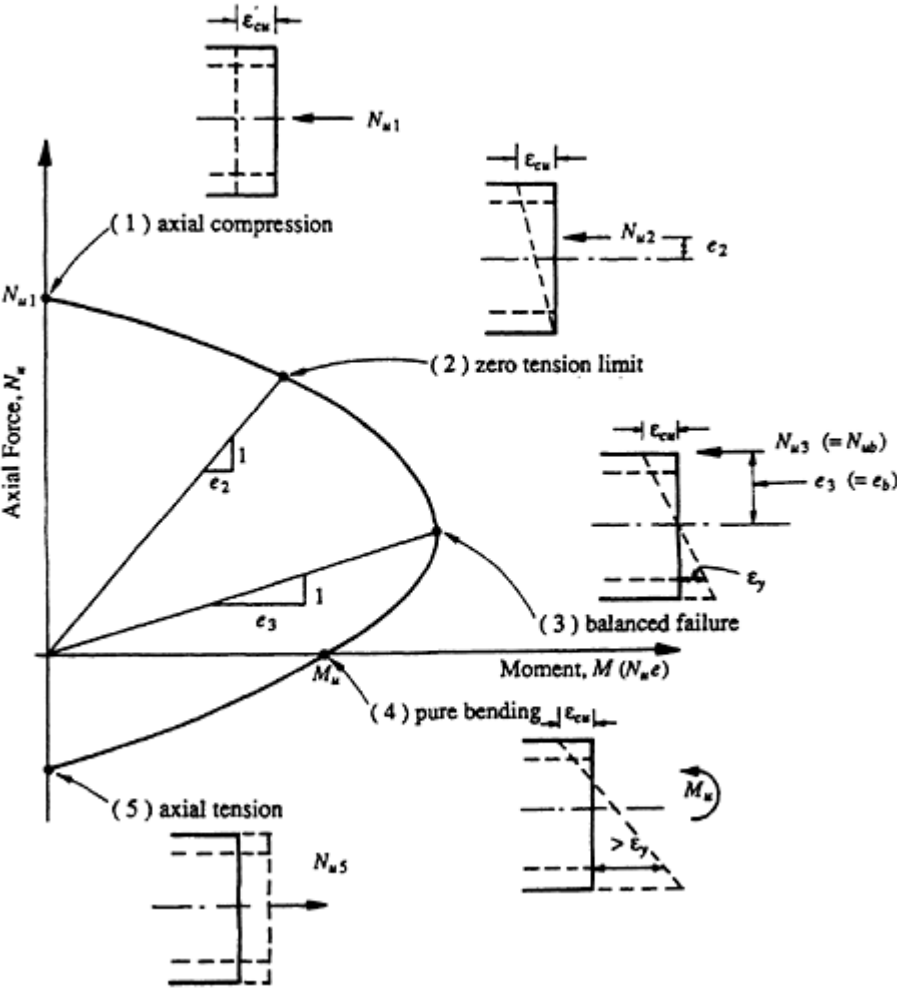


Figure 12.2 A typical strength interaction curve.

interaction curve is *safe* and can be carried by the cross-section. Any point outside the curve represents a combination of axial force and moment that exceeds the strength of the cross-section. Depending on the properties of the cross-section and the relative magnitudes of the axial force and bending moment, the type of failure can range from compressive, when the moment is small, to tensile or flexural, when the axial force is small and bending predominates.

Several critical points are identified on the strength interaction curve in [Figure 12.2](#). Point 1, on the vertical axis, is the point of axial compression (zero bending), and the strength is  $Nu_1$ . The cross-section is subjected to a uniform compressive strain, as shown. Point 2 represents the zero tension point. The combination of axial force  $Nu_2$  and moment  $Nu_2e_2$  at point 2 (when combined with the prestrain caused by prestress) produces zero strain in the extreme concrete fibre. The extreme fibre compressive strain at failure is  $\epsilon_{cu}$ . Between points 1 and 2 on the curve the entire cross-section is in compression.

When the eccentricity of the applied load is greater than  $e_2$ , bending causes tension over part of the cross-section. Point 3 is known as the balanced failure point. The strain in the extreme compressive fibre is  $\epsilon_{cu}$  and the strain in the tensile steel is the yield strain  $\epsilon_y$  (=0.2% offset). The eccentricity of the applied load at the balanced failure point is  $e_3$  (=  $e_b$ ). When a cross-section contains both non-prestressed and prestressed tensile steel with different yield strains and located at different positions on the cross-section, the balanced failure point is not well defined. Point 3 is usually taken as the point corresponding to a strain of  $\epsilon_y$  in the steel closest to the tensile face of the cross-section and is usually at or near the point of maximum moment capacity. At any point on the interaction curve between points 1 and 3, the tensile steel has not yielded at ultimate and failure is essentially compressive. Failures that occur between points 1 and 3 (when the eccentricity is less than  $e_b$ ) are sensibly known as *primary compressive failures*.

Point 4 is the pure bending point, where the axial force is zero, and point 5 is the point corresponding to direct axial tension. At any point on the interaction curve between points 3 and 5, the capacity of the tensile steel (or part of the tensile steel) is exhausted, with strains exceeding the yield strain, and the section suffers a *primary tensile failure*.

Any straight line through the origin represents a line of constant eccentricity called a loading line. Two such lines, corresponding to points 2 and 3, are drawn on [Figure 12.2](#). The slope of each loading line is  $1/e$ . When a monotonically increasing compressive force  $N$  is applied to the cross-section at a particular eccentricity,  $e_i$ , the plot of  $N$  versus  $M$  (=  $N e_i$ ) follows the loading line of slope  $1/e_i$  until the strength of the cross-section is reached at the point where the loading line and the interaction curve intersect. If the eccentricity of the applied load is increased, the loading line

becomes flatter, and the strength of the cross-section at ultimate  $N_u$  is reduced.

The general shape of the interaction curve shown in [Figure 12.2](#) is typical for any cross-section that is under-reinforced in pure bending (i.e. any cross-section in which the tensile steel strain at point 4 exceeds the yield strain). A small increase in axial compression increases the internal compressive stress resultant on the section but does not appreciably reduce the internal tension, thus increasing the moment capacity, as is indicated by the part of the interaction curve between points 4 and 3.

### 12.3.2 Ultimate strength analysis

Individual points on the strength interaction curve can be calculated using an ultimate strength theory, similar to that outlined for pure bending in [Section 4.3](#). The analysis described below is based on the assumptions listed in [Section 4.3.1](#) and the idealized rectangular stress block specified in AS 3600–1988 (and in ACI 318–83) which were presented in [Section 4.3.2](#). At any point on the interaction curve between points 2 and 4, the extreme fibre concrete compressive strain at failure is taken to be  $\varepsilon_{cu}=0.003$ , in accordance with the above two codes. For axial compression at point 1, ACI 318–83 specifies  $\varepsilon_{cu1}=0.003$ , whilst AS 3600 suggests that the maximum uniform strain should be taken as only 0.002, since this is closer to the strain at failure of plain concrete subjected to monotonically increasing compressive load.

Calculation of the ultimate moment  $M_u$  in pure bending (point 4 on the interaction curve) was discussed in [Chapter 4](#). Other points in the strength interaction curve (between points 4 and 2) may be obtained by successively increasing the depth to the neutral axis and analysing the cross-section. With the extreme fibre strain equal to 0.003, each neutral axis position defines a particular strain distribution which corresponds to a point on the strength interaction diagram. The strain diagrams associated with points 2, 3, and 4 are also shown in [Figure 12.2](#).

To define the interaction curve accurately, relatively few points are needed. In fact, if only points 1, 2, 3, and 4 are determined, a close approximation can be made by passing a smooth curve through each point, or even by linking successive points together by straight lines. Such an approximation is often all that is required in design.

Consider the rectangular cross-section shown in [Figure 12.3a](#), with overall dimensions  $D$  and  $b$ . The section contains two layers of non-prestressed reinforcement of areas  $A_{s1}$  and  $A_{s2}$  and two layers of bonded prestressing steel  $A_{p1}$  and  $A_{p2}$ , as shown. A typical ultimate strain diagram and the corresponding idealized stresses and stress resultants are illustrated in [Figures 12.3b](#) and [c](#), respectively. These strains and stresses correspond to a resultant axial force  $N_u$  at an eccentricity  $e$  measured from the plastic centroid

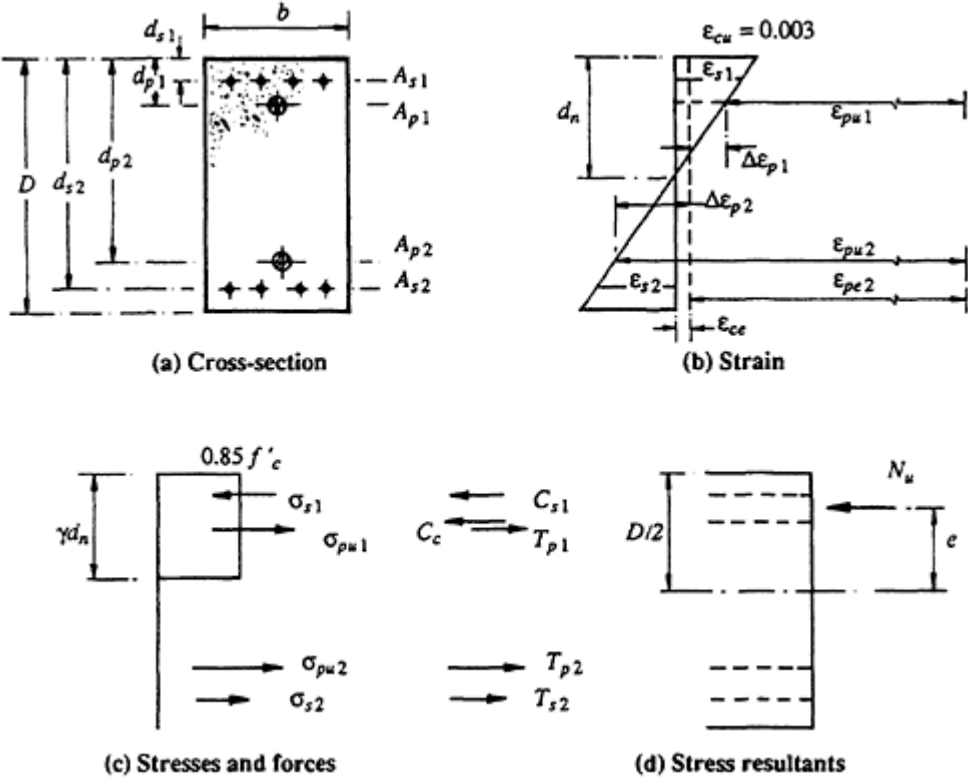


**Figure 12.3** Ultimate stresses and strains on a cross-section in combined compression and uniaxial bending.

of the cross-section (as shown in [Figure 12.3d](#)). Longitudinal equilibrium requires that

$$N_u = C_c + C_{s1} - T_{p1} - T_{p2} - T_{s2} \tag{12.1}$$

and moment equilibrium gives

$$M = N_u e = C_c \left( \frac{D}{2} - \frac{\gamma d_n}{2} \right) + C_{s1} \left( \frac{D}{2} - d_{s1} \right) - T_{p1} \left( \frac{D}{2} - d_{p1} \right) + T_{p2} \left( d_{p2} - \frac{D}{2} \right) + T_{s2} \left( d_{s2} - \frac{D}{2} \right) \tag{12.2}$$

Each of the internal forces can be calculated readily from the strain diagram. The magnitude of the compressive force in the concrete  $C_c$  is the volume of the rectangular stress block, and is given by

$$C_c = 0.85 f'_c \gamma d_n b. \tag{12.3}$$

The magnitude of the strain in the compressive non-prestressed steel  $A_{s1}$  is

$$\epsilon_{s1} = \frac{0.003 (d_n - d_{s1})}{d_n} \quad (12.4)$$

and the compressive force in  $A_{s1}$  is

$$\begin{aligned} C_{s1} &= A_{s1}\epsilon_{s1}E_s \quad \text{if } \epsilon_{s1} < \epsilon_y (= f_y/E_s) \\ &= A_{s1}f_y \quad \text{if } \epsilon_{s1} \geq \epsilon_y \end{aligned} \quad (12.5)$$

The strain in the tensile non-prestressed steel  $A_{s2}$  is

$$\epsilon_{s2} = \frac{0.003 (d_{s2} - d_n)}{d_n} \quad (12.6)$$

and the force in  $A_{s2}$  is

$$\begin{aligned} T_{s2} &= A_{s2}\epsilon_{s2}E_s \quad \text{if } \epsilon_{s2} < \epsilon_y \\ &= A_{s2}f_y \quad \text{if } \epsilon_{s2} \geq \epsilon_y \end{aligned} \quad (12.7)$$

To determine the strain in the prestressing steel at ultimate, account must be taken of the large initial tensile strain in the steel  $\epsilon_{pe}$  caused by the effective prestress. For each area of prestressing steel,

$$\epsilon_{pe1} = \frac{(P_e)_{p1}}{A_{p1}E_p} \quad \text{and} \quad \epsilon_{pe2} = \frac{(P_e)_{p2}}{A_{p2}E_p} \quad (12.8)$$

In [Figure 12.3b](#), it is assumed that the prestressing forces in  $A_{p1}$  and  $A_{p2}$  are such that the effective prestress is axial, producing uniform compressive strain,  $\epsilon_{ce}$ , as shown. If  $P_e$  is the total effective prestressing force acting at the centroidal axis, then the magnitude of  $\epsilon_{ce}$  is

$$\epsilon_{ce} = \frac{P_e}{(nA_{s1} + nA_{s2} + A_c)E_c} \approx \frac{P_e}{[(n-1)A_s + A_g]E_c} \quad (12.9)$$

where  $n$  is the modular ratio  $E_s/E_c$  and  $A_c$  and  $A_g$  are the concrete area and gross cross-sectional area, respectively.

The changes in strain in the bonded prestressing tendons due to the application of  $N_u$  at an eccentricity  $e$  may be obtained from the strain

diagram and are given by

$$\Delta \varepsilon_{p1} = \frac{0.003(d_n - d_{p1})}{d_n} - \varepsilon_{ce1} \quad (12.10)$$

$$\Delta \varepsilon_{p2} = \frac{0.003(d_{p2} - d_n)}{d_n} + \varepsilon_{ce2} \quad (12.11)$$

The final strain in each prestressing tendon is therefore

$$\varepsilon_{pu1} = \varepsilon_{pe1} - \Delta \varepsilon_{p1} \quad \text{and} \quad \varepsilon_{pu2} = \varepsilon_{pe2} + \Delta \varepsilon_{p2} \quad (12.12)$$

The final stress in the prestressing tendons  $\sigma_{pu1}$  and  $\sigma_{pu2}$  may be obtained from a stress–strain curve for the prestressing steel, such as the curve shown in [Figure 2.13](#). If the strain in the prestressing steel remains in the elastic range (and on the compressive side of the cross-section it does), then

$$\sigma_{pu} = \varepsilon_{pu} E_p (\leq \sigma_{py}) \quad (12.13)$$

The forces in the tendons at ultimate are

$$T_{p1} = \sigma_{pu1} A_{p1} \quad \text{and} \quad T_{p2} = \sigma_{pu2} A_{p2} \quad (12.14)$$

With the internal forces determined from Equations 12.3, 12.5, 12.7, and 12.14, the ultimate compressive force  $N_u$  is obtained from Equation 12.1 and the eccentricity  $e$  is calculated using Equation 12.2. The resulting point  $N_u, M (=N_u e)$  represents the point on the strength interaction curve corresponding to the assumed strain distribution.

When the cross-section is subjected to pure compression (point 1 on the interaction curve), the eccentricity is zero and the strength is given by

$$N_{u1} = C_c + A_s f_y - A_{p1} \sigma_{pu1} - A_{p2} \sigma_{pu2} \quad (12.15)$$

where  $C_c = 0.85 f'_c D b$ ,  $A_s$  is the total area of non-prestressed steel, and  $\sigma_{pu1}$  and  $\sigma_{pu2}$  are obtained from the final strain in each prestressing tendon, which is in the elastic range. Therefore,

$$\sigma_{pu} = E_p (\varepsilon_{pe} - \varepsilon_{cu} + \varepsilon_{ce}) \quad (12.16)$$

### Example 12.1

The critical points on the strength interaction curve of the prestressed concrete column cross-section shown in [Figure 12.4a](#) are to be calculated. Steel quantities, prestressing details and material properties are as follows:  $A_{s1}=A_{s2}=2250 \text{ mm}^2$ ;  $A_{p1}=A_{p2}=1000 \text{ mm}^2$ ;  $E_s=200 \times 10^3 \text{ MPa}$ ;

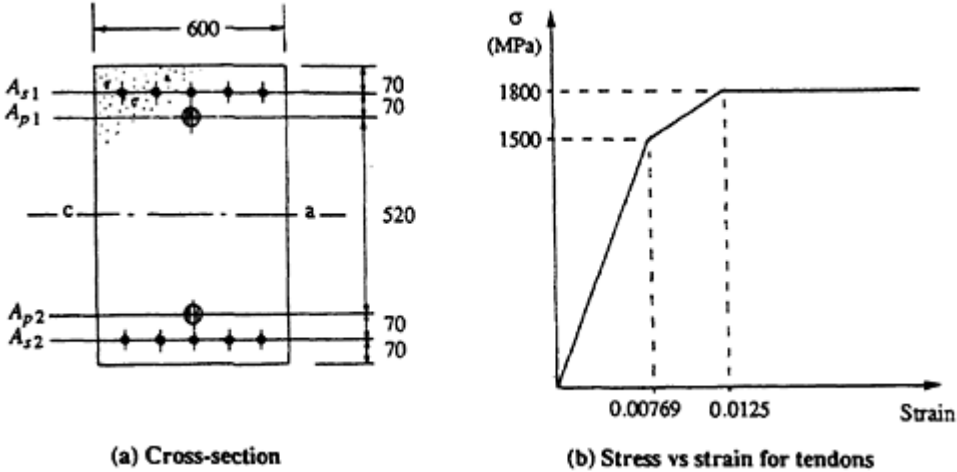


Figure 12.4 Cross-sectional details and idealised stress-strain curve for tendons.

$f_y=400$  MPa;  $f'_c = 40$  MPa;  $E_c=32000$  MPa; and from Equation 4.2,  $\gamma=0.766$ . The properties of the prestressing steel are taken from the idealized stress–strain relationship shown in Figure 12.4b. The total effective prestress is  $P_e=2400$  kN and the effective strain in the prestressing steel is

$$\epsilon_{pe} = \frac{1200}{195 \times 10^3} = 0.00615$$

The magnitude of the average initial strain in the concrete due to  $P_e$  is calculated using Equation 12.9:

$$\epsilon_{ce} = \frac{2400 \times 10^3}{[(5.25 \times 4500) + (600 \times 800)] \times 32000} = 0.000149$$

**Point 1: Pure Compression ( $e=0$ )**

The compressive force carried by the concrete in uniform compression is

$$C_c = 0.85 f'_c D b = 0.85 \times 40 \times 800 \times 600 \times 10^{-3} = 16\,320 \text{ kN}$$

and, from Equation 12.16, the stress in the prestressing steel is

$$\sigma_{pu} = 195 \times 10^3 (0.00615 - 0.002 + 0.000149) = 838 \text{ MPa}$$

Note that the value of  $\epsilon_{cu}$  specified in AS 3600–1988 for pure compression is used here. The strength of the cross-section in axial compression is given by Equation 12.15:

$$N_{u1} = 16\,320 + (4500 \times 400 \times 10^{-3}) - [838(1000 + 1000) \times 10^{-3}] = 16\,440 \text{ kN}$$



**Point 2: Zero tension**

For the case of zero tension,  $d_n=D=800$  mm and Equation 12.3 gives

$$C_c = 0.85 \times 40 \times 0.766 \times 800 \times 600 \times 10^{-3} = 12\,501 \text{ kN}$$

From Equation 12.4,

$$\epsilon_{s1} = \frac{0.003(800 - 70)}{800} = 0.0028 > \epsilon_y (=0.002)$$

The compressive non-prestressed steel has yielded, and from Equation 12.5,

$$C_{s1} = 2250 \times 400 \times 10^{-3} = 900 \text{ kN}$$

The strain in the bottom layer of non-prestressed steel is given by Equation 12.6,

$$\epsilon_{s2} = \frac{0.003(730 - 800)}{800} = -0.000263$$

and, from Equation 12.7,

$$T_{s2} = 2250 \times -0.000263 \times 195\,000 \times 10^{-3} = -115 \text{ kN (compressive)}$$

The change in strain at each level of prestressing steel is compressive and given by Equations 12.10 and 12.11:

$$\Delta \epsilon_{p1} = \frac{0.003(800 - 140)}{800} - 0.000149 = 0.00233$$

$$\Delta \epsilon_{p2} = \frac{0.003(660 - 800)}{800} + 0.000149 = -0.000376$$

and the final strains in the prestressing tendons are obtained from Equations 12.12:

$$\epsilon_{pu1} = 0.00615 - 0.00233 = 0.00382$$

$$\epsilon_{pu2} = 0.00615 - 0.000376 = 0.00577$$

Both strains are in the elastic range and the forces in the tendons are

(Equations 12.15 and 12.16)

$$T_{p1} = 0.00382 \times 195\,000 \times 1000 \times 10^{-3} = 745 \text{ kN}$$

$$T_{p2} = 0.00577 \times 195\,000 \times 1000 \times 10^{-3} = 1126 \text{ kN}$$

The resultant compressive force at ultimate is obtained from Equation 12.1:

$$N_{u2} = 12\,501 + 900 + 115 - 745 - 1126 = 11\,645 \text{ kN}$$

The ultimate moment capacity for the case of zero tension is calculated using Equation 12.2:

$$M_2 = N_{u2} e_2 = \left[ 12\,501 \left( 400 - \frac{0.766 \times 800}{2} \right) + 900(400 - 70) - 745(400 - 140) + 1126(660 - 400) - 115(730 - 400) \right] \times 10^{-3} = 1528 \text{ kNm}$$

Therefore, the eccentricity corresponding to point 2 is

$$e_2 = \frac{M_2}{N_{u2}} = 131.2 \text{ mm}$$

**Point 3:** The balanced failure point

Point 3 corresponds to first yielding in the non-prestressed tensile steel, i.e.  $\varepsilon_{s2}=0.002$  and, therefore, the force in the tensile non-prestressed steel is

$$T_{s2} = 2250 \times 400 \times 10^{-3} = 900 \text{ kN}$$

The depth to the neutral axis at point 3 is therefore

$$d_n = \frac{0.003}{0.003 + 0.002} d_{s2} = 438 \text{ mm}$$

and the compressive force in the concrete is (Equation 12.3)

$$C_c = 0.85 \times 40 \times 0.766 \times 438 \times 600 \times 10^{-3} = 6844 \text{ kN}$$

With  $d_n=438$  mm, the strain in the non-prestressed compressive reinforcement is  $\varepsilon_{s1}=0.0025 > \varepsilon_y$ , and therefore,

$$C_{s1} = 900 \text{ kN}$$

From Equations 12.10, 12.12, 12.13, and 12.14, the force in the top prestressing steel is

$$\begin{aligned} T_{p1} &= A_{p1} \left[ \epsilon_{pe} - \frac{0.003(d_n - d_{p1})}{d_n} + \epsilon_{ce} \right] E_p \\ &= 1000 \left[ 0.00615 - \frac{0.003(438 - 140)}{438} + 0.000149 \right] 195\,000 \times 10^{-3} = 830 \text{ kN} \end{aligned}$$

Equations 12.11 and 12.12 give

$$\epsilon_{pu2} = \epsilon_{pe} + \frac{0.003(d_{p2} - d_n)}{d_n} + \epsilon_{ce} = 0.00782$$

which is just greater than the proportional limit. From [Figure 12.4b](#),

$$\sigma_{pu2} = \left( \frac{0.00782 - 0.00769}{0.0125 - 0.00769} \times 300 \right) + 1500 = 1508 \text{ MPa}$$

and Equation 12.14 gives

$$T_{p2} = 1508 \times 1000 \times 10^{-3} = 1508 \text{ kN}$$

The ultimate strength corresponding to point 3 is obtained from Equations 12.1 and 12.2:

$$N_{u3} = 6844 + 900 - 830 - 1508 - 900 = 4506 \text{ kN}$$

and

$$\begin{aligned} M_3 = N_{u3} e_3 &= \left[ 6844 \left( 400 - \frac{0.766 \times 438}{2} \right) + 900(400 - 70) - 830(400 - 140) \right. \\ &\quad \left. + 1508(660 - 400) + 900(730 - 400) \right] \times 10^{-3} = 2360 \text{ kN m} \end{aligned}$$

The eccentricity at point 3 is

$$e_3 = \frac{2360 \times 10^6}{4506 \times 10^3} = 524 \text{ mm}$$

#### Point 4: Pure bending

For equilibrium of the section in pure bending the magnitude of the resultant compression is equal to the magnitude of the resultant tension, i.e.  $C=T$ . A trial and error approach to determine the depth to the neutral axis

indicates that

$$d_n = 187.7 \text{ mm}$$

The forces in the concrete and the steel are

$$C_c = 0.85 \times 40 \times 0.766 \times 187.7 \times 600 \times 10^{-3} = 2933 \text{ kN}$$

$$C_{s1} = 2250 \times \frac{0.003(187.7 - 70)}{187.7} \times 200\,000 \times 10^{-3} = 847 \text{ kN}; T_{s2} = 900 \text{ kN};$$

and

$$\begin{aligned} T_{p1} &= 1000 \left[ 0.00615 - \frac{0.003(187.7 - 140)}{187.7} + 0.000149 \right] \times 195\,000 \times 10^{-3} \\ &= 1080 \text{ kN} \end{aligned}$$

From Equations 12.11 and 12.12:

$$\epsilon_{p2} = \left[ 0.00615 + \frac{0.003(660 - 187.7)}{187.7} + 0.000149 \right] = 0.01385$$

and [Figure 12.4b](#) indicates that  $\sigma_{pu2} = 1800 \text{ MPa}$ . Therefore,

$$T_{p2} = 1800 \text{ kN}$$

Equation 12.1 confirms that

$$N_{u4} = 2933 + 847 - 1080 - 1800 - 900 = 0$$

and the ultimate moment is

$$\begin{aligned} M_u &= \left[ 2933 \left( 400 - \frac{0.766 \times 187.7}{2} \right) + 847(400 - 70) - 1080(400 - 140) \right. \\ &\quad \left. + 1800(660 - 400) + 900(730 - 400) \right] \times 10^{-3} = 1726 \text{ kNm}. \end{aligned}$$

#### Point 5 Axial tension

The capacity of the section in tension is dependent only on the steel strength. Therefore, taking  $f_y = 400 \text{ MPa}$  and  $f_p = 1800 \text{ MPa}$ , as indicated in [Figure 12.4b](#), the axial tensile strength is

$$N_{u5} = A_s f_y + A_p f_p = [(4500 \times 400) + (2000 \times 1800)] \times 10^{-3} = 5400 \text{ kN}$$

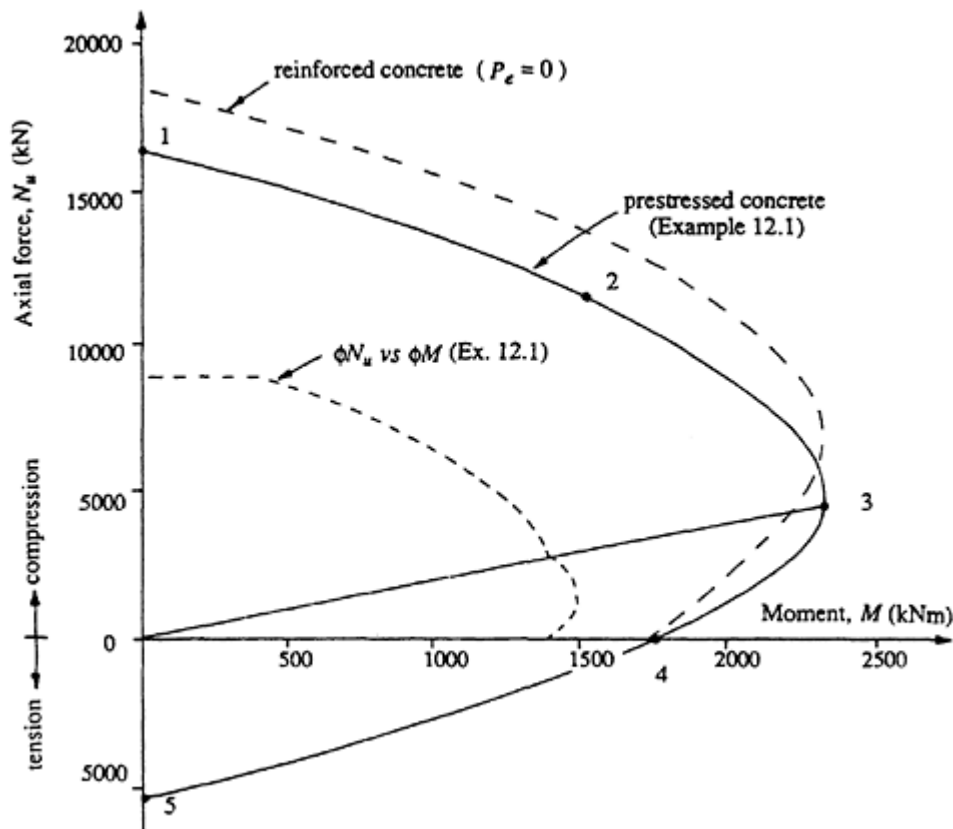


Figure 12.5 Strength interaction curve for [Example 12.1](#).

[Figure 12.5](#) shows the strength interaction curve for the cross-section. The design interaction curve is also shown in accordance with the provisions of AS 3600–1988, as discussed in [Section 12.3.3](#). In addition, [Figure 12.5](#) illustrates the interaction curve for a cross-section with the same dimensions, material properties, and steel quantities (both non-prestressed and prestressed), but without any effective prestress, i.e.  $P_e=0$ . A comparison between the two curves indicates the effect of prestress. In [Example 12.1](#), the prestressing steel induced an effective prestress of 5 MPa over the column cross-section. Evidently, the prestress reduces the axial load carrying capacity by about 15% (at point 1), but increases the bending strength of the cross-section in the primary tension region (points 3 to 4).

### 12.3.3 Design interaction curves

For structural design in accordance with either AS 3600–1988 or ACI 318–83, the design actions  $N^*$  and  $M^*$  (obtained using the appropriate factored load combination for strength as presented in [Section 1.7.3](#)) must lie on or inside the *design interaction curve*. This design curve is obtained

by multiplying each point on the strength interaction curve by the strength reduction factor,  $\phi$ .

### AS 3600–1988

The strength reduction factor in the primary compression region where  $N_u \geq N_{ub}$  (i.e. between points 1 and 3) is  $\phi = 0.6$ . When  $N_u < N_{ub}$  (in the primary tension region), the strength reduction factor is

$$\phi = 0.6 + 0.2 \left( 1 - \frac{N_u}{N_{ub}} \right) \quad (12.17)$$

and  $\phi = 0.8$  at point 4 (pure bending). A minimum eccentricity for the applied load of  $0.05D$  is specified, where  $D$  is the depth of the column in the plane of the bending moment. The AS 3600 design interaction curve for the cross-section analysed in [Example 12.1](#) is drawn in [Figure 12.5](#).

### ACI 318–83

The ACI 318–83 strength reduction factor for members in combined compression and bending is  $\phi = 0.75$  for members with spiral reinforcement and  $\phi = 0.7$  for members with transverse ties. When the axial load is low, however,  $\phi$  may be increased linearly to 0.9 as  $\phi N_u$  decreases from  $0.1f'_c A_g$  or  $N_{ub}$ , whichever is smaller, to zero. To ensure a minimum eccentricity for axially loaded members, the top of the interaction curve is truncated so that the design strength  $\phi N_u$  does not exceed  $0.85\phi N_{u1}$  for spirally reinforced

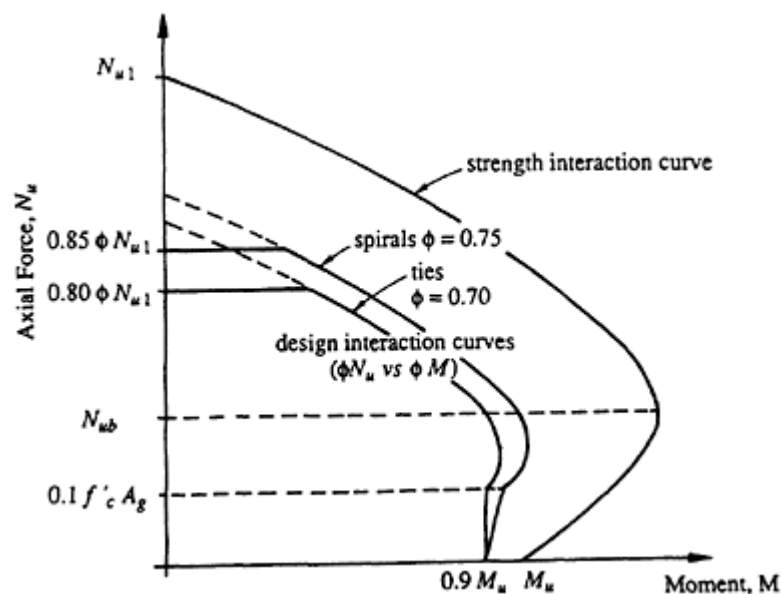


Figure 12.6 Design interaction curve (ACI 318–83).

members or  $0.80\phi N_{u1}$  for members containing conventional ties. A typical design interaction curve, in accordance with ACI 318–83, is illustrated in [Figure 12.6](#).

12.3.4 Biaxial bending and compression

When a cross-section is subjected to axial compression and bending about both principal axes, such as the section shown in [Figure 12.7a](#), the strength interaction diagram can be represented by the three-dimensional surface shown in [Figure 12.7b](#). The shape of this surface may be defined by a set of contours obtained by taking horizontal slices through the surface. A typical contour is shown in [Figure 12.7b](#). Each contour is associated with a particular axial force,  $N$ . The equation of the contour represents the relationship between  $M_x$  and  $M_y$  at that particular value of axial force. In AS 3600–1988, the design expression given in Equation 12.18 is specified to model the shape of these contours. The form of Equation 12.18 was originally proposed by Bresler (1960) and design charts based on the equation have been calibrated by Pannell (1963).

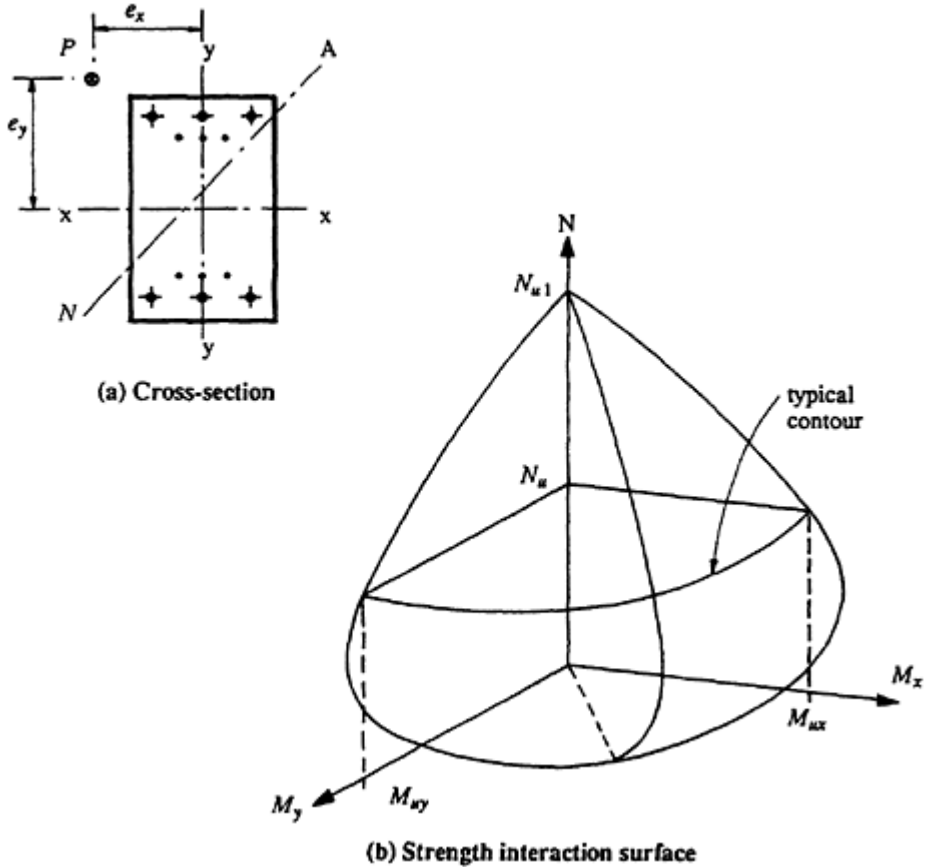


Figure 12.7 Biaxial bending and compression.

If the factored design actions  $N^*$ ,  $M_x^*$ , and  $M_y^*$  fall inside the design interaction surface (i.e. the strength interaction surface multiplied by the strength reduction factor,  $\phi$ ), then the cross-section is adequate. According to AS 3600–1988, a cross-section subjected to biaxial bending should satisfy the following equation,

$$\left(\frac{M_x^*}{\phi M_{ux}}\right)^{\alpha_n} + \left(\frac{M_y^*}{\phi M_{uy}}\right)^{\alpha_n} \leq 1.0 \quad (12.18)$$

where  $\phi M_{ux}$  and  $\phi M_{uy}$  are the design strength in bending calculated separately about the major and minor axis, respectively, under the design axial force  $N^*$ , the factored design moments  $M_x^*$  and  $M_y^*$  are magnified to account for slenderness if applicable (see [Section 12.4](#)), and  $\alpha_n$  is a factor which depends on the axial force and defines the shape of the contour, and is given by

$$\alpha_n = 0.7 + \frac{1.7N^*}{0.6N_{u1}} \text{ but within the limits } 1 \leq \alpha_n \leq 2.$$

Biaxial bending is not a rare phenomenon. Most columns are subjected to simultaneous bending about both principal axes. AS 3600–1988 suggests that biaxial bending need not be considered when the eccentricity about both axes is less than the minimum value (i.e. less than 0.05 times the column dimension in the direction of the eccentricity), or when the ratio of the eccentricities  $e_x/e_y$  falls outside the range 0.2–5.0. In each of the above situations, the code concedes that the cross-section can be designed for the axial force with each bending moment considered separately, i.e. in uniaxial bending and compression.

## 12.4 Slenderness effects

### 12.4.1 Background

The strength of a short column is equivalent to the strength of the most heavily loaded cross-section and, for a given eccentricity, may be determined from the strength interaction curve (or surface). The strength of a long column (or slender column), however, depends not only on the strength of the cross-section, but also on the length of the member and its support conditions. A discussion of the behaviour of a slender pin-ended column was presented in [Section 12.2](#) and the increase in secondary moments due to slenderness effects was illustrated in [Figure 12.1](#). In general, as the length of a compression member increases, strength decreases.



To predict accurately the second-order effects in structures as they deform under load requires an iterative non-linear computer analysis, which generally involves considerable computational effort. For the design of concrete compression members, simplified procedures are available to account for slenderness effects and one such procedure is presented here. A more detailed study of geometric non-linearity and instability in structures is outside the scope of this book.

The critical buckling load,  $N_c$ , of an axially loaded, perfectly straight, pin-ended, elastic column was determined by Euler and is given by

$$N_c = \frac{\pi^2 EI}{L^2} \tag{12.19}$$

where  $L$  is the length of the Euler column between the hinges. In practice, concrete columns are rarely, if ever, pin-ended. A degree of rotational restraint is usually provided at each end of a column by the supporting beams and slabs, or by a footing. In some columns, translation of one end of the column with respect to the other may also occur in addition to rotation. Some columns are completely unsupported at one end, such as a

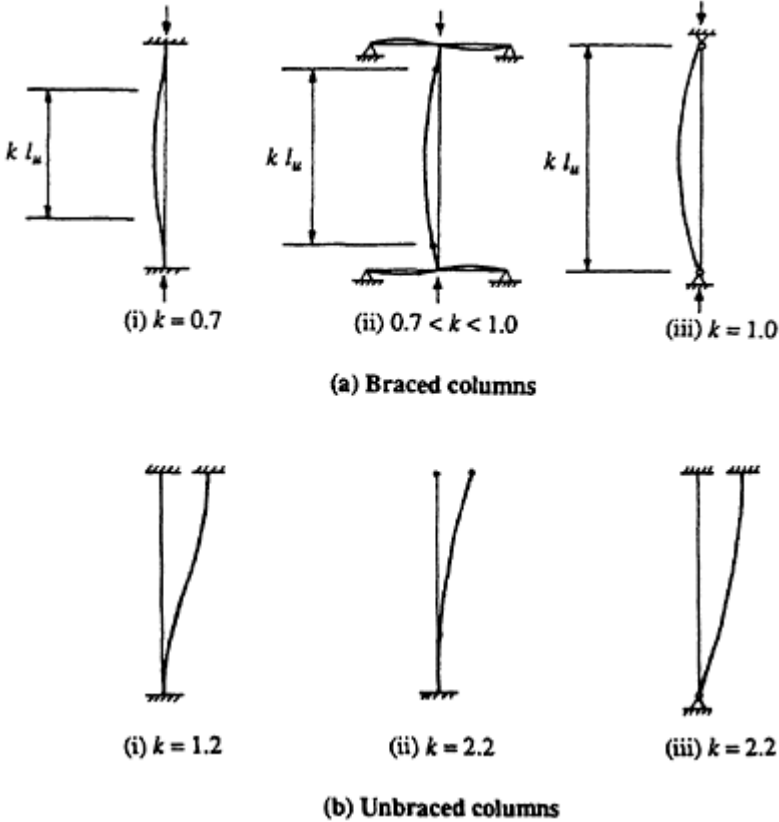
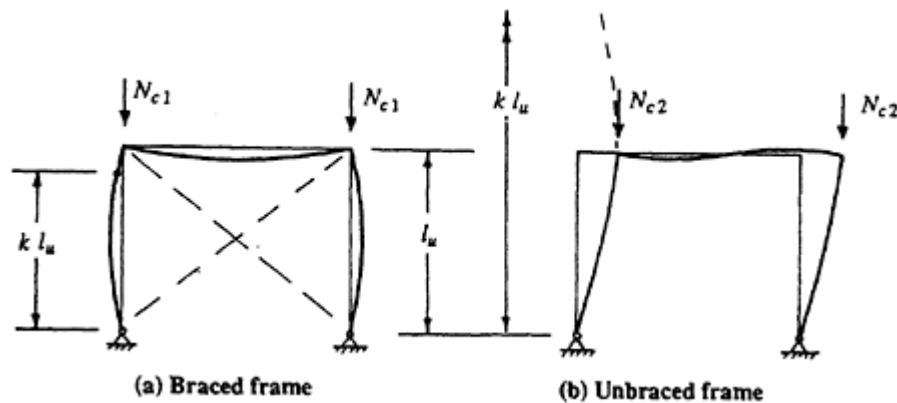


Figure 12.8 Effective length factors,  $k$  (AS 3600–1988).



**Figure 12.9** Effective lengths in a braced and an unbraced portal frame.

cantilevered column. The buckling load of these columns may differ considerably from that given by Equation 12.19.

In general, codes of practice express the critical buckling load of real columns in terms of the *effective length*,  $kl_u$ . ACI 318–83 defines  $l_u$  as the unsupported length of a compression member (and equals  $L$  for an Euler column), and  $k$  is an effective length factor which depends on the support conditions of the column. The critical load of a concrete column is therefore

$$N_c = \frac{\pi^2 EI}{(kl_u)^2} \quad (12.20)$$

In structures that are laterally braced, the ends of the columns are not able to translate appreciably relative to each other, i.e. sidesway is prevented. Most concrete structures are braced, with stiff vertical elements such as shear walls, elevator shafts, and stairwalls providing bracing for the more flexible columns. If the attached elements at each end of a braced column provide some form of rotational restraint, the critical buckling load will be greater than that of a pin-ended column (given in Equation 12.19), and therefore the effective length factor in Equation 12.20 is less than 1.0. Effective length factors specified in AS 3600–1988 for braced columns are shown in [Figure 12.8a](#). The effective length of any column is the length associated with single curvature buckling, i.e. the distance between the points of inflection in the column, as shown in [Figures 12.8a](#) and [12.9a](#). For the column shown in [Figure 12.8a\(ii\)](#), the supports are neither pinned nor fixed. The effective length depends on the relative flexural stiffness of the column and the beams and other supporting elements at each end of the column, and may be calculated readily using end restraint coefficients and effective length graphs or alignment charts contained in codes of practice (such as ACI 318–83R or AS 3600–1988).

For columns in unbraced structures, where one end of the column can translate relative to the other (i.e. sidesway is not prevented), the effective length factor is greater than 1.0, sometimes much greater, as shown in [Figure 12.9b](#). The critical buckling load of an unbraced column is therefore significantly less than that of a braced column. Values of  $k$  specified in AS 3600–1988 for unbraced columns with various support conditions are shown in [Figure 12.8b](#).

To distinguish between a braced and an unbraced column, ACI 318R-83 suggests that a braced column is a compression member located within a storey of a building in which horizontal displacements do not significantly affect the moments in the structure. It is further suggested that a compression member may be assumed to be braced, if it is located in a storey in which the bracing elements (shear walls, elevator shafts, bracing trusses, and other types of bracing) have a total stiffness, resisting lateral movement of the storey, at least six times the sum of the stiffnesses of all the columns within the storey.

In the case of slender prestressed concrete columns, the question arises as to whether the longitudinal prestressing force  $P$  reduces the critical buckling load. In general, a concrete column prestressed with internally bonded strands or post-tensioned with tendons inside ducts within the member is no more prone to buckling than a reinforced concrete column of the same size and stiffness, and with the same support conditions. As a slender, prestressed concrete column displaces laterally, the tendons do not change position within the cross-section and the eccentricity of the line of action of the prestressing force does not change. The prestressing force cannot, therefore, generate secondary moments. However, if a member is externally prestressed, so that the line of action of the prestressing force remains constant, then prestress can induce secondary moments and hence reduce the buckling load. Such a situation could exist, for example, when a member is prestressed by jacking through an abutment.

#### 12.4.2 Moment magnification methods

In lieu of a detailed second-order analysis to determine the effects of short-term and time-dependent deformation on the magnitude of moment and forces in slender structures, codes of practice specify approximate procedures to account for slenderness effects. Both AS 3600–1988 and ACI 318–83 use a *moment magnifier method* to account for slenderness effects in columns. BS 8110 (1985) utilizes a similar approach to account for the additional moment induced in a column due to lateral deflection. In this discussion, the method contained in ACI 318–83 is outlined, although the notation is changed somewhat to conform with the notation used elsewhere in the book.

The idea behind moment magnification is described in ACI 318R–1983

and is based on the concept of using a factor to magnify the column moments to account for the change in geometry of the structure and the resulting secondary actions. The axial load and magnified moment are then used in the design of the column cross-section. The effect of the secondary moments on the strength of a slender column is shown on the strength interaction curve in [Figure 12.10](#). Line OA is the loading line corresponding to an initial eccentricity  $e$  on a particular cross-section. If the column is short, secondary moments are insignificant, the loading line is straight, and the strength of the column corresponds to the axial force at A. If the column is slender, the secondary moments increase at a faster rate than the applied axial force and the loading line becomes curved, as shown. The strength of the slender column is the axial force corresponding to point B, where the curved loading line meets the strength interaction curve. The loss of strength due to secondary moments is indicated in [Figure 12.10](#).

The total moment at failure is the sum of the primary moment  $N_e$  and the secondary moment  $N\Delta$  and may be expressed by a factor  $\delta$  times the primary moment. That is,

$$\delta Ne = Ne + N\Delta = Ne \left( \frac{e + \Delta}{e} \right)$$

and

$$\delta = \frac{e + \Delta}{e}$$

The factor  $\delta$  may be used to magnify the primary moment in order to

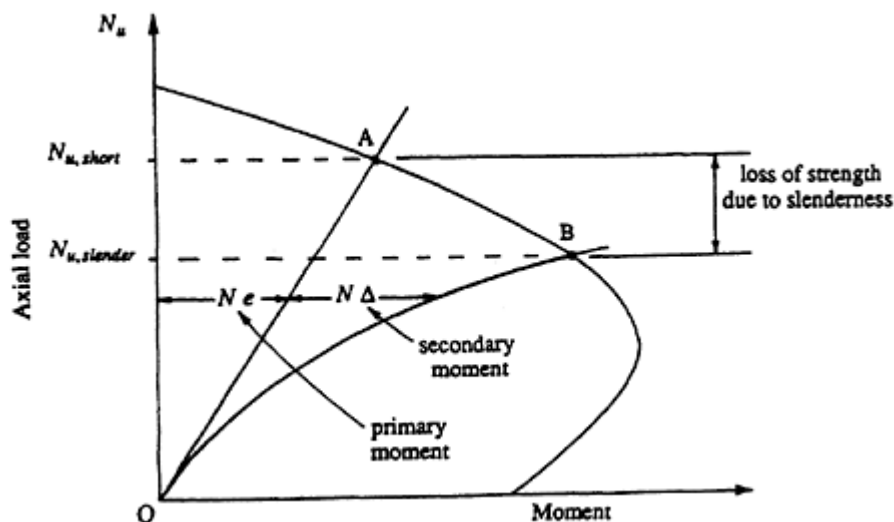


**Figure 12.10** Strength interaction curve for a cross-section in a slender column.

account for slenderness effects. This magnification factor depends on the ratio of the axial force on the column  $N^*$  to the critical buckling load  $N_c$ , the ratio of the design moments at each end of the column  $M_1^*/M_2^*$ , and the deflected shape of the column, which in turn depends on whether the column is braced or unbraced and the rotational restraint at each end of the column.

To determine whether a particular column is slender, and therefore whether moment magnification is required, ACI 318–83 specifies critical values of the slenderness ratio to mark the transition between short and slender columns. The slenderness ratio of a column is defined as the effective length of the column divided by its radius of gyration (taken about the axis of bending),  $kl_u/r$ . For a rectangular cross-section, the radius of gyration may be approximated as 0.3 times the overall column dimension in the direction in which stability is being considered or 0.25 times the diameter of a circular cross-section. For a braced column, the slenderness effect may be ignored when

$$\frac{kl_u}{r} < 34 - 12 \frac{M_{1b}^*}{M_{2b}^*} \quad (12.21)$$

where the subscript b for the end moments refers to a braced column;  $M_{1b}^*$  is the smaller of the two end moments and is taken as positive, if the column is bent in single curvature, and negative, if bent in double curvature;  $M_{2b}^*$  is the larger of the two end moments and is always taken to be positive.

An unbraced column is slender if

$$\frac{kl_u}{r} \geq 22 \quad (12.22)$$

If the slenderness ratio exceeds 100, the code suggests that the approximate moment magnifier method should not be used and that a second-order stability analysis be undertaken. Recent studies, however, have shown that for columns with slenderness ratios between 100 and 120, the moment magnifier method provides a very conservative estimate of strength (Gilbert 1989).

The magnified design moment  $M_m^*$  may be calculated from

$$M_m^* = \delta_b M_{2b}^* + \delta_s M_{2s}^* \quad (12.23)$$

The moment  $M_{2b}^*$  is the larger factored end moment caused by loads that result in no appreciable sidesway (such as uniformly distributed gravity loads on a symmetrical building structure).  $M_{2s}^*$  is the larger factored end moment caused by loads that result in appreciable sidesway (such as lateral

loads on the structure or non-uniform gravity loads). Both  $M_{2b}^*$  and  $M_{2s}^*$  may be calculated using a conventional elastic frame analysis.

The magnification factor  $\delta_b$  applies to the moments in a braced situation. It accounts for secondary moments arising from displacements due to curvature between the ends of the member (such as the secondary moments illustrated in the pin-ended column of [Figure 12.1](#)) and is given by

$$\delta_b = \frac{C_m}{1 - \frac{N^*}{\phi N_c}} \geq 1.0 \quad (12.24)$$

The term  $C_m$  depends on the ratio of the end moments and whether the column is bent in single or double curvature. For members braced against sidesway and with no transverse loads applied to the column between the supports,  $C_m$  is given by

$$C_m = 0.6 + 0.4 \frac{M_{1b}^*}{M_{2b}^*} (\geq 0.4) \quad (12.25)$$

For all other cases,  $C_m=1.0$ . Note that the ratio of the end moments in Equation 12.25 is positive if the column is in single curvature and negative if in double curvature.

The critical buckling load  $N_c$  is given by Equation 12.20. An estimate of  $EI$  for the column at the ultimate limit state is required in order to determine  $N_c$ . This estimate should account, at least approximately, for the change of stiffness caused by material non-linearities, such as cracking, the non-linear stress-strain relationship for concrete in compression, yielding of the steel, and the time-dependent effects of creep. In lieu of more accurate analysis, ACI 318–83 suggests that  $EI$  may be taken as either

$$EI = \frac{0.2E_c I_g + E_s I_s}{1 + \beta_d} \quad (12.26a)$$

or

$$EI = \frac{0.4E_c I_g}{1 + \beta_d} \quad (12.26b)$$

where  $I_s$  is the moment of inertia of the steel area about the centroidal axis of the cross-section,  $\beta_d$  is a factor to account for the effects of creep and is the ratio of the maximum factored dead load moment to the maximum factored total load moment (and is always positive). AS 3600–1988 defines  $EI$  as the ratio of moment to curvature at the point on the interaction curve corresponding to a depth to the neutral axis of  $0.6d$  (the bal-

anced failure point for a column containing non-prestressed tensile reinforcement with  $f_y=400$  MPa) and is therefore given by

$$EI = \frac{200dM_{0.6d}}{1 + \beta_d} \quad (12.26c)$$

The magnification factor  $\delta_s$  only applies to unbraced or sway structures, and models the primary plus secondary moments associated with the lateral drift of the column. This factor magnifies the moments caused by any loads that result in appreciable lateral drift (i.e. a drift exceeding about  $l_u/1500$ ) and is given by

$$\delta_s = \frac{1}{1 - \frac{\Sigma N^*}{\phi \Sigma N_c}} \geq 1.0 \quad (12.27)$$

where  $\Sigma N^*$  and  $\Sigma N_c$  are the summations of the design actions and the critical loads, respectively, for all the columns in the storey.

For a column in a braced structure, the second term in Equation 12.23 (the sway term) is zero, since no loads result in appreciable sidesway. ACI 318–83 specifies that for a pin-ended member in a braced structure or a member with end eccentricities less than  $(15+0.03D)$  mm, the term  $M_{2b}^*$  in Equation 12.23 should be calculated using a minimum eccentricity of  $(15+0.03D)$  mm about each principal axis. In addition, the ratio  $M_{1b}^*/M_{2b}^*$  should be taken as 1.0. The same minimum eccentricities are specified for the determination of the minimum value of  $M_{2s}^*$  in an unbraced structure.

For slender members in biaxial bending, the moment about each axis should be magnified using Equation 12.23 with the restraint conditions applicable to each plane of bending.

### Example 12.2

Consider a 10 m long, pin-ended column in a braced structure. The column cross-section is shown in [Figure 12.4a](#) and the material properties and steel quantities are as outlined in [Example 12.1](#). The strength interaction curve for the cross-section was calculated in [Example 12.1](#) and is illustrated in [Figure 12.5](#). The column is laterally supported at close centres to prevent displacement perpendicular to the weak axis of the section, but is unsupported between its ends in the direction perpendicular to the strong axis. The column is loaded by a compressive force  $N$  at a constant eccentricity  $e$  to produce compression and uniaxial bending about the strong axis. In this example, two loading lines for the column are traced (corresponding to initial eccentricities of  $e=100$  mm and  $e=400$  mm) and the strength of the slender column in each case is established.

Since the column is braced and pinned at each end,  $k=1$  [from [Figure 12.8a\(iii\)](#)],

and therefore  $kl_u=10$  m, with respect to the strong axis. The effective length about the weak axis is small due to the specified closely spaced lateral supports. For bending about the strong axis, the slenderness ratio is

$$\frac{kl_u}{r} = \frac{10\,000}{0.3 \times 800} = 41.7$$

which is greater than the transition limit of 22 (specified in Equation 12.21) and, therefore, the column is slender. For a braced column, Equation 12.23 reduces to

$$M_m^* = \delta_b M_{2b}^*$$

The member is subjected to single curvature bending with equal end moments, and from Equation 2.25,  $C_m=1.0$ . To determine  $EI$  using Equation 12.26a, the gross moment of inertia of the cross-section and the moment of inertia of the steel about the centroidal axis are required. For the cross-section shown in [Figure 12.4a](#),  $I_g=25600 \times 10^6 \text{ mm}^4$  and the moments of inertia of the prestressed and non-prestressed steel are, respectively,

$$I_p = 2 \times 1000 \times 260^2 = 135 \times 10^6 \text{ mm}^4$$

and

$$I_s = 2 \times 2250 \times 330^2 = 490 \times 10^6 \text{ mm}^4$$

The corresponding rigidities are

$$E_c I_g = 32\,000 \times 25\,600 \times 10^6 = 819 \times 10^{12} \text{ N mm}^2$$

and

$$\begin{aligned} E_s I_s + E_p I_p &= (200 \times 10^3 \times 490 \times 10^6) \\ &\quad + (195 \times 10^3 \times 135 \times 10^6) = 124 \times 10^{12} \text{ N mm}^2 \end{aligned}$$

If the ratio of dead load to total load is  $\beta_d=0.7$ , then from Equation 12.26a,

$$EI = \frac{(0.2 \times 819 \times 10^{12}) + (124 \times 10^{12})}{1 + 0.7} = 170 \times 10^{12} \text{ N mm}^2$$



and the critical buckling load is calculated using Equation 12.20:

$$N_c = \frac{\pi^2 \times 170 \times 10^{12}}{10000^2} \times 10^{-3} = 16740 \text{ kN}$$

The loading line for each initial eccentricity is obtained by calculating the magnification factor  $\delta_b$  from Equation 12.24 for a series of values of axial force  $N^*$  and plotting the points  $(N^*, \delta_b N^* e)$  on a graph of axial force and moment.

Sample calculations are provided for the points on the loading lines corresponding to an axial force  $N^*=5000$  kN, using the strength reduction factor specified in ACI 318–83 for a conventionally tied column, i.e.  $\phi = 0.7$ . From Equation 12.24, when  $N^*=5000$  kN,

$$\delta_b = \frac{1}{1 - \frac{5000}{0.7 \times 16740}} = 1.74$$

When  $e=100$  mm, the magnified moment is

$$M_m^* = \delta_b N^* e = 1.74 \times 5000 \times 100 \times 10^{-3} = 872 \text{ kNm}$$

and when  $e=400$  mm,

$$M_m^* = 1.74 \times 5000 \times 400 \times 10^{-3} = 3490 \text{ kNm}$$

Other points on the loading line are as follows:

$N^*$ (kN)	$\delta_b$	$e=100$ mm	$e=400$ mm
		$M_m^*$ (kNm)	$M_m^*$ (kNm)
2000	1.21	241	965
3000	1.34	403	1610
4000	1.52	607	2430
5000	1.74	872	3490
6000	2.05	1230	4920
7000	2.48	1740	--
8000	3.15	2520	-

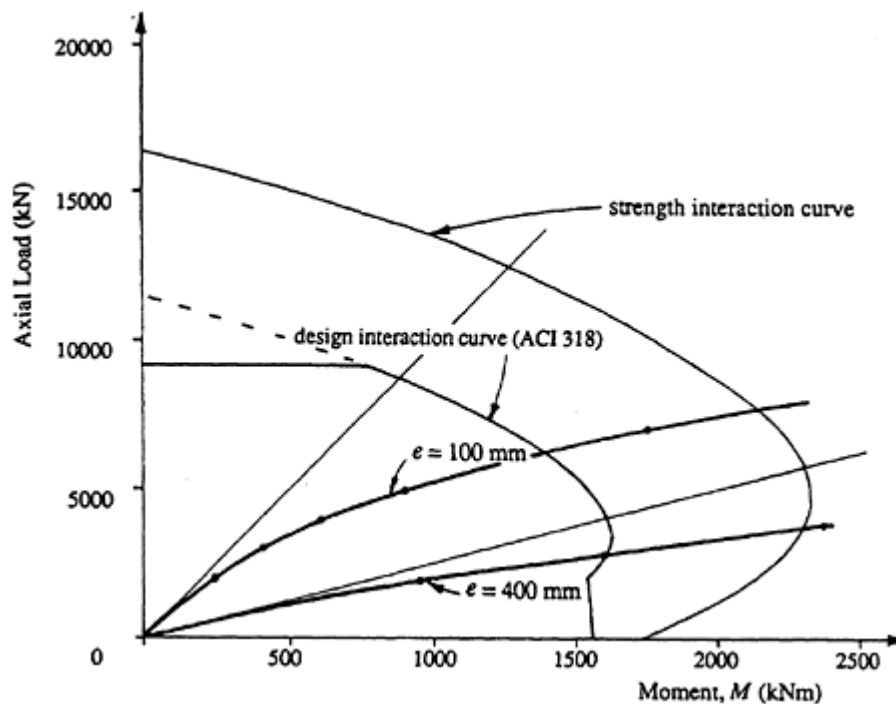


**Figure 12.11** Loading lines and strength of the slender columns of [Example 12.2](#).

The loading lines are plotted on [Figure 12.11](#), together with the strength interaction curve reproduced from [Figure 12.5](#) and the design interaction curve in accordance with ACI 318–83. The strength of each column is the axial load corresponding to the intersection of the loading line and the strength interaction curve. The maximum factored design load  $N^*$  that can be applied to the slender column (and meet the strength design requirements of ACI 318–83) is obtained from the point where the loading line crosses the design interaction curve. Note the significant reduction of strength in both columns due to slenderness, but particularly in the column with the smaller initial eccentricity. Slenderness causes a far greater relative reduction in strength when the initial eccentricity is small, in the primary compression region, than when eccentricity is large and bending predominates. Note also that for very slender columns, the curved loading line crosses the strength interaction curve in the primary tension region, and this is the same region in which prestress provides additional strength (see [Figure 12.5](#)). There is some advantage in prestressing slender columns.

## 12.5 Reinforcement requirements in compression members

The behaviour of a short column loaded to failure depends on the nature of the transverse reinforcement. When the strength of the cross-section is

reached, failure will be brittle and sudden if the column contains no transverse reinforcement in the form of closed ties or spirals (helical reinforcement). Transverse reinforcement imparts a measure of ductility to reinforced and prestressed concrete columns by providing restraint to the highly stressed longitudinal steel and by confining the inner core of compressive concrete. Spirally reinforced columns, in particular, exhibit considerable ductility at failure. Ductility is a critical design requirement for columns in buildings located in earthquake prone regions, where the ability to absorb large amounts of energy without failure is needed.

Codes of practice specify design requirements related to the quantity and disposition of transverse reinforcement in columns. The requirements in ACI 318–83 are summarized below.

For prestressed compression members other than walls, with an average prestress greater than or equal to 1.55 MPa, all longitudinal steel should be enclosed by standard spirals or lateral ties. Lateral ties should be at least 10 mm in diameter or an equivalent area of welded wire fabric (and 12 mm diameter when longitudinal bar diameters exceed 32 mm). The longitudinal spacing between ties should not exceed the smaller of 48 tie bar diameters, 16 longitudinal bar diameters, and the least dimension of the column. The first tie should be located no further than one half the tie spacing above the top of the footing or slab at the bottom end of the member and the last tie should be no further than 75 mm below the lowest reinforcement in any beams framing into the top of the column. Ties should be arranged so that every corner bar is restrained in two directions by the corner of a tie and every other bar (or every alternate bar if bars are spaced closer together than 150 mm) is also restrained by a tie corner.

For spirally reinforced columns, the ratio of spiral reinforcement  $\rho_s$  (defined as the ratio of the volume of spiral reinforcement to the total volume of the core) should satisfy

$$\rho_s = 0.45 \left( \frac{A_g}{A_c} - 1 \right) \frac{f'_c}{f_y} \quad (12.28)$$

where  $A_c$  is the cross-sectional area of the core of the member obtained using the outside diameter of the spiral,  $d_{core}$ . It can be shown that (Naaman 1982)

$$\rho_s \approx \pi \frac{A_s}{A_c} \times \frac{d_{core}}{s}$$

where  $A_s$  is the cross-sectional area of the spiral steel and  $s$  is the pitch of the spiral measured centre to centre. For cast *in situ* construction, the diameter of the spiral bar should be at least 10 mm and the clear spacing between spirals should not be outside the range 25–75 mm.

Compression members with an average prestress of less than 1.55 MPa should have a minimum area of longitudinal non-prestressed reinforcement of  $0.01A_g$ , with a minimum of four bars within rectangular or circular ties and six bars within spirals. The transverse reinforcement requirements should also satisfy the minimum requirements specified for reinforced concrete columns.

## 12.6 Tension members

### *12.6.1 Advantages and applications*

Prestressed concrete tension members are simple elements used in a wide variety of situations. They are frequently used as tie-backs in cantilevered construction, anchors for walls and footings, tie and chord members in trusses, hangers and stays in suspension bridges, walls of tanks and containment vessels, and many other applications.

The use of reinforced concrete members in direct tension has obvious drawbacks. Cracking causes a large and sudden loss of stiffness, and crack control is difficult. Cracks occur over the entire cross-section and corrosion protection of the steel must be carefully considered, in addition to the aesthetic difficulties. By prestressing the concrete, however, a tension member is given strength and rigidity otherwise unobtainable from either the concrete or the steel acting alone. Provided that cracking does not occur in the concrete, the prestressing steel is protected from the environment and the tension member is suitable for its many uses. Compared with compression members, tension members usually have a high initial level of prestress.

The deformation of a prestressed concrete tension member can be carefully controlled. In situations where excessive elongation of a tension member may cause strength or serviceability problems, prestressed concrete is a design solution worthy of consideration.

### *12.6.2 Behaviour*

The analysis of a prestressed concrete direct tension member is straightforward. Both the prestressing force and the external tensile loads are generally concentric with the longitudinal axis of the member, and hence bending stresses are minimized.

Prior to cracking of the concrete, the prestressing steel and the concrete act in a composite manner and behaviour may be determined by considering a transformed cross-section. If required, a transformed section obtained using the effective modulus for concrete (Equation 2.12) may be used to include the time-dependent effects of creep and shrinkage.

Consider a tension member concentrically prestressed with an effective prestressing force  $P_e$ . The cross-section is symmetrically reinforced with an area of bonded prestressing steel  $A_p$ . The transformed area of the tie is therefore

$$A = A_c + n_p A_p = A_g + (n_p - 1) A_p \quad (12.29)$$

where  $n_p$  is the modular ratio given by  $E_p/E_c$ . The uniform stress in the concrete  $\sigma$  due to the prestressing force and the applied external load  $N$  is

$$\sigma = -\frac{P_e}{A_c} + \frac{N}{A} \quad (12.30)$$

and the stress in the prestressing steel is

$$\sigma_p = \frac{P_e}{A_p} + \frac{n_p N}{A} \quad (12.31)$$

For most applications, it is necessary to ensure that cracking does not occur at service loads. To provide a suitable margin against cracking under the day to day loads, and to ensure that cracks resulting from an unexpected overload close completely when the overload is removed, it is common in design to insist that the concrete stress remains compressive under normal in-service conditions. By setting  $\sigma=0$  in Equation 12.30 and rearranging, an upper limit to the external tensile force is established, and is given by

$$N \leq P_e \frac{A}{A_c} = P_e \left( 1 + n_p \frac{A_p}{A_c} \right) \quad (12.32)$$

When a tensile member is stressed beyond the service load range, cracking occurs when the concrete stress reaches the direct tensile strength, which is usually taken as  $0.4\sqrt{f'_c}$  (see Equation 2.4). If the tensile force at cracking is  $N_{cr}$ , then from Equation 12.30,

$$N_{cr} = \left( \frac{P_e}{A_c} + 0.4\sqrt{f'_c} \right) A \quad (12.33)$$

The steel stress at the crack, just after cracking, is

$$\sigma_p = \frac{N_{cr}}{A_p} = \left( \frac{P_e}{A_c} + 0.4\sqrt{f'_c} \right) \frac{A}{A_p} \quad (12.34)$$

and this must be less than the ultimate stress of the steel,  $f_p$ , if failure of the member is to be avoided at first cracking. The steel stress in Equation

12.34 is usually limited to a maximum of about  $f_p/1.2$  in order to obtain a minimum acceptable margin of safety between cracking and ultimate strength. Equation 12.34 can, therefore, be rearranged to obtain an expression for the minimum amount of prestressing steel in a tension member, and is given by

$$A_p \geq \frac{1.2 N_{cr}}{f_p} = \left( \frac{P_e}{A_c} + 0.4\sqrt{f'_c} \right) \frac{1.2 A}{f_p} \quad (12.35)$$

The ultimate strength of the member is equal to the tensile strength of the steel, and is given by

$$N_u = A_p f_p \quad (12.36)$$

and in design, the factored design tensile force must satisfy the design equation,

$$N^* \leq \phi N_u \quad (12.37)$$

where the strength reduction factor for direct tension is the same as for bending ( $\phi = 0.9$  in ACI 318–83 and  $\phi = 0.8$  in AS 3600–1988).

The axial deformation of a prestressed tension member at service loads depends on the load history [i.e. the times at which the prestressing force(s) and the external loads are applied], and the deformation characteristics of the concrete. Stage stressing can be used to carefully control longitudinal deformation. The shortening of a tension member at any time  $t$  caused by an initial prestress  $P_i$  applied to the concrete at a particular time  $\tau_0$  may be approximated by

$$\Delta_{P_i} = \frac{P_i L}{A_c E_{e,0}} \quad (12.38)$$

where  $L$  is the length of the member and  $E_{e,0}$  is the effective modulus of the concrete obtained from Equation 2.12 using the creep coefficient associated with the age of the concrete at first loading,  $\tau_0$ . The elongation at any time caused by an external tensile force  $N$  applied at time  $\tau_1$  may be estimated by

$$\Delta_N = \frac{NL}{\bar{A} E_{e,1}} \quad (12.39)$$

where  $\bar{A}$  is the area of the transformed section calculated using the effective modular ratio,  $E_p/E_{e,1}$ . In addition to deformation caused by loads, shrinkage will cause an additional shortening. A detailed analysis of the time-

dependent deformation of a tension member subjected to any load history can be made using the procedures outlined by Gilbert (1988).

A satisfactory preliminary design of a tension member usually results if the prestressing force is initially selected so that, after losses, the effective prestress is between 10 and 20% higher than the maximum in-service tension. If the compressive stress in the concrete at transfer is limited to about  $0.4f'_{ci}$ , the area of the cross-section  $A_g$  can be determined. The area of steel required to impart the necessary prestress is next calculated. The resulting member can be checked for strength and serviceability, and details may be modified, if necessary.

### Example 7.3

Consider the vertical post-tensioned tension member acting as a tie-back for the cantilevered roof of the grandstand shown in [Figure 12.12](#). In the critical loading case, the tension member must transfer a design working dead load of 800 kN and live load of 200 kN to the footing which is anchored to rock.

The material properties are  $f'_c = 40$  MPa;  $E_c = 32000$  MPa;  $f'_{ci} = 30$  MPa;  $E_{ci} = 27\,500$  MPa;  $f_p = 1840$  MPa;  $E_p = 195000$  MPa; and  $n_p = 6.09$ .

In accordance with the preceding discussion, an effective prestress 10% higher than the maximum applied tension is assumed. Therefore,

$$P_e = 1.1 \times (800 + 200) = 1100 \text{ kN}$$

Owing to the small residual compression existing under sustained loads, the time-dependent loss of prestress is usually relatively small. In this short member, draw-in losses at transfer are likely to be significant. For the purposes of this example, the time-dependent losses are assumed to be 12% and the short-term losses are taken as 15%. The force immediately after transfer and the required jacking force are therefore

$$P_i = \frac{1100}{0.88} = 1250 \text{ kN} \quad \text{and} \quad P_j = \frac{1250}{0.85} = 1470 \text{ kN}$$

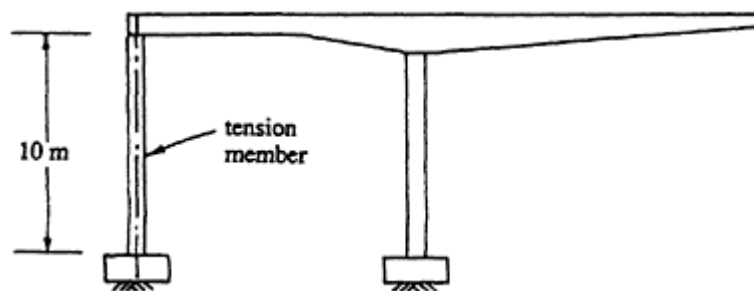


Figure 12.12 Tie-back member analysed in [Example 12.3](#).

If the maximum steel stress at jacking is  $0.85f_p$ , then the area of steel is

$$A_p \geq \frac{1470 \times 10^3}{0.85 \times 1840} = 940 \text{ mm}^2$$

Try ten 12.7 mm diameter strands ( $A_p=1000 \text{ mm}^2$ ) post-tensioned within a 60 mm diameter duct located at the centroid of the cross-section.

The ultimate strength of the member is calculated using Equation 12.36 (using the strength reduction factor and load factors specified in AS 3600–1988):

$$\phi N_u = 0.8 \times 1000 \times 1840 \times 10^{-3} = 1470 \text{ kN m}$$

The design axial force is

$$N^* = (1.25 \times 800) + (1.5 \times 200) = 1300 \text{ kN}$$

which is less than the design strength and is therefore satisfactory. If additional strength had been necessary, non-prestressed steel could be included to increase  $N_u$  to the required level.

If the concrete stress at transfer is limited to  $0.4f'_{ci} = 12 \text{ MPa}$ , the required area of concrete is

$$A_c \geq \frac{P_i}{0.4f'_c} = \frac{1250 \times 10^3}{12} = 104\,200 \text{ mm}^2$$

Try a 350 mm by 350 mm square cross-section with a centrally located 60 mm duct. Therefore, before the duct is grouted,

$$A_c = 350^2 - (0.25\pi \times 60^2) = 119\,700 \text{ mm}^2$$

Under the effective prestress, after all losses and after the duct is fully grouted, the area of the transformed section is obtained using Equation 12.29:

$$A = 350^2 + (6.09 - 1)1000 = 127\,590 \text{ mm}^2$$

and

$$A_c = 121\,500 \text{ mm}^2$$

The uniform stress in the concrete under the full service load is given by



Equation 12.30:

$$\sigma = -\frac{1100 \times 10^3}{121\,500} + \frac{1000 \times 10^3}{127\,590} = -1.21 \text{ MPa}$$

and the steel stress is given by Equation 12.31:

$$\sigma_p = \frac{1100 \times 10^3}{1000} + \frac{6.09 \times 1000 \times 10^3}{127\,590} = 1148 \text{ MPa}$$

Both stresses are satisfactory and cracking will not occur at service loads, even if the losses of prestress have been slightly underestimated.

The minimum area of steel to ensure a factor of safety of 1.2 at cracking is checked using Equation 12.35:

$$A_p = \left( \frac{1100 \times 10^3}{121\,500} + 0.4\sqrt{40} \right) \frac{1.2 \times 127\,590}{1840} = 964 \text{ mm}^2$$

and the area of steel  $A_p=1000 \text{ mm}^2$  adopted here is just sufficient.

If the final creep coefficients associated with the age at transfer,  $\tau_0$ , and the age when the external load is first applied,  $\tau_1$ , are  $\phi^*(\tau_0) = 2.5$  and  $\phi^*(\tau_1) = 2.0$ , then Equation 2.12 gives the appropriate effective moduli:

$$E_{e,0} = \frac{27\,500}{1 + 2.5} = 7860 \text{ MPa} \quad \text{and} \quad E_{e,1} = \frac{32\,000}{1 + 2.0} = 10\,670 \text{ MPa}$$

The shortening caused by prestress is obtained using Equation 12.38:

$$\Delta_P = \frac{1250 \times 10^3 \times 10\,000}{121\,500 \times 7860} = 13.1 \text{ mm}$$

and the elongation caused by  $N$  is given by Equation 12.39. In this Equation,

$$\bar{A} = 121\,500 + 1000 \times \frac{195\,000}{10\,670} = 139\,780 \text{ mm}^2$$

and therefore,

$$\Delta_N = \frac{1000 \times 10^3 \times 10\,000}{139\,780 \times 10\,670} = 6.7 \text{ mm}$$

The net effect is a shortening of the member by

$$\Delta = 13.1 - 6.7 = 6.4 \text{ mm}$$

Shrinkage will cause a further shortening of several mm.

## 12.7 References

- ACI 318–83 1983. *Building code requirements for reinforced concrete*. Detroit: American Concrete Institute.
- ACI 318R–83 1983. *Commentary on building code requirements for reinforced concrete (ACI 318–83)*. Detroit: American Concrete Institute.
- AS 3600–1988. *Australian standard for concrete structures*. Sydney: Standards Association of Australia.
- Bresler, B. 1960. Design criteria for reinforced concrete columns under axial load and biaxial bending. *ACI Journal, Proc.* **57**, 481–90.
- BS 8110 1985. *Structural use of concrete—part I, code of practice for design and construction*. London: British Standards Institution.
- Gilbert, R.I. 1988. *Time effects in concrete structures*. Amsterdam: Elsevier.
- Gilbert, R.I. 1989. A procedure for the analysis of slender concrete columns under sustained eccentric loading. *Civil Engineering Transactions, Institution of Engineers, Australia CE31*, 39–46.
- Naaman, A.E. 1982. *Prestressed concrete analysis and design*. New York: McGraw-Hill.
- Pannell, F.N. 1963. Failure surfaces for members in compression and biaxial bending. *ACI Journal, Proc.* **60**, 129–41.

# Appendix I

## Alternative models for creep and shrinkage

### A.1 Introduction

In Sections [2.5.2](#) and [2.5.3](#), two relatively simple procedures for determining the magnitude and rate of development of the creep coefficient and shrinkage strain were presented. Many more complex procedures have been developed and are recommended by the various concrete authorities. A description and comparison of some of the better known techniques has been presented by Gilbert (1986,1988). In this Appendix, two well known and widely used procedures are outlined.

### A.2 The ACI Committee 209 method (1978)

#### *Creep*

The ACI Committee 209 (1978) adopts a hyperbolic function to represent the relationship between creep and age at first loading:

$$\phi(t, \tau) = \frac{(t - \tau)^{0.6}}{10 + (t - \tau)^{0.6}} \phi^*(\tau) \quad (\text{A.1})$$

where  $\tau$  is the age of the concrete at first loading (in days),  $t - \tau$  is the duration of loading (in days), and  $\phi^*(\tau)$  is the final creep coefficient for concrete first loaded at age  $\tau$  and is expressed as

$$\phi^*(\tau) = 2.35\gamma_1\gamma_2\gamma_3\gamma_4\gamma_5\gamma_6 \quad (\text{A.2})$$

where  $\gamma_1$  to  $\gamma_6$  are correction factors which account for many of the parameters that affect the magnitude of creep.

$\gamma_1$  depends on the age of concrete at the time of first loading,  $\tau$ , and is

given by

$$\text{For moist-cured concrete: } \gamma_1 = 1.25\tau^{-0.118} \quad \text{for } \tau > 7 \text{ days} \quad (\text{A.3})$$

$$\text{For steam-cured concrete: } \gamma_1 = 1.13\tau^{-0.094} \quad \text{for } \tau > 3 \text{ days}$$

$\gamma_2$  is a function of the relative humidity,  $\lambda$  (in percent):

$$\gamma_2 = 1.27 - 0.0067\lambda \quad \text{for } \lambda > 40 \quad (\text{A.4})$$

$\gamma_3$  accounts for the size and shape of the member and depends on the dimension  $h_o$  given by  $4V/S$ , where  $V/S$  is the volume to surface ratio.

When  $h_o \leq 150 \text{ mm}$ ,  $\gamma_3$  is obtained from

$h_o$ (mm)	50	75	100	125	150
$\gamma_3$	1.30	1.17	1.11	1.04	1.00

When  $150 \text{ mm} < h_o < 380 \text{ mm}$ :

$$\gamma_3 = 1.14 - 0.00092h_o \quad \text{when } t - \tau \leq 365 \text{ days} \quad (\text{A.5})$$

$$\gamma_3 = 1.10 - 0.00067h_o \quad \text{when } t - \tau > 365 \text{ days}$$

and when  $h_o \geq 380 \text{ mm}$ :

$$\gamma_3 = \frac{2}{3} [1 + 1.13 \exp(-0.0213V/S)] \quad (\text{A.6})$$

$\gamma_4$  to  $\gamma_6$  account for parameters associated with the composition of the concrete; specifically,  $\gamma_4$  depends on the slump of the fresh concrete,  $s$  (in mm);  $\gamma_5$  is a function of the ratio of the fine aggregate to total aggregate by weight,  $\psi$  (in percent); and  $\gamma_6$  accounts for the air content,  $a$  (in percent):

$$\gamma_4 = 0.82 + 0.00264s \quad (\text{A.7})$$

$$\gamma_5 = 0.88 + 0.0024\psi \quad (\text{A.8})$$

and

$$\gamma_6 = 0.46 + 0.09a < 1.0 \quad (\text{A.9})$$

Under a constant stress  $\sigma_o$  first applied at age  $\tau$ , the load-dependent strain

at time  $t$  is

$$\epsilon(t) = \frac{\sigma_0}{E_c(\tau)} [1 + \phi(t, \tau)] \tag{A.10}$$

where  $E_c(\tau)$  is obtained from Equation 2.6. The concrete strength at age  $\tau$  may be obtained from the 28 day strength using Equation 2.2.

*Shrinkage*

The shrinkage strain at time  $t$ , measured from the start of drying, is given by

For moist-cured concrete: 
$$\epsilon_{sh}(t) = \frac{t}{35 + t} \epsilon_{sh}^* \tag{A.11}$$

For steam-cured concrete: 
$$\epsilon_{sh}(t) = \frac{t}{55 + t} \epsilon_{sh}^*$$

where  $\epsilon_{sh}^*$  is the final shrinkage and may be calculated from

$$\epsilon_{sh}^* = 780 \gamma_2 \gamma_3 \gamma_4 \gamma_5 \gamma_6 \gamma_7 \gamma_8 \times 10^{-6} \tag{A.12}$$

The factors  $\gamma_2$  to  $\gamma_6$  in Equation A.12 depend on the same parameters as the corresponding factors for creep ( $\gamma_2$  to  $\gamma_6$ ), and are given by

$$\begin{aligned} \gamma_2 &= 1.40 - 0.01\lambda \quad \text{for } 40 \leq \lambda \leq 80 \\ \gamma_2 &= 3.00 - 0.03\lambda \quad \text{for } 80 \leq \lambda \leq 100 \end{aligned} \tag{A.13}$$

When  $50 \text{ mm} \leq h_0 \leq 150 \text{ mm}$ ,  $\gamma_3$  is given by

$h_0$ (mm)	50	75	100	125	150	
$\gamma_3$	1.35	1.25	1.17	1.08	1.00	(A.14)

When  $150 \text{ mm} < h_0 \leq 380 \text{ mm}$ :

$$\begin{aligned} \gamma_3 &= 1.23 - 0.0015h_0 \quad \text{for } t \leq 365 \text{ days} \\ \gamma_3 &= 1.17 - 0.0011h_0 \quad \text{for } t > 365 \text{ days} \end{aligned} \tag{A.15}$$

and when  $h_o > 380$  mm:

$$\gamma_3' = 1.2 \exp(-0.00472V/S) \quad (\text{A.16})$$

$$\gamma_4' = 0.89 + 0.00161s \quad (\text{A.17})$$

$$\gamma_5' = 0.30 + 0.014\psi \quad \text{for } \psi \leq 50\% \quad (\text{A.18})$$

$$\gamma_5' = 0.90 + 0.002\psi \quad \text{for } \psi > 50\%$$

$$\gamma_6' = 0.95 + 0.008a \quad (\text{A.19})$$

The term  $\gamma_7$  depends on the cement content,  $c$  (in  $\text{kg/m}^3$ ) and is determined from

$$\gamma_7 = 0.75 + 0.00061c \quad (\text{A.20})$$

Finally,  $\gamma_8$  is a function of the period of initial moist curing  $T_c$  (in days) and is given by

$T_c$	1.0	3.0	7.0	14.0	28.0	90.0
$\gamma_8$	1.2	1.1	1.0	0.93	0.86	0.75

(A.21)

For concrete which is steam cured for a period of between one and three days,  $\gamma_8=1.0$ .

### A.3 The CEB-FIP method (1978)

The method for predicting creep and shrinkage contained in the CEB-FIP Model Code (1978) is based on the method proposed by Rüsçh and Jungwirth (1976).

#### *Creep*

The creep strain at time  $t$  caused by a constant sustained stress  $\sigma_o$  applied at time  $\tau$  is assumed to be

$$\epsilon_c(t, \tau) = \frac{\sigma_o}{E_{c28}} \phi(t, \tau) \quad (\text{A.22})$$

where  $E_{c28}$  is the longitudinal modulus of deformation at 28 days and may be taken as

$f'_c$ (MPa)	20	25	30	35	40	45	50
$E_{c28}$ (GPa)	29	30.5	32	33.5	35	36	37

(A.23)

The creep coefficient  $\phi(t, \tau)$  is therefore defined as the ratio of creep strain at time  $t$  to the instantaneous elastic strain at age 28 days. The total stress produced strain (instantaneous plus creep) at time  $t$  is given by

$$\varepsilon(t, \tau) = \sigma_0 \left[ \frac{1}{E_c(\tau)} + \frac{\phi(t, \tau)}{E_{c28}} \right] \quad (\text{A.24})$$

The creep coefficient is assumed to consist of a reversible delayed elastic component and an irreversible flow component, and is given in Equation A.25. The flow component is further sub-divided into an initial flow component (which occurs within the first 24 hours under load) and a subsequent flow component:

$$\phi(t, \tau) = \phi_d \beta_d(t - \tau) + \beta_a(\tau) + \phi_f [\beta_f(t) - \beta_f(\tau)] \quad (\text{A.25})$$

where  $\phi_d$  is the final delayed elastic creep coefficient (i.e. the ratio of the final delayed elastic strain and the instantaneous strain at 28 days) and is taken to be 0.4. The delayed elastic creep coefficient is associated with the recoverable part of creep. The term  $\beta_d(t - \tau)$  is a function describing the development of the delayed elastic strain with time and may be calculated from

$$\beta_d(t - \tau) = 0.73 \{ 1 - \exp[-0.01(t - \tau)] \} + 0.27 \quad (\text{A.26})$$

$\beta_a(\tau)$  is the rapid initial flow and is given by

$$\beta_a(\tau) = 0.8 \left[ 1 - \frac{f_c(\tau)}{f_c(\infty)} \right] \quad (\text{A.27})$$

The strength ratio  $f_c(\tau)/f_c(\infty)$  is obtained from

$$\frac{f_c(\tau)}{f_c(\infty)} = \frac{\tau^{0.73}}{5.27 + \tau^{0.73}} \quad (\text{A.28})$$

The flow coefficient  $\phi_f$  in Equation A.25 is the sum of two components:

$$\phi_f = \phi_{f1} + \phi_{f2} \quad (\text{A.29})$$

where  $\phi_{f1}$  depends on the relative humidity  $\lambda$  (in percent) and is given by

$$\phi_{f1} = 0.111(0.0002\lambda^3 - 0.043\lambda^2 + 2.57\lambda) - 2.2 \quad (\text{A.30})$$

$\phi_{f2}$  depends on the size of the member and may be obtained from Equation A.31 using the notional thickness  $h_o$  (mm):

$$\phi_{f2} = 1.12[1 + \exp(-0.044h_o^{0.58})] \quad (\text{A.31})$$

where

$$h_o = \gamma \frac{2A_c}{u} \quad (\text{A.32})$$

$A_c$  is the cross-sectional area of the member (in  $\text{mm}^2$ ),  $u$  is the perimeter exposed to drying (in mm), and  $\gamma$  is a humidity coefficient obtained from

$$\begin{aligned} \gamma &= 1.0 + 0.00049 \exp(0.1\lambda) && \text{when } \lambda \leq 98 \\ &= 30 && \text{when } \lambda = 100 \end{aligned} \quad (\text{A.33})$$

The development of the subsequent (or delayed) flow component with time depends on the notional thickness  $h_o$  and is described by the function  $\beta_f(t)$ . When  $50 \text{ mm} \leq h_o \leq 1600 \text{ mm}$ , the function  $\beta_f(t)$  may be calculated from the following expression:

$$\beta_f(t) = \left( \frac{t^\alpha}{t^\alpha + \beta} \right)^{1/3} \quad (\text{A.34})$$

where  $\alpha = 0.8 + 0.55 \exp(-0.003h_o)$  and  $\beta = 770 + 210 \exp(-0.0043h_o)$ .

The elastic modulus at the age of first loading  $E_c(\tau)$  to be used in Equation A.24 is

$$E_c(\tau) = 9.5 [f_c(\tau)]^{1/3} \quad (\text{A.35})$$

and  $f_c(\tau)$  is obtained from Equation A.28.

*Shrinkage*



The mean shrinkage strain which occurs within the time interval  $t_0$  to  $t$  is

given by

$$\varepsilon_{sh}(t, t_o) = \varepsilon_{sho} [\beta_{sh}(t) - \beta_{sh}(t_o)] \quad (\text{A.36})$$

where  $\varepsilon_{sho}$  is a basic shrinkage coefficient obtained from the product of two functions and is given by

$$\varepsilon_{sho} = \varepsilon_{sh1} \varepsilon_{sh2} \quad (\text{A.37})$$

The function  $\varepsilon_{sh1}$  depends on the relative humidity  $\lambda$  and is obtained from

$$\begin{aligned} \varepsilon_{sh1} &= 0.333(0.41\lambda^2 - 37.1\lambda - 372) \times 10^{-6} && \text{when } \lambda \leq 98 \\ &= +100 \times 10^{-6} && \text{when } \lambda = 100 \end{aligned} \quad (\text{A.38})$$

The term  $\varepsilon_{sh2}$  depends on the notional thickness  $h_o$  and may be expressed as

$$\varepsilon_{sh2} = 0.7 + 1.42 \exp(-0.18h_o^{0.45}) \quad (\text{A.39})$$

The development of shrinkage with time is described by  $\beta_{sh}(t)$  and this also depends on the notional thickness:

$$\text{When } 50 \leq h_o \leq 600 \text{ mm:} \quad \beta_{sh}(t) = \frac{t^{0.8}}{t^{0.8} + 0.25h_o} \quad (\text{A.40})$$

$$\text{When } 600 < h_o \leq 1600 \text{ mm:} \quad \beta_{sh}(t) = \frac{t^{1.25}}{t^{1.25} + 8h_o}$$

#### *Temperature effects*

When the ambient temperature during curing is significantly different from 20 °C, the age of the concrete should be adjusted according to the following:

$$t_e = \frac{\alpha}{30} \sum_0^{t_m} \{ [T(t_m) + 10] \Delta t_m \} \quad (\text{A.41})$$

where  $T$  is the mean daily temperature of the concrete occurring during the period  $\Delta t_m$  days.  $\alpha$  depends on the cement type and equals 1 for normal and slow-hardening cements, 2 for rapid-hardening cements and 3 for rapid-hardening, high-strength cements. The adjusted effective age  $t_e$  is used for  $t$  in Equations A.25 and A.34.

## A.4 References

- ACI Committee 209, Subcommittee II 1978. *Prediction of creep, shrinkage and temperature effects 2*. Draft Report. Detroit: American Concrete Institute.
- CEB–FIP 1978. *Model code for concrete structures*. Paris: Comité Euro-International du Béton—Fédération Internationale de la Précontrainte.
- Gilbert, R.I. 1986. *Prediction of creep and shrinkage in concrete—the sorry state of the art*. Unicity Report No. R-234. Kensington: School of Civil Engineering, University of New South Wales.
- Gilbert, R.I. 1988. *Time effects in concrete structures*. Amsterdam: Elsevier.
- Neville, A.M., W.Dilger & J.J.Brooks 1984. *Creep of concrete and its effect on structural behavior*. Amsterdam: North-Holland.
- Rüsch, H. & D.Jungwirth 1976. *Stahlbeton-Spannbeton, Band 2*, Düsseldorf: Werner-Verlag.

# Index

- ACI, American Concrete Institute
- ACI 209 (Committee) [32](#), [41](#), [43](#), [490–3](#)
- ACI [318–83](#):
- bearing stress [225](#)
  - bonded tendons, ultimate stress [140](#)
  - crack control [69](#)
  - column rigidity [477](#)
  - deflection multiplication factor [115](#)
  - design interaction curve [469–70](#), [481](#)
  - design strength [23](#), [147](#)
  - direct design method [401–2](#)
  - drop panels [415](#)
  - ductility [127](#)
  - effective flange width [154](#), [243](#)
  - effective length of a column [473–4](#)
  - effective moment of inertia [111](#)
  - elastic modulus of concrete [37](#)
  - equivalent frame method [398](#)
  - extreme fibre strain [125](#), [459](#)
  - friction losses [104](#)
  - horizontal shear strength [269–70](#), [273–4](#)
  - load combinations [19](#), [21](#)
  - moment magnifier method [474–8](#)
  - maximum tendon spacing in slabs [421](#)
  - minimum level of prestress in slabs [420](#)
  - moment redistribution at ultimate [361](#)
  - permissible concrete stresses [61–2](#)
  - permissible steel stresses [64](#)
  - punching shear [196–7](#)
  - rectangular stress block [125–6](#), [459](#)
  - secondary effects at ultimate [361](#)
  - serviceability [27](#)
  - shear strength of beams [166](#)
  - strength reduction factor [23–4](#)
  - tension member, design of [485](#)
  - transfer length [212–13](#)
  - transverse reinforcement in columns [482](#)
  - unbonded tendons [145](#)
- ACI 435 (Committee) [430](#)
- Age-adjusted effective modulus [41](#), [91](#), [92](#), [252](#), [257](#)
- Age-adjusted effective modulus method [40–1](#), [89](#)
- Age-adjusted transformed section [92](#), [94](#)
- Ageing coefficient [41](#)
- Aggregate interlock [164–5](#)
- Allowable stresses, *see* Stress limits
- Alloy bar [51–2](#)
- Analogous gridwork method [431–2](#)
- Analogous truss [163–4](#), [184–5](#)
- Anchorage length [209](#)
- Anchorage set (slip) [105–6](#)
- Anchorage zone:

- anchorage plates [218](#)
- bearing [214](#), [225](#)
- bursting [215](#), [217](#)
- bursting moment [220](#)
- cracking (splitting) [215](#), [220](#), [221](#)
- methods of analysis [218](#)–25
- post-tensioned members [214](#)–38
- pretensioned members [210](#)–14
- reinforcement requirements [213](#), [218](#), [224](#)–5, [228](#), [233](#)–4, [235](#)–7
- single anchorage [220](#)–1, [225](#)–8
- spalling [217](#), [221](#)–2
- spalling moment [221](#)
- stress isobars and trajectories [214](#)–18, [223](#)
- symmetric prism [222](#), [230](#)
- transfer length [209](#)–10, [212](#)
- transverse forces [209](#), [215](#), [220](#)
- truss analogy [219](#), [237](#)–8
- twin anchorages [221](#)–4, [229](#)–34
- Angle of dispersion [380](#)
- AS, Australian Standard
- AS 1302–1304 [57](#)
- AS 1310–1313 [49](#)–[51](#)
- AS 1480–1982 [387](#)
- AS 1481–1978 [120](#)
- AS 3600–1988:
  - anchorage zones [223](#)–4
  - biaxial bending and compression [470](#)–1
  - bonded tendons, ultimate stress [140](#)
  - crack control [26](#), [63](#), [440](#)–2
  - column rigidity [477](#)–8
  - creep coefficient [46](#)–7
  - deflection calculations (slabs) [431](#)
  - design for serviceability [26](#)–7
  - design interaction curve [469](#)
  - design requirements for shear [170](#)–2
  - design strength [23](#), [126](#), [147](#)
  - direct design method [401](#)–3
  - edge-supported two-way slabs [385](#)–6
  - effective flange width [153](#)–4, [243](#)
  - effective length of columns [472](#)–4
  - effective span [425](#)

- elastic modulus of concrete [37](#)
- extreme fibre strain [125](#), [459](#)
- fire resistance of slabs [422–3](#)
- frame method for flat slabs [399–400](#)
- friction losses [104](#)
- horizontal shear strength [267–9](#), [272–3](#)
- load factors and combinations [20–3](#)
- minimum ultimate curvature [127](#)
- moment coefficients [386](#)
- moment redistribution at ultimate [360](#)
- permissible stresses [62](#)
- prestressing steels [49](#)
- punching shear [197](#), [198–204](#)
- rectangular stress block [125–6](#), [459](#)
- relaxation of steel [53](#)
- secondary effects at ultimate [361](#)
- shear strength of beams [167–73](#)
- span-to-depth ratios [423–8](#)
- shrinkage [47](#)
- strength reduction factors [23–4](#)
- tension members [485](#)
- thermal expansion [48](#)
- transfer length [212](#)
- unbonded tendons [145](#)
- ASTM A416 [50](#)
- ASTM A421 [48](#)
- ASTM A722 [51](#)
  
- Balanced load [9](#), [420](#)
- Band-beam and slab systems, *see* Slabs (post-tensioned)
- Bazant, Z.P. [41](#)
- Beam-type shear 195 *see* Shear strength of beams
- Bearing failure [214](#), [225](#)
- Bond stress, factors affecting [210–12](#)
- Bonded tendons [4](#), [140](#)
- Branson, D.E. [111](#), [438](#)
- Bresler, B. [90](#), [470](#)
- BS, British Standard
- BS 8110, Parts 1 and 2, 1985:
  - bonded tendons [141–2](#)
  - creep coefficient [44–5](#)
  - design for serviceability [27](#)
  - design strength [25](#)
  - effective flange width [153–4](#), [243](#)
  - elastic modulus of concrete [44](#)
  - extreme fibre strain [125](#)
  - friction losses [104](#)
  - horizontal shear strength [271](#), [274–5](#)
  - load factors and combinations [20](#), [22](#)
  - moment redistribution at ultimate [360](#)
  - rectangular stress block [125](#), [127](#)
  - shear strength of beams [166–7](#)
  - shrinkage [45–6](#)
  - transfer length [212](#)
  - unbonded tendons [145–6](#)
- Bursting forces [215](#)
- Bursting moment [220](#)

CAN 3, 1984:

- bearing stress [225](#)
- crack control in slabs [439–40](#)
- design for serviceability [27](#)
- design strength [25](#)
- load factors and combinations [20, 22](#)
- Shear strength, General Method [167](#)
- Shear strength, Simplified Method [168](#)

Cable profile and location [7, 75–7, 321–3, 342–4](#)

Canadian Prestressed Concrete Institute [156](#)

Cantilever construction [323](#)

Capacity reduction factor [23–4, 126, 168](#)

Carry-over factor [335–6](#)

Carry-over moment [334](#)

CEB (1983) [111–12, 114, 120](#)

CEB-FIP 1970 [44](#)

CEB-FIP Model Code, 1978:

- creep predictive model [41, 43, 493–5](#)
- design strength [25](#)
- load factors [20, 23](#)
- relaxation of steel [53–4](#)
- shear strength [167](#)
- shrinkage predictive model [495–6](#)

Cement types [30](#)

Chakrabarti, P. [433](#)

Coefficient of thermal expansion [47–8](#)

Collins, M.P. [167](#)

Column line tendons [394](#)

Column strip [396–8, 433–5](#)

Column strip moment factor [400](#)

Combined load approach [10–11](#)

Compatibility torsion [182, 185–6](#)

Composite members:

- advantages [240–2](#)
- bond between mating surfaces [242](#)
- code provisions [267–71](#)
- determination of prestress [246–8](#)
- effective flange width [243](#)
- flexure-shear cracking [276–7](#)
- horizontal shear [242, 265–7](#)
- loading stages [243–6](#)
- short-term service load analysis [249–51](#)
- time analysis [252–3](#)
- types [240–2](#)
- ultimate flexural strength [265](#)
- ultimate shear strength [275–7](#)
- web-shear cracking [276](#)

Compression field theory [167–8](#)

Compression members:

- biaxial bending and compression [470–1](#)
- braced and unbraced structures [473](#)
- critical buckling load [472](#)
- design interaction curve [468–70](#)
- effective length [473](#)
- geometric non-linearity [455](#)

- moment magnifier method [474–81](#)
  - primary and secondary moments [455](#), [475](#)
  - primary compressive failure [458](#)
  - primary tensile failure [458](#)
  - reinforcement requirements [481–3](#)
  - slender columns [455–6](#), [471–81](#)
  - slenderness effects [471–81](#)
  - slenderness ratio [496](#)
  - stocky columns [456](#)
  - strength interaction curve [457–68](#), [475](#)
  - strength interaction surface [470](#)
  - types [454–5](#)
  - ultimate strength analysis [459–62](#)
- Concordant tendons [324](#), [330](#)
- Concrete:
- admixtures [30](#)
  - aggregates [30](#)
  - coefficient of thermal expansion [47–8](#)
  - composition [30](#)
  - compressive strength (characteristic) [30–1](#)
  - confinement effects [34](#)
  - creep [38–41](#), [44–5](#), [46–7](#)
  - creep coefficient [39–40](#), [42–7](#)
  - deformation of [34–42](#)
  - density [37](#)
  - elastic modulus [36–7](#), [44](#)
  - high strength [31](#)
  - hydration [30](#)
  - instantaneous strain [36–8](#)
  - Poisson's ratio [38](#)
  - shrinkage [41–2](#), [45–6](#), [47](#)
  - strain components [35](#)
  - strength versus time [32–3](#)
  - stress limits [61–4](#)
  - stress-strain curves [31–2](#), [36](#)
  - tensile strength [33](#)
  - water-cement ratio [30](#)
- Continuous members, *see* Statically indeterminate members
- Control joints [440](#)
- Crack control [26](#), [63](#), [358](#), [439–42](#)
- Crack types:
- direct tension [440–2](#)
  - flexural [81](#), [161](#)
  - flexure-shear [161](#), [169–70](#), [276–7](#)
  - web-shear [161](#), [170](#), [276](#)
- Cracked section analysis [81–8](#)
- Cracking moment [81](#)
- Creep:
- coefficient [39–40](#), [42–7](#)
  - delayed elastic component [39](#)
  - factors affecting [38–9](#)
  - flow component [39](#)
  - losses [107–8](#)
  - prediction of [40](#), [42–7](#), [490–5](#)
  - recoverable and irrecoverable [39](#)
  - strain [34–5](#), [38–41](#)
  - tensile [41](#)
  - variation with time [35–6](#), [39](#), [43](#)



Critical buckling load [472](#)  
Critical shear perimeter [198-9](#)  
Cross, H. [334](#)  
Cross-sectional analysis:  
  short-term, uncracked [77-81](#)  
  short-term, cracked [81-8](#)  
  time-dependent, uncracked [89-98](#)  
  time-dependent, cracked [98-102](#)  
Cross-sections (sizing):  
  initial trial dimensions [283-6](#)  
  minimum dimensions based on flexural strength [284-5](#)  
  minimum moment of inertia [284](#)  
  minimum section modulus [68-9](#), [283](#)  
  types [281-3](#)  
Crossing beam analogy [431](#)

Darwin, D. [33](#)  
Decompression moment [169](#)  
Deflection:  
  allowable [27](#)  
  approximate calculation of [108-20](#)  
  coefficients for slabs [430-1](#)  
  composite beams [249-53](#)  
  creep [116](#)  
  instantaneous [110-15](#)  
  limitations [26-7](#)  
  long-term [115-20](#)  
  models for two-way slabs [429-38](#)  
  multiplication factor [115](#), [284](#), [425](#)  
  problems [26](#)  
  shrinkage [116-17](#)  
Deformation of concrete [34-42](#)  
Design action [23](#), [147](#)  
Design strength [23](#), [126](#), [147](#)  
Design procedures:  
  continuous beams [354-75](#)  
  fully-prestressed beams (constant eccentricity) [303-11](#)  
  fully-prestressed beams (draped tendons) [286-303](#)  
  general requirements [17-28](#)  
  partially-prestressed beams [312-18](#)  
  slabs [381-2](#)  
Diagonal compression struts [163-4](#)  
Diagonal tension failure [160](#)  
Direct design method [401-3](#)  
Direct tension cracking in slabs [440-2](#)  
Distribution factor [336](#)  
Disturbed region [214](#)  
Doubly reinforced section [133-4](#)  
Dowel action [164-5](#), [266](#)  
Drop panels [415-16](#)  
Ductility [121-4](#), [127](#), [148](#), [398](#), [400](#), [482](#)

- Edge-supported two-way slabs, *see* Slabs (post-tensioned)
- Effective area of a support [198–9](#)
- Effective depth [124](#)
- Effective length of columns [473–6](#)
- Effective modulus of concrete [40](#)
- Effective span [425](#)
- Effective width of flange [153–4](#), [243](#)
- Elastic modulus of concrete [36–7](#), [44](#)
- Elastic modulus of steel [49](#), [51](#), [57](#)
- Elastic stresses, calculation of [9–15](#)
- Equilibrium torsion [183](#), [186–7](#)
- Equivalent column [398](#)
- Equivalent frame method [398–9](#)
- Equivalent load method [333–4](#), [337](#), [344–5](#)
- Equivalent loads [333–4](#), [337–8](#)
- Ewell, W.W. [431](#)
- 
- Faulkes, K.A. [64](#), [220](#), [361](#)
- Favre, R. [54](#), [89](#)
- Finite element methods [423–4](#), [436–7](#)
- FIP [219](#), [421–2](#)
- Fire resistance period [422–3](#)
- Flat-ducted tendons [377–8](#), [388–9](#)
- Flat plates, *see* Slabs (post-tensioned)
- Flat slabs, *see* Slabs (post-tensioned)
- Flexibility coefficient [329](#)
- Fixed-end moment [334](#)
- Flexural behaviour:  
     at overloads [122–4](#)  
     general [15–17](#)
- Flexural cracks [81](#), [161](#)
- Flexural strength theory: [124–40](#)  
     bonded tendons [127–9](#), [140–5](#)  
     design calculations [147–53](#)  
     flanged sections [153–9](#)  
     idealized rectangular stress blocks [124–7](#)  
     trial and error procedure [129–33](#)  
     ultimate moment [126–7](#), [129](#), [133–5](#), [137](#), [140–2](#)  
     unbonded tendons [145–7](#)
- Flexure-shear cracking [161](#), [169–70](#), [276–7](#)
- Force method, (flexibility method) [325](#)
- Friction losses [104–5](#)
- Fully-prestressed concrete [16](#), [61](#), [64–70](#)
- Fully-prestressed concrete, design procedures [286–7](#), [303–6](#)
- Furr, W.L. [432](#)
- 
- Gergely, P. [220](#)
- Ghali, A. [54](#), [89](#), [326](#), [336](#)
- Gilbert, R.I. [28](#), [33](#), [35](#), [37](#), [40](#), [43](#), [77](#), [89](#), [116](#), [249](#), [400](#), [423–5](#), [427](#), [436–7](#), [476](#), [490](#)
- Guyon, Y. [215–18](#), [222](#)
- 
- Hall, A.S. [197](#), [326](#), [336](#)
- Hanson, N.W. [213](#), [245](#)
- Hawkins, N.M. [197](#)
- Hognestad, E. [164](#)
- Hoyer, E. [211](#)

Hoyer effect [211](#)  
Hsu, T.T.C. [190](#)  
Hydration [30](#)

Illinois method for slab deflection [432-3](#)  
Inclined cracking [161](#)  
Internal couple concept [11-12](#)  
Irwin, A.W. [28](#)  
ISO-3898 [18](#)  
Iyengar, K.T.S.R. [215](#)

Johansen, K.W. [410](#)  
Jungwirth, D. [493](#)

Kaar, P.H. [213](#)  
Kabaila, A.P. [326](#), [336](#)  
Kupfer, H. [33](#)

Leonhardt, F. [239](#)  
Limit state [15](#), [17](#)  
Limit state design [17-28](#)  
Lin, T.Y. [64](#), [361](#)  
Linear transformation [330-2](#)  
Live load factors for serviceability [22-3](#)  
Live load patterns [399](#)  
Load balancing approach [9](#), [12](#), [60](#), [64](#), [74](#), [382-5](#), [394-6](#)  
Load factors and combinations:  
    for serviceability [21-3](#)  
    for stability [21](#)  
    for strength [19-21](#)

Loads:  
    balanced [9](#)  
    characteristic (or specified) [18-19](#), [21-2](#)  
    dead [18](#)  
    factored [19-23](#)  
    live [18-19](#)  
    service [21-3](#)  
    snow [18-19](#)  
    wind [18-19](#)

Long-line pretensioning [241](#)

Loov, R.E. [141](#)

Losses of prestress: [29](#), [102-8](#)  
    anchorage slip [105-6](#)  
    creep [107-8](#)  
    elastic deformation [103-4](#)  
    friction [104-5](#)  
    immediate [102](#)  
    relaxation [108](#)  
    shrinkage [107](#)  
    time-dependent [102-3](#), [106-8](#)

Magnel design diagram [67-8](#), [72](#), [246-8](#)  
Magnel, G. [64](#), [67](#), [220](#)  
Marsh, C.F. [431](#)

- Marshall, W.T. [213](#)  
 Mattock, A.H. [213](#), [361](#)  
 Membrane action [414](#)  
 Mickleborough, N.C. [28](#), [425](#)  
 Middle strip [396–8](#), [433–5](#)  
 Mitchell, D. [167](#)  
 Modular ratio [78](#)  
 Moment-area methods [326](#), [340](#), [345](#)  
 Moment distribution [333](#), [334–6](#), [338](#)  
 Moment-curvature relationship [84–5](#), [358–9](#)  
 Moment magnifier method [474–81](#)  
 Mohr's circle [162](#), [170](#)  
 Murray, D.W. [436](#)
- Naaman, A.E. [482](#)  
 Nawy, E.G. [433](#)  
 Neville, A.M. [29](#), [31](#), [35](#), [38](#), [41](#), [43](#), [48](#), [326](#), [336](#)  
 Nilson, A.H. [361](#), [433–5](#)
- One-way slabs, *see* Slabs (post-tensioned)  
 Over-reinforced beams [123](#)
- Pannell, F.N. [470](#)  
 Parrott, L.J. [45](#)  
 Partially-prestressed concrete [16](#), [61](#), [69](#), [248](#), [312–18](#)  
 Partial safety factors [19](#), [23](#)  
 Pauw, A. [37](#)  
 Pecknoid, D.A. [33](#)  
 Permissible stresses, *see* Stress limits  
 Plastic analysis [17](#), [359](#), [410](#)  
 Plastic hinge, (constant moment hinge) [358–9](#)  
 Plate theory [430](#)  
 Poisson's ratio for concrete [38](#), [430](#)  
 Portland Cement Association [431](#)  
 Post-tensioning:
  - anchorage zones [214–38](#)
  - friction [104–5](#)
  - methods [3–4](#)
  - profiles [7](#), [75–7](#), [321–3](#), [342–4](#)
 Post-Tensioning Institute [421](#)  
 Precast elements [240–2](#)  
 Precast pretensioned trough girder [253](#)  
 Pressure line [330](#)  
 Prestressed concrete:
  - basic concepts [1](#)
  - benefits [1–2](#)
  - introductory example [4–6](#)
  - methods [2–4](#)
 Prestressing force, transverse component [6–9](#)  
 Prestressing steel:
  - relaxation [52–4](#)
  - strain components [127–9](#)
  - types [48–52](#)
 Pretensioning:
  - anchorage zones [210–14](#)
  - method [2–3](#)
  - losses, [3–103](#)

Principal tensile stress [162](#)  
Principle of virtual work [324–32](#), [411](#), [413](#)  
Profile of tendons [7](#), [75–7](#), [321–3](#), [342–4](#)  
Punching shear strength:  
  ACI 318–83 approach [196–7](#)  
  AS 3600 approach [198–204](#)  
  critical shear perimeter [198–9](#)  
  edge column [206–8](#)  
  general [195](#)  
  interior column [204–5](#)  
  minimum moment transferred to column [403](#)  
  torsion strips [200–1](#)  
  with moment transfer [200–4](#)  
  with NO moment transfer [199–200](#)

Rangan, B.V. [190](#), [194](#), [197–8](#), [201–3](#)  
Reinforced concrete [1](#), [2](#)  
Reinforcement, non-prestressed [54–7](#)  
Relaxation of steel [52–4](#), [108](#)  
Ritter, W. [163](#)  
Ritz, P. [414](#)  
Rusch, H. [493](#)

Saemann, J.C. [245](#)  
Sargious, M. [215](#)  
Scanlon, A. [436](#)  
Secondary moments and shears [321](#), [324–32](#), [337](#), [339](#), [361–2](#), [398](#)  
Section modulus, minimum required [68](#), [283](#)  
Selna, L. [90](#)  
Serviceability:  
  design for [25–8](#), [60–120](#)  
  load combinations [21–3](#)  
Sign convention, *see Notation*  
Shear-compression failure [161](#)  
Shear-friction [269–70](#)  
Shear strength of beams:  
  ACI 318–83 approach [179–80](#)  
  anchorage of longitudinal reinforcement [168](#)  
  anchorage of stirrups [165](#), [172](#)  
  AS 3600 approach [167–73](#)  
  BS 8110 approach [180–2](#)  
  concrete contribution [165](#), [169–70](#)  
  critical section [171](#)  
  design equation [172](#)  
  design requirements [170–3](#)  
  maximum and minimum strength [168](#)  
  maximum spacing of stirrups [171](#)  
  minimum transverse steel [167](#), [171](#), [182](#)  
  steel contribution [166](#), [171](#)  
  ultimate strength [165](#)

- web steel requirements [172](#)–3
- Shrinkage:
  - factors affecting [41](#)–2
  - loss due to [107](#)
  - prediction of [42](#)–3, [45](#)–7, [492](#)–3, [495](#)–6
  - strain [35](#), [41](#)–2
- Simpson's rule [327](#)
- Singly-reinforced section [129](#)–33
- Skew bending [184](#)
- Slabs (post-tensioned):
  - balanced load stage [419](#)–21
  - band-beam and slab systems [377](#), [416](#)–17
  - bonded versus unbonded tendons [377](#)–8
  - calculation of slab thickness [423](#)–9
  - cracking in slabs [438](#)–42
  - deflection coefficients [430](#)–1
  - deflection models [429](#)–38
  - edge-supported two-way slabs [376](#)–7, [382](#)–94, [427](#), [431](#), [443](#)–6
  - effects of prestress [378](#)–81
  - finite element models [436](#)–7
  - fire resistance [422](#)–3
  - flat plate slabs [376](#)–7, [394](#)–414, [426](#)–7
  - flat slabs with drop panels [376](#)–7, [415](#)–16, [426](#)–7, [446](#)–52
  - frame analysis [398](#)–400
  - live load patterns [399](#)
  - long-term deflections [442](#)–3
  - non-prestressed reinforcement requirements [380](#), [439](#)–40
  - one-way slabs [376](#)–7, [382](#), [426](#)
  - shear strength, *see* Punching shear strength [402](#)–3
  - span-to-depth ratios [421](#)–2, [423](#)–8
  - yield line analysis of flat slabs [410](#)–14
- Slab system factor [423](#), [426](#)–7
- Slater, W.A. [386](#)
- Slender columns [455](#), [471](#)–81
- Slenderness ratio [476](#)
- Slope [108](#)–9
- Sozen, M.A. [220](#)
- Spalling moment [221](#)
- Span-to-depth ratio:
  - edge-supported slabs [421](#), [425](#), [427](#)
  - flat slabs [421](#)–2, [425](#)–7
  - one-way slabs [421](#), [425](#)–6
- Spandrel beam [200](#)–1
- Spandrel strip [198](#), [200](#), [398](#)
- Spiral reinforcement in columns [482](#)
- Stage stressing [242](#), [372](#), [420](#), [485](#)
- Static moment [397](#), [401](#)
- Statically indeterminate members:
  - advantages and disadvantages [319](#)–21
  - concordant tendons [324](#), [330](#)
  - design of continuous beams [354](#)–75
  - design steps [362](#)–4
  - effects of creep [347](#)–50
  - equivalent load method [333](#)–4, [337](#), [344](#)
  - frames [350](#)–3
  - hyperstatic reactions [323](#), [330](#)–1
  - linear transformation [330](#)–2
  - moment distribution [333](#)–6, [338](#)

- moment redistribution at ultimate [360](#)–1
- non-prismatic members [346](#)–7
- pressure line [330](#), [332](#)
- primary moments and shears [324](#)–5, [330](#)–1
- secondary effects at ultimate [361](#)–2
- secondary moments and shears [321](#), [324](#)–32, [361](#)–2, [398](#)
- tendon profiles [321](#)–3, [342](#)–6
- tertiary effects [351](#)
- virtual work [324](#)–32

Statics ratio method [432](#)

Steel:

- alloy bar [51](#)–2
- low relaxation [50](#), [52](#)–4
- reinforcing bar [54](#)–7
- relaxation [52](#)–4
- strand [50](#)–1
- welded wire fabric [56](#)–7
- wire [48](#)–[50](#)

Stiffness coefficient [335](#)–6

Stirrups [163](#)–7, [171](#)–2

Strand [50](#)–1

Strength of concrete:

- biaxial [33](#)–4
- characteristic compressive [30](#)–1
- cylinder versus cube [31](#)
- gain with age [32](#)–3
- uniaxial [31](#)–2
- tensile [33](#)

Strength, *see* Flexural strength, Shear strength, Torsional strength

Strength reduction factor, *see* Capacity reduction factor

Stress block, rectangular [124](#)–6

Stress limits:

- concrete [61](#)–4
- steel [64](#)
- satisfaction of [64](#)–[74](#)

Stress-strain relationships:

- concrete [31](#)–2, [36](#)–7
- prestressing steel [49](#)–[52](#)
- reinforcing bars [56](#)–7

Stress isobars [215](#)–18, [223](#)

Stress trajectories [214](#)–15, [217](#)

St. Venant's principle [215](#)

Superposition principle [16](#), [74](#), [98](#), [325](#), [354](#)

Symmetric prism [222](#), [230](#)–1

Tasuji, M.E. [33](#)

Tendon profile, *see* Cable profile and location

Temperature effects on creep and shrinkage [496](#)

Tension members:  
  advantages and applications [483](#)  
  axial deformation [485](#)  
  behaviour [483–6](#)  
  design example [486–9](#)

Tension stiffening effect [82](#), [110–12](#)

Tesar, M. [215](#)

Theorem of complementary shear stress [266](#)

Thornton, K. [361](#)

Time-dependent behaviour [89–102](#)

Timoshenko, S. [430](#)

Torsional cracking [184](#), [188–9](#)

Torsional strength:  
  additional longitudinal steel [185](#), [187](#)  
  AS 3600 provisions [185–94](#)  
  beam with transverse reinforcement [186–7](#)  
  beam without transverse reinforcement [186](#)  
  combined torsion, bending and shear [187–9](#)  
  design equation [187](#), [189](#)  
  detailing of stirrups [188](#)  
  effect of prestress [184](#)  
  maximum strength [187](#)  
  minimum closed hoops [185](#)  
  truss analogy (3-D) [184–5](#)

Transfer length [209–14](#)

Transfer of prestress [60](#)

Transformed sections [77–8](#), [92](#), [94](#)

Transmission length, (*see* transfer length)

Transverse reinforcement in columns [481–3](#)

Transverse tendon forces [6–9](#)

Trost, H. [41](#)

Trough girder [253](#)

Ultimate curvature [126–7](#)

Ultimate load stage [17](#), [122–4](#)

Ultimate strength design [121](#), [124](#)

Ultimate flexural strength:  
  code-oriented procedures [140–7](#)  
  general [23](#), [121–47](#)

Under-reinforced beams [123](#)

Upper bound approach [414](#)

Vanderbili, M.D. [432](#)

Variable angle truss model [167](#)

Vibration in buildings [27–8](#)

Virtual force [326](#)

Virtual work, *see* Principle of virtual work

VSL [380](#)

Volume integration [327–8](#)

Walters, D.B. [433–5](#)

Warner, R.F. [64](#), [220](#), [361](#)

Washa, G.W. [245](#)

Web-crushing [164](#), [168](#)

Web-shear cracking [161](#), [170](#), [276](#)

Westergaard, H.M. [386](#)

Wide beam method for slab deflection [433–5](#)



Wire mesh, welded [56–7](#)

Wires [48–50](#)

Woinowsky-Krieger, S. [430](#)

Work products, external and internal [326](#), [411–13](#)

Yield line theory, [385](#), [410–14](#)

Yield lines [410–11](#)

Yield stress [49](#), [51](#), [55–7](#)

Yogananda, C.V. [215](#)

Zia, P. [190](#)